

UNCLASSIFIED

AD NUMBER

ADB018948

LIMITATION CHANGES

TO:

Approved for public release; distribution is unlimited.

FROM:

Distribution authorized to U.S. Gov't. agencies only; Test and Evaluation; NOV 1976. Other requests shall be referred to Air Force Flight Dynamics Lab., Wright-Patterson AFB, OH 45433.

AUTHORITY

AFWAL ltr 9 Aug 1985

THIS PAGE IS UNCLASSIFIED

AD

BO 18948

Authority ~~AFWAL~~ 1tr,
9 Aug 85-



REMOVED AT REQUEST OF THE NATIONAL ARCHIVES

✓ AFFDL-TR-76-97
Volume I

2

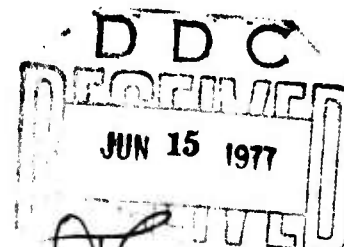
AD B018948

ADVANCED DESIGN COMPOSITE AIRCRAFT (ADCA) STUDY

GRUMMAN AEROSPACE CORPORATION
BETHPAGE, NEW YORK 11714

NOVEMBER 1976

TECHNICAL REPORT AFFDL-TR-76-97 Volume I
FINAL REPORT FOR JULY 1975 - AUGUST 1976



Distribution limited to U.S. Government agencies only; test and evaluation data, November 1976. Other requests for this document must be referred to the Structures Division (FBS), Air Force Flight Dynamics Laboratory, Wright-Patterson AFB, Ohio 45433

DDC FILE COPY

AIR FORCE FLIGHT DYNAMICS LABORATORIES
AIR FORCE WRIGHT AERONAUTICAL LABORATORIES
AIR FORCE SYSTEMS COMMAND
WRIGHT-PATTERSON AIR FORCE BASE, OHIO 45433

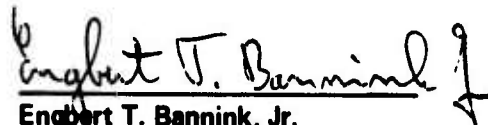
NOTICES

When Government drawings, specifications, or other data are used for any purpose other than in connection with a definitely related Government procurement operation, the United States Government thereby incurs no responsibility nor any obligation whatsoever, and the fact that the Government may have formulated, furnished, or in any way supplied the said drawings, specifications, or other data is not to be regarded by implication or otherwise as in any manner licensing the holder or any other person or corporation, or conveying any rights or permission to manufacture, use, or sell any patented invention that may in any way be related thereto.

This technical report has been reviewed and is approved for publication.

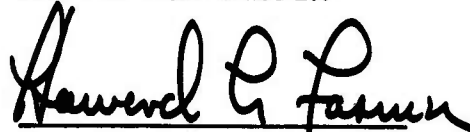


Larry G. Kelly, Acting Chief
Advanced Structures Development Branch
Structural Mechanics Division
Air Force Flight Dynamics Laboratory



Engbert T. Bannink, Jr.
Aerospace Engineer
Structural Mechanics Division
Air Force Flight Dynamics Laboratory

FOR THE COMMANDER



Howard L. Farmer, Col USAF
Chief, Structures Division

Copies of this report should not be returned unless return is required by security considerations, contractual obligations, or notice on a specific document.

SECURITY CLASSIFICATION OF THIS PAGE (When Data Entered)

19 REPORT DOCUMENTATION PAGE		READ INSTRUCTIONS BEFORE COMPLETING FORM
1. REPORT NUMBER	2. GOVT ACCESSION NO.	3. PERFORMING ORG. REPORT NUMBER
18 AFFDL TR-76-97-VOL-1		
4. TITLE (and Subtitle)	5. TYPE OF REPORT & PERIOD COVERED	
6 ADVANCED DESIGN COMPOSITE AIRCRAFT (ADCA) STUDY. Volume I.	9 FINAL TECHNICAL REPORT. JULY 1975 - AUG 1976	
	10 PERFORMING ORG. REPORT NUMBER	
	30	
7. AUTHOR(s)	8. CONTRACT OR GRANT NUMBER(s)	
10 H. FORSCH	15 F33615-75-C-3124	
9. PERFORMING ORGANIZATION NAME AND ADDRESS	10. PROGRAM ELEMENT, PROJECT, TASK AREA & WORK UNIT NUMBERS	
GRUMMAN AEROSPACE CORPORATION BETHPAGE L.I. NEW YORK 11714	16 62201F/13680131-17 01	
11. CONTROLLING OFFICE NAME AND ADDRESS	12. REPORT DATE	
AIR FORCE FLIGHT DYNAMICS LABORATORY ATT AFFDL/FBS - ITEM NO. 0002 SEQUENCE NO. A00B WPAER OHIO 45433	11 NOV 1976	
14. MONITORING AGENCY NAME & ADDRESS (if different from Controlling Office)	13. NUMBER OF PAGES	
12 451p.		
	15. SECURITY CLASS. (of this report)	
	UNCLASSIFIED	
	15a. DECLASSIFICATION/DOWNGRADING SCHEDULE	
D		
16. DISTRIBUTION STATEMENT (of this Report)		
DISTRIBUTION LIMITED TO GOVERNMENT AGENCIES ONLY; TEST AND EVALUATION DATA, NOVEMBER 1976. OTHER REQUESTS FOR THIS DOCUMENT MUST BE REFERRED TO THE STRUCTURES DIVISION (FBS), AIR FORCE FLIGHT DYNAMICS LABORATORY, WRIGHT PATTERSON AFB OHIO		
45433		
17. DISTRIBUTION STATEMENT (of the abstract entered in Block 20, if different from Report)		
APPROVED FOR PUBLIC RELEASE, DISTRIBUTION UNLIMITED		
18. SUPPLEMENTARY NOTES		
19. KEY WORDS (Continue on reverse side if necessary and identify by block number)		
ADVANCED COMPOSITES GRAPHITE EPOXY BORON EPOXY		
20. ABSTRACT (Continue on reverse side if necessary and identify by block number)		
<p>THE ADCA PROGRAM DEFINED THE PAYOFFS AND RAMIFICATIONS OF THE UNRESTRAINED APPLICATION OF ADVANCED COMPOSITES MATERIALS TO A COMPLETELY NEW AIRCRAFT. THE SPECIFIC OBJECTIVE WAS TO OBTAIN A SMALLER, LIGHTER AND LESS COSTLY AIRCRAFT, CAPABLE OF PERFORMING THE SUPERSONIC PENETRATION INTERDICTION FIGHTER MISSION AT LOWER LIFE CYCLE COSTS THAN A METAL COUNTERPART.</p> <p>THE PROGRAM INDICATED THAT SIGNIFICANT COST AND WEIGHT SAVINGS OVER AN EQUIVALENT METAL AIRCRAFT COULD BE ACHIEVED BY THE LOGICAL APPLICATION OF ADVANCED COMPOSITE</p> <p>(cont on p. ii)</p>		

DD FORM 1 JAN 73 1473 EDITION OF 1 NOV 65 IS OBSOLETE

UNCLASSIFIED

SECURITY CLASSIFICATION OF THIS PAGE (When Data Entered)

388 847

mt

Typist:
capitalize only the
first letter in each
sentence, + ADCA.

SECURITY CLASSIFICATION OF THIS PAGE(When Data Entered)

Secret (S)

MATERIALS TO 80% OF AIRFRAME. THE FINAL SAVINGS WERE A 26% REDUCTION IN VEHICLE TAKE-OFF-GROSS WEIGHT AND A 21% REDUCTION IN THE CUMULATIVE AVERAGE FLY-AWAY COSTS. THESE SAVINGS WERE PRIMARILY DUE TO THE RESIZING OF THE VEHICLE WHICH WAS MADE POSSIBLE BY THE WEIGHT SAVINGS RESULTING FROM APPLICATION OF COMPOSITES. ASIDE FROM THESE SAVINGS, THIS PROGRAM HAS ALSO DEMONSTRATED THAT THE CAPABILITY EXISTS, WITH CURRENT TECHNOLOGY, TO DESIGN AND FABRICATE AN AIRFRAME UTILIZING UP TO 80% COMPOSITE MATERIAL.



UNCLASSIFIED

SECURITY CLASSIFICATION OF THIS PAGE(When Data Entered)

FOREWORD

The work reported herein was performed under the sponsorship of the Air Force Flight Dynamics Laboratory, Air Force Systems Command, Wright-Patterson Air Force Base, Ohio 45433. Mr. L. Kelly, AFFDL/FBS is the Air Force Program Manager and Cpt. E. Bannink, AFFDL/FBS is the Air Force Project Engineer.

The work was performed by the Advanced Composites/Advanced Aircraft Systems Groups, Grumman Aerospace Corporation, Bethpage, New York 17714, under Contract F-33615-75-C-3124, Project Task 1368-01-31. The inclusive dates of contract performance are July 1975 to Aug. 30, 1976. Submittal Date of this report is November 1976.

Key Grumman personnel associated with the program and their respective areas of responsibility are:

R. Caporali	Program Director	P. Schwartz	Weights
R. Hadcock	Program Manager	H. Borstell	Materials & Processes
H. Forsch	Project Engineer	D. Pearce	Power Plant
R. McNiece	Asst. Project Engineer	R. Erlandson	Mechanical Systems
J. Sicari	Structural Design	W. Evans	Aerodynamics
S. Johnson	Structural Analysis	T. Ervolina	Propulsion
C. Waters	Dynamics	C. Gianetto	Guidance & Control
W. McDowell	Loads	W. Bruning	Operations Analysis
D. Sharp	Structural Mechanics	D. Colquhoun	Configuration Design
	J. Katz	Engineering Specifications	

White Section	<input type="checkbox"/>
Red Section	<input checked="" type="checkbox"/>
UNANNOUNCED	<input type="checkbox"/>
JUSTIFICATION	
BY	
DISTRIBUTION AVAILABILITY CODES	
EXC. AVAIL. ADD. OR SPECIAL	
B	

TABLE OF CONTENTS

<u>Section</u>		<u>Page</u>
I	INTRODUCTION AND SUMMARY	1
II	MISSION ANALYSIS	3
	2.1 Overview	3
	2.2 Mission Perspective	3
	2.3 Mission Performance Consideration	4
	2.4 Point Performance Considerations	6
	2.5 Payoff Analysis	6
III	CONFIGURATION SCREENING	13
	3.1 Composite Materials	13
	3.2 Engine Candidates	13
	3.3 Mission Requirements	16
	3.4 Avionics	17
	3.5 Candidate Wing Shapes	17
	3.6 Parametric Screening	19
	3.6.1 F404-GE-400	21
	3.6.2 F101-GE-100	21
	3.6.3 Summary	22
IV	VEHICLE DEFINITION	23
	4.1 General Arrangement	23
	4.2 Tandem Crew Configuration	25
	4.3 Weight and Balance	28
	4.4 Aerodynamics and Vehicle Performance	36
	4.4.1 Aerodynamic Configuration Features	38
	4.4.2 Vehicle Aerodynamic Characteristics	41
	4.4.3 Wing Design	47
	4.4.4 Canard Design	54
	4.4.5 Longitudinal Control Considerations	56
	4.4.6 Wind Tunnel Testing	58
	4.4.7 Vehicle Performance	70
	4.5 ADCA Propulsion System	90
	4.5.1 Inlet Design	91
	4.5.2 Nozzle Design	92
	4.6 Flight Control	94
	4.6.1 Flight Controls Mechanization	98
	4.7 Systems	101
	4.7.1 Control Surface Actuation	105
	4.7.2 Hydraulic Systems	105
	4.7.3 Electric Power System	108
	4.7.4 Bleed Air and Environmental Control Systems	109
	4.7.5 Power Plant Installation	112
	4.7.6 Accessory Drive and Emergency Power Systems	115
	4.7.7 Fuel System Schematic	117

TABLE OF CONTENTS (Cont)

Section		Page
V	AIRFRAME STRUCTURAL DEFINITION AND DETAIL DESIGN	121
5.1	Composite Materials Design Considerations	121
5.1.1	Materials Selection	121
5.1.2	Design Practices	127
5.1.3	Design Allowables	127
5.1.4	Hardware Selection	137
5.1.5	Integral Fuel Tank Sealing Concepts	137
5.1.6	Radar Characteristics	139
5.1.7	Design/Manufacturing Interface	140
5.2	Loads and Criteria	140
5.2.1	Preliminary Design Loads Estimates	140
5.2.2	Aeroelastic Effects	145
5.2.3	Aeroelastic Tailoring Benefits Evaluation (Wing)	147
5.2.4	Aeroelastic Tailoring Benefits Evaluation (Fin-Rudder)	161
5.2.5	Summary of Aeroelastically Corrected, Balanced Aircraft Loads for Preliminary Design	163
5.3	ADC Overall Structural Arrangement	165
5.4	Wing Structural Arrangement and Detail Design Concepts	167
5.4.1	Wing Structural Arrangement	167
5.4.2	Detail Structural Design Concept	168
5.4.3	Wing Design Cycle	174
5.4.4	Laminate Tailoring Options	177
5.4.5	COMBO (Composite Box Optimization) Procedure	178
5.4.6	Finite Element Model (FEM)	181
5.4.7	Finite Element Model Optimization for Increased Twist	195
5.4.8	Vibration and Flutter Considerations	207
5.5	Canard Structural Arrangement and Detail Design Concept	252
5.5.1	Canard Structural Arrangement	252
5.5.2	Detail Structural Design Concept	252
5.5.3	Canard Vibration and Flutter Consideration	254
5.6	Vertical Fin Structural Arrangement and Detail Design	283
5.6.1	Vertical Fin Structural Arrangement	283
5.6.2	Vertical Fin Structural Design Concept	283
5.6.3	Fin Vibration and Flutter Consideration	284

TABLE OF CONTENTS (Cont)

Section		Page
5.7	Fuselage Structural Arrangement and Detail Design . . .	327
5.7.1	Structural Arrangement	328
5.7.2	Detail Structural Design Concept	331
5.7.3	Landing Gear and Landing Loads	332
5.7.4	Fuselage Flight Design Conditions	341
5.7.5	Acoustic Levels	342
5.7.6	Internal Pressurization	343
5.7.7	Engine Nacelle Structure Temperature	347
5.7.8	Fuselage Internal Load Distribution	350
5.7.9	Fuselage Bending and Torsional Stiffness	352
5.7.10	Fuselage Shell Sizing and Tradeoffs	354
5.8	Design of Critical Areas.	365
5.8.1	Wing to Fuselage Attachment	365
5.8.2	Canard to Fuselage Attachment	371
5.8.3	Vertical Fin to Fuselage Attachment	377
5.8.4	Main Landing Gear Attachment.	377
5.8.5	Engine Mounts	381
5.8.6	Fuselage Manufacturing Splice-FS 450	381
5.8.7	Hoist Fitting	382
5.8.8	Control Surface Attachment	382
5.9	Manufacturing Plan	388
5.10	Environmental Considerations	390
5.10.1	Repair Techniques	390
5.10.2	Impact Resistance	391
5.10.3	Lightning Strike Protection Systems	392
5.10.4	Erosion Protection Coatings	392
5.10.5	Moisture Absorption Protection Systems	393
VI	COST	395
6.1	Cost Estimating Methodology	395
6.1.1	Airframe Cost	395
6.1.2	Propulsion Cost	395
6.1.3	Avionics Cost	395
6.1.4	Spares and Support Costs	396
6.1.5	Operating Cost	396
6.2	Cost Analysis	397
6.2.1	Initial Sizing and Tradeoff Studies	397
6.2.2	Initial Cost Comparisons	397
6.2.3	Reliability and Maintainability Analysis	402
6.2.4	Updated Vehicle Sizing Studies	403
6.2.5	Resized Vehicle Cost Comparisons	407
6.2.6	Composite Airframe Cost Breakdown	407
6.2.7	Fuel Consumption Comparison	413
6.2.8	Optimum Composite Usage Tradeoff	413
6.2.9	Production Feasibility.	413
VII	TECHNOLOGY DEVELOPMENT PLAN	417
VIII	REFERENCES	425

LIST OF ILLUSTRATIONS

Figure		Page
1	ADCA Program Schedule	2
2	Combat Radius	5
3	Mission Profile	5
4	Takeoff and Landing	7
5	Maneuverability Is Required for Self Defense	7
6	Acceleration Requirements	8
7	Bounding the Tactical Requirements	8
8	ADCA vs Existing Capability	9
9	Design/Performance/Cost Trade Analysis	10
10	Life Cycle Costs vs Penetration Speed	11
11	Sensitivity of Life Cycle Costs to Combat Losses	11
12	Initial Assessment	12
13	ADCA General Arrangement	24
14	ADCA Inboard Profile	26
15	Tandem Crew Configuration	27
16	Advanced Composite Wing Box Weight Savings	29
17	Advanced Composite Empennage Weight Savings	29
18	Advanced Composite Weight Savings - Rudders, Flaps, Doors, Etc.	30
19	Advanced Composite Fuselage Weight Savings	30
20	Advanced Composite Weight Savings - Miscellaneous Components	31
21	ADCA C.G. Travel Plot	33
22	Takeoff Gross Weight Comparison	35
23	Weight-to-Bearing Strength, Composites vs Titanium	37
24	ADCA Mission Profile Supersonic Penetration Interdiction Fighter (SPIF) Mission	37
25	The Compound Planform Wing	40
26	Vehicle Longitudinal Characteristics, RSS Design, Variable Camber and Canard	40
27	Minimum Drag Status	42
28	Trimmed Lift Curves	43
29	Trimmed Drag Polars	44
30	Maximum Lift Coefficient	44
31	ADCA Estimated Longitudinal Aero Coefficients	46
32	ADCA Lateral/Directional Static Derivatives	48
33	ADCA Lateral/Directional Dynamic Derivatives	49
34	ADCA Rudder Effectiveness	50
35	ADCA Aileron Effectiveness	51
36	Load Distribution Optimized for Supersonic Cruise	52
37	Optimum Span Load Distributions	53
38	Wing Twist Distribution	54
39	Canard Size, Wing Location and Stability are Traded Off Within Practical Design Limits	55
40	Canard Sizing	55
41	Canard Sizing Criteria, Time and Stability Boundaries	56
42	Slab Canard Provides Best "G" Capability and Control Anticipation	57

LIST OF ILLUSTRATIONS (Cont)

Figure		Page
43	Slab Canard Provides Instantaneous Response	58
44	Missile Avoidance Capability	59
45	Slab Canard Has Best Low Speed Pitch Acceleration	59
46	ADCA Low Speed Wind Tunnel Model	61
47	ADCA Low Speed Wind Tunnel Model.	61
48	Effect of Variable Camber on Drag Polar	62
49	Canard Effect on Induced Drag	62
50	Canard Effect on Longitudinal Characteristics, Uncambered Wing	63
51	Linear Longitudinal Characteristics of Canard Configuration	63
52	Canard Provides Trim Over a Broad C_L Range, Linearity Maintained	64
53	Lift and Drag Improvements With Canard Camber	64
54	Wing and Canard Effects on Trimmed Drag Polar	65
55	Trimmed Drag Improvement With Canard Size and Camber, Wing Camber, and RSS	65
56	Canard Lift Loss Due to Downwash on Wing	66
57	Effect of Canard Height on Directional Stability	66
58	Moderate Height Canard Improves Lateral/Directional Characteristics	67
59	Effect of Canard Height on Lateral/Directional Stability	67
60	Aileron Effectiveness Maintained Throughout Angle of Attack and Sideslip Angles Tested.	68
61	Influence of Canard on Aileron Effectiveness	68
62	Directional Stability and Rudder Effectiveness, Canard Off	69
63	Directional Stability and Rudder Effectiveness, Canard On	69
64	1/25-Scale High Speed Tunnel Model	71
65	ADCA Alternate Missions	75
66	Alternate Store Installation	76
67	ADCA SPIF Mission Supersonic/Subsonic Radius Tradeoff	77
68	ADCA Sea Level Interdiction	78
69	ADCA Ferry Range	78
70	ADCA Maneuverability Summary	79
71	ADCA Acceleration Capability	80
72	Operational Flight Envelope	81
73	Operational Flight Envelope.	81
74	Maximum Sustained Load Factor	82
75	Maximum Sustained Load Factor	83
76	Maximum Sustained Load Factor	83
77	Maximum Sustained Load Factor	84
78	Maximum Instantaneous Load Factor	84
79	Maximum Instantaneous Load Factor	85
80	Specific Excess Power	86
81	Specific Excess Power	86
82	Specific Excess Power	87
83	Specific Excess Power	87
84	Specific Excess Power	88
85	Specific Excess Power	88

LIST OF ILLUSTRATIONS (Cont)

Figure		Page
86	Specific Excess Power, Intermediate Power	89
87	Specific Excess Power, Intermediate Power	89
88	Takeoff and Landing Ground Roll Distance	90
89	Fixed-Inlet Design	91
90	Matched-Inlet Performance	92
91	Nozzle Installation Considerations	93
92	Baseline F101 Nozzle/Airframe Integration	94
93	Fly-By-Wire Permits Control Configuring for Superior Performance and Flying Qualities	95
94	Pitch Channel Block Diagram	96
95	Normal Acceleration Response to Step Command	97
96	Roll Channel Block Diagram	98
97	Bank Angle Response to Roll Command	99
98	Rolling Maneuver in Accelerated Flight (2g)	100
99	Yaw Channel Block Diagram	101
100	Sideslip Response to Step Yaw Rate Command	102
101	Sideslip Response to Pulse Yaw Command	103
102	Aircraft Response to Turbulence	104
103	ADCA Flight Controls, General Arrangement	106
104	ADCA Preliminary Hydraulic Systems Block	107
105	ADCA Electrical Power System	108
106	ADCA Environmental Control System	110
107	ADCA Typical Power Plant Installation	113
108	ADCA Preliminary Accessory Drive and Emergency Power Systems	116
109	ADCA Fuel System Schematic	119
110	Joint Bonding/Moisture Barrier Concept	122
111	Effect of Humidity on Gr/Ep Allowables at 250° F (0/90/±45) Laminates with 10% 90° Layers	122
112	Effect of Humidity on B/Ep Allowables at 250° F (0/90/±45) Laminates with 10% 90° Layers	124
113	Mach Number vs Altitude	125
114	Boron and A/S Graphite Materials Cost Trends	126
115	Allowable Tensile Strength $\sigma_{G/\pm 45^\circ G/90^\circ G}$ Laminate Type AS Graphite Epoxy, Room Temperature, No Holes	129
116	LHS Graphite/Epoxy Laminate, No Holes	130
117	LHS Graphite/Epoxy Laminate, No Holes	131
118	Predicted Axial Stress-Strain Curves	132
119	Predicted Anisotropic Coupling, Axial Stress/Shear Strain Curves, Graphite/Epoxy Laminate without Holes	133
120	Stress Concentration And Die-Away For Anisotropic Laminate With Circular Hole	136
121	Integral Fuel Tank Sealing Concepts	138
122	Advanced Sealing Concept	139

LIST OF ILLUSTRATIONS (Cont)

Figure		Page
123	ADCA Wing Loads	141
124	ADCA Canard Swept Air Loads (Limit).	142
125	ADCA Vertical Tail Swept Air Loads (Limit).	143
126	Design 105A, Ultimate Vertical Shear Fuselage.	144
127	Design 105A, Ultimate Vertical Bending Moment Fuselage	144
128	Flexibility Factor, Lift, Wing	148
129	Flexibility Factor, Pitching Moment, Wing	148
130	Flexibility Factor, Lift, Canard	149
131	Flexibility Factor, Lift, Canard	149
132	Flexibility Factor, Lift, Canard, Antisymmetric Deflection	150
133	Flexibility Factor Pitching Moment, Canard, Antisymmetric Deflection	150
134	Flexibility Factor, Rolling Moment, Canard, Antisymmetric Deflection	151
135	Flexibility Factor, Lift, Inboard Flaperon, Symmetric Deflection	151
136	Flexibility Factor, Pitching Moment, Inboard Flaperon, Symmetric Deflection	152
137	Flexibility Factor, Lift, Inboard Flaperon, Antisymmetric Deflection	152
138	Flexibility Factor, Pitching Moment, Inboard, Flaperon, Antisymmetric Deflection	153
139	Flexibility Factor, Rolling Moment, Inboard Flaperon, Antisymmetric Deflection	153
140	Flexibility Factor, Lift, Outboard Flaperon, Symmetric Deflection	154
141	Flexibility Factor, Pitching Moment, Outboard Flaperon, Symmetric Deflection	154
142	Flexibility Factor, Lift, Outboard Flaperon, Unsymmetric Deflection	155
143	Flexibility Factor, Pitching Moment, Outboard Flaperon, Unsymmetric Deflection	155
144	Flexibility Factor, Rolling Moment, Outboard Flaperon, Unsymmetric Deflection	156
145	Flexibility Factor, Lateral Force, Vertical Tail.	156
146	Flexibility Factor, Rolling Moment, Vertical Tail.	157
147	Flexibility Factor, Yawing Moment, Vertical Tail.	157
148	Flexibility Factor, Lateral Force, Rudder.	158
149	Flexibility Factor, Rolling Moment, Rudder.	158
150	Flexibility Factor, Yawing Moment, Rudder.	159
151	ADCA Wing Box Twist Distribution	160
152	Flexibility Factor, Lateral Force, Vertical Tail.	162
153	Flexibility Factor, Lateral Force, Rudder.	162
154	ADCA Limit Fuselage Airload	165
155	Structural Arrangement	166

LIST OF ILLUSTRATIONS (Cont)

Figure		Page
156	Wing Structural Concept	169
157	Wing Structural Concept	171
158	Advanced Wing Box Concept	175
159	ADCA Wing Design Cycle	176
160	Wing Twist Control Sensitivity	178
161	Finite Element Layer Directions	182
162	Finite Element Model Layer Directions	183
163	Finite Element Model Upper Cover Node and Element Numbers . .	184
164	Upper Cover Layup	186
165	Lower Cover Layup	186
166	Upper Cover Stress Resultants	187
167	Lower Cover Stress Resultants	188
168	Upper Cover Layer Stress (KSI), Layer No. 1	189
169	Upper Cover Layer Stress (KSI), Layer No. 2	190
170	Upper Cover Layer Stress (KSI), Layer No. 3	191
171	Upper Cover Layer Stress (KSI), Layer No. 4	192
172	Top Cover Principal Stress, Layer No. 1	193
173	ADCA Wing Vertical Deflection	194
174	Alternate Rib and Spar Idealization	196
175	Streamwise Twist Distribution at Ultimate Load	198
176	ADCA Wing Upper Cover	199
177	Finite-Element Optimization Procedure	200
178	ADCA Wing Upper Cover	203
179	Upper Cover Layup: Converged Design After MCR/ASOP/ FASTOP Cycling	204
180	Upper Cover Stress Resultants: Converged Design After MCR/ ASOP/FASTOP Cycling	205
181	Streamwise Twist Distribution at Ultimate Load	206
182	Wing Dynamic Idealization Beam Model	211
183	ADCA Wing-Node Lines and Flutter Envelope, Clean Wing	213
184	Wing Beam Model, Clean, No Fuel, M = 0.6, Sea Level	214
185	Wing Beam Model, Clean, No Fuel, M = 0.6, 20,000 Ft	215
186	Wing Beam Model, Clean, No Fuel, M = 0.6, 40,000 Ft	216
187	Wing Beam Model, Clean, No Fuel, M = 0.8, Sea Level	217
188	Wing Beam Model, Clean, No Fuel, M = 0.8, 20,000 Ft	218
189	Wing Beam Model, Clean, No Fuel, M = 0.8, 40,000 Ft	219
190	Wing Beam Model, Clean, No Fuel, M = 1.3, Sea Level	220
191	Wing Beam Model, Clean, No Fuel, M = 1.3, 11,000 Ft	221
192	Wing Beam Model, Clean, No Fuel, M = 1.3, 20,000 Ft	222
193	Wing Beam Model, Clean, No Fuel, M = 1.3, 40,000 Ft	223
194	Wing Beam Model, Clean, No Fuel, M = 1.6, 21,500 Ft	224
195	Wing Beam Model, Clean, No Fuel, M = 1.6, 40,000 Ft	225

LIST OF ILLUSTRATIONS (Cont)

Figure		Page
196	Wing Node Lines and Flutter Envelopes, Clean, Full Fuel	227
197	Wing Beam Model, Clean, Full Fuel, $M = 0.8$, Sea Level	228
198	Wing Beam Model, Clean, Full Fuel, $M = 0.8$, 20,000 Ft	229
199	Wing Beam Model, Clean, Full Fuel, $M = 0.8$, 40,000 Ft	230
200	Wing Beam Model, Clean, Full Fuel, $M = 1.3$, Sea Level	231
201	Wing Beam Model, Clean, Full Fuel, $M = 1.3$, 11,000 Ft	232
202	Wing Beam Model, Clean, Full Fuel, $M = 1.3$, 20,000 Ft	233
203	Wing Beam Model, Clean, Full Fuel, $M = 1.3$, 40,000 Ft	234
204	ADCA Wing - Sidewinder Installation	236
205	Wing Node Lines and Flutter Envelopes, Tip-Mounted Sidewinder, Without Fuel	238
206	Wing Beam Model, Tip-Mounted Sidewinder, No Fuel, $M = 0.8$, Sea Level	239
207	Wing Beam Model, Tip-Mounted Sidewinder, No Fuel, $M = 0.8$, 20,000 Ft	240
208	Wing Beam Model, Tip-Mounted Sidewinder, No Fuel, $M = 0.8$, 40,000 Ft	241
209	Wing Beam Model, Tip-Mounted Sidewinder, No Fuel, $M = 1.3$, Sea Level	242
210	Wing Beam Model, Tip-Mounted Sidewinder, No Fuel, $M = 1.3$, 11,000 Ft	243
211	Wing Beam Model, Tip-Mounted Sidewinder, No Fuel, $M = 1.3$, 20,000 Ft	244
212	Wing Beam Model, Tip-Mounted Sidewinder, No Fuel, $M = 1.3$, 40,000 Ft	245
213	Wing Finite Element Dynamic Idealization	247
214	Wing Node Shapes, Symmetric	248
215	Wing Node Shapes, Symmetric	249
216	Wing Finite Element Model, Clean, No Fuel, Symmetric, $M = 0.8$, Sea Level	250
217	Wing Finite Element Model, Clean, No Fuel, Antisymmetric, $M = 0.8$, Sea Level	251
218	Canard Structural Concept	253
219	Preliminary Canard Node Lines and Flutter Boundary	256
220	Preliminary Canard V-g- plot, $K(Act.) = 29 \times 10^6$ in lb/rad, $M = 0.8$, Sea Level	257
221	Preliminary Canard V-g- plot, $K(Act.) = 29 \times 10^6$ in lb/rad, $M = 1.5$, 17,750 Ft	258
222	Preliminary Canard V-g- plot, $K(Act.) = 20 \times 10^6$ in lb/rad, $M = 0.8$, Sea Level	259
223	Preliminary Canard V-g- plot, $K(Act.) = 20 \times 10^6$ in lb/rad, $M = 1.5$, 17,750 Ft	260
224	Canard Dynamic Idealization	262
225	Final Canard Mode Shapes	265
226	Final Canard V-g- plot $K(Act.) = 20 \times 10^6$ in lb/rad, $M = 0.6$, Sea Level	267
227	Final Canard V-g- plot $K(Act.) = 20 \times 10^6$ in lb/rad, $M = 0.6$, 20,000 Ft	268

LIST OF ILLUSTRATIONS (Cont)

Figure		Page
228	Final Canard V-g- plot K(Act.)= 20 x 10 ⁶ in lb/rad, M = 0.6, 40,000 Ft	269
229	Final Canard V-g- plot K(Act.)= 20 x 10 ⁶ in lb/rad, M = 0.8, Sea Level	270
230	Final Canard V-g- plot K(Act.)= 20 x 10 ⁶ in lb/rad, M = 0.8, 20,000 Ft	271
231	Final Canard V-g- plot K(Act.)= 20 x 10 ⁶ in lb/rad, M = 0.8, 40,000 Ft	272
232	Final Canard V-g- plot K(Act.)= 20 x 10 ⁶ in lb/rad, M = 1.3, Sea Level	273
233	Final Canard V-g- plot K(Act.)= 20 x 10 ⁶ in lb/rad, M = 1.3, 11,000 Ft	374
234	Final Canard V-g- plot K(Act.)= 20 x 10 ⁶ in lb/rad, M = 1.3, 20,000 Ft	375
235	Final Canard V-g- plot K(Act.)= 20 x 10 ⁶ in lb/rad, M = 1.3, 40,000 Ft	376
236	Final Canard V-g- plot K(Act.)= 20 x 10 ⁶ in lb/rad, M = 1.5, 17,750 Ft	277
237	Final Canard V-g- plot K(Act.)= 20 x 10 ⁶ in lb/rad, M = 1.5, 20,000 Ft	278
238	Final Canard V-g- plot K(Act.)= 20 x 10 ⁶ in lb/rad, M = 1.5, 40,000 Ft	279
239	Final Canard V-g- plot K(Act.)= 20 x 10 ⁶ in lb/rad, M = 1.8, 27,200 Ft	280
240	Final Canard V-g- plot K(Act.)= 20 x 10 ⁶ in lb/rad, M = 1.8, 40,000 Ft	281
241	Final Canard V _L Flutter Envelope, Sea Level	282
242	Final Canard Flutter Envelope, 20,000 Ft	282
243	Final Canard Flutter Envelope, 40,000 Ft	283
244	Fin Assembly and Installation	285
245	Fin Assembly and Installation	287
246	Fin-Rudder Dynamic Idealization	289
247	ADCA Fin Mode Shapes, $\beta = 15^\circ$, Slab	292
248	ADCA Fin Mode Shapes, $\beta = 0^\circ$, Slab	293
249	Slab Fin Tailored, $\beta = 15^\circ$, M=0.8, Sea Level	295
250	Slab Fin Tailored, $\beta = 15^\circ$, M=1.3, Sea Level	296
251	Slab Fin Untailored, $\beta = 0^\circ$, M=0.8, Sea Level	297
252	Slab Fin Untailored, $\beta = 0^\circ$, M=1.3, Sea Level	298
253	Fin-Rudder, Frequency vs Actuator Stiffness	300
254	ADCA Fin-Rudder Mode Shapes, $\beta = 15^\circ$	302
255	ADCA Fin-Rudder Mode Shapes, $\beta = 0^\circ$	303
256	Fin-Rudder Untailored, $\beta = 0^\circ$, M=0.8, Sea Level	304
257	Fin-Rudder Untailored, $\beta = 0^\circ$, M=0.8, 20,000 ft	305
258	Fin-Rudder Untailored, $\beta = 0^\circ$, M=0.8, 40,000 ft	306
259	Fin-Rudder Untailored, $\beta = 0^\circ$, M=1.3, Sea Level	307
260	Fin-Rudder Untailored, $\beta = 0^\circ$, M=1.3, 20,000 ft	308
261	Fin-Rudder Untailored, $\beta = 0^\circ$, M=1.3, 40,000 ft	309
262	Fin-Rudder Tailored, $\beta = 15^\circ$, M=0.8, Sea Level	310

LIST OF ILLUSTRATIONS (Cont)

Figures		Page
263	Fin-Rudder Tailored, $\beta = 15^\circ$, $M = 0.8$, 20,000 ft	311
264	Fin-Rudder Tailored, $\beta = 15^\circ$, $M = 0.8$, 40,000 ft	312
265	Fin-Rudder Tailored, $\beta = 15^\circ$, $M = 1.3$, Sea Level	313
266	Fin-Rudder Tailored, $\beta = 15^\circ$, $M = 1.3$, 11,000 ft	314
267	Fin-Rudder Tailored, $\beta = 15^\circ$, $M = 1.3$, 20,000 ft	315
268	Fin-Rudder Tailored, $\beta = 15^\circ$, $M = 1.3$, 40,000 ft	316
269	Fin-Rudder Tailored, $\beta = 15^\circ$, $M = 0.6$, 21,500 ft	318
270	Fin-Rudder Tailored, $\beta = 15^\circ$, $M = 1.6$, 40,000 ft	319
271	Fin-Rudder Tailored, $\beta = 15^\circ$, $M = 1.8$, 27,200 ft	320
272	Fin-Rudder Tailored, $\beta = 15^\circ$, $M = 1.8$, 40,000 ft	321
273	Fin-Rudder Tailored, $\beta = 15^\circ$, $M = 0.6$, Sea Level	322
274	Fin-Rudder Tailored, $\beta = 15^\circ$, $M = 0.6$, 20,000 ft	323
275	Fin-Rudder Tailored, $\beta = 15^\circ$, $M = 0.6$, 40,000 ft	324
276	Fin-Rudder V_L Flutter Speed Envelope	325
277	Fin-Rudder Flutter Envelope, 20,000 ft	325
278	Fin-Rudder Flutter Envelope, 40,000 ft	326
279	Fuselage Design Requirements	327
280	Fuselage Structural Arrangement	329
281	Fuselage Structural Arrangement-Station 280	332
282	Fuselage Structural Arrangement-Station 427	333
283	Fuselage Structural Arrangement-Station 650	334
284	ADCA Nose Gear Tire Data	339
285	Brake Sizing	341
286	ADCA Fuselage Ultimate Vertical Bending Moment	342
287	ADCA Fuselage Ultimate Vertical Shear	343
288	ADCA Fuselage Ultimate Vertical Shear	344
289	Overall ADCA Sound Pressure Levels	345
290	ADCA Predicted Sound Pressure Levels for Aircraft Zones 1-6	346
291	ADCA Predicted RMS Acceleration Levels for Aircraft Zones 1-6	347
292	ADCA Nacelle Structural Temperatures at ADCA Design Seppd Envelope F-101-GE-100 Engine Standard Day-Steady State-No Shroud	348
293	F101-GE-100 Estimated Engine Surface Temperature, Standard Day	349
294	Estimated Effect of Altitude on Engine Surface Temperature	350
295	ADCA Fuselage Bending Stiffness	353
296	ADCA Fuselage Torsional Stiffness	353
297	ADCA Fuselage Side Panel Weight Study	355
298	ADCA Fuselage Top Deck Weight vs Compressive Load Intensity	357
299	COMFU Program Design Cycle	359

ILLUSTRATIONS (Cont)

<u>Figures</u>		<u>Page</u>
300	Wing/Fuselage Attachment-Front Spar	366
301	Wing/Fuselage Attachment-Rear Spar	367
302	Wing/Fuselage Attachment-Rear Spar	369
303	Wing/Fuselage Attachment-Mid Spar	372
304	Wing/Fuselage Attachment-Mid Spar	373
305	Canard/Fuselage Attachment	375
306	ADCA Main Landing Gear Attachment	379
307	Engine Mount	383
308	Fuselage Manufacturing Splice	385
309	Hoist Fitting Attachment	387
310	Control Surface Attachment	388
311	Repair Procedure, ADCA Wing.	391
312	Moisture Barrier/Edge Protection Concept	394
313	Boron and A/S Graphite Materials Cost Trends	396
314	Cumulative Average Flyaway Costs	398
315	Life-Cycle Costs	399
316	Cruise Mach No. Sensitivity, Composite Baseline F101(1), Baseline Mission	400
317	ADCA Mach 2 Cruise Cost Comparison	401
318	Cost Analysis Input Constraints	406
319	Vehicle Design Parameters	407
320	ADCA Cost Comparisons	408
321	ADCA Unit Cost Comparisons	409
322	Fuel Consumption Comparison	414
323	Composite Utilization Rate Payoff	415
324	Cover-to-Substructure Attachment Techniques	419
325	Advanced Assembly Technique for Skin-to-Substructure Fastening	420
326	Advanced Sealing Concept	422

TABLES

Table		Page
1	Weight Reductions Over Metal Airframes (As Used for Sizing Studies)	14
2	Current and Growth Engine Candidates	15
3	Candidate Engine Comparison	16
4	Other Sizing Input Data	16
5	Avionics System	18
6	Typical Configuration Screen	20
7	Summary Group Weight Statement	32
8	Payload and Design Factors	38
9	Vehicle Performance	38
10	Control Surface and Function Summary	41
11	Mission Drag Status	42
12	Revised Performance Comparison	72
13	Vehicle Characteristics	73
14	Point Performance	74
15	Mission Performance Summary	74
16	ADCA Cabin Heat Load Comparison	111
17	Composite Design Allowables	123
18	Composite Materials (Organic Matrices)	126
19	General Design Practices for Structures Utilizing Composite Materials	128
20	Tensile Strength of Graphite/Epoxy with Holes	134
21	Limit Air Loads (lb)	143
22	ADCA Balanced Aircraft Airloads	164
23	Second Wing Twist Optimization	202
24	Wing Beam Model Influence Coefficient Matrix	209
25	Wing Mass Properties, Clean, No Fuel	210
26	Wing Beam Modal Frequencies, Clean, No Fuel	212
27	Wing Flutter Speed Summary, Clean, No Fuel	212
28	Wing Mass Properties, Full Fuel	226
29	Wing Frequency Comparison	226
30	Wing Flutter Speed Summary, Full Fuel	235
31	Sidewinder & Launcher Mass Properties	235
32	Wing Frequency Comparison	235
33	Wing Flutter Speed Summary-Sidewinder Mounted Beam Model	237
34	Wing Tip Pylon and Mount Flexibilities	237
35	Wing Frequency Comparison-Clean, No Fuel	246
36	Wing Flutter Speed Comparison-M = 0.8, Clean, No Fuel	246
37	Preliminary Canard Calculated Frequencies	255
38	Preliminary Canard Frequency Comparison	255
39	Preliminary Canard Flutter Speed Comparison	261
40	Final Canard Gross Weight Properties	261
41	Final Canard Distributed Mass Properties	263
42	Canard Beam Root Flexibilities ($\times 10^6$)	263
43	ADCA Canard Beam Model Influence Coefficients $\times 10^6$	264
44	Canard Vibration Analyses	266
45	ADCA Canard Flutter Speed Summary	266

LIST OF TABLES (Cont)

<u>Table</u>		<u>Page</u>
46	Preliminary ADCA Fin Vibration and Flutter Speed Comparison	289
47	ADCA Vertical Tail Beam Model Influence Coefficients	290
48	ADCA Slab Fin Mass Properties	291
49	ADCA Slab Fin Frequency Comparison	291
50	ADCA Slab Fin Vibration Comparison of Rotation in First Bending Mode	294
51	ADCA Slab Fin Flutter Speed Comparison	294
52	ADCA Rudder Mass Properties	299
53	ADCA Fin-Rudder Frequency Comparison	301
54	ADCA Fin-Rudder Flutter Speed Comparison	301
55	ADCA Fin-Rudder Flutter Speed Summary	317
56	ADCA Preliminary Landing Gear Loads (Limit)	335
57	ADCA Preliminary Landing Gear Loads (Limit)	336
58	ADCA Preliminary Landing Gear Loads (Limit)	337
59	Preliminary Brake Sizing Energy Requirement- Min. Weight Brake	340
60	Critical Ultimate Longeron Load	351
61	Critical Ultimate Side Panel Shears	351
62	COMFU Results	360
63	Mesh Systems Compared with Flame Spray	393
64	Subsystem Technology Improvement Factors	404
65	R & M Parameter Forecasts	405
66	Cost Analysis Input Variables	406
67	ADCA Composite Airframe RDT&E Cost Breakdown (12 development Aircraft, No G & A, No Fee)	410
68	ADCA Composite Airframe Production Cost Breakdown (300 Aircraft, No G & A, No Fee)	410
69	ADCA Component Production Cost Breakdown (300 Air- craft, No G & A, No Fee) Wing	411
70	ADCA Component Production Cost Breakdown (300 Air- craft, No G & A, No Fee) Body	411
71	ADCA Component Production Cost Breakdown (300 Air- craft, No G & A, No Fee) Fin and Canard	412
72	ADCA Component Production Cost Breakdown (300 Air- craft, No G & A, No Fee) Air Induction Section	412

List of Symbols

AR	Aspect Ratio
a_y	Lateral Acceleration
B	Wing Span
\bar{c}	Chord
c	Mean Aerodynamic Chord
C_D	Drag Coefficient
$C_{D_{BE}}$	Back End Drag Coefficient
$C_{D_{MIN}}$	Minimum Drag Coefficient
$C_{D_{TRIMMED}}$	Trimmed Drag Coefficient
C_L	Lift Coefficient
$C_{L_{ic}}$	Lift Coefficient Due To Canard Incidence
$C_{L_{MAN}}$	Maneuver Lift Coefficient
C_{L_q}	Lift Coefficient Due To Pitch Damping
C_{L_α}	Lift Curve Slope, Total Aircraft
$C_{L_{\alpha B}}$	Body Lift Curve Slope
$C_{L_{\alpha w}}$	Wing Lift Curve Slope
C_{L_δ}	Lift Coefficient Due To Specified Deflection
C_ℓ	Rolling Moment Coefficient
C_{ℓ_P}	Roll Damping Coefficient Due To Roll Rate
C_{ℓ_q}	Roll Damping Coefficient Due To Pitch
C_{ℓ_r}	Rolling Moment Coefficient Due To Yaw Rate
C_{ℓ_γ}	Rolling Moment Coefficient Due To Sideslip
C_{ℓ_β}	Rolling Moment Coefficient Due To Aileron Deflection
$C_{\ell_{\delta a}}$	
$C_{M_{C_L}}$	Pitching Moment Curve Slope
$C_{M_{ic}}$	Pitching Moment Coefficient Due To Canard Incidence
C_{m_0}	Zero Lift Pitching Moment Coefficient
C_{m_α}	Pitching Moment Coefficient With Respect To Angle of Attack

List of Symbols (Cont)

C_m	Pitching Moment Coefficient
C_{m_q}	Pitch Damping Coefficient Due To Pitch Rate
C_{m_α}	Pitching Moment Coefficient Due to Angle of Attack
$C_{m_{\alpha_B}}$	Pitch Damping Coefficient Due to Angle of Attack For Body
$C_{m_{\alpha_W}}$	Pitch Damping Coefficient Due To Angle of Attack For Wing
C_{m_δ}	Pitching Moment Coefficient Due to Specified Deflection
C_{N_β}	Effective Directional Stability Coefficient
C_{n_p}	Yaw Damping Coefficient Due to Roll Rate
C_{n_r}	Yawing Moment Coefficient Due to Yaw Rate
C_{n_β}	Yawing Moment Coefficient Due to Sideslip
$C_{n_{\delta a}}$	Yawing Moment Coefficient Due to Aileron Deflection
$C_{n_{\delta r}}$	Yawing Moment Coefficient Due to Rudder Deflection
C_r	Yawing Moment Coefficient
C_v	Nozzle Coefficient
C_{v_p}	Translational Damping Coefficient Due to Roll
C_{v_γ}	Side Force Coefficient Due to Yaw Rate
C_{v_β}	Side Force Coefficient Due to Pitch Rate
$C_{v_{\delta r}}$	Side Force Coefficient Due to Rudder Deflection
C_{16}	Shear Strain/Axial Stress Flexibility Coefficient
D	Bolt Diameter
D_{BE}	Back End Drag
E_{11}^c	Layer Longitudinal Compressive Modulus
E_{11}^t	Layer Longitudinal Tensile Modulus
E_{22}^c	Layer Transverse Compressive Modulus

List of Symbols (Cont)

E_{22}^t	Layer Transverse Tensile Modulus
F	Predicted Failure Stress
F_{bru}	Layer Ultimate Bearing Stress
F_{cu}	Layer Ultimate Compression Stress
F_{ils}	Interlaminar Ultimate Shear Stress
F_{xTU}	Ultimate Tensile Stress in X Direction
F_1^{cu}	Layer Longitudinal Ultimate Compressive Stress
F_1^{tu}	Layer Longitudinal Ultimate Tensile Stress
F_2^{cu}	Layer Transverse Ultimate Compressive Stress
F_2^{tu}	Layer Transverse Ultimate Tensile Stress
f	Test Failure Stress
G_z	Interlaminar Shear Modulus
G_{12}	Layer Shear Modulus
I	Moment of Inertia
I_c	Pitch Inertia
K_{ay}	Lateral Acceleration Gain
K_F	Forward Loop Gain
K_{NZ}	Feedback Gain, Normal Acceleration
K_p	Roll Command
K_{pc}	Roll Command Gain
$K_{pc\alpha}$	Cross Feed Gain
K_q	Feedback Gain Pitch Rate
K_{rc}	Yaw Command Gain
ℓS_c	Canard Volume
M	Mach Number
N_p	Neutral Point
N_z	Normal Load Factor

List of Symbols (Cont)

P	Failing Load
P_c	Roll Command
p	Aircraft Roll Rate
Q, q	Dynamic Pressure
q	Pitch Rate
r	Yaw Rate
r_c	Yaw Command
S	Surface Area
s	Seconds
T	Thrust
TR	Taper Ratio
T_A	Actuator Time Constant
T_{PC}	Roll Command Prefilter Time Constant
T_{rc}	Yaw Command Prefilter Time Constant
T_{wo}	Washout Time Constant
t	Thickness
t'	Thickness of One Ply
V_F	Flutter Speed
V_L	Limit Airspeed
W	Weight, Width of Specimen
X	Center of Gravity Location in Fuselage Coordinates
α	Angle of Attack
α_{11}	Coefficient of Longitudinal Thermal Expansion
α_{22}	Coefficient of Transverse Thermal Expansion
β	Sideslip Angle, Kick Angle of 0° Plies

List of Symbols (Cont)

$\Delta\delta_{C_{MAX}}$	Maximum Incremental Canard Deflection
δ_A	Aileron Deflection
δ_{AC}	Commanded Aileron
$\dot{\delta}_A$	Aileron Rate
$\dot{\delta}_{C_{MAX}}$	Maximum Canard Rate
δ_P	Pedal Deflection
δ_R	Rudder Deflection
δ_{ST}	Stick Deflection
η	Percent Chord
η_L	Lift Flexibility Factor
η_ℓ	Rolling Flexibility Factor
η_m	Pitch Flexibility Factor
η_n	Yaw Flexibility Factor
θ	Pitch Angle, Angle of Crossplies
$\ddot{\theta}$	Pitch Acceleration
Λ	Sweep Angle
ν_{12}	Major Poissons Ratio
ρ	Density
σ_V	RMS Side Gust Velocity
σ_W	RMS Vertical Gust Velocity
σ_X	Axial Stress in X Direction
σ_Y	Axial Stress in Y Direction
τ_{XY}	Shear Stress
ϕ	Bank Angle
Ω_{DR}	Dutch Roll Natural Frequency

Section I

INTRODUCTION AND SUMMARY

The objective of the ADCA program is to define the payoffs and ramifications of the unrestrained application of composite materials to a completely new aircraft. The specific objective is to obtain a smaller, lighter and less expensive aircraft, capable of performing an identical advanced tactical mission at lower life cycle costs than a metal counterpart.

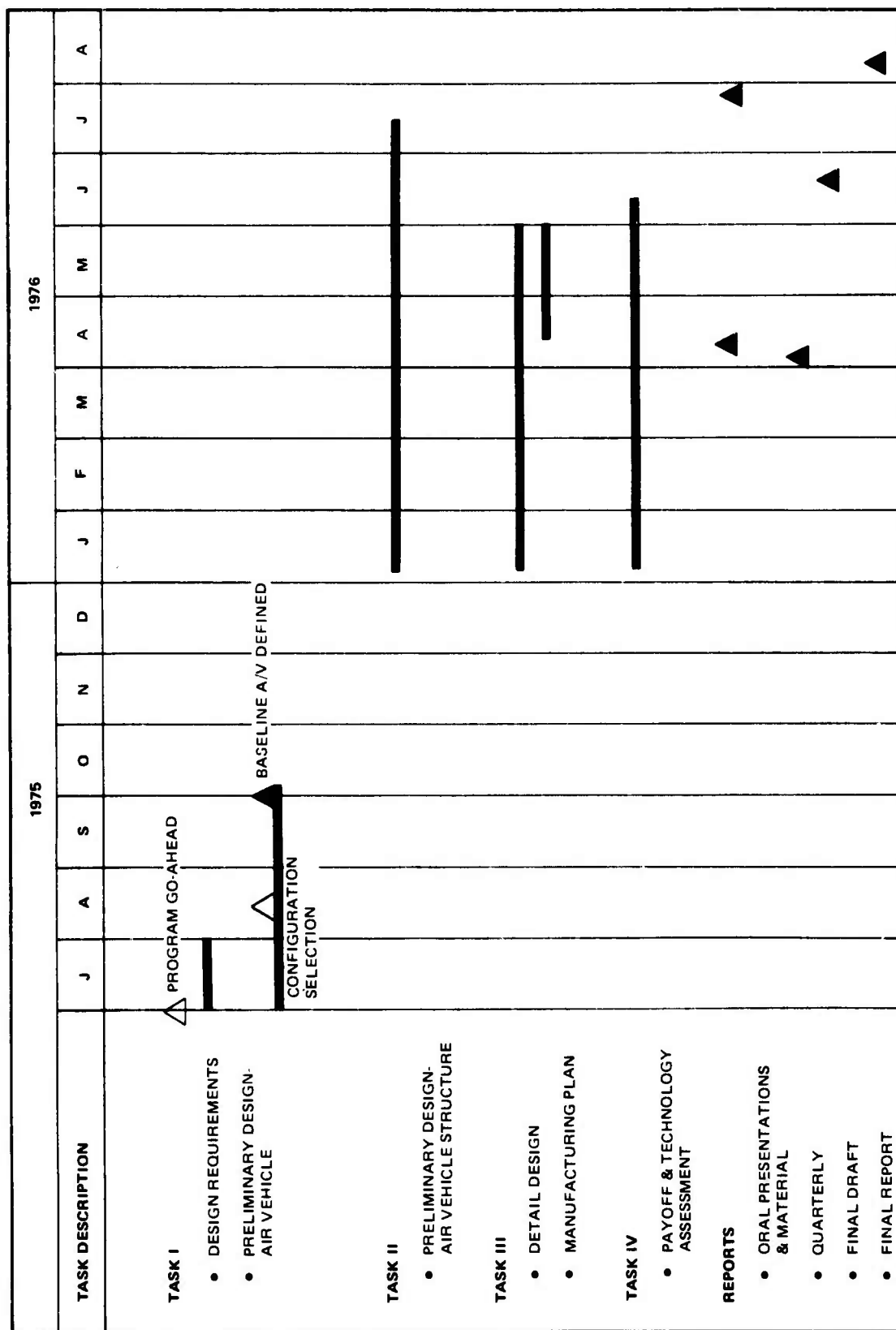
To meet these program objectives, the Supersonic Penetration Interdiction Fighter (SPIF) mission was selected (as specified in the Statement of Work) based on the fact that this mission provides the most demanding requirements and yields the maximum potential payoff from the unrestrained use of composite materials. Furthermore, the SPIF mission addresses, better than any other, the serious 1980 threat of advanced SAMs and new interceptors.

This final report outlines the procedures and results of the ADCA study. This one year program (Figure 1) initiated in July 1976, consisted of four tasks:

- I - Design Requirements
- II - Preliminary Design
- III - Detail Design
- IV - Payoff and Technology assessment.

In addition to these four tasks a partially in-house funded wind tunnel test was conducted to provide aerodynamic substantiation of vehicle performance. These tests are still in progress, however the work completed to date is summarized.

This program indicated that significant cost and weight savings over an equivalent metal aircraft could be achieved by the logical application of advanced composite materials to 80% of the airframe. The final savings were a 26% reduction in vehicle take-off-gross weight and a 21% reduction in the cumulative average fly-away costs. These savings were primarily due to the resizing of the vehicle which was made possible by the weight savings resulting from application of composites. Aside from these savings, this program has also demonstrated that the capability exists, with current technology, to design and fabricate an airframe utilizing up to 80% composite material.



Section II

MISSION ANALYSIS

2.1 OVERVIEW

Air Force tactical forces must be able to carry out offensive strike missions against high value targets. But increasingly sophisticated ground defenses and severe threat environments are making these targets unavailable to existing systems. The Supersonic Penetration Interdiction Fighter (SPIF) concept holds promise of restoring the balance to the offensive. Designed specifically for supersonic attack, SPIF will penetrate area defenses and terminal threats, achieve a high level of strike effectiveness, and survive both surface-to-air and air-to-air threats.

However, achieving this step function in offensive capability requires the selective application of advanced technologies to provide the improved performance, smaller size and affordable cost of a feasible SPIF design. Advanced composite structures are almost unique as a technology for meeting these three mandated criteria. Advanced composites, in short, will make SPIF happen!

2.2 MISSION PERSPECTIVE

The major concern in future conflicts is the massive, heavily armored assault by a force equipped, and supported, for rapid advancement. In addition to offensive ground elements this force would include the severe defensive fire power of surface-to-air missiles (SAM's), antiaircraft artillery (AAA), and advanced interceptors for protection. Tactical fighters will be employed for penetration and strike in advance of the attacking force; a rapid and well coordinated attack can be expected.

Primary mission emphasis for SPIF would be counter-air, which includes air-field and concentration area attack, and defense suppression well into enemy territory. This mission, stripping the enemy of his defenses, air cover and supply bases, would be an effective counter stroke.

A typical coordinated SPIF strike force would be protected by fighter cover in the combat area with escort aircraft for immediate defense suppression and jamming support. Since the strike force would be making a supersonic raid, the escort aircraft would be SPIF's, configured for the protective role. The nominal strike force would be composed of four aircraft with strike elements making coordinated attacks while the escort aircraft suppress any impending threat enroute.

2.3 MISSION PERFORMANCE CONSIDERATION

Supersonic cruise pays off! Analysis of a SPIF penetrating enemy territory at high altitude reveals that:

- Probability of loss to surface-to-air defenses decreases approximately 15% (almost linearly) with an increase in penetration Mach number from 0.9 to 2.0
- Probability of loss from air-to-air defenses decreases by 85% as penetration Mach number is increased from 0.9 to 1.6, with the rate of improvement rapidly decreasing above 1.6M.

A nominal 1.6M cruise speed over enemy territory was imposed on ADCA with the understanding that the optimum speed might be slightly above or slightly below this value, subject to a more lengthy and extensive analysis.

The flight radius of an SPIF must be addressed in two segments: from base to the Forward Edge of the Battle Area (FEBA) and, from FEBA to the desired target. The former is derived from consideration of the enemy's surface attack capabilities and available friendly runways and takeoff and landing design constraints. A base-to-FEBA radius of 150 nm puts the airfield beyond the majority of threats but still vulnerable while a distance of 250 nm from FEBA provides relative safety. A nominal leg of 200 nm, coupled with a short takeoff and landing capability (see below) provided a practical solution and was subsequently imposed on ADCA.

The required FEBA-to-target distance is obviously a function of the targets location. Figure 2 illustrates the distribution of all potential targets beyond FEBA. A penetration of 150 nm into enemy territory puts most of the targets within range. A radius of 250 nm puts the majority of high value targets within striking distance (not indicated in Figure 2). A nominal FEBA-to-target range of 200 nm was selected for ADCA, thereby imposing a total radius requirement of 400 nm. The suggested profile to accomplish this mission is shown in Figure 3. The capability of existing and planned aircraft to perform the SPIF mission is compared with ADCA on Figure 2.

Available runway length is both a prime design factor and operational consideration. Figure 4 summarizes the number of usable runways available to SPIF as a function of runway length for a typical scenario. Superimposed on this plot is an estimate of damage levels that might occur in the event of enemy strikes. The results

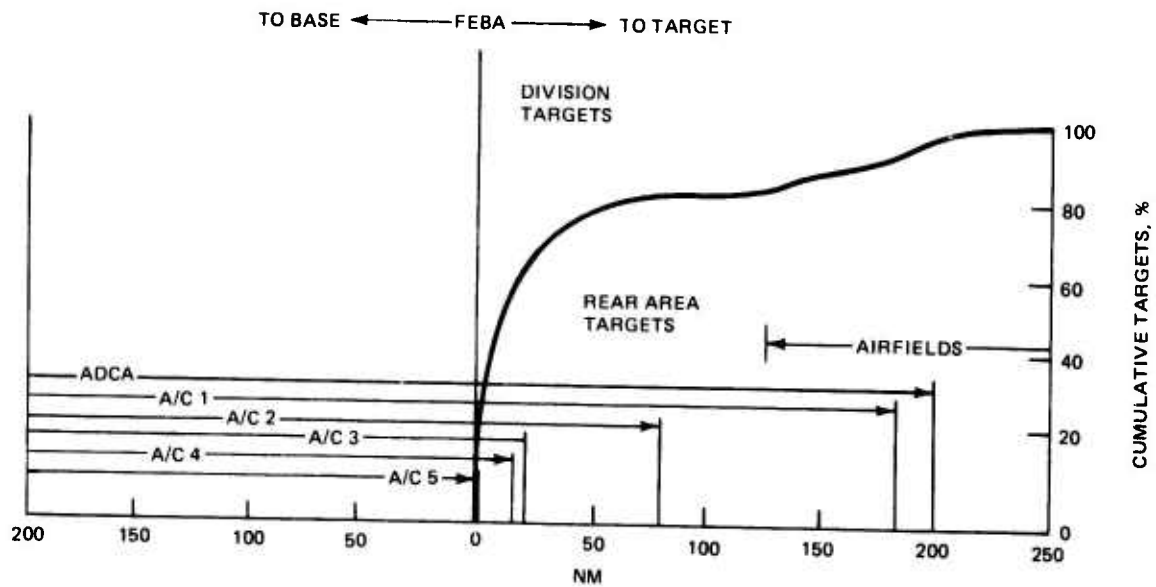


Figure 2. Combat Radius

- (2) 2000 LB A/G WEAPONS
- (2) 250 LB A/A WEAPONS
- PROVISION FOR GUN & AMMO
- NO RANGE EXTENSION DEVICES
- COMBAT FUEL = 15% TOTAL FUEL
- LAUNCH A/G WEAPONS

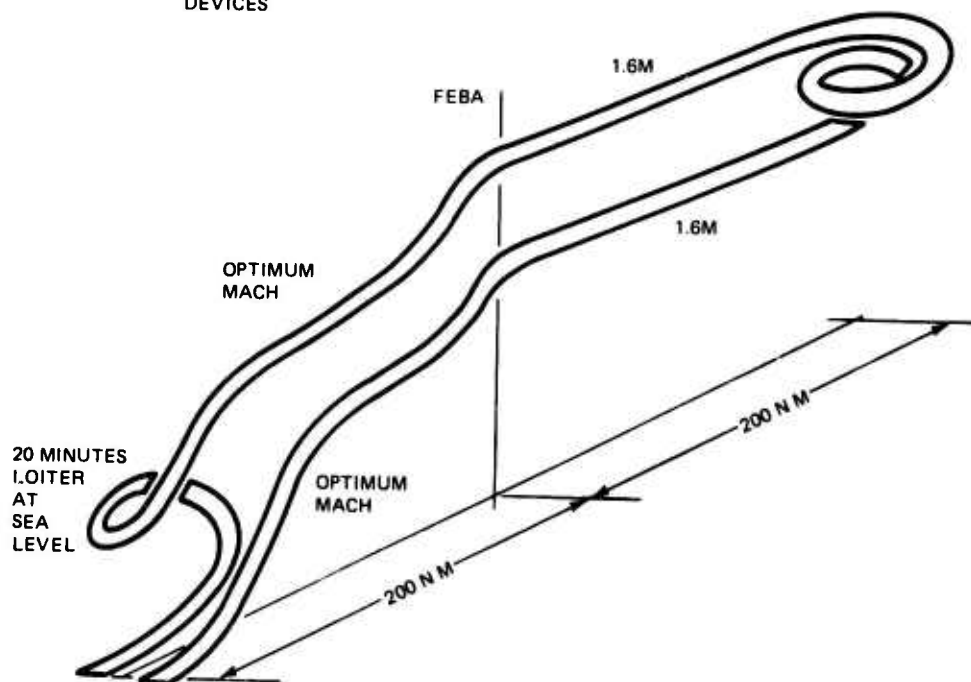


Figure 3. Mission Profile

indicate a region of available runway length that could be used for design purposes. A takeoff and landing distance (ground roll) of 3200 ft each, has been selected for the ADCA. This capability will typically allow the use of at least 70 existing runways.

2.4 POINT PERFORMANCE CONSIDERATIONS

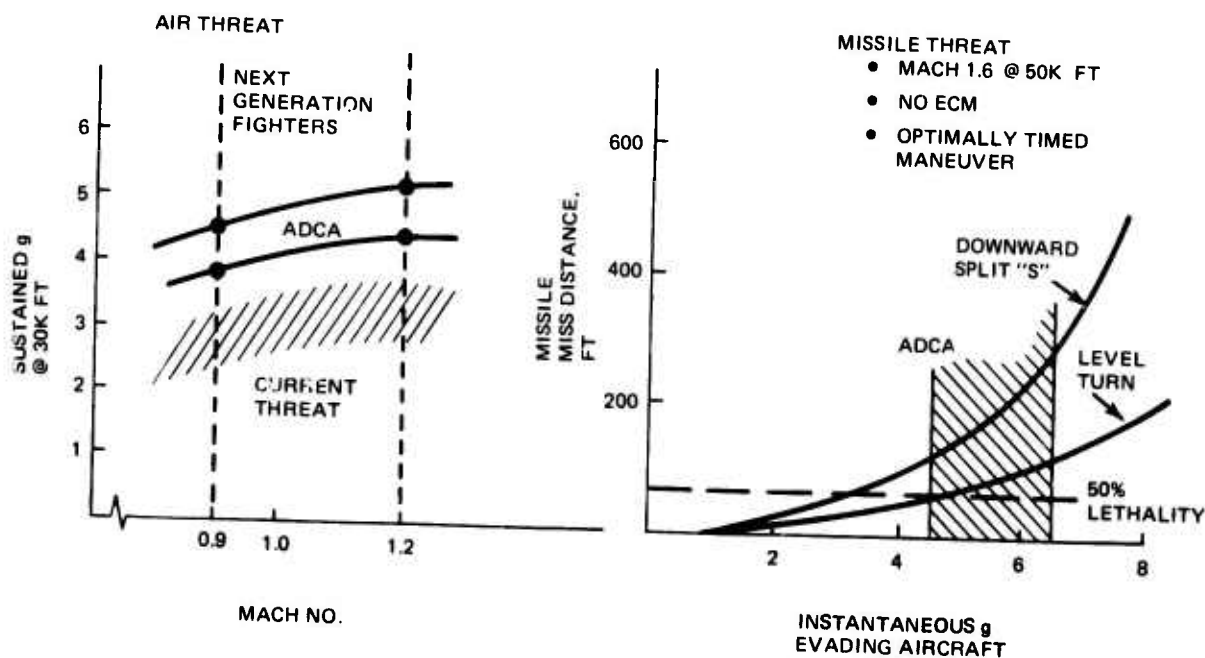
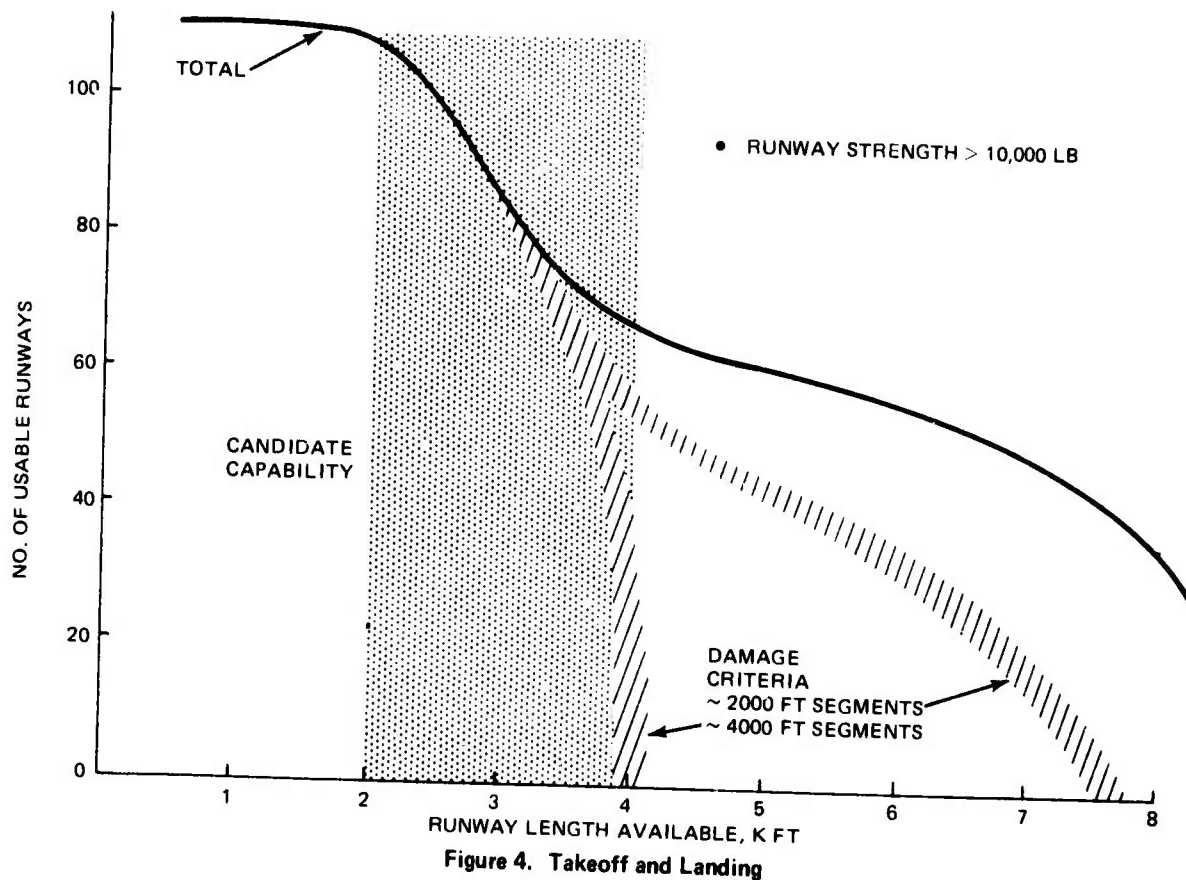
Point performance constraints were imposed on ADCA to ensure that a flexible, versatile system was considered and studied. In this process, a number of performance items were reviewed relative to the current threat and existing designs. These items include among others, acceleration and maneuverability. Figure 5 presents the sustained and instantaneous g levels required to outperform the anticipated airborne and missile threats. Nominal ADCA levels are highlighted. Level flight acceleration from 0.8M to 1.6M at 35,000 ft is shown in Figure 6 for current threat aircraft. As indicated, the minimum acceleration time of 80 seconds required to match the lowest threat was imposed in ADCA.

Figure 7 summarizes the tactical requirement desired in a SPIF aircraft and imposed on ADCA for its derivation and analysis. A suggested tradable (study) range is indicated in Figure 7, with selected sensitivities to the nominal levels within this tradable range presented in Section 4.

Finally, Figure 8 presents the relative average of four performance items as a function of relative supersonic radius. The overall capability of an ADCA (or SPIF) designed to meet the selected nominal requirements of Figure 7 is shown to exceed both the threat, and existing and future enemy aircraft.

2.5 PAYOFF ANALYSIS

The flow diagram in Figure 9 illustrates the logic used in performing the Design/Performance/Cost tradeoff analysis. Major inputs include ADCA performance/design parameters and a consideration of the threat and scenario. Life Cycle Cost (LCC) analysis was completed on a number of parametric designs. A survivability analysis was conducted on typical ADCA designs in order to assess the losses expected in a high threat environment. Total force levels were computed by combining an initial buy of 300 aircraft plus the attrited aircraft expected ($N_o + N_{attr.}$). Payoff analysis is portrayed by the cost to obtain a fixed level of effectiveness, i.e., sorties flown to targets killed as a function of design tradeoffs.



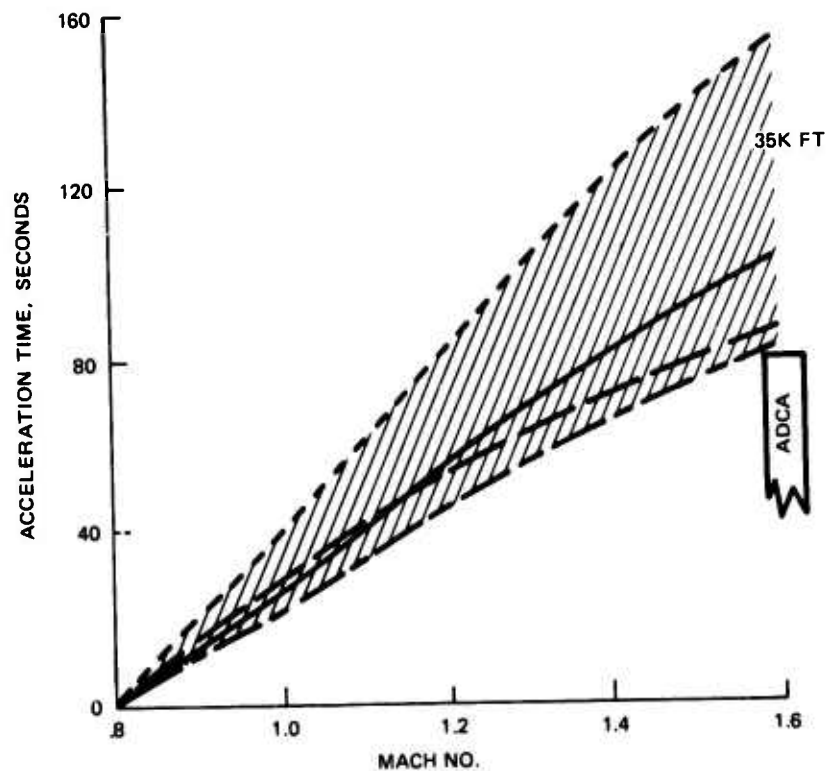


Figure 6. Acceleration Requirements

Requirement	Nominal	Tradeable Range
Radius (Optimum Mach), nm (Subsonic/Supersonic)	200/200	150-250
Supersonic Cruise M	1.6	Up To 2.0
Supersonic Cruise Altitude, Ft	Optimum	
Acceleration, sec	80	55-80
Maneuverability		
Instantaneous g @ Cruise M/Alt	5.0	4.5-6.5
Sustained g @ .9M/30K Ft	3.8	3.0-5.0
Sustained g @ 1.2M/30K Ft	4.4	4.0-5.0
Avionics Weight, lb	1350	850-1700
A/G Weapons Weight, lb	4000	4000-8000
Takeoff and Landing Distance, Ft (Ground Roll)	3200	2000-5000

Figure 7. Bounding The Tactical Requirements

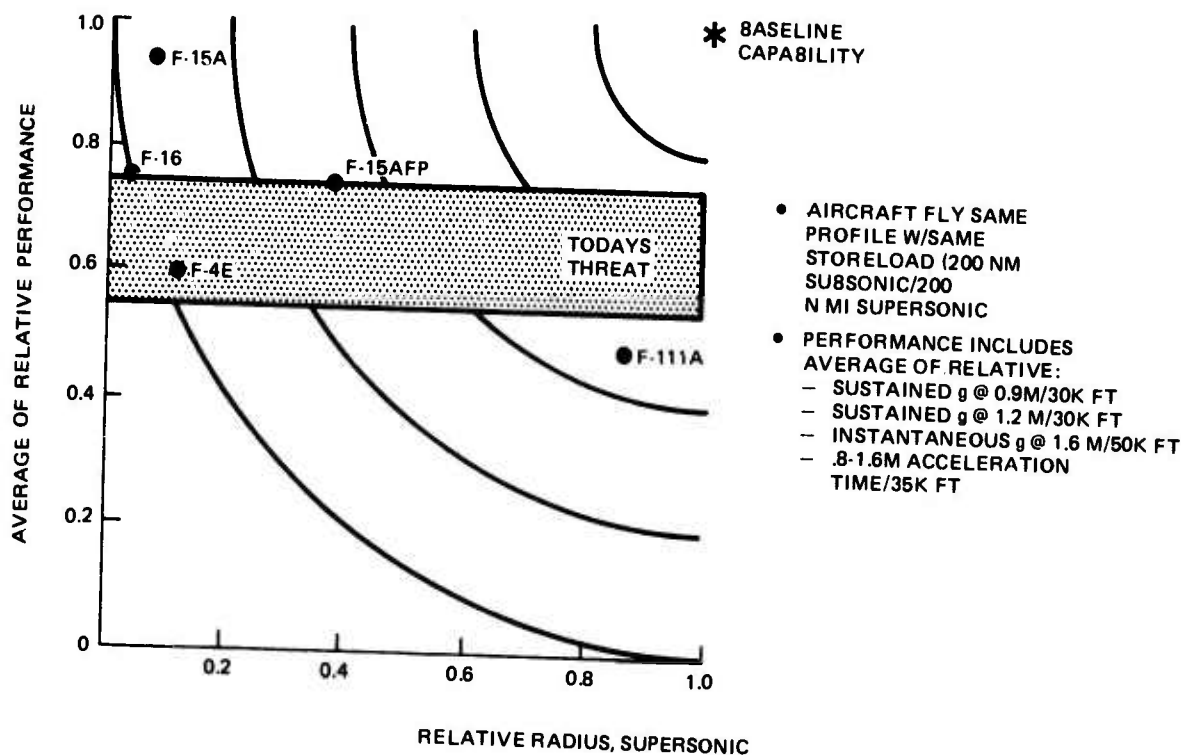


Figure 8. ADCA vs Existing Capability

An example of a design tradeoff analysis is presented in Figure 10. The results show the increase of LCC for a buy of 300 aircraft as penetration Mach number is varied. When combat losses for 5000 sorties are accounted for, further increases in LCC are projected. It is apparent that although high ECM and a large raid size were assumed, the cost impact of losses would be significant. When losses due to only SAM's are considered, the cost curve is fairly flat in this region, thus precluding a clear choice of a preferred design dash speed. However, when air-to-air losses are included, large savings in LCC are realized with supersonic dash out to Mach 2.0.

To test the sensitivity of the assumptions governing losses, the curves in Figure 11 were constructed. This plot degrades overall combat losses from a high level of 100% down to 0 in 25% increments. It should be noted that a step in the cost curve occurs when changing inlet designs from a fixed to variable inlet geometry. The results show that when there is no combat attrition, a subsonic aircraft is the least expensive and preferred design. As losses increase to a high level of 100% of those shown in Figure 10, the preferred dash speed shifts dramatically out to Mach 2.0. If, on the

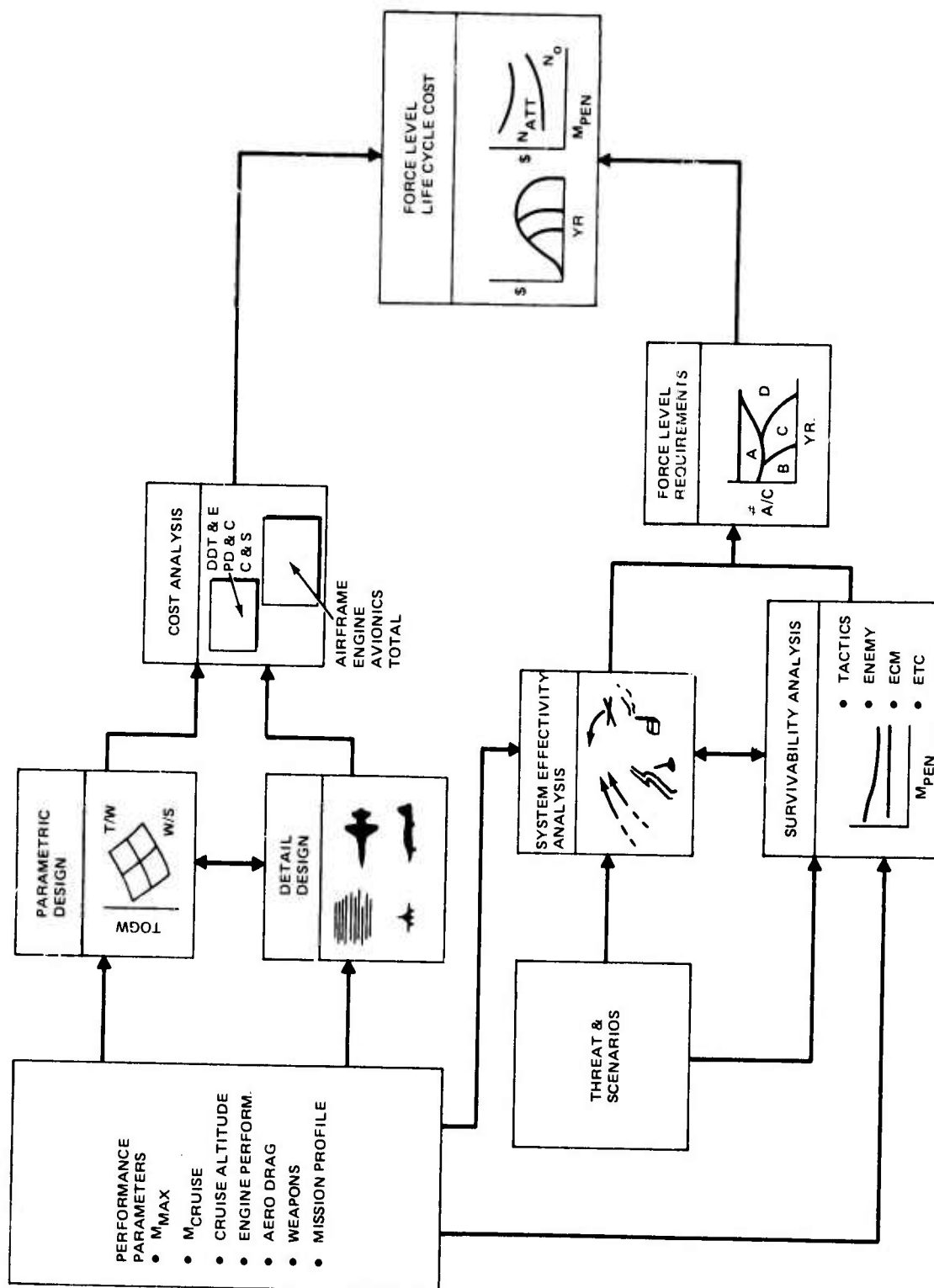


Figure 9. Design/Performance/Cost Trade Analysis

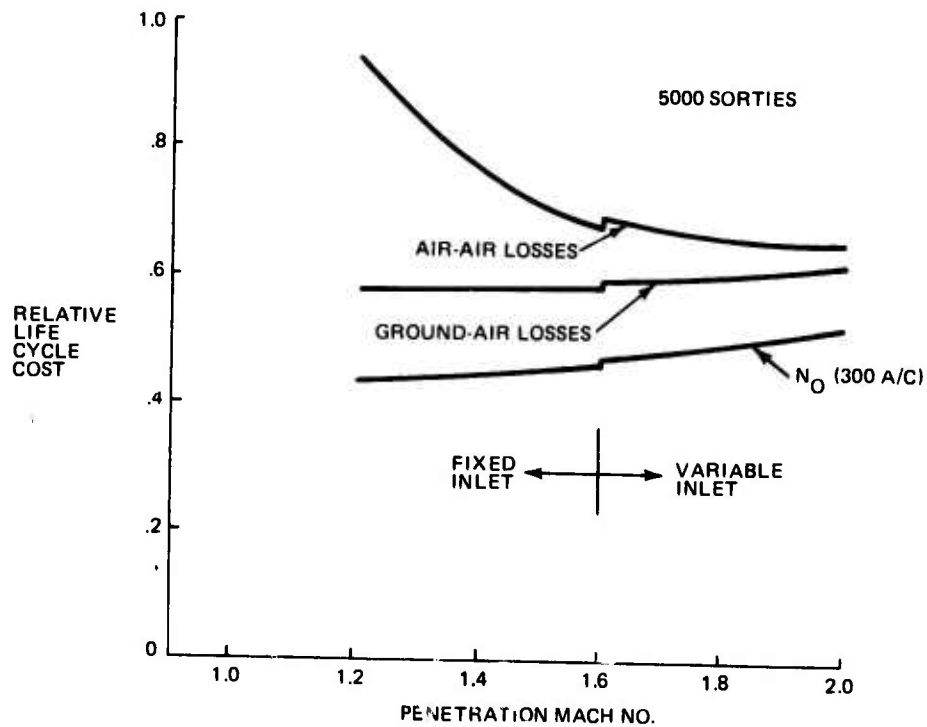


Figure 10. Life Cycle Costs vs Penetration Speed

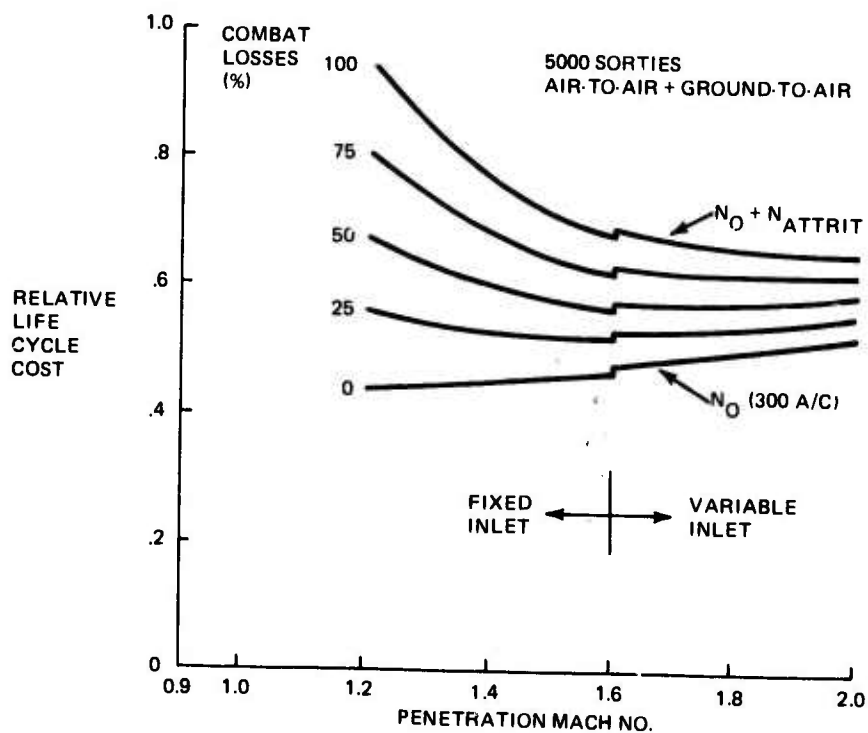


Figure 11. Sensitivity of Life Cycle Costs to Combat Losses

other hand, losses can be held to only 50% of the computed value, a moderate dash of Mach 1.6 will be beneficial and sufficient in terms of costs and reduced complexity.

A review of ADCA survivability analysis indicates the following:

- Probability of mission success is highly dependent on assumptions for tactics, raid size, penetration aids, and use of support aircraft
- Probability of loss from surface-to-air defenses decrease approximately 15% with increase in penetration speed from Mach 0.9 to 1.6
- Probability of loss to air-to-air defense decreases approximately 85% as penetration Mach number is increased from 0.9 to 1.6M - less of an effect above 1.6M
- Combined SAM and AAA defenses exhibit significant reduction in effectiveness as penetration Mach number is increased from transonic to supersonic.

Figure 12 illustrates the typical results of applying the payoff assessment methodology. For this example, and to this point in time, the impact of cruise speed and materials has been isolated. The data of Figure 12 show the distinct advantage of an ADCA in the SPIF role, favoring both use of advanced composites and supersonic penetration.

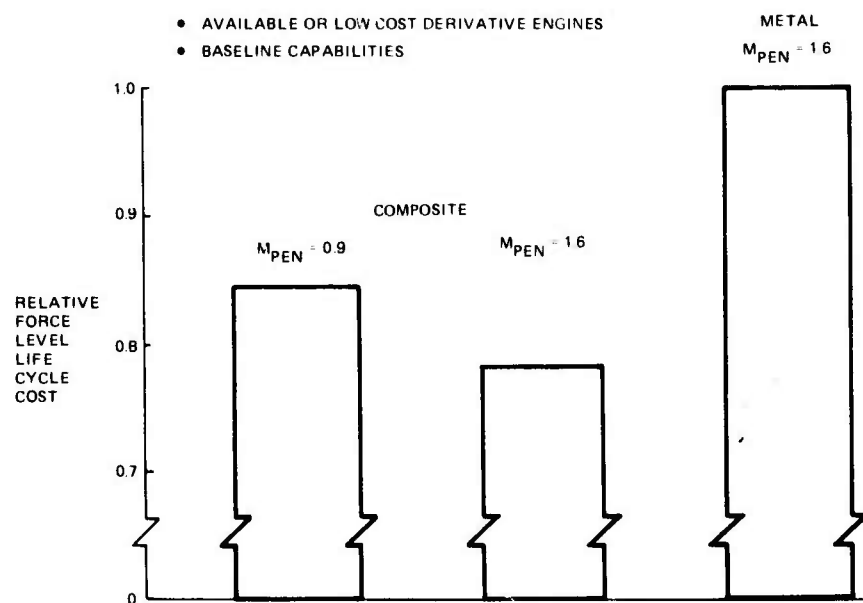


Figure 12. Initial Assessment

Section III

CONFIGURATION SCREENING

Configurations capable of performing the desired SPIF mission were evaluated using Grumman's Rapid Aerospace Vehicle Evaluation System (RAVES) sizing programs. Primary inputs for the studies were:

- Strength-to-weight ratios of composite materials
- Performance characteristics of the candidate engines
- Mission requirement constants
- Gross aerodynamic planform characteristics.

Each of these items will be discussed briefly in order to provide the rationale for the inputs used in determining the chosen configuration.

3.1 COMPOSITE MATERIALS

The fundamental drivers in arriving at a particular ADCA configuration were, understandably, the properties of the composites themselves. Grumman, in over ten years of experience with composite materials, has accumulated a wealth of data indicating the structural weight savings achievable as a function of the amount and type of composite material used. These data were used, in combination with the known experiences of other aerospace corporations, to formulate the component-by-component weight savings that could reasonably be expected by a relatively low cost (Design-to-Cost) composite design and manufacturing approach. The composite usage goals and expected weight savings resultant from such an approach are shown in Table 1. Also shown in this figure are the weight savings that might be achieved in the same time period by using advanced metal materials. These metal inputs were used for the metal baseline study discussed elsewhere in this report.

3.2 ENGINE CANDIDATES

Engines considered for the ADCA configuration were, by direction, confined to those either presently in use, undergoing tests, or readily derivable from a current model. Table 2 lists the candidates considered during the preliminary screening process as well as several of their more important characteristics. The "fine-mesh" evaluations centered about three models; the Pratt & Whitney F100(B); the General Electric F404-GE-100, and the General Electric F101-GE-100. The TF30 series

TABLE 1. WEIGHT REDUCTIONS OVER METAL AIRFRAMES
(AS USED FOR SIZING STUDIES)

Component	Weight Savings, %	Composites Goal, %	Advanced Metal Aircraft Weight Savings, %
Fixed Wing—No Twist Control	28	87	9
—With Twist $\Lambda = 20^\circ$	26.5	} 87	N/A
40°	23		
60°	17		
—Double Delta	23.5		
Swing Wing—No Twist Control	20	} 65	9
—With Twist Control	17		N/A
Tails & Canards—Slab	23	} 79	9
—Fixed	30		9
Body	20	72	3
Air Induction—Fixed Inlet	22	80	5
—Variable Inlet	20	80	5
Landing Gear	16	40	10

engines were found to be non-competitive simply by virtue of their substantially lower thrust to weight ratios. Other, more advanced, J101 versions were avoided in keeping with the stated intention of determining what could be achieved with readily available hardware. Performance characteristics supplied by the engine manufacturers were suitably modified for installation effects and provided as inputs to the screening process. Results are discussed later when the various options are presented, but it is noted at this time that engine selection did not evolve completely from the quantitative screening process. Subjective judgements also influenced the selection. Table 3 shows some of the non-performance related considerations that influenced the selection of the proposed ADCA engine.

TABLE 2. CURRENT AND GROWTH ENGINE CANDIDATES

Status	Designation	Sea Level Static (SLS) Rating, Lb	Turbine Inlet Temp, °F	Bypass Ratio (BPR)	Overall Pressure Ratio (OPR)	Thrust/Weight	Mean Qualification Time (MQT) or Potential Availability
Available or Under Development	F100-PW-100	24,000 class	2500 class	0.7	23	8.0 class	Oct 1973
	J101-GE-100	15,000 class	2500 class	0.2	25	8.0 class	42 MFGA
	F404-GE-400	16,000 class	2500 class	0.35	25	8.0 class	June 1979
	F101-GE-100	30,000 class	2600 class	2.0	26	8.0 class	June 1976
	TF30-P-412	20,300	2150	0.9	20	5.1	May 1971
	TF30-P-100	25,100	2400	0.7	20	6.3	Dec 1971
Growth Projections	F100(B)	25,000 class	2500 class	0.7	23	8.0 class	48 MFGA
	J101/J-7A9	16,000 class	2500 class	0.35	25	8.0 class	Late 70's
	J101 Growth Step 3	17,500 class	2700 class	0.22	27	8.5 class	42 MFGA
	J101 Growth Step 5	19-20,000	2700 class	0.3	27	9.0 class	42 MFGA (Must Follow Step 3)
Note: MFGA — Projected MQT Timing In Months From Go-Ahead							

TABLE 3. CANDIDATE ENGINE COMPARISON

F101	<ul style="list-style-type: none"> • Under development for B-1 (QT in '76) • Meets ADCA mission/performance requirements • Lightest TOGW with single engine installation • PFRT performance deficiencies identified (not critical) • Growth capability available • Approx unit cost \$1.2M
F404	<ul style="list-style-type: none"> • Development program for F-18 not established (QT in '79) • Lightest twin engine aircraft • YJ101 highly successful in F-17 flight test but early on maturity cycle • Additional growth capability available • Approx unit cost \$0.6M
F100	<ul style="list-style-type: none"> • Basic engine QT '73 for F-15 • ADCA requires growth version (B) • Potential development program cost \$200M • Other growth options possible but not identified • Approx unit cost \$1.1 to 1.6M

3.3 MISSION REQUIREMENTS

Other original mission requirement constants are listed in Table 4. The various design weights are those required for the ADCA study while the range and cruise Mach number requirements came from the Operations Analysis studies discussed in the previous section. Maximum Mach number and limit load factor requirements are consistent with the desire to at least provide parity with the threat while keeping weight and cost required to perform the desired mission to a minimum. The combat fuel allowance of 15% is admittedly arbitrary but appears to be a reasonable minimum required for evasive maneuvering.

TABLE 4 OTHER SIZING INPUT DATA

• Uninstalled Avionics Weight:	1350 lb
• Max Mach No.:	1 (S.L.)/2(Alt)
• Cruise Mach No.:	1.6
• Fixed Weight (Gun Provision, Armor, APU's, etc)	400 lb
• Combat Fuel Allowance:	15% of Total Fuel
• Flight Design Gross Weight:	TOGW - 20% Fuel
• Landing Design Gross Weight:	TOGW - 60% Fuel +8000 lb Stores
• Combat Weight:	TOGW - 50% Fuel
• Radius:	200 nm Subsonic +200 nm Supersonic
• Limit Load Factor: (Flight Design Gross Weight)	6.5g

3.4 AVIONICS

Probably the most subjective choice of requirements is the uninstalled avionics weight of 1350 lb. The avionics system for the ADCA was sized and developed to perform a SPIF mission and is based on 1975 to 1980 technology. The basic system provides the ADCA with an all-weather capability and is consistent with the delivery requirements of most inventory weapons as well as those under development. At the heart of the fire control portion of the avionics system is a Synthetic Aperture Radar (SAR) with a 28-in. planar array antenna and sufficient digital processing to recognize the prime SPIF targets at ranges in excess of the outer launch envelope limit of GBU-15 type weapons. The radar has an inherent air-to-air capability and could accommodate the delivery of the Sparrow missile for an A/A configuration.

Autonomous delivery of laser-guided ordnance required an electro-optics (E-O) subsystem including a laser rangefinder/designator, FLIR and/or a T.V. Since the performance of these devices is very sensitive to prevailing weather conditions, i.e., visibility, ceiling and relative humidity, which are generally unfavorable for the prime SPIF scenario, they were not included in the basic fire control subsystem. For off-design missions, such as the battlefield interdiction mission where it is anticipated that laser-guided ordnance and E-O sensors would have a high utilization rate, the E-O sensor suit would be accommodated in a self-contained missionized pod, thus unburdening the basic avionics system by nearly 400 lb. The major elements comprising the basic ADCA avionics system along with their weights are shown in Table 5.

3.5 CANDIDATE WING SHAPES

Aerodynamic planforms considered, encompassed virtually all wing types and control concepts available, consistent with the balance requirements implied by efficient subsonic and supersonic cruise. The delta planform exhibited the best supersonic aerodynamic characteristics, while aerodynamics consistent with transonic maneuvering required more conventional transonic swept-wing configurations. The trisonic wing selected for the ADCA baseline is an optimized combination of the two. Variable sweep was considered because of the obvious potential for matching the configuration to the various flight regimes, while a fixed wing subsonic/supersonic compromise was provided by the double delta (trisonic) planform. Aerodynamic inputs provided for the various planforms were the result of an amalgamation of historic Grumman and NASA

TABLE 5. AVIONICS SYSTEM

Subsystem	Weight, lb	Total Weight
Communications		92
• UHF Comm	14	
• Backup UHF	10	
• VHF Comm	7	
• Secure Voice	6	
• Digital Data Link	31	
• IFF Transponder	21	
• Interference Blanker	3	
Navigation		119
• Inertial (IMU)	10	
• TACAN	28	
• AHRS	19	
• Air Data Computer	20	
• UHF/ADF	7	
• LORAN	17	
• Radar Altimeter	10	
• ILS	8	
Fire Control		556
• Synthetic Aperture Radar	420	
• Central Computer	35	
• Armament Control	101	
• E-O Sensor Suit & Pod	(380)	
Electronic Support Measures		419
• Radar Homing and Warning	122	
• DECM	204	
• Chaff Dispenser	33	
• Tail Warning Radar	60	
Displays & Controls		166
• Vertical Situation Display	66	
• Head-Up Display	32	
• Multi-Function Display	68	
Total:	1,352	

data with results obtained from recent Grumman advanced configuration studies. In general, the aerodynamic inputs provided for the screening process represented subsonic and supersonic cruise parameters consistent with a modest improvement over recently demonstrated values, while transonic and supersonic maneuverability parameter estimates were based on wind tunnel demonstrations of recent Grumman designs.

3.6 PARAMETRIC SCREENING

Table 6 shows a typical configuration screen resulting from combining the inputs discussed above with the nominal mission requirements of Table 4. As noted, the delta and variable sweep configurations are materially heavier and can, therefore, be readily discarded. The higher weights for the delta are the result of the low wing loading required to provide acceptable takeoff and maneuvering performance while the variable sweep configuration is primarily the victim of the reduced weight savings made possible by using composites on such a vehicle. Providing the delta with a retractable canard offers a substantial improvement, but the lack of an effective pitch control device still results in a materially heavier solution than either the transonic or trisonic designs. Considering the various engine options within the trisonic and transonic columns lead to the conclusion that the most cost-effective solutions are either two F404 engines or a single F101. The four combinations circled in Table 6 are, therefore, left for further consideration. Considering the accuracy limitations of the screening process, these four solutions are regarded as substantially equal.

Detailed studies of the transonic and trisonic configurations showed that while the trisonic weight could be met, the transonic wing with aft-tail configuration resulted in a less efficient supersonic cruise vehicle than had been assumed in the early studies. As a result, the "drawn" vehicles tended to be several thousand pounds heavier. The increased size of the transonic/tailed configuration is primarily the result of supersonic trim drag induced by the down-loaded tail. Attempts to materially reduce or eliminate the trim penalty resulted in unsatisfactorily high levels of subsonic instability with its attendant control problems. A transonic wing/canard configuration which would achieve the desired weight goal was postulated but discarded since it essentially represented a special case of the trisonic (double delta) family. In brief, the trisonic configuration survived the detailed screen by virtue of:

- The lower weight (and, therefore, cost) of the trisonic planform as shown by the detailed studies, and
- The greater design (and mission) flexibility provided by the double delta trisonic planform which could in the limit include optimal transonic or supersonic variations.

Regarding engine selection, detailed studies showed both two F404's or one F101 to be acceptable and, in fact, nearly equal in performance and configuration weight.

TABLE 6. TYPICAL CONFIGURATION SCREEN

- Available or Low Cost Derivative Engines
- Baseline Mission
- Size for Most Critical of: 3.8 "g" Sustained @ 0.9M/30,000 ft
3200 ft Takeoff Ground Roll w/10,000 lb A/G Weapons
3200 ft Landing Ground Roll

Air Vehicle Engines	TOGW, lb/Accel Time (M=0.8 to M=1.6/35,000 ft.) ~ sec				
	Delta	Delta With Retractable Canard	Trisonic With Canard	Transonic With Aft Tail	Vari-Sweep With Aft Tail
(1) F404	No Solution	No Solution	No Solution	No Solution	No Solution
(2) F404	42,630/110	39,378/83	37,489/72	37,976/73	40,620/83
(3) F404	45,679/55	45,187/52	44,047/49	44,299/49	47,609/55
(1) F100B	No Solution	No Solution	No Solution	No Solution	43,013/166
(2) F100B	49,199/59	48,148/55	47,201/52	47,446/52	51,499/59
(1) F101	45,203/136	39,922/91	37,826/79	37,941/78	41,470/92

While the "one F101" configuration did ultimately become the lightest by several hundred pounds; the slightly better point performance of the "two F404" configuration made either equally suitable for purposes of the ADCA study. To a large extent, the final choice of one F101 (double circled solution of Table 6) was largely subjective, but might be more readily explained by considering each engine in a bit more detail.

3.6.1 F404-GE-400

The F404 engine development program for the U.S. Navy F-18 application was at the time of the study not on a firm approved schedule. An engine qualification test (QT) was possible by 1979, but is tied directly to a go-ahead for the F-18 program.

The engine provided the lightest twin engine aircraft design in the ADCA studies. The basic YJ101 turbojet engine (which is the basis for the F404 growth version) had passed a Preliminary Flight Rating Test (PFRT) and was highly successful in the F-17 flight test program. However, the engine had not accumulated the engine operating hours to reach the maturity level where most of the operational or design problems will have surfaced. Growth potential up to the 20,000 lb thrust class is available primarily through turbine temperature increase in the J101/F404 design. Significant growth steps, over 17,000 lb class, will require development well into the 1980's.

3.6.2 F101-GE-100

This 2.0 bypass ratio, afterburning turbofan is currently under development for the U.S. Air Force B-1 bomber. The program is on schedule with engine Qualification Test (QT) in July 1976 and Defense System Acquisition Review Council (DSARC) III production decision expected by November 1976. The F101 cycle is unique in that its performance characteristics have, by coincidence, been tailored to the ADCA transonic and supersonic sizing conditions. It is also the only current engine that has been specifically designed for sustained supersonic cruise.

The engine, as is, meets the ADCA mission/performance requirements with the lightest TOGW (single engine installation) of all candidates evaluated in detail. Deficiencies in engine performance identified since PFRT are not critical to the ADCA design. The F101 has growth potential available through increased turbine temperature and overall pressure ratio.

Production unit cost of the F101 is competitive with the other candidates at an estimated \$1.2 million for large production quantities. Comparable estimates for the F404 put its unit cost at or just below \$0.6 million.

Of the two candidates, the F101 was the closest to qualification during the configuration studies for ADCA and, therefore, has the lowest risk associated with its potential availability in the time period under consideration.

In essence then, the choice of the single F101 configuration is largely the result of the "reality" of the engine, it gives an acceptable answer "as is." A secondary consideration was the subsonic efficiency of the F101. While the design mission has a relatively long supersonic cruise leg, only about 40% of the total fuel is expended supersonically, placing less of a premium on supersonic efficiency than one might intuitively expect. Considering this, in conjunction with the fact that most aircraft hours are accumulated in training and most training would be subsonic, led to the realization that an engine such as the F101 would result in substantial and increasingly important fuel savings.

3.6.3 Summary

While either the two F404 trisonic configuration or the single F101 trisonic configuration could have served equally well for the stated purpose of the ADCA study, the single F101 was chosen to lend the confidence that would be demanded for a real hardware program intended to satisfy the requirements delineated earlier in this report.

Section IV

VEHICLE DEFINITION

The screening process, outlined in Section III, evaluated various combinations of engines and airframes. As noted in that section, the preferred vehicle selected as a baseline to evaluate structural details is a trisonic configuration with an afterburning F101-GE-100 engine. This vehicle with its large unbroken surfaces and minimum number of access panels, is particularly suited to the use of composite materials while simultaneously meeting the demands of a difficult, supersonic mission.

The output of the screening process, however, was only the starting point for the configuration. This computer representation was given added credibility by careful design and integration of components and systems. In addition, continuing analyses, tradeoffs, and testing were performed upon the configuration to develop a reliable, achievable, baseline design.

In particular, the achievement of excellent supersonic performance coupled with transonic maneuver parity necessitated innovation and the integration of all technologies. The selected hybrid wing planform and close coupled canard successfully meet these diverse requirements.

4.1 GENERAL ARRANGEMENT

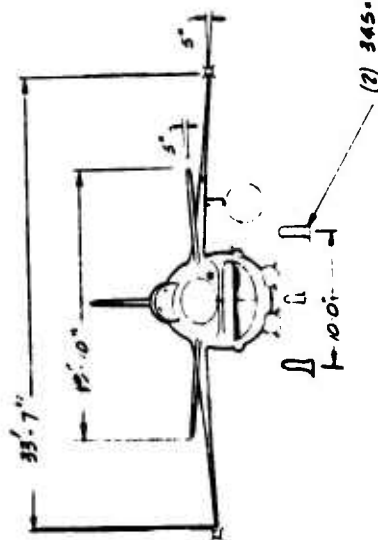
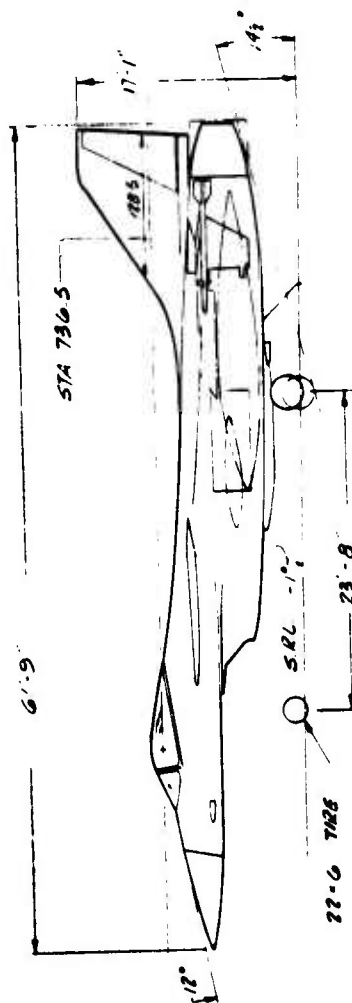
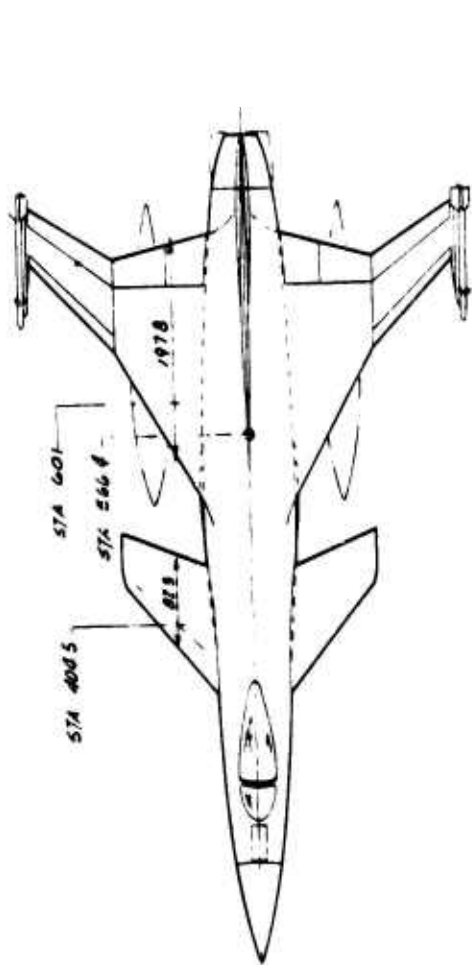
The aircraft, Figure 13, has a single F101-GE-100 afterburner-equipped turbofan engine with variable C-D nozzle. Engine removal is accomplished by a built-in rail system, which requires no major breaks in the primary fuselage structure. The inlet system is a simple fixed ramp design.

The fuselage utilizes multi-purpose major structural bulkheads and frames. The entire body structure is "idealized" for composite construction. A one-piece windshield and manual side-opening canopy complete the cockpit enclosure. Conventional "free-fall" landing gear has been incorporated into the design. Equipment and weapons access is achieved via access panels and main landing gear bay doors. The M-61 gun is located for optimum operation and accessibility with ammo loading achieved by either drum removal or external loading.

The fuel system consists of integral fuselage and wing tanks with a self-sealing fuselage bladder tank containing sufficient protected "get-home" fuel. Total useable fuel quantity was 11,750 lbs of JP-4 fuel.

DATA

SURFACE	AREA m^2	R	TR	%	ALL
WING	411	2.75	.75/50	3.5-5	60°/145°
CANARD	90	2.10	.9	4-3	50°
VERT TAIL	80	.875	.75	4-3	55°
SURFACE CONTROLS					
CANARD	90	2.75	.75/50	3.5-5	60°/145°
INBOARD FLAP/SLAT	40	2.10	.9	4-3	50°
OUTBOARD FLAP/SLAT	20	.875	.75	4-3	55°
OUTBOARD LE DROOP	21				
RUDER	21				
WEIGHTS					
EMPTY	21556 lbs	USEFUL LOAD	18997 lbs	TOTAL	FUEL
				40553 lbs	12675 lbs
PROPULSION					
		NOZZLE		RATED THRUST (LBS)	
F101 GF-100		VARIABLE C/D		30 000 LB CLASS	
A/B TURBOFAN					
MAX CROSS SECTIONAL AREA - 319 m^2					
TOTAL WETTED AREA - 1931 m^2					



(2) 345-9787-25

Figure 13. ADCA General Arrangement

The aircraft is configured with both a landing drag chute and an over-run arresting hook. The vehicle conforms to all Air Force Ground Handling geometry requirements.

The inboard profile (Figure 14) depicts vehicle systems and subsystems arranged for best performance and most reliable operation. The location of avionics, weapons and crew systems in the forward section provides for direct access and easy maintenance.

Consideration of internal packaging during the design development ensures realistic vehicle lines and makes for a design that is operationally sized from the outset.

At the conclusion of Phase I the vehicle payload was increased by Air Force direction in order to better satisfy mission requirements. At the same time fuselage speed brakes, and a landing drag chute, which had both been previously considered were incorporated into the general arrangement. The general arrangement was also revised to reflect the air-to-air missiles being moved from the pylon station to the wing tip. Provisions for a pylon station are, however, still provided for alternate missions and ferry flight. The revised vehicle payload which reflected a gun and ammo weight of 600 lb and a store capability of 5000 lb increased the fuel required to perform the identical mission to 12,675 lb. The increased fuel (925 lb) was accommodated by using part of the available growth tank volume so that no change was required to the vehicle external configuration. Since wing surface area was not increased, the wing loading increased from 90 psf to 99 psf. These revised weights are reflected in all further vehicle performance data.

4.2 TANDEM CREW CONFIGURATION

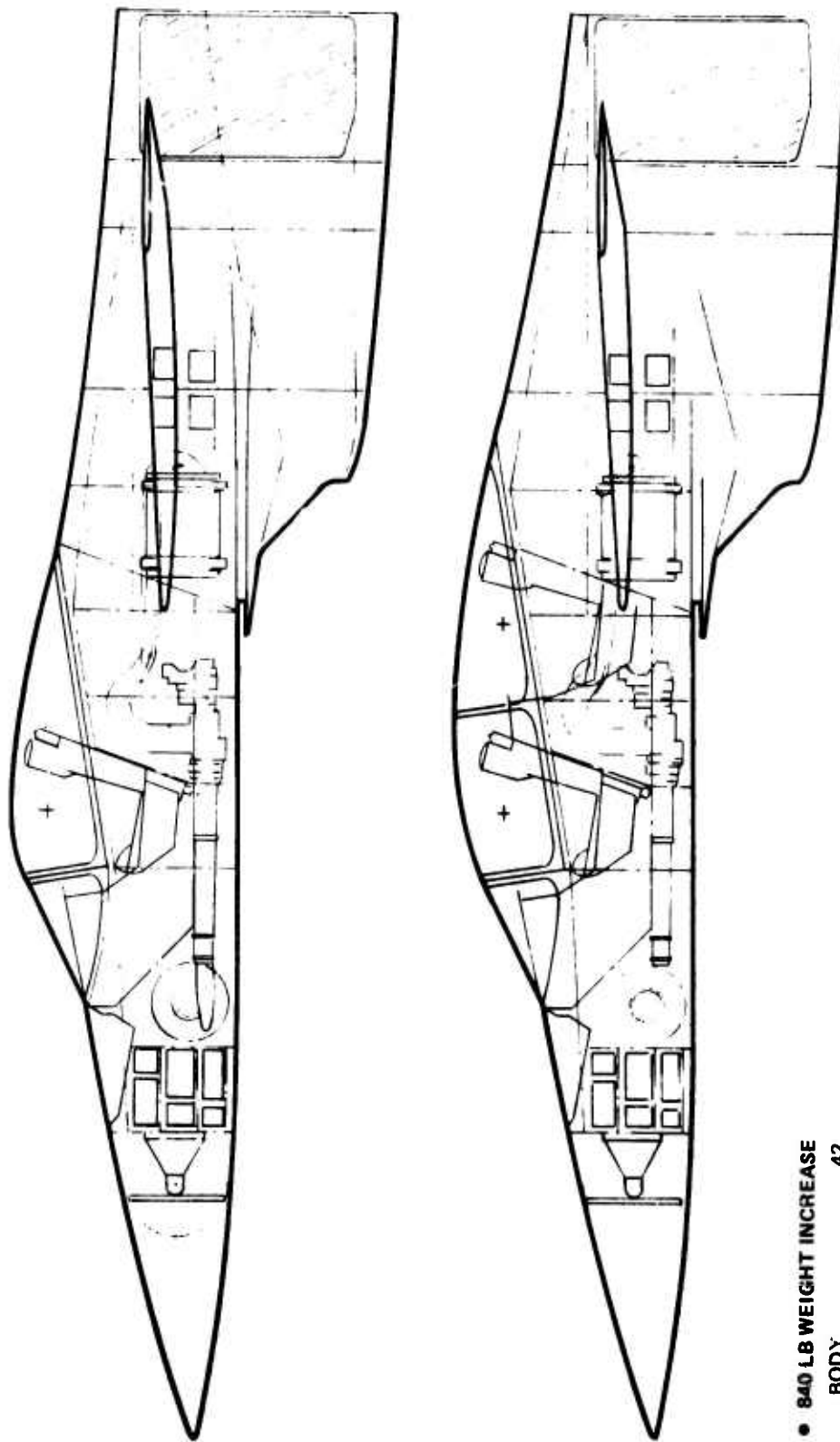
The ADCA aircraft can incorporate a two-place cockpit. The additional (rear) crew station meets all geometry requirements for a second pilot except for vision requirements. The desired fuselage body camber, precludes providing the additional height required for the standard design point eye position. This cockpit geometry, however, is presently incorporated in the TF-15 aircraft. The tandem crew configuration is shown in Figure 15.

An enlarged canopy and revised upper (Forward Section) fuselage skin panels are the only major structural rework required. Primary fuselage bulkhead and frames could be built into the single place vehicle that would only require relocation of avionics units to provide for the installation of the rear seat. The additional growth required in the ECS system could be added behind the present ECS units.

The M-61 gun and ammo installation, if required, would remain untouched. Structure

[illegible]

26



• 840 LB WEIGHT INCREASE

BODY	42
CANOPY	83
E.C.S.	134
FURN. & EQUIP	286
CREW	240
EQUIPMENT	55
	<u>840 LB</u>

3.8% INCREASE IN TOGW TO
MAINTAIN CONSTANT MISSION

Figure 15. ADCA Tandem Crew Configuration

required to install the instrumentation associated with the aft pilot appears to be of a secondary nature.

4.3 WEIGHT AND BALANCE

The reduction (percent) in structural weight due to advanced composites and 1980 metals is shown in Table 1. These savings are applied to the weight estimates from our statistical analysis that has a population of some 42 aircraft constructed with conventional materials.

The stated savings are based on detailed studies of recent composite applications and conceptual studies on the effects of items such as twist control. These savings are within the range represented in Figures 16 through 20.

The 1980 metal baseline levels represent F-14, F-15 and F-16 technology. Various components of these vehicles were compared with estimates of their weight in conventional materials from our statistical analysis to evaluate the effects of 1980 metals.

The weight statement shown in Table 7 represents the final weights of the ADCA vehicle. This vehicle has changed in several ways since the end of Phase I of this project. A drag chute system and grounding provisions have been added, along with a gun and ammunition weighing 600 lb. The store carrying capability has been increased to 5000 lb without degrading the basic SPIF mission. The air-to-air missiles were moved to the wing tips to eliminate the pylon and further reduce drag. The wing weight was updated, using the Weights Group W-5 (AMSA) program to reflect the latest thickness variations and stiffness requirements. The body weight shown is an output of the Weights Group W-9 Semi-Analytical Fuselage Estimate (SAFE) program.

Programs such as Aero Surface Multi-Station Analysis (AMSA) for wings, and SAFE for fuselage allowed the weights group to move away from statistical weights to semi-analytical weights. These programs analyze the major structural components of the wing (i.e., wing box) and fuselage (i.e., shell and longerons) based on the loads, geometry and stiffness requirements. Only secondary structure is left to statistical analysis. Sensitivity to geometry, loads, material and stiffness changes can be more accurately assessed, and tradeoff studies performed with these programs. The SAFE program allows a fuselage to be subdivided into any number of convenient sections, it can handle complicated geometry, and allows for effectiveness factors on longerons. These programs were developed under the Rapid Aerospace Vehicle Evaluation System (RAVES) system and were slanted toward quick

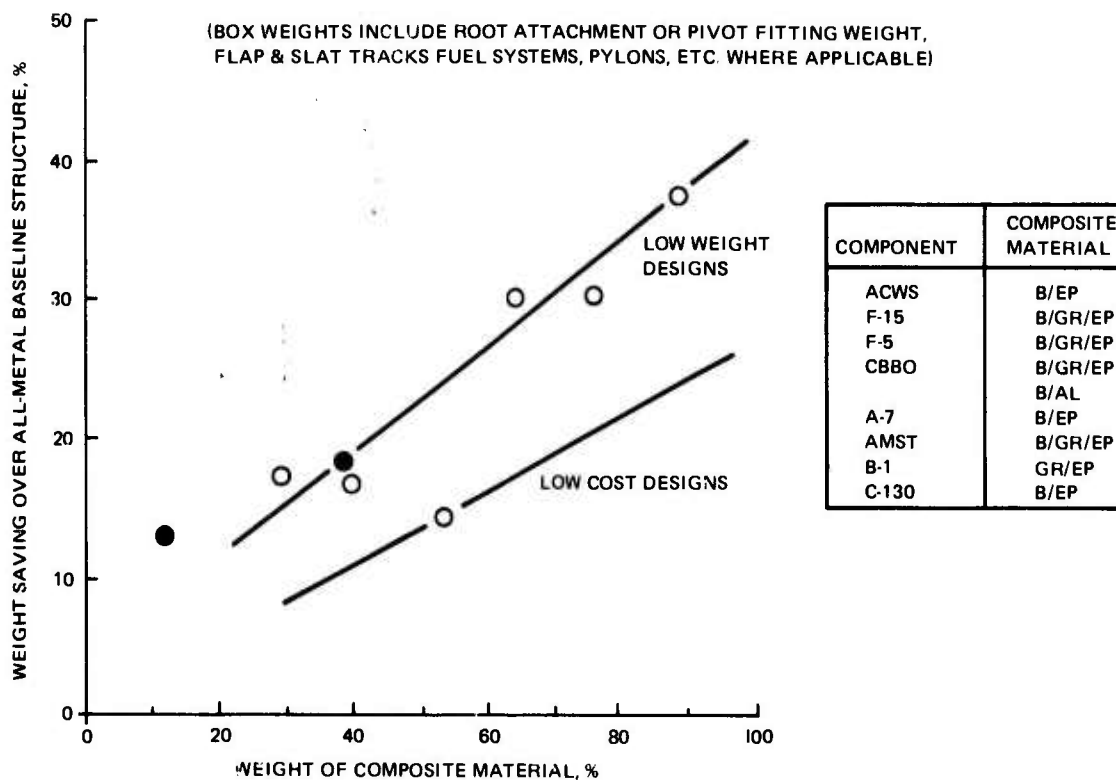


Figure 16. Advanced Composite Wing Box Weight Savings

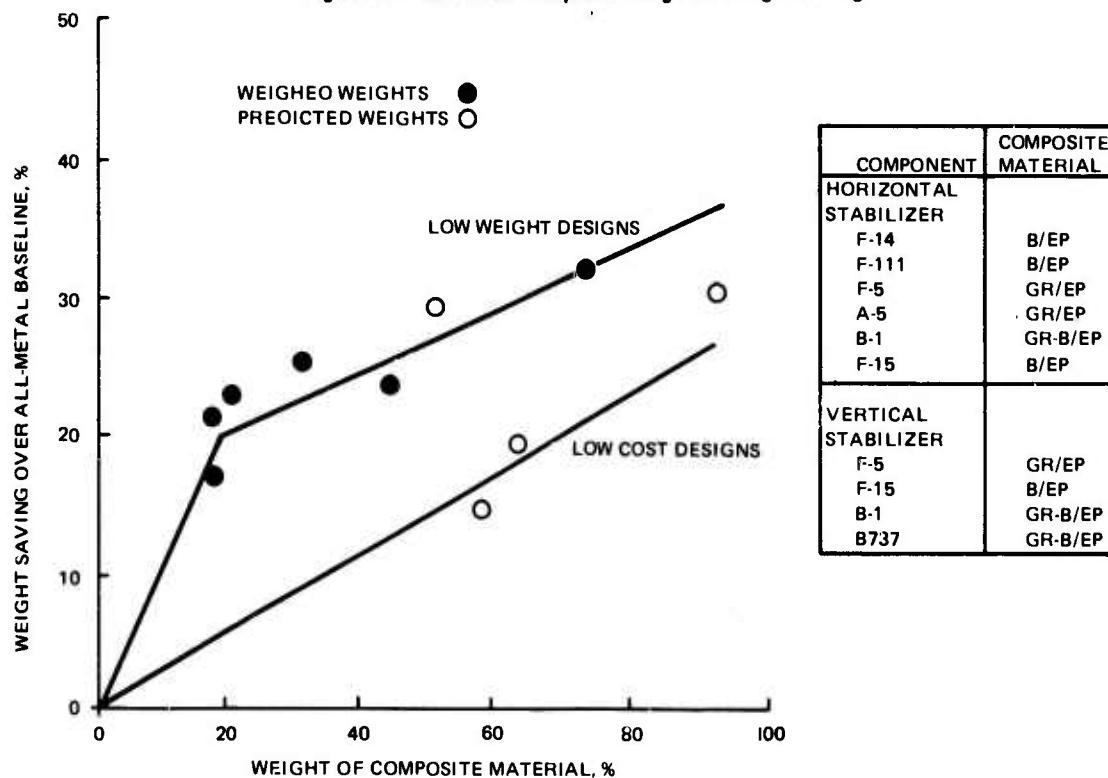


Figure 17. Advanced Composite Empennage Weight Savings

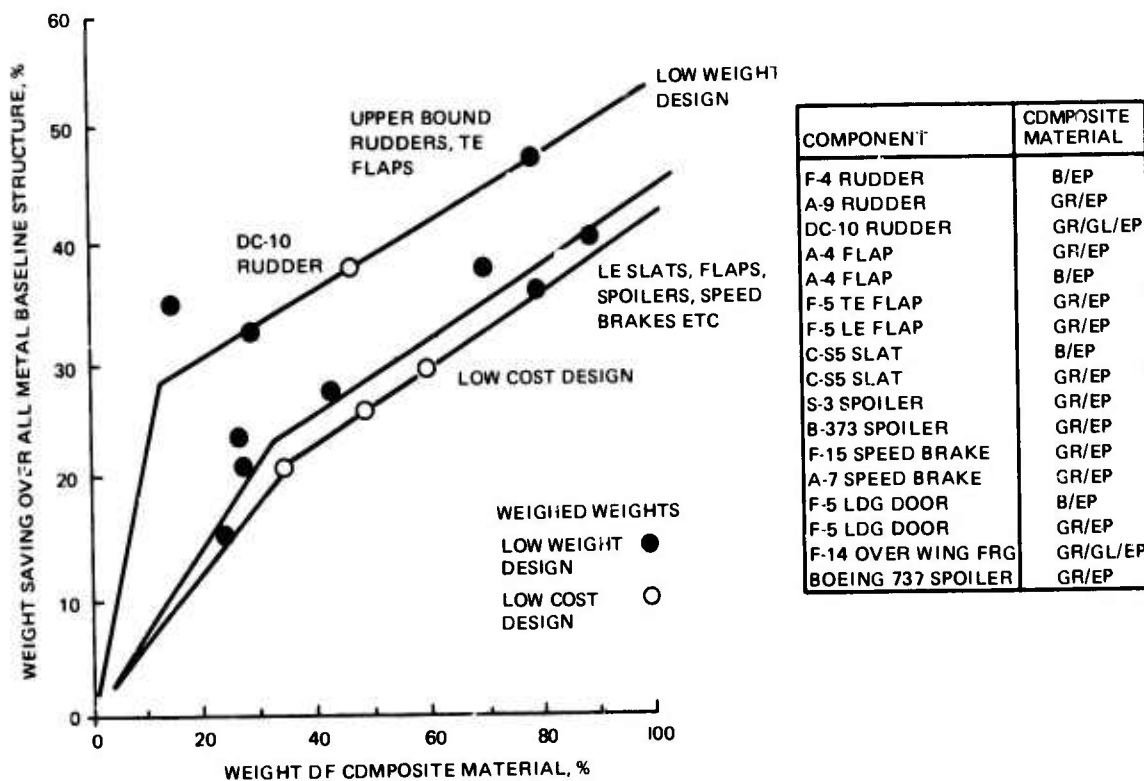


Figure 18. Advanced Composite Weight Savings - Rudder, Flaps, Doors, Etc.

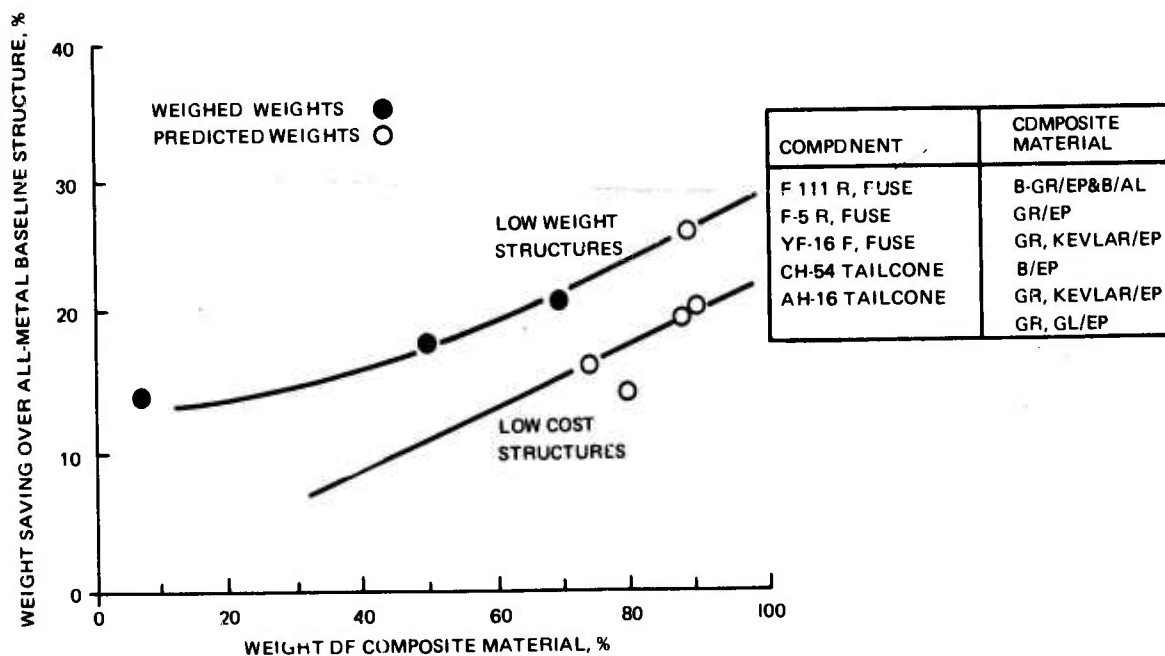


Figure 19. Advanced Composite Fuselage Weight Savings

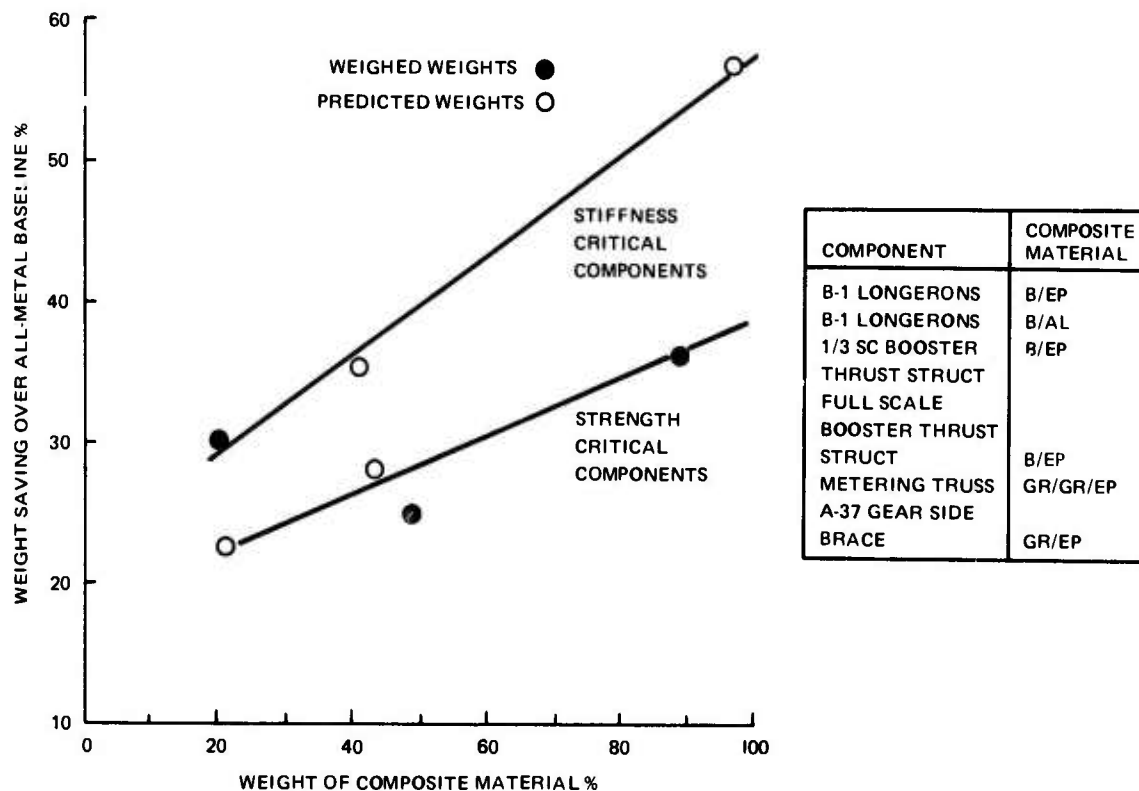


Figure 20. Advanced Composite Weight Savings - Miscellaneous Components

turnaround terminal operation.

Both AMSA and SAFE are metal-oriented programs. To reach composite values, a percentage saving for composites is applied to the weights these programs calculated. These savings were based on many in-house studies done at Grumman, and information gathered from studies done by other companies. To develop added confidence in these values, the wing was evaluated using the Weights Group W-12 Composite Aero Surface Multi-Station Analysis (CAMSA) program. This recently developed program is similar to AMSA except it evaluated the wing box in composite material. Based on our B-1 horizontal stabilizer experience, correlation factors were developed for the program. The weight this program predicts for the wing box confirms the attainability of our estimates of composite savings compared to metal values.

Figure 21 shows the cg travel for the SPIF mission. The fuel usage plan illustrated was chosen to minimize cg travel during the mission and maintain similar handling characteristics of the vehicle for various legs of the mission. This plan saves

TABLE 7. SUMMARY GROUP WEIGHT STATEMENT

Group	Configuration	ADCA	\bar{x}	$w\bar{x}$
Wing (Incl. Surfaces)		3,208	664.	2,130,112
Canard Including C/T		1,143	410.	469,145
Tail (Incl. Surfaces)		316	729.	230,364
Body		3,320	497.	1,650,040
Alighting Gear		1,591	541.	860,731
Arresting Gear		72	660.	47,520
Engine Section		87	719.	62,553
Air Induction		882	512.	451,584
Moisture/Lightning Protection		275	540.	148,500
Drag Chute System		76	780.	59,280
Structure Subtotal - Lbs.		10,970	557	6,109,829
Struct/Togw//Struct/W.E.				
Propulsion				
Engine Installation *		4,235	729.	3,087,315
Accessory Gearbox *		90	653.	58,770
Engine Shroud		50	717.	35,850
Exhaust System *				
Engine Controls *		25	717.	14,500
Starting System *		49	689.	33,761
Propeller *				
Lube System *		70	700.	49,000
Fuel System		565	568.	320,920
Flt. Cont. (Incl. Auto-Pilot)		978	569.	556,482
Auxiliary Power Plant (EPU)		165	575.	94,875
Instruments		160	410.	65,600
Hydraulic And Pneumatic		481	560.	269,360
Electrical		584	560.	327,040
Avionics (Install-Factor=1.25)		1,690	370.	625,300
Armament		160	299.	47,840
Furnishings And Equipment		286	290.	82,940
Air Conditioning		338	340.	114,920
Anti-Ice Group		50	265.	13,250
Load And Handling Group		10	560.	5,600
Gun And Ammo		600	350.	210,000
Contingency				
Weight Empty - Lbs.		21,556	562.4	12,123,152
Crew		240	280.	67,200
Fuel - Unusable		127	573.	72,771
Usable		12,675	573.	7,262,775
Oil		100	710.	71,000
Stores - A/G		5,000	564.	2,820,000
A/A		500	707.	353,500
Racks, Launchers		300	612.	183,600
Equipment		55	280.	15,400
Useful Load		18,997		
ZFZ Stores Gross Weight†		22,378	560.1	12,533,123
Zero Fuel Gross Weight		27,878	563.4	15,706,623
Take-Off Gross Weight		40,553	566.4	22,969,398

*Main Engine(s) Only

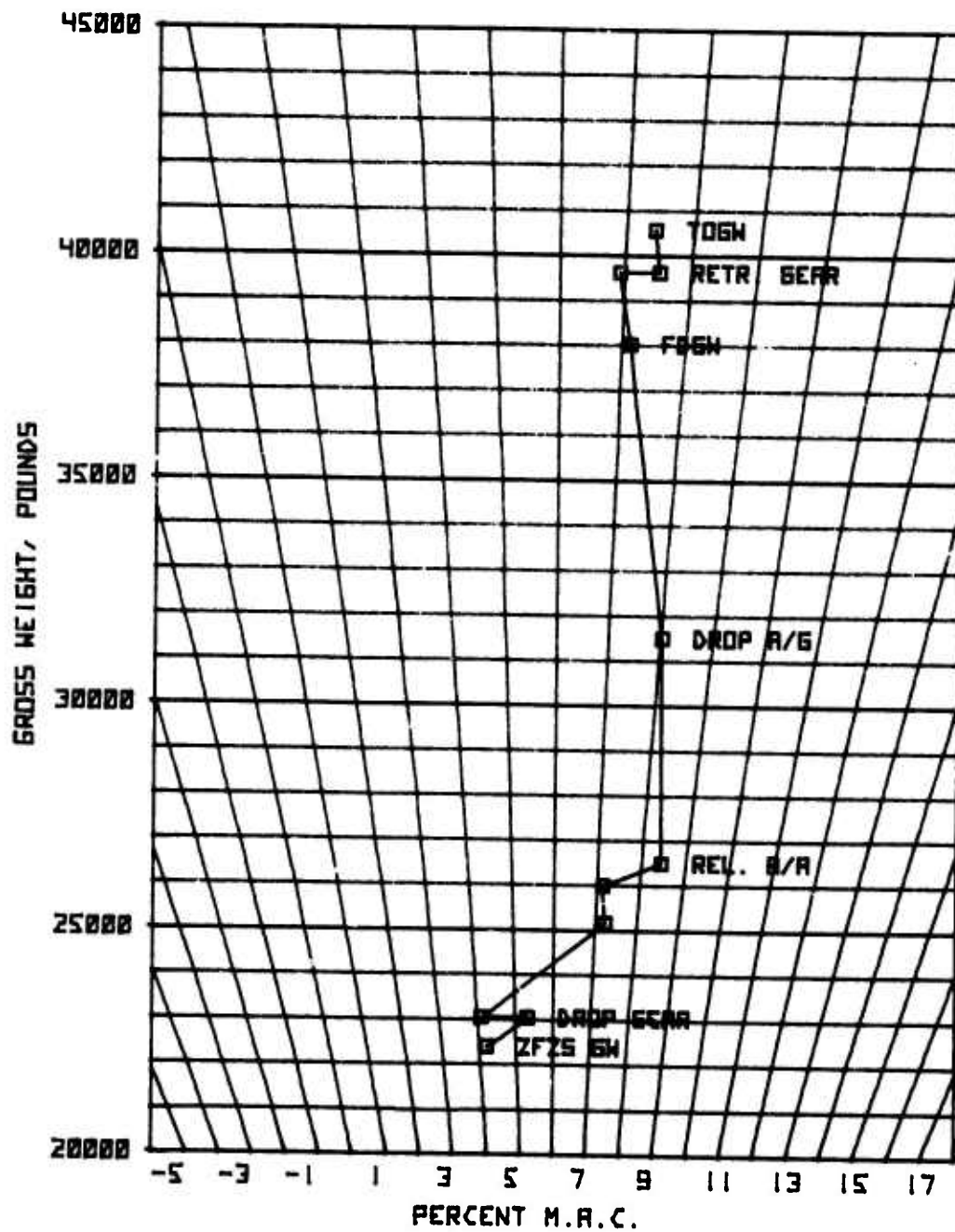


Figure 21. ADCA C.G. TRAVEL PLOT

the protected aft fuel tank as the "get home" fuel tank and uses all other tanks at such a rate as to empty them at the same time. The cg seems to have a forwardmost position of 4% MAC and an aftmost position of 8.5% MAC.

The geometry of the baseline vehicle was frozen at the end of Phase I. Using this geometry and the latest information on drag, the vehicle was run using the W-2 Computerized Initial Sizing Program (CISE) program to determine fuel required to complete the SPIF mission. The CISE program is a multidisciplinary program which simulates flying a vehicle through the mission and iterates to find a vehicle which will meet mission requirements. Using this program, three other vehicles were evaluated. The first was an equivalent all-metal baseline, the second was a composite substitution vehicle, and the third was an all-composite vehicle with an advanced (not off-the-shelf) engine. To keep the comparison as valid as possible, the same restrictions were placed on these vehicles as on our baseline vehicle. The results are shown in Figure 22. The weights shown are from CISE runs, which are statistical data. The summary group weight statement uses the baseline CISE run as a starting point, and using the drawing of the baseline vehicle (Figure 13), a more detailed analysis was utilized to recalculate the various components. The weight of the actual baseline vehicle does not match the weight of the CISE baseline vehicle for those reasons. Because drawings and loads do not exist for the other vehicles in the study, the comparison, to remain fair, was run on the results of the CISE runs.

The study showed that even though a composite substitution vehicle is only 5% lighter than the all metal baseline, a vehicle designed around composites from the sizing stage is about 24% lighter. This is due to the iterated effect of the changes on the vehicle size. The penalty for using an off-the-shelf engine rather than an advanced engine is over 5% in the composite baseline. A similar penalty is also inherent in the metal baseline.

Another study performed was one that judged the effect of varying the percentage of composites in the structural weight. This was done by using a "rubber" F-101 engine and a constant wing loading. The percentage of composite was changed by making individual components all metal until the whole vehicle was metal. The 100% composite savings were estimated knowing that the low bearing allowables of composites make it impractical to use only composites. We were able to estimate the resultant savings due to this by comparing weight-to-bearing strength of composites to titanium. Based on this information

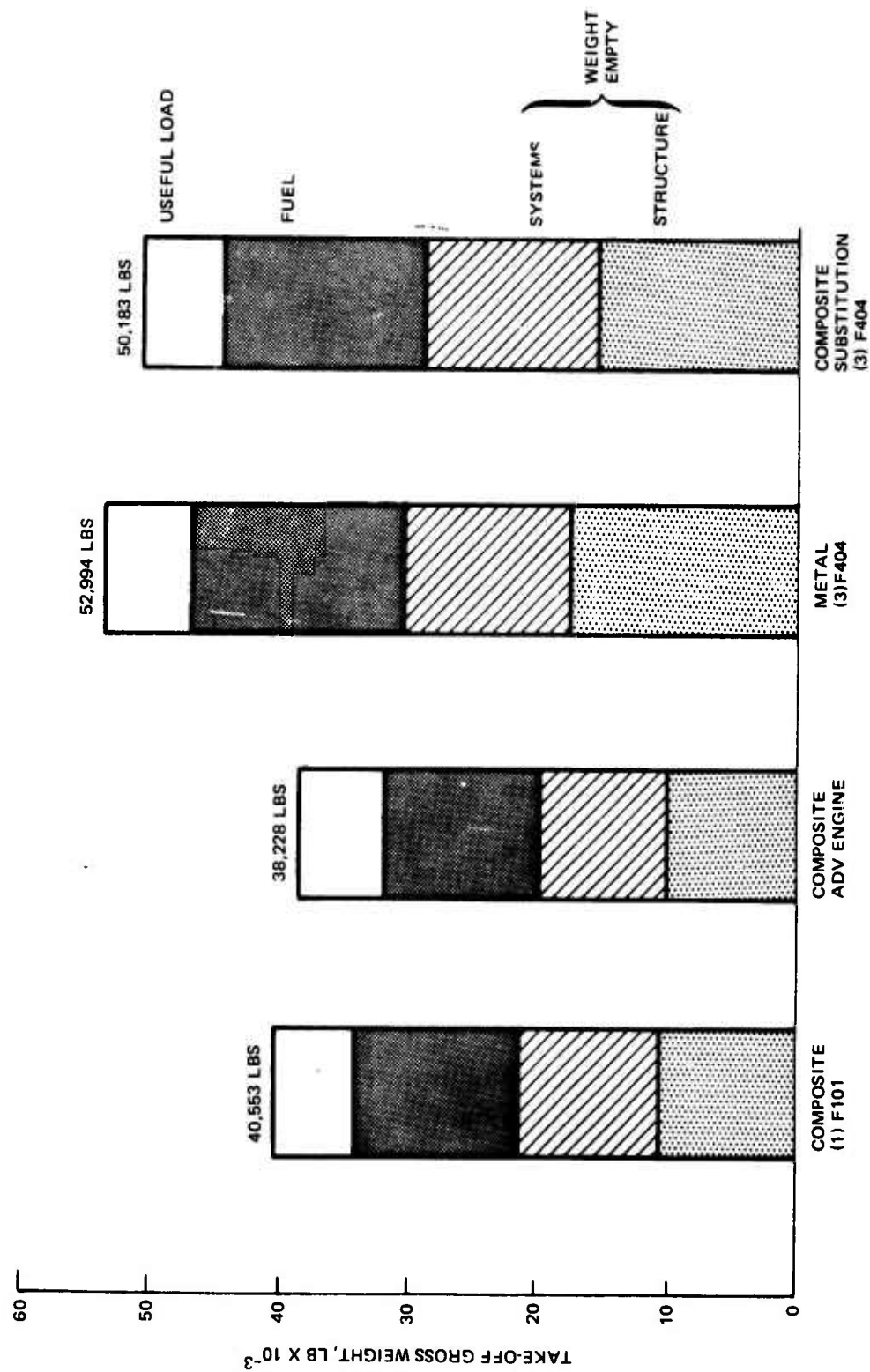


Figure 22. Takeoff Gross Weight Comparison

the curve in Figure 23 was developed. It indicated that the optimum percentage of composites for weight is at about 75%. Due to limitations in time, this study was run using the CISE program with growth factors to try and simulate the baseline vehicle. The all-metal vehicle doesn't match the all-metal baseline because it has different limitations. This study is just trying to show sensitivity and a trend.

4.4 AERODYNAMICS AND VEHICLE PERFORMANCE

The design mission selected for the ADCA study is that of a Supersonic Penetration Interdiction Fighter (SPIF). This selection provides a demanding set of requirements, but yields the maximum potential payoff for the unrestrained use of composite materials. Furthermore, this mission addresses, better than any other, the serious problems of survivability and mission effectiveness in the advanced SAM and Ground Control Intercept (GCI) threat environment of the 1980's and beyond.

The mission profile is illustrated and detailed in Figure 24. It is a 400 n mi radius, deep strike mission, with equal sub- and supersonic legs, delivering a 5,000 lb payload to the target at supersonic speed. The 1.6 Mach cruise speed was selected based upon design/performance/cost tradeoff analysis. This included consideration of performance parameters, design complexity, threat environment, and potential aircraft losses, upon life cycle cost and mission effectiveness.

The weapons payload, and other significant design factors are listed in Table 8. These were selected by the Flight Dynamics Laboratory to be representative of the 1980's time frame, and to burden the ADCA design study with a meaningful design challenge. The vehicle carries gun and ammunition, and 5,500 lb of advanced air to ground and air to air weaponry.

The performance requirements listed in Table 9 were chosen at the onset of the ADCA vehicle design study. They were imposed to ensure that a flexible, versatile system would be developed to outperform all existing airborne and missile threats. This is no mean feat, when one seeks to combine across-the-board dominance in combat maneuverability, with supersonic cruise, and a primary ground attack role. As Table 9 shows, the ADCA performs this difficult task very well. The vehicle takeoff gross weight is 40,553 lb, including 12,675 lb of fuel and a full complement of weapons. It uses an existing GE-F101 engine, and is a realistic and practical design for a 1980's time frame IOC.

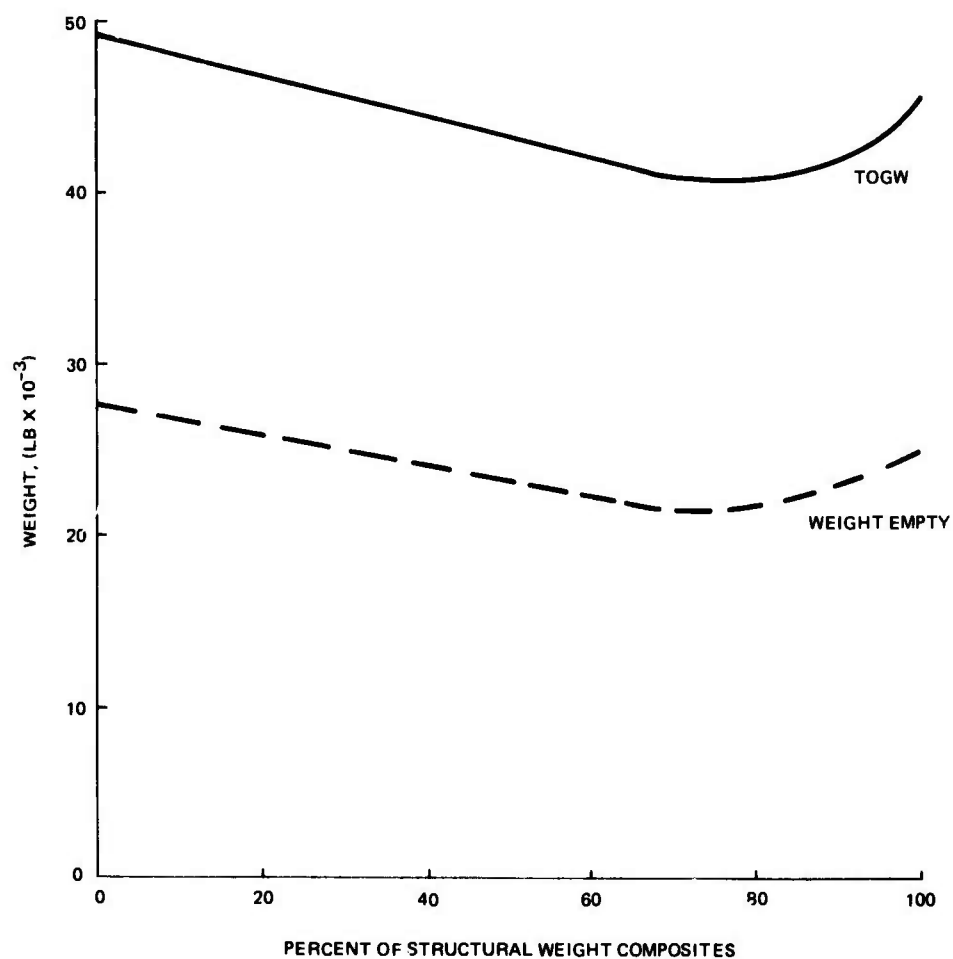


Figure 23. Weight-to-Bearing Strength, Composites vs Titanium

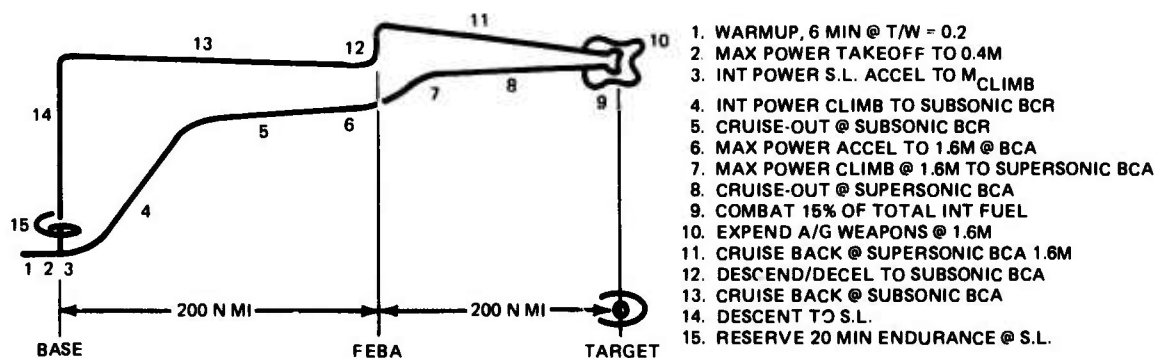


Figure 24. ADCA Mission Profile Supersonic Penetration Interdiction Fighter (SPIF) Mission

TABLE 8. PAYLOAD AND DESIGN FACTORS

Avionics Complement	1,350 lb (uninstalled)
Armament:	
2 Advanced Air-to-Ground Guided Weapons	5,000 lb
2 Advanced Air-to-Air Missiles	500 lb
M-61 Gun and Ammo.	600 lb
Maximum Mach No.	1.0 @ Sea Level
	2.0 @ Altitude
Limit Load Factor	6.5 @ Flight Design Gross Weight

TABLE 9. VEHICLE PERFORMANCE

	Requirement	A/G Stores Retained	A/G Dropped
Maneuverability:			
Instantaneous g @ M = 1.6/50K ft	4.5	6.5 (Limit Load)	
Sustained g @ M 0.9/30K ft*	3.0	3.1	3.7
Sustained g @ M 1.2/30K ft	4.0	4.1	4.9
Sustained g @ M 1.6/50K ft	---	2.1	2.6
Acceleration Time			
M. 8 to 1.6 @ 35K ft	80 sec	83 sec	66.5 sec
Takeoff/Landing Distance, ft	3200/3200	3150/2550	
(Ground Roll: SL, Tropic Day)			

*Mach 0.9 sustained g has been corrected downward in accordance with wing twist available with a realistic design.

4.4.1 Aerodynamic Configuration Features

The aerodynamic configuration of the ADCA vehicle was developed to provide efficient cruise and outstanding maneuverability at all flight speeds, while making optimum use of composite material structural design concepts.

Self-defense and alternate mission capability, coupled with the weapons load flexibility of the resultant design can serve as a standard for the operational requirements achievable in a supersonic cruise aircraft.

The hybrid wing planform, illustrated in Figure 25, has a highly swept leading edge and low thickness ratio in the wave-drag sensitive root region. Outboard, a thin supercritical wing segment of moderate sweep provides increased aspect ratio and high transonic maneuverability. This planform results in efficient cruise at all Mach numbers.

Relaxed Static Stability (RSS) and Control Configured Vehicle (CCV) technology have been combined with uncompromised control power to attain the maximum maneuvering capabilities of the airframe. The combined effect of neutral point shift with Mach number, shown in Figure 26, wing variable camber programming with Mach number and lift, and positive canard lift to trim at all flight conditions, results in highly efficient cruise and maneuver performance. Canard control power allows unrestricted use of wing trailing edge flaps to provide takeoff and landing performance which is more than sufficient to meet alternate mission and overload requirements.

With the possible exception of the canard, the control surfaces are simple and perform in a very conventional manner. This is summarized in Table 10. In subsonic flight, more than adequate roll control is provided by differential inboard flaperons, while the outboard flaperons are brought into play only in the low "q" power approach regime, permitting best utilization of inboard flaps for high lift. This approach places no stiffness requirement on the wing to enhance control effectiveness. At supersonic flight speeds, differential canard deflection provides powerful roll control. Their use at subsonic speeds is avoided due to a countering moment from the wing. However, such application in concert with yaw stabilization by the rudder provides direct side force control, should that capability prove operationally desirable for the ADCA (e.g., cross-wind landing, subsonic ground attack or air combat maneuvering).

The aircraft has relaxed directional stability (CCV in yaw), permitting a significantly smaller vertical tail than would otherwise be the case (almost 50% larger). An extremely stiff, aeroelastically tailored vertical tail provides exceptional directional stability and rudder power. These characteristics were incorporated into a control system simulation and resulted in a smaller and lighter vertical fin. Control system simulations conducted to date have indicated instantaneous vehicle response characteristics, and performance exceeding any requirement, while employing reasonable control rates throughout.

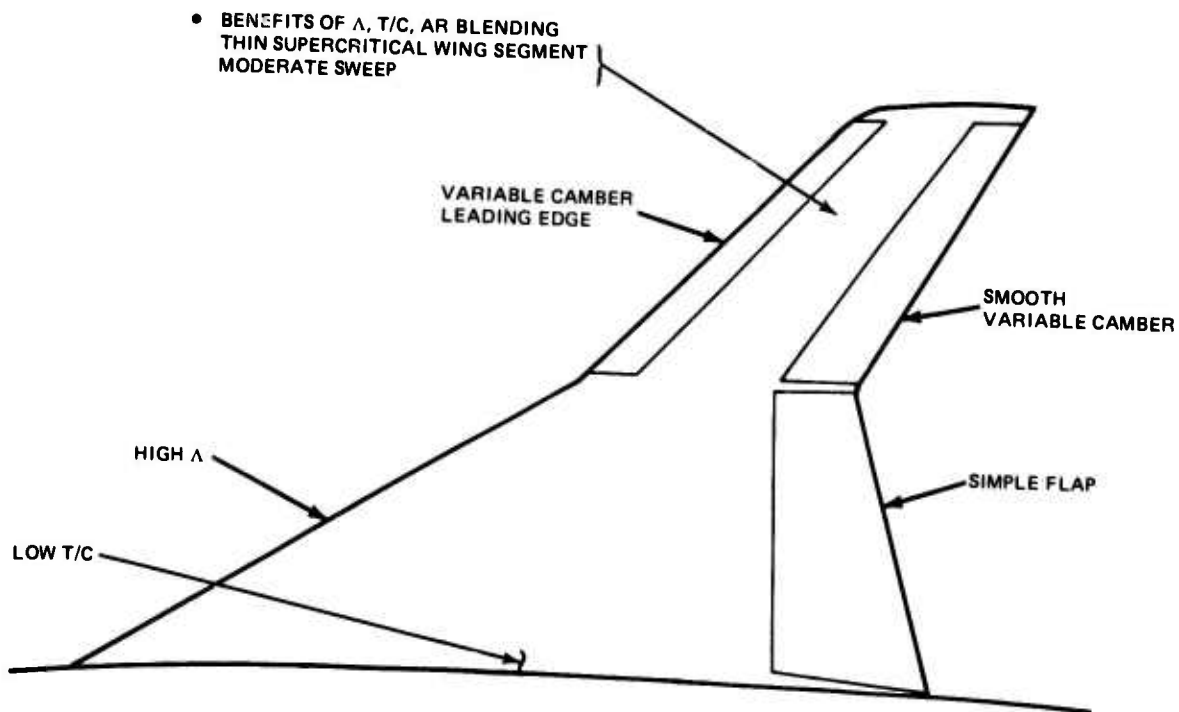


Figure 25. The Compound Planform Wing

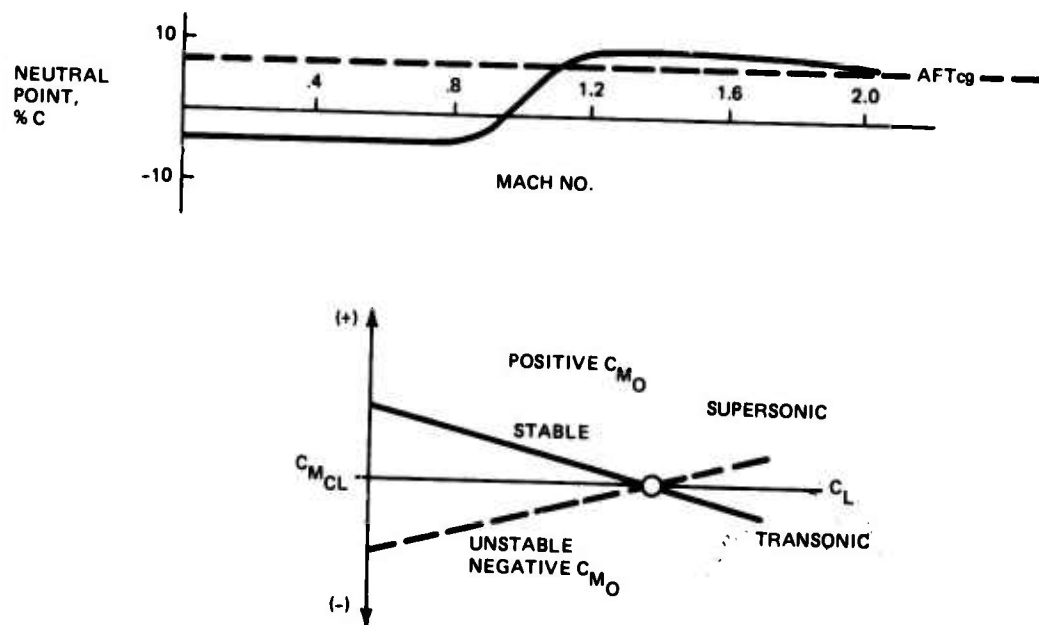


Figure 26. Vehicle Longitudinal Characteristics, RSS Design, Variable Camber and Canard

TABLE 10. CONTROL SURFACE AND FUNCTION SUMMARY

Control Surface Summary			
Surface	Area	Max Throw	Rate
Canard	90 Ft ²	±30°	50°/Sec
Inboard Flaperons	40 Ft ²	±30°	50°/Sec
Outboard Flaperons	20 Ft ²	20°	30°/Sec
Outboard L.E. Droop	11 Ft ²	20°	30°/Sec
Rudder	24 Ft ²	±30°	50°/Sec
Control Function Summary			
Function	Flight Condition	Surface Function Throw	
Roll	Subsonic Q < 400 psf	Inboard/Outboard Flaperons ±15°/15°	
	Q > 400 psf	Inboard Flaperons ±15°	
	Supersonic	Inboard Flaperon/Differential Canard ±15°/±15°	
Pitch	Subsonic & Supersonic	Canard	±20°
Yaw	Subsonic & Supersonic	Rudder F(Q)	±30° Max ±10° Max

4.4.2 Vehicle Aerodynamic Characteristics

4.4.2.1 Lift and Drag

Minimum drag variation with Mach number is shown in Figure 27. Wave drag was obtained using the Supersonic Area Rule Computer Code, and the drags associated with a fixed inlet were estimated from test data. Statistical data were used for antenna and cooling and ventilating drags. Mission drag status (C_{DMIN} with stores on) is given in Table 11. This is compared to the original target values that were established using the Grumman "CISE" code, and very conservative store drag levels. The clean aircraft drag level at Mach 1.6 is the result of favorable structural weight tradeoffs with thickness distributions only (not absolute thicknesses) at the inboard wing rear spar, in the canard, and in the vertical tail. The vertical tail was reduced in size and thickness based upon very favorable aeroelastic tailoring benefits, and the aircraft's exceptional directional stability

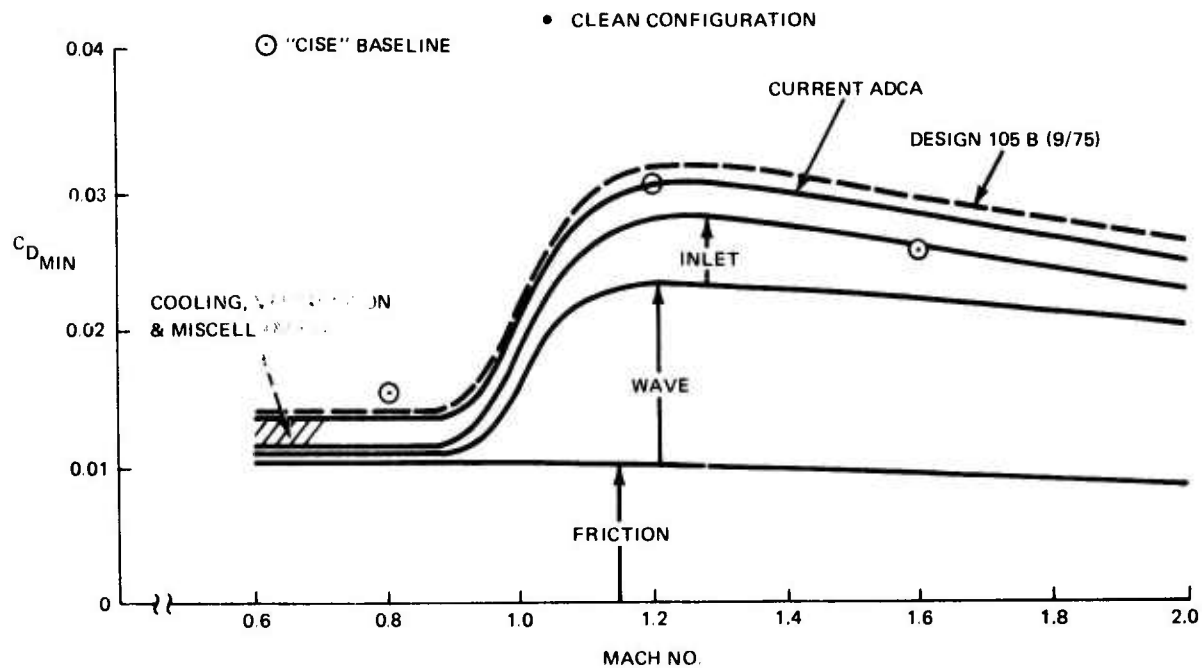


Figure 27. Minimum Drag Status

TABLE 11. MISSION DRAG ($C_{D\text{ MIN}}$) STATUS

			C _D MIN (counts)			
			Mach No.	0.8	1.2	1.6
Original Target	Aircraft	Clean		155	304	256
	Stores	2 A/A		16	31	30
		2 A/G		17	54	54
	Target Total			188	389	340
ADCA	Aircraft	Clean		137	306	283
	Stores	2 A/A		14	26	24
		2 A/G		17	27	34
	Current Total			168	359	341

and control characteristics. The new, lower, store-drag levels are the result of moving the air-to-air missiles to the wing tips, which also eliminates the underwing pylons, and an up to date analysis of advanced supersonic missile data and installation factor wind tunnel data for that missile interpolated between tangent mounted and semi submerged values. This is expected to be fully representative of the ADCA store installation. The mission drags are everywhere equal to or better than the original target levels.

Vehicle low speed aerodynamic characteristics ($M = 0.2$) have been based upon Grumman ADCA model wind tunnel data. Subsonic compressibility effects have been estimated by standard Data Compendium (DATCOM) techniques. The Mach 0.9 drag polar was constructed through the maneuver design point using the results of the transonic wing design effort. That effort utilized the Grumman subsonic wing-body computer code, and transonic data from other in-house two dimensional airfoil and complete configuration wind tunnel programs. Lift and drag characteristics are presented in Figures 28, 29 and 30.

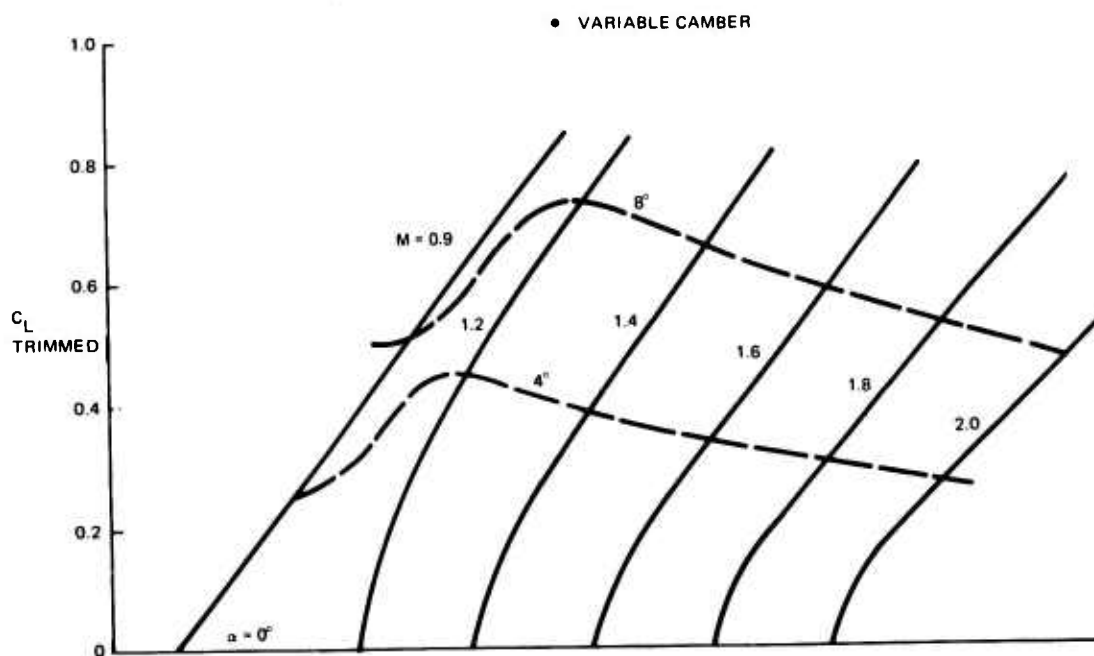


Figure 28. Trimmed Lift Curves

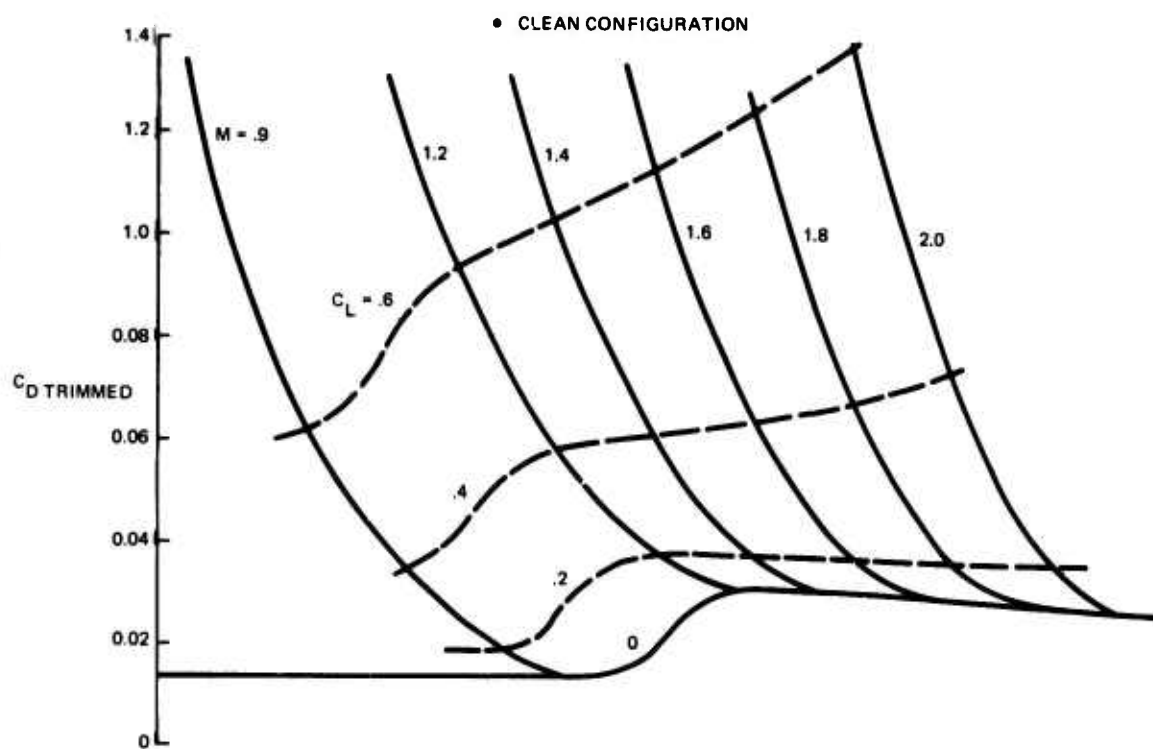


Figure 29. Trimmed Drag Polars

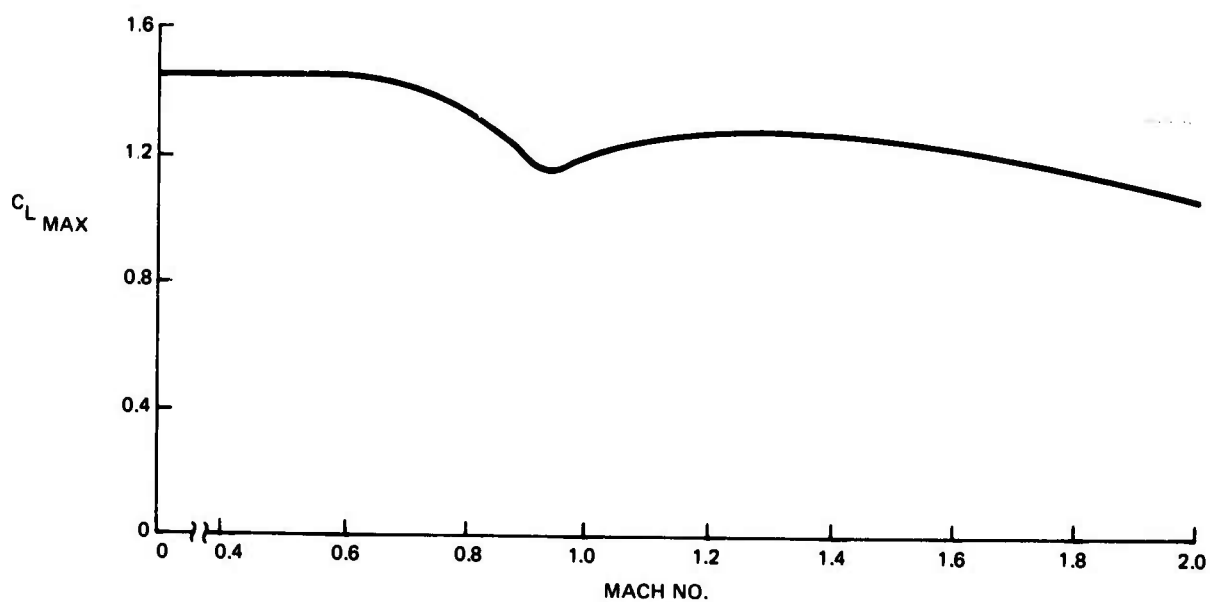


Figure 30. Maximum Lift Coefficient

The supersonic vehicle characteristics are based upon results obtained using the Woodward wing-body computer code. The drag due to lift is based upon variable camber providing optimum loadings in the low to moderate angle of attack range. It is recognized, however that the linear theory is limited in its validity by lift coefficient and angle of attack, and that this limitation varies with Mach number. The variable camber drag-due-to-lift is replaced by conventional wing polars at the higher lift coefficients.

Vehicle characteristics initially were based upon statistical data, DATCOM estimation methods, and area rule wave drag computer results. This has been thoroughly updated to incorporate subsonic ADCA model wind tunnel data, and the results of an extensive design and analysis effort that utilized complex subsonic and supersonic wing-body and area rule computer codes.

4.4.2.2 Stability and Control

ADCA longitudinal aero characteristics have been updated and are presented in Figure 31. These data reflect the configuration changes incorporated in configuration 105B particularly the reduced canard area. Use has been made of the ADCA model to adjust estimated subsonic levels to account for preliminary test results.

The data are presented in a format compatible with both applied loads requirements for flexibilizing the data, and guidance and control requirements for incorporation of the data in control system studies.

The data presented in Figure 31 are based on the results of applying a first approximation derivatives computer program to the configuration. These results have been adjusted to reflect wind tunnel test results in those areas where compatible results were available. Calculations based on the methods presented in Datcom were used to incorporate the canard vortex interference on the wing damping derivatives.

Two levels of canard control effectiveness are presented; canard, and canard plus interference. The canard level is required to determine the canard loads and flexibility coefficients. The canard plus interference level is required to determine the actual total incremental loads due to canard deflection.

Estimated lateral/directional aero coefficients for the ADCA configuration 105B were updated to reflect a revised vertical tail contribution to C_y based on low speed wind tunnel correlation results. These changes effect C_{n_r} and C_{y_p} throughout the Mach range and other coefficients at Mach 0.9.

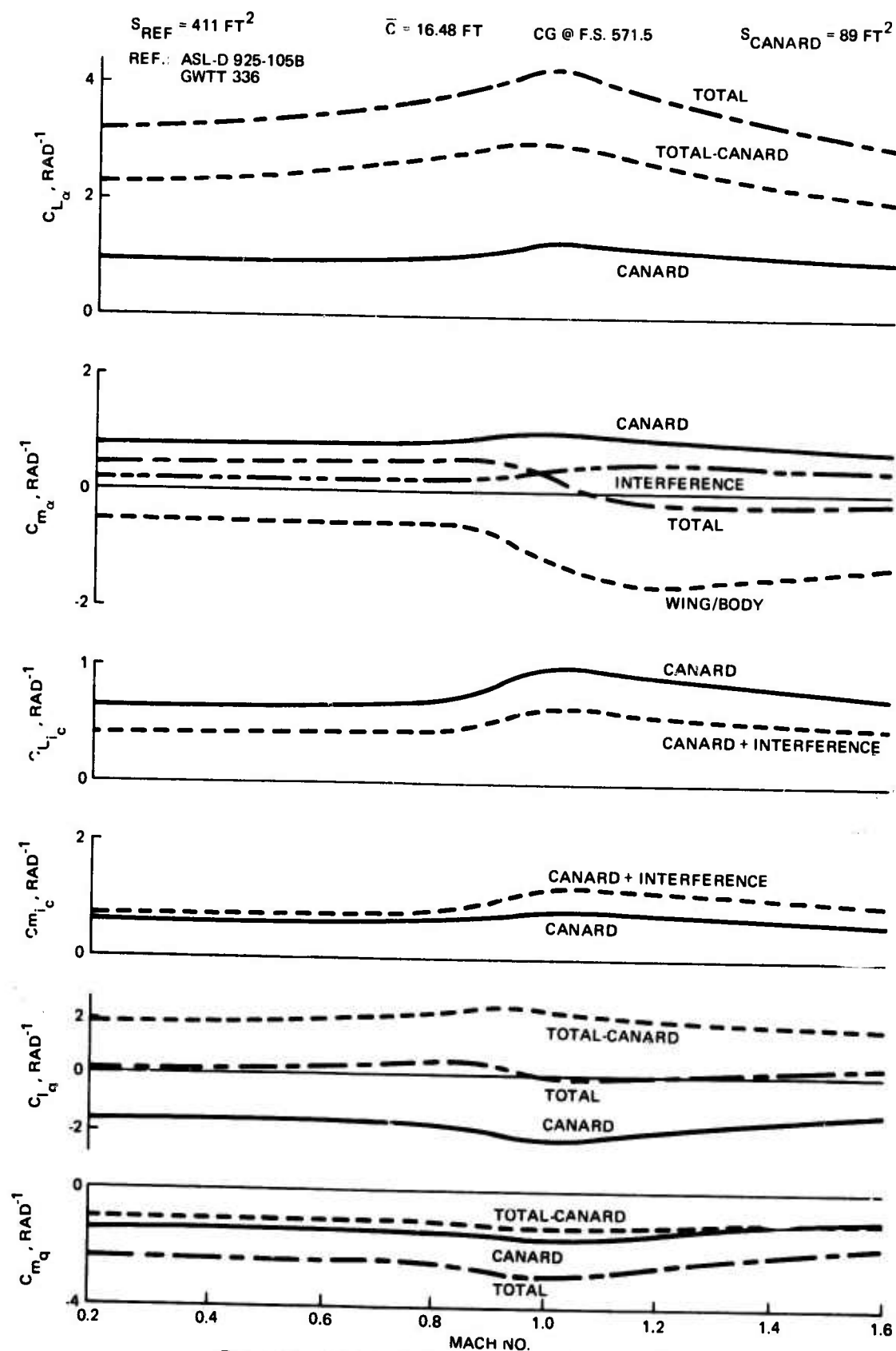


Figure 31. ADCA Estimated Longitudinal Aero Coefficients

The lateral/directional static, dynamic and control derivatives are plotted versus Mach number in Figures 32 through 35. In addition, the vertical tail contributions for a 10% area reduction have been estimated, though not shown here. All of this information has been assimilated into a 5 degree-of-freedom analog simulation of the vehicle control system for full stability and control analysis. This analysis also incorporated aeroelastic effects on total system performance. Control system parameters, control rate requirements, and vertical tail size reduction, were investigated at critical points in the flight envelope.

4.4.3 Wing Design

The ADCA mission and point performance requirements present the challenge of providing a broad range of aerodynamic capabilities, over a wide Mach number spectrum. The compound-planform-wing/canard combination was developed to meet these diverse supersonic, transonic, and low speed requirements. Wing shapes were then defined to maximize performance at the supersonic cruise (Mach 1.6), and transonic maneuver (Mach 0.9) flight conditions.

In the wing design effort, extensive use was made of computer codes capable of analyzing complex configurations. The Woodward Program and the Grumman Subsonic Wing-Body Program were used to design the wing camber and twist to optimize the supersonic cruise and transonic maneuver points. These wing designs were developed concurrently in the attempt to realize the full practical capabilities of a single composite wing.

In both studies, fuselage geometry had to be consistent and optimum at both design points and several fuselage camber shapes and angles of attack were investigated during the analytical design phase. These fuselage parameters were necessary to obtain a common wing root incidence while preserving low supersonic cruise drag and the fuselage pitching moment required to trim the supercritical wing at transonic maneuver conditions. Once the fuselage cruise and maneuver angles of attack were determined, the wing could be optimized in detail at each design point.

4.4.3.1 Supersonic Cruise

The wing and canard were designed for least drag at the supersonic cruise condition ($M = 1.6$, $C_L = 0.20$, $\alpha_{FRL} = 2^\circ$ to fuselage reference line). Pitching moment constraints were imposed to obtain a trimmed condition. Leading edge camber and twist were constrained to practical shapes and analyzed with and without leading edge suction. The com-

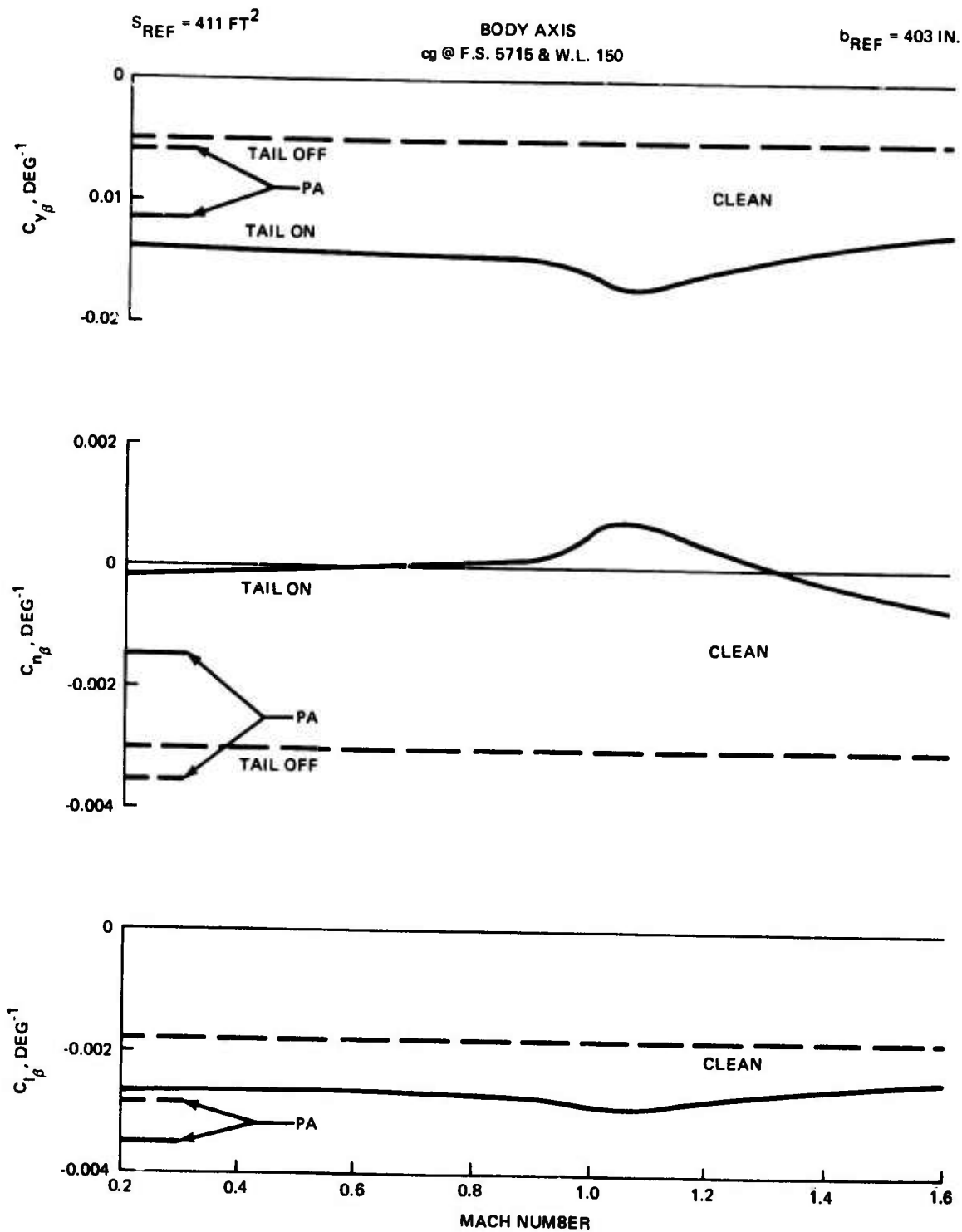


Figure 32. ADCA Lateral/Directional Static Derivatives

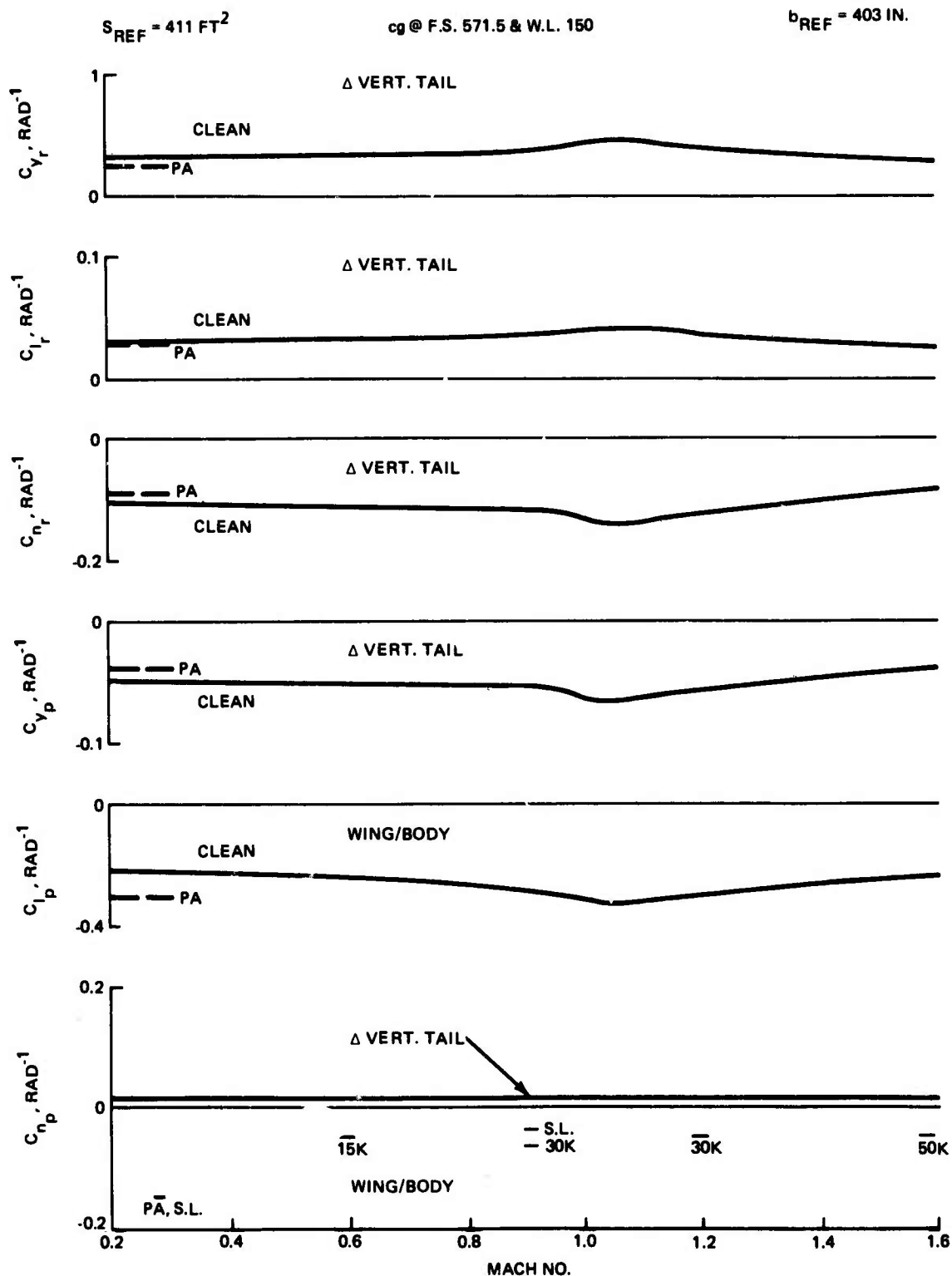


Figure 33. ADCA Lateral/Directional Dynamic Derivatives

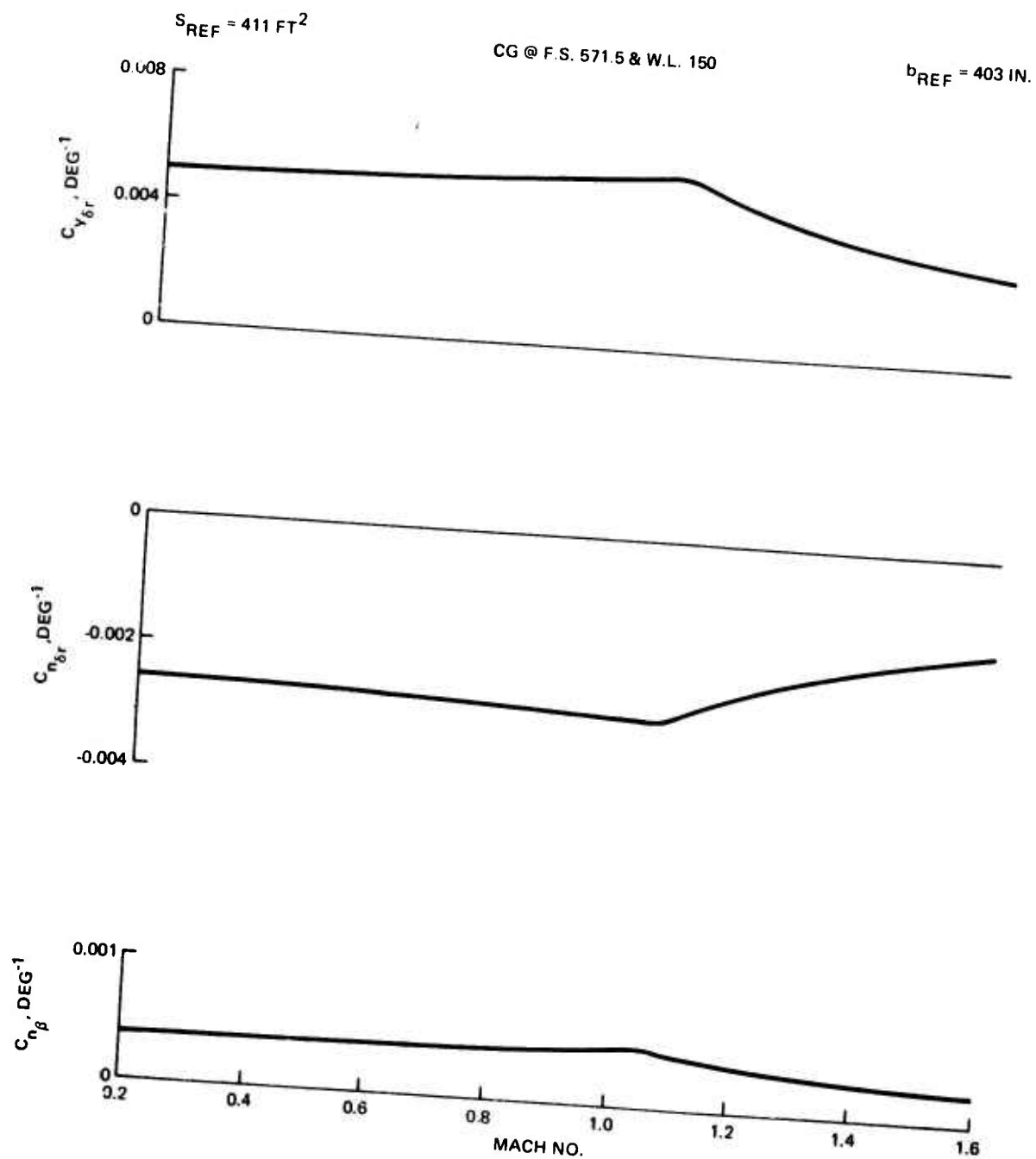


Figure 34. ADCA Rudder Effectiveness

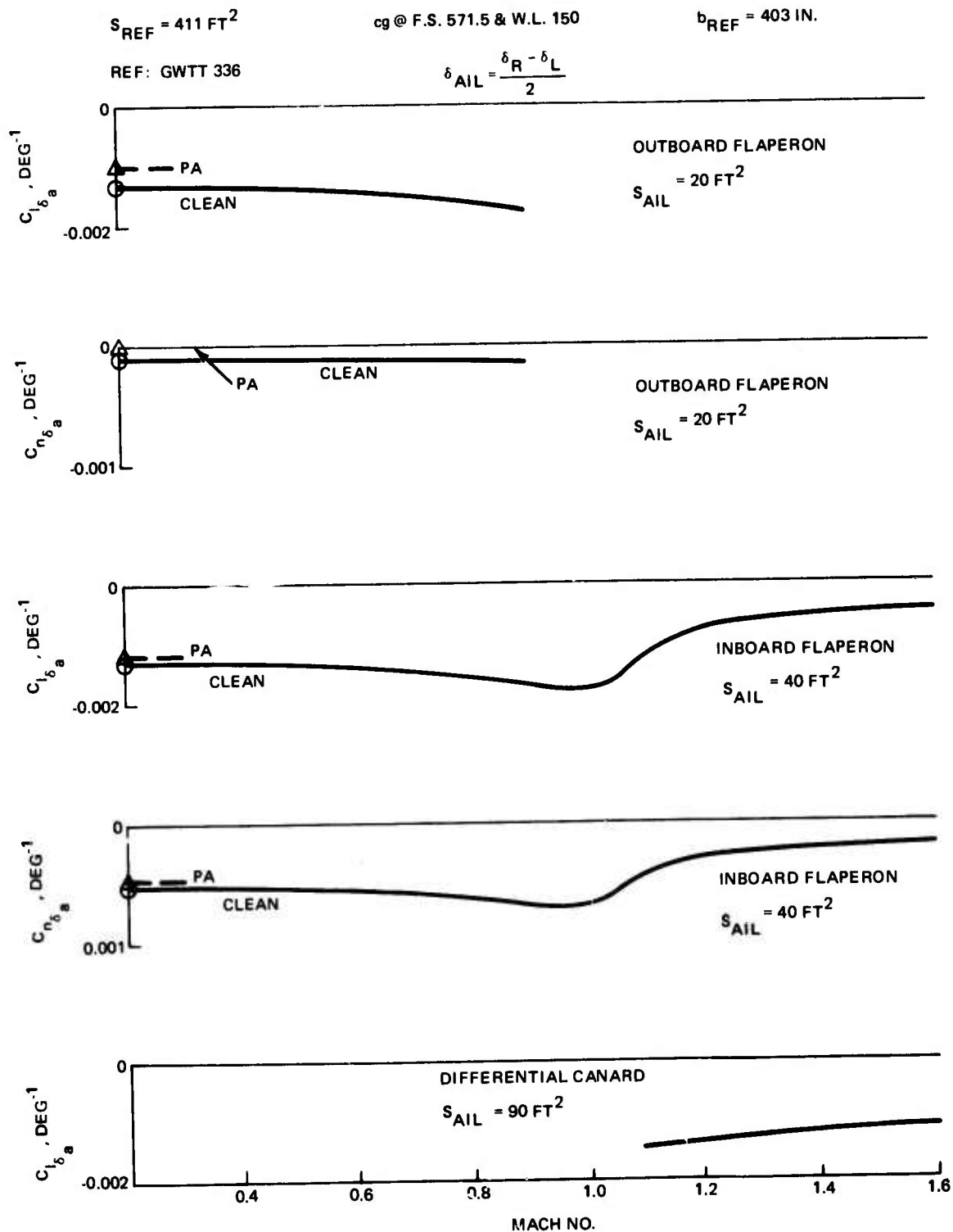


Figure 35. ADCA Aileron Effectiveness

puter model was modified for analysis to account for the subsonic leading edge on the inboard wing and the lift loadings were modified based upon data obtained from Grumman Highly Maneuverable Aircraft Technology (HIMAT) wind tunnel results. The final wing shape provides the near-optimum loading shown in Figure 36 and realizes low induced drag at cruise lift.

4.4.3.2 Transonic Maneuver

The wing and canard were optimized for maximum sustained performance at the transonic maneuver point ($M = 0.9$, $C_L = 0.75$, $\alpha_{FRL} = 12^\circ$). The camber distribution on the inboard wing section was determined by the supersonic wing design while the outboard section has supercritical airfoil camber. The twist distribution tailors the span load to minimize the combined induced and pressure drags. The load sharing between the wing, body, and canard is designed to produce a trimmed condition without excessive lift on any part. The supersonic cruise and transonic maneuver load distributions on the wing and canard are shown in Figure 37.

The load distribution at the sustained maneuver point permits non-supercritical treatment of the larger chord inboard wing which is compatible with the supersonic cruise

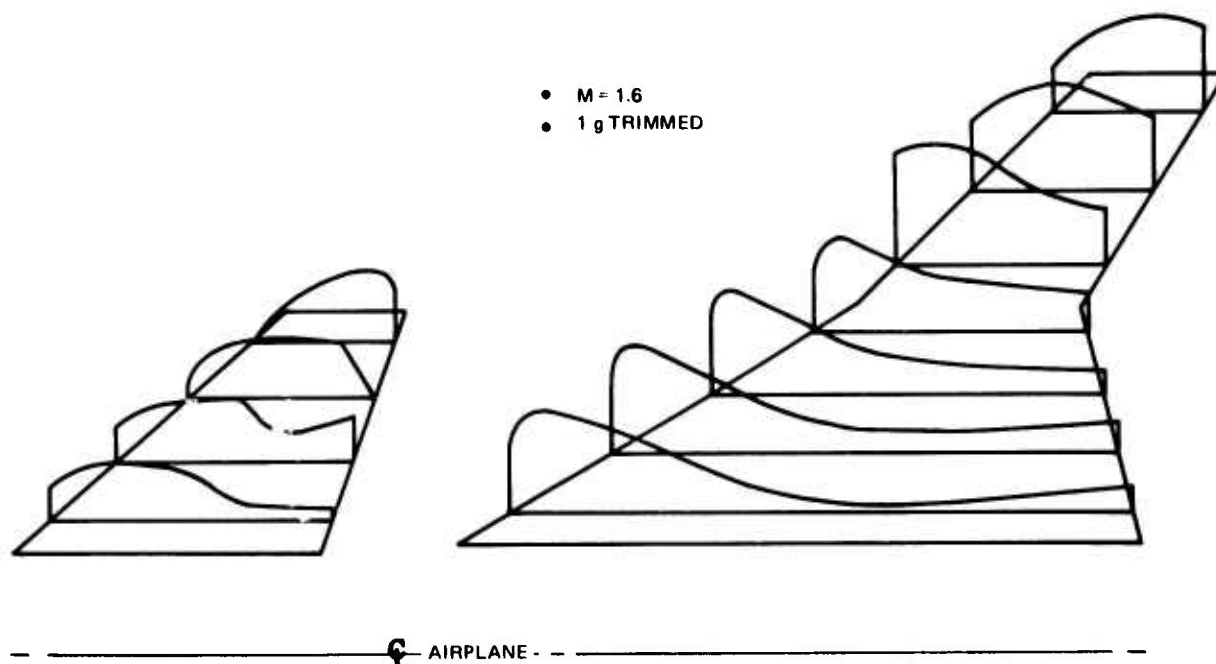


Figure 36. Load Distribution Optimized for Supersonic Cruise

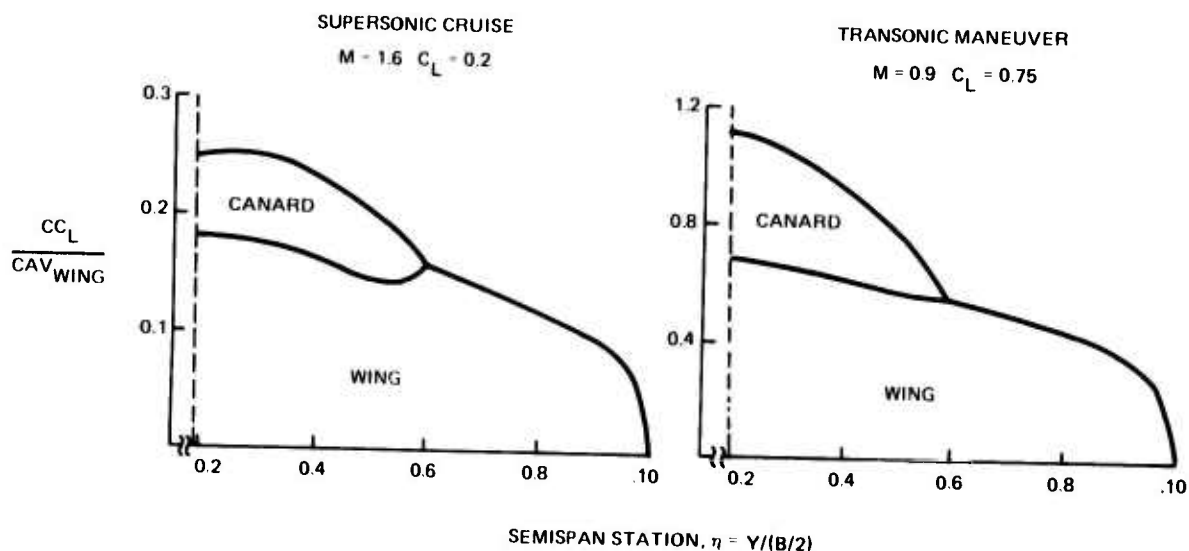


Figure 37. Optimum Span Load Distributions

shape requirement and design simplicity. The outboard loading is obtainable with an existing family of thin supercritical airfoils. These variable camber airfoils have been tested at Grumman and the data were used in estimating the wing characteristics.

4.4.3.3 Aeroelastic Wing Twist

The supersonic cruise wing shape is of overriding importance due to its direct impact on mission performance and takeoff gross weight. The structural wing box therefore was constrained to match the defined optimum supersonic cruise shape under a 1 g load. Within the design constraint of minimizing structural weight increase, and the strength requirement at ultimate load factor (9.75 g) tailored and untailored aeroelastic wing twist characteristics were determined. The various desired and available wing twist distributions are shown in Figure 38. The tailored wing represents an attempt to provide increased washout at the transonic maneuver condition. The result is a negligible improvement in sustained g capability due to a tailoring over the untailored case. This is disappointing perhaps, but not too surprising since there is no significant center of pressure variation between the supersonic cruise and supercritically loaded transonic maneuver conditions investigated here. Drooping the outboard leading edge device provides an additional 3° of washout also shown in Figure 38, to provide an increase in maneuver g capability.

These results are discussed in more detail in Section 5.2.3.

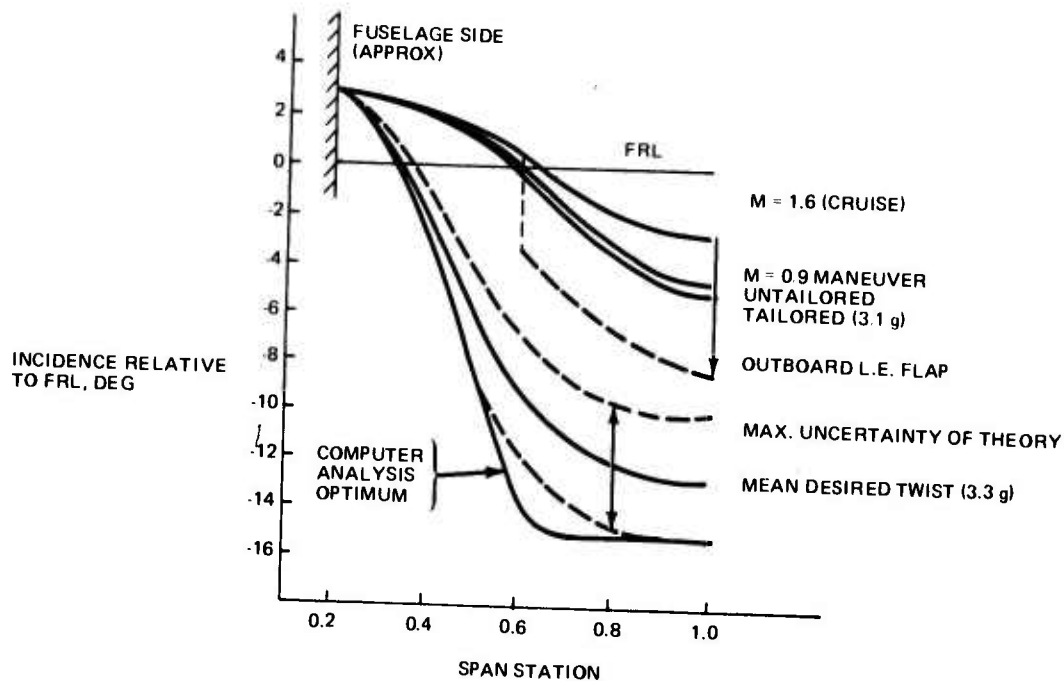


Figure 38. Wing Twist Distribution

4.4.4 Canard Design

The current canard size is the result of tradeoff studies involving vehicle stability level and wing location, while satisfying trim requirements over the flight C.G. range. Moving the wing forward and increasing canard size each decrease vehicle stability. Practical design considerations limit the forward movement of the wing and, therefore, provides a lower bound of canard size as a function of vehicle stability. The current design in Figure 39 represents a compromise of canard size, vehicle stability and wing location.

Figure 40 shows, in planview, some of the configurations considered in the canard sizing study. The impact of the canard control actuation was also considered. Slab canards as well as fixed canards with leading and trailing edge devices were investigated.

Canards were sized to satisfy both trim and stability requirements. The maximum allowable instability level is applied at the most aft center of gravity location and forms the right hand bound of the canard volume shown in Figure 41. Trim requirements are applied at the most forward center of gravity location and form the left hand bounds of

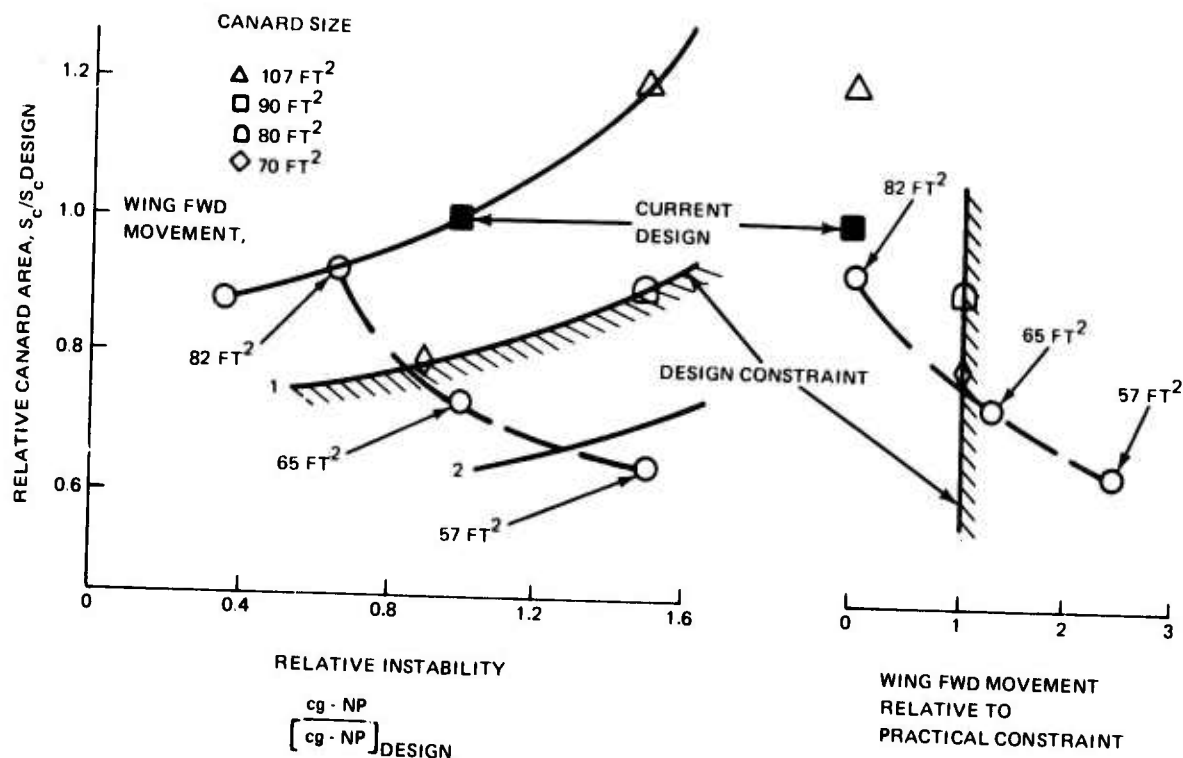


Figure 39. Canard Size, Wing Location and Stability Are Traded Off Within Practical Design Limits

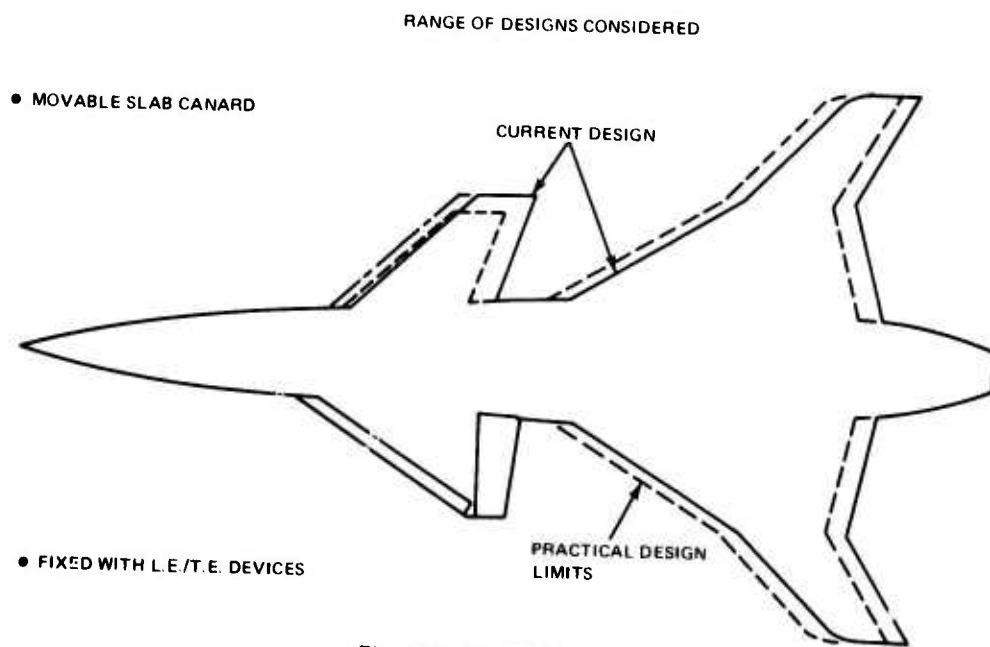


Figure 40. Canard Sizing

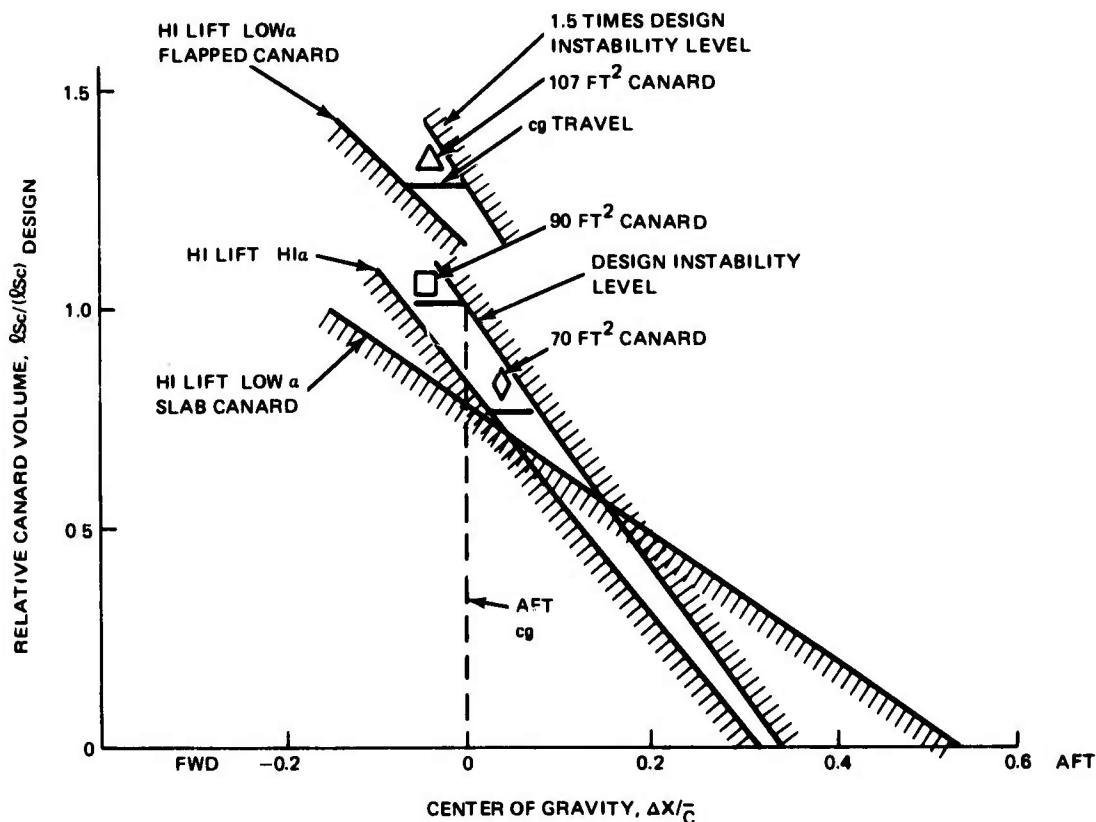


Figure 41. Canard Sizing Criteria, Time and Stability Boundaries

Figure 41. Two trim conditions were considered, as potentially critical; a high lift, high angle of attack trim requirement and a high lift, low angle of attack trim requirement. Which of these two bounds is more critical is configuration dependent. The center of gravity range for a given canard volume must lie between the most critical design boundaries.

4.4.5 Longitudinal Control Considerations

The slab canard configuration with its supplemental trim lift provides increased "g" capability with increasing stability level as shown in Figure 42. This capability is superior to the wing/elevon configuration whose shorter control arm requires increased negative lift to trim the increased stability levels. The slab canard configuration also exhibits superior levels of the control anticipation parameter (well exceeding the MIL-F-8785B category B Level 1 requirements) at all stability levels shown. The wing-elevon configuration can meet these requirements only at the higher stability levels where "g"

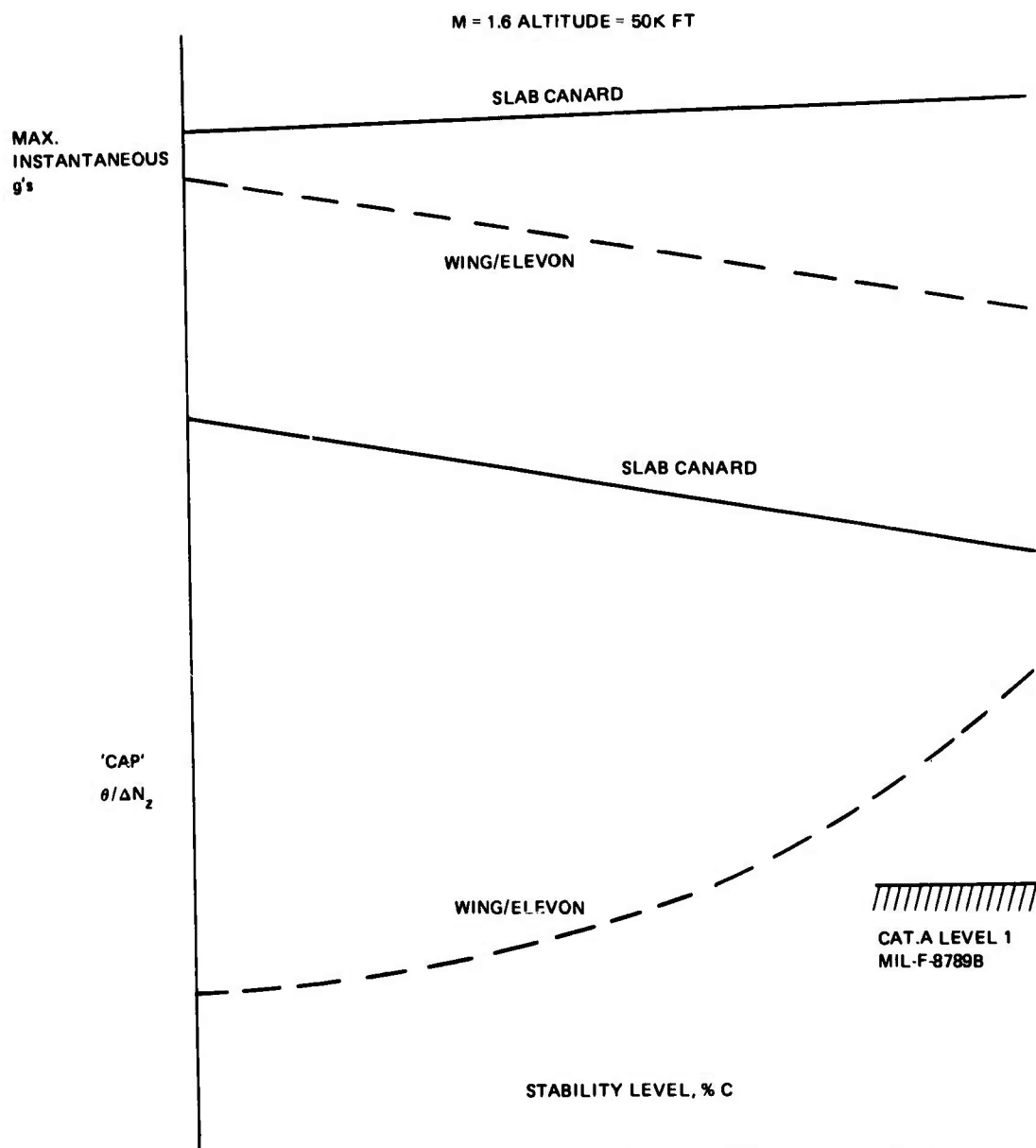


Figure 42. Slab Canard Provides Best 'G' Capability and Control Anticipation

capability is reduced. The high pitch acceleration capability of the slab canard configuration is superior to the wing alone configuration and approaches the F-14 high performance fighter level shown in Figure 43. This high pitch acceleration capability allows almost instantaneous attainment of its greater "g" capability. The improved maneuver and missile

avoidance capability of the slab canard configuration is reflected in Figure 44 which indicates a lateral range 2.5 times greater than that of the wing-elevon configuration. Figure 45 shows that the slab canard configuration maintains its superior subsonic pitch acceleration in both directions whereas the wing/elevon configuration would become control limited and not be able to pitch down at the higher instability levels.

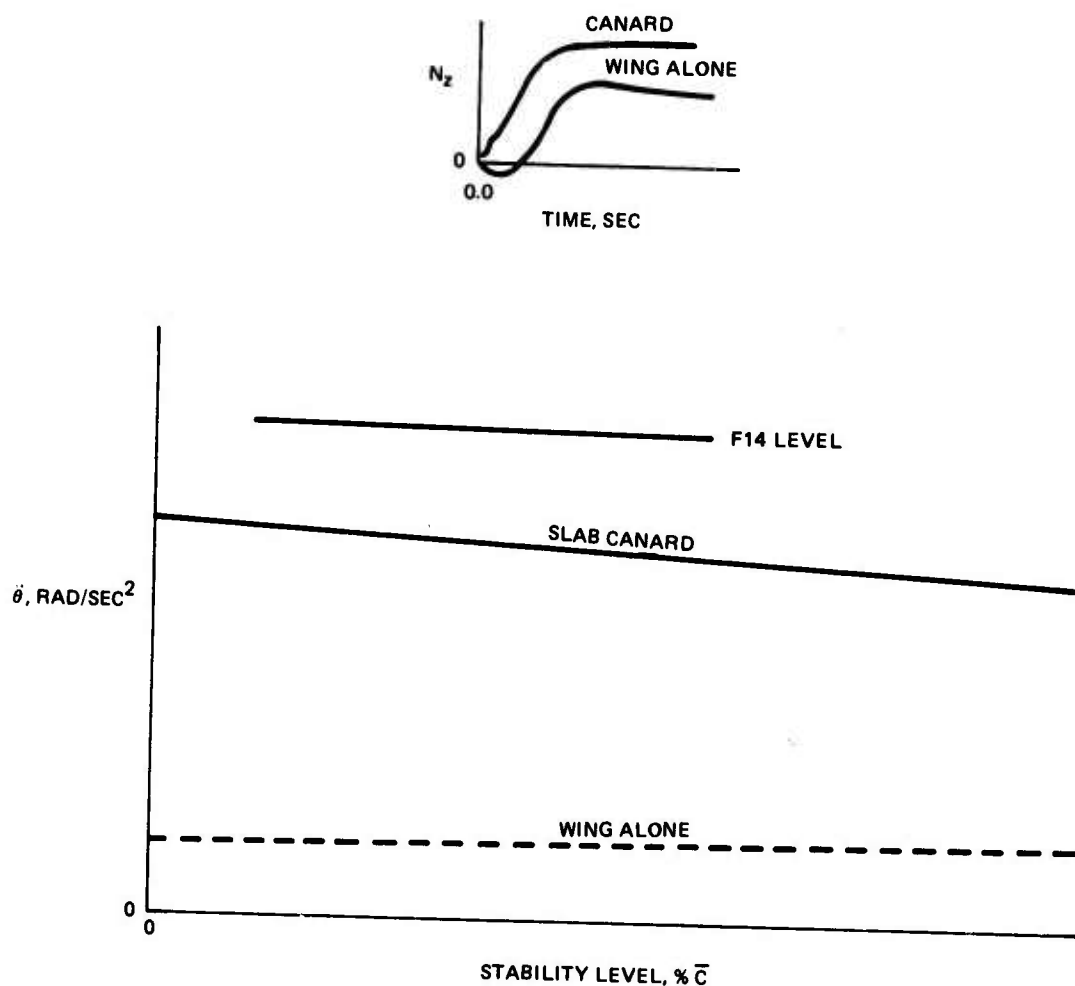


Figure 43. Slab Canard Provides Instantaneous Response

4.4.6 Wind Tunnel Testing

In support of the ADCA aerodynamic analysis, two wind tunnel tests have been conducted, with a third test scheduled for July 1976:

1. Low speed: 1/12-scale AAC airplane at Grumman Low Speed Wind Tunnel Facility, tested August 18 to Sept. 19, 1975, Test GWTT336

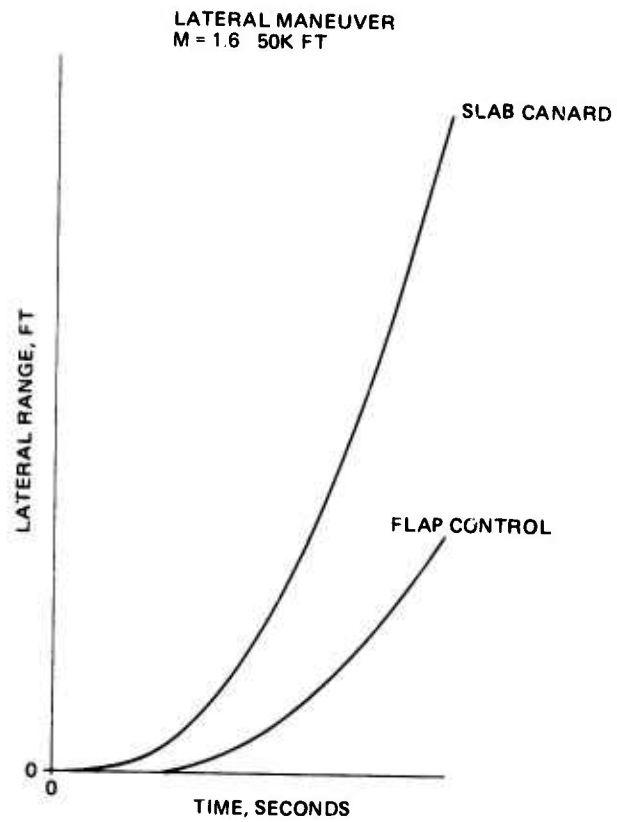


Figure 44. Missile Avoidance Capability

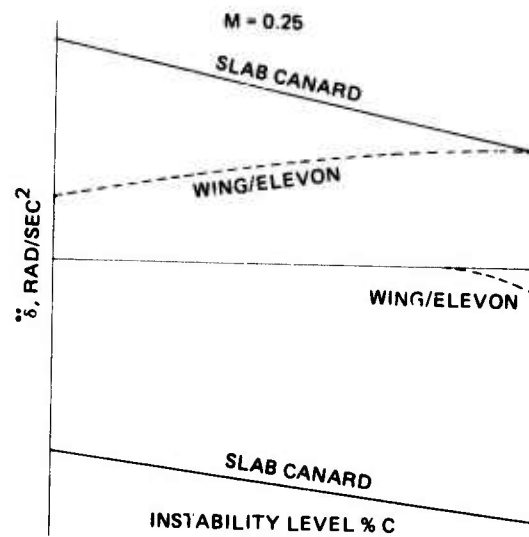


Figure 45. Slab Canard Has Best Lowspeed Pitch Acceleration

2. Transonic: 1/25-scale Advanced Fighter Model at Arnold Engineering Development Center, Propulsion Wind Tunnel Test TC444, tested April 19 to May 5, 1976

3. Supersonic: Test of above model at AEDC Facility during July of this year is scheduled.

To date wind tunnel test data reduction and analysis is incomplete pending the supersonic test results.

A 1/12-scaled model of the ADCA canard-wing aircraft was tested in Grumman's low speed wind tunnel facility between August 18 and September 19, 1975. The test was conducted under a nominal dynamic pressure of 37 psf using a six component strain gauge - sting balance. The model was tested to an angle of attack of 24° , and 20° of sideslip. Modular design of the wind tunnel model presented the capability of major configurational changes in a single wind tunnel test so that planform sizing, positioning and comparison investigations could be made. Two wing planforms, three canard control surfaces, and single and twin tail configurations were tested. There were 123 configurational changes here in the test. The ADCA planform wing results are presented here.

Figures 46 and 47 illustrate the model, with its uncambered and untwisted wing, and simple hinged control surfaces. The effect of variable camber on the drag polar is shown in Figure 48 for an array of wing leading and trailing edge deflections. The canard further improves polar shape, lift and moment characteristics and provides control power to high angle of attack, as shown in Figures 49 through 52. Drag reduction available with both wing and canard camber are illustrated in Figures 53 to 55. An analysis of the canard on wing lift interference is presented in Figure 56. Canard downwash reduces wing lift by one-half the amount of the lift on the canard. This, coupled with the zero to slightly negative roll effectiveness obtained with differential canard deflection, indicate an outboard net interference lift on the wing. Figures 57 to 59 show the striking lateral-directional improvements obtained in properly locating the canard, and the inherent spin resistant properties of the final design. Finally, in Figures 60 through 63, the canard's beneficial interference effects on both inboard and outboard wing flaperon effectiveness, and upon rudder effectiveness are strikingly demonstrated.

This wind tunnel test program has demonstrated that the ADCA is a CCV in the most complete sense, with favorably interacting control surfaces providing absolute control authority about all axes, and at all vehicle attitudes so far investigated- even through combined angles of attack and sideslip of 23° and 20° respectively.

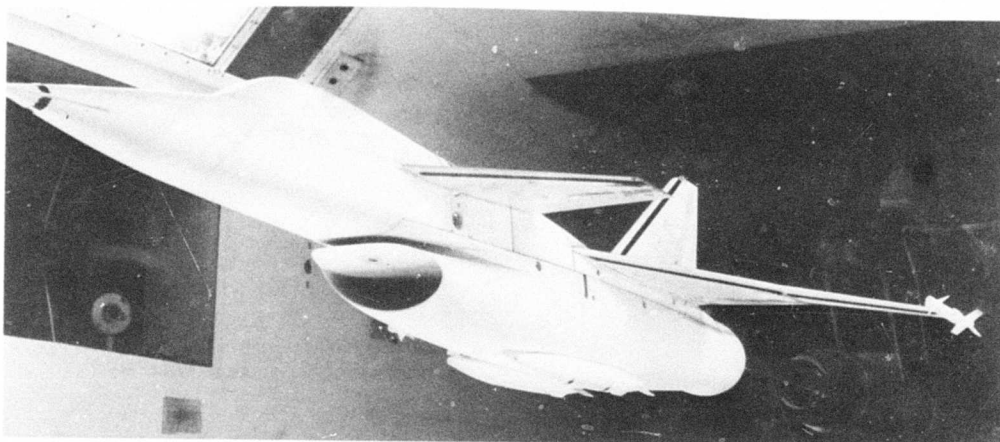


Figure 46. ADCA Low Speed Wind Tunnel Model

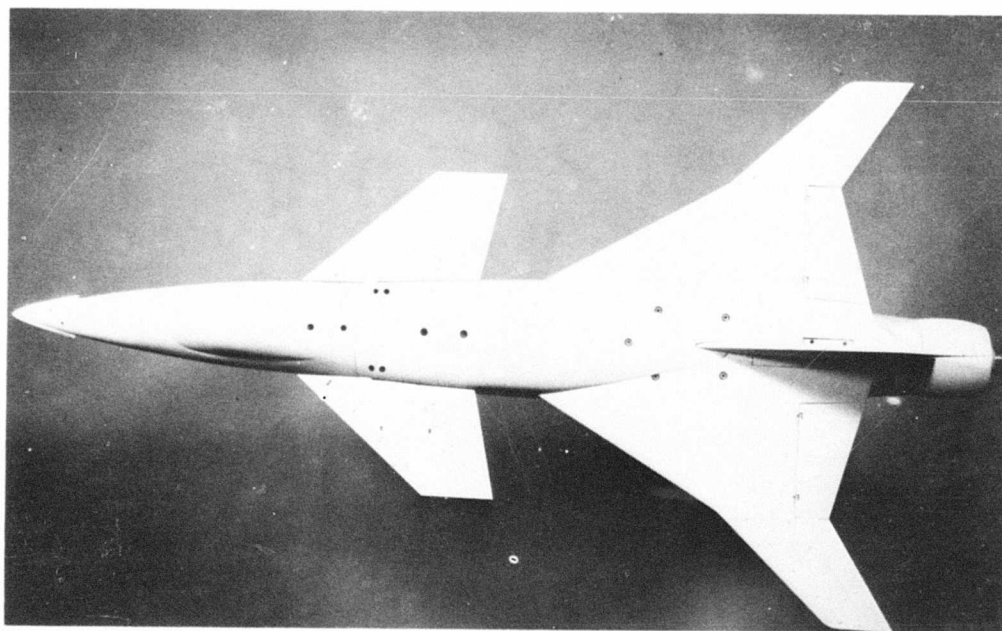


Figure 47. ADCA Low Speed Wind Tunnel Model

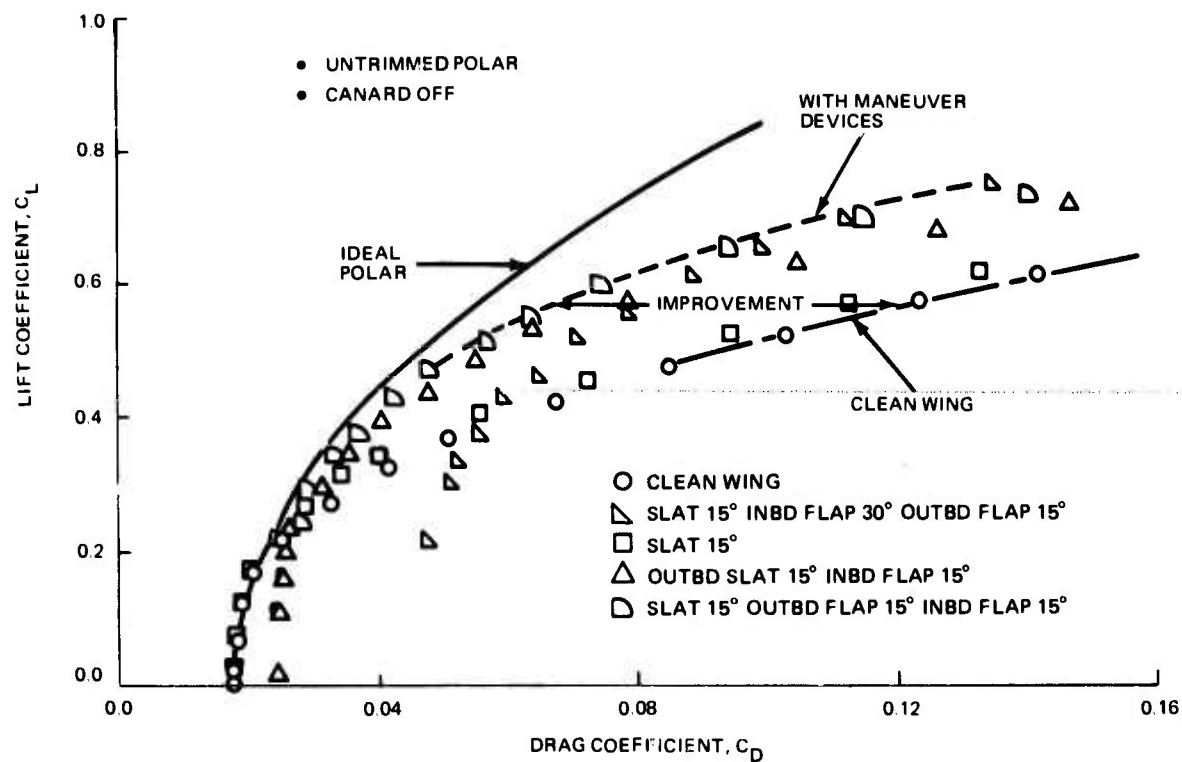


Figure 48. Effect of Variable Camber On Drag Polar

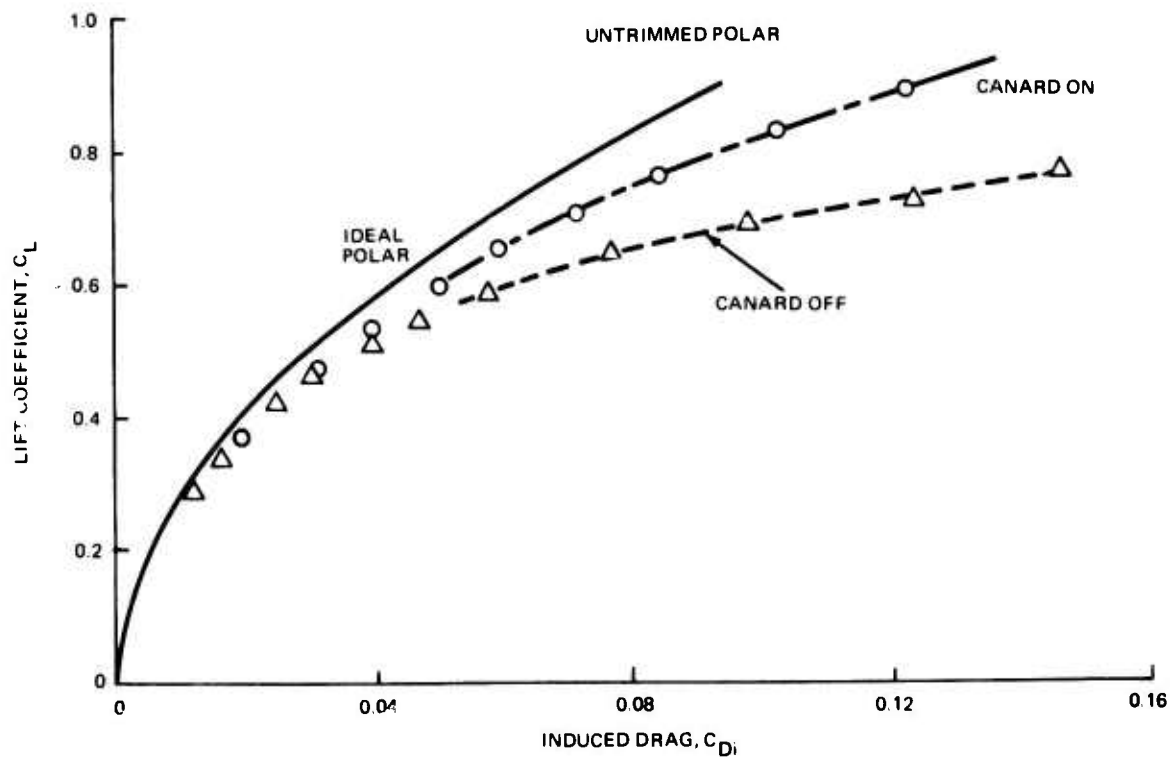


Figure 49. Canard Effect On Induced Drag

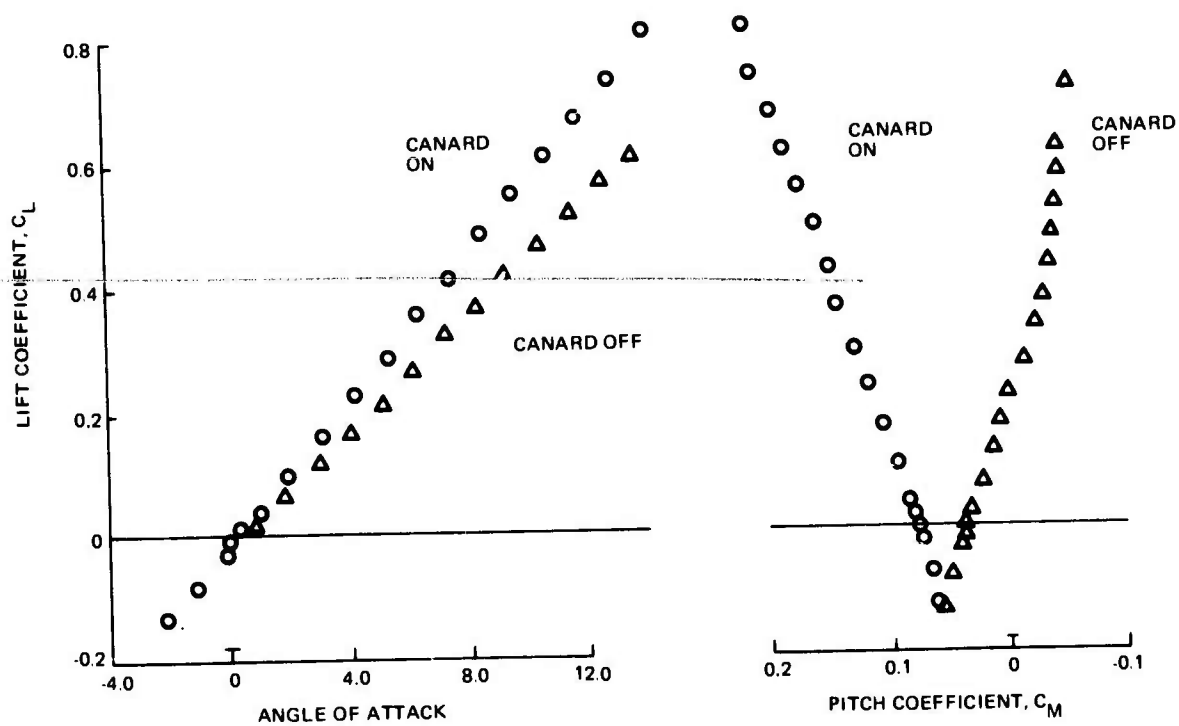


Figure 50. Canard Effect On Longitudinal Characteristics, Uncambered Wing

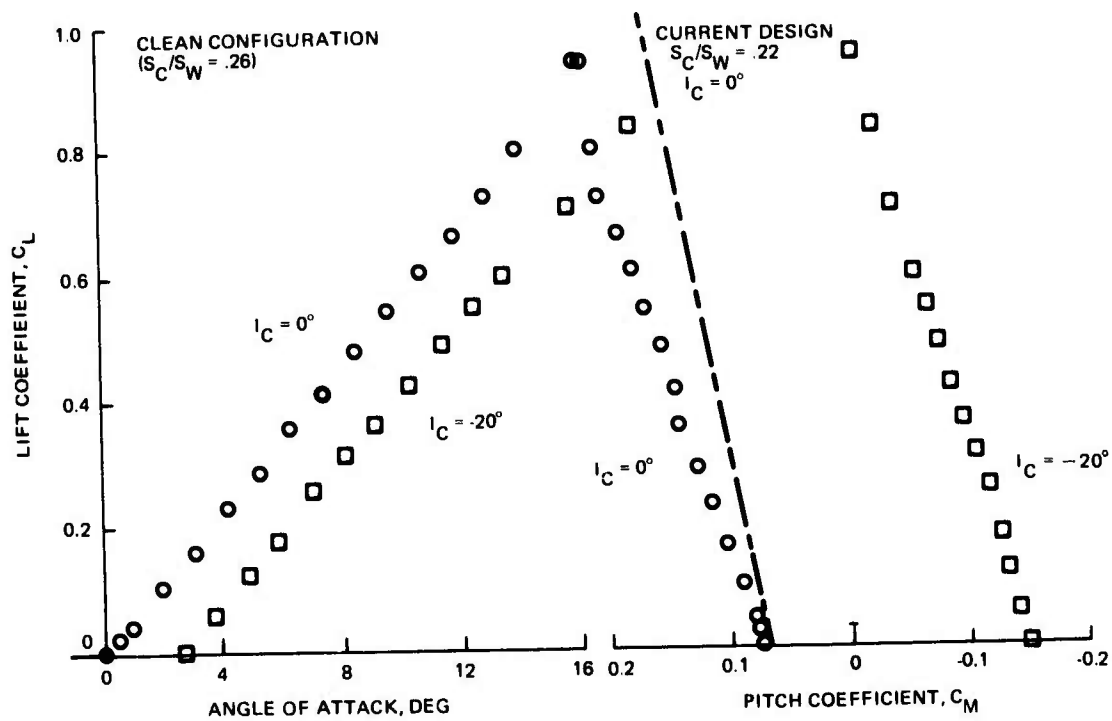


Figure 51. Linear Longitudinal Characteristics of Canard Configuration

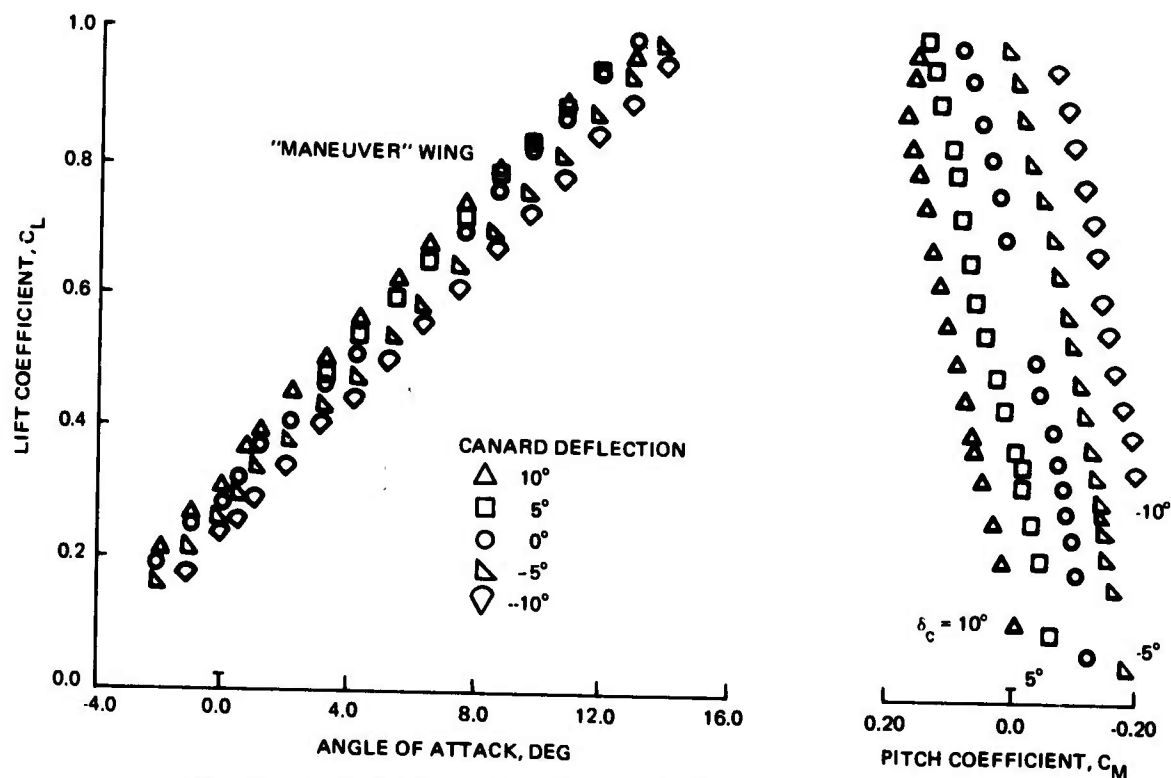


Figure 52. Canard Provides Trim Over A Broad C_L Range, Linearity Maintained

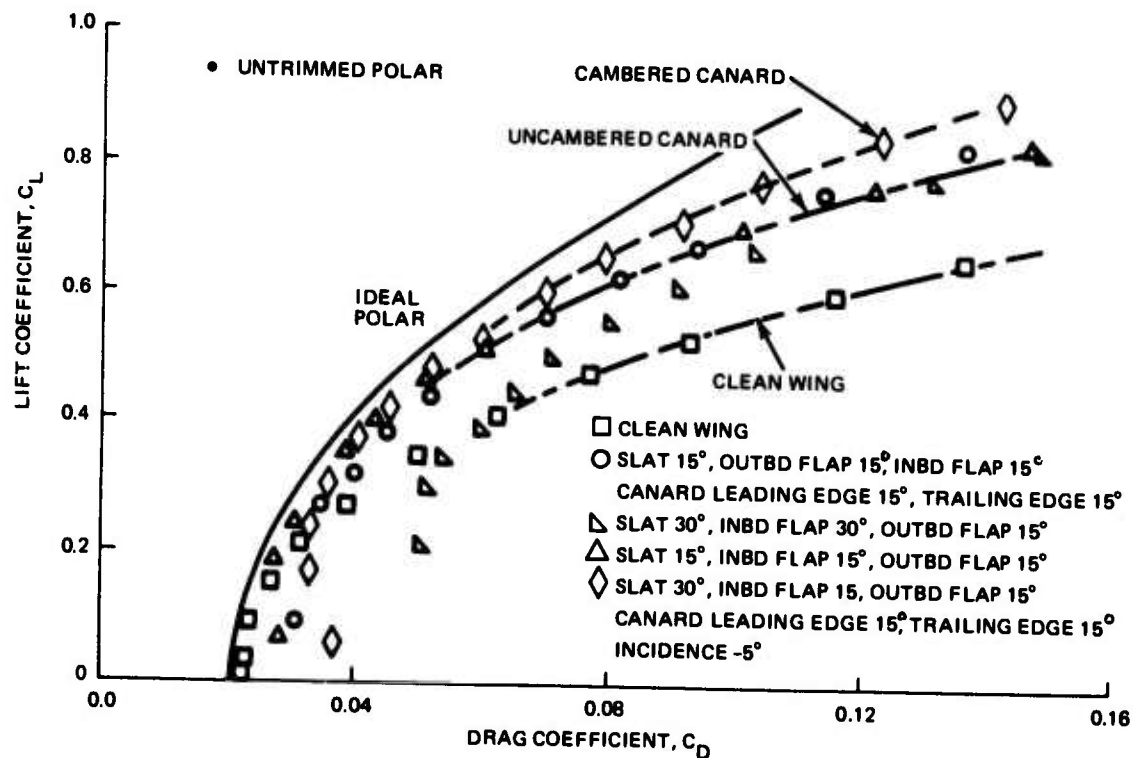


Figure 53. Lift and Drag Improvements With Canard Camber

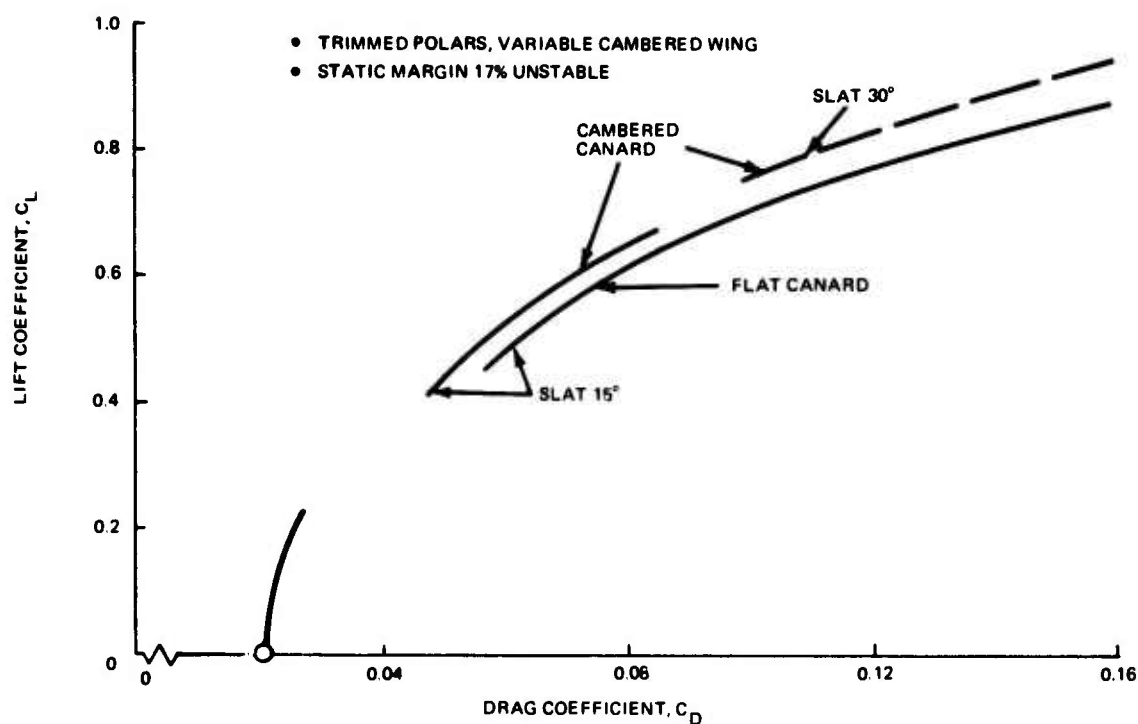


Figure 54. Wing and Canard Camber Effects On Trimmed Drag Polar

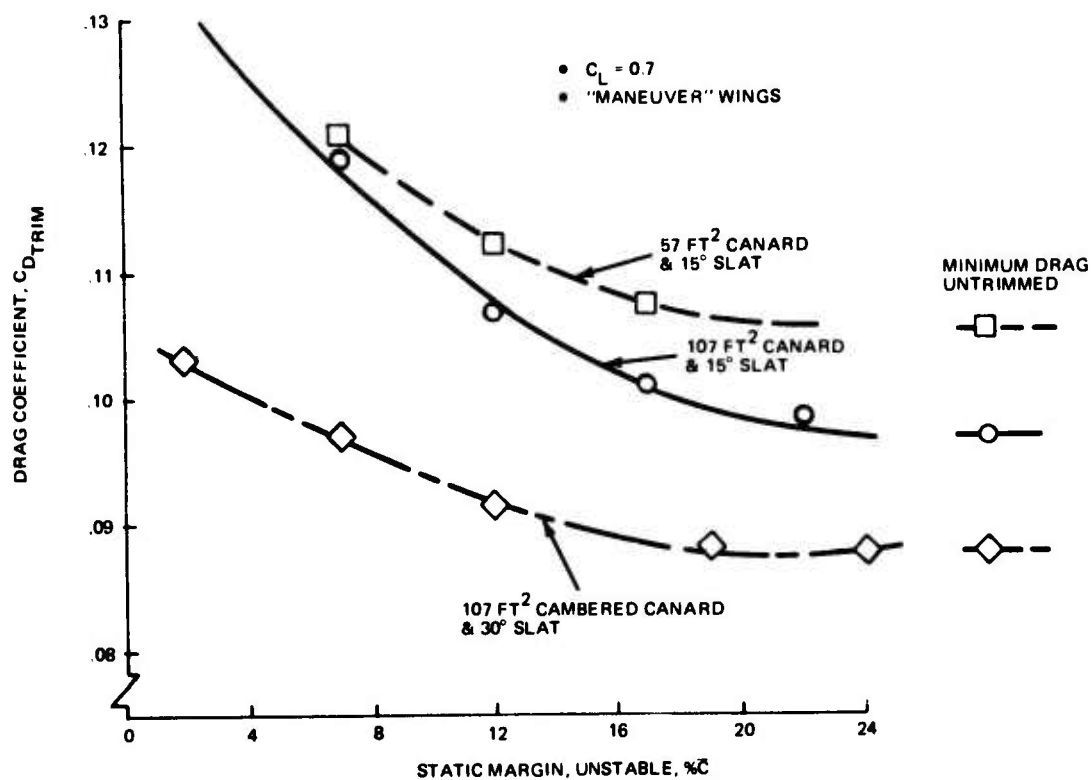


Figure 55. Trimmed Drag Improvement With Canard Size and Camber, Wing Camber, and RSS

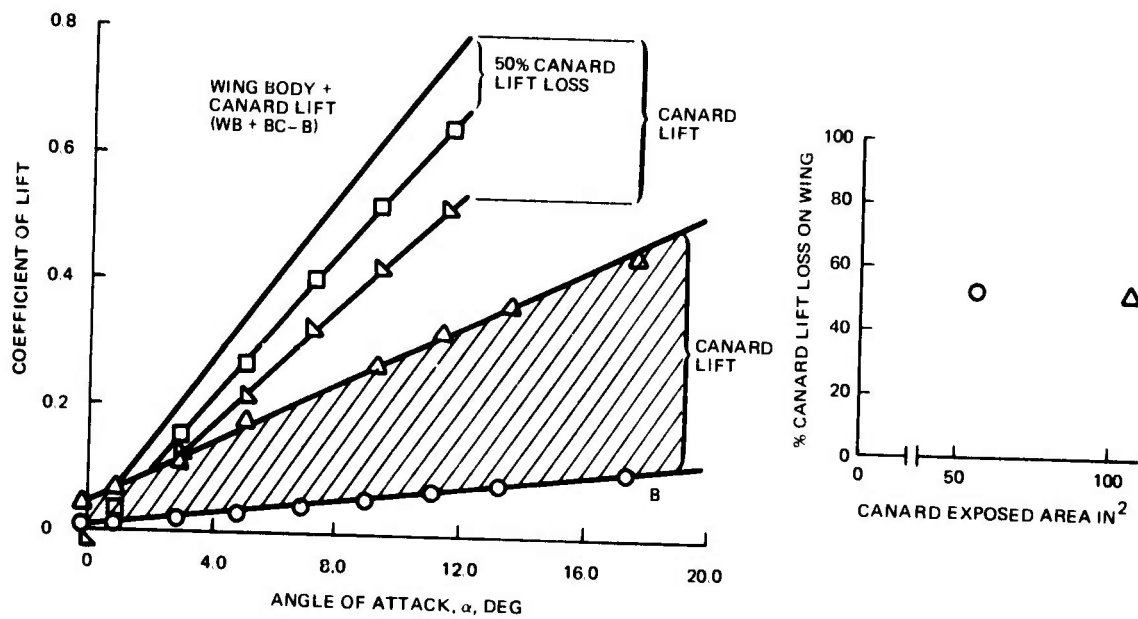


Figure 56. Canard Lift Loss Due to Downwash On Wing

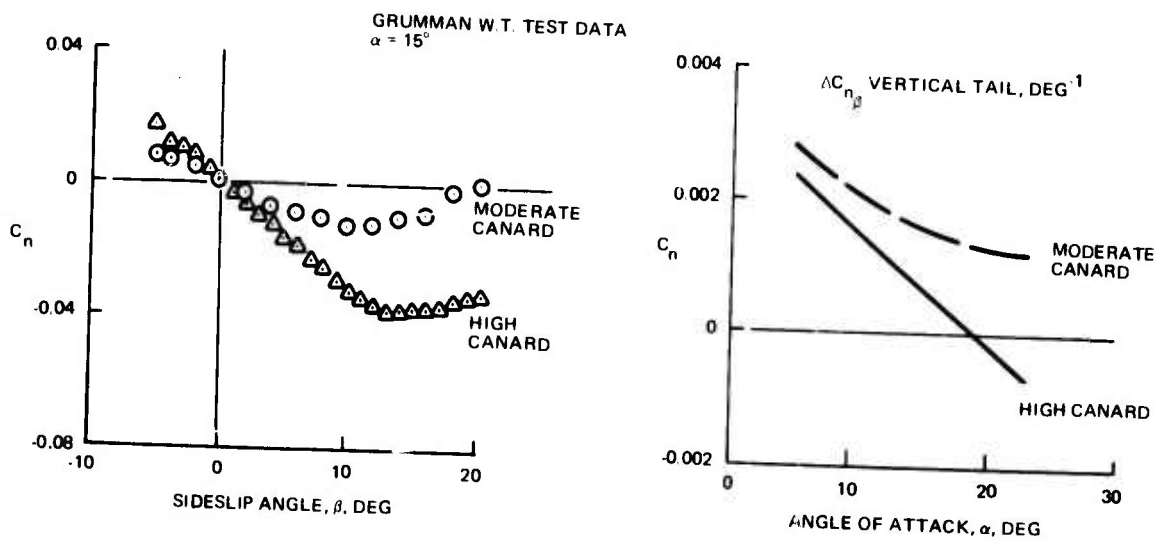


Figure 57. Effect of Canard Height on Directional Stability

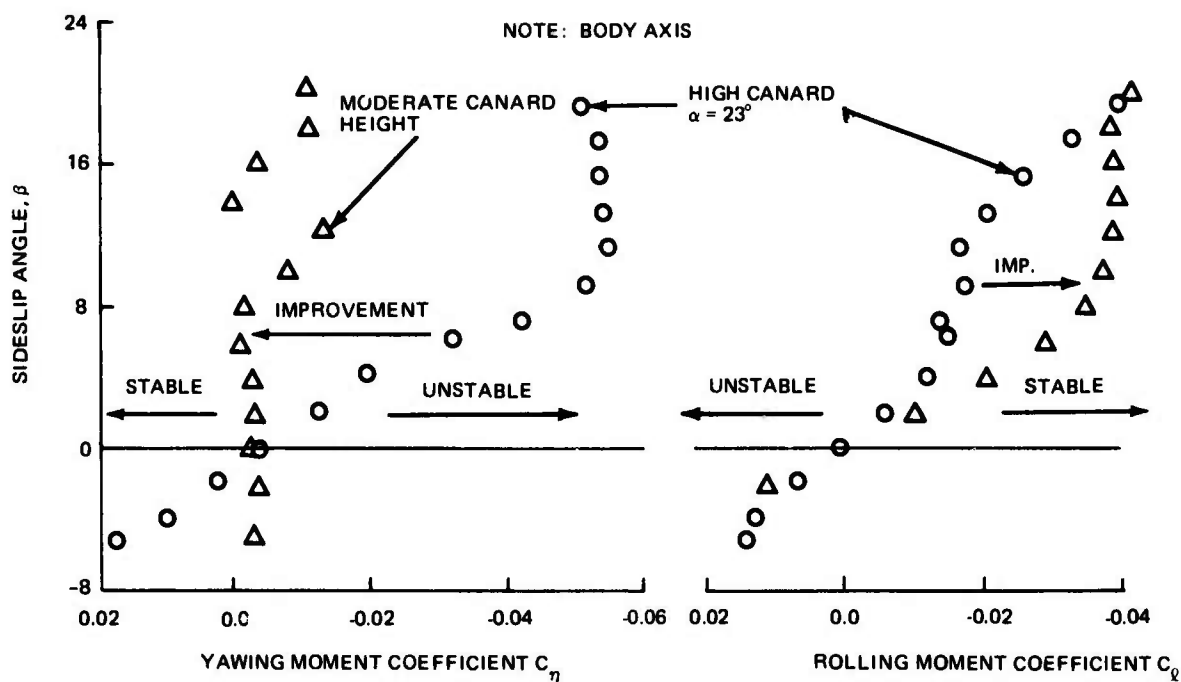


Figure 58. Moderate Height Canard Improves Lateral/Directional Characteristics

- GRUMMAN LOW SPEED WIND TUNNEL TEST DATA
- DERIVATIVES AT $\beta = 0$

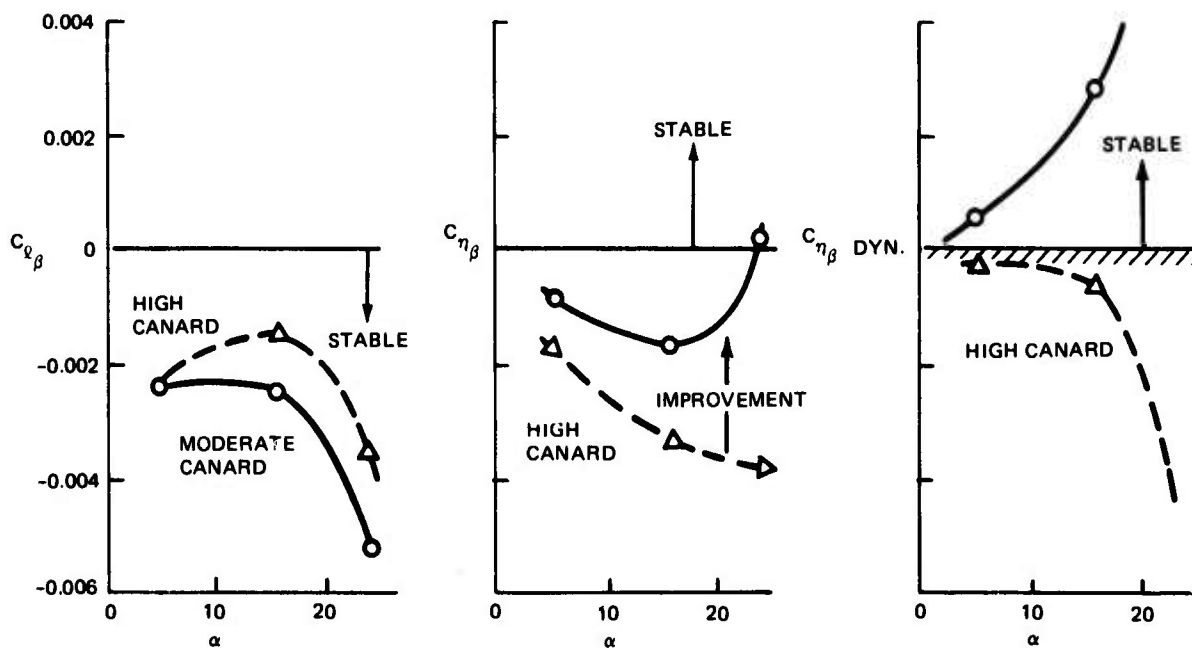


Figure 59. Effect of Canard Height On Lateral/Directional Stability

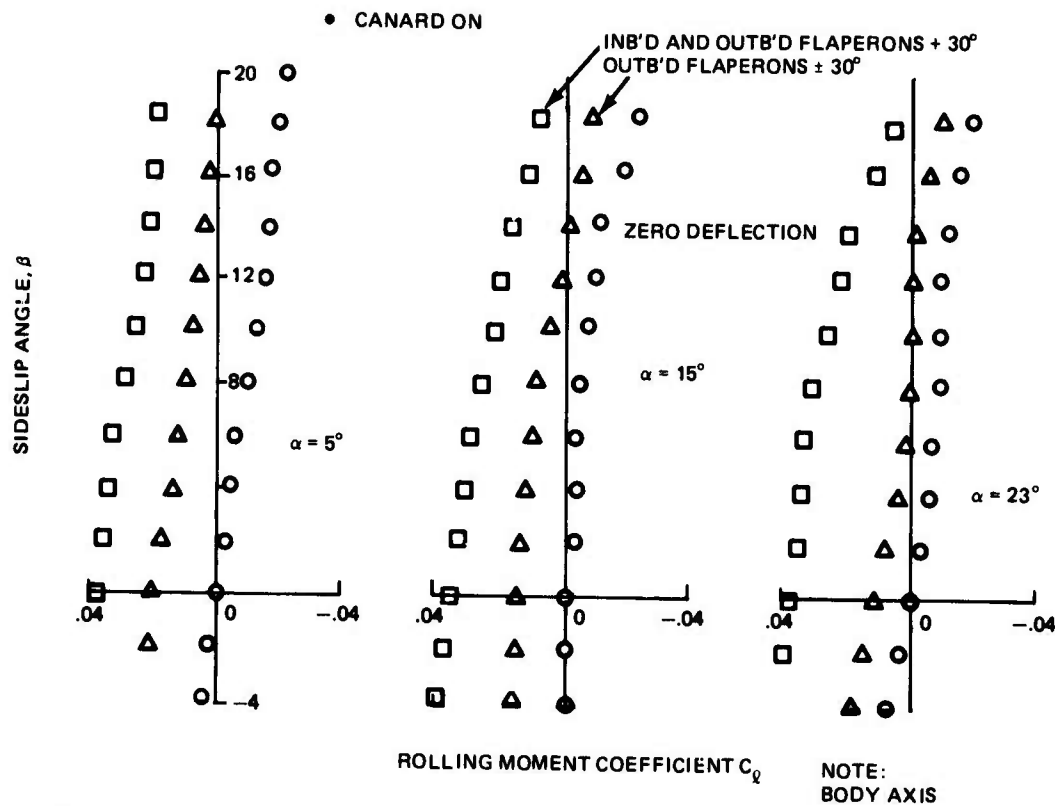


Figure 60. Aileron Effectiveness Maintained Throughout Angle of Attack And Sideslip Angles Tested

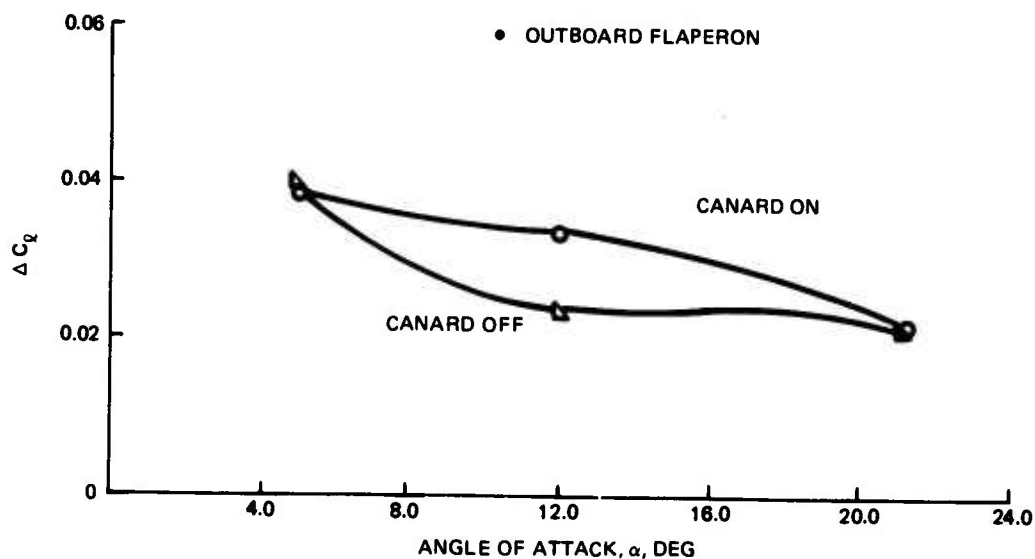


Figure 61. Influence of Canard On Aileron Effectiveness

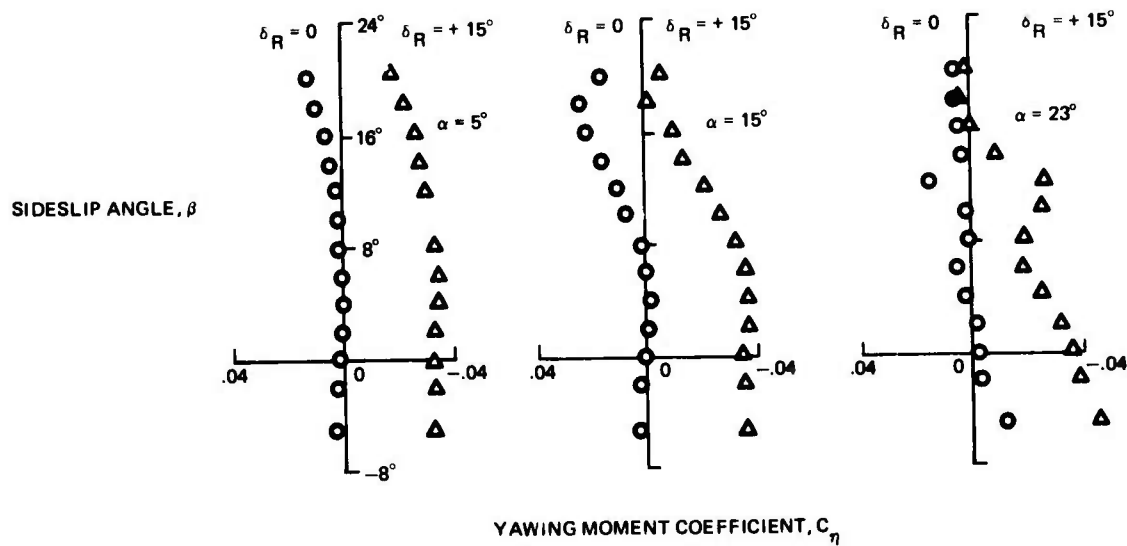


Figure 62. Directional Stability and Rudder Effectiveness, Canard Off

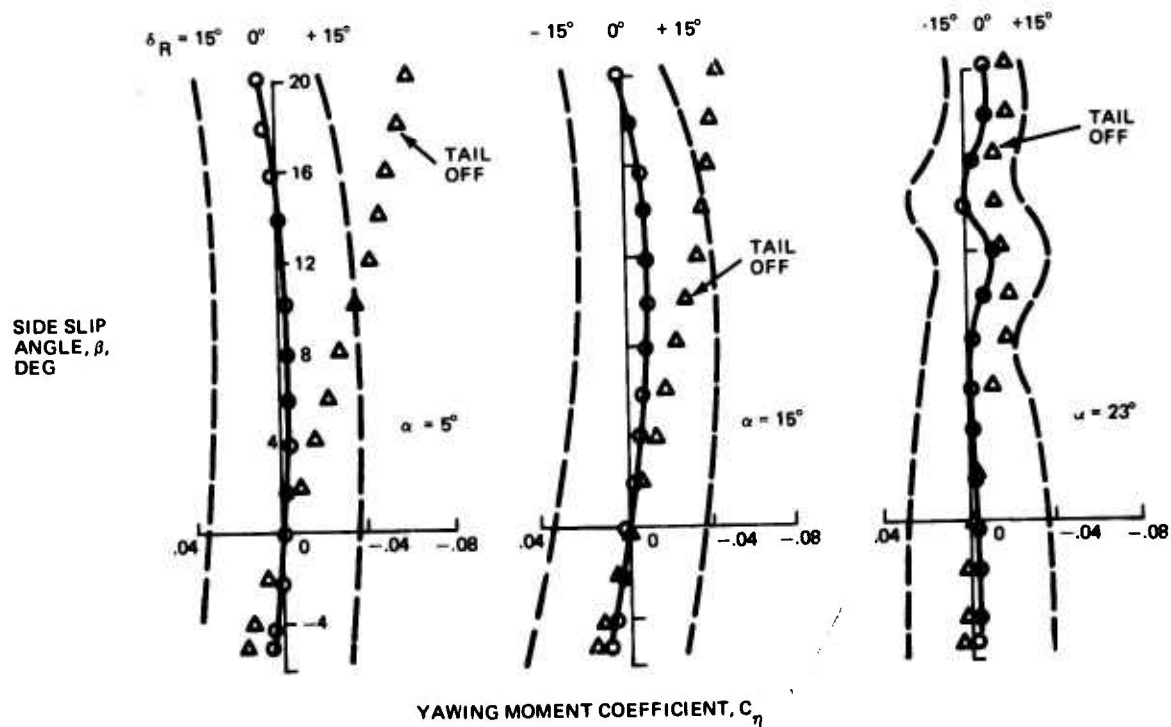


Figure 63. Directional Stability and Rudder Effectiveness, Canard on

The success achieved during the low speed testing program has lead directly to model fabrication and scheduling of extensive high speed testing. The transonic-supersonic tests, were part of a cooperative AFFDL - Grumman wind tunnel test program to evaluate advanced configuration concepts. Three separate double delta wing models were built. Subsonic testing has been completed, with supersonic testing currently underway. Figure 64 is a photograph of a partially completed 1/25-scale high speed ADCA model. Model force and moment data, static and dynamic wing root bending moment data, and extensive wing surface pressure data provided by 100 pressure taps will:

- Define the aerodynamic loads and performance of a Mach 0.9 maneuver wing configuration, with ideal twist for transonic air combat maneuvering
- Define the aerodynamic loads and performance at Mach 0.9 of an optimum Mach 1.6 cruise wing configuration. The performance increment between this and the above transonic wing defines range of transonic sustained g capability, as well as data variations with aeroelastic twist at higher g
- Provide comparable loads and performance data at Mach 0.9 for a variable camber version of the optimum Mach 1.6 cruise wing
- Document the transonic-supersonic performance of a planar wing reference configuration.

The range of wing shapes and aerodynamic loading conditions encompassed by these tests will provide the necessary aerodynamic data base to evaluate alternative tailored or variable-camber wing designs.

4.4.7 Vehicle Performance

During the third and final quarter no vehicle performance work was conducted. To date there are no aero, propulsion or weight changes affecting performance of the ADCA vehicle. Therefore the performance of the second quarter report remains the same and is repeated in this final report for completeness.

A baseline configuration consistent with the ADCA mission definition was identified through the screening process described in Subsection 3.6. Since that time the aerodynamic characteristics have been further investigated and results presented in Subsection 4.4 of this report. The drag polar, CL_{max} , store drag and other pertinent information was used to generate the performance reported in this section. By Air Force direction, the vehicle

(as originally configured) was revised as follows; without change to the external vehicle shape and size:

- A/G weapons weight increased from 4,000 to 5,000 lb
- Provisions for gun upgraded to a 600 lb gun installation
- Updated aero analysis

These changes result in an increase in the fuel required for the SPIF mission. This additional fuel could be accommodated by increasing the forward fuselage fuel tank size. At the same time, the air-to-air missiles were relocated from the pylon to the wing tip. The pylon was eliminated, however wing store station capability is provided at B. L. 91.1. The point and mission performance of this along with the maneuverability figures demonstrate the excellent agility level, a result of the versatility designed into the vehicle. Table 12 presents a revised performance comparison. The salient characteristics of the selected baseline configuration are summarized in Table 13.

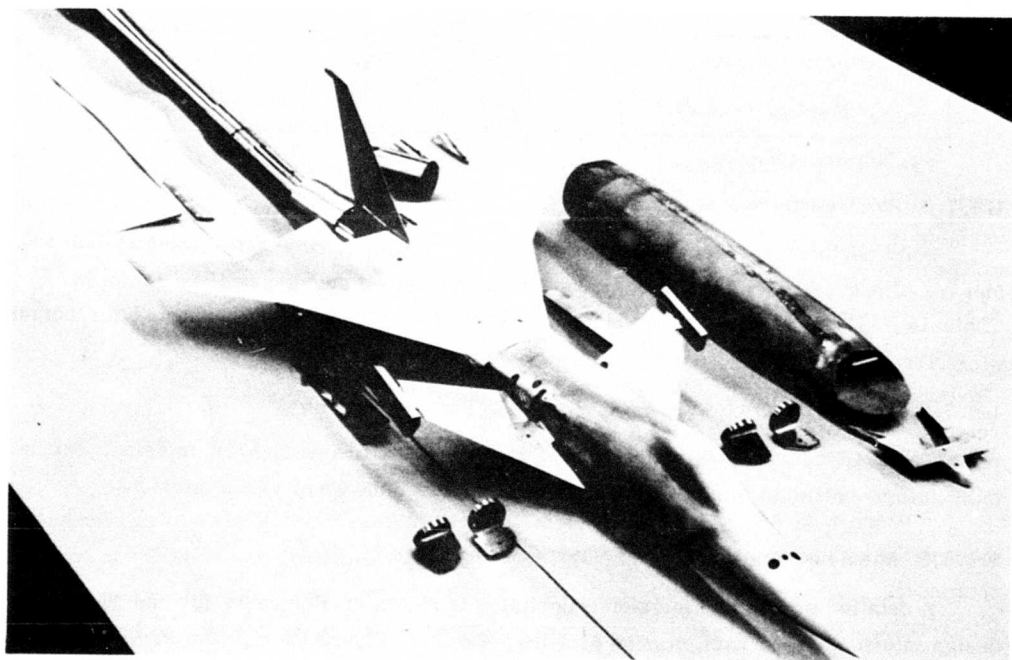


Figure 64 1/25-Scale High-Speed Tunnel Model

TABLE 12. REVISED PERFORMANCE COMPARISON

	Initial Performance	Final Performance
SPIF Mission		
Radius, n mi	200/200	200/200
TOGW, lb	37,357	40,553
Internal Fuel, lb	11,750	12,675
Payload A/G Weapons, lb	(2) 2,000	(2) 2,500
A/A Missiles, lb	390	500
Gun weight	Provision For	M,61 Type 600 lb
Combat weight, lb	31,482	34,215
Sustained g's		
M=0.9 30,000 ft	3.68	3.1*
M=1.2 30,000 ft	4.50	4.1
M=1.6 50,000 ft	2.23	2.1
Instantaneous g's		
M=1.6 50K ft	6.5	6.5
Acceleration Time, sec		
M=0.8 to M=1.6 35K ft	78	83

*With twist correction

4.4.7.1 Point Performance

Point performance is calculated for the SPIF mission configuration loading with 50% fuel remaining. Values for air-to-ground weapon retained and dropped are shown in Table 14. The sustained g's at Mach 0.9 at 30,000 ft have been corrected for actual wing twist distribution.

4.4.7.2 Mission Performance

Table 15 summarizes mission performance for the design SPIF mission, sea level interdiction, battlefield interdiction (alternate payload) and ferry range missions.

4.4.7.3 Missions/Tradeoffs

A detailed profile and mission description is shown in Figure 24 for the SPIF design mission. Alternate mission profiles, shown in Figure 65 use the same mission rules for takeoff, combat and landing reserves. The different mission legs are noted on

THIS REPORT HAS BEEN DELIMITED
AND CLEARED FOR PUBLIC RELEASE
UNDER DOD DIRECTIVE 5200.20 AND
NO RESTRICTIONS ARE IMPOSED UPON
ITS USE AND DISCLOSURE.

DISTRIBUTION STATEMENT A

APPROVED FOR PUBLIC RELEASE,
DISTRIBUTION UNLIMITED.

TABLE 13. VEHICLE CHARACTERISTICS

Power Plant		Weights			Dimensions	
No. & Mod	F101-GE-100	Loading	Lb	L.F.	Wing	
Manufacturer	General Electric	Empty	21556		Span	33'-7"
Engine Specification No.	CP45B0002B	TOGW	40553	(6.1)	Incidence	1°
Type	Augmented Turbofan,	FDGW	38018	6.5	Anhedral	5°
	Mixed Flow	Max Takeoff	47553	(5.2)	Sweepback	60°/46.5°
Length with A/B	180.7"	Max Landing	42104		Length	61'-9"
Diameter (Max)	55.2"	() Estimated			Height	17'-1"
Weight (Dry)	4235 lb				Tread	23'-8"
Tailpipe	Variable C-D					
Augmentation	A/B					

Fuel			Ordnance
Location	No. Tanks	Gal.	SPIF Mission
Fuselage-Bladder	2	427	(2) A/A Missiles-
Fuselage-Integral	4	1081	Wing Tip
Wing-Integral	1	442	(2) 2500 lb A/G
Wing-Ext Drop	2	1200	Weapons-Fuselage
			(1) M-61 20mm Gun
			Integral

the profile. Air-to-ground weapons are dropped at the radius point, while air-to-air weapons are retained for the entire mission. The ferry range calculation includes no air-to-ground weapons or air-to-air missiles and a military power takeoff is used. Maximum afterburner takeoff is used for all other missions.

The ADCA vehicle has the potential of carrying low drag external stores on the fuselage, utilizing the concept of conformal weapon carriage. The aircraft is shown in

TABLE 14. POINT PERFORMANCE

SPIF Configuration		
<ul style="list-style-type: none"> ○ (2) A/G Weapons ○ (2) A/A Missiles ○ 50% Fuel 		
Sustained g's	M=0.9, 30K $N_z = 3.1^*$	(3.7*)
	M=1.2, 30K $N_z = 4.12$	(4.9)
	M=1.6, 50K $N_z = 2.13$	(2.6)
Instantaneous g's	M=1.6, 50K $N_z = 6.5$	(Structural Design Limit)
Acceleration Time: M=0.8 to M=1.6, 35K Ft=83 sec (66.5 sec)		

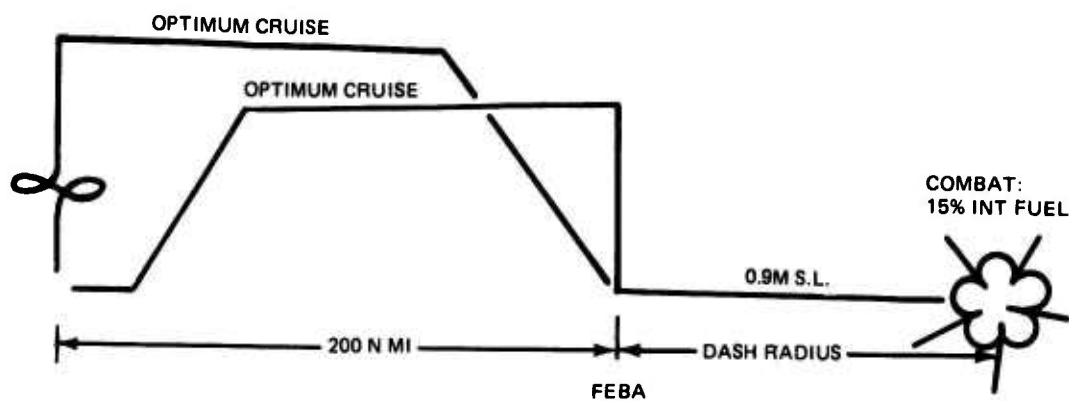
* Adjusted from 3.3 to 3.1 for available wing twist
 () A/G Weapons Dropped

TABLE 15. MISSION PERFORMANCE SUMMARY

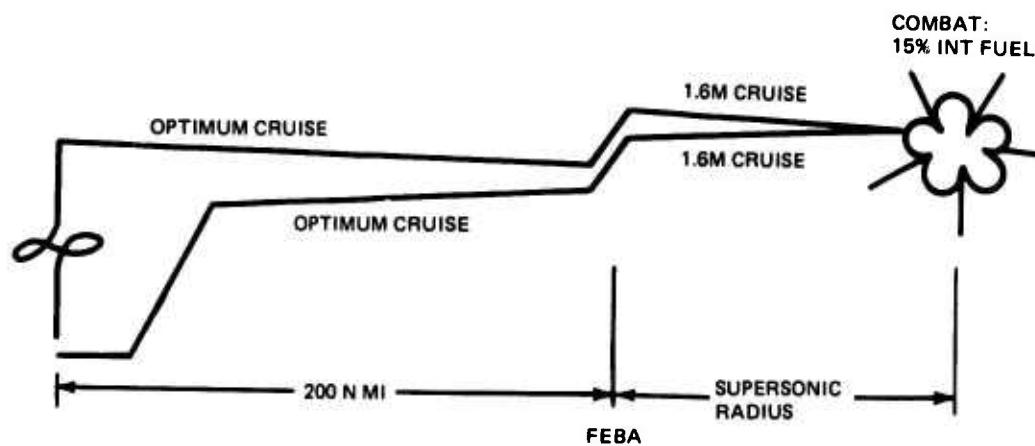
	SPIF	Sea Level Interdiction	Battlefield Interdiction (Alternate Payload)	Ferry	Ferry
TOGW, lb	40,553	40,553	44,521	34,753	43,753
Internal Fuel, lb	12,675	12,675	12,675	12,675	12,675
External Fuel, lb	0	0	0	0	7,800
Payload Bombs, lb	2(2500)	2(2500)	8(1000)	0	0
Missiles	2 A/A	2 A/A	Bluff 2 A/A	0	0
Radius, n mi (Up to FEBA/Beyond FEBA)	200/200	200/186	200/118	2,534	3,453
Penetration Speed, M	1.6	0.9	1.6	0.9	0.85-0.9
Altitude In	50,000	0	50,000	37,000*	31,000*
Altitude Out	62,000	0	61,000	50,000**	49,500**

* Altitude at start of cruise
 ** Altitude at end of cruise

- SEA LEVEL INTERDICTION



- BATTLEFIELD INTERDICTION



- FERRY

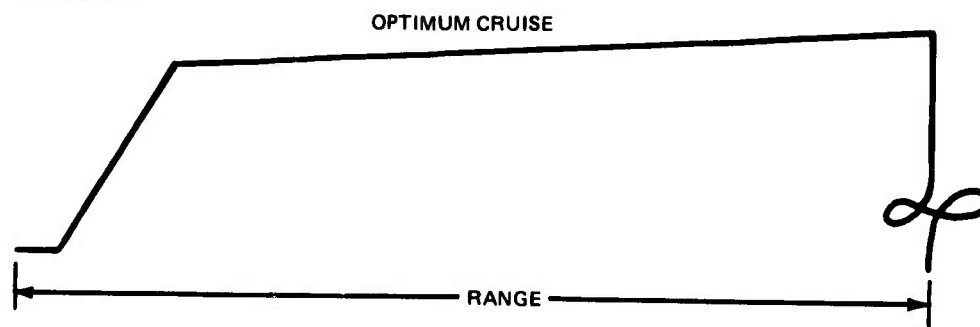


Figure 65. ADCA Alternate Missions

Figure 66 configured with eight, 1,000 lb, bluff shape GP bombs. Eight Lode-14 bomb racks are installed in the lower fuselage structure. An external fairing encloses the weapons reducing the aerodynamic drag penalties normally associated with the external stores loadings. This fairing structure would be jettisoned upon release of stores to "clear-up" the vehicle for supersonic return flight. The only penalties to the baseline configuration would be the structural rework associated with the incorporation of the Lode-14 bomb racks and attaching hardware for the external fairing.

The SPIF mission radius was selected to reach certain targets as outlined in Section II. However, to demonstrate alternate capability the ADCA subsonic/supersonic radii were traded. Figure 67 shows that decreasing the subsonic base to FEBA radius to 100 n mi yields a supersonic radius of 239 n mi at Mach 1.6, at a penetration altitude of better than 50,000 ft. Similarly, when the subsonic radius is increased to 300 n mi the supersonic radius degraded to 162 n mi. This flexibility allows mission tailoring for specific airfield/target locations.

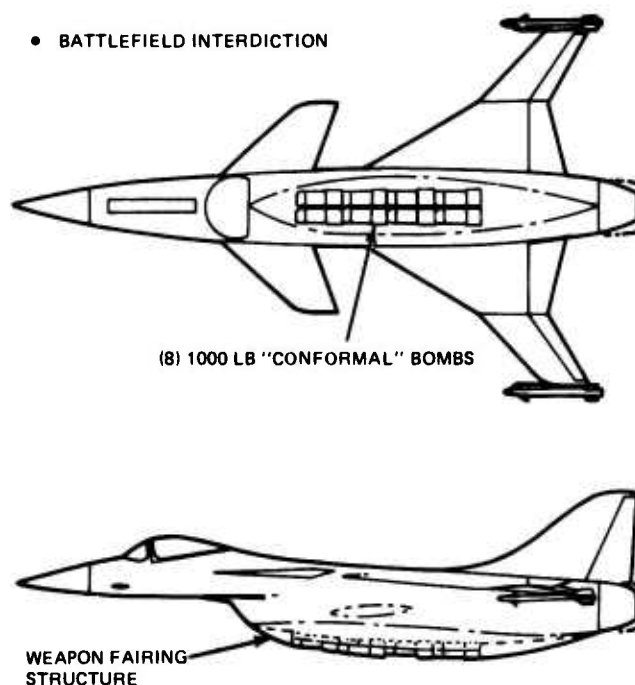


Figure 66. Alternate Store Installation

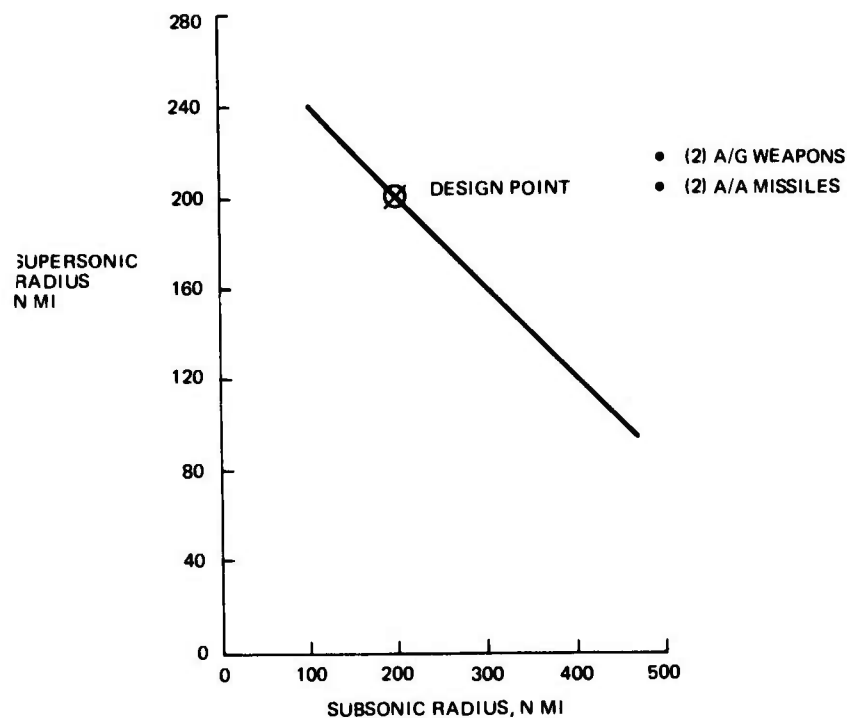


Figure 67. ADCA SPIF Mission Supersonic/Subsonic Radius Tradeoff

Considering the potential tactical advantage of a sea level penetration, the baseline vehicle was evaluated for an array of FEBA to target radii as a function of cruise speed. These results are shown in Figure 68. It should be noted that the F101 engine is capable of achieving Mach 0.94 at intermediate power. Cruise speeds above this require operation in a region below minimum partial afterburner.

The speed corresponding to 200 n mi radius beyond FEBA is $M = 0.87$ and at $M = 0.90$ ($V = 595$ KTAS) the penetration distance is reduced to 179 n mi. For all cases, the air-to-ground weapons are released at the radius and the air-to-air missiles are retained for the entire mission. Two hundred nautical miles base to FEBA is held fixed with sea level penetration distance as a fallout.

A ferry range of 2600 n mi requires between 200 and 300 gal. of external fuel which presents no problem to the ADCA baseline design. The ADCA aircraft is designed to carry up to two, 600-gal. drop tanks, which increases the ferry range to 3453/3134 n mi (tanks dropped/tanks retained). With only internal fuel and no pylons, the range is 2534 n mi. Figure 69 presents the ferry range variation with external fuel.

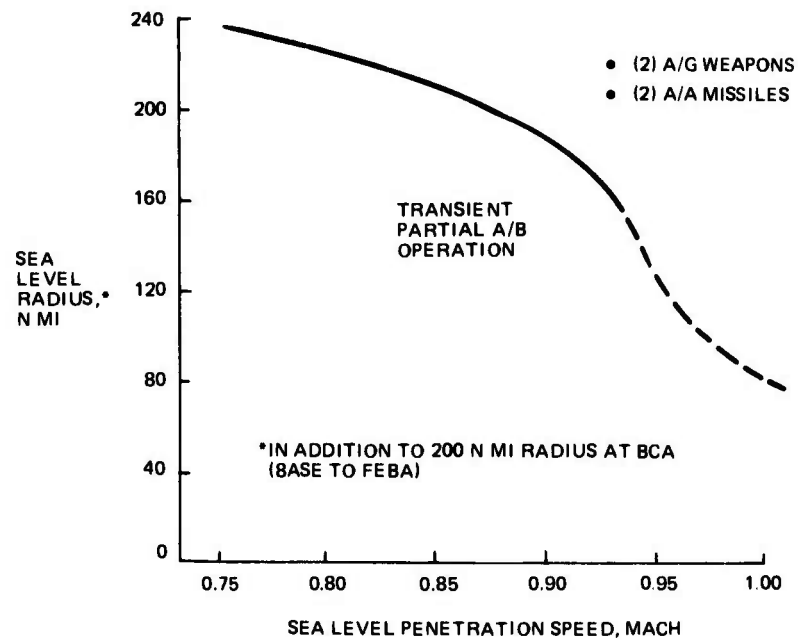


Figure 68. ADCA Sea Level Interdiction

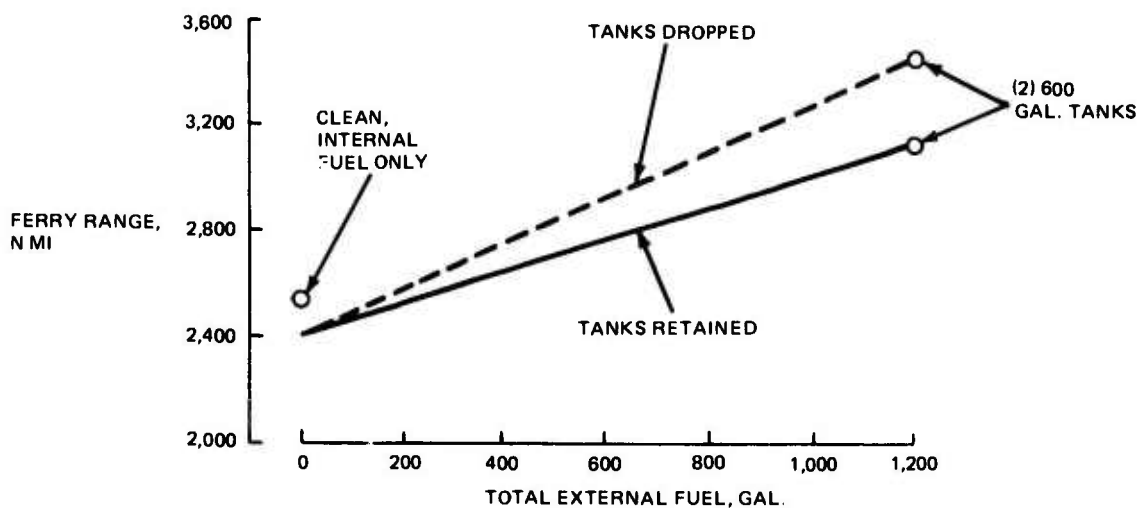


Figure 69. ADCA Ferry Range

The current ADCA alternate store installation for the battlefield interdiction mission is eight, 1000 lb bluff weapons carried conformally. Wave drag analysis of the stores installation has indicated a lower drag than predicted resulting in the radii shown on Table 15 being slightly conservative.

4.4.7.4 Maneuverability

The 18 illustrations presented in the following subsections illustrate the excellent maneuverability of the ADCA aircraft in the SPIF mission configuration. Whether the aircraft has air-to-ground weapons retained or weapons dropped, it is a formidable match for any threat, giving the ADCA excellent self-protection capability.

4.4.7.5 Load Factor Sensitivity

Selected sustained and instantaneous load factor variations with gross weight are illustrated in Figure 70 for several operational conditions and give an indication of the vehicle's superior agility. For example, at Mach 1.6, 50,000 ft, the aircraft has the capability of exceeding the structural design limit of 6.5 g's giving it an excellent missile avoidance capability.

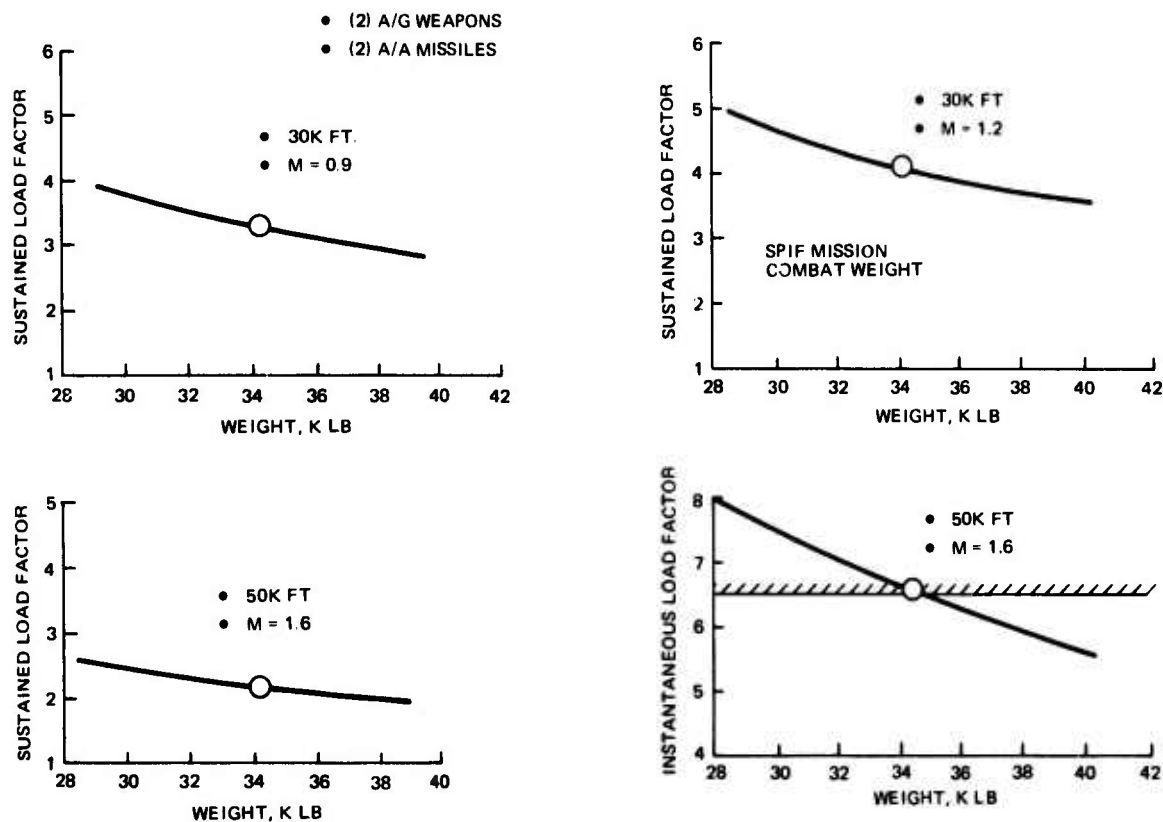


Figure 70. ADCA Maneuverability Summary

4.4.7.6 Acceleration Sensitivity

Excellent acceleration capability is demonstrated by the ADCA. With two air-to-ground weapons, two air-to-air missiles and 50% fuel, the ADCA can accelerate from Mach 0.80 to Mach 1.60 at 35,000 ft in 83 seconds. When the air-to-ground weapons are released the acceleration time decreases to 66.5 seconds; this is equivalent or better than the current threat interceptor. Figure 71 shows a time history with Mach number for three mission weights.

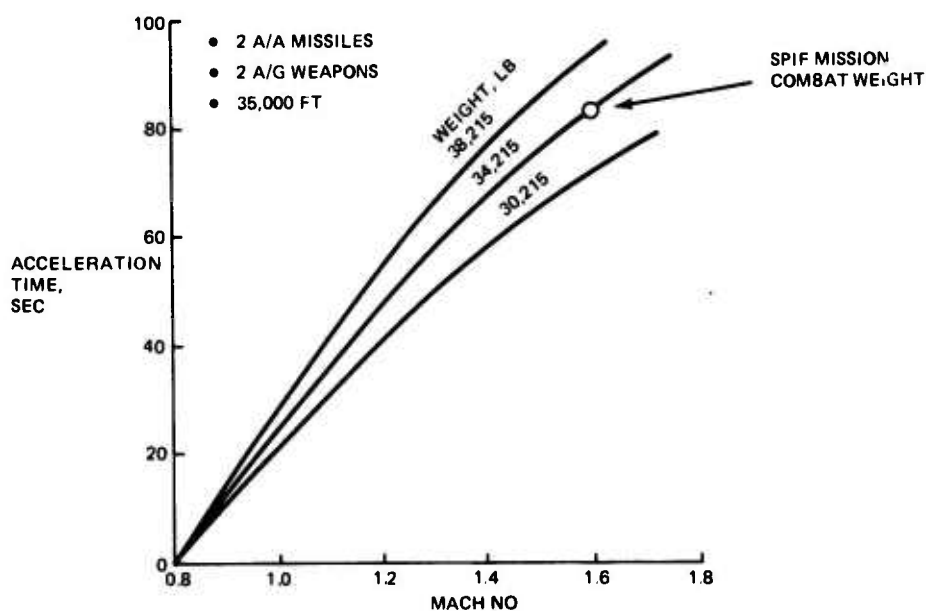


Figure 71. ADCA Acceleration Capability

4.4.7.7 Flight/Operational Envelope

The level flight high speed envelope is illustrated in Figures 72 and 73 for the SPIF mission configuration with and without air-to-ground weapons. Steady state flight conditions are shown for both intermediate and maximum thrust. The shaded area indicates transient operation where the engine is limited to one minute operation. The left hand side is limited by clean $C_{L_{max}}$ and engine operational envelope.

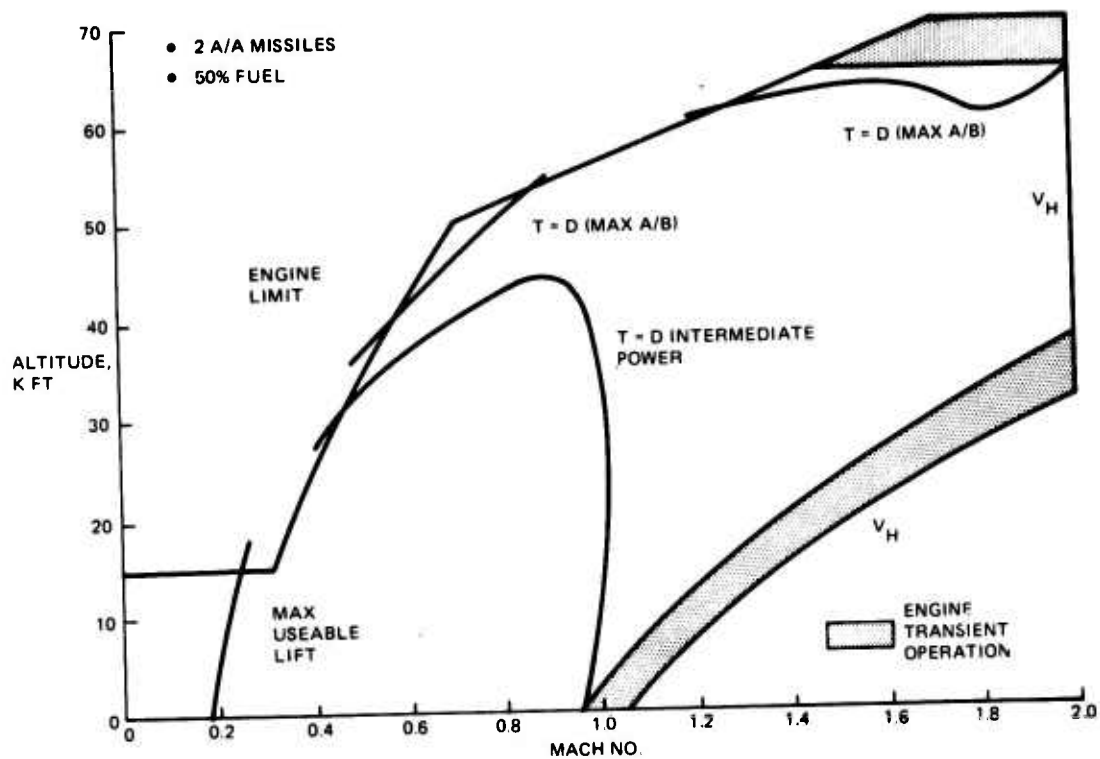


Figure 72. Operational Flight Envelope

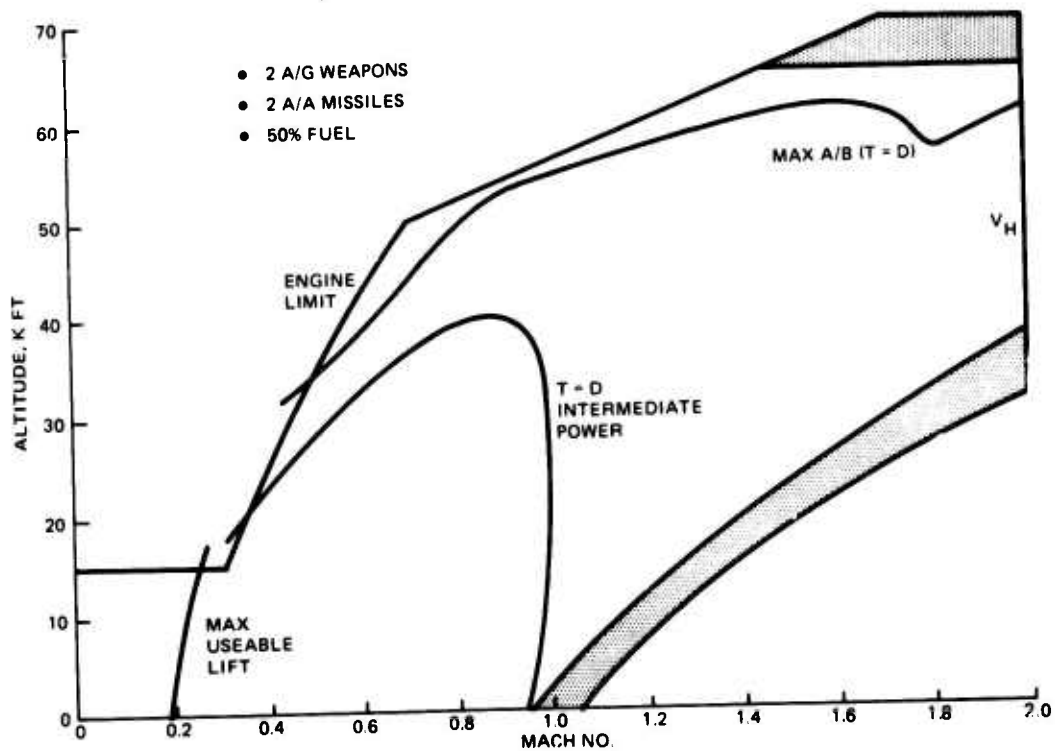


Figure 73. Operational Flight Envelope

For flight maneuvering the limit factors are +6.5 and -3 g's for the entire flight envelope up to V_L . Flight envelope can be obtained using these limits and the sustained, instantaneous and level flight presented herein.

4.4.7.8 Sustained g's

Figures 74 thru 77 present sustained g's for the operating envelope of the ADCA aircraft with and without air-to-ground weapons. The curves are done for a combat condition of 50% fuel at both maximum and intermediate power.

4.4.7.9 Instantaneous g's

Instantaneous g capability is illustrated in Figures 78 and 79. The aircraft configured with two air-to-air missiles, 50% fuel, with and without air-to-ground weapons, is shown. No thrust corrections have been applied to the C_{Lmax} , yielding some conservatism in the values shown. Over a large spectrum of the flight envelope the aircraft is capable of pulling 5 or more g's for excellent missile avoidance.

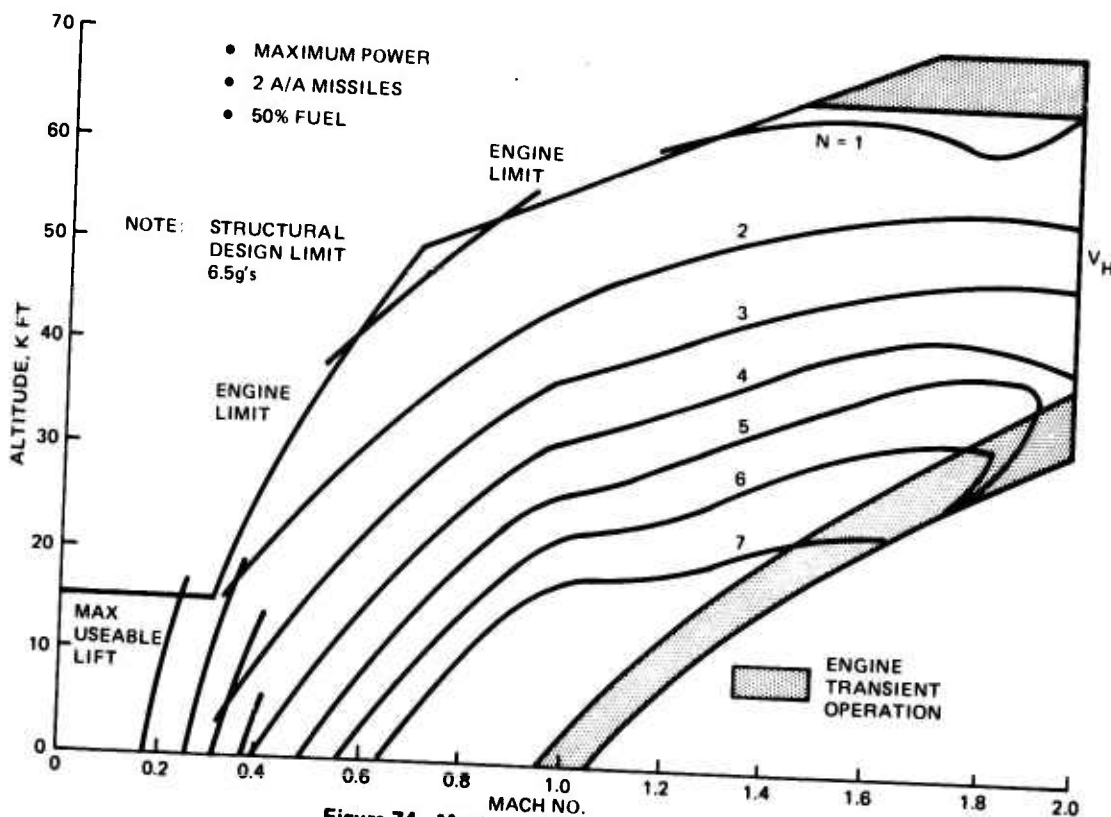


Figure 74. Maximum Sustained Load Factor

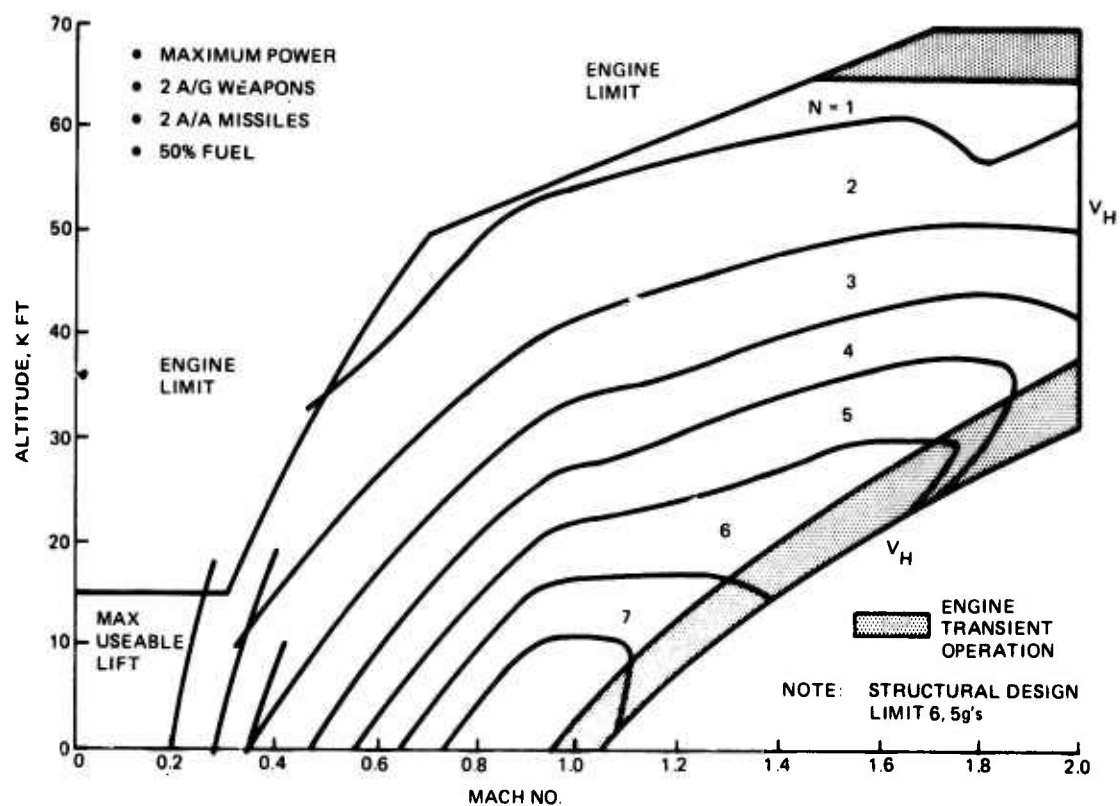


Figure 75. Maximum Sustained Load Factor

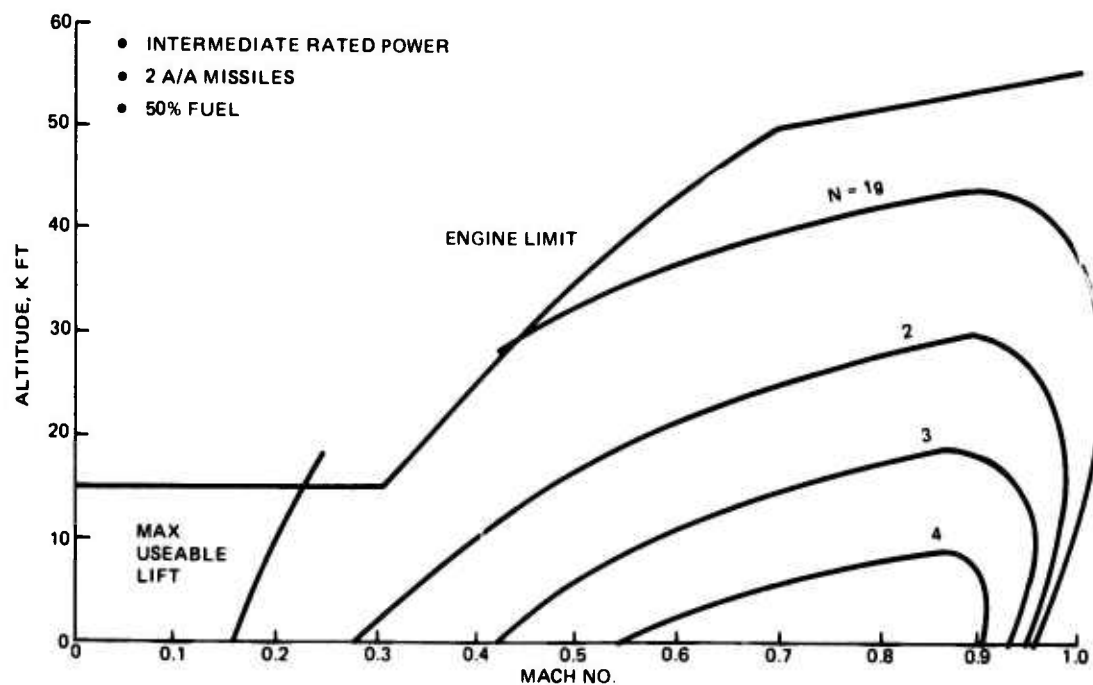


Figure 76. Maximum Sustained Load Factor

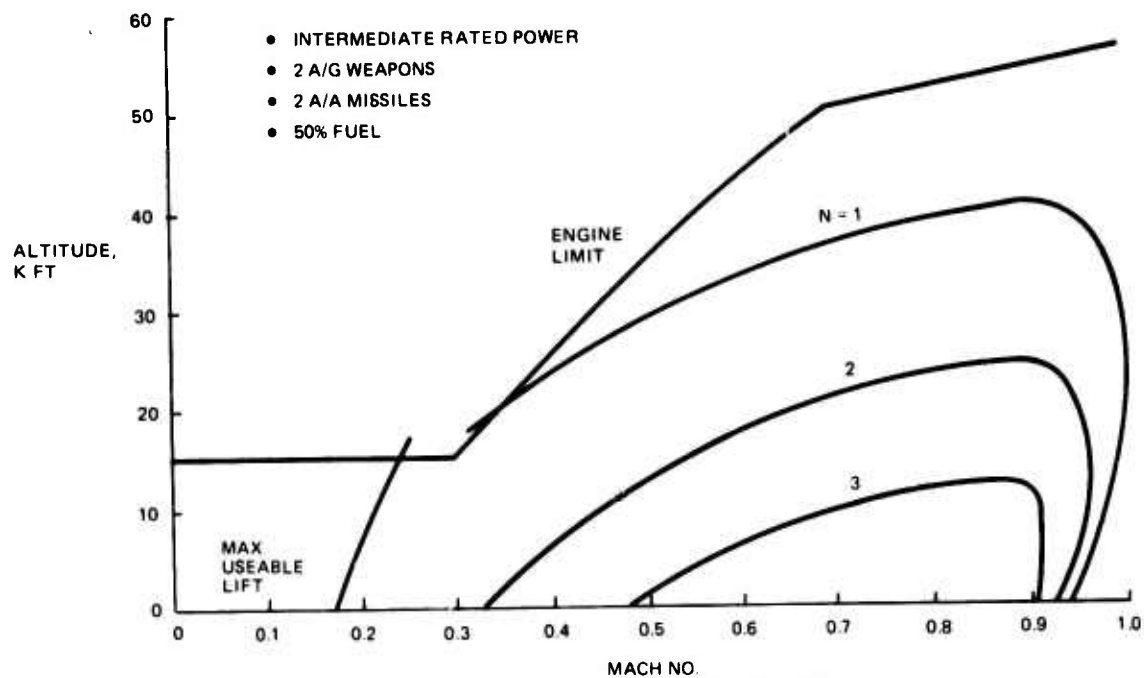


Figure 77. Maximum Sustained Load Factor

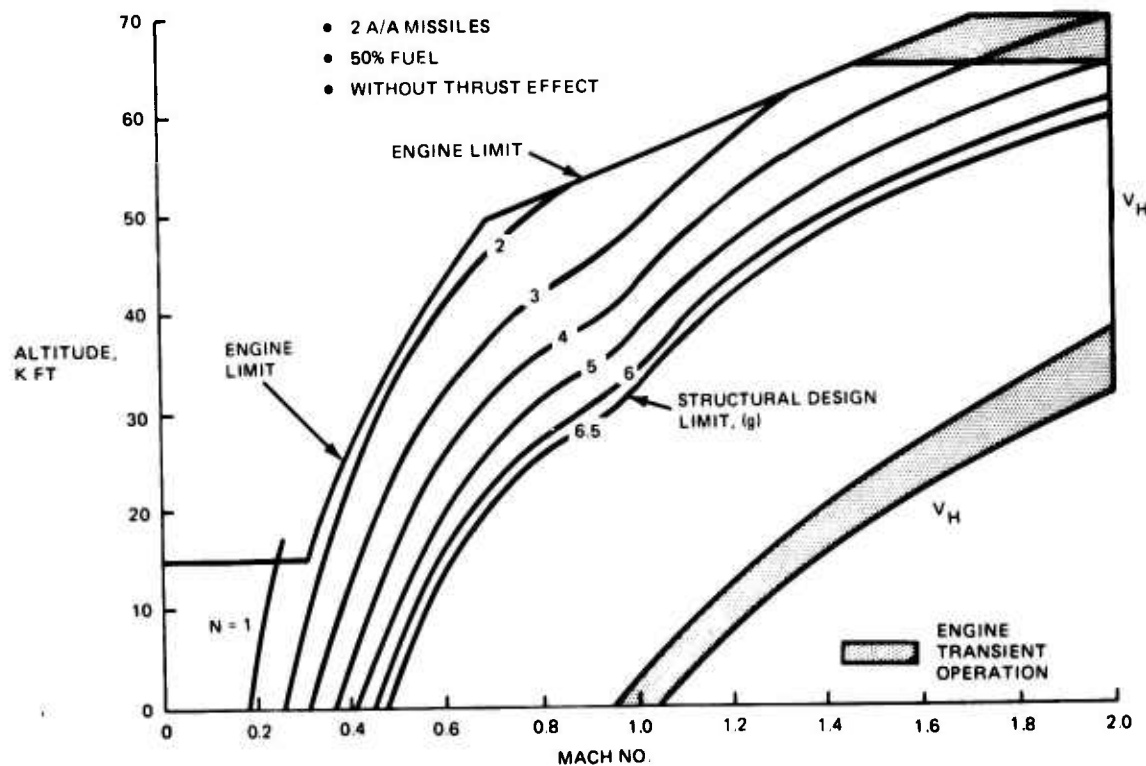


Figure 78. Maximum Instantaneous Load Factor

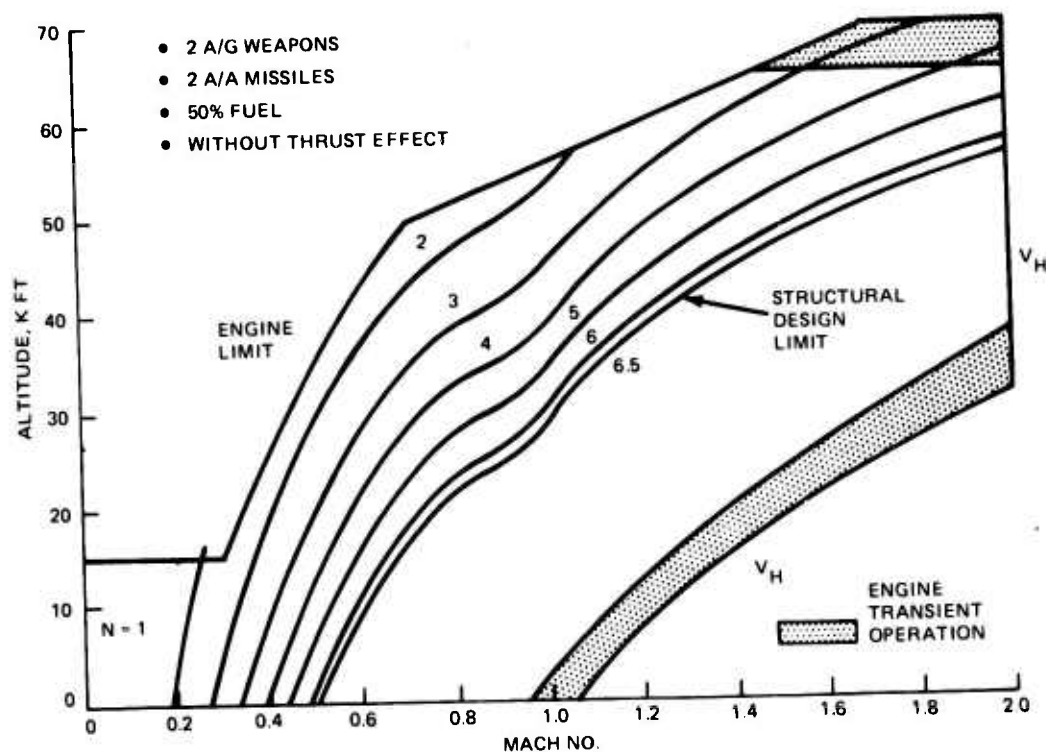


Figure 79. Maximum Instantaneous Load Factor

4.4.7.10 Specific Excess Power Contours

Specific excess power (P_S) was calculated using the energy maneuverability program for the SPIF mission payload, 50% fuel with and without air-to-ground weapons. Excellent P_S is demonstrated with the 2 air-to-ground and 2 air-to-air weapons. Superior performance is achieved when the air-to-ground weapons are dropped and the air-to-air missiles retained. The 1 g, 3 g and 5 g P_S values, as a function of altitude and Mach number, are presented in Figures 80 through 85 for maximum power. Intermediate power contours for both configurations at 1 g conditions are shown in Figures 86 and 87. These figures demonstrate excellent combat effectiveness throughout the flight envelope for both maximum and intermediate power.

4.4.7.11 Takeoff and Landing

The ADCA aircraft as configured uses a ground rotation angle of 12 degrees which yields an effective $C_{L_{max}}$ useable of 1.14, for takeoff and landing only. It should be noted that low speed wind tunnel test data indicates a $C_{L_{max}}$ (with no ground angle restriction) in excess of 1.40 is achievable. Figure 88 presents ground roll distances for maximum

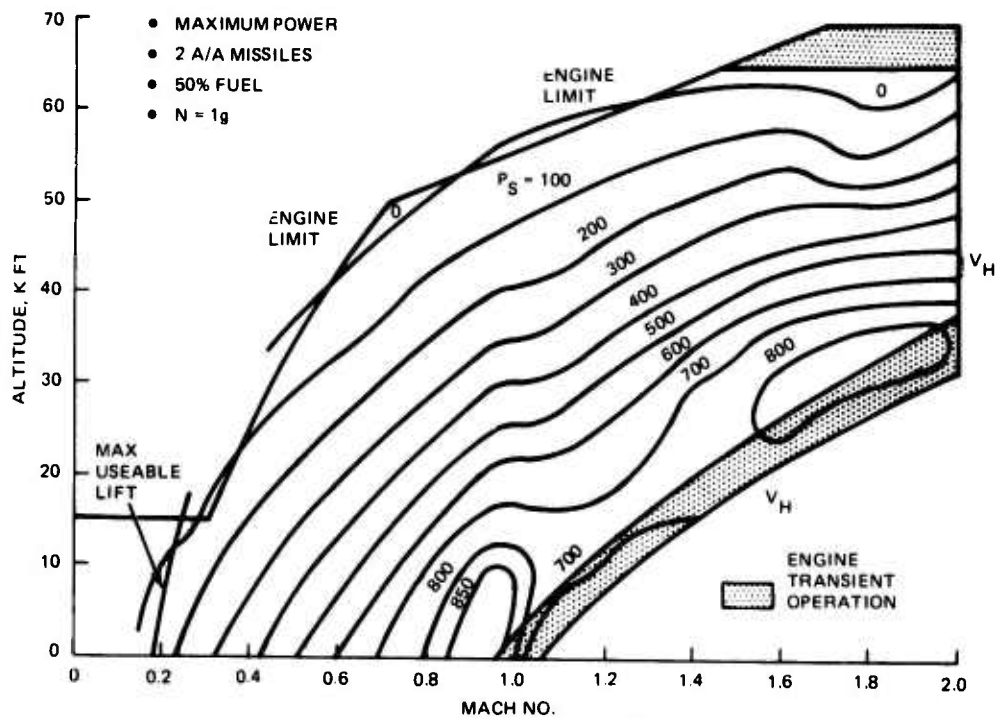


Figure 80. Specific Excess Power

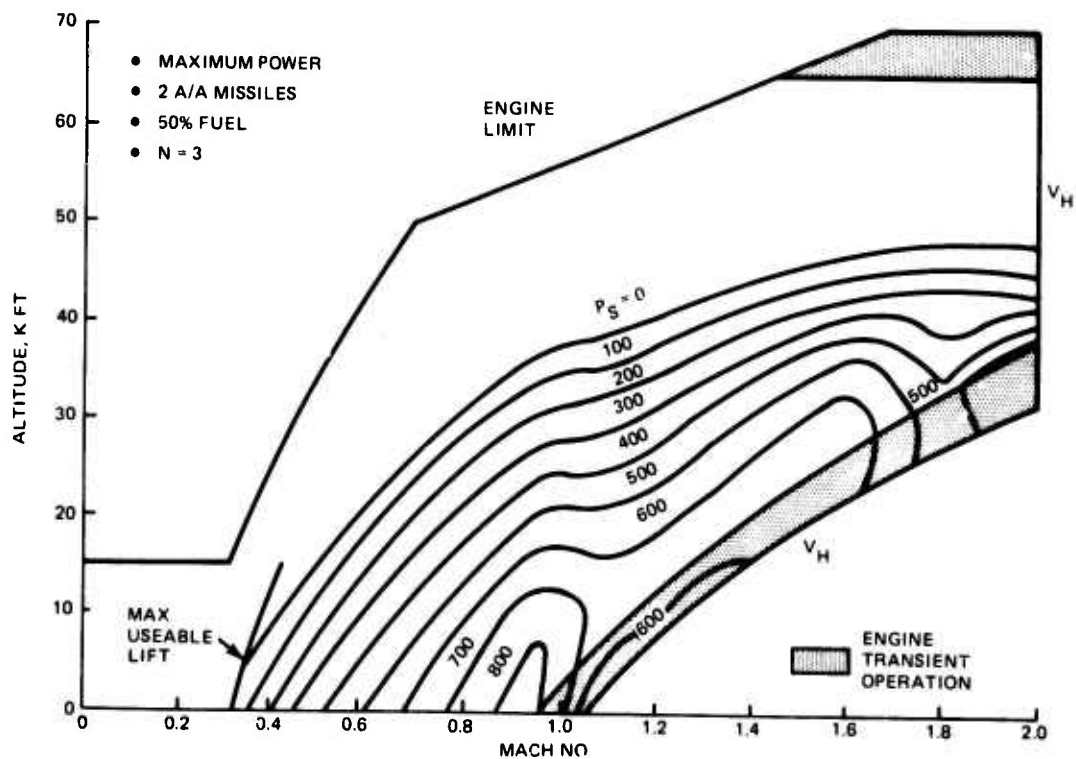


Figure 81. Specific Excess Power

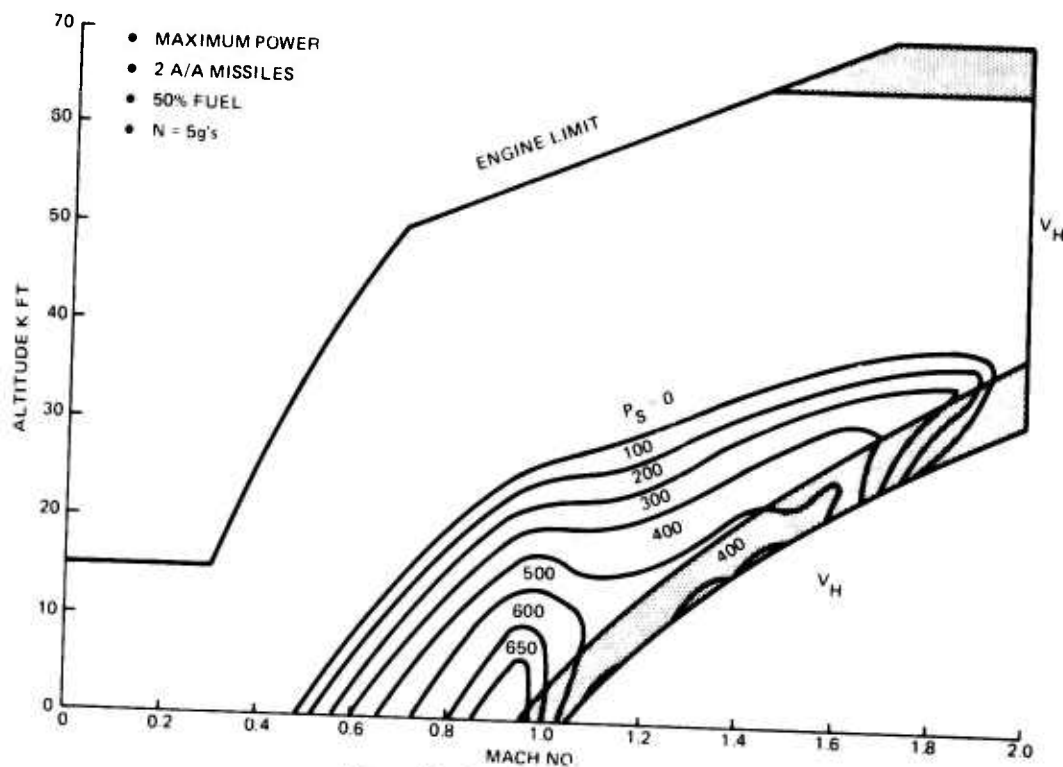


Figure 82. Specific Excess Power

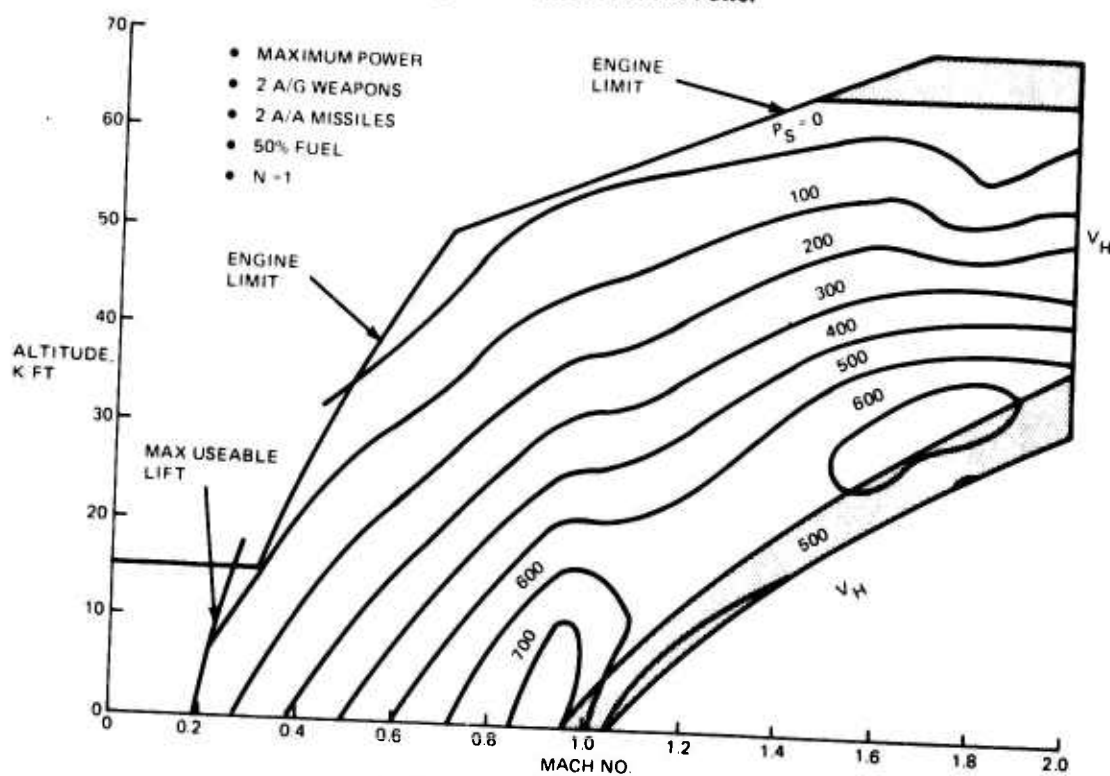


Figure 83. Specific Excess Power

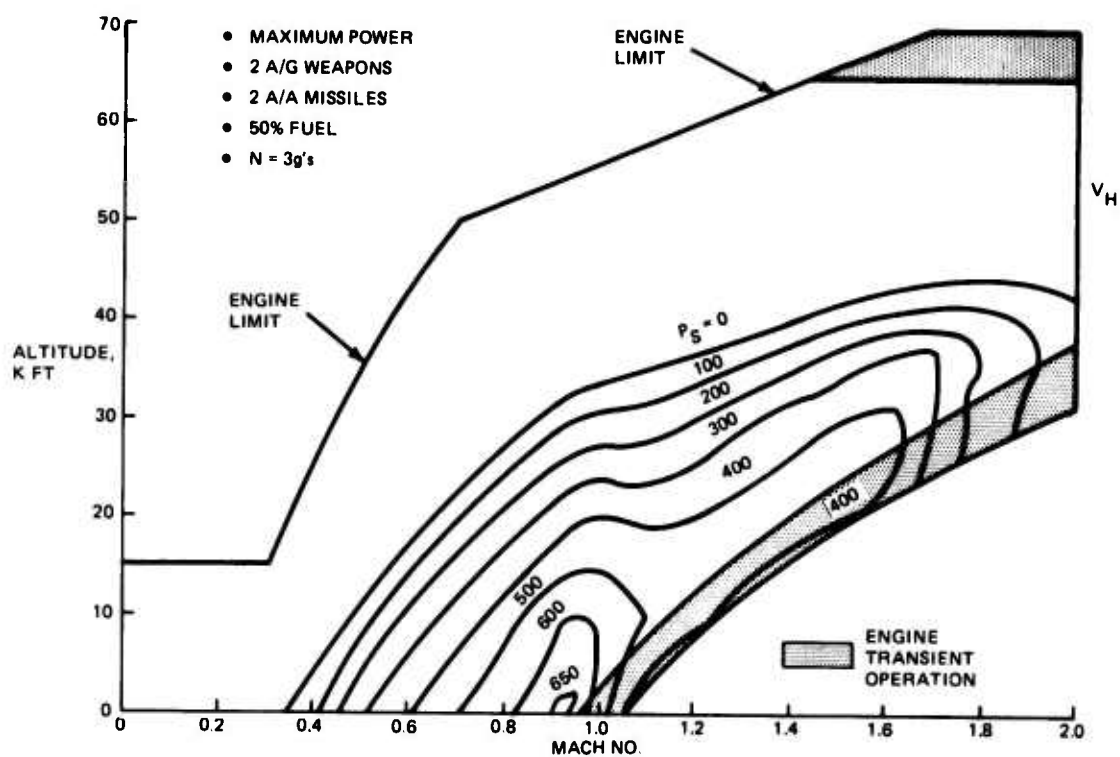


Figure 84. Specific Excess Power

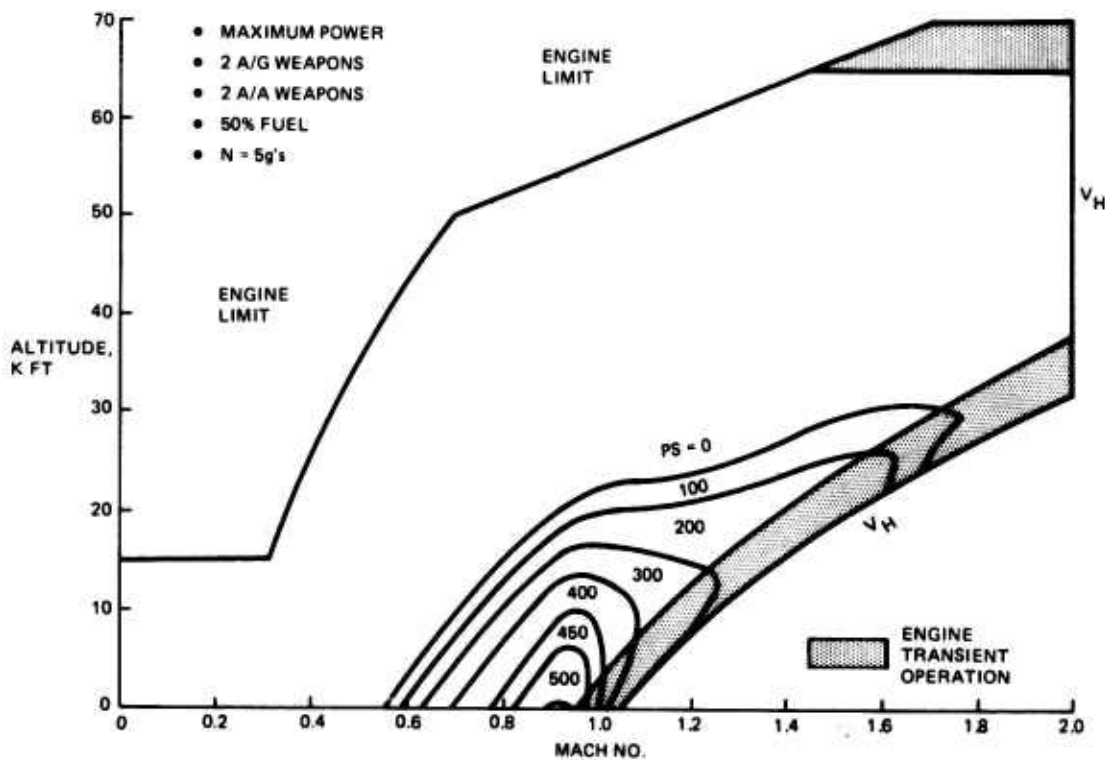


Figure 85. Specific Excess Power

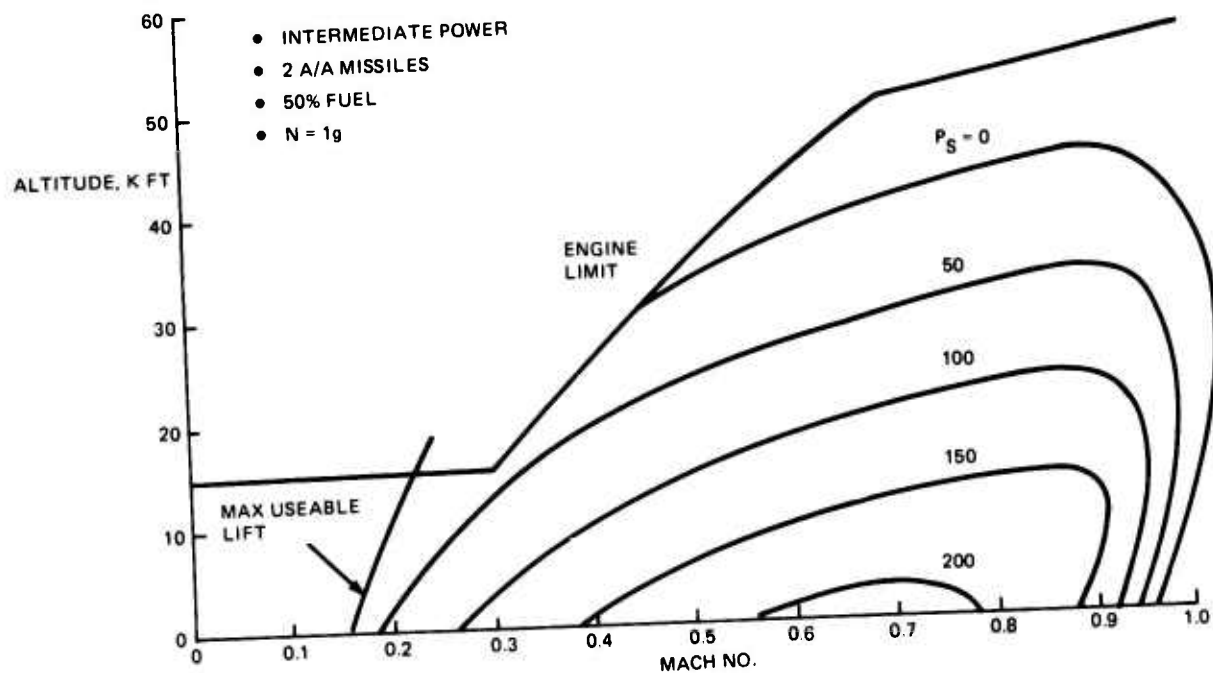


Figure 86. Specific Excess Power

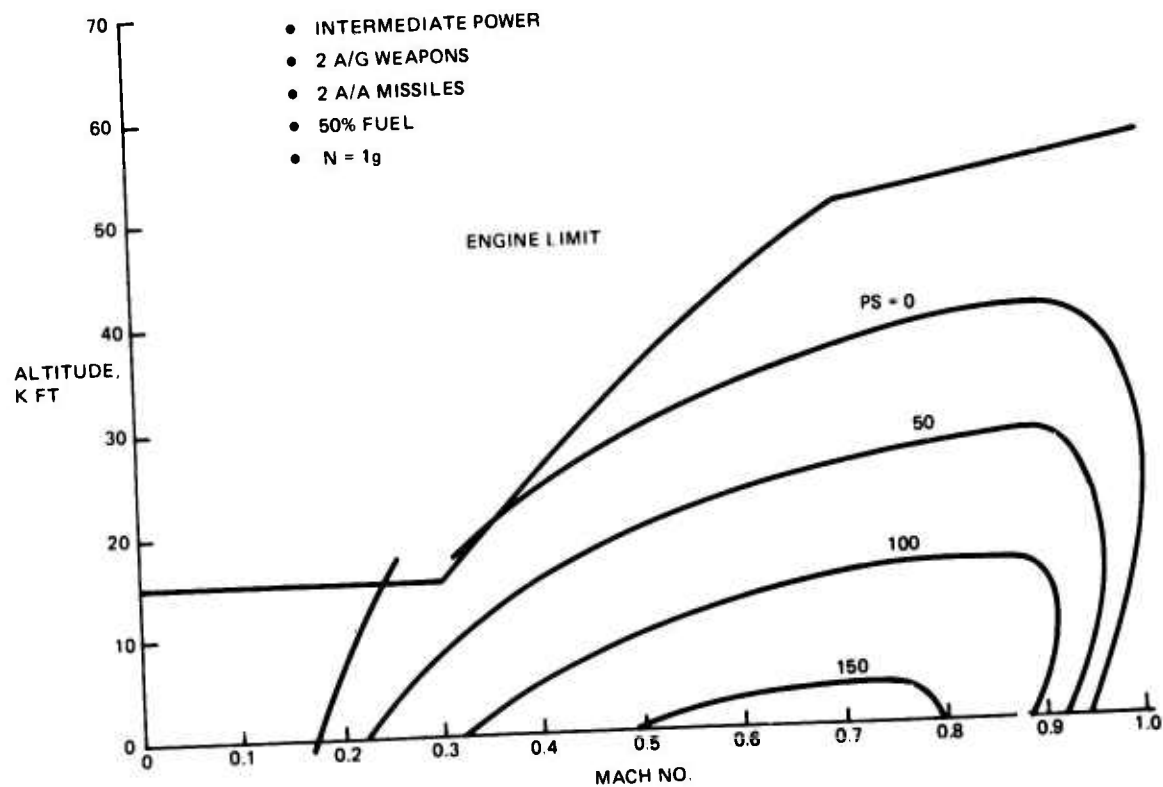


Figure 87. Specific Excess Power

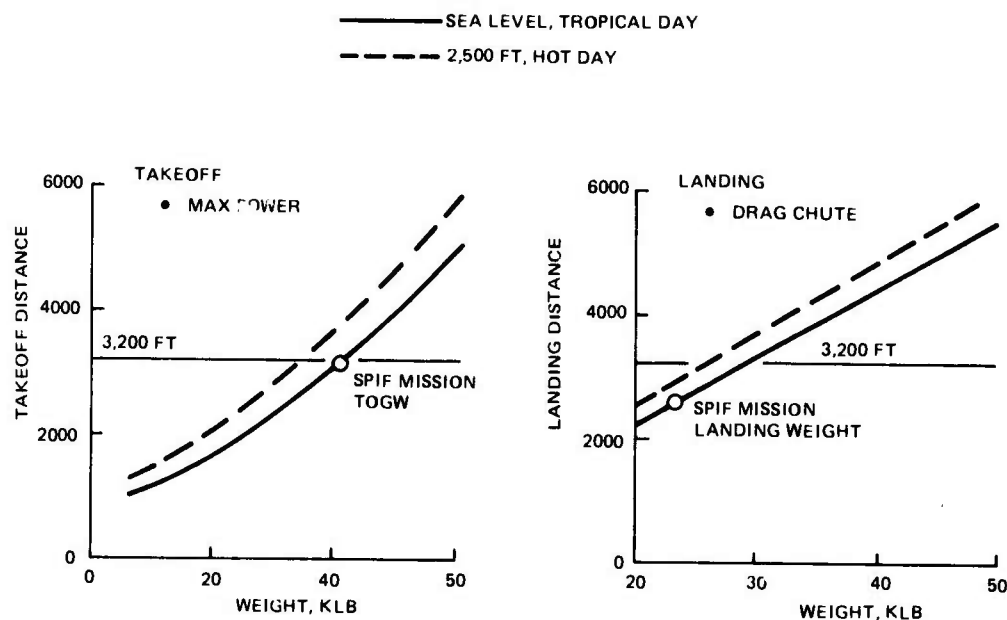


Figure 88. Takeoff and Landing Ground Roll Distance

afterburner takeoff and landing with drag chute vs weight for both tropical day at sea level and hot day at 2500 ft altitude. The aircraft meets the 3200 ft ground roll restriction for takeoff and landing at basic SPIF mission takeoff and landing weights with reserve for tropical day, sea level.

Improvement in takeoff performance is achievable if growth potential in the basic F101 engine were to be utilized. The current growth projections indicate capability for up to 25% more takeoff thrust at sea level, tropic day conditions; without exceeding the current F101 engine installation envelope.

4.5 ADCA PROPULSION SYSTEM

The ADCA propulsion system incorporates one General Electric 30,000 lb thrust class F101-GE-100 afterburning turbofan engine, currently under development by the USAF for the B-1 program. The installation features a fixed geometry external compression inlet designed for efficient supersonic cruise performance and a low drag aft-fuselage contour, blended with the single convergent-divergent nozzle. Evaluation studies of available engine designs indicated that the F101 has a unique cycle that provides a good combination of supersonic/subsonic performance and sufficient thrust to meet transonic acceleration and maneuvering requirements. Installed engine performance was derived

from the General Electric F101-GE-100 engine performance deck No. 090172, using estimated performance characteristics of the inlet system, aircraft systems' bleed air and power extraction requirements and the interference drag associated with the nozzle installation.

4.5.1 Inlet Design

The ADCA inlet is a fixed geometry external compression design as shown in Figure 89. This low cost inlet system, designed to meet $M_{\text{cruise}}/M_{\text{burst}} = 1.60/2.00$ requirements, was found to be superior to candidate normal shock and variable ramp designs. The inlet is underslung, as with the F-16, and is 18 ft aft of the aircraft nose.

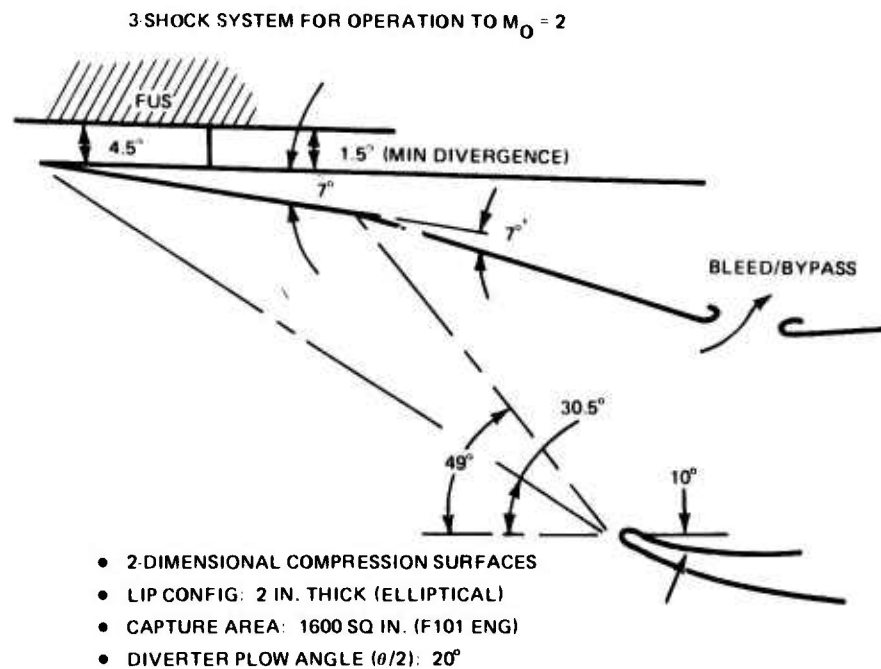


Figure 89. Fixed-Inlet Design

The fixed ramp turning angles of $7^\circ/7^\circ$ provide the same compression at $M_0 = 1.60$ as does the F-14. The throat-to-capture area ratio is also identical, i.e., $A_t/A_c = 0.68$. To assure that operation to $M_0 = 2.00$ is a reasonable development goal, an F-14 was flown to $M_0 = 2.05$ with the ramps locked at the $M_0 = 1.60$ position, and demonstrated successful operation including wind-up-turns at 6 g's.

For operational requirements to Mach numbers greater than $M = 2.0$, a simplified control-variable position ramp inlet design has been identified as an optional installation. Inlet total pressure recovery, including estimated flow field effects, are shown in Figure 90. An additional 3% greater pressure recovery may be provided at $M_0 = 2.2$ by suitably tailoring the forebody contours. There is no significant forebody effect at $M_0 = 1.6$.

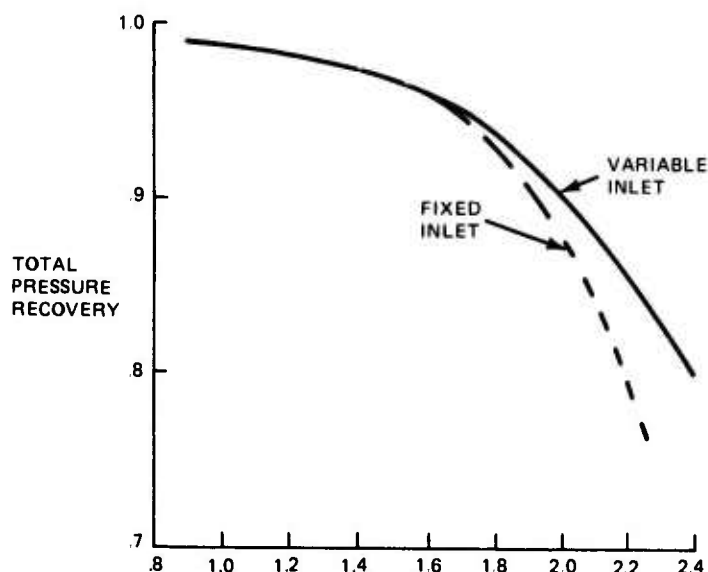


Figure 90. Matched-Inlet Performance

4.5.2 Nozzle Design

Several candidate nozzle concepts were studied in the ADCA single and twin engine configurations. Vectored axisymmetric and asymmetric nozzle designs were compared to the conventional axisymmetric nozzle installations. The relative merits, in terms of nozzle weight and performance characteristics are shown in Figure 91. The aircraft performance benefits resulting from vectored thrust (improved instantaneous g's and landing/takeoff capability) and asymmetric nozzle lift enhancement through supercirculation effects were not sufficient to offset their potential nozzle installation deficiencies.

Both the vectored nozzle and the asymmetric (two dimensional) nozzle concepts incurred a weight penalty over the basic axisymmetric nozzle installation. In general, the asymmetric nozzles are heavier than comparable axisymmetric designs because they

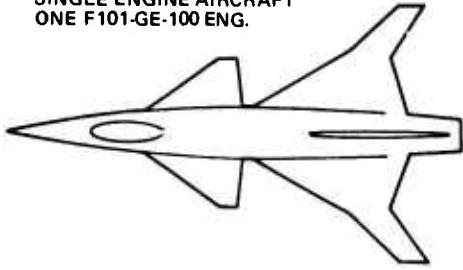

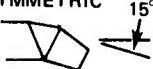

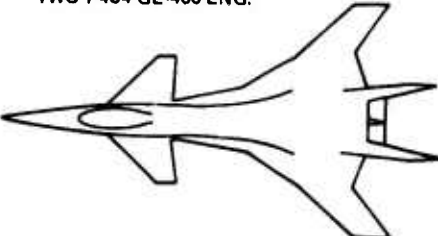

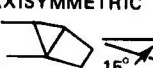

	NOZZLE TYPE	$\Delta WT/A/C, lb$	$\Delta C_V \%$ INT. LOSS		$\Delta D_{INT}/F_{Gi}^*$	
			@ M = .9	@ M = 1.6	@ M = .9	@ M = 1.6
SINGLE ENGINE AIRCRAFT ONE F101-GE-100 ENG. 	AXISYMMETRIC 	0	0	0	0.027	-0.008
	VECTORED AXI-SYMMETRIC 	218	0.6	0.04	0.027	-0.008
	ASYMMETRIC (ADEN TYPE) 	748	0.26	1.38	0.034	0.003
TWIN ENGINE AIRCRAFT TWO F404-GE-400 ENG. 	AXISYMMETRIC 	0	0	0	0.079	0.045
	VECTORED AXISYMMETRIC 	190	0.6	0.04	0.079	0.045
	ASYMMETRIC (ADEN TYPE) 	398	0.26	1.38	0.038	0.011
*RELATIVE TO MAX A/B SINGLE AXI INSTALLATION						

Figure 91. Nozzle Installation Considerations

can not take advantage of the hoop stress principle due to the two-dimensional aspects of their design. The additional internal nozzle coefficient (C_V) losses associated with the vectored and asymmetric nozzles are based on information provided by the engine manufacturers and available reports. These data sources were also used to assist in estimating the relative nozzle interference drag penalties of these designs. The comparison indicates the lower backend drag associated with the single engine installation.

The ADCA design incorporates the existing variable convergent-divergent nozzle of the F101-GE-100 engine. This nozzle in the single engine configuration permits a tight external wrapping of the fuselage around the backend of the engine and blending of the external lines with the nozzle to form a low drag area progression of the aft fuselage/nozzle closure. Experimental wind tunnel testing of similar single engine configurations, conducted by Grumman on the HIMAT program, provided design guidelines in achieving the optimum aft-fuselage contour upstream of the nozzle-connect station. The HIMAT data

also provided a firm basis for estimating the nozzle backend drag of the ADCA configuration. Figure 92 based on a compilation of afterbody drag data from several nozzle test programs, illustrates the bucket of the C_D (backend) vs equivalent boattail angle where the design must be optimized for minimum drag. This narrow region is between 2° and 4°.

Within the practical constraints of the F101 size, the ADCA equivalent aft fuselage boattail angle is 5-1/2°, which is near optimum. This provides a low level of afterbody drag without forcing changes to the overall aircraft or engine designs.

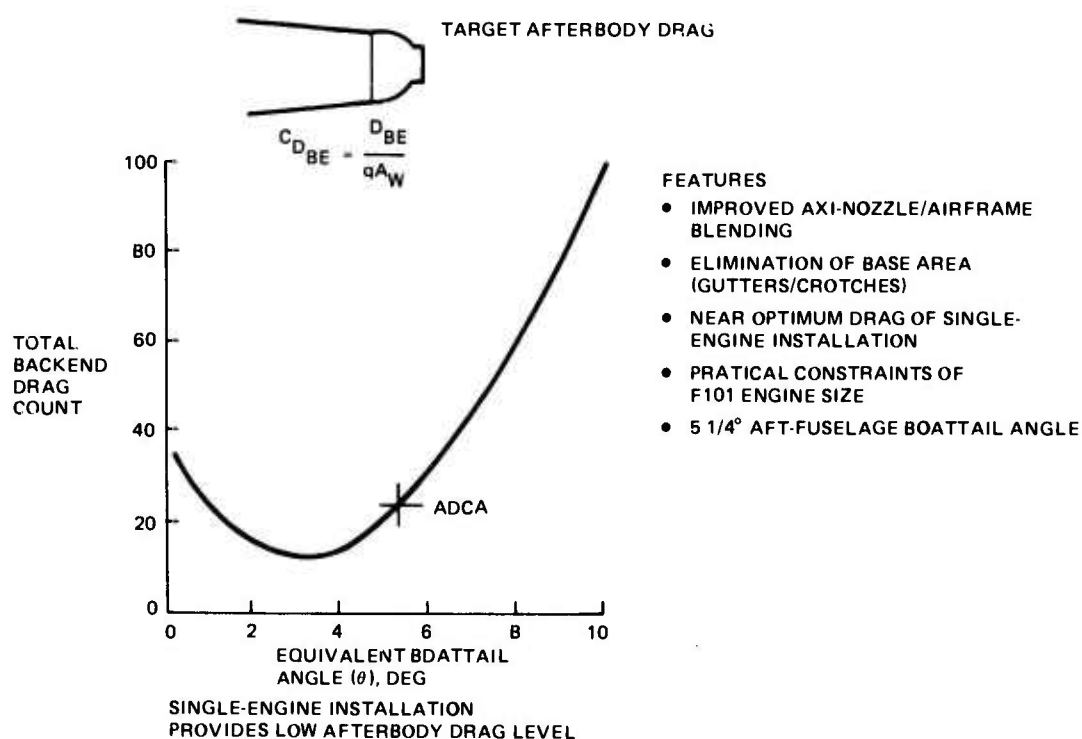


Figure 92. Baseline F101 Nozzle/Airframe Integration

4.6 FLIGHT CONTROL

A digital fly-by-wire concept was considered since it allows for design freedom which otherwise would not be available. Optimum use of control surfaces and surface combinations, ease of control law modification and gain schedules and utilization of relaxed static stability to tailor aircraft performance are among the benefits available to the designer. The general design philosophy is illustrated in Figure 93. A description of the flight control system hardware concepts is given in Subsection 4.7. All stability and control

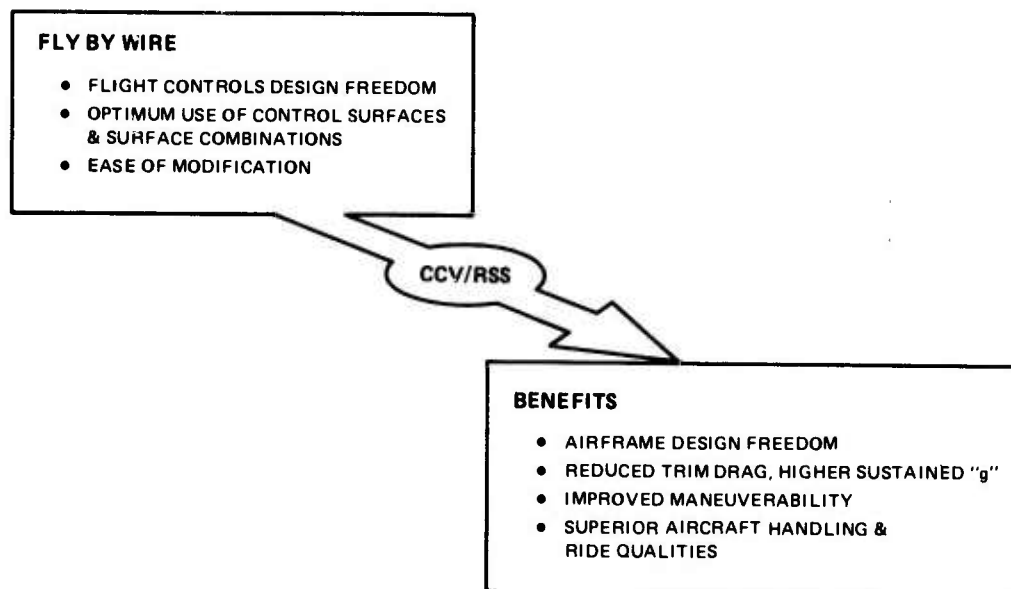


Figure 93. Fly-By-Wire Permits Control 'Configuring' for Superior Performance and Flying Qualities

system work in this study phase emphasized control sizing and required control surface rates. This work was required for overall configuration sizing.

Aircraft control about all axis is effected by direct pilot force through a sidarm controller and rudder pedals. This action will command the electrical equivalent of aircraft g's and rate in the pitch and yaw channels and rate in the roll channel. The error signals produced by these commands and the feedback signals provide the driving inputs to power actuators for surface actuation. Pitch control is achieved by an all movable canard, yaw control by a flap type rudder, and roll control by flaperons and differential canard. For those subsonic flight regimes of low dynamic pressure ($q < 400$ psf), both the inboard and outboard flaperons were used for roll control. At high dynamic pressure, inboard flaperons are used, and differential canards are introduced at supersonic speeds. Control surface power, authority, and maximum rate are critical design requirements for this configuration since it is Control Configured Vehicle (CCV) for part of the flight envelope. The importance of these requirements are recognized and the values shown for authorities and rates appear to be satisfactory. Pitch control inputs during rapid rolls were investigated in order to show the control power is satisfactory during these maneuvers for maintaining the desired aerodynamic stiffness in pitch and yaw.

A block diagram of the pitch channel control system logic is shown in Figure 94. Aircraft N_z and pitch rate are fed back and compared to the command input. A washout circuit is added as an additional control input for low dynamic pressure in order to improve the aircraft response in these flight regimes. Typical aircraft responses are shown for four flight conditions in Figure 95.

A block diagram of the roll channel control system logic is shown in Figure 96. The aircraft roll rate is fed back and compared to the command input. A lag is added to the input command to prevent excessive rate limiting of the power actuator and to effectively set the aircraft's roll time constant. Typical aircraft rolls for 1 g and 2 g's are shown in Figures 97 and 98. In these figures, bank angle rather than roll rate is shown. The system is presently set for a steady roll rate of approximately $200^\circ/\text{sec}$ for full cockpit control input in areas of the flight envelope where the aircraft has at least this capability. In other areas the system will attain a roll rate equal to the maximum roll capability of the aircraft.

A block diagram of the yaw channel control system logic is shown in Figure 99. Aircraft a_y and yaw rate are fed back and compared to the command input. Lateral acceleration (a_z) is included to give the aircraft the apparent defined directional stability. The input command also includes P_c for the purpose of additional aircraft coordination during rolls. Typical responses for step and pulse yaw rate commands are shown in

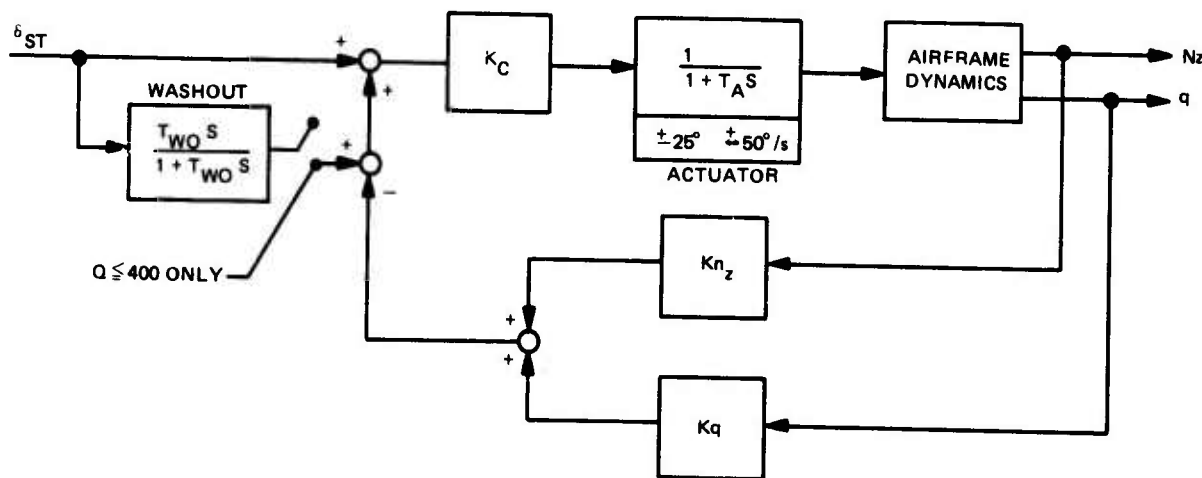
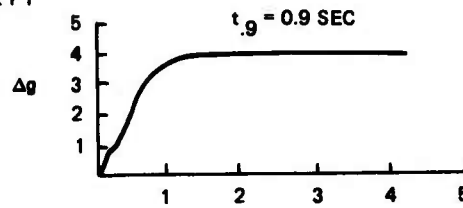


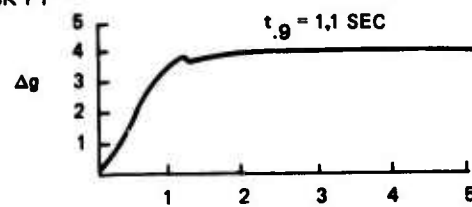
Figure 94. Pitch Channel Block Diagram

M = 1.6 ALTITUDE - 50K FT



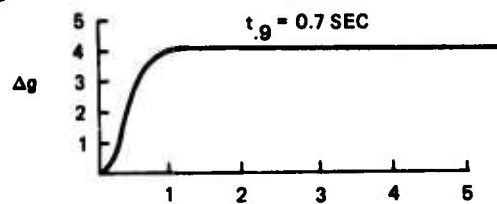
$\Delta\delta_{C\text{ MAX}} = 9^\circ$
 $\dot{\delta}_{C\text{ MAX}} = 50^\circ/\text{s}$

M = 0.6 ALTITUDE - 15K FT



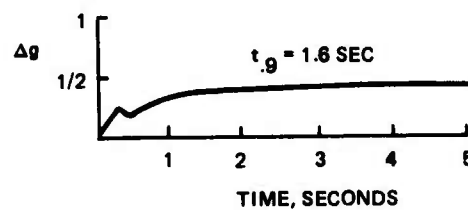
$\Delta\delta_{C\text{ MAX}} = 19^\circ$
 $\dot{\delta}_{C\text{ MAX}} = 50^\circ/\text{s}$

M = 0.9 ALTITUDE - SL



$\Delta\delta_{C\text{ MAX}} = 2^\circ$
 $\dot{\delta}_{C\text{ MAX}} = 40^\circ/\text{s}$

APPROACH



$\Delta\delta_{C\text{ MAX}} = 15^\circ$
 $\dot{\delta}_{C\text{ MAX}} = 50^\circ/\text{s}$

Figure 95. Normal Acceleration Response to Step Command

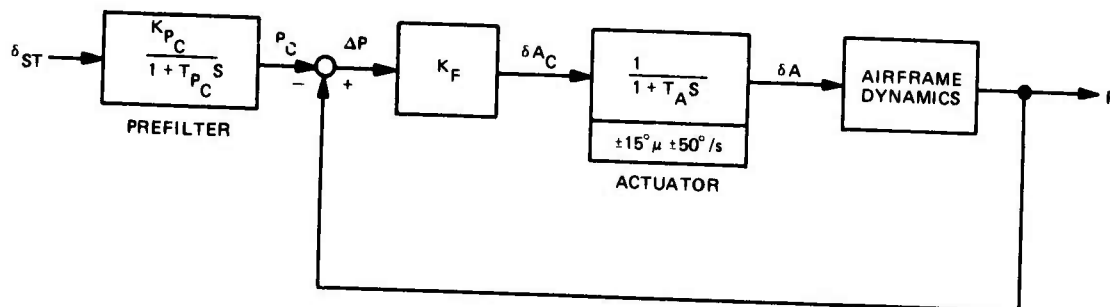


Figure 96. Roll Channel Block Diagram

Figures 100 and 101 to demonstrate both static and dynamic stability. The system parameters were set to give a system response equivalent to W_d 2.5 to 3.0 rad sec.

System response to turbulence at Mach 0.9 at 500 ft altitude is shown in Figure 102. The Dryden form for the random turbulence velocities was used. As shown in the figure, the control surface rates are low and well within the system capability.

It was assumed that system gains and time constants in the pitch and yaw channels will be programmed to achieve the desired response characteristic (this is not considered a difficult task for a digital fly-by-wire system). The roll channel gain was considered as constant.

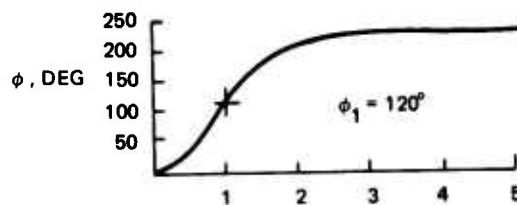
4.6.1 Flight Controls Mechanization

A fly-by-wire design concept was mechanized for the ADCA configuration. The control system/airframe configuration was tailored to comply with the Level 1 flying qualities for a Class IV airplane in MIL-F-8785 (ASG). To accomplish this work, a five-degree-of-freedom analog computer simulation was used. Design in the time domain is, of necessity, for a control system workable in Flexstab. The pertinent criteria used for gain selection and shaping were as follows:

- Short period dynamic characteristics
- Dutch roll dynamic characteristics
- Roll performance
- Adverse yaw maneuvers
- Full stick rolls at maximum "g" conditions (pitch-roll-yaw coupling).

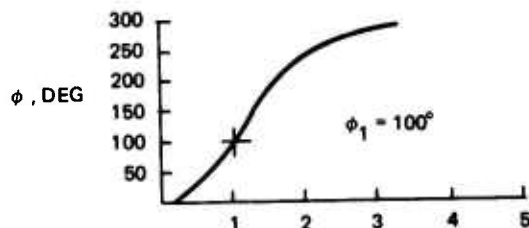
The power approach flight condition was completed. The control configuration including gains and required shaping in all three channels have been determined for this flight condition.

$M = 1.6 \mu$ ALTITUDE = 50K FT



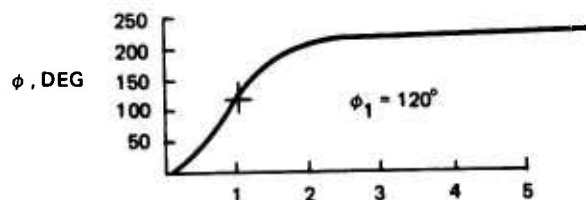
$\delta A \text{ MAX} = 5^\circ$
 $\dot{\delta A} \text{ MAX} = 50^\circ/\text{s}$

$M_0 = 0.6 \mu$ ALTITUDE 15K FT



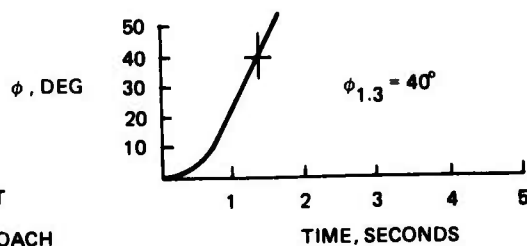
$\delta A \text{ MAX} = 5^\circ$
 $\dot{\delta A} \text{ MAX} = 50^\circ/\text{s}$

$M_0 = 0.9 \mu$ ALTITUDE = SL



$\delta A \text{ MAX} = 5^\circ$
 $\dot{\delta A} \text{ MAX} = 50^\circ/\text{s}$

APPROACH



$\delta A \text{ MAX} = 15^\circ$
 $\dot{\delta A} \text{ MAX} = 40^\circ/\text{s}$

$\phi_1 > 90^\circ \mu$ COMBAT
 $\phi_{1.3} > 30^\circ \mu$ APPROACH

Figure 97. Bank Angle Response to Roll Command

$M = 0.6$ ALTITUDE = 15K FT $N_z = 2g$ (WORST CASE)

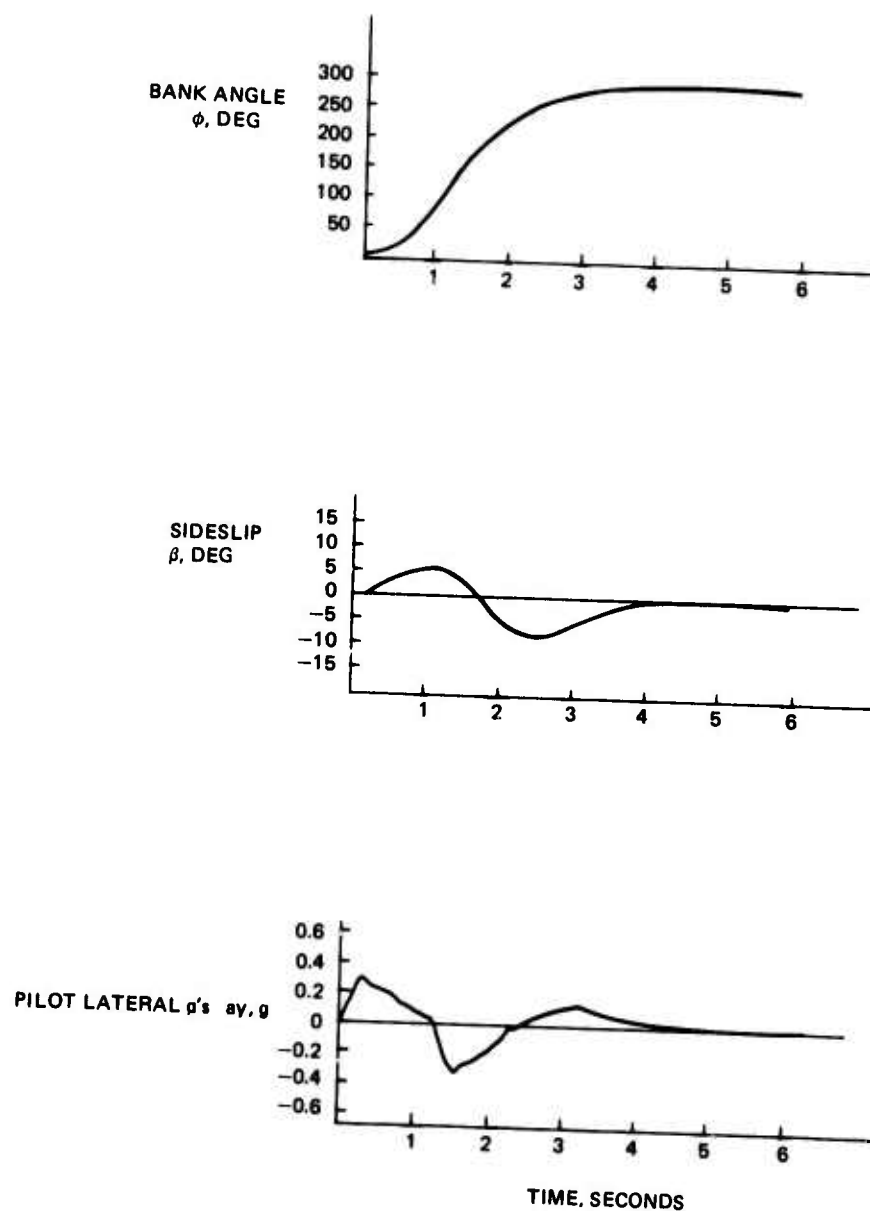


Figure 98. Rolling Maneuver in Accelerated Flight (2g)

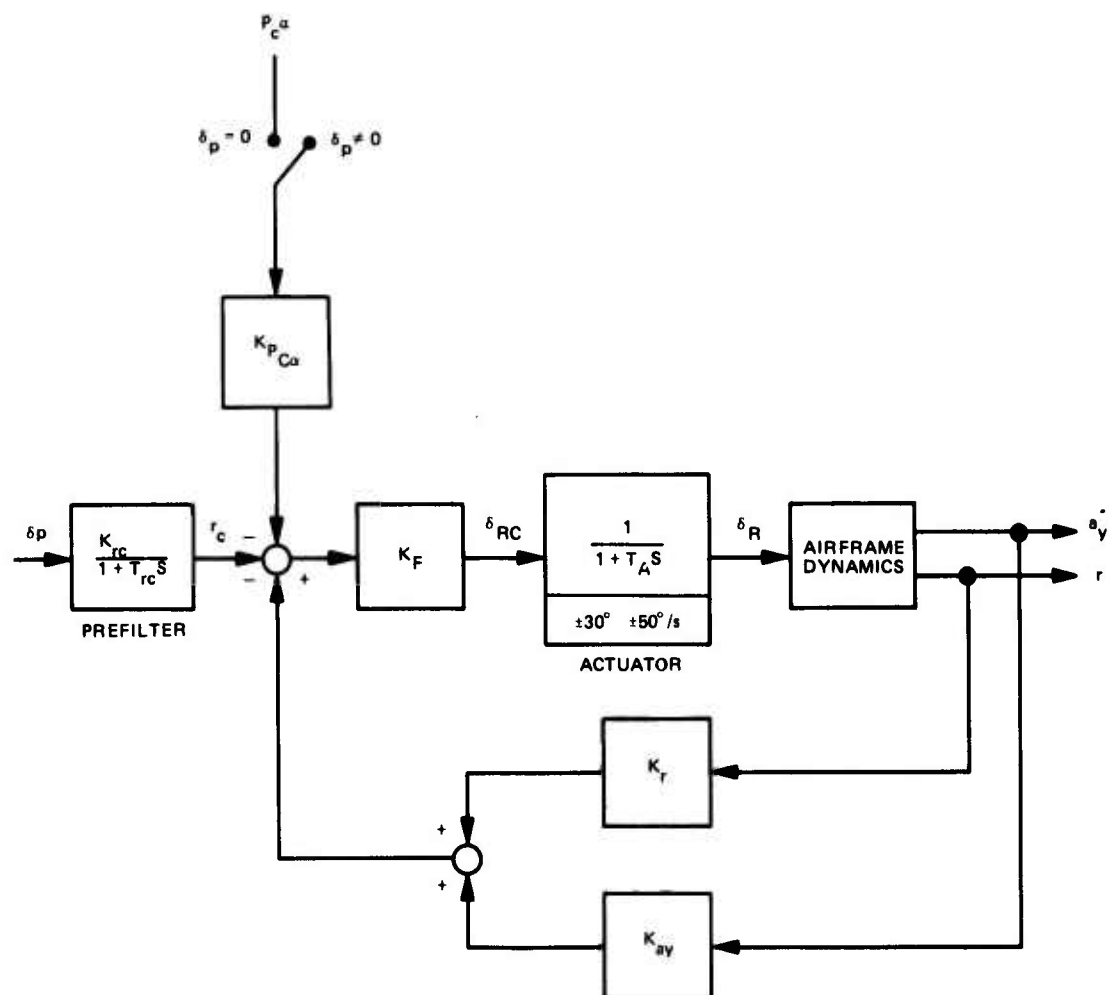


Figure 99. Yaw Channel Block Diagram

4.7 SYSTEMS

In a parallel effort during the development of the ADCA vehicle a preliminary investigation of the vehicle systems was undertaken. Accounting for system characteristics at this time ensures the existence of a vehicle that is compatible with both the system demands and requirements. This in turn minimizes the amount of design adjustment necessary as the vehicle becomes more operationally oriented.

A brief outline of the system characteristics follows.

CRITERIA: $\Omega_{DR} = 2 \text{ to } 3 \text{ rps}$

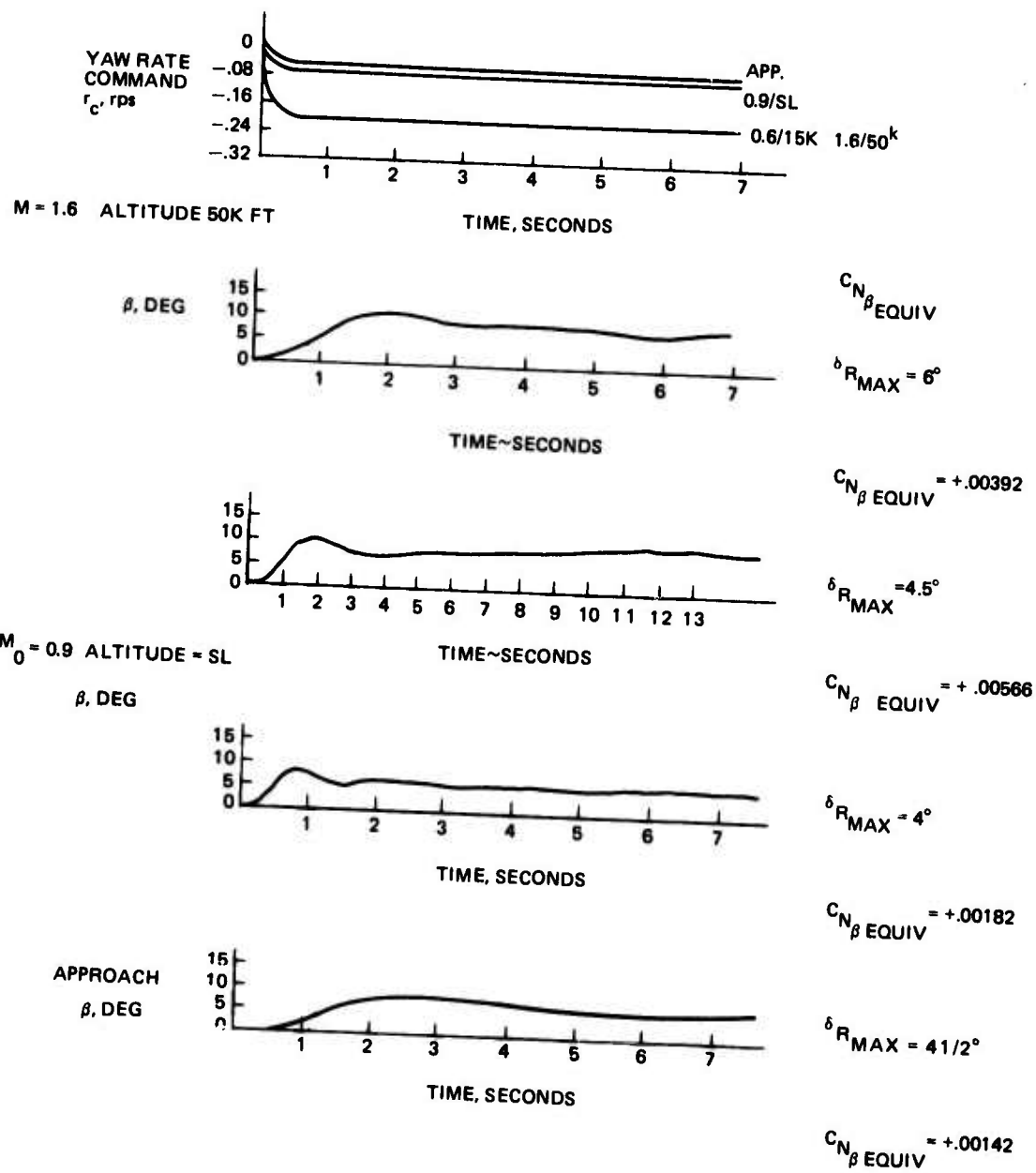
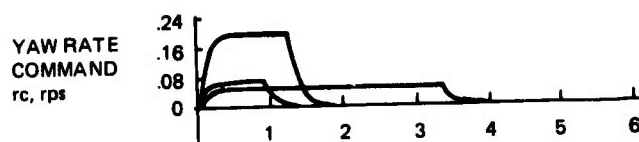


Figure 100. Sideslip Response to Step Yaw Rate Command



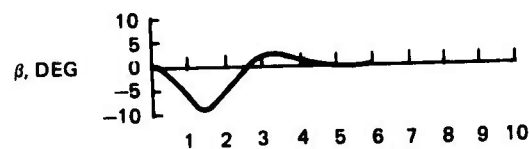
CRITERIA: $\delta R > 0.4$

M = 1.6 ALTITUDE = 50^K FT



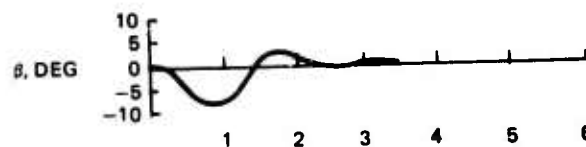
$\delta R_{MAX} = 8^\circ$

M = 0.6 ALTITUDE = 15^K FT



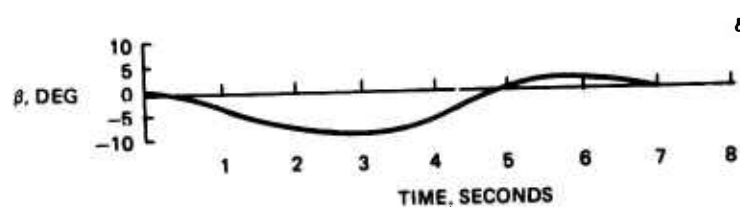
$\delta R_{MAX} = 4^\circ$

M = 0.9 ALTITUDE = SL



$\delta R_{MAX} = 4^\circ$

APPROACH



$\delta R_{MAX} = 7^\circ$

Figure 101. Sideslip Response to Pulse Yaw Command

M = 0.9 ALTITUDE = 500 FT

DRYDEN MODEL: $\sigma\omega = 6.7 \text{ fps}$ $\sigma_v = 10.2 \text{ fps}$

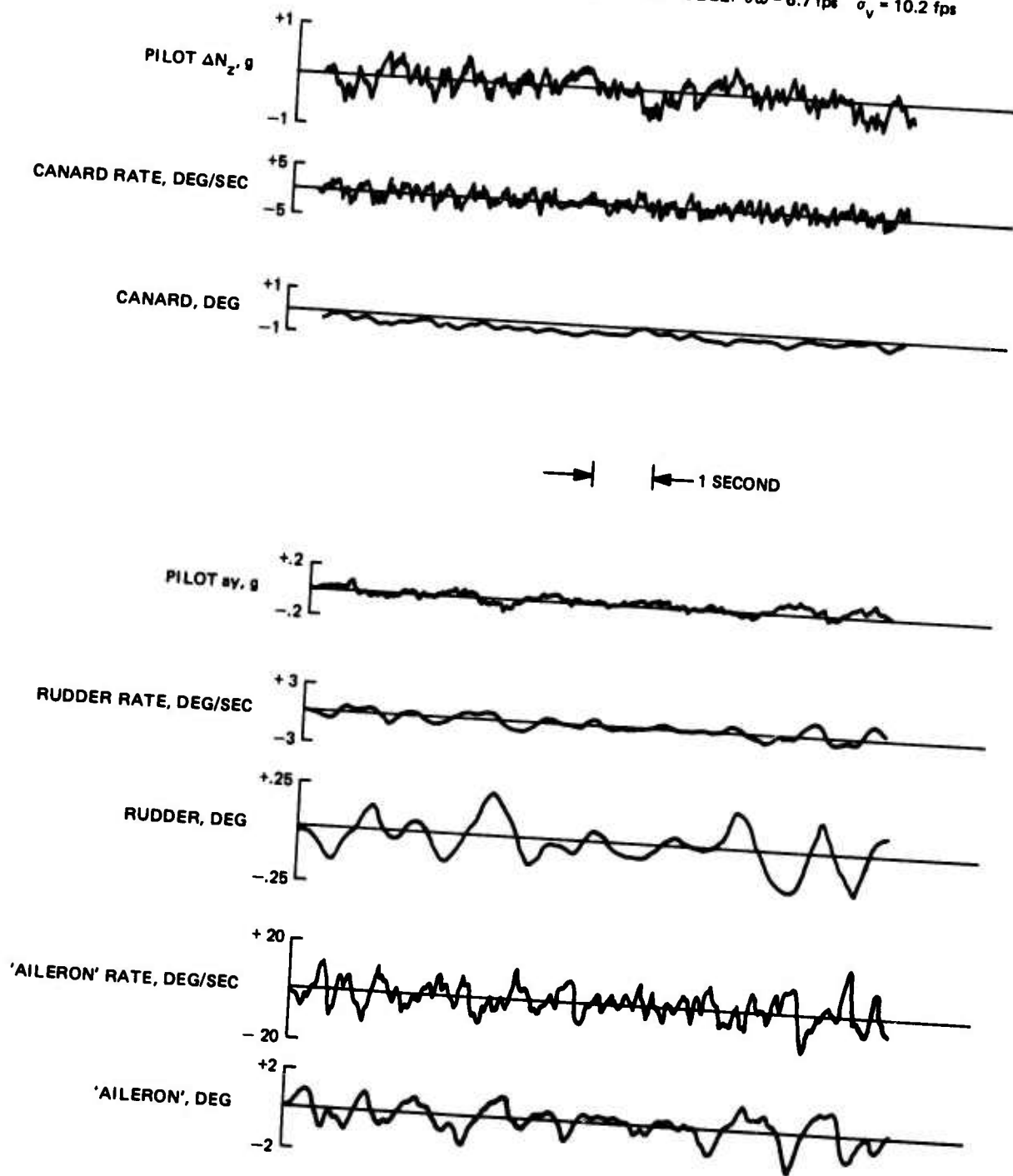


Figure 102. Aircraft Response to Turbulence

4.7.1 Control Surface Actuation

The primary flight control surfaces of the ADCA vehicle consist of left and right independently actuated canards, wing (inboard and outboard) flaperons and a single fin mounted rudder. Leading and trailing edge surfaces on the outboard portion of the wing provide additional active camber control. The inboard flaperons serve as high-lift devices when deflected symmetrically downward, and act as lift spoilers when deflected upward from neutral, during ground roll braking operations.

A preliminary ADCA flight control actuation arrangement is shown in Figure 103.

All primary flight control surfaces (with the exception of the outboard leading edge and trailing edge surfaces) are driven by irreversible, mechanical input, dual tandem servo actuators. The actuators are "rip-stop constructed" and are sized to support limit air load hinge moments on a single hydraulic system.

The surface actuators are commanded mechanically from remotely located "triplex" command actuators. These actuators, tentatively selected in an active/on-line configuration, accept electronic signals from the redundant central computers and are powered by the three independent aircraft hydraulic systems.

The outboard leading edge and trailing edge surfaces are actuated by mechanical rotary (power hinge) actuators. This type of actuation selection was dictated by the severe space limitation imposed by the thin ADCA wing. The mechanical rotary actuator performs the function of both a hinge and a power actuator resulting in a reduced size and weight high stiffness structural joint with minimum free play. All rotary actuators in each subsystem are interconnected via a rigid torque tube transmission system to a central power drive unit (PDU) located in the fuselage. Two hydraulic motors power each PDU and with both systems operable are capable of driving the flaps at the required rate of $30^\circ/\text{sec}$ under full limit hinge moment.

4.7.2 Hydraulic Systems

As shown in Figure 104, the preliminary hydraulic systems configuration of the ADCA utilizes three independent hydraulic systems.

System No. 1 serves primary flight controls, wing camber drives and utility (wheel brakes, landing gear etc.) subsystems. It is powered by one pump driven by a bleed air or hydrazine powered emergency power unit (EPU).

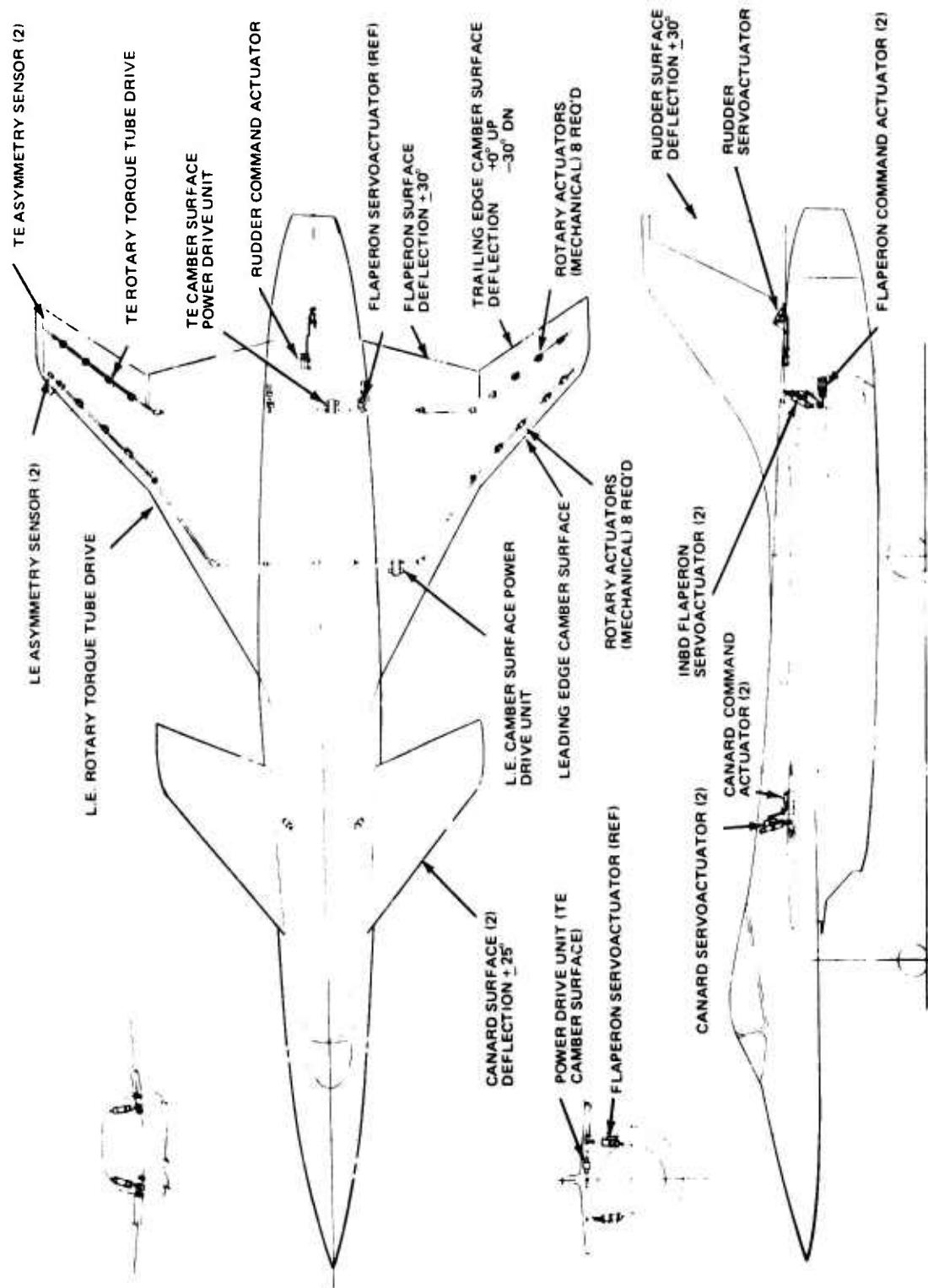


Figure 103. ADCA Flight Controls, General Arrangement

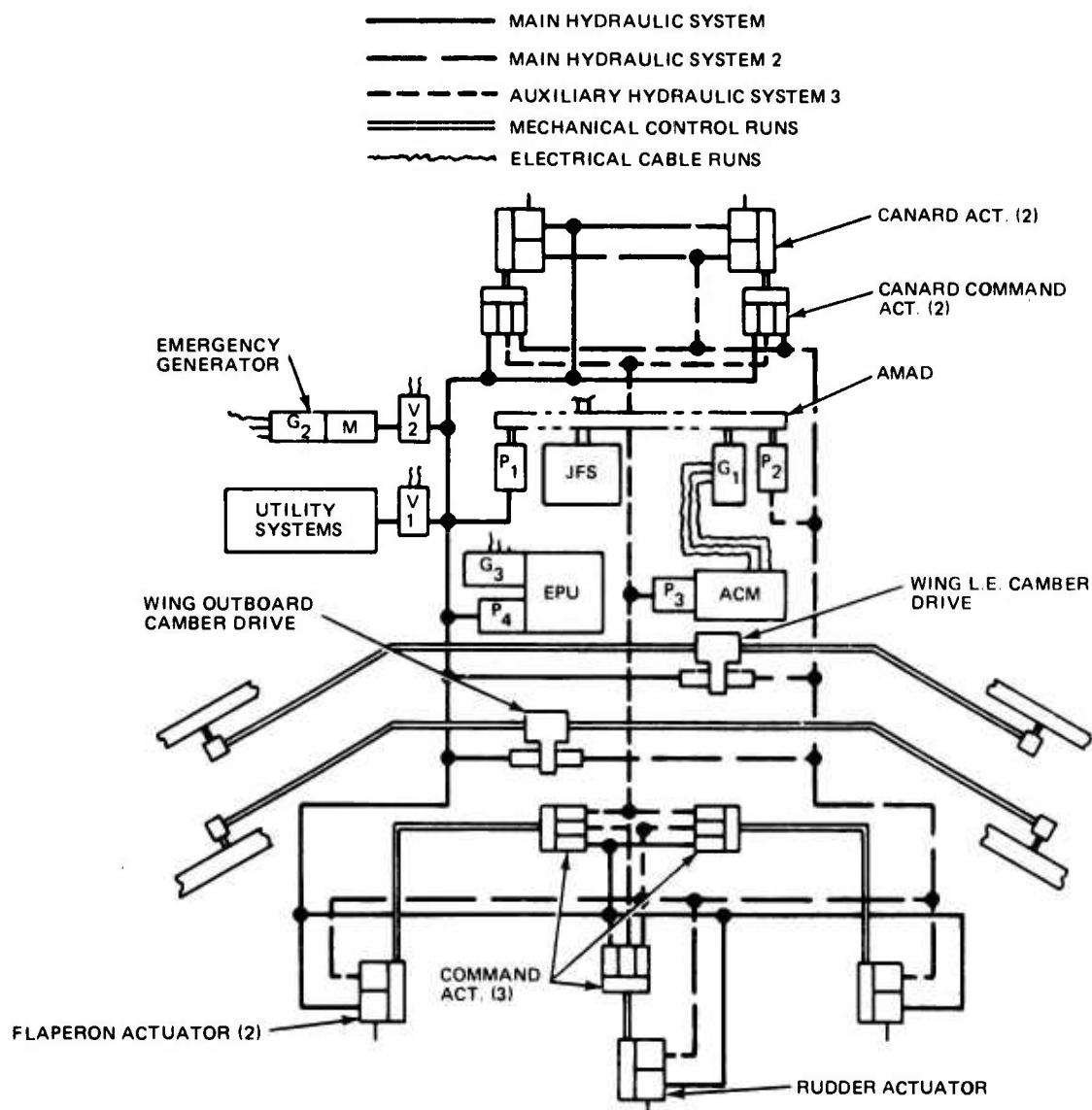


Figure 104. ADCA Preliminary Hydraulic Systems Block Diagram

System No. 2 serves primary flight control subsystems but provides emergency operation of wing camber drives. It is powered by one pump driven by the Airframe Mounted Accessory Drive (AMAD).

System No. 3 serves the command (secondary) actuators of the primary flight control systems exclusively. It is powered by an electrically driven pump power module similar to those used on A-6 and F-14 aircraft as a backup for primary flight controls.

To enhance reliability/survivability, valve V1 isolates subsystems not required in clean flight. Valve V2 is a normally open shut-off valve for the emergency generator. It automatically opens to drive the generator in the event of a complete loss of AMAD driven generators.

4.7.3 Electric Power System

The ADCA Electric Power System is presented on Figure 105. Mission completion power is provided by a single engine driven 40/50 KVA Integrated Drive Generating (IDG) system. A 5 KVA emergency generator is driven at constant speed by a dual mode (hydrazine/engine bleed air) turbine and provides sufficient power for safe flight and landing under night and icing conditions.

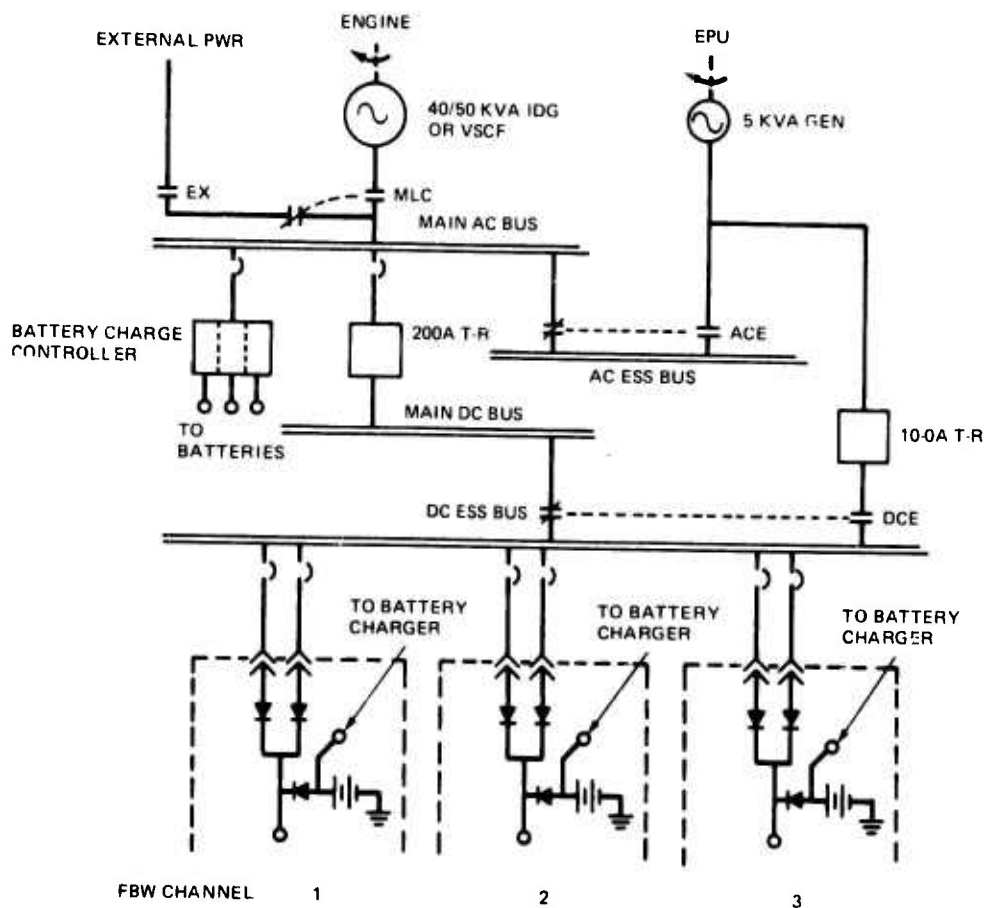


Figure 105. ADCA Electrical Power System

The aircraft's dc power requirements are supplied by fully qualified unregulated transformer-rectifiers (T-R's).

Each channel of the fly-by-wire (FBW) flight controls is powered by dual diode isolated feeders from the dc essential bus. Self contained nickle-cadmium batteries insure power interrupt free service to the FBW electronics. A battery charge/controller is incorporated to insure proper battery state and rate of charge thereby maximizing battery performance and service life.

The ADCA electric power system design places maximum emphasis on the selection of service proven high reliability components which significantly reduce program development costs and risk. Additionally, this design makes exclusive use of Air Force inventory equipment yielding lower operational costs through common support provisions and logistics. Following is a list of major power components and application criteria:

- | | |
|---------------------|--------------|
| * 40/50 kva IDG | - F-15, F-16 |
| 200A T-R | - C-141, C-5 |
| 100A T-R | - F-4, C-135 |
| EPU and Accessories | - F-16 |

Sufficient power capacity exists in the primary generating system (approximately 50% growth) to meet future system changes and for expanded requirements.

4.7.4 Bleed Air and Environmental Control Systems

The bleed air system provides precooled air at a maximum pressure of 60 psig, for use in environmental control, jet blast rain removal and anti-icing. The system has been configured in accordance with Paragraph 3.2.4 of Air Force specification MIL-E-38453 A. The bleed air system consists of a high pressure regulator and shut-off valve, a bleed air driven ejector is employed in conjunction with a ram air modulating system for temperature control of the precooler cooling air.

The environmental control system provides, cockpit air conditioning, pressurization, and moisture control, electronic equipment cooling and pressurization, and gun gas purge. See Figure 106. These functions are all dependent upon the refrigeration subsystem

— — *Should a suitable Variable Speed Constant Frequency (VSCF) Generating System become available, it should be considered for application to ADCA.

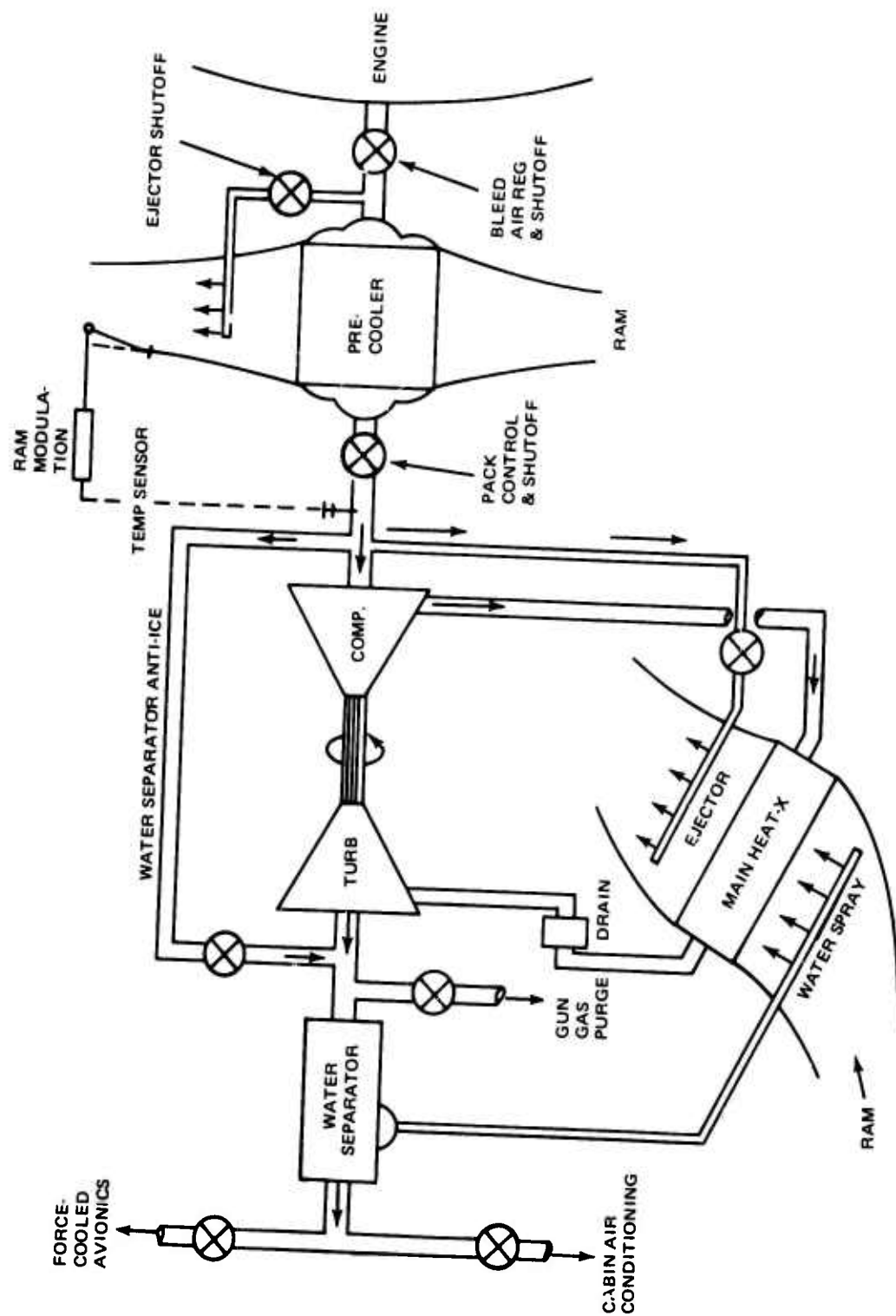


Figure 106. ADCA Environmental Control System

which has been configured in accordance with Paragraph 3.1.1 of MIL-E-33453 A. The refrigeration subsystem consists of pack capacity controls, a bootstrap air cycle machine, an air to air heat exchanger, and a water separator. A bleed air driven ejector is used to provide a means of drawing ambient cooling air through the heat exchanger during ground operation. If an onboard APU is employed as a bleed air and power source for ground checkout, the APU air would be supplied directly to the air cycle compressor inlet. APU operation may preclude the use of the bleed air ejector, with the heat exchanger depending upon the APU bleed flow capacity. In this case, the ejector would be replaced with a fan employing an electric or hydraulic power drive.

The bleed air and environmental control system will incorporate off-the-shelf components for most of the controls, the air cycle machine, and water separator, thereby assuring low risk and minimum cost. However, a considerable weight saving is achieved with the design of optimum heat exchangers using the proven techniques of today's high temperature units. The estimated weight of the bleed air and environmental control system is 350 lb with optimum heat exchangers, and 430 lb with off the shelf units.

A comparative evaluation of the cabin heat loads of the ADCA and an identical all metal aircraft, indicated a small difference in total load as shown in Table 16. This was attributed to the fact that the only area where a heat transfer path is long enough, to take

TABLE 16. ADCA CABIN HEAT LOAD COMPARISON

Contributing Factors	Sea Level Hot Day, M=0.95		50K Ft Hot Day, M=1.6	
	ADCA	Metal	ADCA	Metal
Solar Radiation, Btu/hr	5578	5578	6853	6853
Bulkheads, Btu/hr	5040*	5868	1730*	2586
Insulated External Skin, Btu/hr	713	713	423	423
Canopy Windshield, Btu/hr	7197	7195	3560	3560
Metabolic, Btu/hr	400	400	400	400
Avionics, Btu/hr	7500	7500	7500	7500
Total Btu/hr	26428	27256	20466	21322

*Significant heat load reduction occurs in bulkhead heat transfer due to the long heat transfer path fin effects.

advantage of the low thermal conductivity of composite material, is in bulkhead fin effect.

All avionic equipment is of the air cooled type; either by temperature and humidity controlled air ducted directly to the individual "boxes", or by convection to the temperature controlled compartment environment. A 25% increase was imposed on all avionic cooling requirements, in accordance with Paragraph 3.1.1.2.2.1 of MIL-E-38453 A in order to arrive at the preliminary design of the bleed air and environmental control system.

The crew oxygen system will be designed and installed in accordance with MIL-D-19326. It is anticipated that the supply will be a GFE 20 liter GCU-84/A liquid oxygen converter in accordance with MIL-C-29803. Consideration was also given to the On-Board Oxygen Generators (OBOG) being developed under a joint Air Force/Navy program. Grumman is participating in the OBOG development as a result of contracts N62269-72-C-0144, N62269-73-0307, N62269-74-C-0243 and an anticipated carry-on. As a result, Grumman felt it is premature to consider these systems as candidates at this time. Should these systems progress sufficiently, they should be considered as a candidate supply. Other components utilized in the system will either be Government furnished or off-the-shelf components utilized in similar systems.

4.7.5 Power Plant Installation

A typical power plant installation is shown in Figure 107. The approach used employs an aircraft mounted accessory drive. The engine is installed from the ground cart by rails and rollers. Quick disconnect fittings are used to minimize the installation time, which should be within the 30 minute standard.

The accessory drive shown in this study is the one being developed for the F-16 airplane. The scheduled 1976 qualification data is within the ADCA guidelines.

For engine installation, the fuselage is removed at the aft engine/vertical fin mounting bulkhead. Rails are installed on either side of the fuselage and supported to ground aft of the fuselage bulkhead after mating ground cart rails to these fuselage rails, the engine is rolled forward into the airplane. The rollers are shown installed on the engine ground handling mount points by single quick disconnect pins. A cradle under the engine may be required to stabilize the rollers, however, it is not believed to be necessary.

Engine mounts are then attached, using quick connect fittings. One forward mount takes vertical, thrust and side loads; the second takes only vertical and thrust loads. The single aft mount link takes vertical loads only.

BEST AVAILABLE COPY

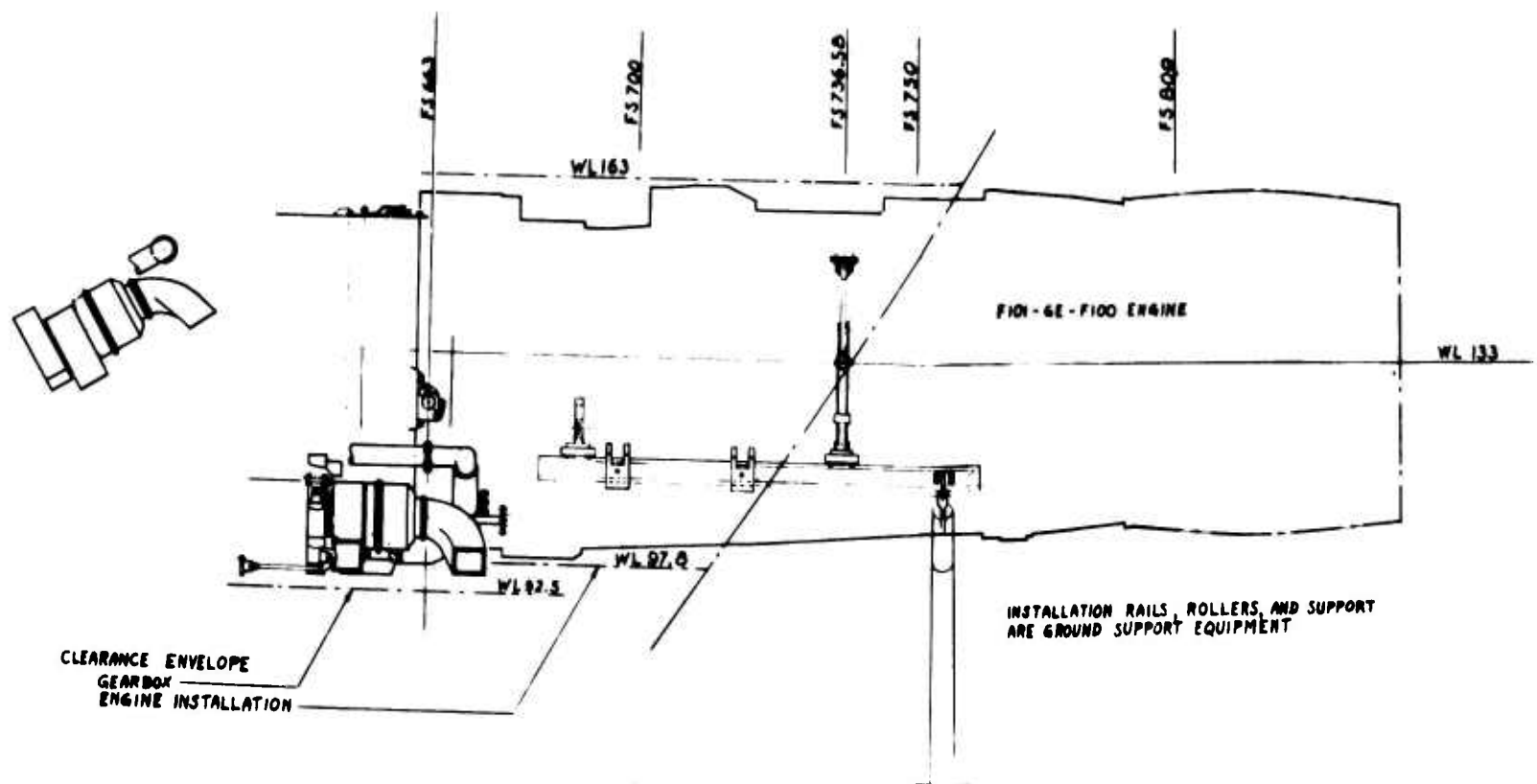
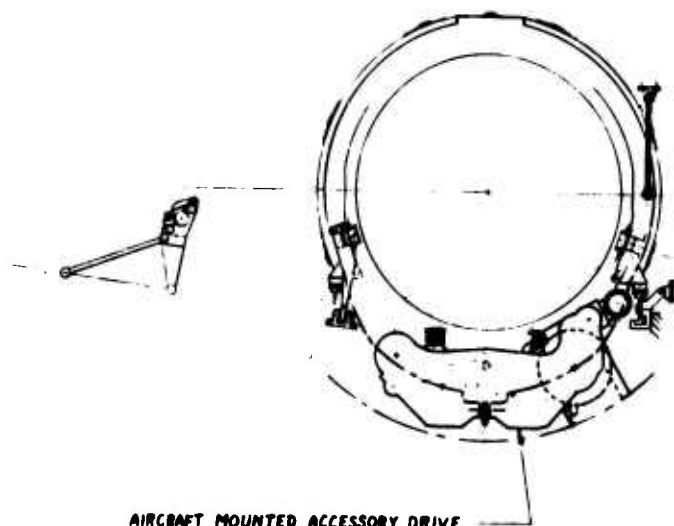
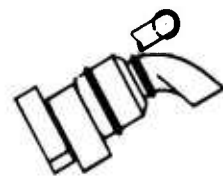


Figure 107. ADCA Typical Power Plant Installation



AIRCRAFT MOUNTED ACCESSORY DRIVE
E-16 SHOWN



CLEARANCE ENVELOPE
GEARBOX
ENGINE INSTALLATION

Note that prior to installation, certain hardware items should be added to the engine to speed up the overall installation time and to reduce the fuselage access door requirements. Components requiring further consideration for this pre-installation assembly include: power takeoff shaft (the forward end splines into the remote gearbox) main fuel line flexible line assembly, bleed air lines, and the fan inlet flange flexible seal assembly. Quick attachment fittings will be supplied for these items which will all mate to the respective airframe components near the engine forward mount plane.

4.7.6 Accessory Drive and Emergency Power Systems

The accessory drive is mounted on the aircraft and driven by the engine power takeoff (PTO) shaft. Normal back-up power is supplied here. However, since loss of hydraulic or electric power might be catastrophic in this control configured aircraft, an independent system has been selected to provide limited power for aircraft control until emergency procedures can be taken. A block diagram of these systems is shown in Figure 108. In this preliminary selection, the systems currently under development for the F-16 aircraft were chosen as they appear to provide the power and redundancy levels required for the ADCA.

The accessory drive system is being developed by Sundstrand Corp., and the emergency power unit by the Garrett Corp.

The accessory drive gear box has two hydraulic pump pads, an integrated drive generator (IDG) pad and a jet fuel starter (JFS) pad. A back-up generator is driven by a hydraulic motor as shown. The JFS drives through a torque converter and overrunning clutch so that it is inactive after the engine is started. The gear box also features a manual device to decouple the engine from the gear box. Thus the JFS can be used to drive the accessories for ground check-out without starting the main engine. The JFS can also be used to restart the main engine in case of flame-out during flight.

In the event of failure of the accessory drive power supply, such as a PTO shaft failure, the Emergency Power Unit (EPU) will automatically start up and supply a reduced amount of hydraulic and electric power. The EPU will utilize engine bleed air to drive a power turbine, maintaining constant speed by a control valve. If bleed air is insufficient to maintain speed, stored monopropellant will be used to augment the bleed air. If bleed air is lost completely, the unit will operate on the monopropellant alone. The mono-

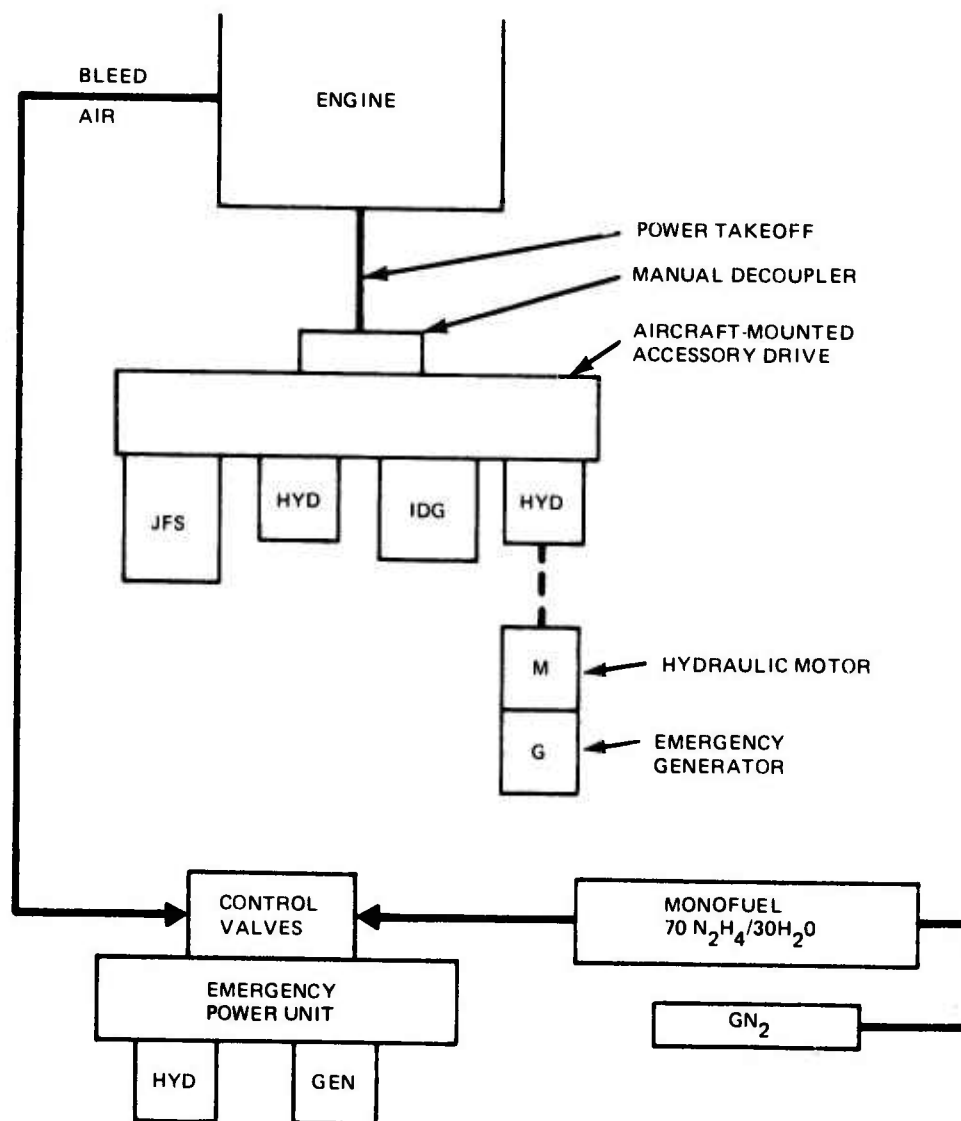


Figure 108. ADCA Prelim Accessory Drive and Emergency Power Systems

propellant is a mixture of 70% hydrazine and 30% water and is decomposed spontaneously by a Shell 405 catalyst. Enough monopropellant will be stored to provide 10 to 20 minutes of operation.

Approximate power ratings for these systems are as follows:

Accessory Drive

- (2) Hydraulic Pumps - 43 gpm at 3000 psi each
- IDG - 50 kva
- JFS - 200 hp class

Emergency Power Unit

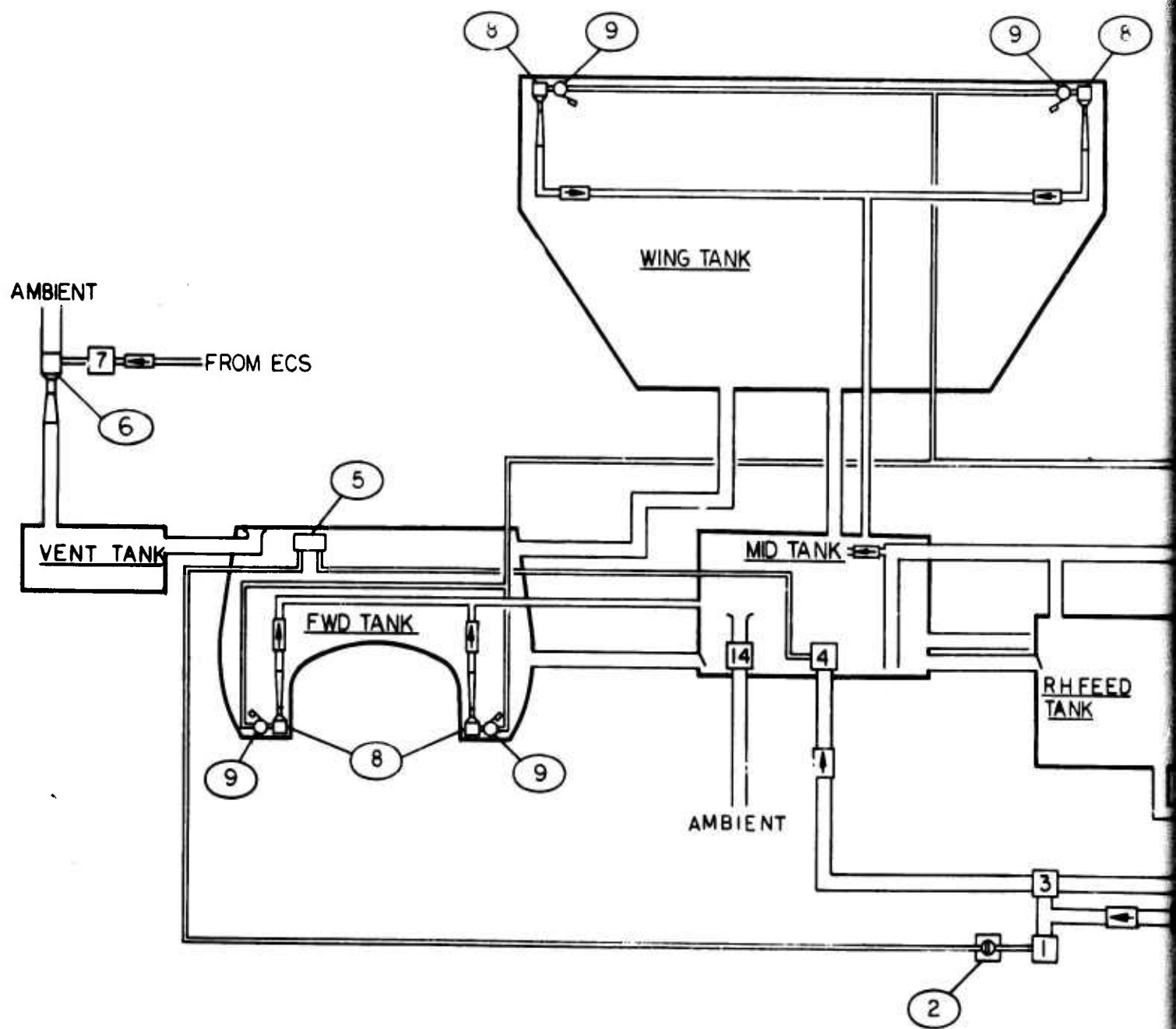
- Hydraulic Pump - 25 gpm at 3000 psi
- Alternator - 8.4 shp at 12000 rpm

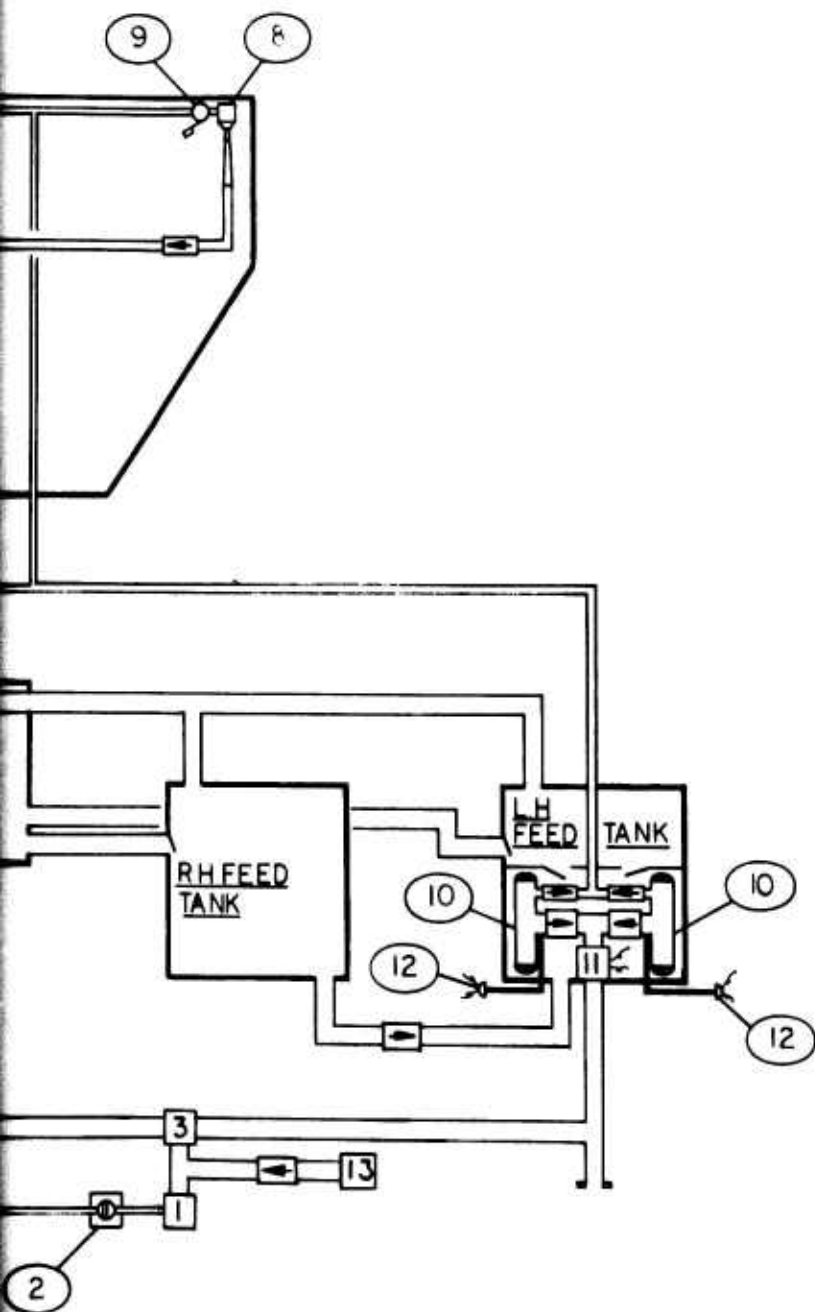
4.7.7 Fuel System Schematic

A schematic of the basic fuel system is shown in Figure 109. The system consists of a vent tank which is located high in the fuselage forward of the fuel tanks, and seven tanks; a wing tank; forward saddle-shaped fuselage tank; mid fuselage tank, and four aft fuselage tanks. The left aft fuselage tank serves as the feed tank and is compartmented to provide approximately 10 sec negative-g operation. Two electrically driven double-ended boost pumps are located in the negative-g compartment and provide positive scavenging for all attitudes. These pumps also supply pressurized fuel to the ejector pumps located in the wing and forward fuselage tanks. Ejector pumps were selected for these locations due to space limitations in the wing tank and also for lower cost as well as high reliability. The mid fuselage tank feeds to the aft tanks by gravity and no pump is required. The aft right hand tank is connected to the negative-g tank by a line beneath the engine inlet duct. In case of electrical pump failure the entire system can feed by gravity with a minor amount of trapped fuel. The two lower aft fuselage tanks, including the negative-g tank, have selfsealing bladders. The vent tank, wing tank, and the other fuselage tanks are of composite material construction, integral with the basic fuselage/wing structure.

The fueling adapter has provisions for ground fueling or defueling. An in-flight refueling receptacle was provided, as was in-flight dump capability.

Engine bleed air, after cooling by the environmental control system, provides the motive force for the air ejector pump which pumps ambient air into the vent tank. A nominal tank pressure of 3 to 4 psig is anticipated. During in-flight refueling operations, displaced vent air will flow back past the ejector and out the vent line.





ITEM	QTY	NOMENCLATURE
1	1	PRESSURE FUELING ADAPTER
2	1	PRECHECK VALVE
3	1	FUELING/DEFUELING SELECTOR
4	1	FUELING SHUTOFF VALVE
5	1	HI-LEVEL PILOT VALVE
6	1	AIR EJECTOR PUMP
7	1	AIR PRESSURE REGULATOR
8	4	FUEL EJECTOR PUMP
9	4	FLOAT OR. SHUTOFF VALVE
10	2	DOUBLE END BOOST PUMP
11	1	ELECT. OR. FUEL ISOLATION VALVE
12	2	FUEL PRESSURE SWITCH
13	1	IN-FLIGHT REFUELING RECEPTACLE
14	1	DUMP VALVE

Figure 109. ADCA Fuel System Schematic

Section V

AIRFRAME STRUCTURAL DEFINITION AND DETAIL DESIGN

5.1 COMPOSITE MATERIALS DESIGN CONSIDERATIONS

5.1.1 Materials Selection

Various factors have been taken into account in formulating a list of candidate composite materials for the ADCA. The first of these factors is availability in the late 1970's, early 1980's of fully qualified systems. Full qualification of new fiber/matrix systems requires a significant investment of both money and time. The boron and graphite fibers used in current qualified systems were developed over ten years ago. The only new fibers which may be developed to the point of qualification by 1980 are the pitch-based graphite fibers and the boron-on-carbon monofilaments. Neither of the fibers are likely to have mechanical properties significantly different from current graphite and boron fibers, but they should be far less expensive.

Organic matrix systems are being developed which have the potential for being less sensitive to moisture pick-up and the associated high temperature compression strength degradation experienced by the current epoxies. The emerging thermoplastic matrices (polyimides, polyarylsulfones and polyphenylenes) show promise and their use could result in a significant reduction in processing costs. However, they are not yet fully qualified nor has their sensitivity to moisture been fully determined.

Lightning strike and triboelectric charging protection must be applied to critical areas of the ADCA structure in accordance with MIL-B-5087. These systems must not only protect the structure but also the subsystems and an allowance has been made for the weight of both external and internal aluminum foil in critical areas which could also function as a moisture barrier, Figure 110.

During the preliminary design phase of the program, allowance was made for both the compression strength degradation of composites after humidity exposure and weight penalties incurred by using foil for lightning strike/moisture protection. The basic dry properties of today's qualified systems, Table 17, have been used and adjusted for "wet" strength as shown in Figures 111 and 112. In addition, the mission which evolved from this Task has been evaluated for structural temperatures. These temperatures do not exceed the 250°F temperature, Figure 113, above which long term humidity/thermal

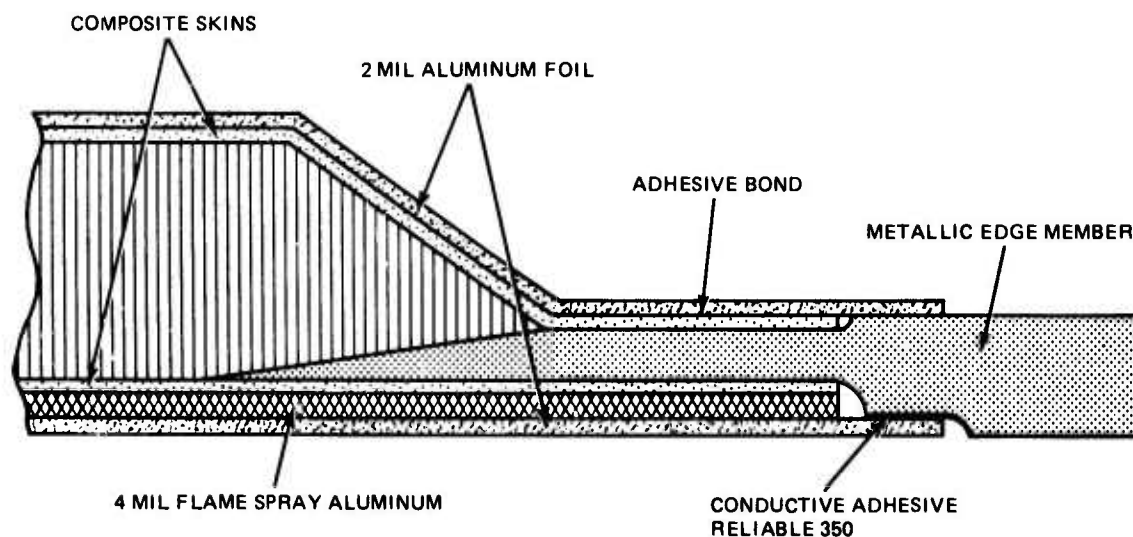


Figure 110. Joint Bonding/Moisture Barrier Concept

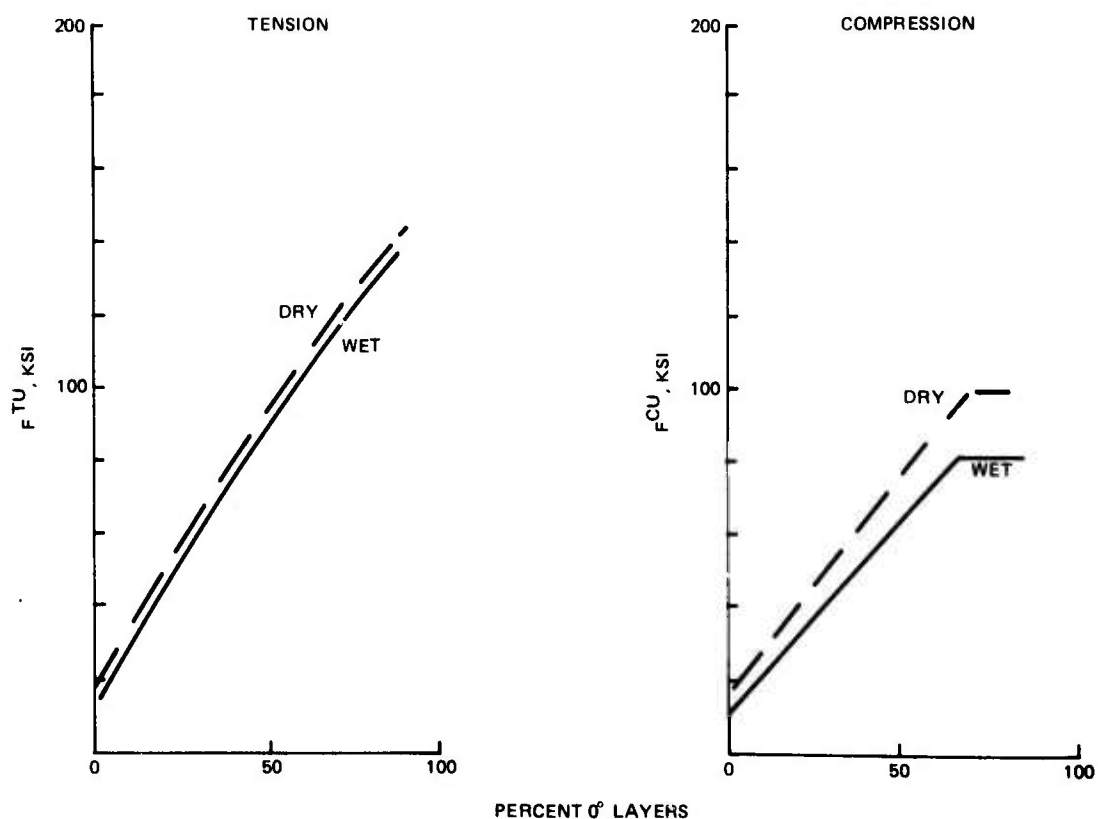


Figure 111. Effect of Humidity on Gr/Ep Allowables at 250°F (0/90/±45) Laminates with 10% 90° Layers

TABLE 17. COMPOSITE DESIGN ALLOWABLES

Property		Unidirectionally Non-Woven											
		Boron/Epoxy AV5505 3M SP290 Unitary				Boron/Epoxy AV5505 3M SP290 In Hybrids				Graphite/Epoxy			
		350° F		350° F		350° F		350° F		3501/AS		T300 N5208/X934	
No.	Holes	RT	350° F	RT	350° F	RT	350° F	RT	350° F	RT	350° F	RT	350° F
F ₁ tu	ksi	178	154	165	152	165	152	169	152	169	165	169	165
F ₂ tu	ksi	10.5	6	10.5	6	10.5	6	6.0	3	6.0	4.3	4.3	3.3
F ₁ cu*	ksi	480	480	480	480	480	480	162	137	162	141	141	90
F ₂ cu	ksi	40	12	40.0	12	40.0	12	25	15	25	20	28	16.8
With 5/16													
F ₁ tu gross	ksi	80	80	80.0	80.0	80.0	80.0	76	76	76	76	76	21
F ₂ tu gross	ksi	5.0	3.0	5.0	3.0	5.0	3.0	3.2	2.0	3.2	2.1	1.2	1.2
F ₁ cu gross	ksi	185	180	185.0	180.0	185.0	180.0	76	76	76	76	21	21
F ₂ cu gross	ksi	12.0	5.5	12.0	5.5	12.0	5.5	12.5	7.5	12.5	10.0	14.0	8.4
E ₁₁ t	msi	30.3	28.3	30.3	28.3	30.3	28.3	18.5	17.7	18.5	22.0	42.0	42.0
E ₂₂ t	msi	2.8	.9	2.8	.9	2.8	.9	1.6	1.1	1.6	1.5	1.0	.65
E ₁₁ c	msi	31.8	30.6	31.8	30.6	31.8	30.6	18.5	17.7	18.5	22.0	42.0	42.0
E ₂₂ c	msi	2.8	.9	2.8	.9	2.8	.9	1.6	1.1	1.6	1.5	1.0	.65
G ₁₂	msi	.723	.232	.723	.232	.723	.232	.65	.20	.65	.52	.70	.21
ν ₁₂		.25	.25	.25	.25	.25	.25	.25	.25	.25	.25	.25	.25
G _z	ksi	250	134	250	134	250	134	104	98	104	140	>80	>80
F _{11s}	ksi	7.0	4.5	7.0	4.5	7.0	4.5	7.1	5.1	7.1	14.2	4.3	3.6
F _{bru} D/t > 2	ksi	140.0	64.0	140.0	64.0	140.0	64.0	66.0	48.0	66.0	66.0	66.0	48.0
a ₁₁	in./in.° F	2.5	2.5	2.5	2.5	2.5	2.5	.25	.25	.25	.30	.58	.58
a ₂₂	in./in.° F	13.0	22.0	13.0	22.0	13.0	22.0	15.2	20.0	15.2	11.0	16.5	20.0
t'	in.	.0051		.00525		.00525		.00525		.00525		.0055	
ρ	Lb/in. 3	.075		.075		.075		.055		.055		.061	
Reference		AFML-TR-70-231	AFML-TR-72-232	AFML-TR-72-232	AFML-TR-72-232	AFML-TR-72-232	AFML-TR-72-232	AFML-TR-72-232	AFML-TR-72-232	AFML-TR-72-232	AFML-TR-72-232	AFML-TR-72-232	AFML-TR-72-232
Notes		* Interlaminar shear modulus G _z is cut off on comp strength											
+ Estimated value													
x Hole diameter correction factor													
		Dia	3/16	1/4	5/16	3/8	1/2						
		CF	1.142	1.07	1.0	.95	.87						

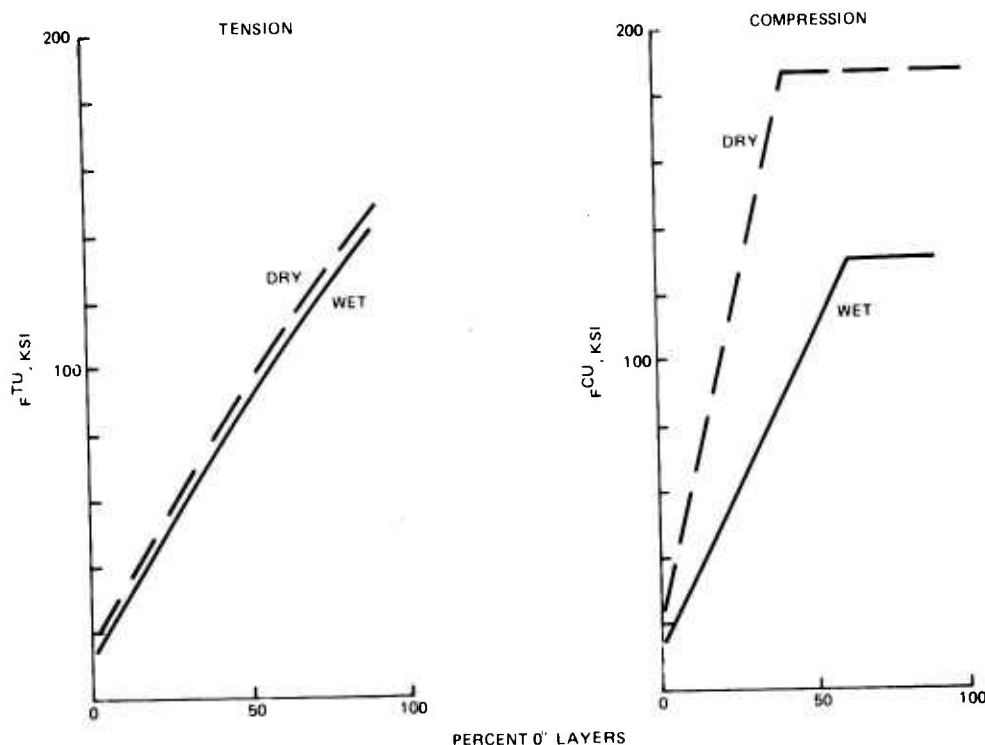


Figure 112. Effect of Humidity on B/Ep Allowables at 250°F (0/90/±45) Laminates with 10% 90° Layers

exposure in conjunction with thermal "spikes" can reduce the matrix glass transition temperature and cause a very significant degradation of the strength and stiffness of epoxy matrices.

The only metal matrix systems qualified today are boron aluminum and Borsic/aluminum. Graphite/aluminum appears to be at least ten years from qualification and its properties are not yet very promising. Aluminum matrix composites were candidates for the regions of the airframe in the engine bay and for firewalls.

Candidate composites, in terms of availability in the 1980 time period are shown in Table 18. Actual selection of specific materials or mixtures of materials was made from structural weight-vs-cost tradeoffs. Projected material prices shown in Figure 114 were used to project materials cost data. A design-to-cost approach was used in conjunction with an aggressive design/manufacturing interface which accounted for developing new low fabrication cost concepts and aimed for structural simplicity. Structural simplicity in combination with large integrally molded components should significantly reduce logistics and assembly costs.

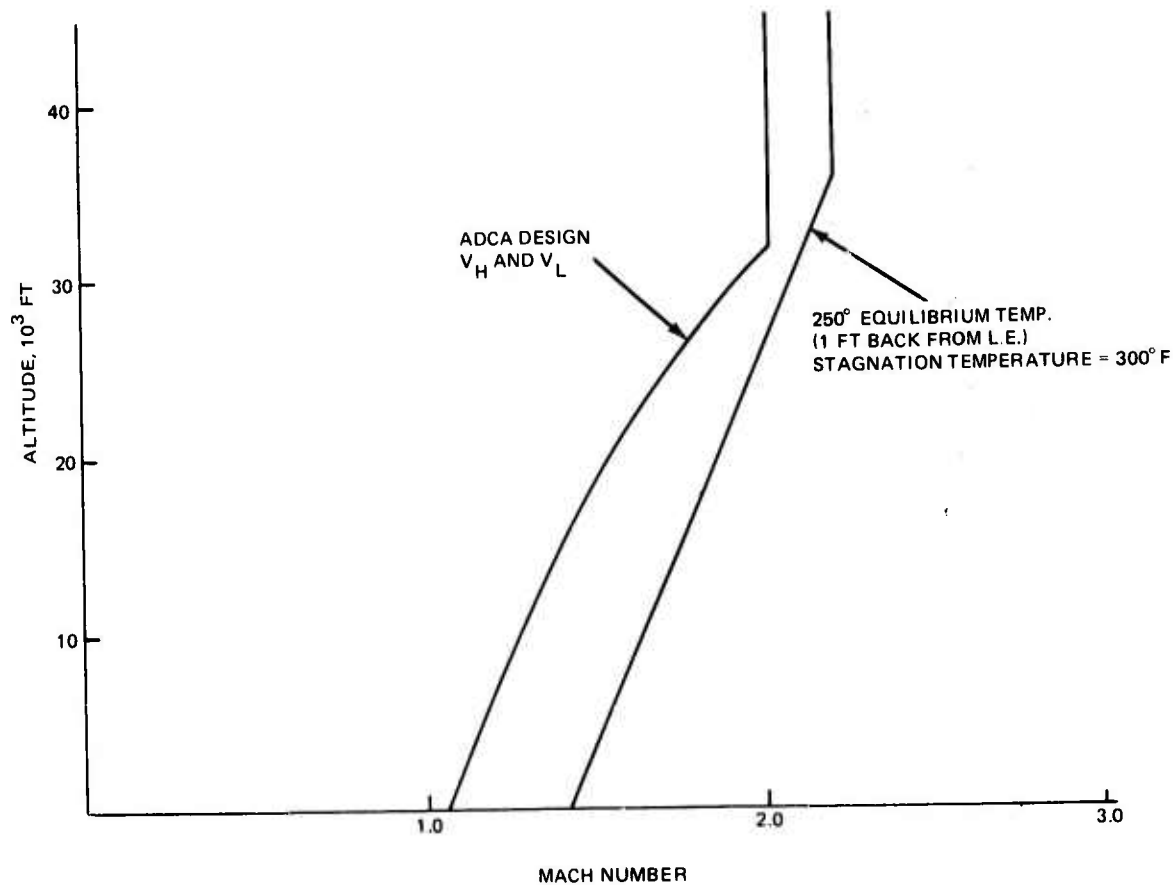


Figure 113. Mach Number vs Altitude

Additional factors influencing materials selection and structural design were damage tolerance, repairability and durability. Graphite/boron and graphite/woven fiberglass or Kevlar hybrid laminates have exhibited significant damage tolerance and were candidates for the wing and fuselage respectively.

In terms of repairability and durability the following facts were considered. To eliminate problems associated with corrosion of aluminum honeycomb core, only composite core (glass, Kevlar or graphite) was utilized for those portions of the ADCA airframe where honeycomb sandwich construction appeared to be the most attractive. Also, to eliminate any fastener corrosion problems, only titanium or stainless steel fasteners were used in laminates containing graphite fibers.

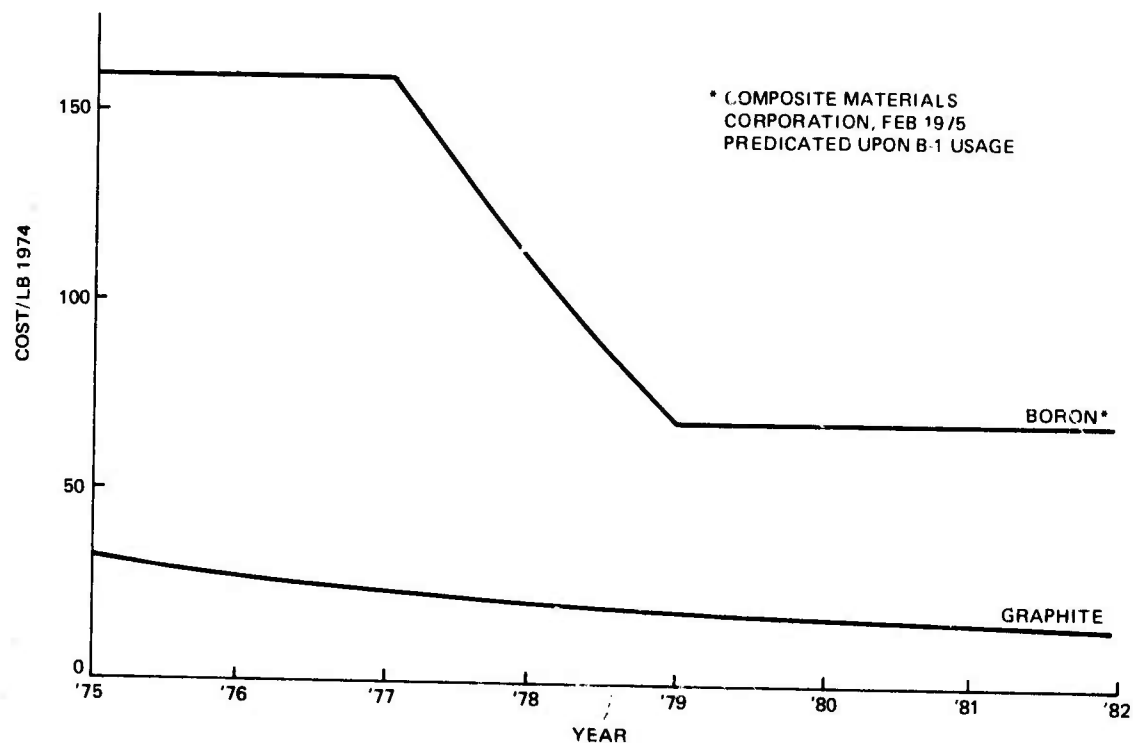


Figure 114. Boron and A/S Graphite Materials Cost Trends

TABLE 18. COMPOSITE MATERIALS (ORGANIC MATRICES)

Qualified (1975)	Near Term (1978) Qualification
B/Ep AVCO 5505, 3M SP 290 (B on W)	B/Ep AVCO 5505 (B on C Monofilament)
Gr/Ep LHS Non Woven Unidirect Hercules 350I/AS 300/N 5208 T300/X 934 LHS Woven T300/X 934 (HMF 330C, HMF 3177 etc)	Gr/Ep LHS T300 Properties with Pitch Fiber Thermoplastic Matrices Polyimide, Polyarylsulfone (PAS), Nylon, PPO etc. with B, Gr, K49 or Glass Fibers
HM Non Woven Unidirect Hercules HM 5/3002M UHM Non Woven Unidirect Celanese GY70/HYE 1534	
Kevlar 49/Ep Non Woven Unidirect Kevlar 49/CE 330" Woven Kevlar 49/Ep 181 Style	
Glass/Ep Woven & Non Woven E & S Glass/Ep	

5.1.2 Design Practices

The successful design of advanced composite structures results from a basic understanding of the materials; the weaknesses as well as the strong points. The design practices presented in Table 19 were generated to take maximum advantage of composite materials. They were established by studies including experimental testing or by engineering judgement, for primary structure. There are acceptable alternate methods and practices but those listed have been successfully demonstrated.

5.1.3 Design Allowables

5.1.3.1 Allowable Stresses for Anisotropic Laminates Without Holes

Figure 115 shows the effect on ultimate tensile strength of kicking the 0° plies through a small angle β . It appears that for a laminate having 50% 0° plies, that a kick of up to 15° can be tolerated without loss of tensile strength. A family of axial stress, shear stress envelopes, has been established for the $15^\circ/90^\circ/\pm 45^\circ$ laminates. The envelopes are based on a simple fiber failure criterion and apply only to all-graphite (type AS) laminates without holes. The envelopes shown in Figure 116 are based on a fiber failure strain of $9120 \mu \text{ in./in.}$ (equivalent to a layer longitudinal allowable stress of 169,000 psi) and also assumes that the transverse stress (σ_y) is zero, typical of a high aspect ratio wing panel. The four envelopes in Figure 116 are for 10%, 30%, 50% and 70% of the plies at 15° kick; in each case 10% of the plies are at 90° and the remainder are balanced $\pm 45^\circ$ plies.

A non-linear strength analysis program "STR 3" has been developed for analyzing composite laminates. Overall strength of the laminate, under uniaxial or combined in-plane loading, is computed using the mechanical properties and orientation of the constituent layers, assuming each layer to be quasi-homogeneous and orthotropic. The layers are assumed to have linear elastic stress-strain behavior in the longitudinal and transverse directions; the non-linearity of the shear stress-strain behavior is represented by a cubic relation. The program incorporates two "failure" criteria - failure of a fiber by exceeding its allowable stress, and yielding of a layer following a modified version of the Hill von Mises yield criterion. For a filament-controlled laminate, yielding of a layer does not constitute failure of the laminate. Figure 117 shows the results of STR 3 for a $15^\circ/19^\circ/\pm 45^\circ$ graphite epoxy laminate having 50% of the layers at 15° . The fiber failure results are in good agreement with the simple strain criterion envelope. The inner curve shows

TABLE 19. GENERAL DESIGN PRACTICES FOR STRUCTURES UTILIZING COMPOSITE MATERIALS

Practice	Reason
<ul style="list-style-type: none"> Filamentary controlled laminates — minimum of three layer orientations 	To prevent matrix & stiffness degradation
<ul style="list-style-type: none"> A $+\theta$ & a $-\theta$ ply are in contact with each other wherever possible 	To minimize interlaminar shear
<ul style="list-style-type: none"> $\pm\theta^\circ$ layers are added as required 	In-plane shear is carried by tension & compression in the $\pm\theta$ layers
<ul style="list-style-type: none"> $\pm\theta$ plies (at least one pair) on extremes of laminate. However, for specific design requirements (applied moments) 0° or 90° plies may be more advantageous 	Increases buckling for thin laminates; better damage tolerance; more efficient bonded splice
<ul style="list-style-type: none"> When adding plies, try to maintain symmetry 	To minimize warping & interlaminar shear
<ul style="list-style-type: none"> Maintain a homogeneous stacking sequence, banding several plies of the same orientation together 	Increased strength
<ul style="list-style-type: none"> Minimize stress concentrations using softening strips 	Composites are essentially elastic to failure
<ul style="list-style-type: none"> When possible, stack 0° plies into localized groups 2–3 in. wide, 8–10 in. apart within cover laminate 	To provide distinct load paths within laminate separated by a highly damage tolerant zone composed primarily of $\pm\theta$ layers
<ul style="list-style-type: none"> When adding plies use a 0.3 in. overlap in major load direction using a wedge type pattern 	It requires approximately 0.3 in. to develop strength of ply
<ul style="list-style-type: none"> Limit use of epoxy composites to maximum service temperature of 250°F 	Strength degradation of matrix above 250°F after thermo-humidity exposure
<ul style="list-style-type: none"> Use co-cured bonded subassemblies whenever possible 	Reduces part count & assembly hours
<ul style="list-style-type: none"> 3D edge distance & 6D pitch for bolted joints 	Lower cost due to prohibitive bond fit tolerance
<ul style="list-style-type: none"> Use Ti or A286 stainless steel fasteners in Gr/Ep 	Minimizes fastener corrosion problems
<ul style="list-style-type: none"> Design bonded step joints rather than scarf joints 	More consistent results, design flexibility & lower cost
<ul style="list-style-type: none"> Use Ti rather than Al for splice plates 	Lower residual thermal stresses on adhesive
<ul style="list-style-type: none"> Bonded joints — No 90° plies in contact with Ti 	Reduction in lap shear strength
<ul style="list-style-type: none"> Bonded joints — $\pm\theta^\circ$ plies on first & last steps 	To reduce peak loading at beginning & end of joint

the envelope at which layers yield transversely to their fiber direction. Figure 118 shows the predicted axial stress-strain curve for this laminate.

The STR 3 program has also been used to provide a comparison between two laminates, as shown below.

Both laminates are of graphite/epoxy without holes. Laminate 'A' is a typical ADCA laminate. 'B' is a $0^\circ/\pm 35^\circ$ laminate (chosen for its high Poisson's ratio dictated by a high camber requirement) which is rotated through 20° to give the required anisotropy. Both laminates have similar values for the modulus E_{11} and the shear strain/axial stress coupling C_{16} ; they differ in their effective shear moduli and Poisson's ratios.

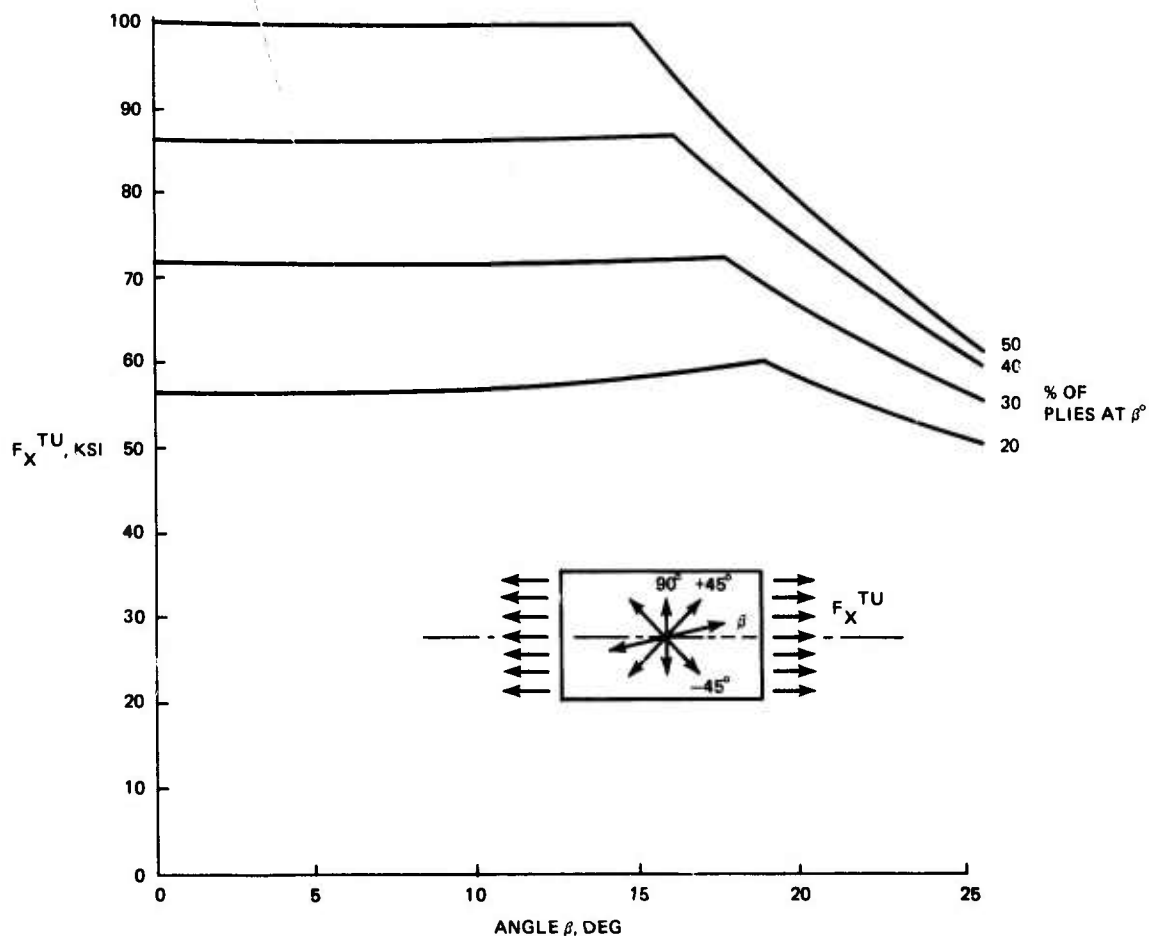


Figure 115. Allowable Tensile Strength $\beta_G/\pm 45^\circ G/90^\circ G$ Laminate Type AS Graphite Epoxy, Room Temperature, No Holes

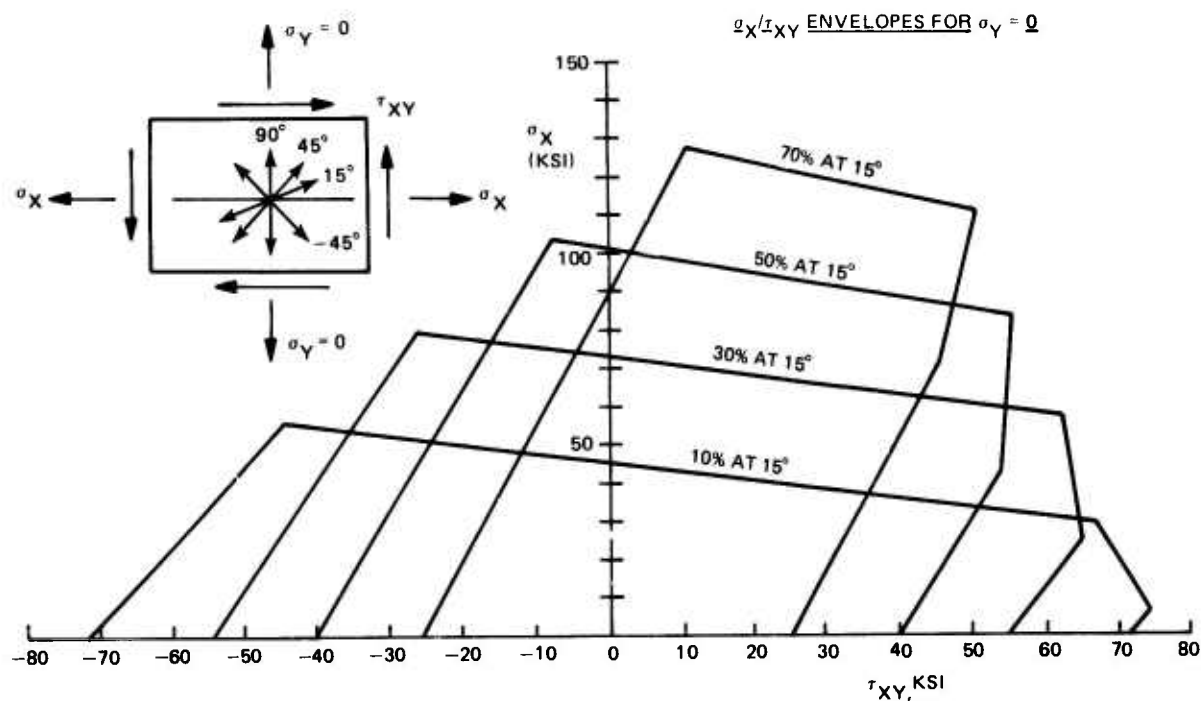


Figure 116. LHS Graphite/Epoxy Laminate. No Holes

Typical ADCA, Laminate 'A'

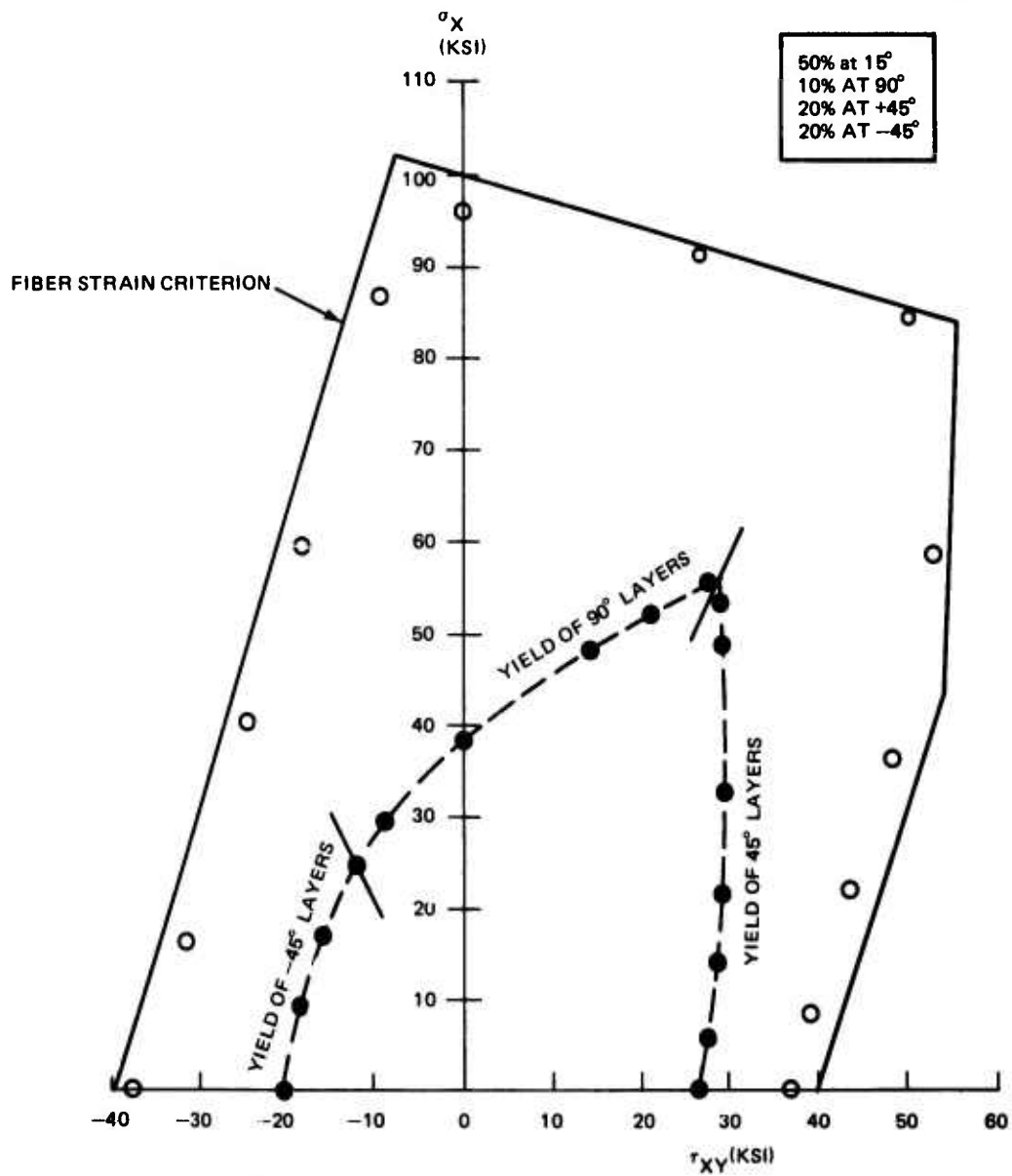
$$\begin{aligned} E_{11} &= 8.13 \times 10^6 \\ G &= 2.47 \times 10^6 \\ \nu &= 0.495 \\ C_{16} &= 0.0817 \times 10^{-6} \\ 50\% &\text{ at } -15^\circ \\ 10\% &\text{ at } 90^\circ \\ 20\% &\text{ at } 45^\circ \\ 20\% &\text{ at } -45^\circ \end{aligned}$$

Typical Hi MAT, Laminate 'B'

$$\begin{aligned} E_{11} &= 8.22 \times 10^6 \\ G &= 1.73 \times 10^6 \\ \nu &= 0.834 \\ C_{16} &= 0.0815 \times 10^{-6} \\ 44\text{-}1/2\% &\text{ at } -15^\circ \\ 44\text{-}1/2\% &\text{ at } 55^\circ \\ 11\% &\text{ at } 20^\circ \end{aligned}$$

The results of the STR 3 program are shown in Figures 118 and 119. The laminates differ markedly in their behaviour, laminate A fails by fracture of the -15° layers and, although the non-linearity caused by transverse yielding of the 90° layers and then the 45° layers can be discerned, the laminate is reasonably well-behaved. Laminate B by contrast fails by yielding of the matrix at a comparatively low axial stress and is

$\sigma_X: \tau_{XY}$ ENVELOPE FOR $\sigma_Y = 0$



FROM STR 3:

- FIBER FAILURE
- TRANSVERSE YIELDING OF A LAYER

Figure 117. LHS Graphite/Epoxy Laminate. No Holes

more non-linear than A, particularly in its anisotropic shear strain/axial stress coupling behavior. Laminate B in fact typifies a matrix dominated laminate, whose properties are sensitive to the matrix stiffness and strength.

5.1.3.2 Anisotropic Laminates With Holes

- Layer Allowable Stress - For the purpose of resizing the finite element model, an allowable layer longitudinal stress of 76,000 psi has been used in ASOP 3. This represents a "far field" allowable which accounts for the presence of an open hole within the field without having to calculate the detailed stress distribution around the hole.

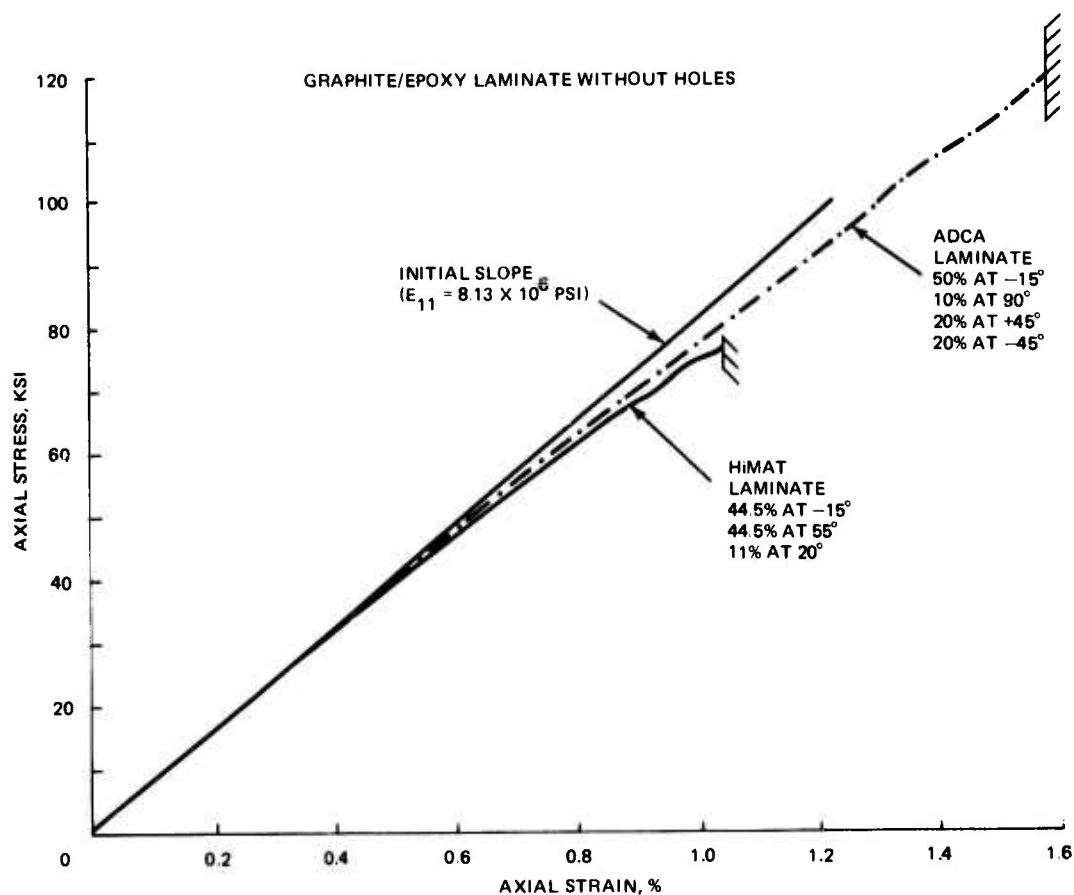


Figure 118. Predicted Axial Stress-Strain Curves

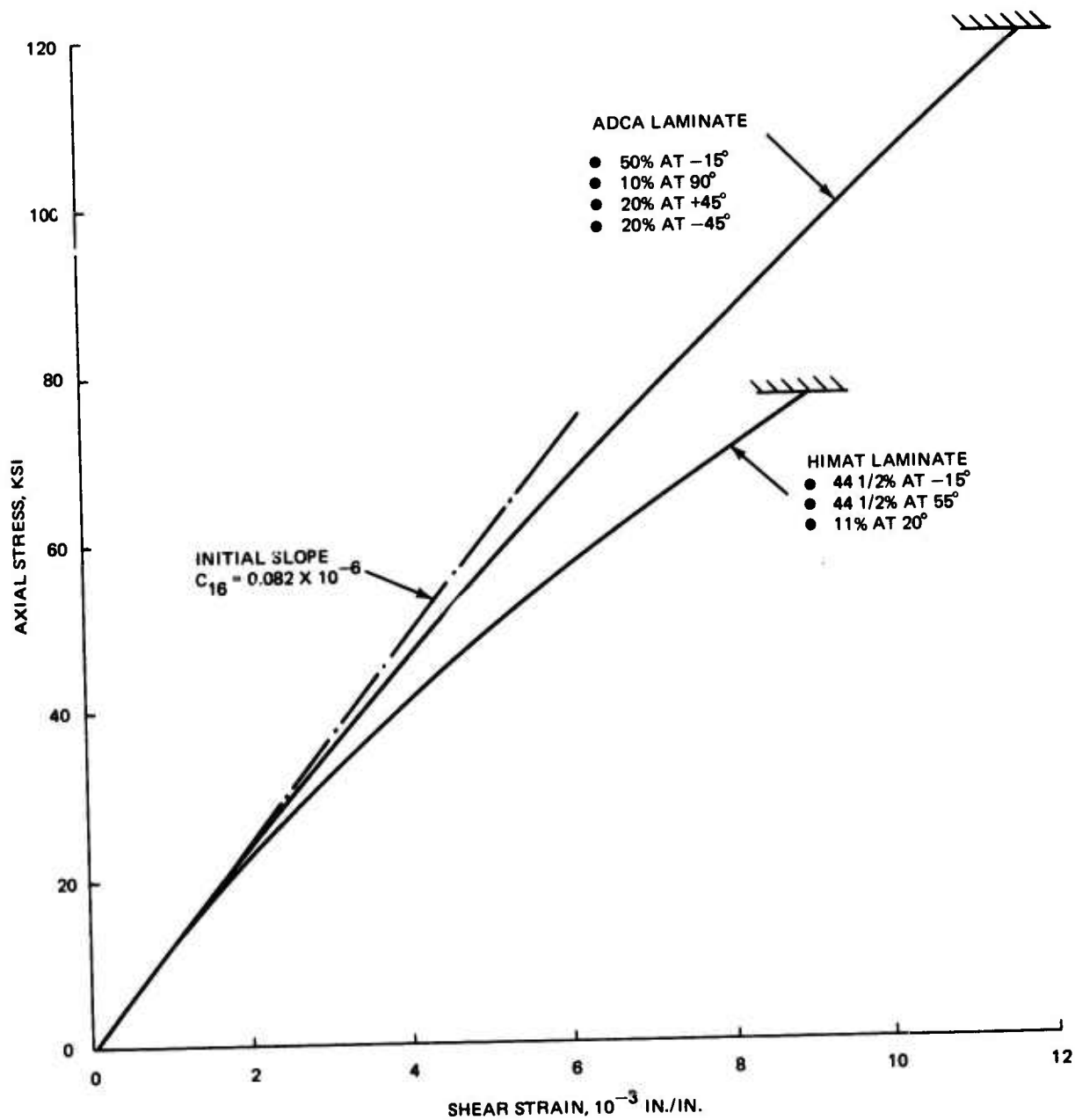


Figure 119. Predicted Anisotropic Coupling, Axial Stress/Shear Strain Curves, Graphite/Epoxy Laminate Without Holes.

To verify the value used, 37 tensile tests performed at Grumman on orthotropic graphite/epoxy laminates with open holes were analyzed. The results, Table 20, cover seven different layups, tested at temperatures from -67°F to 180°F . Calculating the 'B' level layer allowable gives a value of 78,000 psi, which is sufficiently close to the value used so that no changes need be made.

TABLE 20. TENSILE STRENGTH OF GRAPHITE/EPOXY WITH HOLES

LHS GR/Ep Laminates with Holes							
Source, Layup, Temperature (0°/90°/±45°)	W	D	t	P	F Pred, ksi	f Test, ksi	Ratio
Grumman, 18/4/28, R.T.	1.5	0.181	0.269	20.25	41.40	51.4	1.24
	1.506	0.182	0.279	19.10		48.3	1.17
	1.506	0.183	0.277	20.40		51.6	1.25
	1.492	0.182	0.302	23.65		60.4	1.46
	1.492	0.183	0.302	21.05		53.7	1.30
	1.492	0.181	0.291	22.30		56.9	1.37
Grumman, 18/4/28, 180°F	1.505	0.182	0.280	20.3	41.4	51.4	1.24
	1.504	0.182	0.279	31.0		53.1	1.28
	1.506	0.182	0.281	20.75		52.5	1.27
	1.497	0.182	0.298	23.05		58.6	1.42
	1.490	0.182	0.300	22.3		57.0	1.38
	1.497	0.180	0.281	22.35		56.9	1.37
Grumman, 4/18/28, 180°F	1.504	0.186	0.251	10.1	21.8	25.6	1.17
	1.514	0.186	0.236	10.85		27.3	1.25
	1.503	0.187	0.249	10.0		25.3	1.16
Grumman, 4/1/12, R.T.	0.5	0.125	0.080	1.91	31.5	42.8	1.36
	0.5	0.125	0.080	1.84		41.2	1.31
Grumman, 8/8/16, R.T.	3.0	0.376	0.168	19.5	28.2	38.7	1.37
	3.0	0.376	0.168	21.25		42.2	1.50
	3.0	0.376	0.168	18.8		37.3	1.32
Grumman, 8/8/16, R.T.	3.0	0.501	0.168	19.0	25.8	37.7	1.46
	3.0	0.501	0.168	18.7		37.1	1.44
	3.0	0.501	0.168	20.95		41.6	1.61
Grumman, 2/2/32, R.T.	1.25	0.2	0.189	6.43	18.0	27.2	1.51
	1.25	0.2	0.189	6.39		27.0	1.50
	1.25	0.2	0.189	6.0		25.4	1.41
Grumman, 8/2/20, R.T.	1.25	0.2	0.158	7.83	33.7	39.8	1.18
	1.25	0.2	0.158	7.71		39.2	1.16
	1.25	0.2	0.158	7.91		40.2	1.19
Grumman, 2/8/20, R.T.	1.25	0.2	0.158	4.76	21.4	24.2	1.13
	1.25	0.2	0.158	4.86		24.7	1.15
	1.25	0.2	0.158	4.86		24.7	1.15
Grumman, 18/4/28, -67°F	1.497	0.187	0.302	20.0	41.40	50.9	1.229
	1.515	0.188	0.252	16.8		42.2	1.020
Grumman, 4/18/28, -67°F	1.502	0.186	0.248	8.72	21.85	22.1	1.012
	1.513	0.186	0.245	9.04		22.9	1.042
	1.514	0.188	0.251	9.64		24.9	1.110

37 Tests Mean Ratio = 1.284
Std. Dev. = 0.148

∴ "B" Level Allowable = $(1.284 - 1.732 \times 0.148) 76,000 = 78,000$ psi

NOTE: F_{Pred} is based on a layer strength of 76,000 psi appropriate to a 5/16" diameter open hole and a specimen width/hole diameter = 6.

Corrections for hole size and W/D are given in CTN-75.1

W = Specimen width
D = Hole Diameter
t = Specimen thickness
P = Failing Load

● **Stress Distribution Around a Hole in an Anisotropic Laminate** - The use of a constant layer allowable in the above is a simplification; in actual fact the allowable strength will vary with the stress concentration in the critical layer at the hole, and the die-away of the stress away from the hole (Ref. 1). In order to approach this problem, the Savin differential equation (Ref. 2) has been programmed to give the stress distribution in the region of a hole in an infinite anisotropic plate which is subjected to an axial tensile stress. The COMHOL program considers an elliptical hole, with the circular hole as a limiting case. The laminate stresses and the layer stresses around the hole boundary, as well as the die away of the maximum laminate tangential stress away from the hole, are calculated.

Some preliminary results from this program are shown in Figure 120. The laminate stress concentration at the hole, measured tangentially to the β direction, is plotted against the percentage of the β plies and shows the expected increase in stress concentration with percentage. Also plotted is the die-away of the stress concentration with distance from the hole, measured normal to the β direction. There is no significant difference in the results for the orthotropic ($\beta = 0^\circ$) laminate and the anisotropic ($\beta = 15^\circ$) laminate, leading to the conclusion that the design allowable stresses for the orthotropic laminate may be applied to the anisotropic laminate. The allowable stresses for graphite/epoxy laminates given in Reference 3 can therefore be used.

5.1.3.3 Increased Tensile Allowables

The possibility of using an increased allowable stress for the wing lower cover has been examined. The current allowable layer longitudinal stress is 76,000 psi, which represents a "far field" allowable that accounts for the presence of an open hole within the field. If bolt holes in the lower cover can be eliminated by the "stitching" concept (discussed in Subsection 5.4.2) then the only holes to be accounted for would arise from battle damage. Since the cover need carry only 1.25 x limit load with such damage, the layer allowable could be increased to 91,000 psi. This would save approximately 100 lb per vehicle. If, in addition, crack arresters could be used in the cover, in the form of 0.25-in. wide strips of glass fiber in each layer, then the fiber allowable could be increased to the full unnotched layer allowable of 169,000 psi. This would save approximately 198 lb per vehicle.

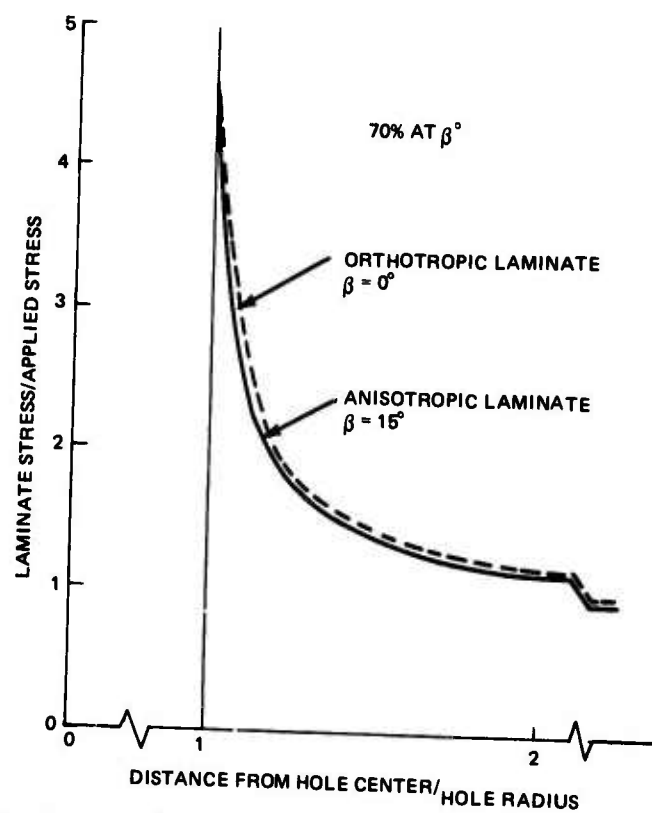
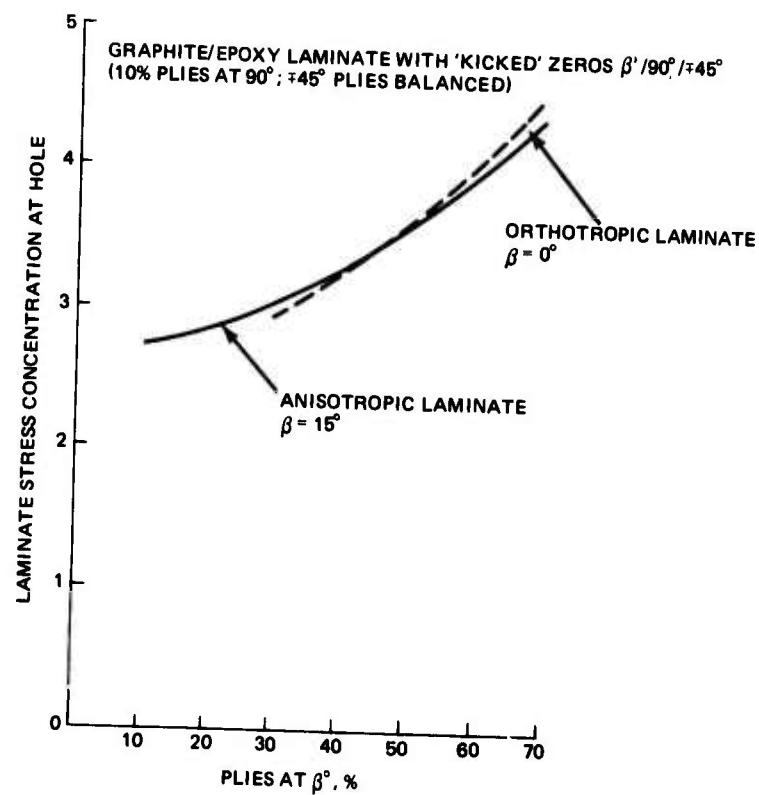


Figure 120. Stress Concentration And Die-Away For Anisotropic Laminata With Circular Hole

5.1.4 Hardware Selection

The selection of hardware to be utilized in composite components involves unique design considerations. These considerations include:

- Galvanic corrosion effects
- Reduced fastener pull-through capability
- Fastener installation forces.

Previous programs have demonstrated that potentially severe and expensive galvanic corrosion problems can be eliminated by restricting hardware utilized in graphite/epoxy to fasteners made of titanium, A286 stainless steel, and monel. During the past ten years titanium hardware utilization has increased, so that today, titanium hardware is available in nearly all common configurations and sizes including repair hardware.

Because of the fastener pull-through capability, tension head fasteners should always be used in composite components even when the primary loading is in shear. The manufactured head, (nut side) of the fastener is also important in this regard, particularly in the case of blind fasteners. The conventional blind fastener is installed and produces the required pull-up load by expanding the shank either by forcing in an oversized mandrel or by locally failing the shank in compression. Both of these techniques produce an undesirable result in that the manufactured head of the fastener does not sit flush against the composite surface. Because of this, and the bulbous shape of the manufactured head, under a tension load the head acts as a wedge and greatly reduces the tension capability of the joint. In addition, the installation forces of the fastener shank expanding, produce very high bearing loads against the edge of the fastener hole locally crushing the composite.

The only blind fastener currently available that overcomes these difficulties is the Jo-Bolt. This fastener is locked in place by expansion of a sleeve over the shank. This sleeve sits square and flush against the composite surface and does not produce any radial loads on the edge of the hole. However, the small thickness of this expanded sleeve results in a very small footprint which reduces the pull through capability. Development work is necessary to provide a blind fastener for use in composites that overcomes the above mentioned problem, while at the same time providing an increased footprint.

5.1.5 Integral Fuel Tank Sealing Concepts

Use of the aircraft structure as a fuel tank is an exceptionally weight efficient method of containment, because it eliminates the need for the additional weight associated

with bladder tanks. While this method does save weight, it does make sealing more difficult. Figure 121 shows three potential sealing concepts for application on the ADCA. The first two make use of the channel seal groove method and the last of the faying surface seal. Both methods are used on current military aircraft. The channel groove sealing method has as its main advantages simple resealability through further injection and minimum sealant weight. The advantages of the faying surface/fillet sealing method are the need for only a single row of fasteners, when structurally adequate, and less expensive initial cost.

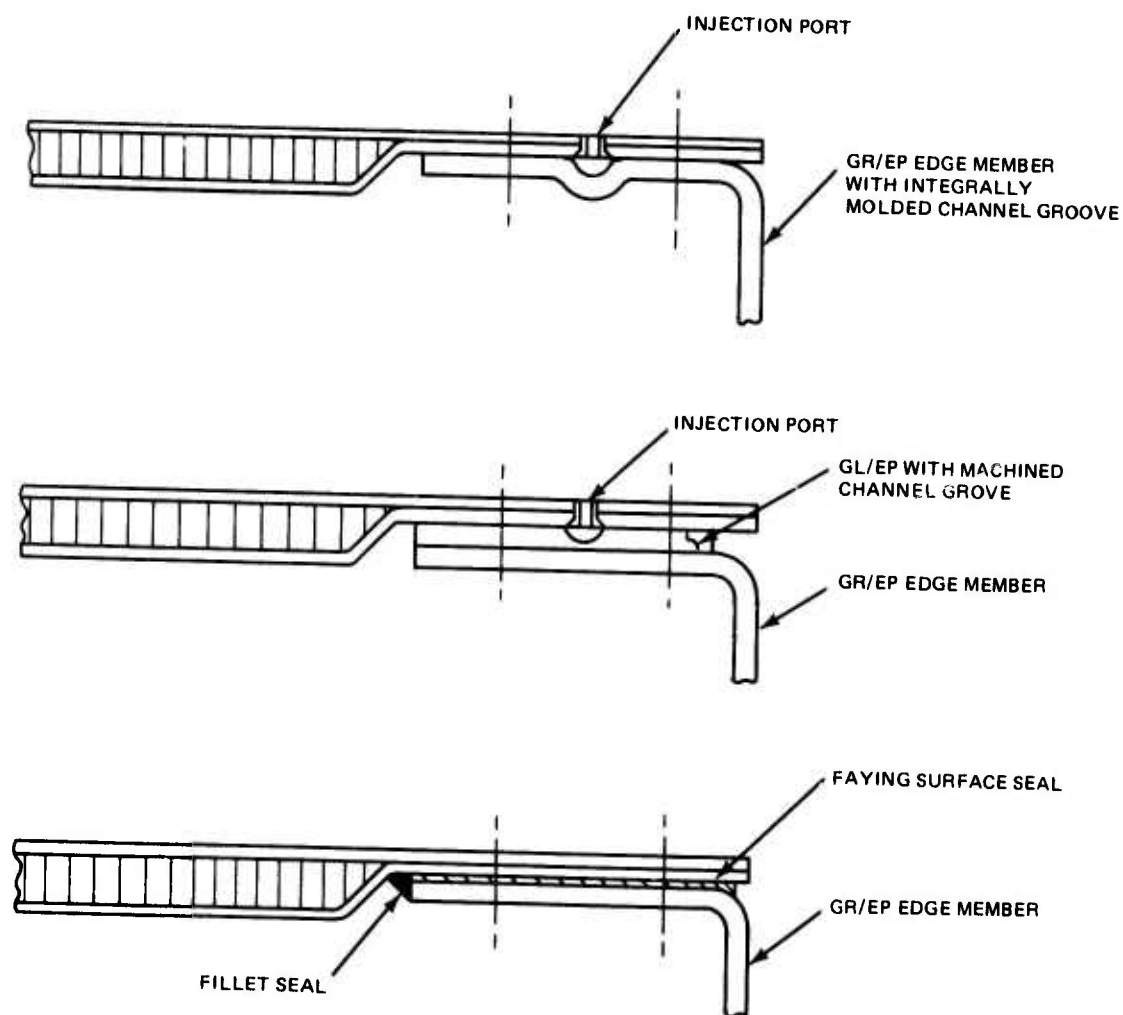


Figure 121. Integral Fuel Tank Sealing Concepts

An advanced sealing concept, shown in Figure 122, uses a thermoplastic adhesive as the sealing agent. It is also the intent of this concept to utilize the adhesive as a shimming material, simplifying box assembly operation. Softening of the adhesive would be accomplished by application of local ultrasonic energy, as would resoftening of the adhesive if local resealing or skin removal for major structural repair were required.

5.1.6 Radar Characteristics

Tests were performed at Grumman to determine the reflectivity, absorption and transmission characteristics of hybrid (boron graphite) composite material at different radio frequencies. Measurements at S, C, X and K-band frequencies for horizontally and vertically polarized energy on composite samples of different sizes, shapes and thicknesses

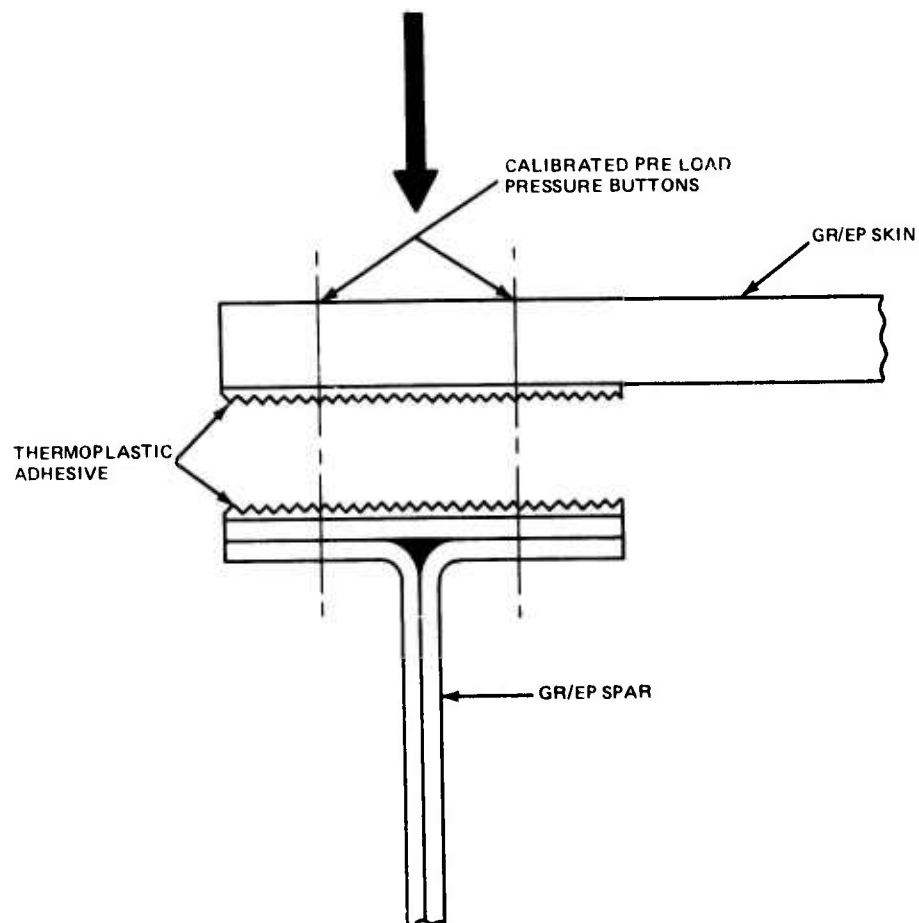


Figure 122. Advanced Sealing Concept

indicated that the reflectivity of composite material is on average about 1 db lower than that of metallic materials. In essence, the use of hybrid composite material will result in only a slight reduction in radar cross section signature when compared to metal aircraft. The slight difference between the composite and metals will neither increase or reduce radar cross section. Transmission of radar energy through graphite or hybride graphite/boron epoxy composite material is nil.

Since the aircraft skin material acts as the antenna ground plane for on-board communications, navigations and countermeasures antenna, tests were conducted at Grumman to determine if composite materials acting as the antenna ground plane would have any adverse effect on the shape or patterns of those antennas. The results of the tests indicated that patterns taken over metal and composite ground planes were in close agreement. Tilt of antenna lobes were the same; shape and width of lobes are similar and peaks of lobes are within 1 db of each other. In essence, a hybrid composite ground plane will influence radiation patterns of antennas mounted on them in much the same manner as a metallic ground plane.

5.1.7 Design/Manufacturing Interface

To achieve a low cost, efficient composite structure a strong design/manufacturing interface must exist from design inception. The intent of this interfacing, between design, tooling, manufacturing and quality control, is to determine the individual discipline requirements, capabilities and limitations and then to compromise as necessary, to achieve the maximum program benefits.

5.2 LOADS AND CRITERIA

5.2.1 Preliminary Design Loads Estimates

At each stage of the ADCA design cycle, design loads appropriate to that level were defined. As a starting point for the structural design, "worst case" airloads were estimated for the wing, canard, fin and fuselage. These loads provided the preliminary strength requirements for each surface design.

A symmetric maneuver, $N_z = 6.5$, condition was considered for the definition of the preliminary "worst case" wing loads. The effect of the canard downwash in re-distributing lift was taken into account. A lifting surface method programmed for a digital computer was used to obtain the spanwise and chordwise distributions of lift. The ultimate shear, bending moment and torsion loads are shown in Figure 123.

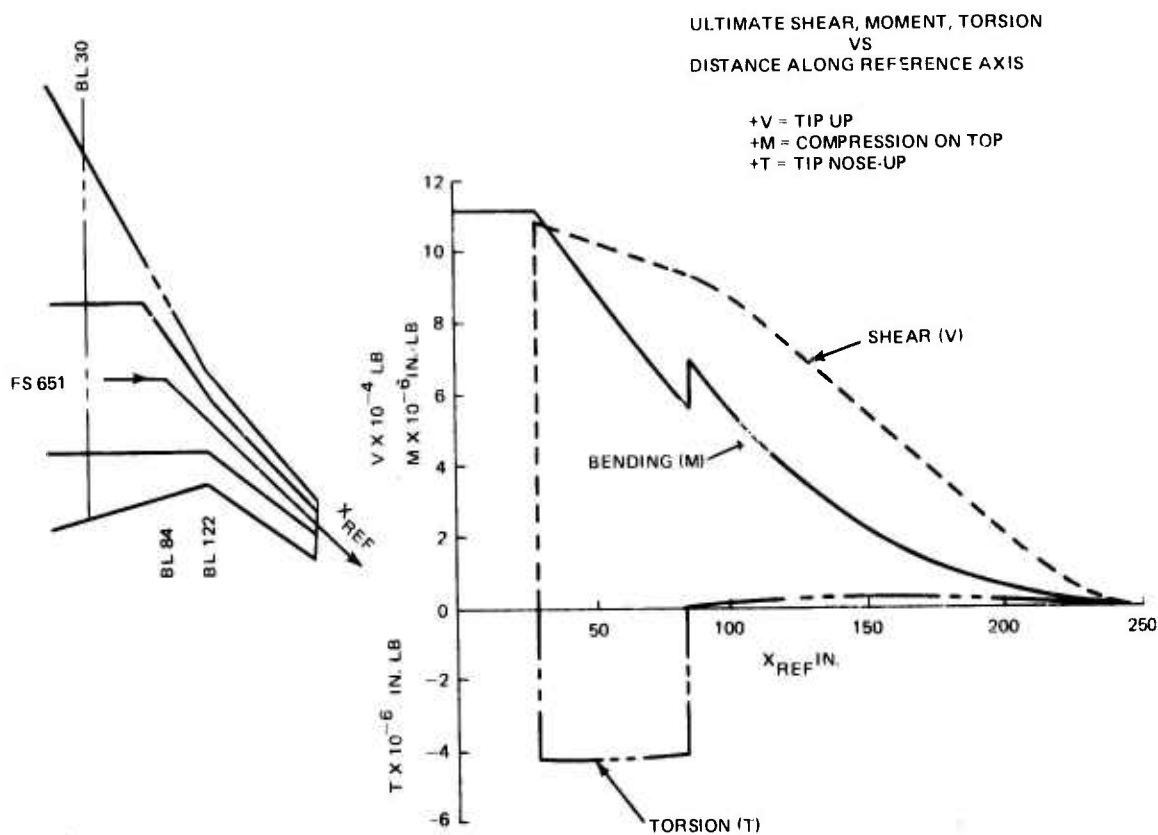


Figure 123. ADCA Wing Loads

The "worst case" canard design loads were derived for an $N_z = 5.2$ rolling maneuver. Because the canards are used to roll the vehicle, this is more critical than an $N_z = 6.5$ symmetric maneuver. Estimates were made of the rolling acceleration needed for suitable maneuverability and the antisymmetrical portion of the load was calculated to obtain that rolling acceleration. The load distributions were again obtained using lifting surface methods. A summary of the limit airloads, shear, bending moment and torsion are shown in Figure 124.

The preliminary "worst case" fin loads were based on the empirical fact that the tail load on fighters usually approaches but does not exceed the weight of the aircraft. This value of tail load was, therefore, assumed and distributed using lifting surface theory. Two chordwise center of pressure locations were used to allow for rudder effects. Figure 125 shows the resulting swept limit air loads.

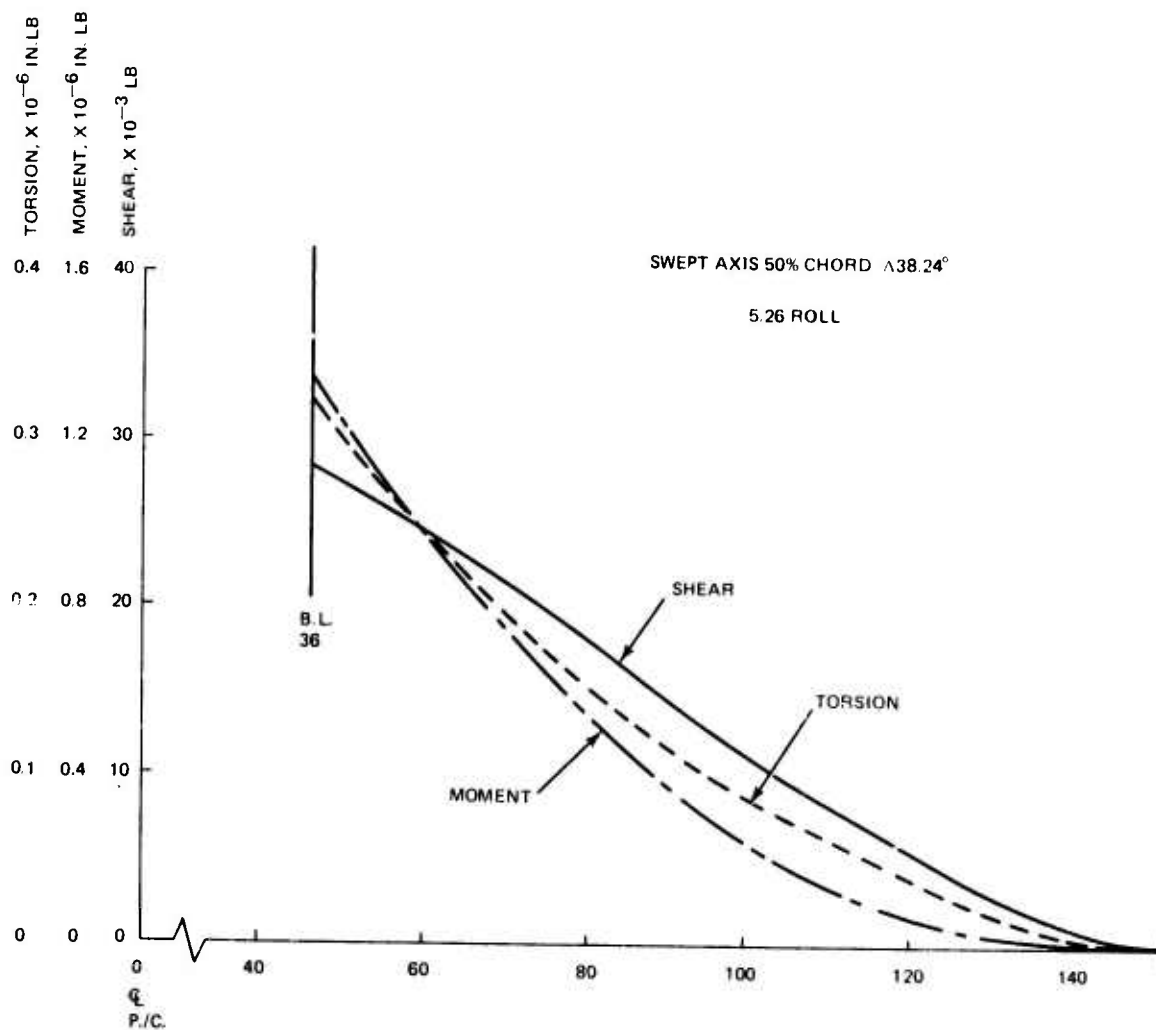


Figure 124. ADCA Canard Swept Air Loads (Limit)

Preliminary fuselage airloads were calculated for two symmetrical maneuvers at the flight design gross weight of 34,965 lb for a limit load factor of 6.5g. Two different overall aircraft center-of-pressure positions were used to allow for uncertainties in the estimated aerodynamic data. The two positions used represent conditions which maximize aerodynamic loads on different parts of the fuselage. The effects of carry-over loads from the wings and canards are included as is the lift of the fuselage itself.

Ultimate net fuselage loads were calculated for the two conditions by combining the canard, wing, and fuselage airloads with the distributed inertia for the flight design gross

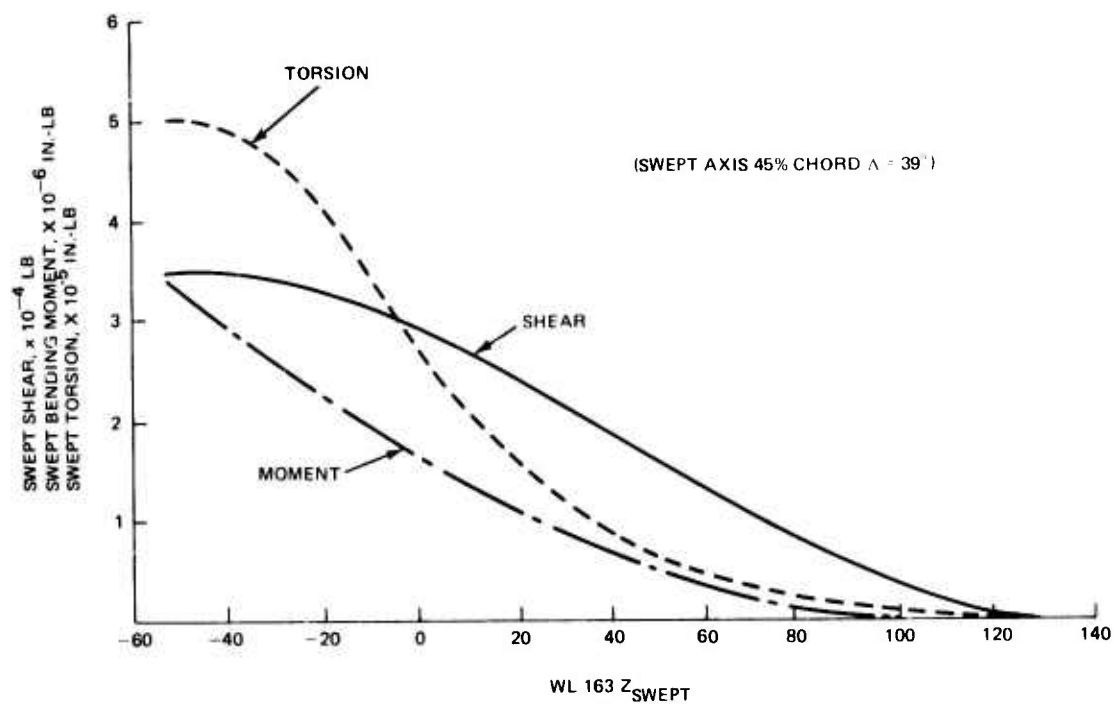


Figure 125. ADCA Vertical Tail Swept Air Loads (Limit)

weight and multiplying by the ultimate factor of 1.50. The ultimate net fuselage vertical shear and bending moment are presented in Figures 126 and 127, respectively. The limit airloads for the two conditions are summarized in Table 21 below.

TABLE 21. LIMIT AIR LOADS (LBS.)

Component	Condition 1	Condition 2
Wing (2 Sides)	158,170	140,170
Canard (2 Sides)	1,204	32,280
Fuselage	67,898	54,822

Condition 2, which has the most forward wing center-of-pressure, imposes the highest shear and bending on the forward fuselage and the maximum shear just forward of the wing front beam attachment point. The critical aft fuselage shear and bending occurs in Condition 1, which has the most aft wing center-of-pressure.

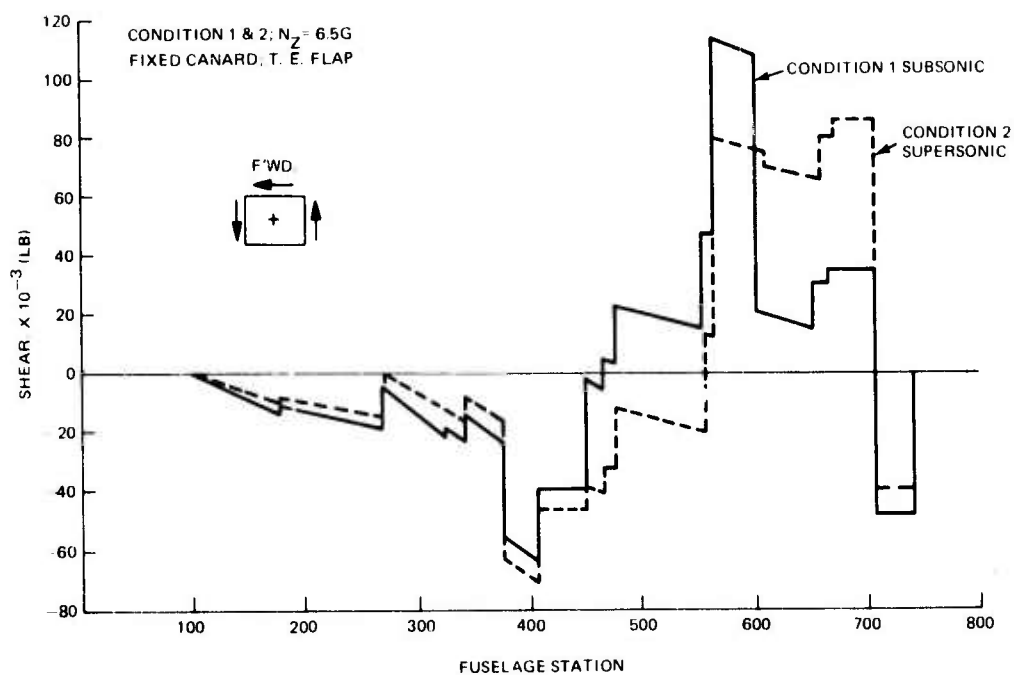


Figure 126. Design 105A, Ultimate Vertical Shear Fuselage

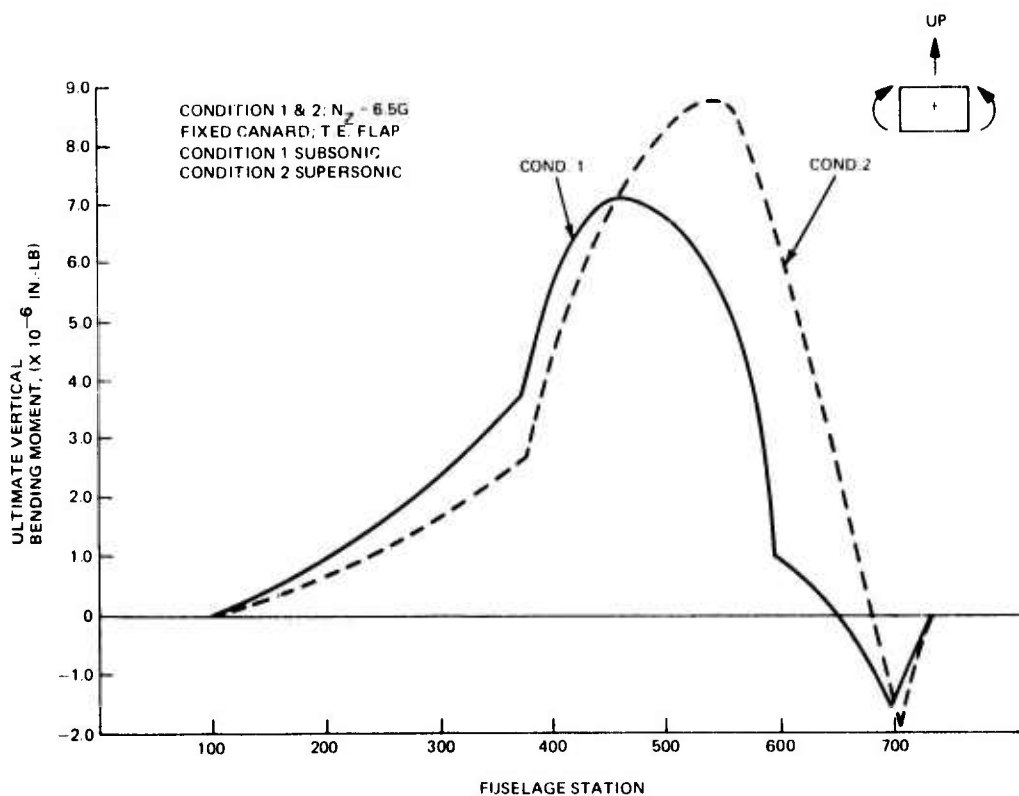


Figure 127. Design 105A, Ultimate Vertical Bending Moment Fuselage

5.2.2 Aeroelastic Effects

The "worst case" loads for the wing, canard and fin were used in conjunction with stiffness and twist requirements to define the preliminary cover and substructure designs for each surface. Beam type idealizations were formulated for each surface and the structural flexibility influence coefficients calculated. The effective canard actuator pitch spring as well as the rudder rotational spring were properly represented. The effect of the structural flexibility on the component load distributions was then considered.

The aeroelastic corrections to the rigid force and moment coefficient data for the wing, canard, inboard and outboard flaperons, vertical tail, rudder, and certain damping terms are given in Figures 128 through 150. The results are presented in the form of flexible to rigid aerodynamic derivative ratios (η) for each coefficient. Moment data is referenced to a nominal flight design gross weight center-of-gravity position as noted on the figures. The equations below demonstrate the relationship of the flexible component data to the rigid component data.

Aircraft Angle of Attack, α :

$$C_{L\alpha}^{TOTAL FLEX} = \eta_{L\alpha W} C_{L\alpha W} + \eta_{L\alpha C} [C_{L\alpha}^{TOTAL} - C_{L\alpha W} - C_{L\alpha B}^{RIGID}] + C_{L\alpha B}^{RIGID}$$

$$C_{m\alpha}^{TOTAL FLEX} = \eta_{m\alpha W} C_{m\alpha W} + \eta_{m\alpha C} [C_{m\alpha}^{TOTAL} - C_{m\alpha W} - C_{m\alpha B}^{RIGID}] + C_{m\alpha B}^{RIGID}$$

Canard Deflection, δ_c :

$$C_{L\delta_c(SYM)}^{FLEX} = \eta_{L\delta_c} C_{L\delta_c(SYM)}^{RIGID}$$

$$C_{m\delta_c(SYM)}^{FLEX} = \eta_{m\delta_c} C_{m\delta_c(SYM)}^{RIGID}$$

$$C_{L\delta_c(ANTISYM)}^{FLEX} = \eta_{L\delta_c(ANTISYM)} C_{L\delta_c(ANTISYM)}^{RIGID}$$

$$C_{m\delta_c(ANTISYM)}^{FLEX} = \eta_{m\delta_c(ANTISYM)} C_{m\delta_c(ANTISYM)}^{RIGID}$$

$$C_{l\delta_c(ANTISYM)}^{FLEX} = \eta_{l\delta_c(ANTISYM)} C_{l\delta_c(ANTISYM)}^{RIGID}$$

Inboard Flaperon Deflection, $\delta_{FI/B}$:

$$C_{L\delta F I/B (SYM)}^{FLEX} = \eta_{L\delta F I/B (SYM)} C_{L\delta F I/B (SYM)}^{RIGID}$$

$$C_{m\delta F I/B (SYM)}^{FLEX} = \eta_{m\delta F I/B (SYM)} C_{m\delta F I/B (SYM)}^{RIGID}$$

$$C_{L\delta F I/B (ANTISYM)}^{FLEX} = \eta_{L\delta F I/B (ANTISYM)} C_{L\delta F I/B (ANTISYM)}^{RIGID}$$

$$C_{m\delta F I/B (ANTISYM)}^{FLEX} = \eta_{m\delta F I/B (ANTISYM)} C_{m\delta F I/B (ANTISYM)}^{RIGID}$$

$$C_{L\delta F I/B (ANTISYM)}^{FLEX} = \eta_{L\delta F I/B (ANTISYM)} C_{L\delta F I/B (ANTISYM)}^{RIGID}$$

Outboard Flaperon Deflection, $\delta_{FO/B}$:

$$C_{L\delta F O/B (SYM)}^{FLEX} = \eta_{L\delta F O/B (SYM)} C_{L\delta F O/B (SYM)}^{RIGID}$$

$$C_{m\delta F O/B (SYM)}^{FLEX} = \eta_{m\delta F O/B (SYM)} C_{m\delta F O/B (SYM)}^{RIGID}$$

$$C_{L\delta F O/B (ANTISYM)}^{FLEX} = \eta_{L\delta F O/B (ANTISYM)} C_{L\delta F O/B (ANTISYM)}^{RIGID}$$

$$C_{m\delta F O/B (ANTISYM)}^{FLEX} = \eta_{m\delta F O/B (ANTISYM)} C_{m\delta F O/B (ANTISYM)}^{RIGID}$$

$$C_{L\delta F O/B (ANTISYM)}^{FLEX} = \eta_{L\delta F O/B (ANTISYM)} C_{L\delta F O/B (ANTISYM)}^{RIGID}$$

Sideslip Angle, β :

$$C_{Y\beta A/P}^{FLEX} = \eta_{Y\beta VT} C_{Y\beta VT}^{RIGID} + (C_{Y\beta A/P}^{RIGID} - C_{Y\beta VT}^{RIGID})$$

$$C_{L\beta A/P}^{FLEX} = \eta_{L\beta VT} C_{L\beta VT}^{RIGID} + (C_{L\beta A/P}^{RIGID} - C_{L\beta VT}^{RIGID})$$

$$C_{n\beta A/P}^{FLEX} = \eta_{n\beta VT} C_{n\beta VT}^{RIGID} + (C_{n\beta A/P}^{RIGID} - C_{n\beta VT}^{RIGID})$$

Rudder Deflection, δ_R :

$$C_{Y\delta R}^{FLEX} = \eta_{Y\delta R} C_{Y\delta R}^{RIGID}$$

$$C_{L\delta R}^{FLEX} = \eta_{L\delta R} C_{L\delta R}^{RIGID}$$

$$C_{n\delta R}^{FLEX} = \eta_{n\delta R} C_{n\delta R}^{RIGID}$$

Yaw Damping, $\frac{r_b}{2V}$:

$$C_{Y_{rVT}}^{FLEX} = \eta_{Y_{rVT}} C_{Y_{rVT}}^{RIGID}$$

$$C_{Z_{rVT}}^{FLEX} = \eta_{Z_{rVT}} C_{Z_{rVT}}^{RIGID}$$

$$C_{N_{rVT}}^{FLEX} = \eta_{N_{rVT}} C_{N_{rVT}}^{RIGID}$$

Pitch Damping, $\frac{q_c}{2V}$:

$$C_{Lq}^{CANARD FLEX} = \eta_{Lq} C_{Lq}^{CANARD RIGID}$$

$$C_{mq}^{CANARD FLEX} = \eta_{mq} C_{mq}^{CANARD RIGID}$$

5.2.3 Aeroelastic Tailoring Benefits Evaluation (Wing)

As previously mentioned, the wing results presented in Figures 128 and 129 were developed for a beam-type structural idealization, where the objective of increased washout under load directly contributed to the laminate orientation selection. The number of layers was sized to meet strength and stiffness requirements. The 0° cover layers (those running parallel to the main load carrying axis) were then rotated 15° forward to increase the wing washout. Using this beam model as a base, a more refined finite element structural idealization was formulated. This finite element model was used for all subsequent aeroelastically corrected loads calculations.

The load distribution on the wing, resulting from an aerodynamically optimum twist at Mach 1.6 and an altitude of 50,000 ft for the cruise condition, was imposed on the finite element structural influence coefficient matrix to determine the flexible twist for that condition. The loading was based on an aircraft combat weight of 34,168 lb (TOGW less 50% fuel). The 1.0 g exposed wing airload per side was determined to be 9,406 lb acting at 0.557 c, (FS 661.792, and BL 109.471). The twist differential between the achieved and the optimum was defined to be the built-in twist. This built-in twist distribution of the wing box varied from +3.0° at the fuselage side to -1.2° at the tip. A similar load distribution, based upon aeroelastically optimum twist, was developed for the sustained-maneuver design point at Mach = 0.9, at an altitude of 30,000 ft, and a load factor of 3.32. The ex-

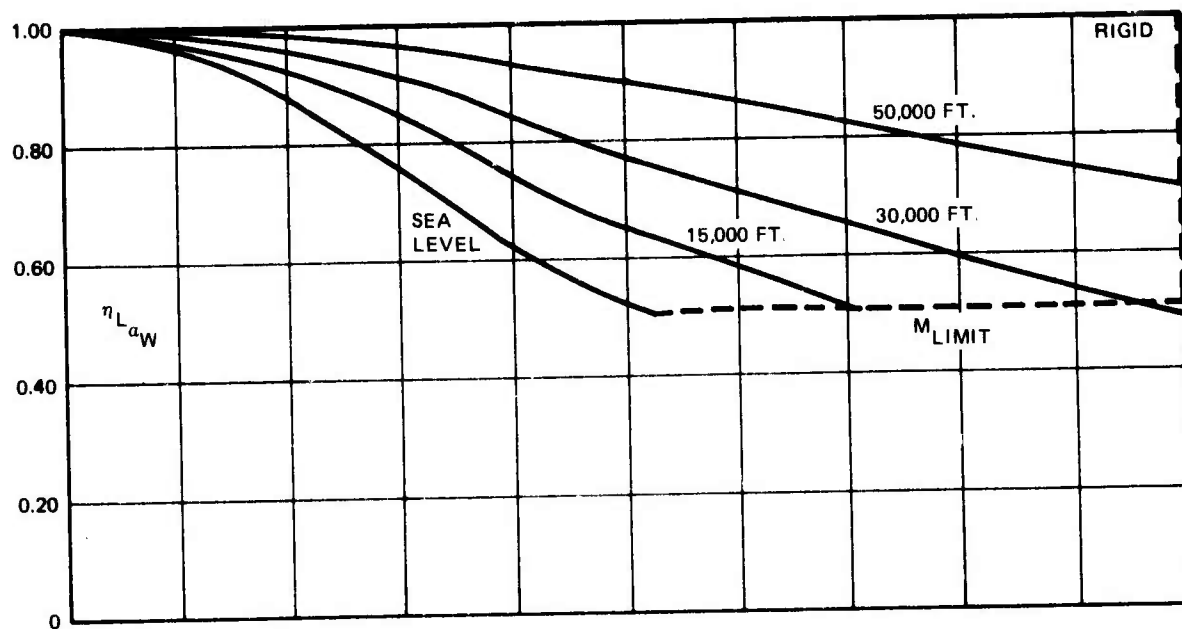


Figure 128. Flexibility Factor, Lift, Wing

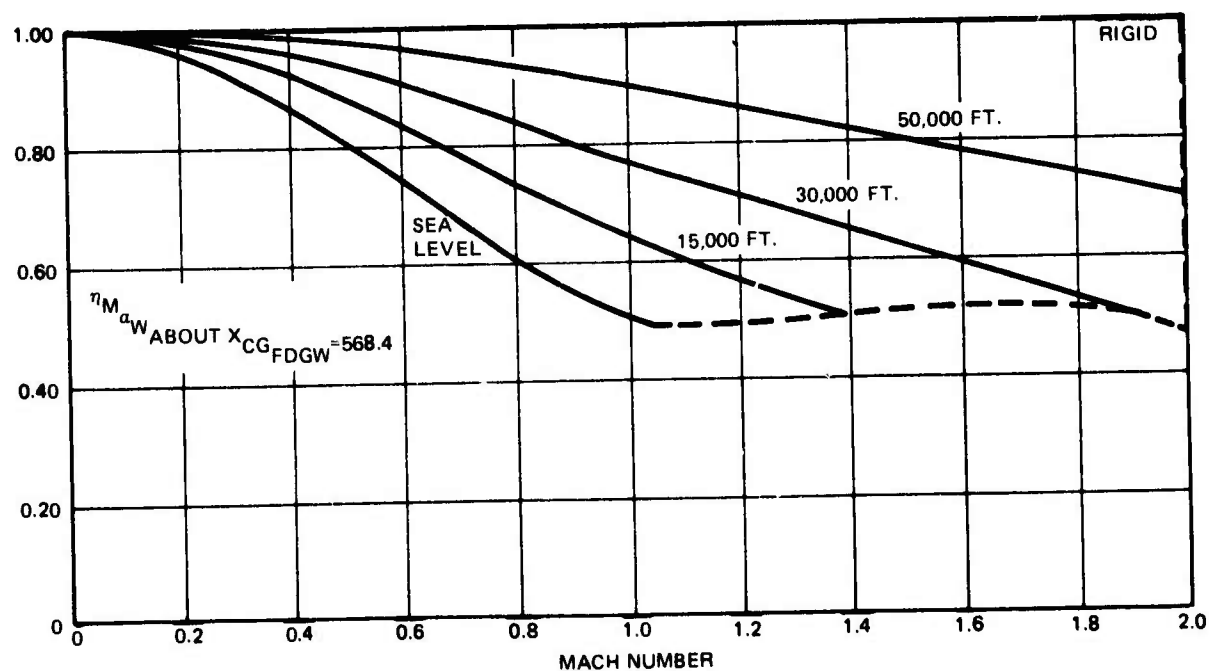


Figure 129. Flexibility Factor, Pitching Moment, Wing

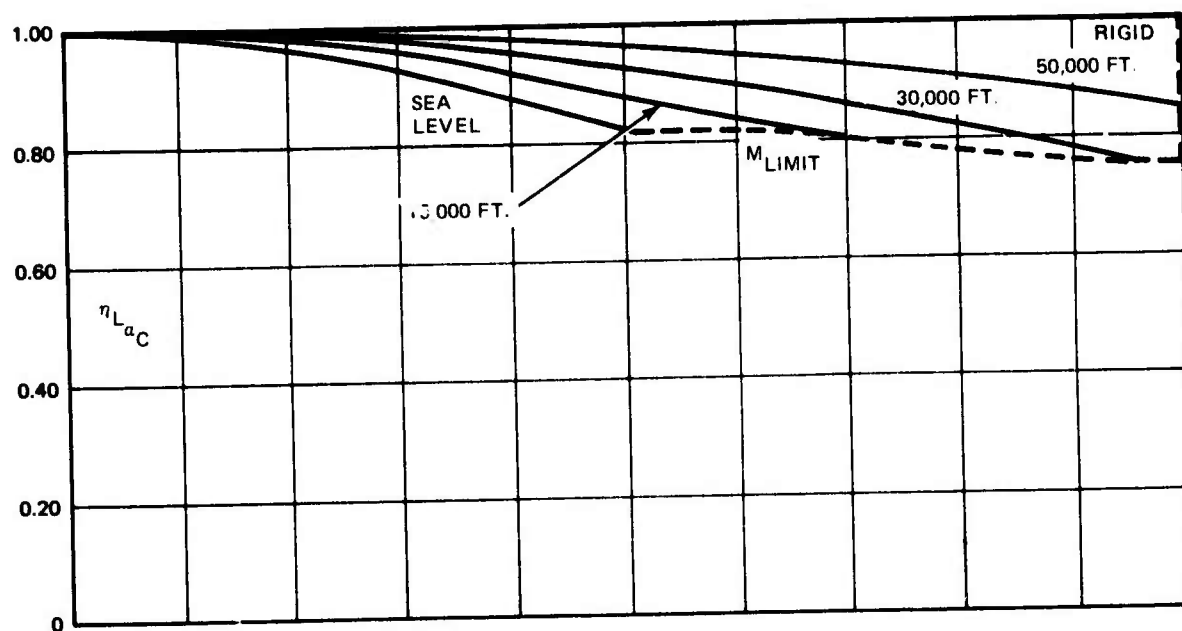


Figure 130. Flexibility Factor, Lift, Canard

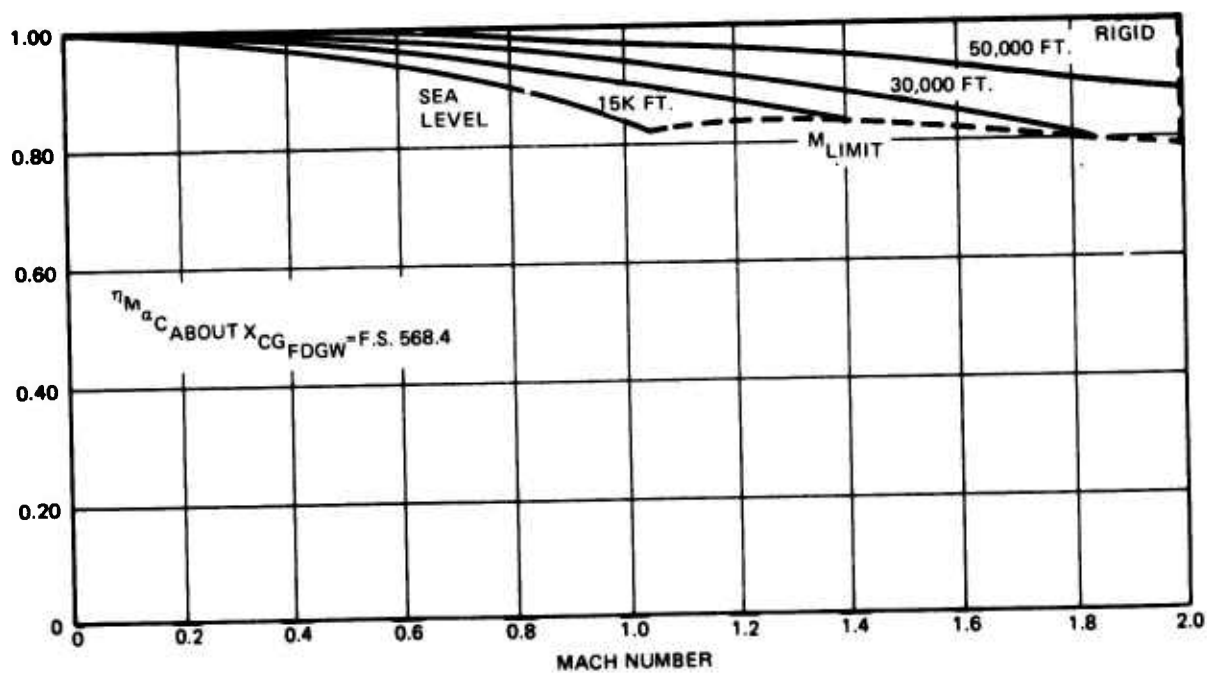


Figure 131. Flexibility Factor, Pitching Moment, Canard

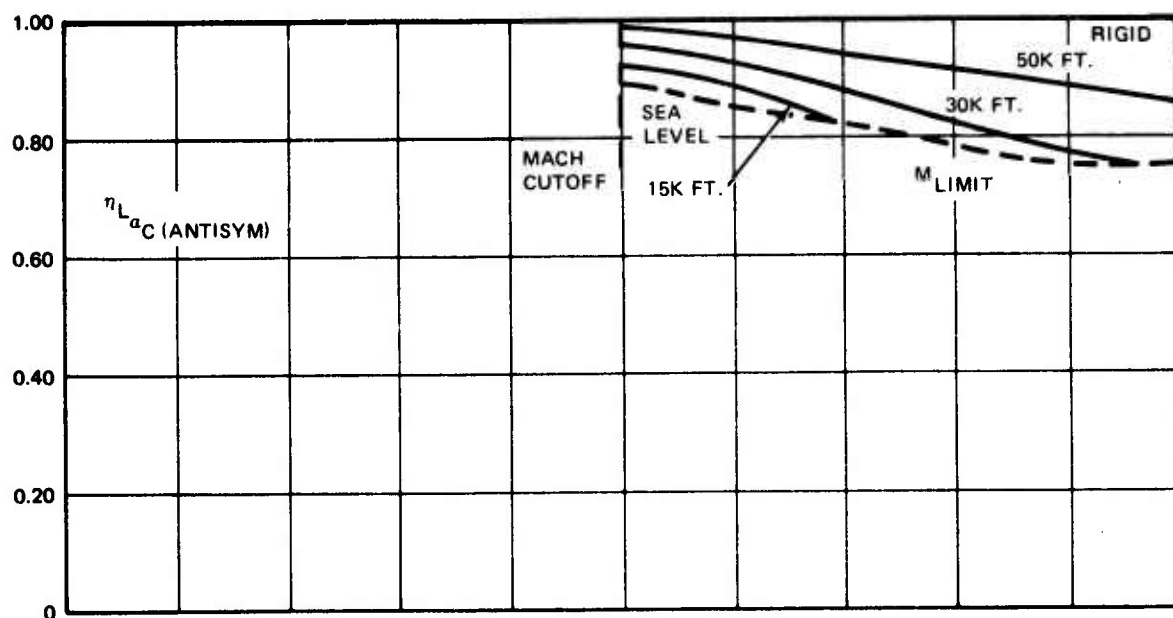


Figure 132. Flexibility Factor, Lift, Canard, Antisymmetric Deflection

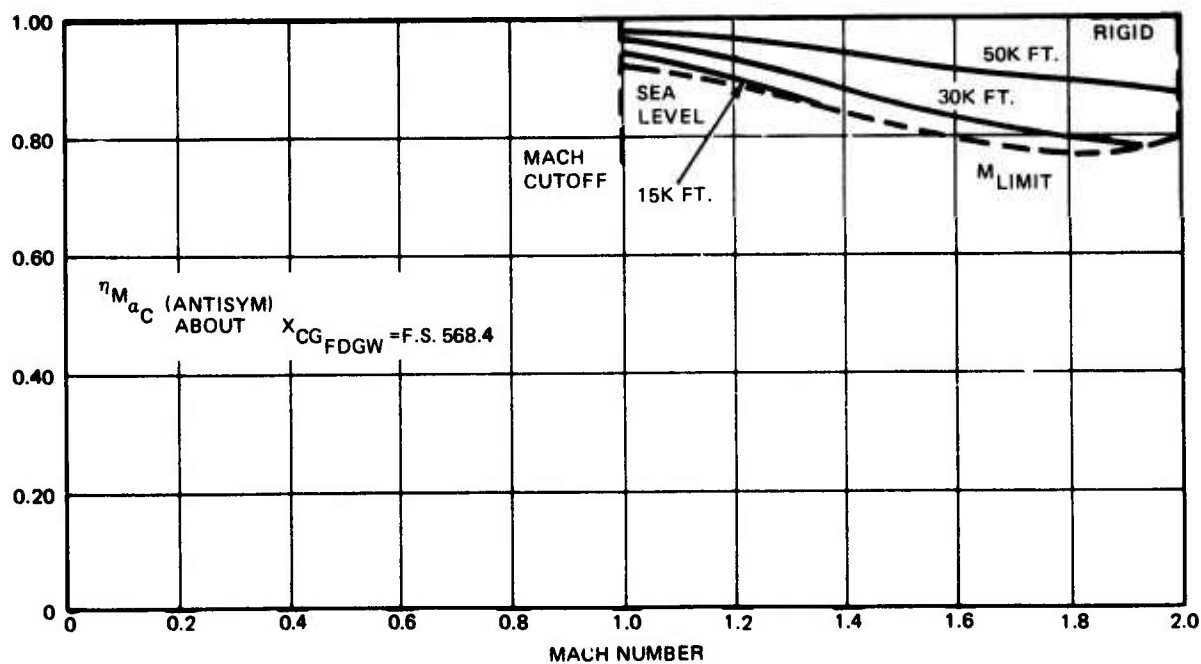


Figure 133. Flexibility Factor, Pitching Moment, Canard, Antisymmetric Deflection

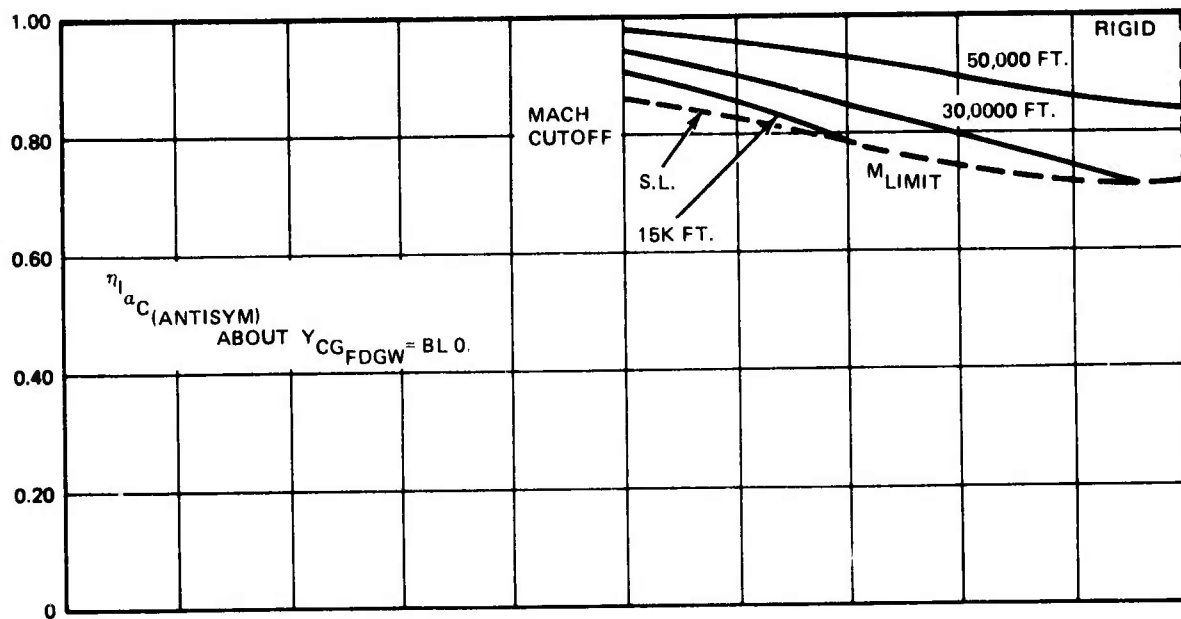


Figure 134. Flexibility Factor, Rolling Moment, Canard, Antisymmetric Deflection

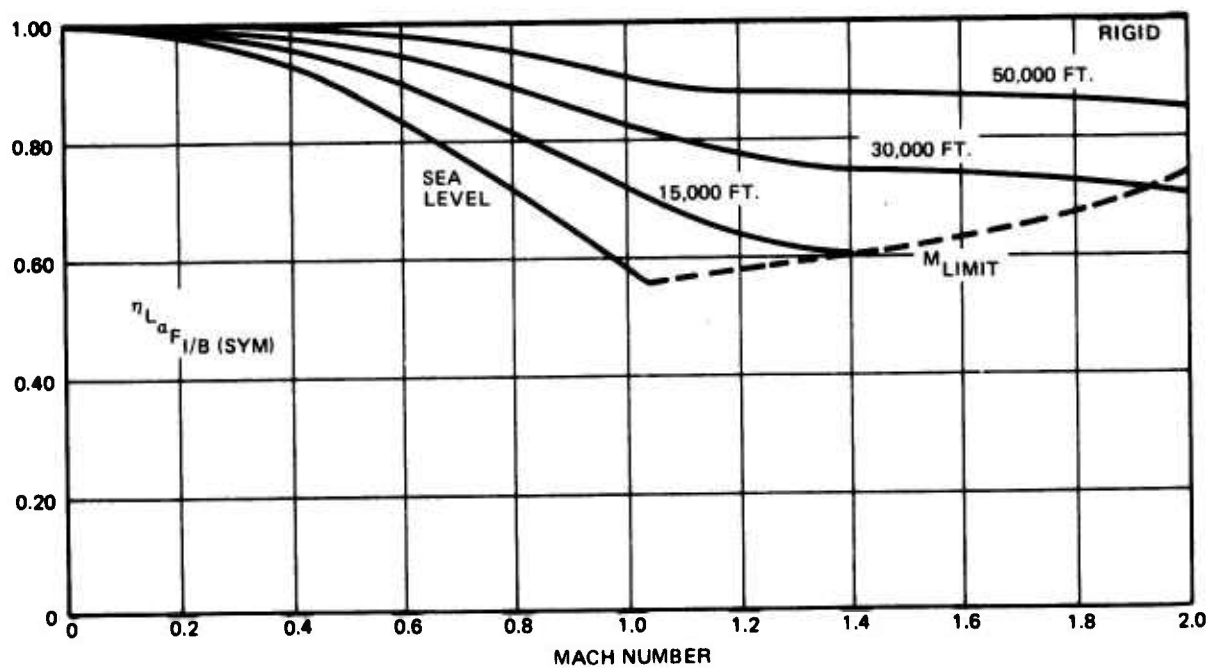


Figure 135. Flexibility Factor, Lift, Inboard Flaperon, Symmetric Deflection

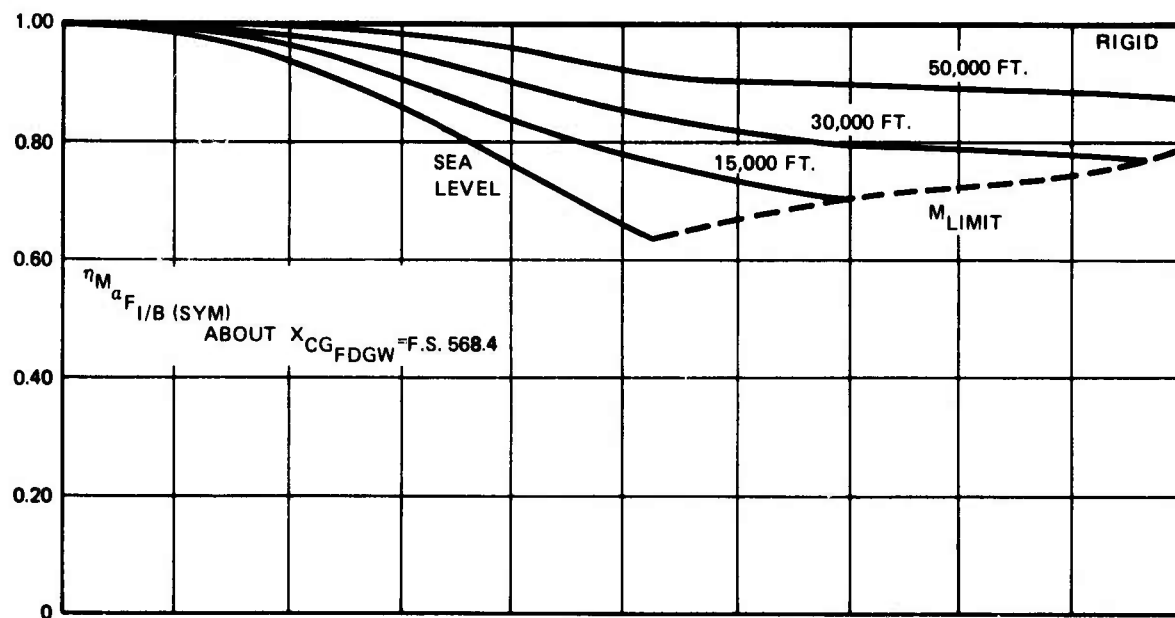


Figure 136. Flexibility Factor, Pitching Moment, Inboard Flaperon, Symmetric Deflection

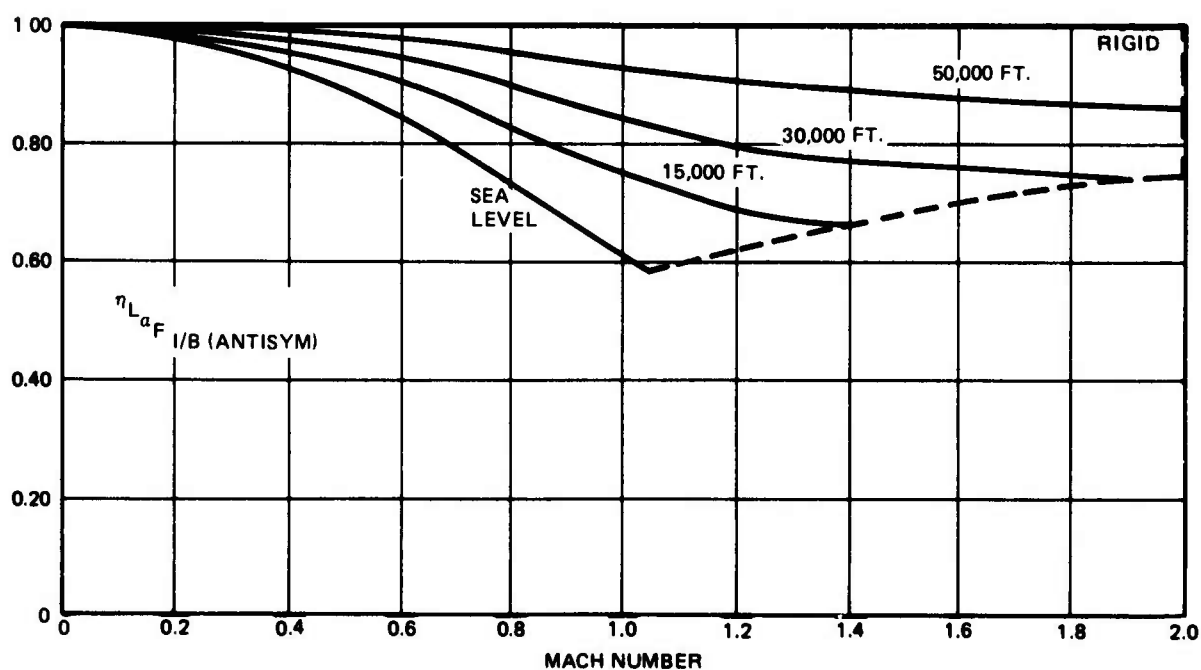


Figure 137. Flexibility Factor, Lift, Inboard Flaperon, Antisymmetric Deflection

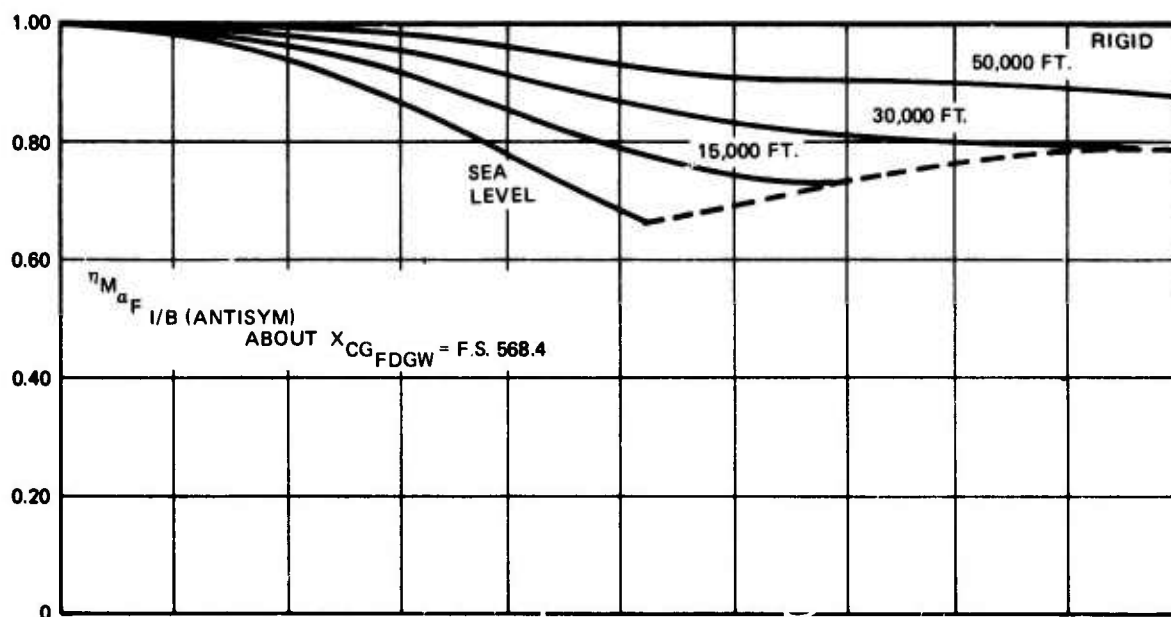


Figure 138. Flexibility Factor, Pitching Moment, Inboard Flaperon, Antisymmetric Deflection

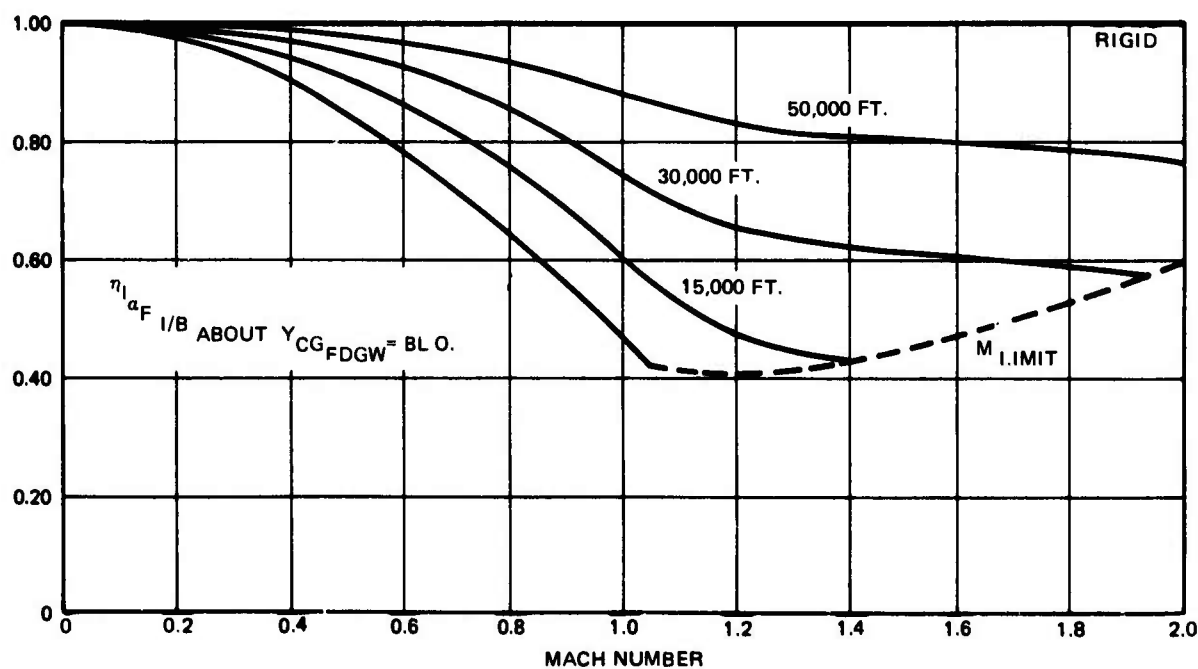


Figure 139. Flexibility Factor, Rolling Moment, Inboard Flaperon, Antisymmetric Deflection

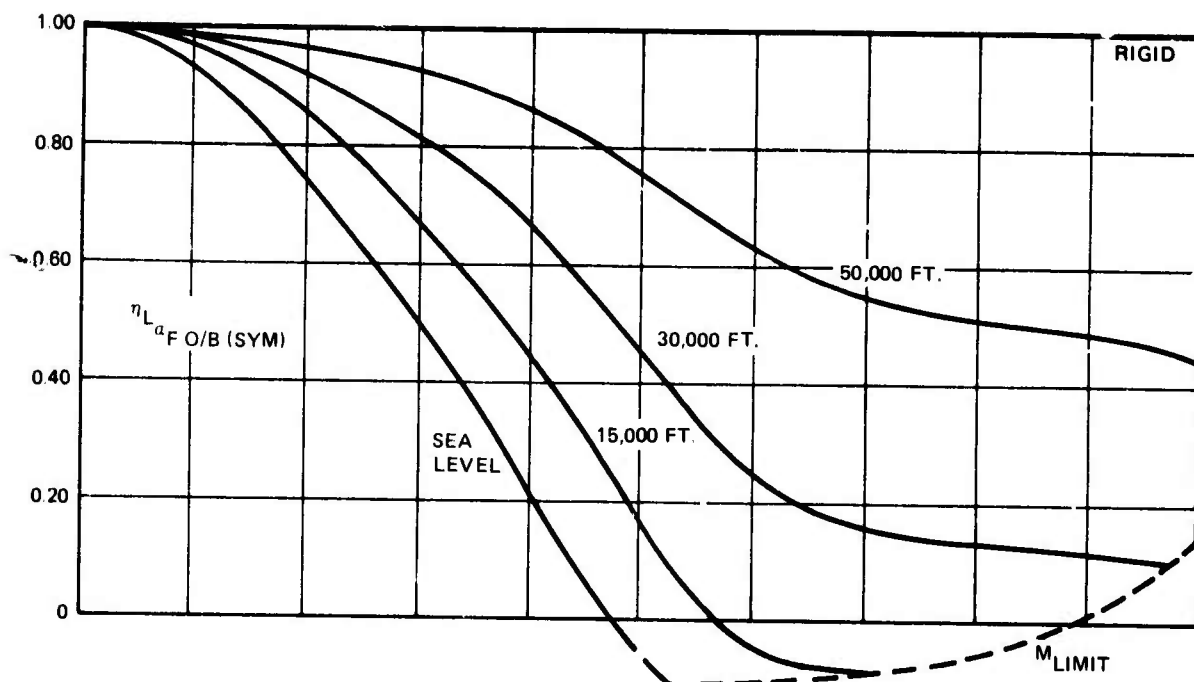


Figure 140. Flexibility Factor, Lift, Outboard Flaperon, Symmetric Deflection

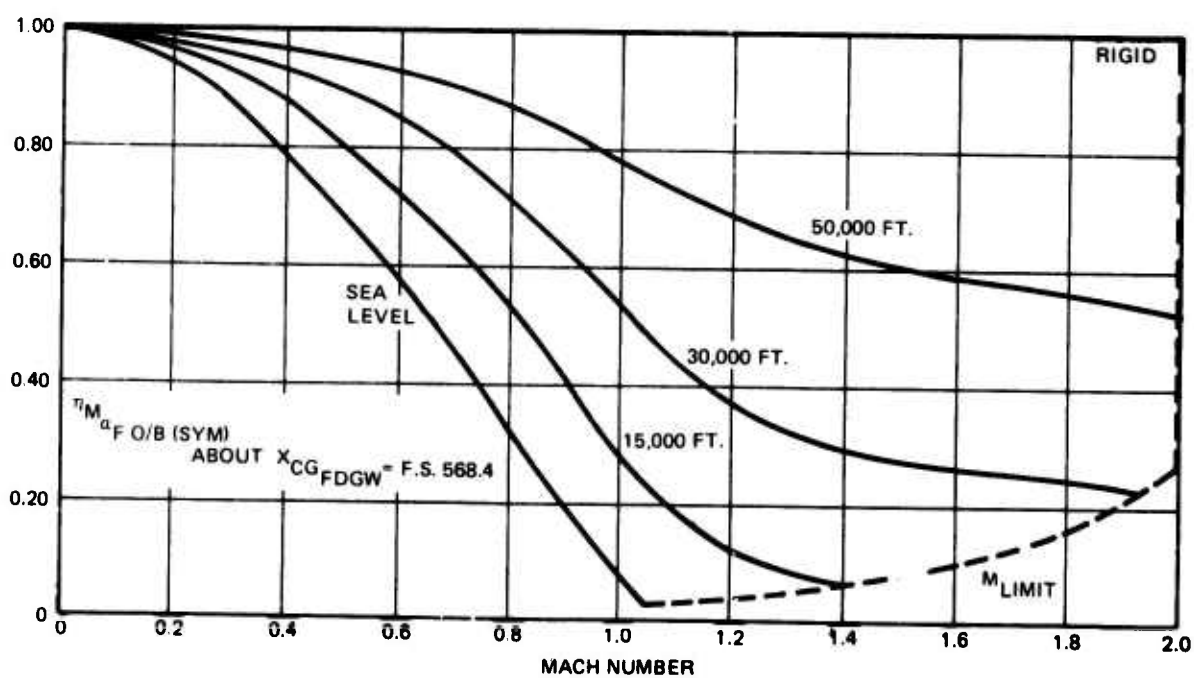


Figure 141. Flexibility Factor, Pitching Moment, Outboard Flaperon, Symmetric Deflection

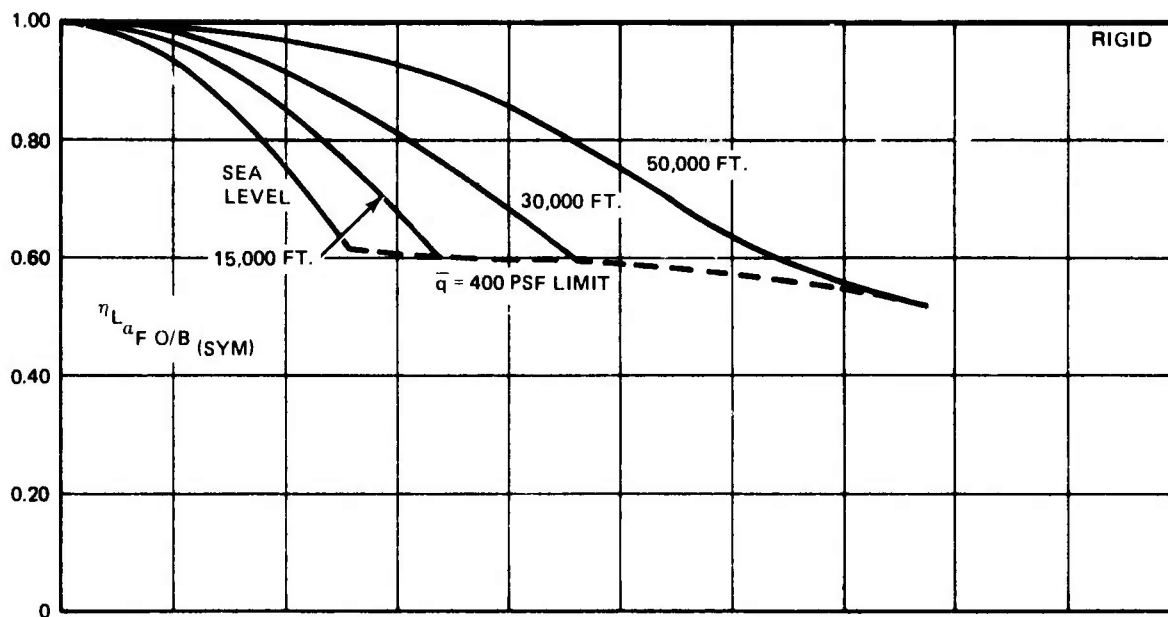


Figure 142. Flexibility Factor, Lift, Outboard Flaperon, Unsymmetric Deflection

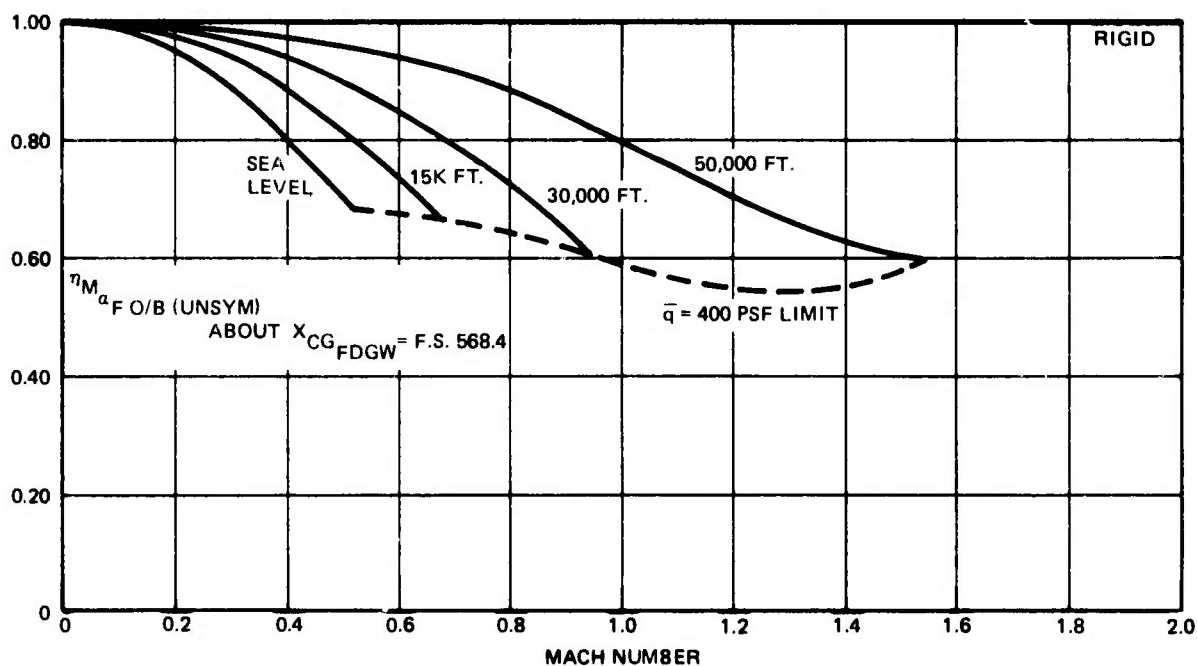


Figure 143. Flexibility Factor, Pitching Moment, Outboard Flaperon, Unsymmetric Deflection

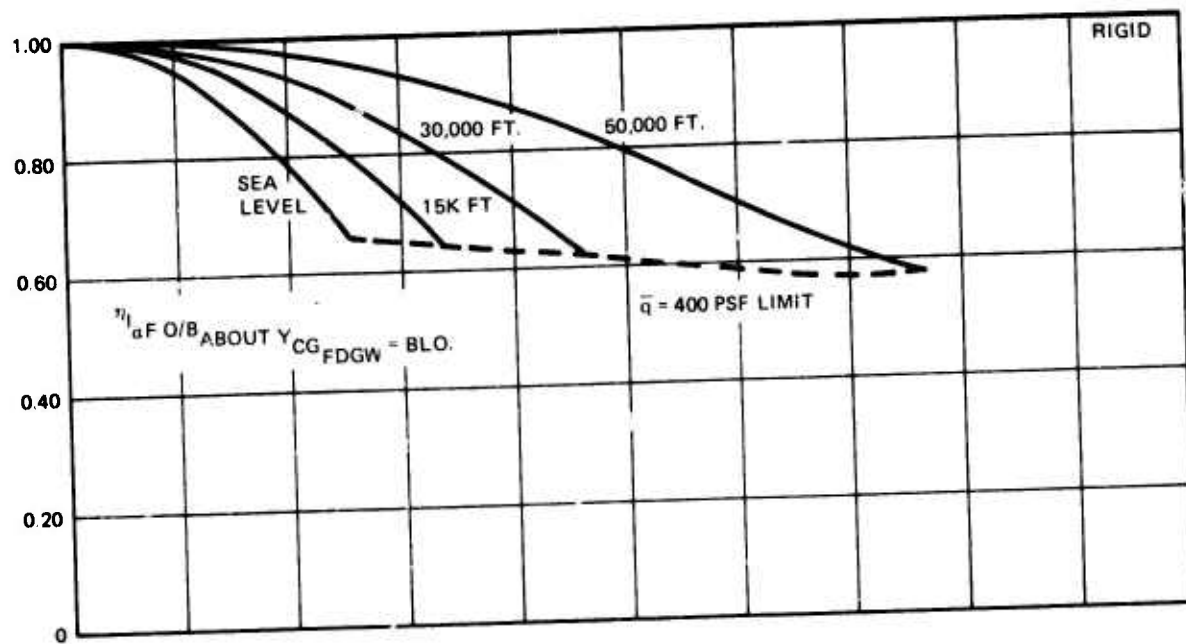


Figure 144. Flexibility Factor, Rolling Moment, Outboard Flaperon, Unsymmetric Deflection

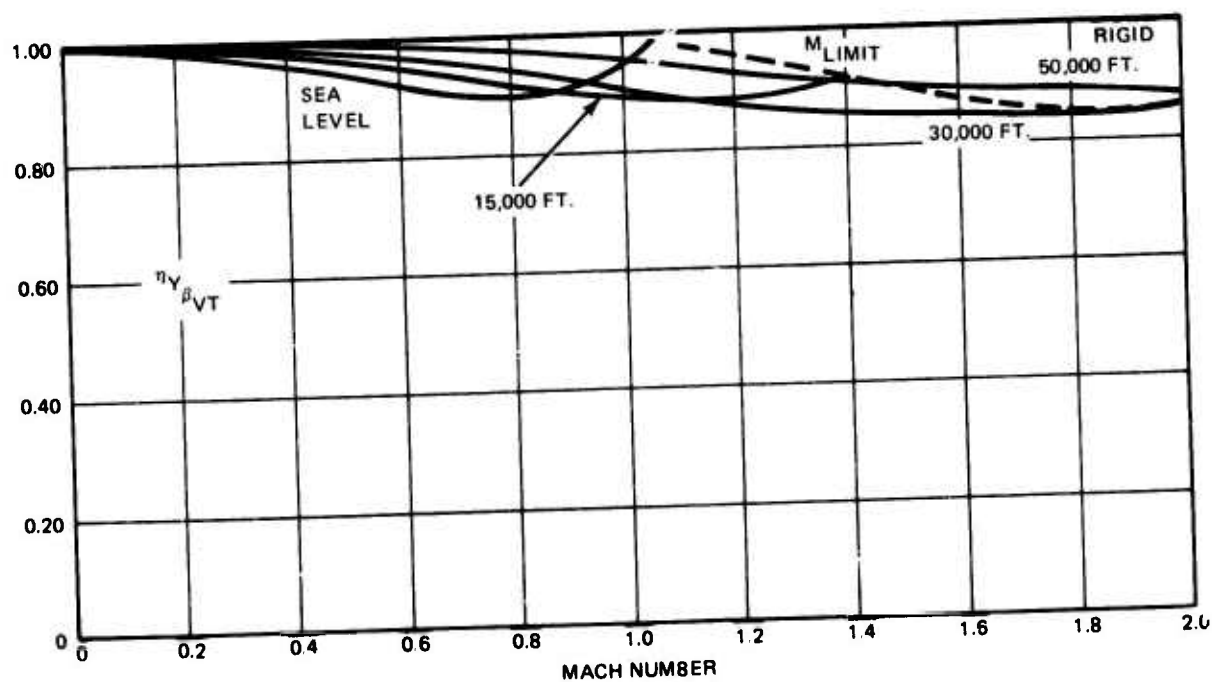


Figure 145. Flexibility Factor, Lateral Force, Vertical Tail

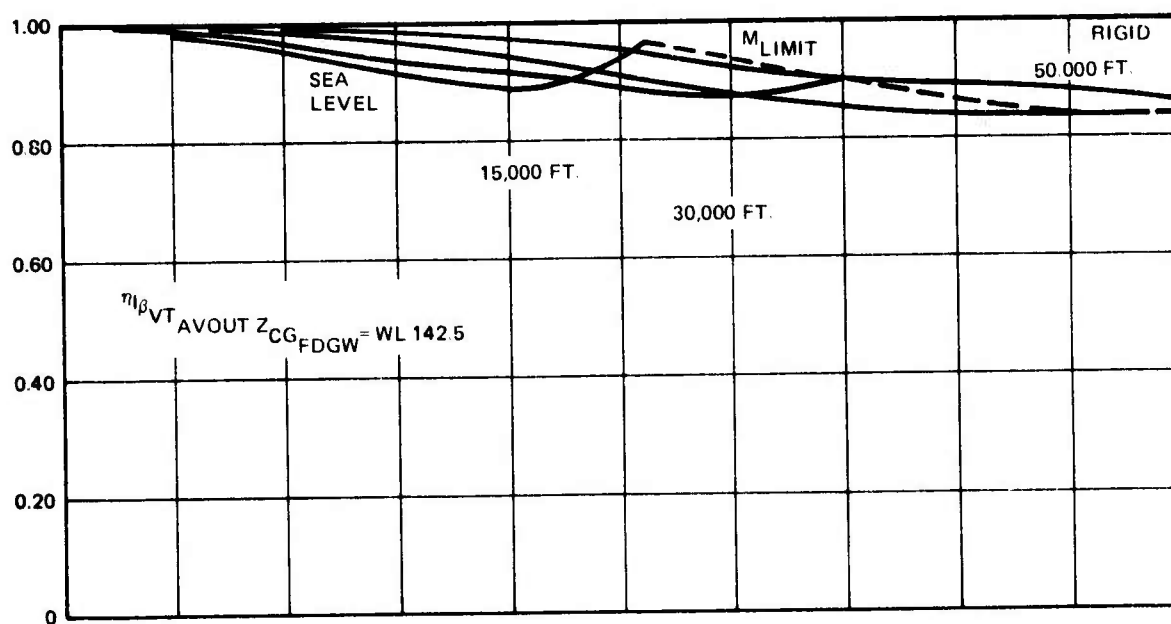


Figure 146. Flexibility Factor, Rolling Moment, Vertical Tail

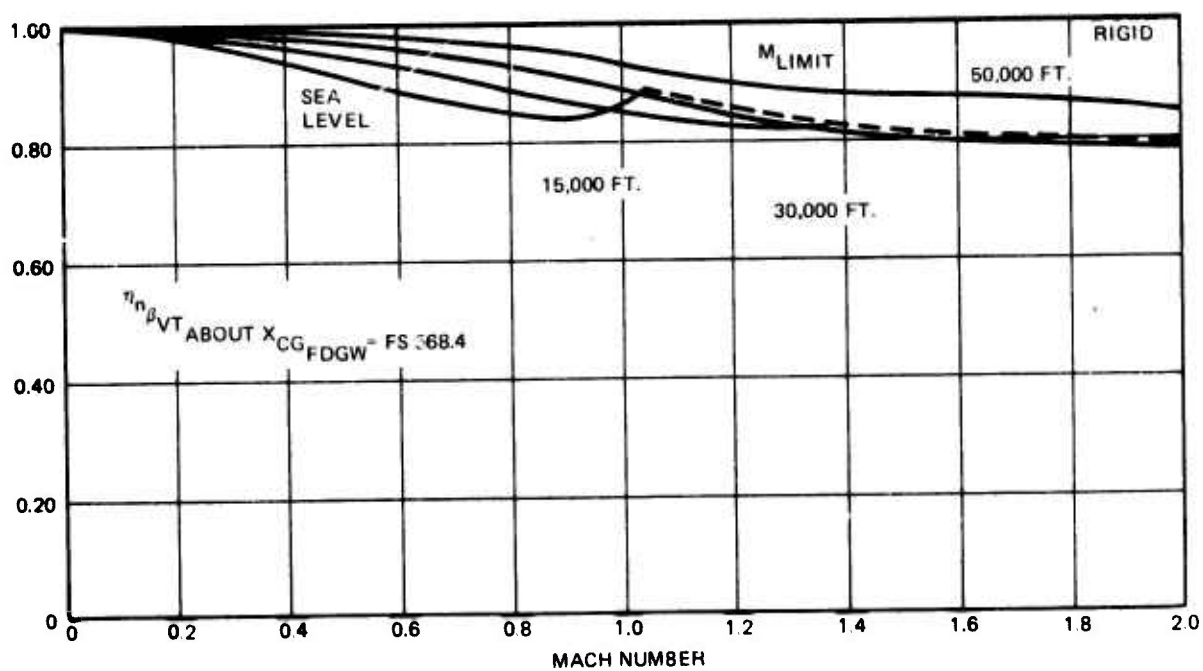


Figure 147. Flexibility Factor, Yawing Moment, Vertical Tail

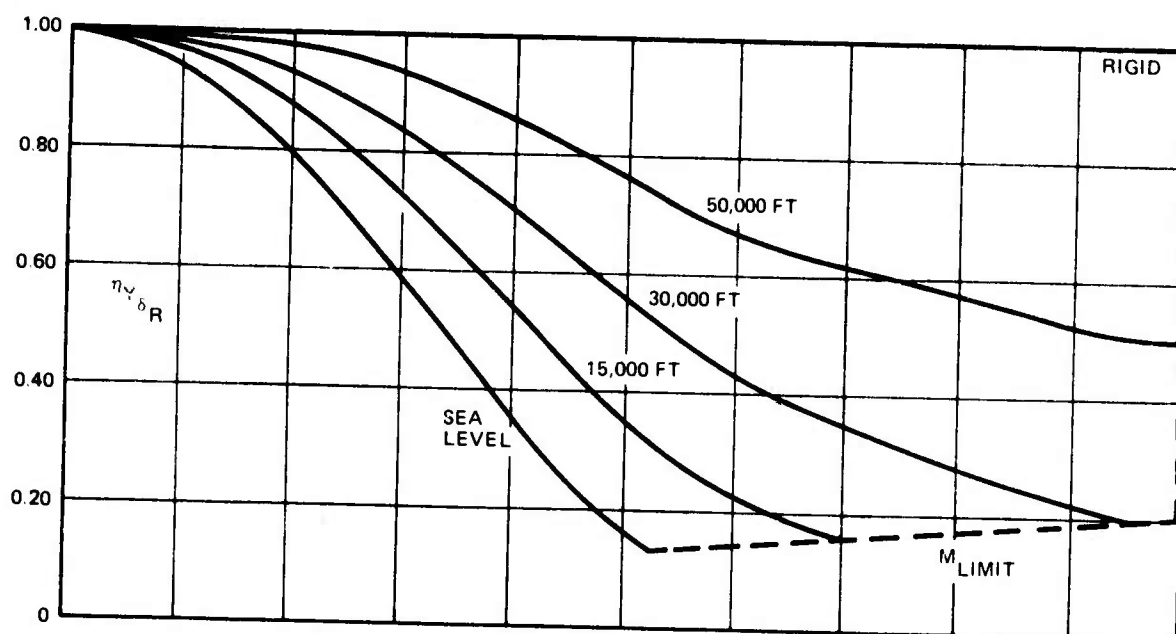


Figure 148. Flexibility Factor, Lateral Force, Rudder

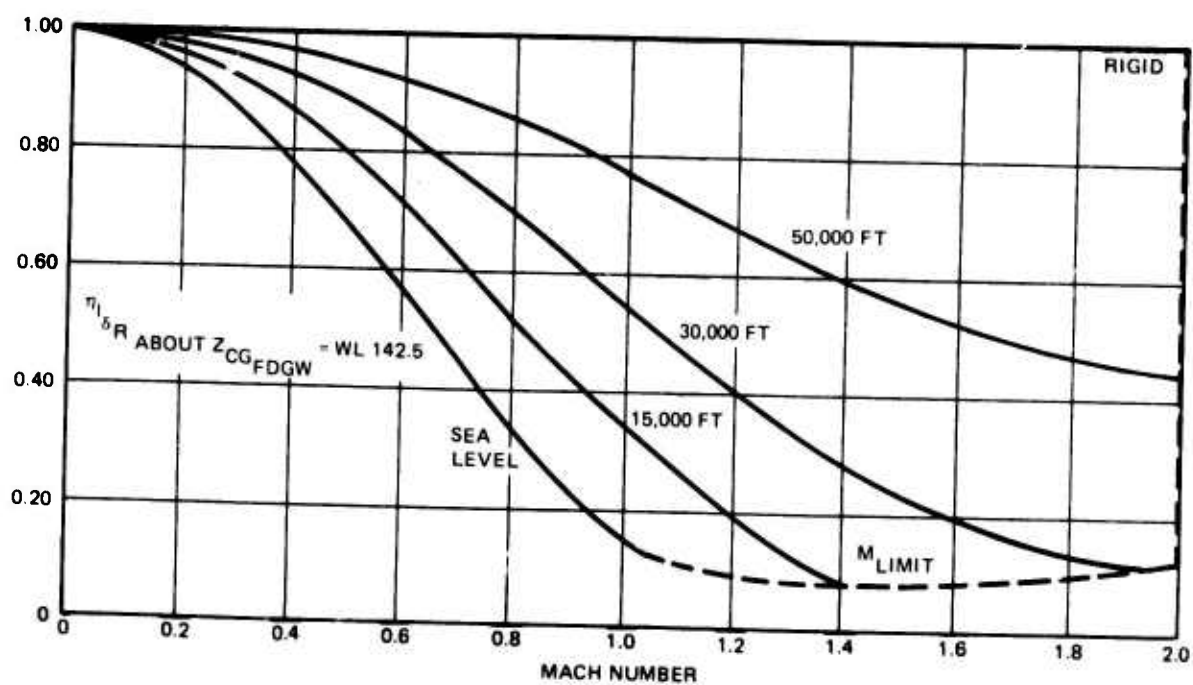


Figure 149. Flexibility Factor, Rolling Moment, Rudder

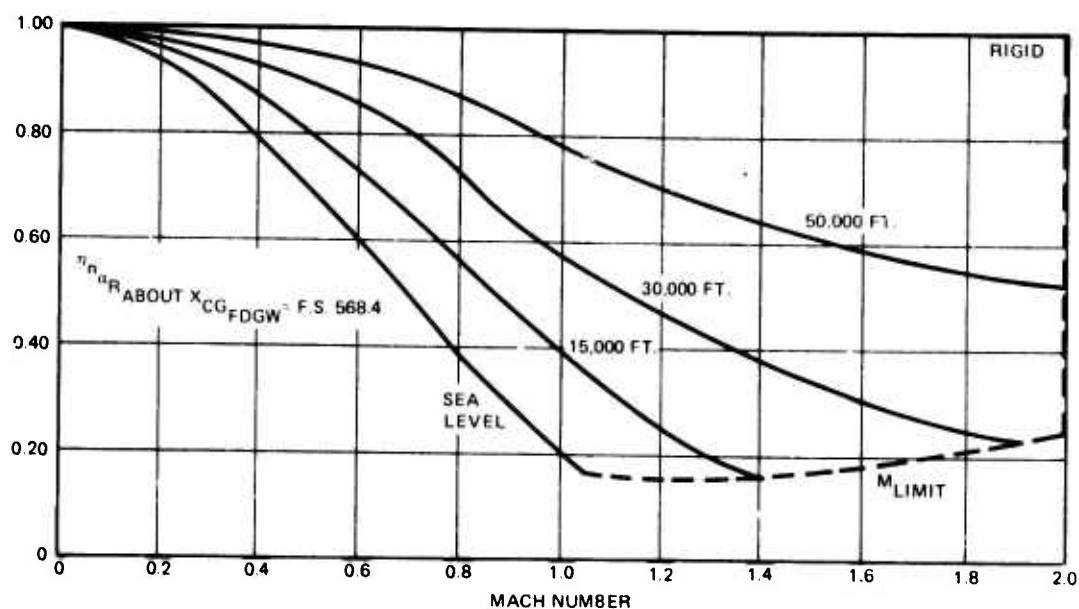


Figure 150. Flexibility Factor, Yawing Moment, Rudder

posed wing load at 3.32 g was determined to be 30,452 lb per side acting at 0.578 c, (FS 666.008, and BL 109.793). The resultant elastic twist for this case, plus the built-in twist, determined the transonic maneuver point twist configuration for aerodynamic performance evaluations. This total twist variation was $+3.0^\circ$ to -4.9° , fuselage side to tip.

A parallel effort was conducted for a finite element model of an untailored wing. The same load distributions were applied to obtain a corresponding twist at the sustained maneuver design point. Analysis indicates a net gain of 0.5° in the overall tip twist from the untailored to the tailored wing (See Figure 151). This is based on untailored wing results of a built-in spanwise twist variation of $+3.0$ to -1.6° , and a sustained maneuver design point total twist variation of $+3.0$ to -4.4° . * As the $M = 0.9$ load distribution was based upon an optimum twist quite different from that which was attained, the calculations should be iterated until the load distribution and the resultant twist are compatible. However, this first result is considered fairly indicative of the difference in the two wing structural models.

*It should be noted that the difference in elastic twist at the tip, between tailored and untailored wings, is 0.9° , but the overall difference is reduced to 0.5° because of a 0.4° change in the built-in twist.

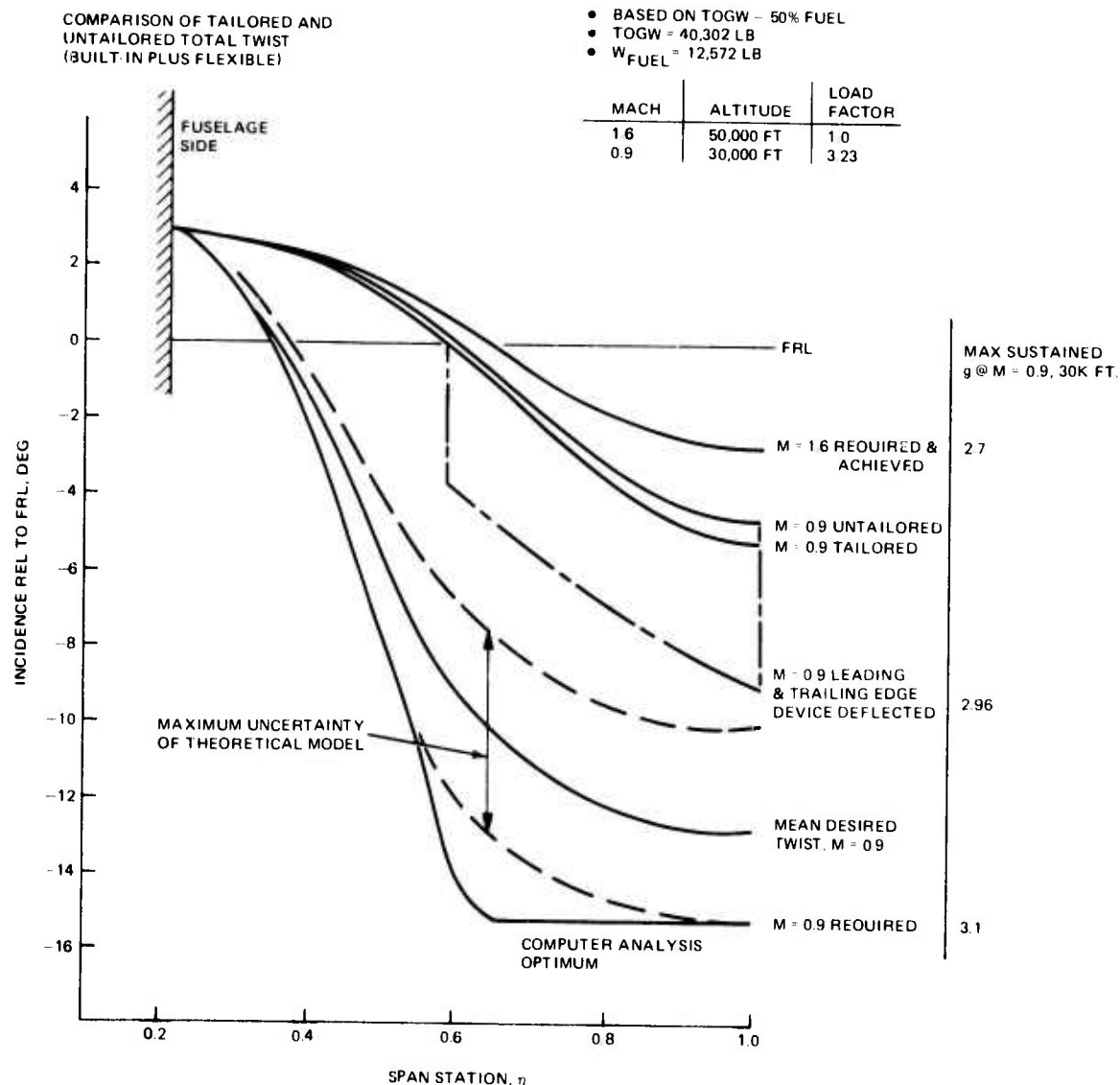


Figure 151. ADCA Wing Box Twist Distribution

An increase in twist will translate into an increase in sustained-maneuver load factor and a reduction in induced drag. The aerodynamic improvement, with regard to sustained "g" capability at transonic ($M = .9$) speeds, was evaluated based on the transonic wind tunnel test program results. The wings that were tested in this program included the lg $M = 1.6$ shape wing; this same wing with increased leading and trailing edge deflection resulting

in effectively more twist, and the computer analysis aerodynamically optimum wing ($M = .9$, 30,000 feet).

The sustained "g" capability, based upon the limited transonic tests, are presented in Figure 151. As can be seen, camber and twist, as a result of leading and trailing edge device deflection, have a significant impact on the sustained "g" capability, in that nearly 96% of the maximum sustained "g" can be obtained by control system deflection on the cruise design 1g ($M = 1.6$ cruise) wing. By including the aeroelastic twist contribution, nearly 98% of the maximum "g" capability can be achieved.

It was apparent from these tests that the real-world benefits gained from passive twist control, at best, would be very slight for this configuration and that much higher pay-offs could be achieved by optimizing control surface induced twist and camber. Further program efforts to increase wing-tip twist were abandoned. However, since a 25% increase over the untailored wing twist could be achieved at no cost or weight penalty, the aeroelastically tailored wing was still maintained as a baseline.

The completed analyses of flexible airload distributions on the wing indicates small excursions of the spanwise center of pressure for these two models. Therefore, the difference in wing bending moment, and thus any benefit of tailoring as to load alleviation, was deemed minimal.

5.2.4 Aeroelastic Tailoring Benefits Evaluation (Fin-Rudder)

The fin-rudder results, presented previously, refer to the base-case fin which includes a cover laminate meeting strength and stiffness requirements, with the 0^0 plies rotated 15^0 aft from the main load-carrying axis. The effective rudder actuator stiffness of 20×10^6 in. lb/rad in rotation is modeled. Tailoring in this manner demonstrated a significant flutter speed improvement as well as increased fin effectiveness. To evaluate this aeroelastic benefit, a beam-type model was generated for a similar untailored fin, i.e., the 0^0 layers were not rotated.

The comparison of tailored to untailored configurations indicates a significant improvement in flexible load carrying capability of up to 20%, in the transonic and supersonic range of the ADCA flight envelope at the higher dynamic pressures, i.e., along the V_L line. The effect of tailoring the fin is carried over onto the rudder so that similar enhancement of the rudder effectiveness is seen (Figures 152 and 153).

Aeroelastic tailoring of the fin-rudder system in the context of a relaxed stability design can have significant impact on flight loads and control system requirements. A

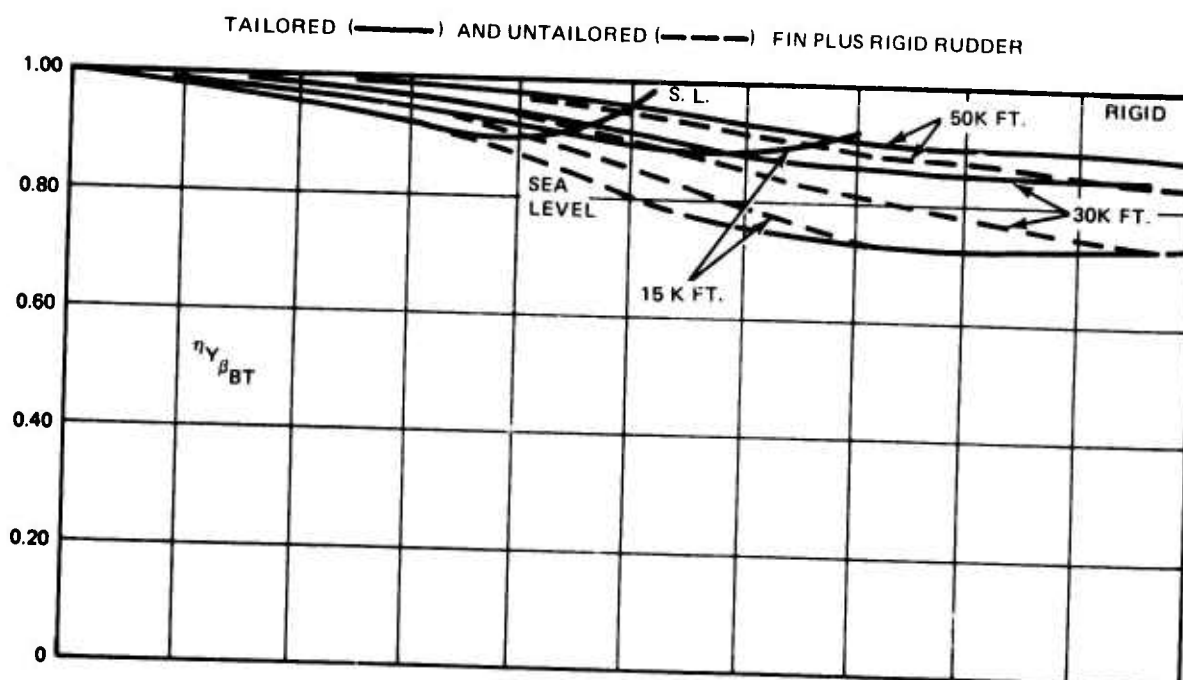


Figure 152. Flexibility Factor, Lateral Force, Vertical Tail

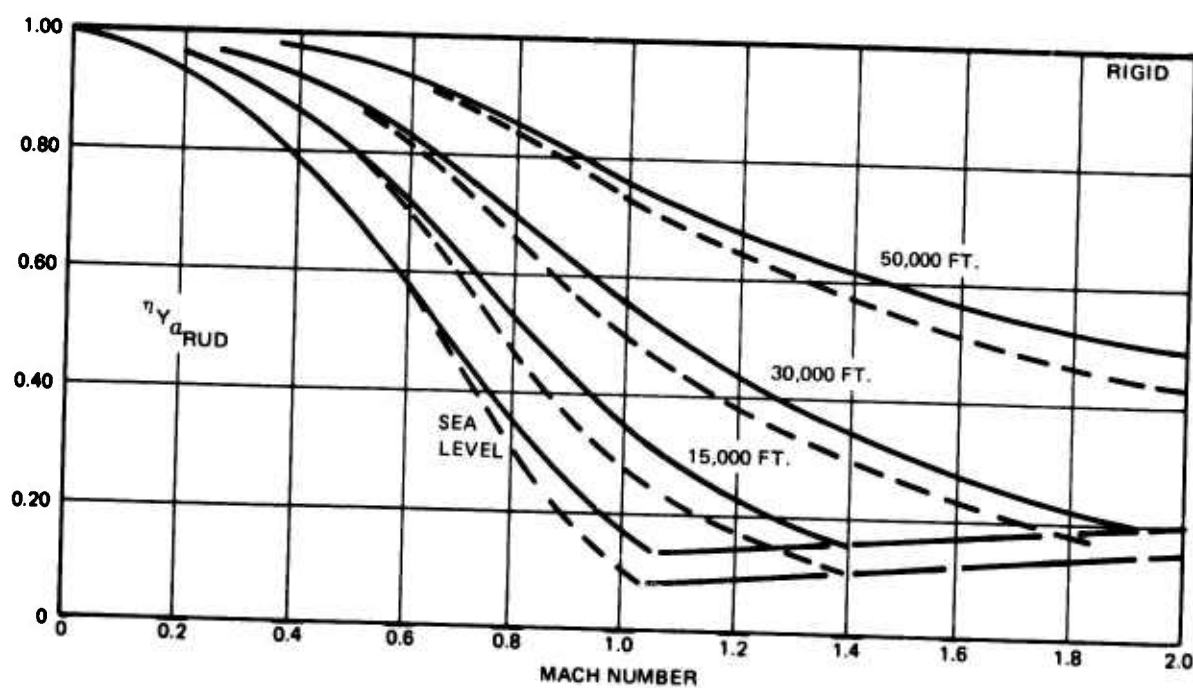


Figure 153. Flexibility Factor, Lateral Force, Rudder

more effective flexible vertical tail, significantly increasing the lateral-directional stability of the aircraft, would tend to sharply decrease lateral maneuver loads on fuselage and fin and at the same time increase rolling performance. An increase in rudder control effectiveness would reduce lateral fuselage loads and/or reduce the response requirements of the control system. Conversely, a more effective vertical fin, while maintaining the original stability levels, would allow a reduction in tail size and thus a decrease in drag.

5.2.5 Summary of Aeroelastically Corrected, Balanced Aircraft Loads for Preliminary Design

The preceding data based upon beam type structural idealization and relating the flexible to rigid surface lift contributions was finally used to correctly balance the entire aircraft. Updated aircraft weight estimates were incorporated and the built-in wing twist was taken into account. Eleven flight conditions were considered. They are referenced to a nominal flight design gross weight of 37,878 lb, a longitudinal cg position of FS 564.2 and roll and pitch axes inertia values of 20,011 slug-feet sq, and 149,078 slug-feet sq, respectively. The loads are distributed to five major component areas of the aircraft: wing, canard; forward fuselage; and fuselage in presence of wing and canard and are given in Table 22.

The symmetric conditions represent dynamic pull-ups at the point of maximum normal load factor and a maximum nose downward pitch acceleration of 6 rad/sec^2 induced by a symmetric canard deflection. Condition 11, representing the maximum symmetric canard load, is essentially Condition 2 just prior to the introduction of this canard deflection. Condition 1 represents the supersonic cruise condition which determines the built-in wing twist. Condition 5 is the transonic sustained-g maneuver point with the addition of the loads due to the aforementioned pitch acceleration. The roll conditions represent aircraft loads at the point of maximum roll rate plus a sharp reversal of roll control to induce an opposing roll acceleration of 12 rad/sec^2 . Subsonic roll control is effected primarily by the inboard flaperons. Supersonic roll control is effected by both the inboard flaperons and an antisymmetric canard deflection.

In all cases the combination of airload plus inertial load resulted in conditions less critical than the preliminary "worst case" predictions for each surface. The strength adequacy of the current design as presented is, therefore, demonstrated.

The limit fuselage airload distribution is included for the selected structural design conditions in Figure 154.

TABLE 22. ADCA BALANCED AIRCRAFT AIRLOADS

	Mach	Altitude 10 ³ Ft	q lb/in ²	n _z	L wing/ side	L b(w)	L canard/ side	L b(c)	L fwd fuse
Built-in Twist Condition	1.	50	3.0142	1.0	9,628	4,170	5,372	2,015	1,599
	2.	50	3.0142	6.5	77,669	33,637	13,728	16,259	12,900
	3.	0	8.3323	3.25	53,413	23,375	-13,762	13,308	6,805
	4.	0	8.3323	6.5	87,258	38,186	12	21,741	11,117
Sustained 'g' Maneuver	5.	30	2.4744	3.25	52,092	22,796	-11,903	12,979	6,636
	6.	30	2.4744	6.5	85,105	37,244	3,042	21,205	10,843
	7.	50	0.9537	3.25	51,756	22,649	-11,430	12,895	6,594
	8.	50	0.9537	6.5	84,374	36,923	4,070	21,022	10,750
Subsonic Roll Left Right	9.	0	8.3323	5.2	89,348	24,121	23,604	13,733	7,022
					20,888		17,758		
Supersonic Roll Left Right	10.	50	3.0142	5.2	57,498	20,347	46,053	9,835	7,803
					36,478		18,471		
Condition 2 Without Pitch Acceleration	11.	50	3.0142	6.5	57,444	24,878	42,134	12,025	9,541

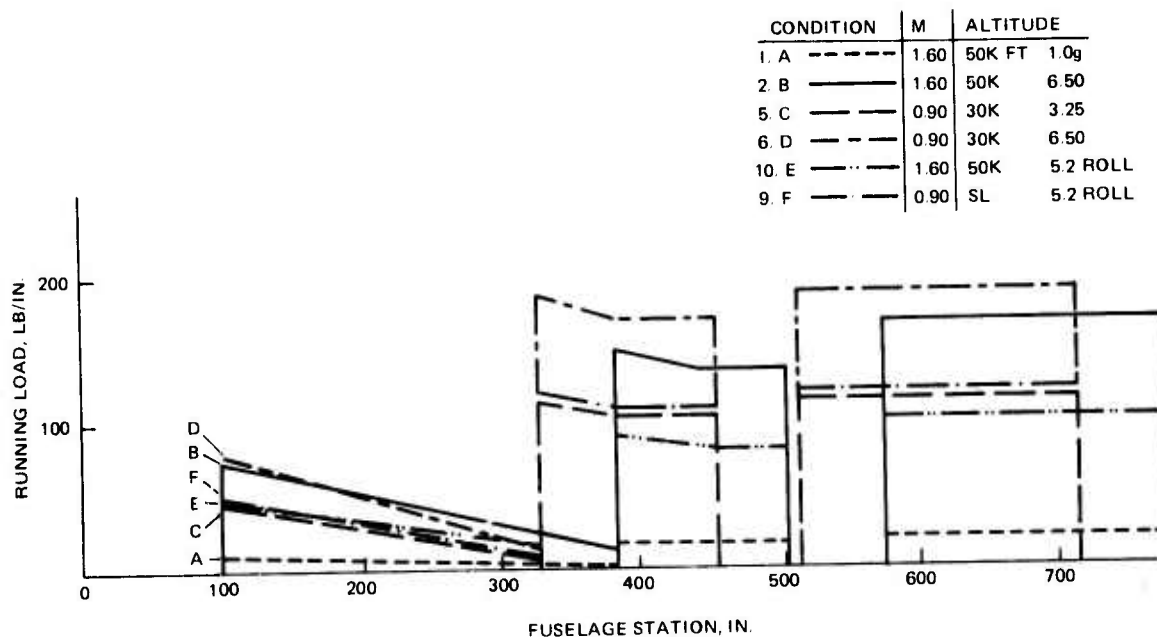


Figure 154 ADCA Limit Fuselage Airload

5.3 ADCA OVERALL STRUCTURAL ARRANGEMENT

The ADCA structural arrangement, as shown in Figure 155, has been configured to:

- Minimize the number of parts
- Minimize the number of joints
- Give maximum flexibility to design integral structure
- Provide the required structural integrity
- Provide adequate access
- Permit the use of a thru wing
- Permit the most advantageous use of composite materials

The aircraft structure is comprised of four major structural assemblies: the wing which is configured as a "thru" box multi-spar structure continuous from tip to tip; the canard which is a fully moveable slab surface of full depth honeycomb construction; the vertical fin which, like the canard, is a full depth honeycomb structure, and the fuselage which is of semi-monoque construction comprising 17 major bulkheads and frames, a structural outer shell, a structural duct and 6 longerons.

BEST AVAILABLE COPY

The design emphasizes large one-piece advanced composite moldings, modularized construction, and continuity of primary structural load paths.

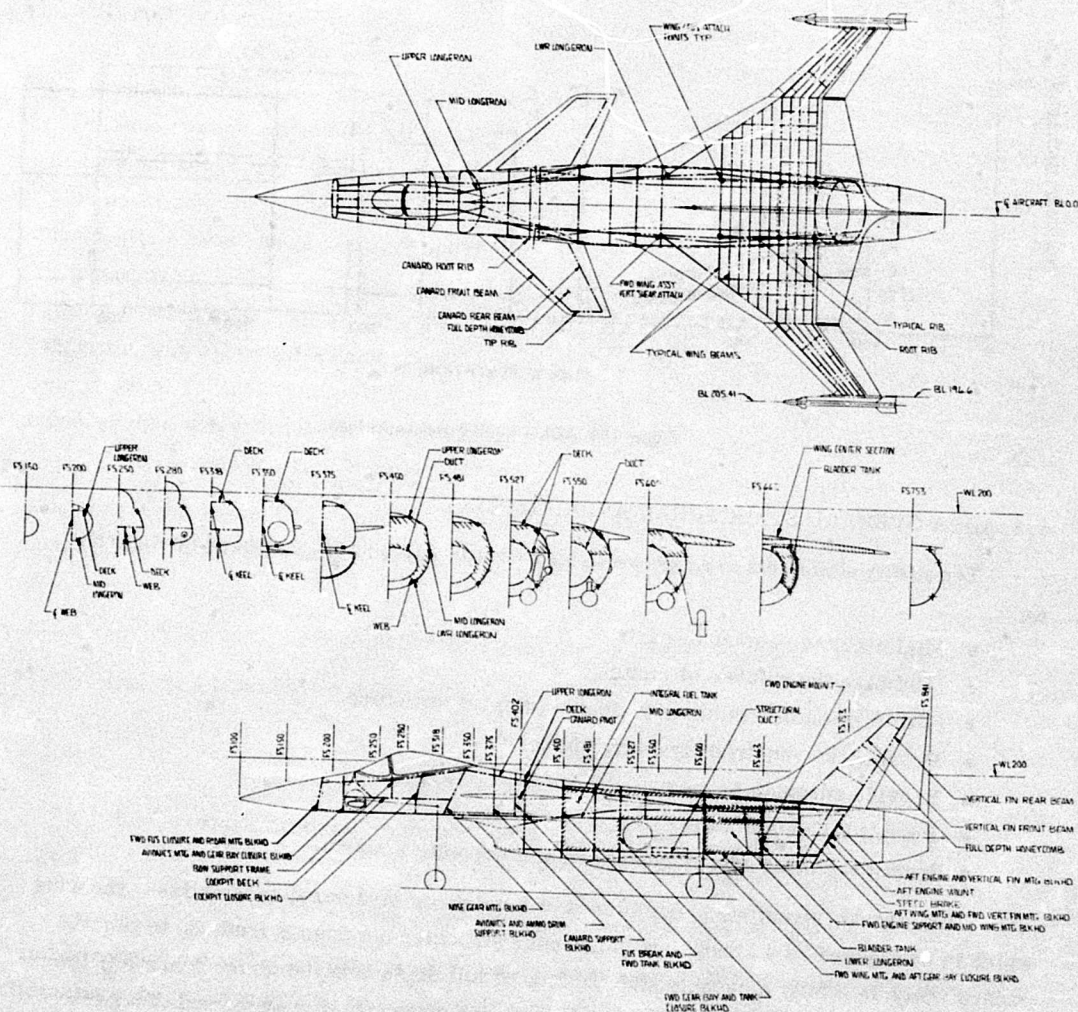


Figure 155. Structural Arrangement

5.4 WING STRUCTURAL ARRANGEMENT AND DETAIL DESIGN CONCEPTS

5.4.1 Wing Structural Arrangement

The ADCA structural wing box is configured as a single unit multi-spar structure with a span of 393.2 in. and a maximum width of 160.2 in. Maximum depth at Butt Line (BL) 30 is 7.87 in. The structural box doubles as a fuel tank from Fuselage Station (FS) 600 to 701.401 and to BL 120.95. The outer panel, from BL 120.95 to BL 196.6 is dry. The wing center section has 11 spars, and the outer panel 5. The spars provide shear carrying capability to the wing box, as well as stabilizing the wing skins against buckling. In addition, they resist the internal fuel pressure loads and provide support for the crushing loads due to bending radius of curvature. Attachment to the fuselage is accomplished at the front, mid-main and rear spars at BL 30. The front and rear spar fuselage attachments are made with single pins picking up the spars at their neutral axis to preclude imposing high secondary loads to the attaching bulkheads due to wing bending. The mid-main spar attachment is also made with single pins, however, the attachment lug hangs down through the lower cover. The lug is attached to a vertical link, which in turn attaches to the fuselage bulkhead. The links permit the wing bending deflections without inducing high secondary loads in the fuselage bulkhead, while still carrying the primary vertical shears.

Ribs are provided at six locations in the wing center section. Four of the six are full chord and the remaining two are stub-sections. Each rib performs specific prime functions as outlined below:

- BL 30 Rib - Provides primary root load redistribution capability
- BL 76.22 - Provides inboard laminate transition kick point, front spar kick support and flap hinge support
- BL 91.13 - Provides outboard laminate transition kick point
- BL 120.95 - Provides tank scaling, front and rear spar kick supports and redistribution capability
- BL 50.95 and 106.04 - Provides flap hinge support.

In the wing outer panel two full chord and six stub ribs are utilized. The most inboard full rib is provided primarily for load redistribution but also serves as a trailing edge actuator support. The most outboard or tip rib serves to close the structural box and has been

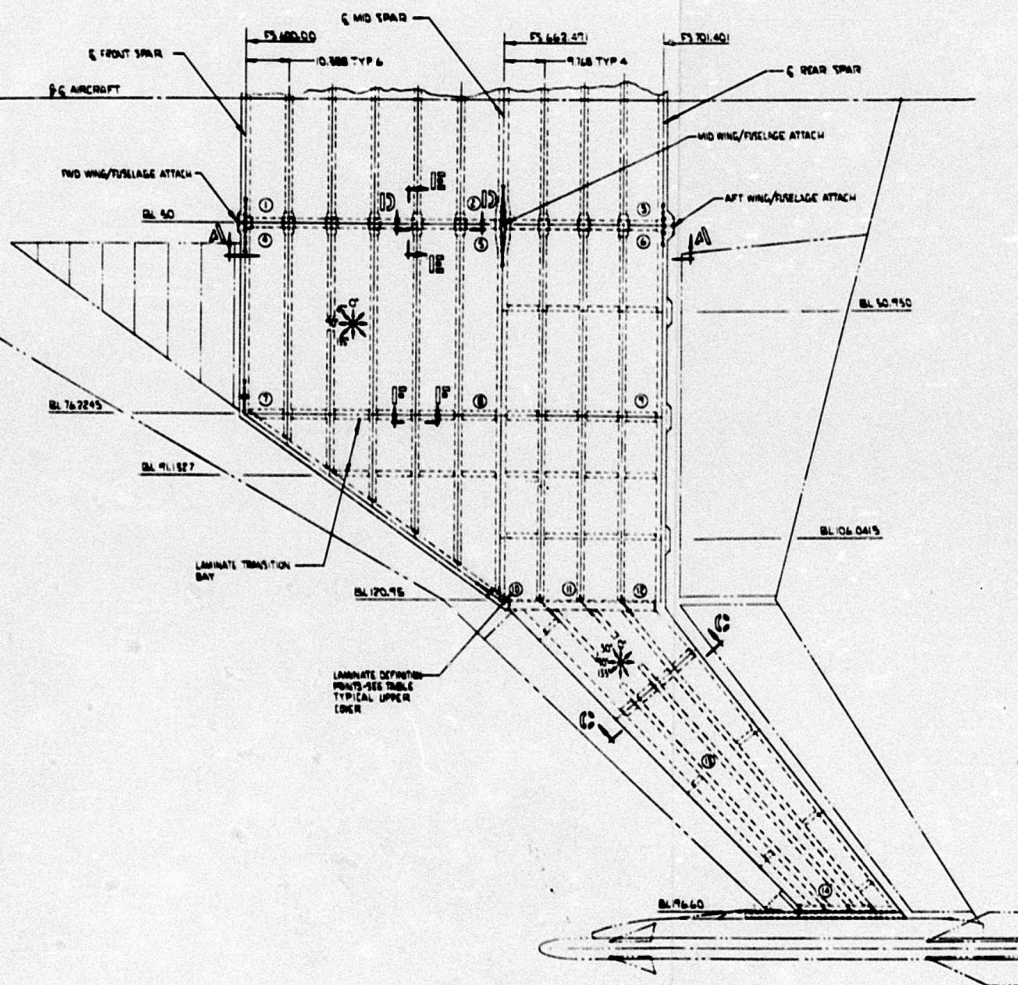
integrated with an adapter for the tip-mounted missile launcher. The six stub ribs are provided for actuator support of the leading and trailing edge devices.

The wing skins provide the basic axial and torsional shear load carrying capability as well as the required bending (EI) and torsional (GJ) stiffness material. In addition, for the ADCA vehicle, the skins will be aeroelastically tailored to provide desired wing twist. The tailoring will be accomplished between BL 91.13 and 196.60. Relative to a common axis, this means that two laminate orientations will be used, one outboard of BL 91.3 and one inboard of BL 76.22. Between BL 76.11 and 91.13 an integral laminate transition will take place.

5.4.2 Detail Structural Design Concept

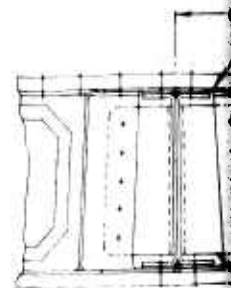
The ADCA wing structural design concept is shown in Figures 156 and 157. The entire wing structure is fabricated using advanced composite materials, with the exceptions of the BL 120.95 rib and the combination tip rib/missile launcher adapter, which are currently configured as titanium parts. The basic concept employs Gr/Ep, spars and ribs attached to one piece Gr/Ep skins with blind fasteners at the upper or compression skin and a combination of fasteners and bonded joints at the lower or tension skin. Section A-A, alternate section A-A and detail B of Figure 157 depict the two baseline design concepts currently being considered for the lower skin joint, through the wing center section. The upper skin joint is similar for both. The first concept (section A-A) shows bolted joints at the front and rear spars to effect fuel tank sealing and at the mid main spar, which carries the mid wing attachment. At the inter spars, a unique type of joint is being employed in an effort to eliminate the majority of mechanical fasteners from the lower skin. For this joint concept dry yarns of graphite (other composite materials will also be investigated) will be "punched" or "stitched" through the uncured skin laminate such that two ends of yarn will result at each stitch position. Number of ends per yarn and stitch pitch will be determined as a function of the internal fuel pressure loads, which the yarns in conjunction with the back-to-back channel section spars will resist. Subsequent to the yarn insertion, the skin would be cured on an inside tool to give precise control of the mating surface. The back-to-back channel sections which would be used along each yarn run would be precured parts featuring integral web stiffeners and reinforcements, fabricated using a trapped rubber molding technique. The tools for making these parts would be fabricated using the skin mold as a master. For assembly of the spars to the skin, adhesive

BEST AVAILABLE COPY

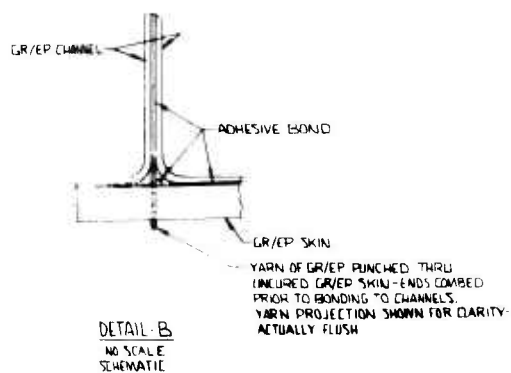


POINT	NUMBER OF PILES	TOTAL
1	1	1
2	2	2
3	3	3
4	4	4
5	5	5
6	6	6
7	7	7
8	8	8
9	9	9
10	10	10
11	11	11
12	12	12
13	13	13
14	14	14
15	15	15
16	16	16
17	17	17
18	18	18
19	19	19
20	20	20
21	21	21
22	22	22
23	23	23
24	24	24
25	25	25
26	26	26
27	27	27
28	28	28
29	29	29
30	30	30
31	31	31
32	32	32
33	33	33
34	34	34
35	35	35
36	36	36
37	37	37
38	38	38
39	39	39
40	40	40
41	41	41
42	42	42
43	43	43
44	44	44
45	45	45
46	46	46
47	47	47
48	48	48
49	49	49
50	50	50
51	51	51
52	52	52
53	53	53
54	54	54
55	55	55
56	56	56
57	57	57
58	58	58
59	59	59
60	60	60
61	61	61
62	62	62
63	63	63
64	64	64
65	65	65
66	66	66
67	67	67
68	68	68
69	69	69
70	70	70
71	71	71
72	72	72
73	73	73
74	74	74
75	75	75
76	76	76
77	77	77
78	78	78
79	79	79
80	80	80
81	81	81
82	82	82
83	83	83
84	84	84
85	85	85
86	86	86
87	87	87
88	88	88
89	89	89
90	90	90
91	91	91
92	92	92
93	93	93
94	94	94
95	95	95
96	96	96
97	97	97
98	98	98
99	99	99
100	100	100

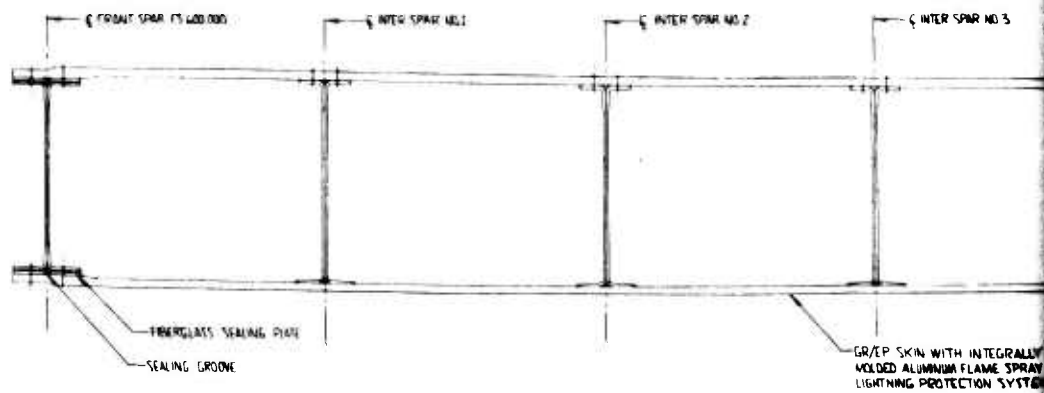
Figure 158. Wing Structural Concept

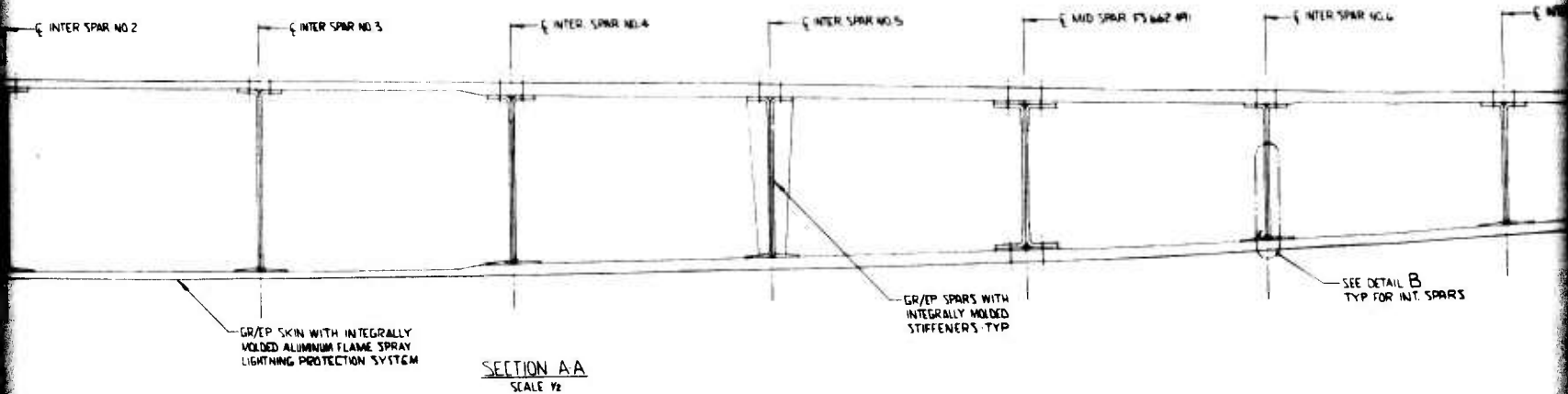
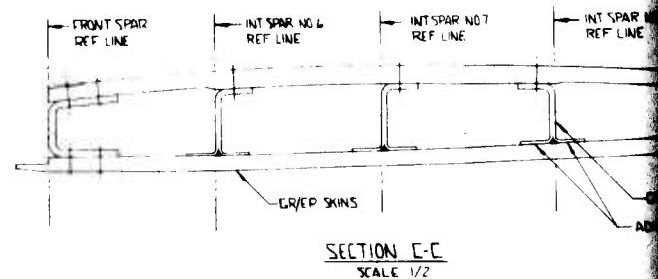
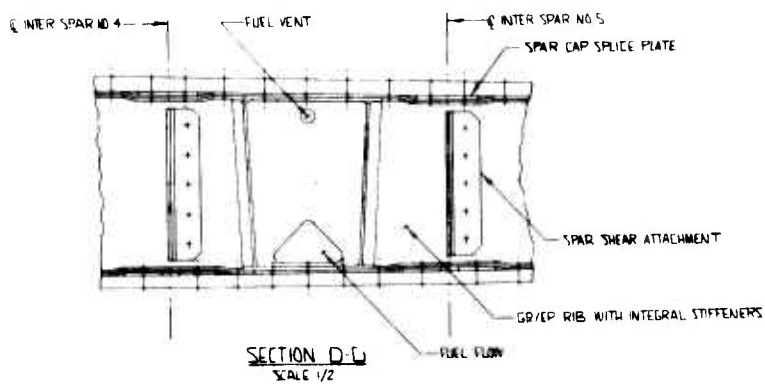
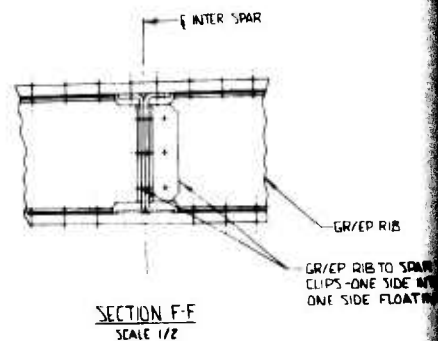
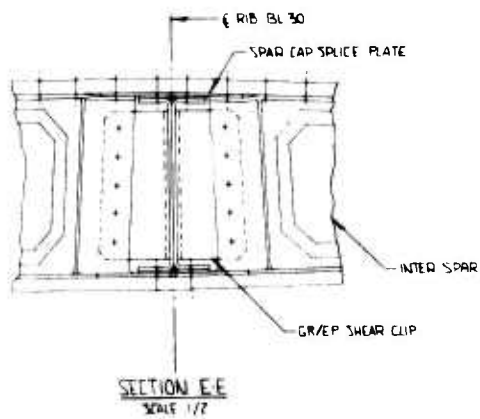


SECTION E-E
SCALE 1/2



INTER SPAR NO 4





BEST AVAILABLE COPY

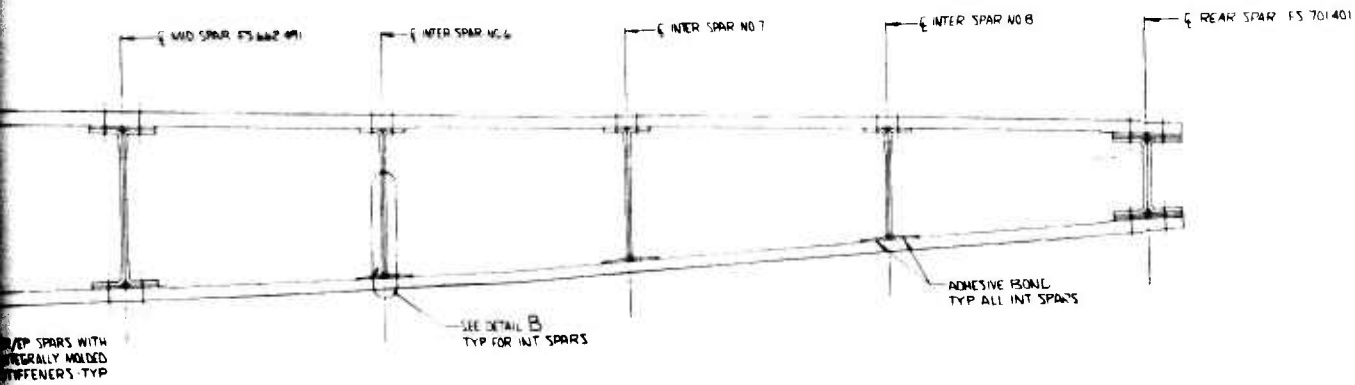
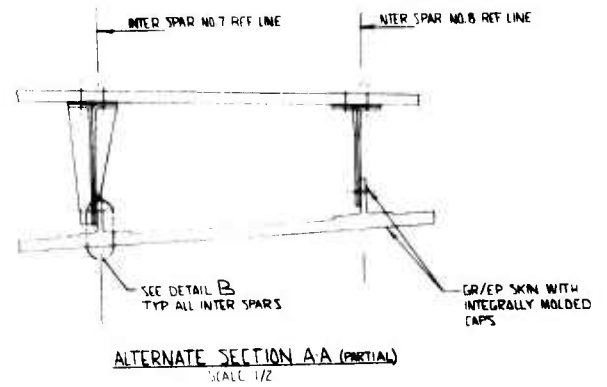
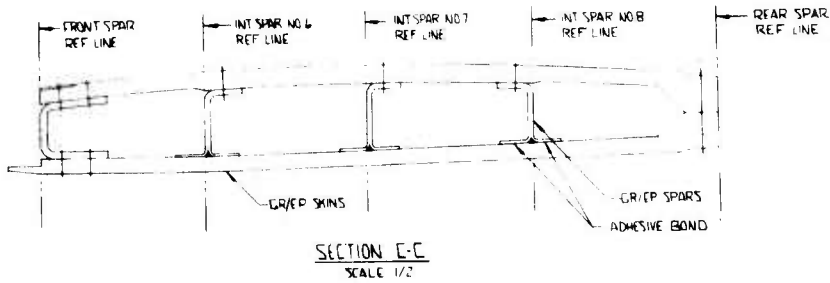
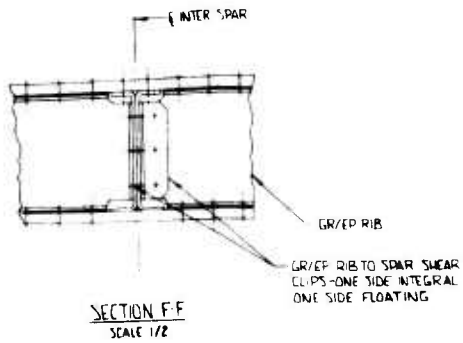


Figure 157. Wing Structural Concept

would be applied to the channel flanges and webs; the yarns molded in the skin would be held vertical with the ends combed, the spar halves would be brought together trapping and bonding the yarns and simultaneously bonding the flanges to the skin. The resulting joint would resist spar shears through the bond and fuel pressure as tension loads in the yarns. Peak loads on the adhesive at the web/flange intersection hardpoint would be minimized if not eliminated.

The second concept as shown in alternate section A-A is identical in basic concept and intent as the first, except that the spar cap at the lower skin would be integrally molded with the skin. The same graphite yarn approach would be used to handle the fuel pressure loads. Advantages associated with this approach would be in using air passage skin tooling, relaxed tolerances on spar height control for subsequent assembly operations and elimination of a secondary bond cycle. The one disadvantage is that an extra line of fasteners would be required at each spar to attach the web to the integrally molded upstanding cap leg. At the upper skin joint a symmetrical blind fastener joint is employed to minimize flange bending, more uniformly introduce the fuel pressure tensile loading to the spar webs, and preclude fastener "pull-thru" problems.

Another advanced wing box concept that shows promise is presented in Figure 158. This concept employs stitching of the lower skin cap to the lower skin while both parts are uncured. A continuous chain type stitch would be employed, requiring access from one side of the part only to effect the joining operation. In addition, the spar webs and lower skin would be cured as one piece integral molding, minimizing the number of separate detail parts and subsequent assembly operations, resulting in lower part cost. An advanced wing box assembly technique is also utilized with the concept, in an effort to further reduce assembly cost by minimizing any final upper skin to spar shimming operation. The technique makes use of a quick curing "assembly adhesive" and temporary assembly hardware (Cleco's). The sequence of operations would be as follows:

- Locate upper spar caps to upper skin and pilot drill
- Attach caps to skin with Cleco's
- Apply assembly adhesive to caps
- Locate upper skin cap assembly to previously cured lower skin/integral web assembly
- Remove Cleco's and upper skin
- Install permanent cap to web fasteners

- Replace upper skin and install permanent skin to cap blind fasteners.

The wing skins are of all Gr/Ep plain panel construction utilizing two basic laminate orientations as shown in Figure 156. The orientations have been selected to yield both maximum structural efficiency and desired wing twist for improved vehicle performance. Typical skin axial loads range from approximately 19,000 to 30,000 lb/in. at BL 120.95 and from 8000 to 28,000 lb/in. at BL 30.

5.4.3 Wing Design Cycle

The ADCA wing design cycle consists of three levels of effort, each with an increasing degree of sophistication of loads and structural model definition, see Figure 159.

The initial cycle begins with a "worst case" set of loads based on engineering judgment, and a preliminary torsional stiffness based on mass distribution and the desired flutter speed. In addition, a set of ply angles is selected which will yield a practical laminate with favorable twist behavior under load without compromise of the torsional stiffness or bending strength. These inputs are now cycled through the Composite Beam Optimization Program (COMBO) anisotropic beam model program (Ref. 4) which outputs a definition of an optimum box beam structure including a flexibility matrix. A flutter analysis is now performed and the results compared to the flutter requirements; if necessary the torsional stiffness can be adjusted and the calculations repeated to bring the flutter speed sufficiently close to the target value.

(This "COMBO" procedure is also used on the canard and fin and the resulting flexibility matrices are used to calculate control effectiveness, to rebalance the flexible aircraft, and as an input to the "FLEXSTAB" program.)

A finite element model of the wing is now generated using the cover laminates defined by the COMBO beam results; the chosen ply angles are retained and the plus and minus 45° plies are maintained equal in number. During this phase, extensive use of the Grumman "RAVES" programs is made to generate and analyze the finite element model, and to present the results. This better defined structural model is then optimized, using Automated Structural Optimization Program (ASOP III) (Ref. 5), based on the same "worst case" loads and holding the plus and minus 45° plies defined by COMBO as minima in order to preserve the torsional stiffness requirement. The flexibility matrix of this model is then utilized to perform a more detailed flutter analysis. If inadequate, the FEA optimization cycle can be re-

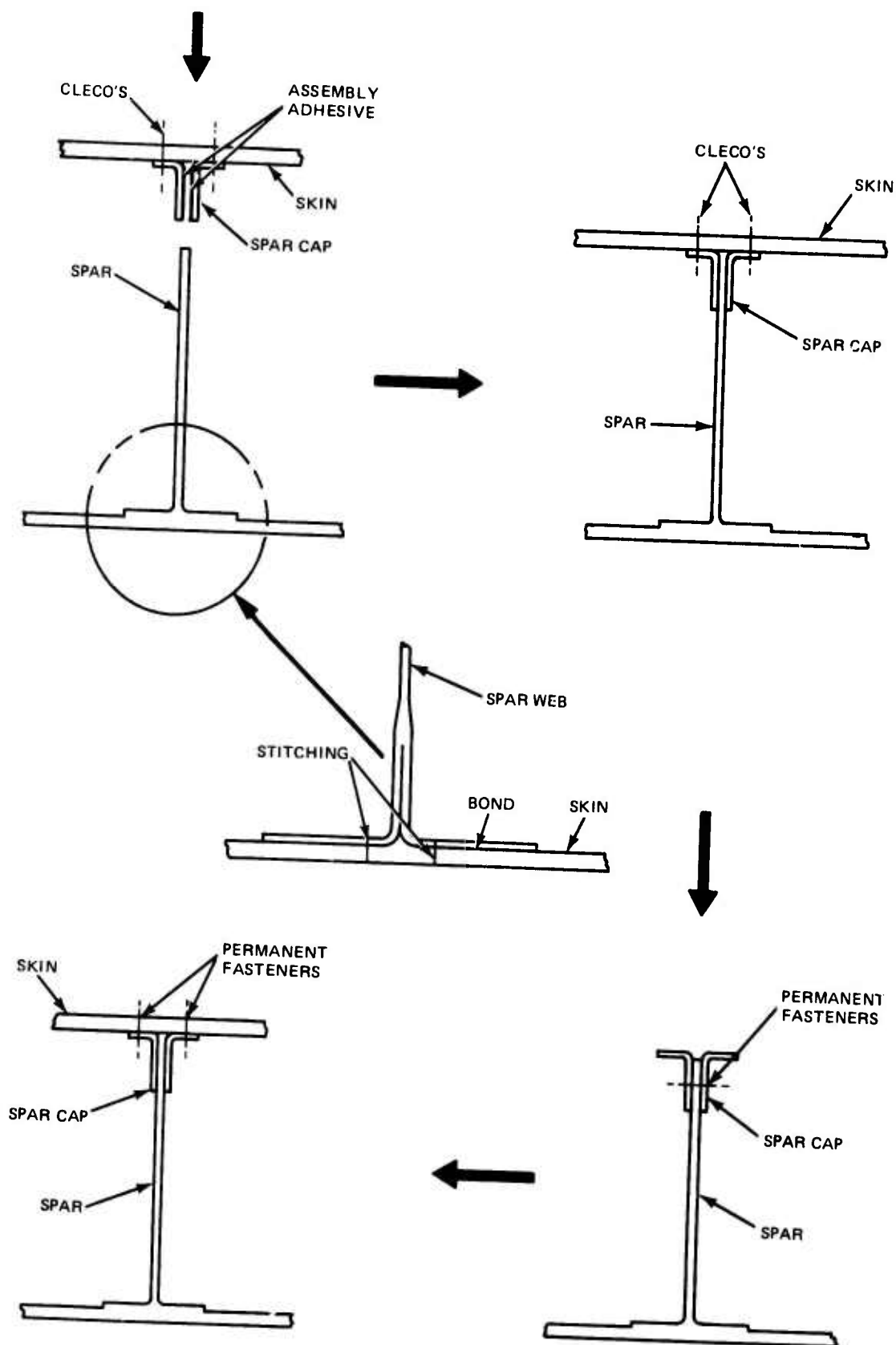


Figure 158. Advanced Wing Box Concept

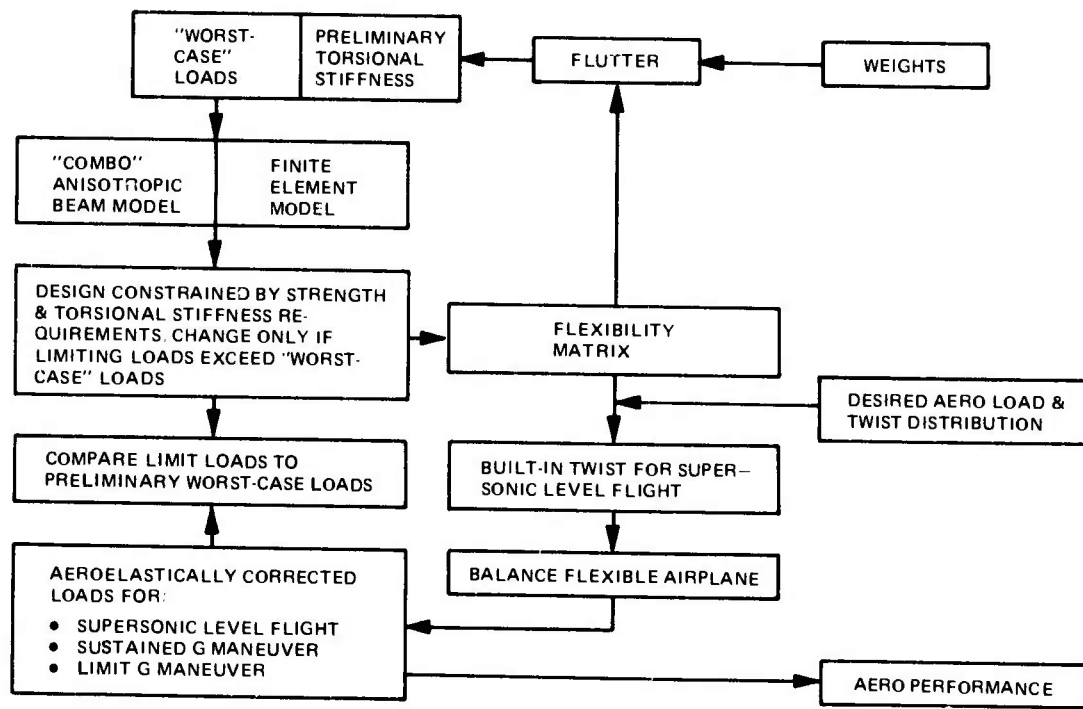


Figure 159. ADCA Wing Design Cycle

peated using Flutter and Strength Optimization FASTOP (Ref. 6) until an optimized design adequate for both strength and flutter requirements are achieved.

Starting with the defined aerodynamic twist and load distribution at the cruise condition (1.6M, 1g) and utilizing the flexibility matrix of the optimized FEA model, the wing "jig" shape (zero load shape) can be defined. At the maneuver design point (0.9M, 3.2g), aerodynamic loads based on supercritical airfoil theory and the desired twist distribution, are applied to the flexibility matrix and the actual twist distribution calculated, adding in the "jig" shape twist. The aerodynamic loads should then have been corrected for this revised twist distribution and the analysis recycled until the structural twist matched the aerodynamic twist consistent with the applied loads. However, by this stage it was clear that the performance payoff for aeroelastic tailoring was insignificant and the analysis was stopped.

Before the payoff was evaluated, a considerable effort was put into further increasing the structural twist. Using the recently developed Multiple Constraint Resize (MCR) program interactively with ASOP and FASTOP a potential design was created which satisfied

the strength and flutter requirements and has 25% more twist than the earlier aeroelastically tailored finite element model. See Section 5.4.7.

5.4.4 Laminate Tailoring Options

Acroelastic tailoring implies a lifting surface which can distort so as to enhance aerodynamic performance while meeting both strength and flutter requirements. Tailoring can be achieved by using advanced composite materials in such combinations and orientations that the resulting laminates are anisotropic, whereby the bending and twisting deformations of the surface are coupled. There are three techniques with which this coupling can be achieved:

- Unbalancing the $\pm\theta^\circ$ plies
- Rotating the entire laminate
- Kicking the 0° plies through a small angle with the $\pm\theta^\circ$ plies balanced.

The first two of the three techniques were developed at Grumman in the establishment of the computer program TWST (Twist Control Program for Composites) between February and May 1972. Although both of these techniques are effective in coupling the bending and twisting deflections, they both produce a large reduction in the shear modulus. This, in most cases, results in an unacceptable weight penalty to the structure.

The concept of kicking off the 0° plies, developed at Grumman in April 1975, does not suffer this penalty. In fact, there is a slight increase in the shear modulus and axial strength when the kick angle is less than 15° , Figures 115 and 160.

A comparison between unbalancing the $\pm\theta^\circ$ (45°) angle plies and kicking the 0° plies is presented in Figure 160 for an all graphite laminate of a 41.5° sweep wing. (ADCA outer wing.) The comparison is shown as plots of the twist control parameter against the shear modulus of the laminate. The curves demonstrate that if the laminate is tensile strength designed (which entails a high percentage of 0° plies), kicking the 0° plies through a small angle gives a more effective twist control than unbalancing the $\pm 45^\circ$ angle plies; while if the laminate is shear-stiffness designed for flutter prevention (which entails a high proportion of $\pm 45^\circ$ angle plies), unbalancing the angle plies to provide twist control leads to an unacceptable loss in shear modulus.

These basic concepts were used to select the baseline laminates for the composite wing. Further studies, with a finite-element model of the wing, considered unbalanced

$\pm \theta^\circ$ plies in combination with kicked 0° plies. These studies are discussed in Subsection 5.4.7.

5.4.5 COMBO (Composite Box Optimization) Procedures

A study, initiated early in 1975, indicated that a procedure should be developed to permit rapid tradeoffs of candidate advanced composite wings. Such a procedure should define the effect of composite materials selection, layer orientation, and cover and substructure configuration on such factors as weight, cost, aeroelastic tailorability, and flutter and divergence speeds.

For a preliminary weight distribution and planform, the torsional stiffness required for flutter and divergence prevention is empirically estimated. A preliminary definition of the optimum wing twist, in terms of increased performance and reduced drag, is derived for two loading conditions (1g level flight and maneuver design condition, for example). Pre-

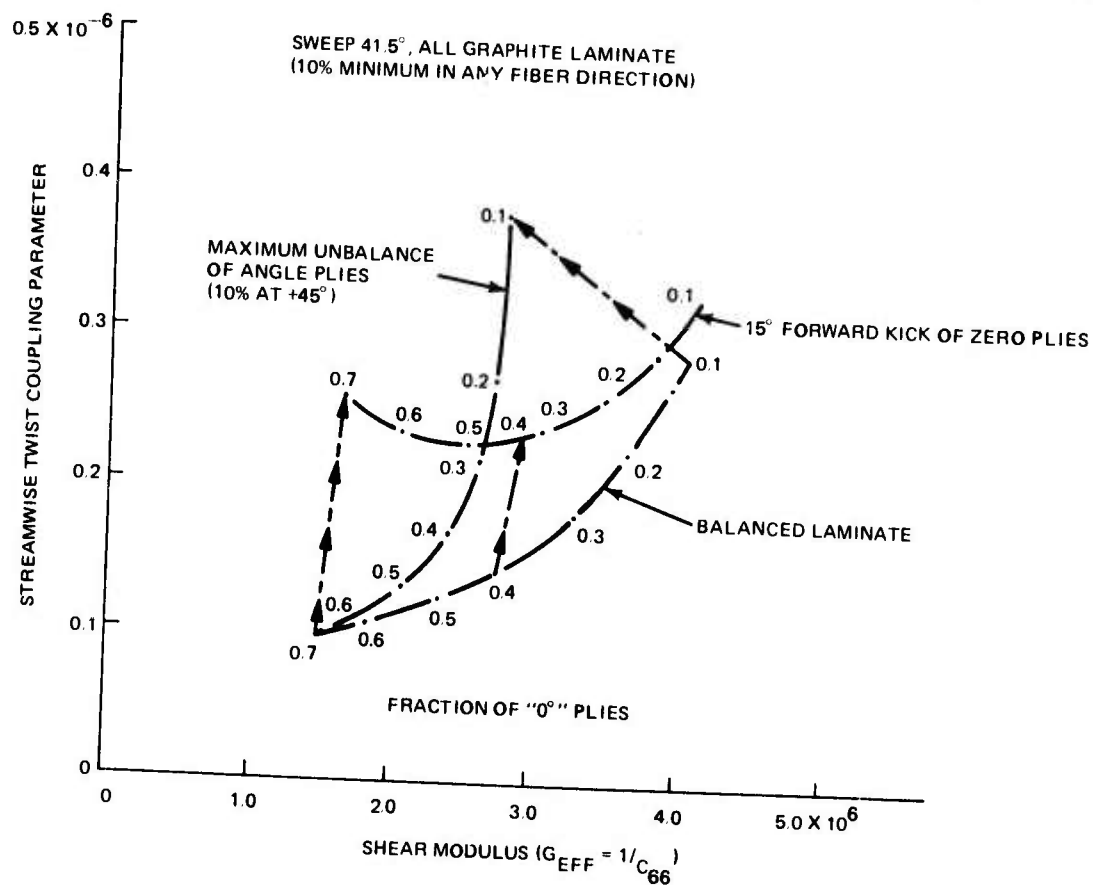


Figure 160. Wing Twist Control Sensitivity

liminary loads for a strength design are generated and then combined with the stiffness and twist requirements, for the beam-design process outlined below.

The lifting surface is first idealized into a number of rectangular bays. The laminated box covers are assumed to be composed of fibers running in four directions: β , 90, and $\pm \theta$ degrees, where the zero direction coincides with the 50% chord of the structural box and β is a small angle (typically $< 15^\circ$), so that the β direction is nominally spanwise.

COMBO first uses conventional preliminary-design techniques to size the covers and spars to meet strength and GJ requirements. In this initial-sizing step, the cover laminate is assumed to be orthotropic (i.e., the number of $+\theta$ and $-\theta$ plies are assumed to be equal and the spanwise fibers are assumed to be parallel to the 50% chord). The program contains both a multispar and a honeycomb option, and in each option vertical shear, torsion, bending stresses, and cover buckling are among the criteria used in the initial sizing.

Next, the covers are tailored to obtain the desired elastic twist at each station along the span. To accomplish this step, the conventional beam formulas were modified to incorporate the elastic coupling between bending and torsion induced by the anisotropic covers. The resultant equation:

$$\begin{pmatrix} -\frac{d^2 w}{dx^2} \\ \frac{-d\alpha_\beta}{dx} \end{pmatrix} = \begin{bmatrix} F_{11} & F_{12} \\ F_{12} & F_{22} \end{bmatrix} \cdot \begin{pmatrix} M_x \\ M_{x_y} \end{pmatrix} \quad (1)$$

relates the bending curvature ($d^2 w/dx^2$) and the chordwise twist rate ($d\alpha_\beta/ds$) to the known bending and twisting moments. In order to obtain the streamwise twist rate ($d\alpha/dx$) the components in the streamwise direction of $d\alpha_\beta/dx$ and $d^2 w/dx^2$ (which is also the bending-angle rate) are added; i.e.,

$$\frac{d\alpha}{dx} = \frac{d\alpha_\beta}{dx} \cos \Lambda + \frac{d^2 w}{dx^2} \sin \Lambda \quad (2)$$

Equations (1) and (2) are used to relate the change in the streamwise angle of attack ($\Delta\alpha$) across each bay to the material properties and material distribution. Four options are available to achieve the desired values of $\Delta\alpha$. These options are:

1. Adding 0° fiber layers in each bay.
2. Unbalancing the $\pm\theta$ layers; i.e., deleting some of the $+\theta$ layers, and adding an equal number of $-\theta$ layers, or vice versa.
3. Rotating the entire laminate in all bays in both upper and lower covers.
4. Rotating the spanwise layers only; i.e., the angle β orienting the spanwise plies is set to a small non-zero value. To avoid manufacturing splices, β is usually set to the same value in all bays.

In the first option, 0° fibers are added to reduce $d\alpha/dx$ in Eq (2) by decreasing d^2w/dx^2 . Since the 0° fibers are strength critical in the initial design, these layers cannot be subtracted; therefore, this option is only useful when it is necessary to decrease the angle-of-attack distribution of a swept wing.

In both options 1 and 2, Eq (1) and (2) are used, together with the relations which define the F_{ij} 's to solve for the specific number of fibers to achieve the desired $\Delta\alpha$ across each panel. (In options 3 and 4, where weight is exchanged and the entire laminate is rotated or only the spanwise layers are rotated, there is only one variable to adjust—the fiber rotation angle—and it is only possible to match the desired angle of attack at one specified span location.)

In options 2, 3 and 4, tailoring is accomplished by reorienting the plies; therefore, in the tailoring step, no weight is added to the initial strength-stiffness design when these methods are used. However, some weight may have already been added, if the GJ distribution has been increased for flutter adequacy due to the bending-torsion coupling requirement. As discussed in 5.4.4 options 2 and 3 cause a decrease in G and the weight penalty may be significant.

After tailoring the material, the COMBO program checks the stresses and deflections of the final design. The program also computes the relative weights and costs of major structural components for use in trade studies. The cost analysis includes both fabrication and material charges.

Finally, COMBO computes the structural-stiffness and influence-coefficient matrices required as input data for conventional flutter and aeroelastic-load-prediction programs.

The design is then checked for flutter and divergence by using existing computer programs. If necessary, the torsional-stiffness requirements are modified in accordance with the previously discussed guidelines and the cycle is repeated.

5.4.6 Finite Element Model (FEM)

The ADCA wing is a double-delta planform with a thickness/chord ratio of 0.03 at the root, 0.05 at the BL 121 break and 0.05 at the tip. The wing box has a very large constant chord of approximately 101 in. to BL 76 at which point the front beam sweeps aft and the chord reduces to 39 in. at BL 121. The outer panel is swept aft while tapering to a tip chord of 24 in. at BL 197. The vertical wing fuselage supports are at the front, main, and rear spars at BL 30. The drag attachment is at this butt line.

The center box has 11 beams that are normal to airplane center except for the front beam which, as previously mentioned, sweeps aft from BL 76 to BL 121. The outer panel has five beams. Full ribs exist at BL 0, 30, 76, 121, one normal to the outer panel box centerline at about BL 142, and at the tip. Partial ribs and formers redistribute flap and slat loads into the wing box at other locations.

The finite element model depicts the wing box semi-span due to symmetry of the structure. The wing covers were divided into 54 panels each. Full depth spars and ribs were assumed to exist throughout. To reduce the complexity of the model only five intermediate beams were assumed to exist inboard of BL 122, two outboard. Minimum stiffnesses of these beams were chosen to correspond to the estimated stiffness of the total number of actual intermediate beams.

For preliminary load distribution, the supports at BL 30 were all assumed to be rigid and analysis was made of an aluminum structure with preliminary gages. The analysis was made utilizing the S3 programs of the Grumman RAVES system. From this analysis a better definition of the substructure was made. By this time the COMBO program had been utilized for establishment of preliminary layups for the covers and front and rear beams to satisfy torsional stiffness and strength requirements for an "untailed" layup, i.e., a 0° , $\pm 45^\circ$, 90° layup with balanced $\pm 45^\circ$'s. The COMBO "zeros" were normal to the airplane centerline between BL 0 and BL 84, and parallel to the box mid-line between BL 84 and the tip. However, as a wing cover splice was planned for BL 122, the layup described in Figure 161, $\lambda_5 = 41.9^\circ$, was used in the finite element model. This structure was re-analyzed as a composite (graphite-epoxy) structure, again using Grumman RAVES program, S-3. Deflections, twists, and internal load distributions were obtained as well as structural influence coefficients for preliminary flutter checks or aeroelastic corrections. RAVES programs S50 and S51 were used to obtain plots of fiber stresses and deflections.

A study of different approaches to tailoring for increased washout showed the desirability of kicking the outer panel "zero" layers 15° forward (less sweep, $\theta_5 = -15^\circ$), Figure 161. This was incorporated into the model, along with a flexible support at the mid-spar and adjustments of the geometry to account for changes in skin thickness, and updating of the spars to meet strength requirements. This model was analyzed again by the RAVES programs which as yet do not recycle to optimize the structure with respect to strength. The results showed some negative margins of safety inboard of BL 122. The GJ calculated from the imposition of a unit couple to the tip was in good agreement with the requirements. The tip twist was 15.8° nose down at ultimate load, compared to 12.2° on the previous "untailored" model.

Subsequently, it was decided to eliminate the manufacturing splices in the wing covers. This would have left the outer panel 90° and $\pm 45^\circ$ layers misaligned with the center section layers by only 3.1° , so the entire outer panel layup was rotated 3.1° to eliminate this misalignment. The 15° kicked outer panel layers were then carried inboard to BL 76

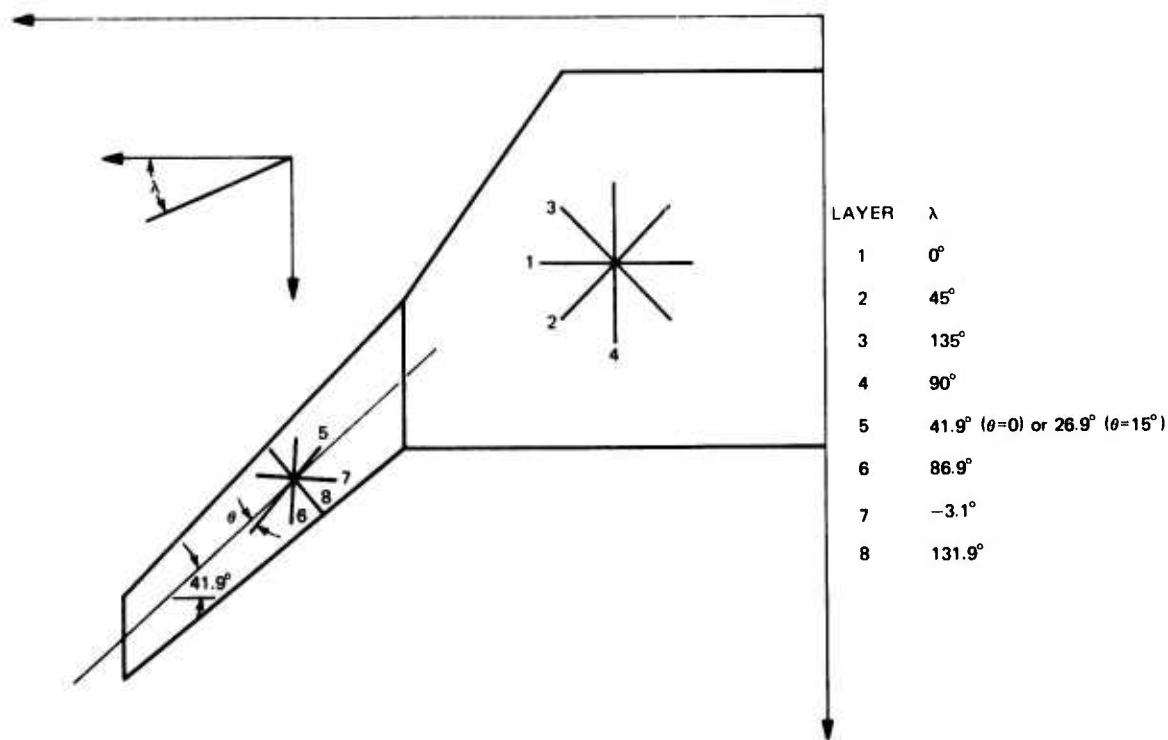


Figure 161. Finite Element Model Layer Directions

resulting in the layup directions of Figure 162. Analysis of this model was performed using the ASOP-3 program as it has a recycling capability for stress optimization. It also has the capacity to maintain equality of the $\pm 45^\circ$ layers to sustain the "balance" of the laminate. This analysis showed the need for additional layers between BL 76 and BL 122 to satisfy strength, but some layers between BL 0 and BL 122 which were originally supplied to meet torsional stiffness requirements remained understressed. A final cover configuration was then derived. Because flutter speed is less sensitive to inboard torsional stiffness, some material was removed to make the box more efficient. Structural influence coefficients were generated, and a flutter check was made which showed satisfactory performance.

Figures 163 through 171 show panel numbers, cover layups, stress resultants, and filament stresses for this tailored model Composite Structure, Modified Cover (CSMC.) Figures 172 and 173 show plots of principal layer stress and deflection obtained using the RAVES S50 and S51 programs.

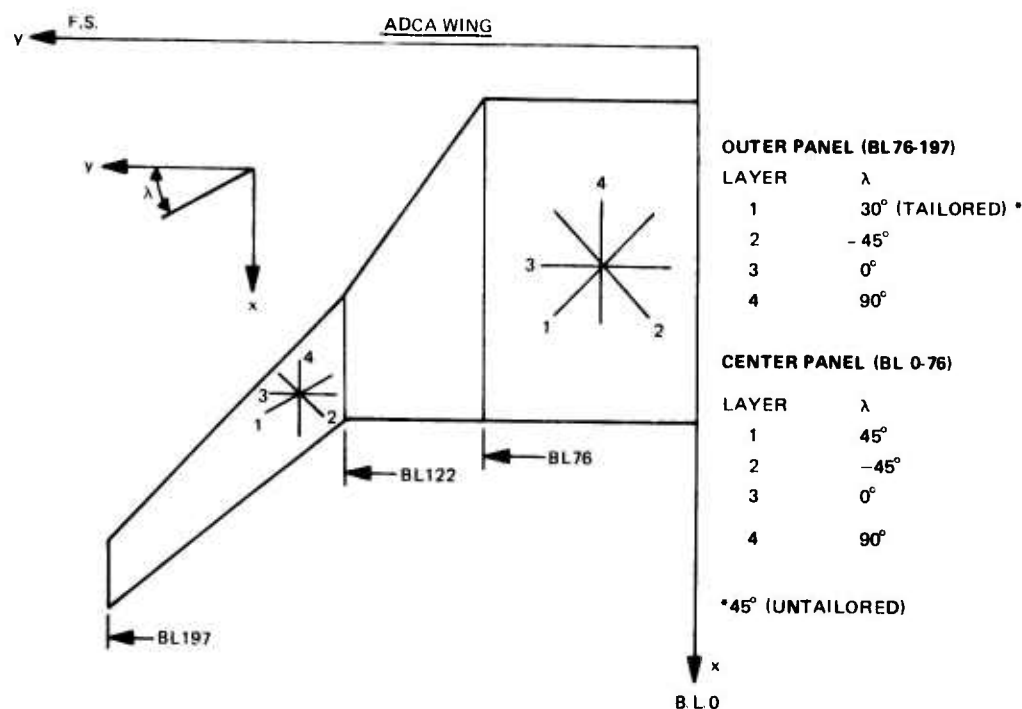
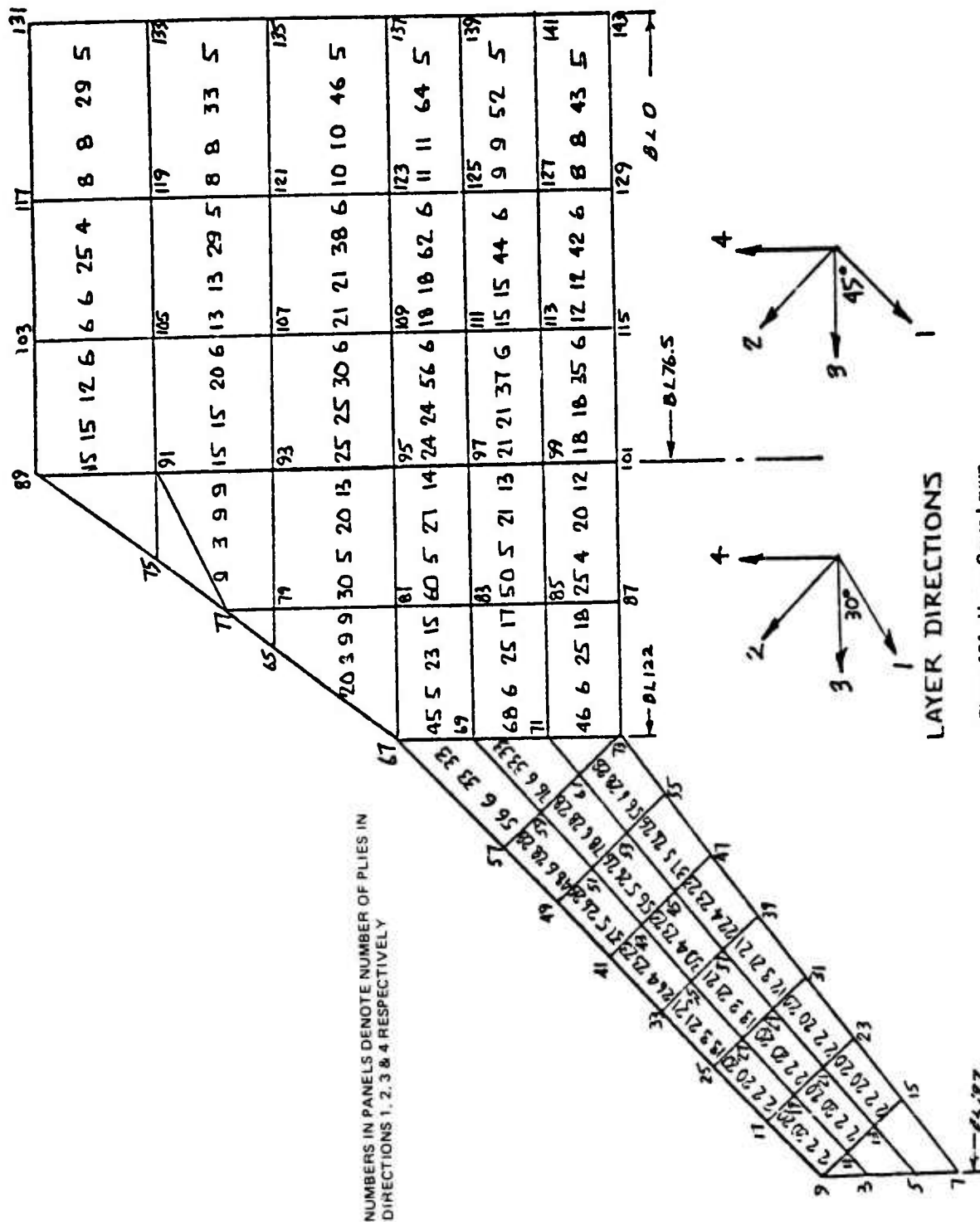


Figure 162. Finite Element Model Layer Directions

BEST AVAILABLE COPY



BEST AVAILABLE COPY

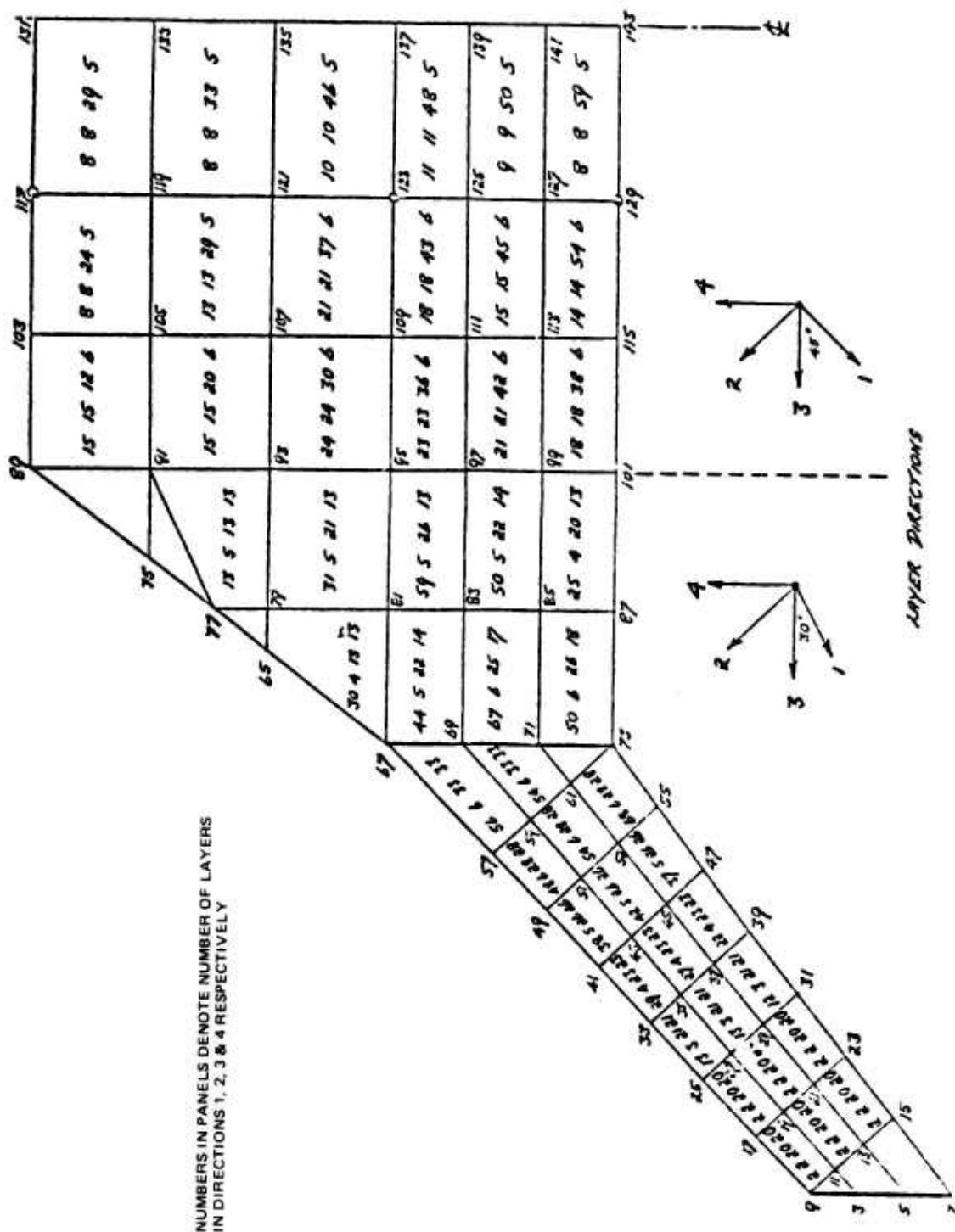


Figure 165. Lower Cover Layout

Figure 126: Moment Center Stress Resultants. The diagram illustrates the distribution of stress resultants (N, N_v, N_{xv}) in lb/in. across various members of a structure. The table below provides the numerical values for these resultants, organized by member and layer direction.

Member	N	N _v	N _{xv}
89	-2308	-5397	-7654
103	-1044	-413	-325
117	-1023	-1262	-344
123	71	105	119
75	-7617	-10975	-12199
105	-1366	-1501	-494
125	-2950	-3363	-604
77	-2997	-10975	-12199
107	-1366	-1501	-494
121	-2950	-3363	-604
65	-1256	-1730	-19181
79	-2627	-3925	-2169
109	-5962	-6419	-4943
81	-2672	-29378	-20579
83	-4345	-2863	-656
85	-11755	-6149	-864
67	-17871	-29378	-20579
69	-3197	-2863	-656
71	-8808	-6149	-4943
73	-27183	-18020	-22136
75	-5866	-1279	-575
77	-1562	-5775	-717
79	-1872	-12840	-17180
81	-3485	-816	-300
83	-9474	-4695	-3768

The diagram also includes two vector diagrams illustrating the layer directions (1, 2, 3) at specific points. The first diagram shows the layer directions at a point where the moment is 84.0. The second diagram shows the layer directions at a point where the moment is 84.122. The layer directions are defined by the angles between the layers and the horizontal axis.

Figure 166. Upper Cover Stress Resultants

TEST RESULTS COPY

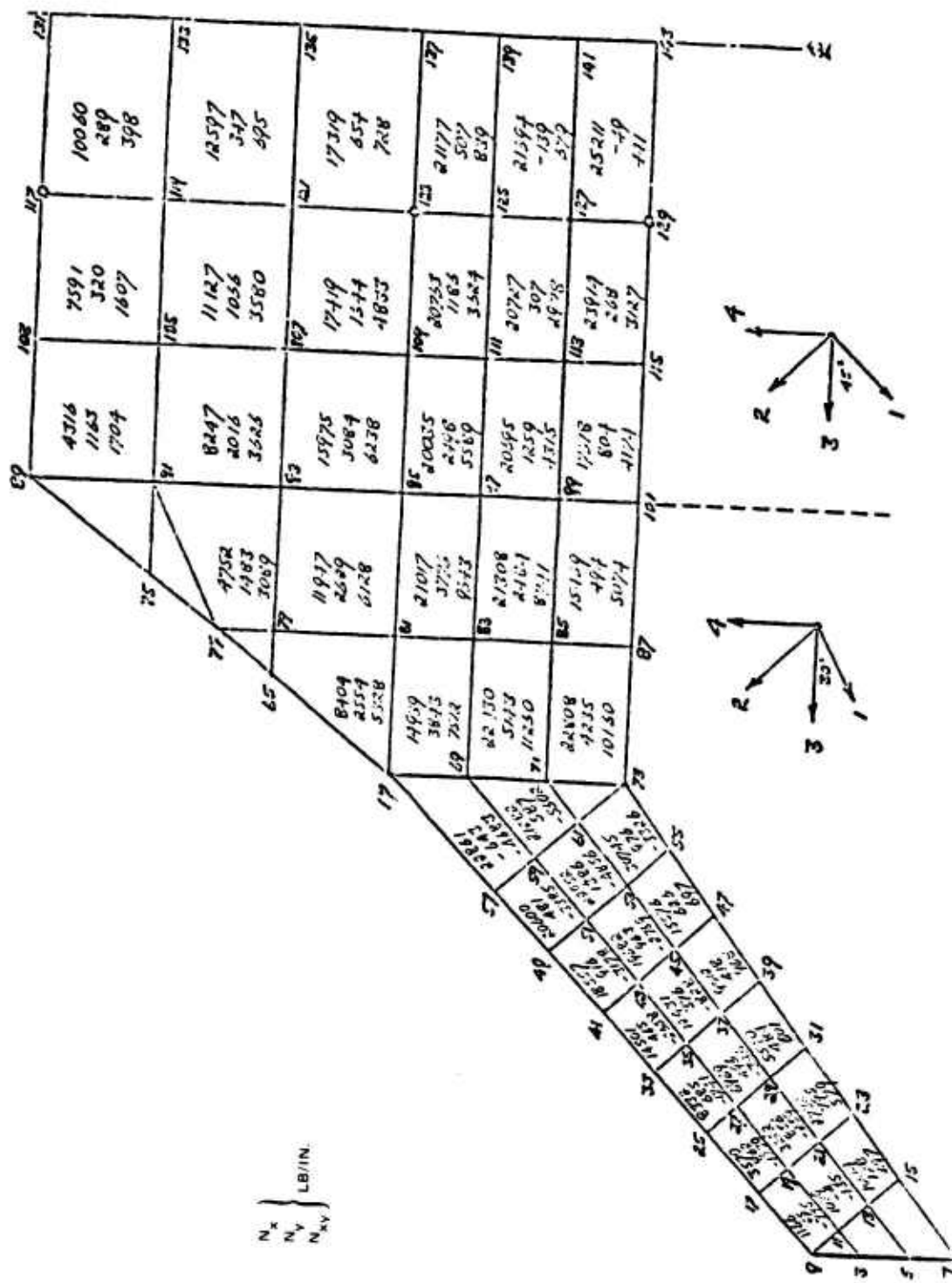
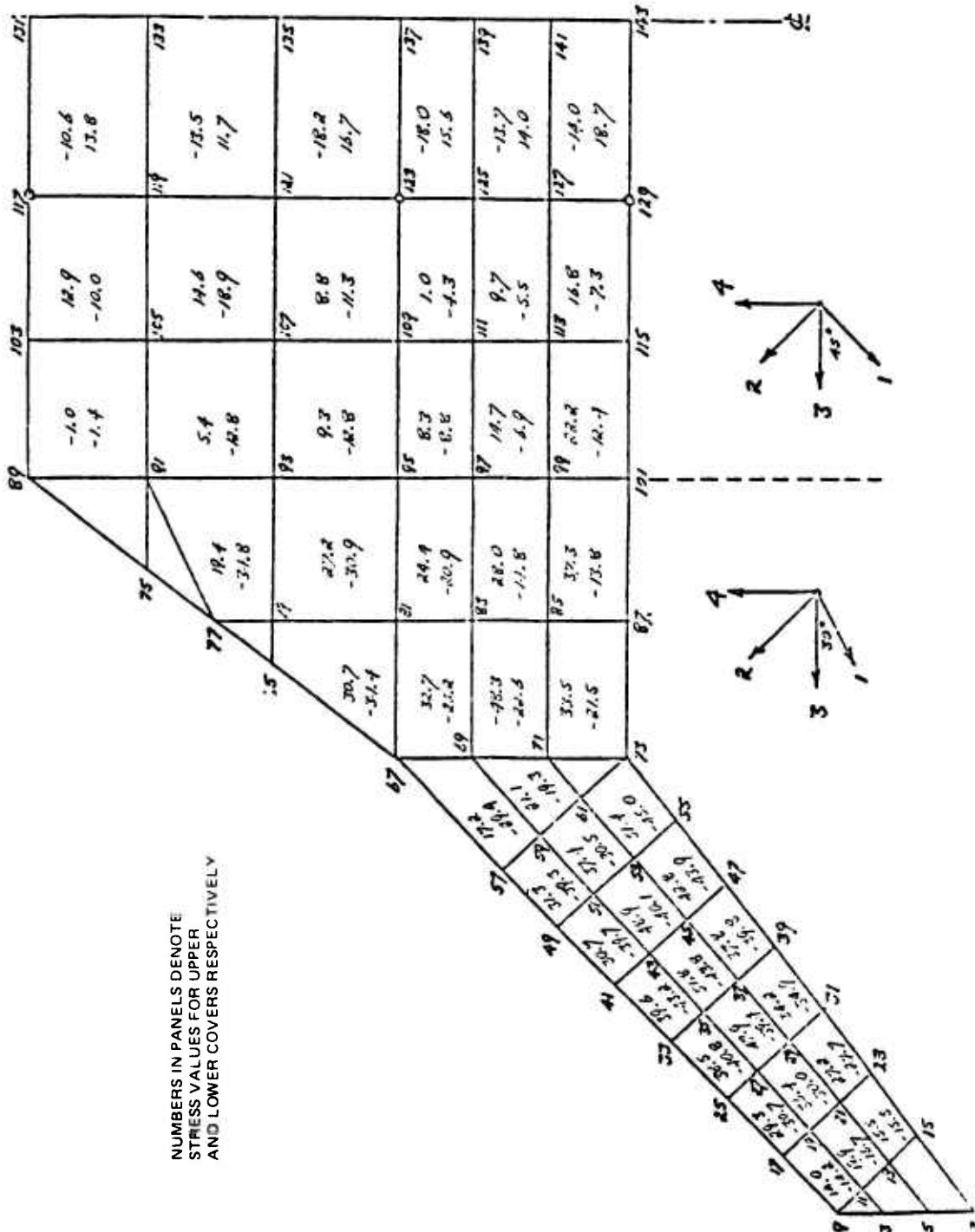
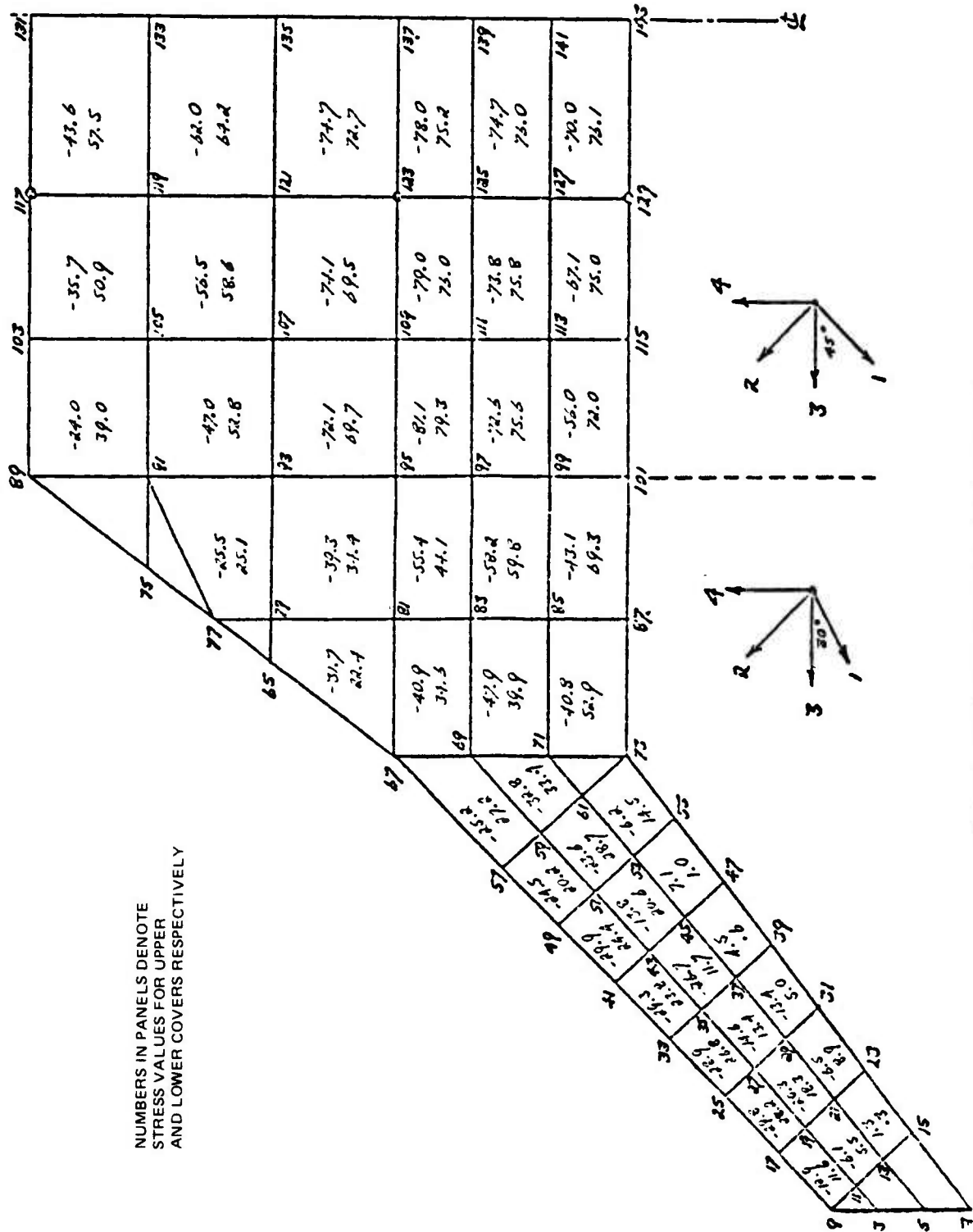


Figure 167. Lower Cover Stress Resultants

BEST AVAILABLE COPY



BEST AVAILABLE COPY



BEST AVAILABLE COPY

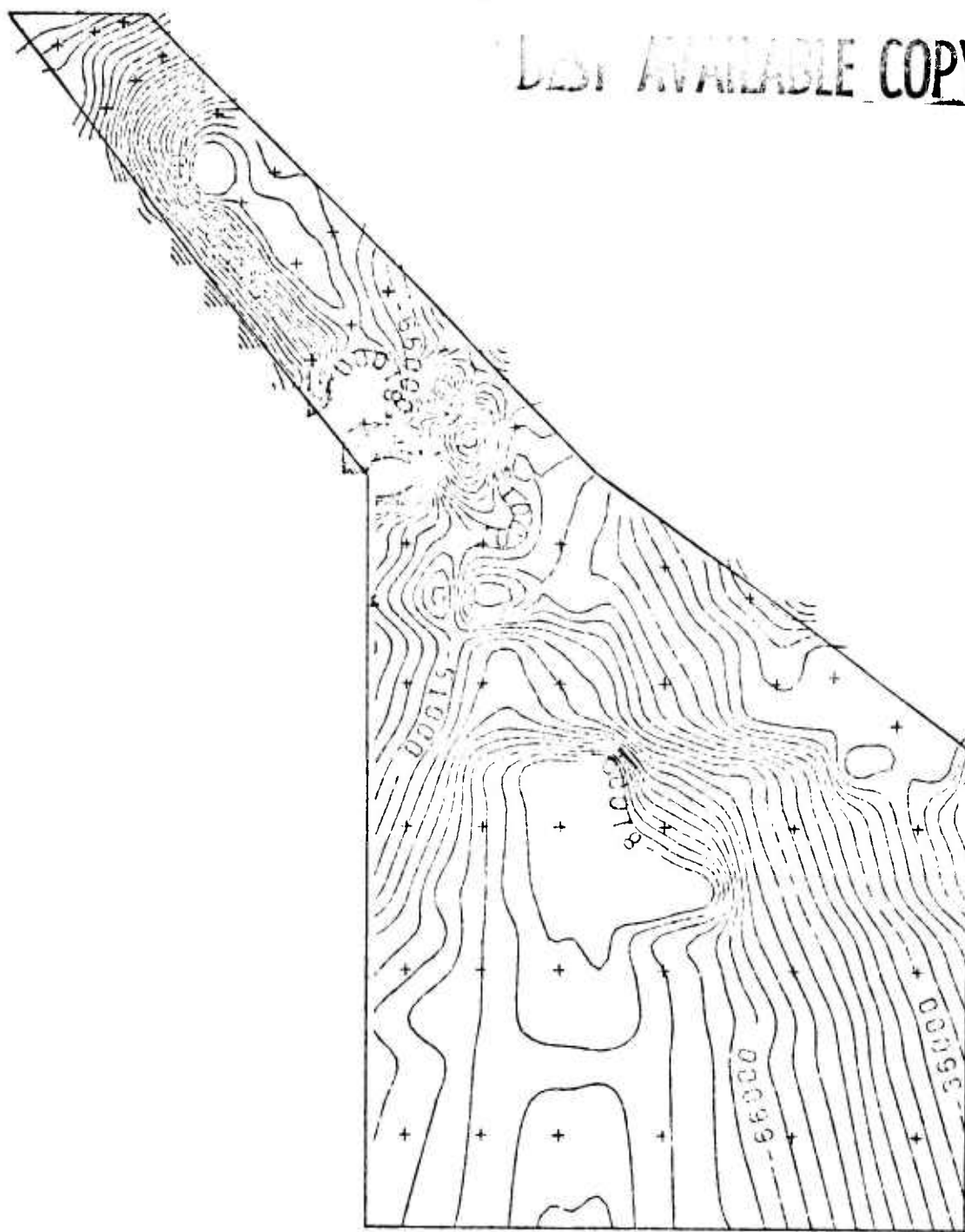


Figure 172. Principal Stress, Top Cover, Layer No. 1

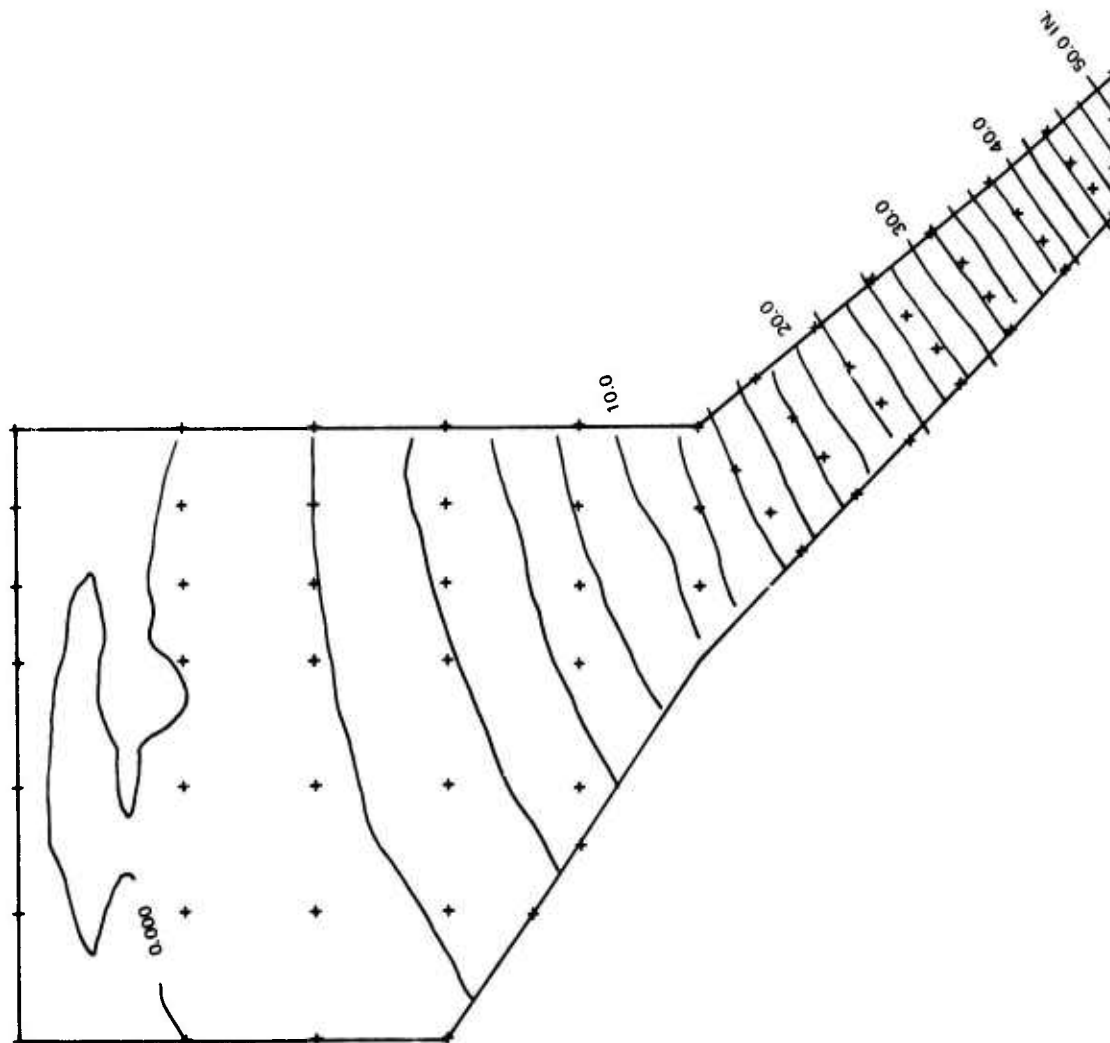


Figure 173. ADCA Wing Vertical Deflection

Using the structural influence coefficients from this model and the desired wing twist at 1.0 g, a built-in twist was derived. Figure 151 shows the desired twist curves at $M = 1.6$, 1.0 g and $M = 0.9$, 3.2 g. The tailored 1g twist attained matches the required by adding in the built-in twist described above. The tailored and untailored twist curves at $M = 0.9$, 3.2 g attained are also shown. As can be seen, they fall significantly short of the desired twist at $M = 0.9$.

A parallel effort was conducted for a finite element model of an untailored wing. The same load distributions were applied to obtain revised distributions for the built-in twist and twist at the sustained maneuver design point. Analysis indicates a net change in the

tip twist of 0.5° at 3.2g (Reference Figure 151). The elastic change is larger, 0.9° or 24% of the tailored value, but this is reduced by the revised built-in twist requirement. The increase in twist from the untailored to the tailored would translate into an increase in sustained maneuver load factor, and a reduction in induced drag.

All of the analyses described previously were run with a full grid of spars and ribs. Several runs were made with the rib idealization shown in Figure 174. This resulted in gage changes to the ribs and some slight influences on the spars. The changes to the covers were minimal and no difference in twist could be calculated.

All of the above work was premised on tailoring without adding weight over the strength and stiffness design.

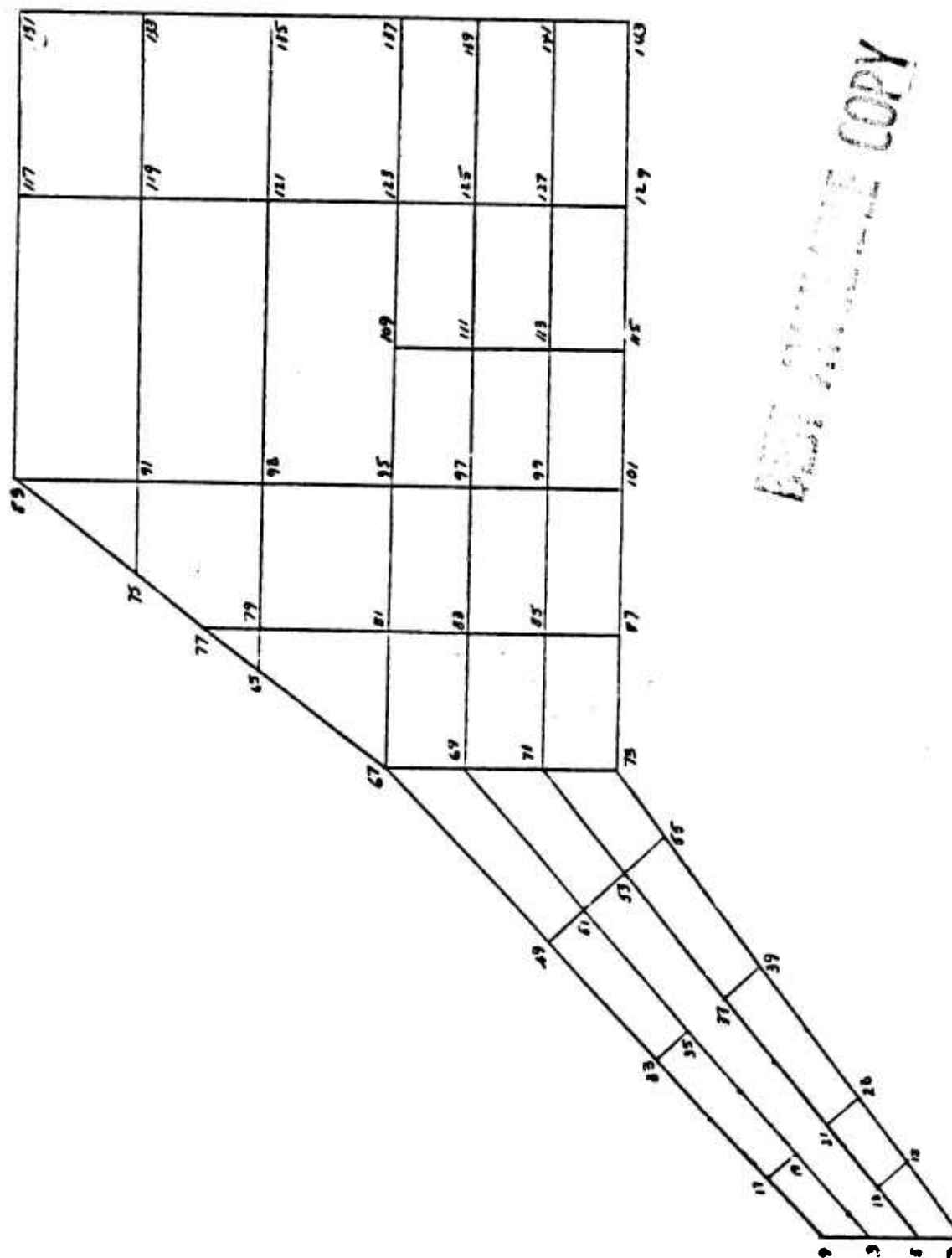
5.4.7 Finite-Element Model Optimization for Increased Twist

Because the twist distribution curves, for the baseline CSMC wing of the preceeding section, fall significantly short of the desired distribution in the sustained g condition, additional studies were performed using the newly developed Multiple Constraint Resizing (MCR) program. The first of these studies used MCR alone to determine where material could be added to the CSMC wing - which was already strength and flutter adequate - so as to increase the twist. The second study coupled MCR interactively with the ASOP III (Ref. 5) and FASTOP (Ref. 6) programs to produce a new design.

The MCR algorithm is based on an optimality criterion which employs the derivatives, with respect to each member weight, of the flutter speed, V_F , and the elastic streamwise twist angle, θ , at several spanwise stations, j . In addition, the procedure uses approximate relations to predict the change in the θ_j 's and V_F as the structure changes.

5.4.7.1 Optimization of Stiffness-Constrained Design

The first optimization study started with a finite-element model which satisfied both strength and flutter-speed requirements. In this design (CSMC), the spanwise fibers in the outboard portion of the wing were rotated 15° forward. As indicated in Figure 175, the tip twist angle for this design is -16.2° (nose-down) based on a "worst-case" load distribution (subsection 5.2.1). For reference, the twist-angle distribution for the untailored design is also presented. It is seen that reorienting the outboard spanwise fibers has resulted in an increase in the nose-down tip twist of 4.0° at ultimate load. The goal of the study described here was to increase this nose-down twist as much as possible.



Handwritten text: "COPY" and "174" (likely a reference number).

Figure 174. Alternate Rib and Spar Idealization

A groundrule established for the first optimization study was that the existing laminate thicknesses of the baseline CSMC wing could not be decreased; plies could only be added to accomplish the increased twist. Also, it was decided to address a single-twist constraint and only the composite wing covers were eligible for redesign. The target sustained-g, tip-twist angle was -17.0° at ultimate load, and the upper cover laminate for this redesign is shown in Figure 176. Similar optimizations were performed for the other desired twist angles, and the results are summarized in the following table. It is seen that only a small increase in twist could be achieved by adding material. In fact, it was determined that a limiting value existed; i.e., the addition of an infinite amount of weight could only increase the magnitude of the tip twist angle to -17.65° . The limiting values are shown by the hatched lines on Figure 175.

Converged Results ("Worst Case" Loads)		
Weight Increase, lb/side	Twist @ BL 122, Wing Break	Twist @ BL 197, Wing Tip
0	-5.15°	-16.2°
24.9	-5.47°	-16.5°
51.8	-5.70°	-16.7°
73.7	-5.70°	-17.0°
∞	-6.25°	-17.65°

Twist given in elastic twist under worst case ultimate loads; as-built twist is not included.

5.4.7.2 Coupled Optimization for Twist Angle, Flutter Speed, and Strength

A second optimization study was performed in which interactions among twist-angle, flutter-speed, and strength requirements were considered. Here, MCR, ASOP-III (Ref. 5) and the flutter-analysis capability of FASTOP (Ref. 6) were employed together as indicated in Figure 177. Before proceeding with the discussion of the ADCA optimization cycle, these programs will be briefly described.

ASOP-III (Automated Structural Optimization Program) employs a Fully Stressed Design (FSD) algorithm to optimize both composite and metallic structures subject to

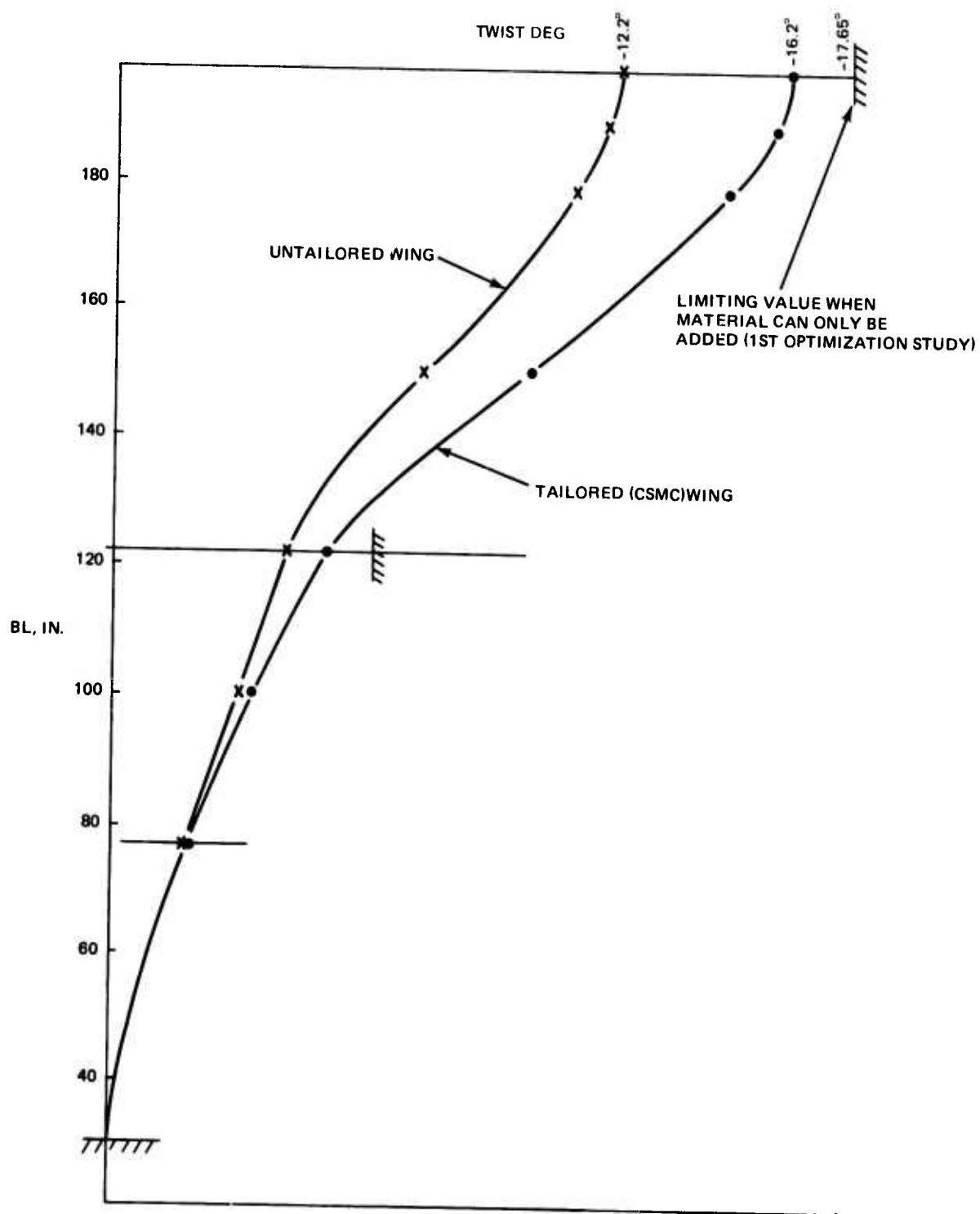


Figure 175. Streamwise Twist Distribution at Ultimate Load

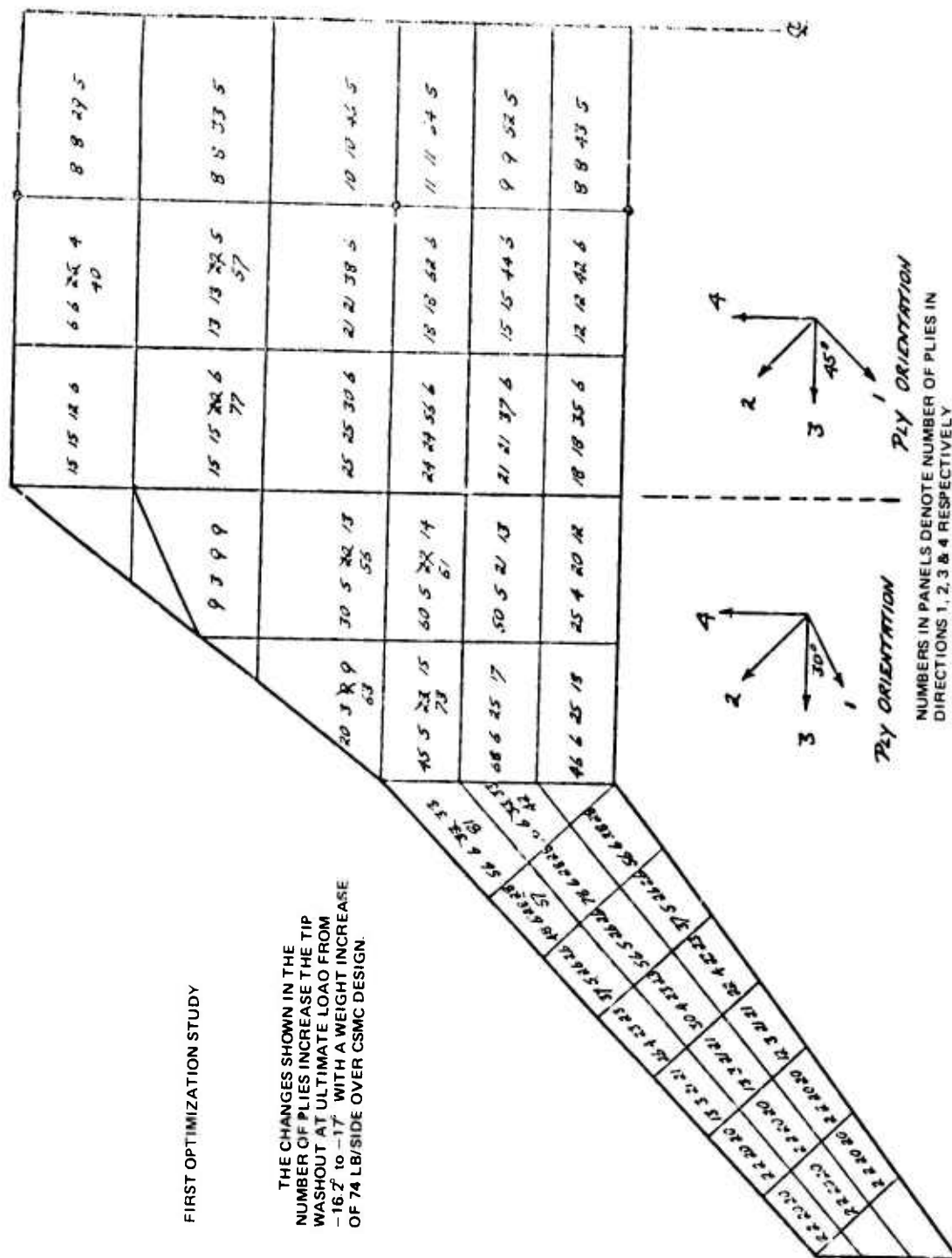


Figure 176. ADCA Wing, Upper Cover

strength requirements. A typical composite member is treated by ASOP-III as a stack of orthotropic membrane elements, where each element represents all plies with a common fiber direction. In normal usage, several ASOP-III analysis-redesign cycles are performed until convergence is achieved. In the converged design, each element is either fully stressed or at its minimum manufacturing-gage limit. The required thicknesses of composite materials are then converted to numbers of plies by dividing by the thickness per layer and conservatively rounding upward to obtain integral numbers of plies.

FASTOP (Flutter And Strength Optimization Program) is normally employed to perform weight optimization of a lifting surface subject to combined flutter and strength requirements. However, while the flutter module in FASTOP is capable of optimizing both composite and metallic structures, the strength (FSD) module currently addresses only

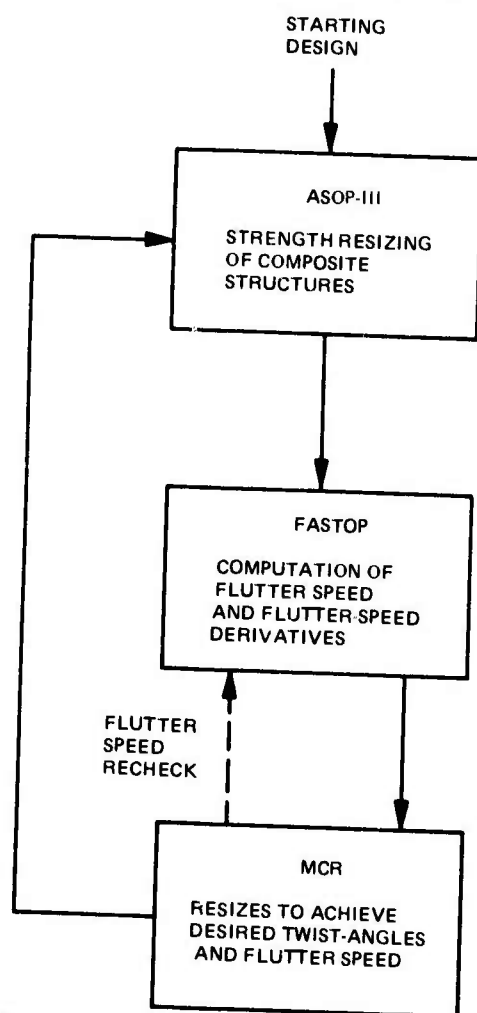


Figure 177. Finite-Element Optimization Procedure

metallic structures. Also, MCR includes the capability for flutter resizing. Therefore, in this study, the ASOP-III program was employed for strength design, MCR was employed for flutter and twist resizing, and only the flutter-analysis and flutter-derivative calculation capability of the FASTOP system was employed.

The optimization procedure shown in Figure 177 is initiated by performing several FSD cycles using the ASOP-III program. FASTOP is then used to compute the flutter speed and flutter-speed derivatives. These quantities in turn are used in MCR, where resizing is performed simultaneously for twist and flutter-speed requirements. In this initial MCR step, no element is permitted to fall below its strength minimum (as previously predicted by ASOP-III) or fall below its minimum manufacturing-size requirement, and elements that are resized upward are classified as twist/flutter critical. MCR also performs a finite-element deflection analysis to check the twist angles of the redesigned structure, and, if desired, FASTOP may be used to check the flutter speed. At this point, one cycle of Figure 177 has been completed.

The new design is now passed to ASOP-III to start a second cycle. Here, ASOP-III treats any element previously resized upward (for twist-angle and flutter-speed requirements) as a minimum-gage value; i.e., it may resize that element upward to satisfy strength requirements but not downward. However, any strength-critical elements from the first cycle may be resized either way in this second ASOP-III step. Similarly, in the second MCR resizing, strength-critical elements are considered as minimum-gage, but elements that are twist/flutter critical may be resized either way.

The ASOP-III/MCR resizing loop is repeated until convergence is achieved. The converted design is a minimum-weight structure satisfying the desired flutter-speed and twist-angle requirements without violating strength or minimum manufacturing size requirements.

The starting point for the second optimization study was a version of the CSMC wing in which the GJ requirement was discarded. The $\pm 45^\circ$ layers were reduced to minimum gage (one ply), while the 0° and 90° layers were unchanged, and the design was run through five cycles of ASOP-III to correct any strength deficiencies. The flutter speed of the resulting design was calculated to be 488 kt, and the tip washout under the "worst case" ultimate loads was -19.6° .

The goal of the second study was to increase the flutter speed to 800 kts and to increase the washout as much as possible. After several cycles, in which the tip twist was increased with each redesign, it was decided to fix the target constraints at 800 kts and -20° and allow the procedure to converge to a minimum weight design. The results are summarized in Table 23.

TABLE 23. SECOND WING TWIST OPTIMIZATION STUDY

DESIGN	TIP TWIST AT "WORST CASE" D. U. L. (deg)	FLUTTER SPEED (k eas)	WEIGHT OF REDESIGN lb/side
START	-19.6	488	603
CONVERGED	-20.0	803	688
CSMC (for comparison)	-15.8	790	751

Figures 178 and 179 show the starting and final laminates for the upper cover, figure 180 shows the stress resultants in the final version, and figure 181 shows the twist distribution achieved compared to the previous finite-element models.

A comparison of figures 179 and 180 with the corresponding figures 164 and 166 for the CSMC wing show that the cycling procedure has moved the spanwise axial load N_x forward in the outboard positions of the wing, and added large numbers of unbalanced $\pm 45^{\circ}$ layers along the outboard leading edge while removing material along the entire trailing edge.

This may be understood as a forward shift of the flexural axis with a stiff torque tube between the front and second beams. The unbalance of the $\pm 45^{\circ}$ layers is less easily understood, since the studies of Subsection 5.4-4 indicate that this is not an efficient way of providing bending/torsion coupling in a wing. The derivatives - which show the change of twist and flutter speed with layer thickness - were next examined for each layer in each panel of the outboard upper cover. This provided considerable insight into the behaviour of the wing:

- Most of the derivatives show that increasing washout is detrimental to the flutter speed
- Subtracting plies from the nominally spanwise layer is the most effective way of increasing the washout, by reducing the bending stiffness, but this reduces the flutter speed and is not allowed by the bending strength requirement

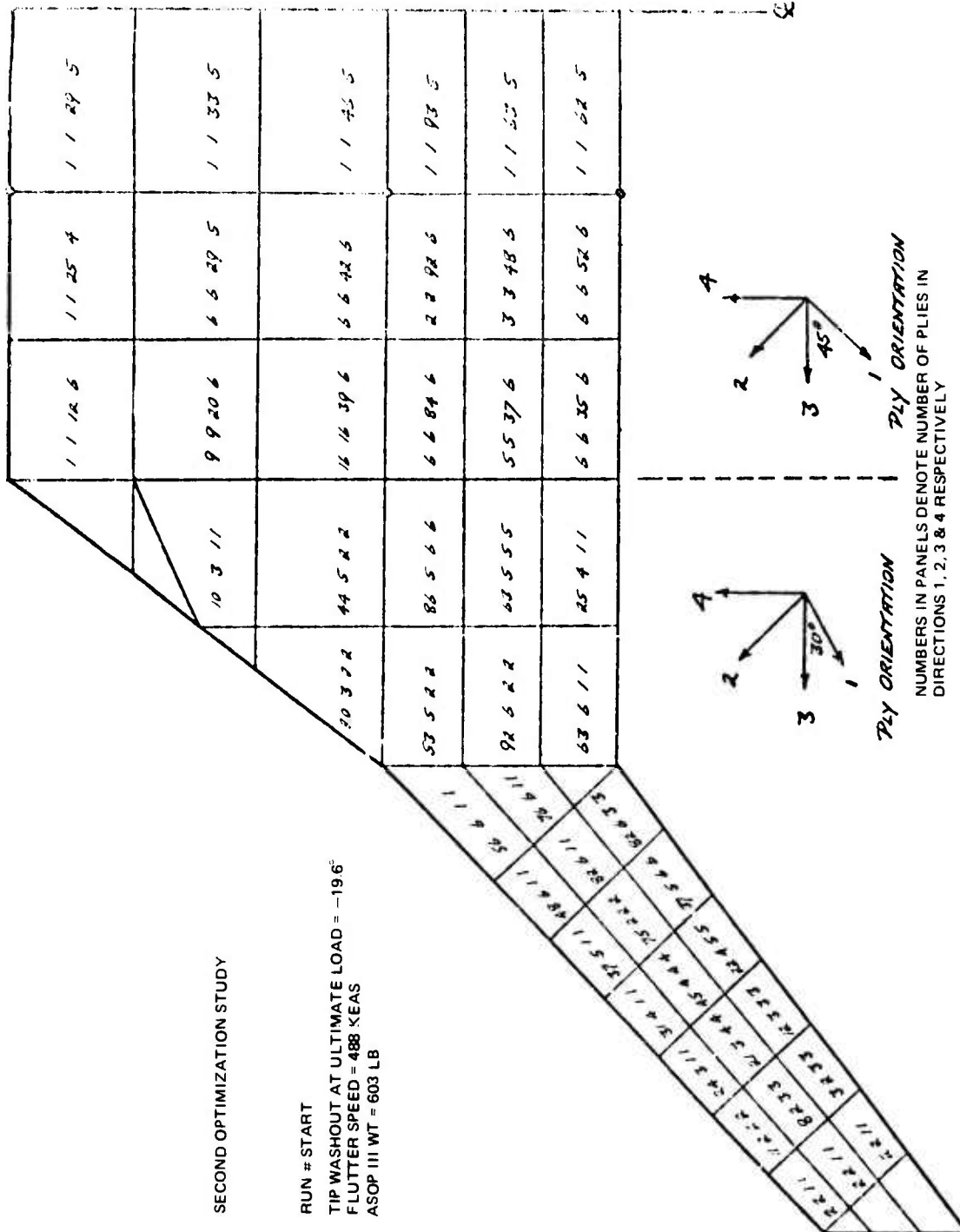


Figure 178. ADCA Wing. Upper Cover

SECOND OPTIMIZATION STUDY

NUMBERS IN PANELS DENOTE NUMBER OF PLIES IN DIRECTIONS 1, 2, 3 & 4 RESPECTIVELY. WHERE UNDERLINED, NUMBER OF PLIES IS DESIGNED BY TWIST AND FLUTTER REQUIREMENT. REMAINDER DESIGNED BY STRENGTH OR MIN. GAUGE.

[illegible]

Figure 179 Upper Cover Layout:
Converged Design After
MCR/ASOP/FASTOP Cycling

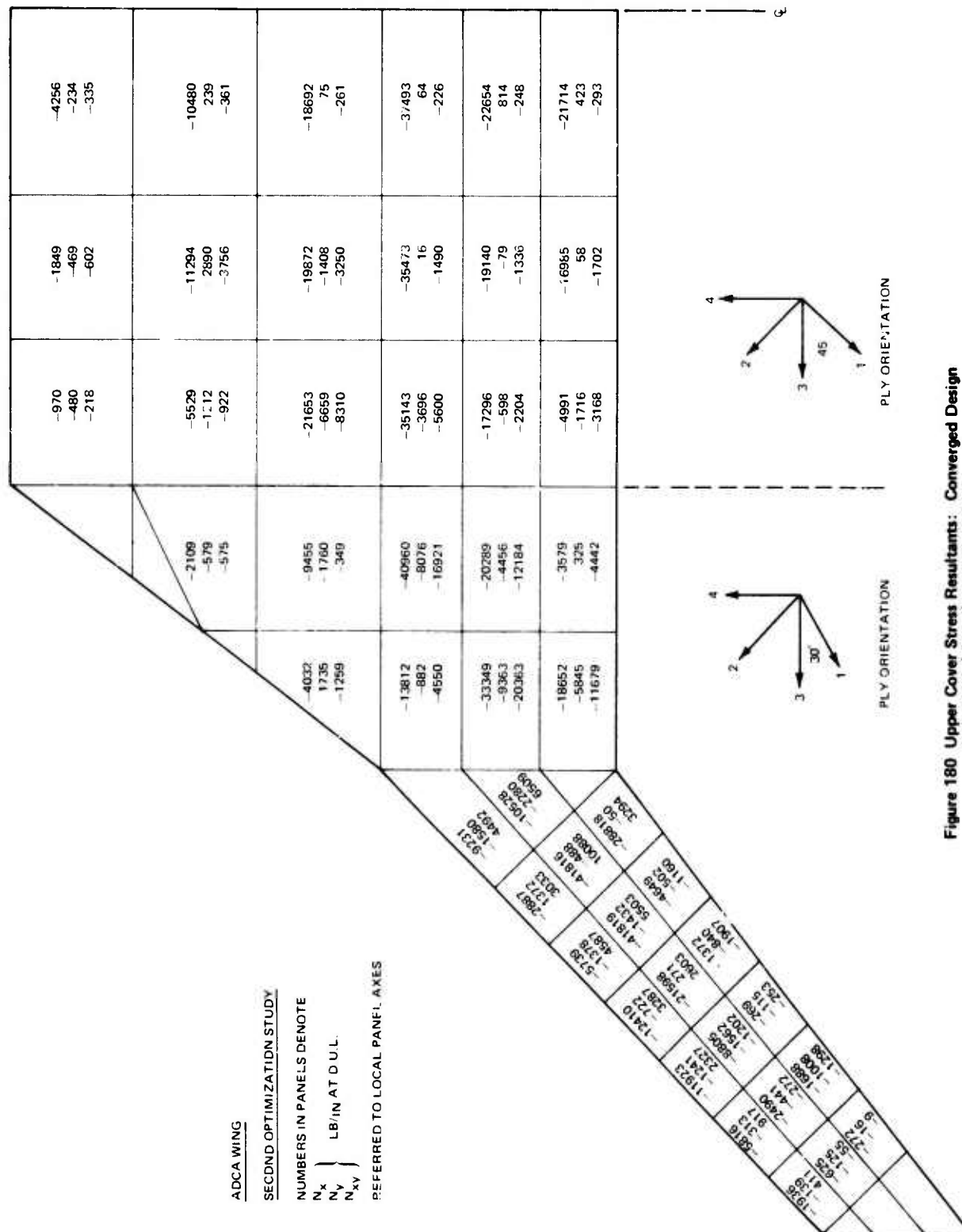


Figure 180 Upper Cover Stress Resultants: Converged Design
 After MCR/ASOP/FASTOP Cycling

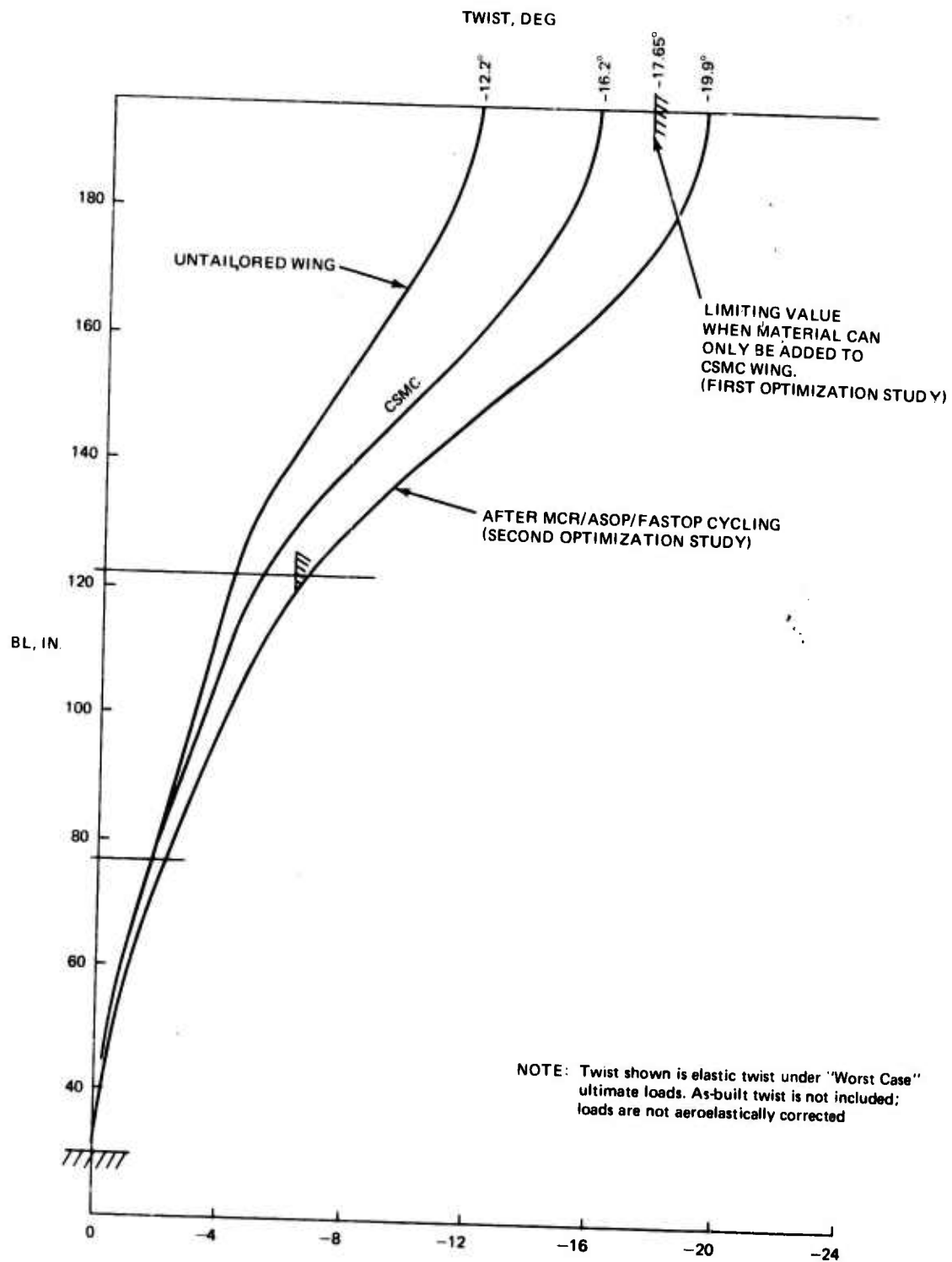


Figure 181. Streamwise Twist Distribution at Ultimate Load

- Adding plies to the $\pm 45^\circ$ layers (3 and 4) is the most effective way of increasing the flutter speed; Layer 4 being more effective than Layer 3 but having a more detrimental effect on the washout.
- The derivatives are all small: the largest twist derivative occurs in layer 1 of panel 9 (see Figure 163) and is 0.0137 radians/lb. Since one layer weighs only 0.027 lb, the tip twist changes only 0.021 degrees for each additional ply. Similarly the largest flutter derivative occurs in layer 4 of panel 29 and is 13.39 knots/lb, therefore the flutter speed changes 0.36 knots for each additional ply
- Unbalancing the $\pm 45^\circ$ plies is indeed a comparatively ineffective way of providing the bending/twisting coupling. So much so, that forcing the $\pm 45^\circ$ plies into balance throughout the wing (i.e. layers 3 & 4 outboard of B. L. 76 and layers 1 & 2 inboard of B. L. 76) resulted in a loss of flutter speed of only 23 knots and a gain in washout of 0.09° .

It may be concluded from this examination that, while the laminates which result from MCR/ASOP/FASTOP cycling give a minimum weight design which meets the constraints, the flutter speed and washout are relatively insensitive to the laminate in a given panel. The important aspects of the cycling are in the redistribution of bending material, to shift the flexural axis forward, and the provision of a torsional stiffness through balanced $\pm 45^\circ$ plies. This accounted for 290 kts of the total increase in flutter speed. Unbalance of the $\pm 45^\circ$ plies, by relatively large amounts, gave the remaining 23 kts of the increase.

Obviously, the design shown in figure 179 is not yet a practical structure and further refinement in a finer grid finite element model, plus more design loading cases and flutter checks at other Mach numbers, weights and store conditions would be required. However, it is already clear at this stage that the linked MCR/ASOP/FASTOP cycling has demonstrated the potential design of a wing which has 25% more twist than the CSMC wing, and that the resulting laminates can be smoothed for ease of manufacture, etc., without incurring large penalties in washout or flutter speed.

5.4.8 Vibration and Flutter Considerations

The technical intent of the flutter integrity program for the ADCA is twofold. First within the limits of a preliminary design effort, adequate flutter margins for each surface must be demonstrated. Secondly the independence of the bending and torsional stiffness

available through advanced composite technology demands the definition of required torsional stiffness such that the weight penalty associated with flutter integrity is near minimum.

Results for the ADCA wing using the final beam-type dynamic model are included. The model reflects the increased aircraft weight to meet SPIF mission requirements. Adequate flutter margins for the clean wing, both empty and with full fuel, and tip-mounted Sidewinder cases are demonstrated. A finite element analysis for the wing has been completed and is discussed in detail above. The results of the finite element analysis have been used to verify the beam model flutter results and excellent similarity in flutter characteristics is demonstrated.

5.4.8.1 Methodology

To define torsional stiffness requirements for preliminary design, historical data relating the fundamental torsion frequency to planform and flight envelope parameters was compiled. Having determined the required ω_α for flutter integrity, a statistical approximation for the spanwise weight distribution is used in conjunction with an inverse Rayleigh solution to determine the compatible GJ distribution. These data together with strength and twist requirements form the basic input to the COMBO program. COMBO uses a modified beam approach to simultaneously meet these requirements. The output from COMBO includes anisotropic stiffness matrices for each panel on the idealized beam. These are subsequently integrated to form the overall beam influence coefficients.

Vibration analyses using the stiffness, thus defined, and more refined mass properties are then completed. In all cases, panels perpendicular to the main beam axis are assumed rigid. Finally, rational flutter analyses are completed to verify the preliminary requirements. Analyses utilized the Doublet Lattice approach for the subsonic regime and the Mach Box Program supersonically. Analyses for the wing finite element model were accomplished within the FASTOP system so that any required resizing for flutter could be easily implemented.

Mass and stiffness data as well as vibration and flutter analyses results for each of the surfaces is detailed below.

5.4.8.2 Wing Flutter Analysis

The ADCA wing design aimed towards the realization of conventional aeroelastic tailoring benefits. These have been discussed previously. The structural implications of

TABLE 24. WING BEAM MODEL INFLUENCE COEFFICIENT MATRIX*

	1	2	3	4	5	6	7	8	9	10	11	12	13	14	15	16
1	0.6073															
2	1.9190	7.2832														
3	3.0947	12.561	24.833													
4	3.9872	16.568	35.966	60.793												
5	4.9351	20.824	47.791	89.080	147.49											
6	5.9389	25.331	60.313	119.03	213.16	342.08										
7	6.9428	29.838	72.835	148.99	278.82	479.22	743.40									
8	7.9467	34.345	85.358	178.95	344.49	616.37	1026.8	1593.5								
9	0	0	0.0187	0.561	0.0958	0.1378	0.1799	0.2220	0.00236							
10	0	0	0.0581	0.1745	0.2980	0.4288	0.5597	0.6905	0.00236	0.00734						
11	-0.0327	-0.1467	-0.2459	-0.2084	-0.1685	-0.1263	-0.0840	-0.0417	0.00177	0.00551	0.0173					
12	-0.0327	-0.1467	-0.2459	-0.1427	0.0521	0.2584	0.4646	0.6709	0.00177	0.00551	0.0173	0.0332				
13	-0.0327	-0.1467	-0.2459	-0.1427	0.1657	0.6408	1.1159	1.5910	0.00177	0.00551	0.0173	0.0332	0.0502			
14	-0.0327	-0.1467	-0.2459	-0.1427	0.1657	0.8311	1.7262	2.6213	0.00177	0.00551	0.0173	0.0332	0.0602	0.1056		
15	-0.0327	-0.1467	-0.2459	-0.1427	0.1657	0.8311	2.0047	3.5153	0.00177	0.00551	0.0173	0.0332	0.0602	0.1056	0.1828	
16	-0.0327	-0.1467	-0.2459	-0.1427	0.1657	0.8311	2.0047	3.8726	0.00177	0.00551	0.0173	0.0332	0.0602	0.1056	0.1828	0.3162

*See Figure 182 Coordinate Definition

such design directives include increasing the washout from the basic strength and stiffness designed wing. It has been previously demonstrated that tailoring for increased washout is detrimental to flutter speed. Thus, the flutter integrity of the wing had to be verified with specific caution. Preliminary analyses were accomplished using an anisotropic dynamic beam model. Those results have been verified utilizing the finite element model.

The preliminary wing was sized using the COMBO program for strength, stiffness and twist per g requirements. Several variations of ply layup were considered. The final approach used the laminate defined by strength and stiffness requirements with the 0° layers for the outboard wing kicked 15° forward from the main beam axis. This allows the optimum twist for the $M = 1.6$ cruise condition to be achieved while achieving, as much as possible, the optimum twist for the $M = 0.9$ maneuver condition within minimum weight constraints.

The wing beam model dynamic idealization is shown in Figure 182 where the panels and rotational degrees of freedom are taken perpendicular to the beam reference axis. Corresponding flexibility influence coefficients for the final iteration beam model are included in Table 24.

Distributed weights data for the clean wing without fuel is included in Table 25. These reflect the increased vehicle weight to meet the limits of the study area for the SPIF mission requirements.

**TABLE 25. WING MASS PROPERTIES
CLEAN, NO FUEL**

Panel	Weight, lb	Arm*, in.	Unbalance, lb-in.	$I_{yy_{cg2}}$ lb-in.	$I_{yy_{EA2}}$ lb-in.
1	390.0	-12.1	-4719.0	1,215,878	1,272,978
2	308.0	1.4	432.3	596,460	597,065
3	141.8	-10.5	-1488.9	32,012	47,645
4	153.1	8.3	1270.7	58,062	68,609
5	178.4	6.4	1141.8	50,233	57,540
6	111.3	2.7	300.5	17,688	18,499
7	90.5	2.6	235.3	11,614	12,226
8	81.2	4.2	341.0	8,067	9,499
*Refers to perpendicular distance from panel cg to beam axis; positive indicates aft cg					

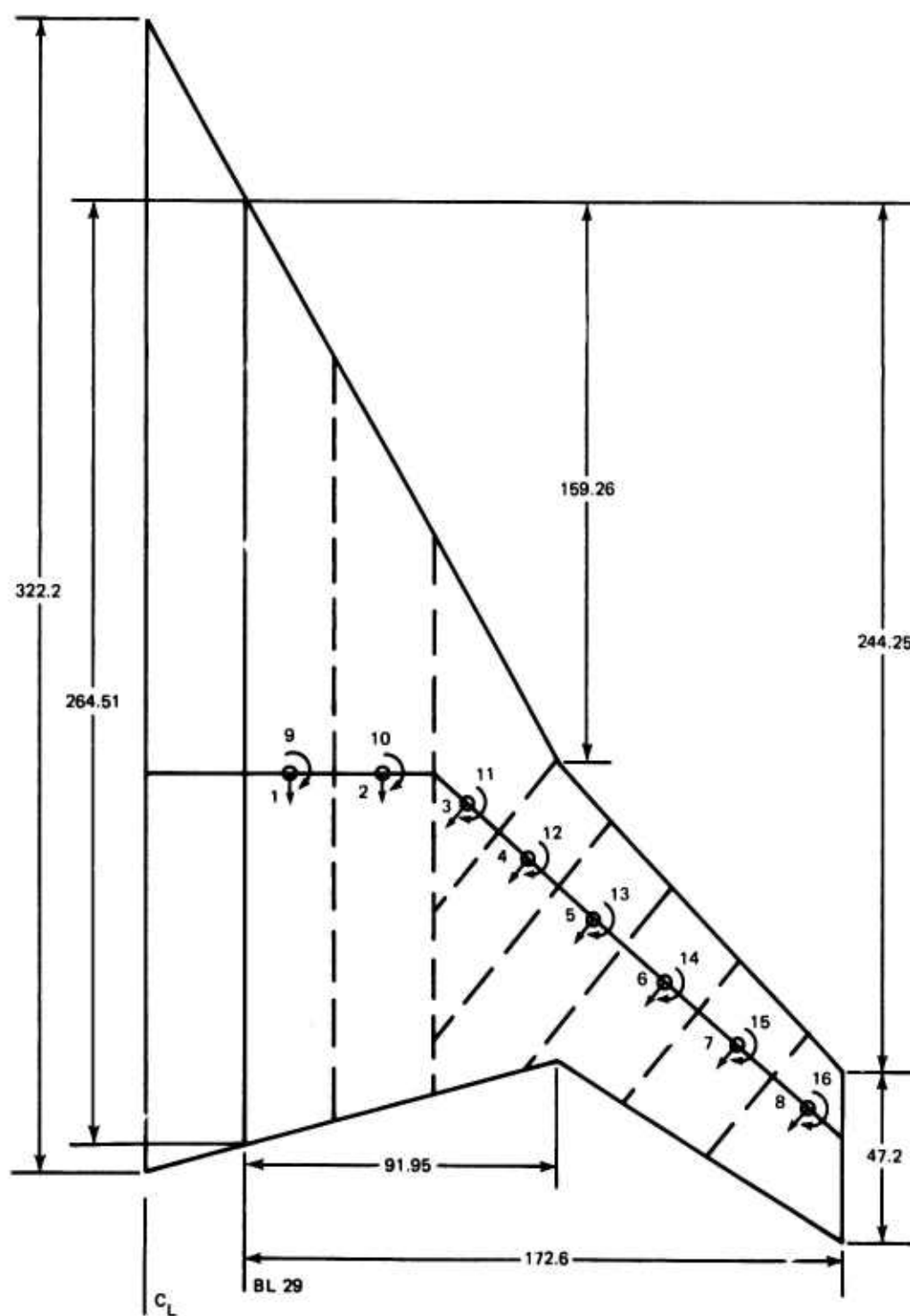


Figure 182. Wing Dynamic Idealization Beam Model

Vibration analyses were completed for the above and the resultant frequencies are summarized in Table 26. Node line plots for these modes are included in Figure 183.

TABLE 26. WING BEAM MODAL FREQUENCIES
CLEAN, NO FUEL

Mode	Frequency, Hz
1st Bending	6.21
2nd Bending	20.31
Torsion	32.03

Flutter analyses were completed throughout the entire flight regime and the resultant flutter envelope is shown in Figure 183, where adequate flutter boundaries are demonstrated. Since this provides the baseline case for the wing analyses, V-g- plots are included in Figures 184 through 195. The basic flutter mechanism is seen to be a ternary involving wing first and second bending as well as torsion. The results are summarized in Table 27.

TABLE 27. WING FLUTTER SPEED SUMMARY
CLEAN, NO FUEL

Mach	Altitude, 1000 ft	V _f , KEAS	V _f /V	Ref V -g- ω Plot, Figure
0.6	SL	837	2.11	184
	20	820	3.06	185
	40	801	4.71	186
0.8	SL	809	1.54	187
	20	771	2.16	188
	40	739	3.27	189
1.3	SL	NF**	-	190
	11*	NF	-	191
	20	NF	-	192
	40	NF	-	193
1.6	21.5*	NF	-	194
	40	NF	-	195
*Altitude appropriate to V _L envelope				
**No Flutter				

It should be noted that the vibration and flutter results included above refer to cantilevered modes with a representative root spring included.

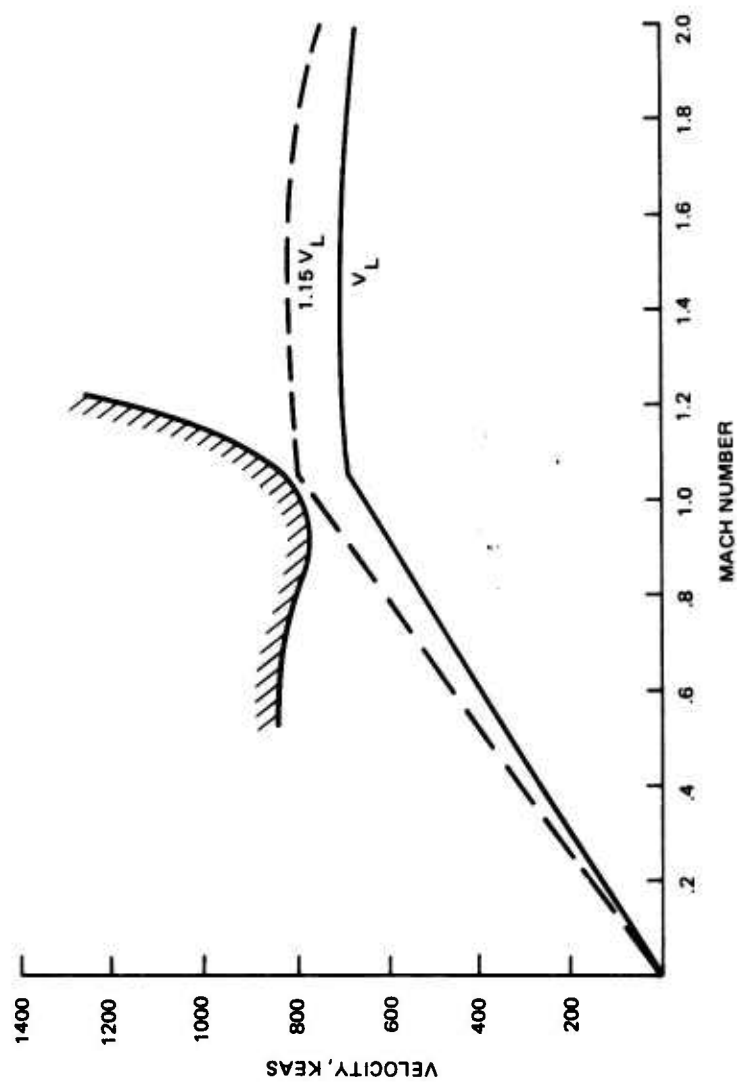
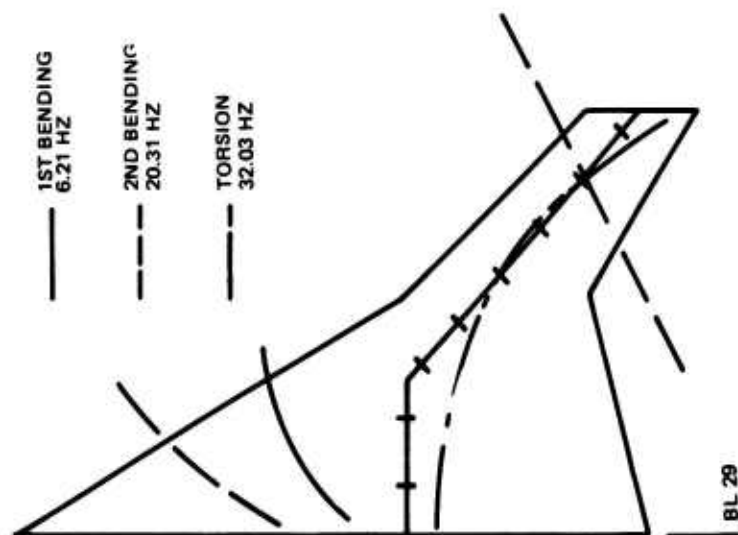


Figure 183. ADCA Wing - Node Lines and Flutter Envelope, Clean Wing

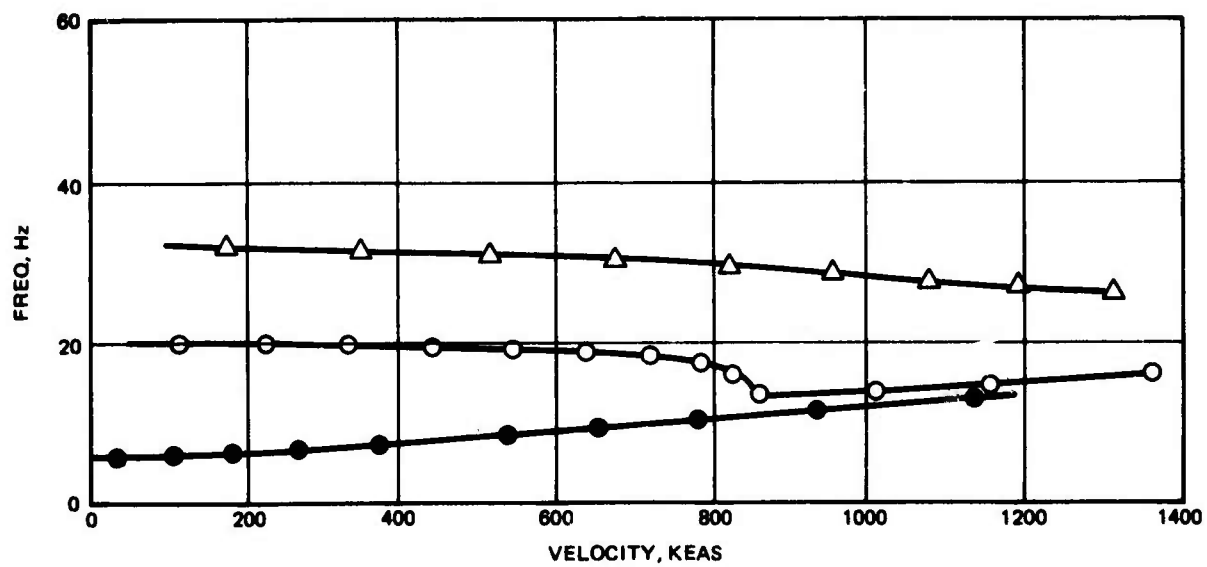
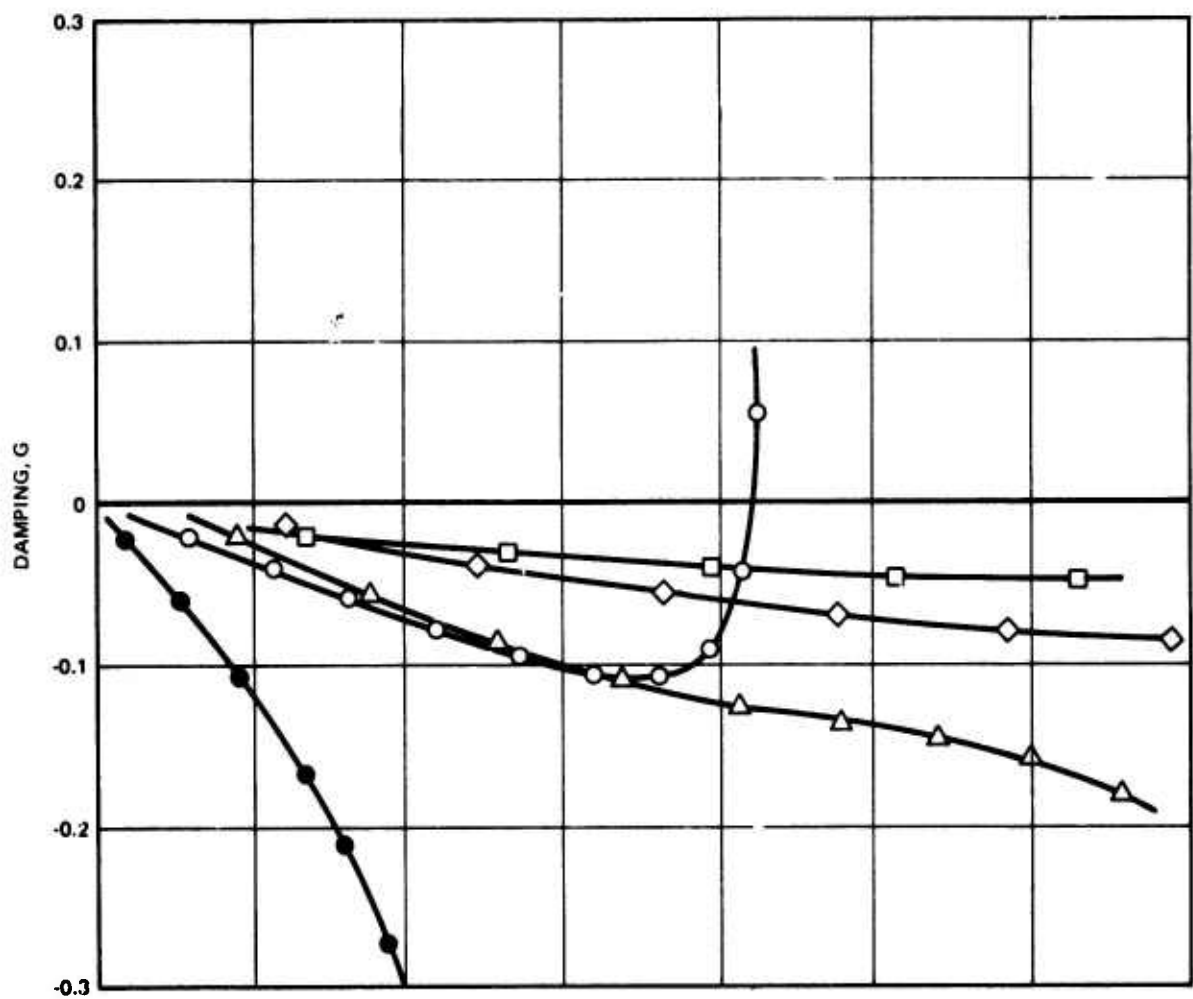


Figure 184. Wing Beam Model, Clean, No Fuel, $M = 0.6$, Sea Level

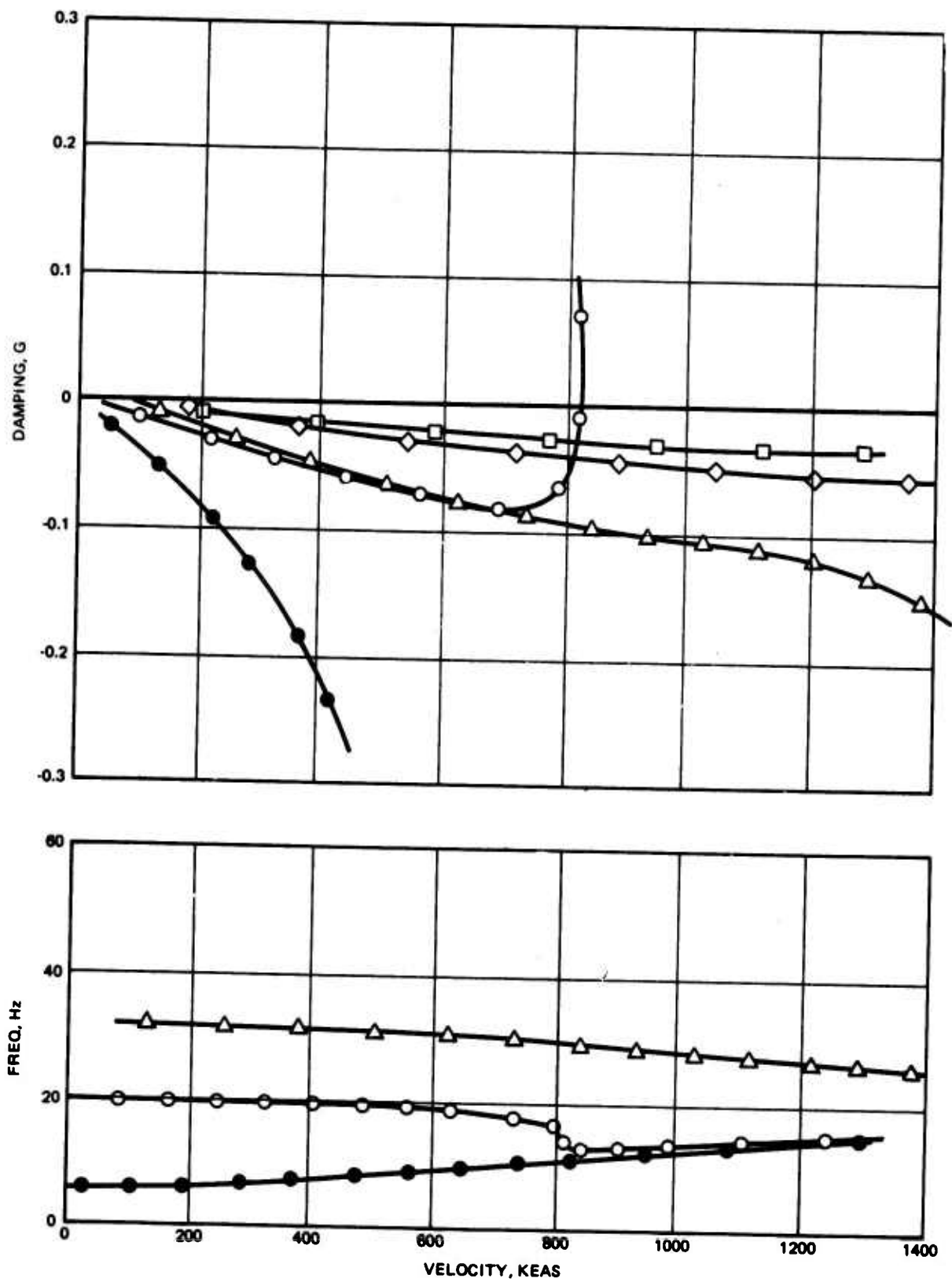


Figure 185. Wing Beam Model, Clean, No Fuel, $M = 0.6$, 20,000 Ft

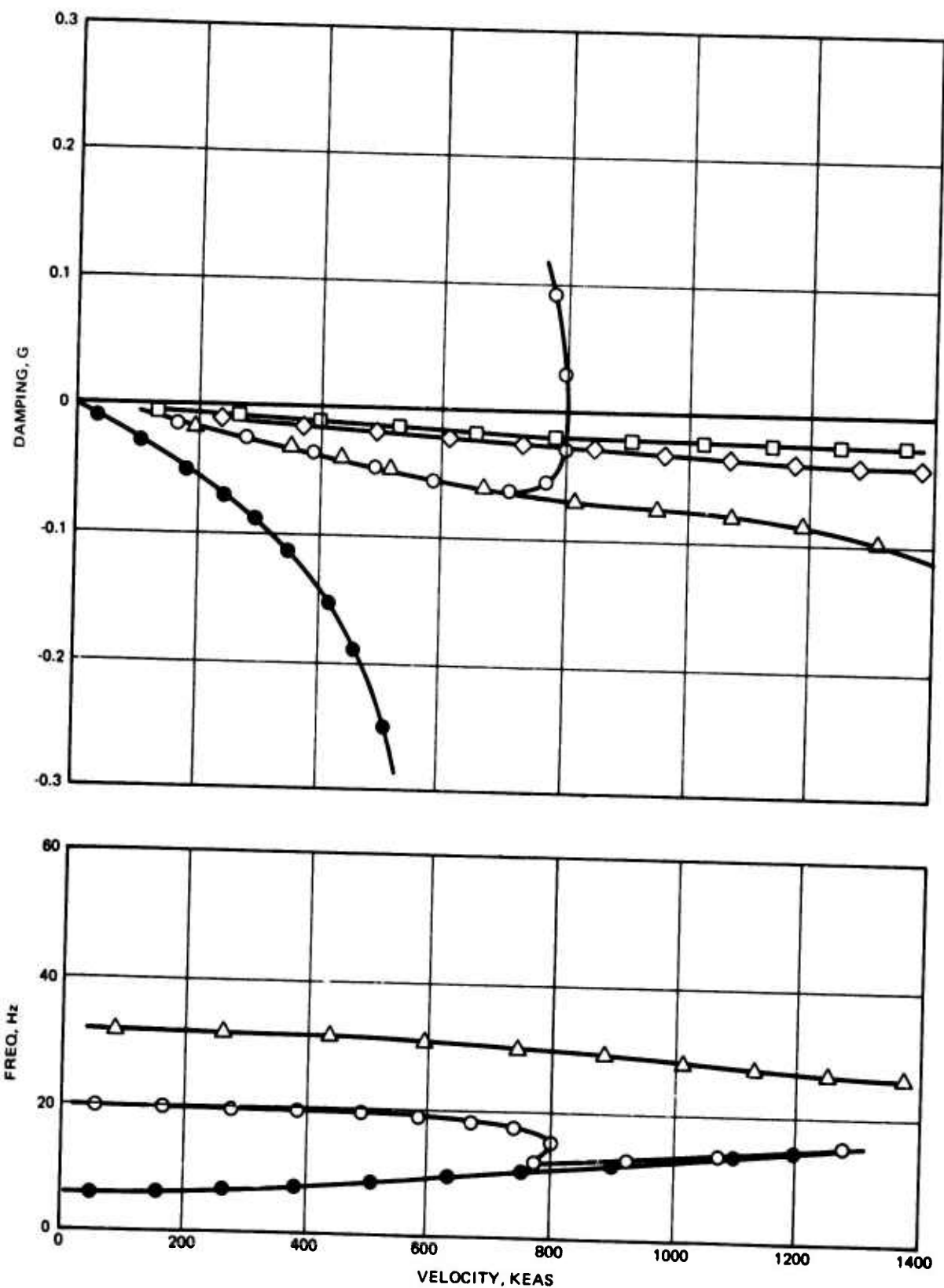


Figure 186. Wing Beam Model, Clean, No Fuel, $M = 0.6$, 40,000 Ft

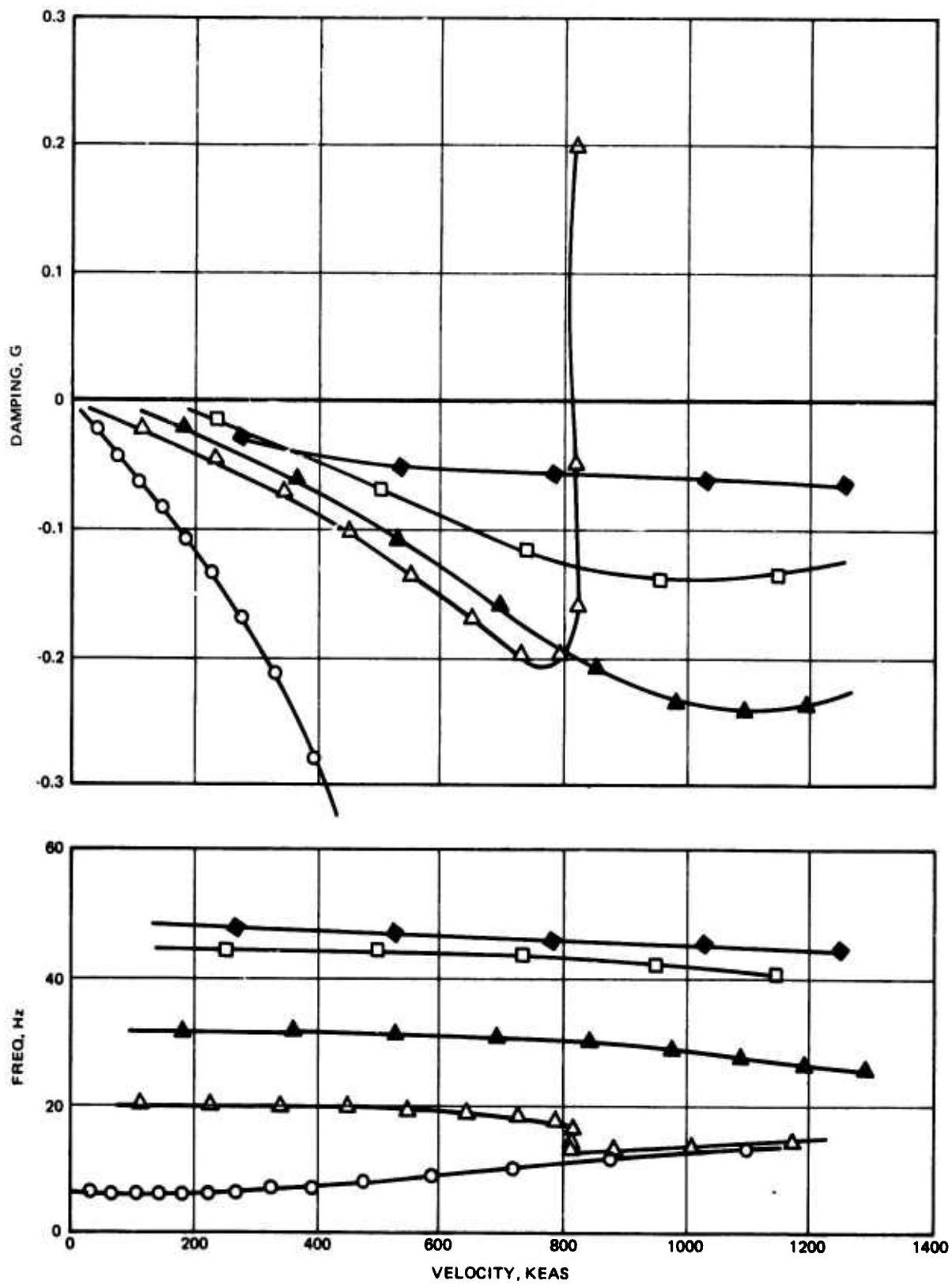


Figure 187. Wing Beam Model, Clean, No Fuel, M = 0.8, Sea Level

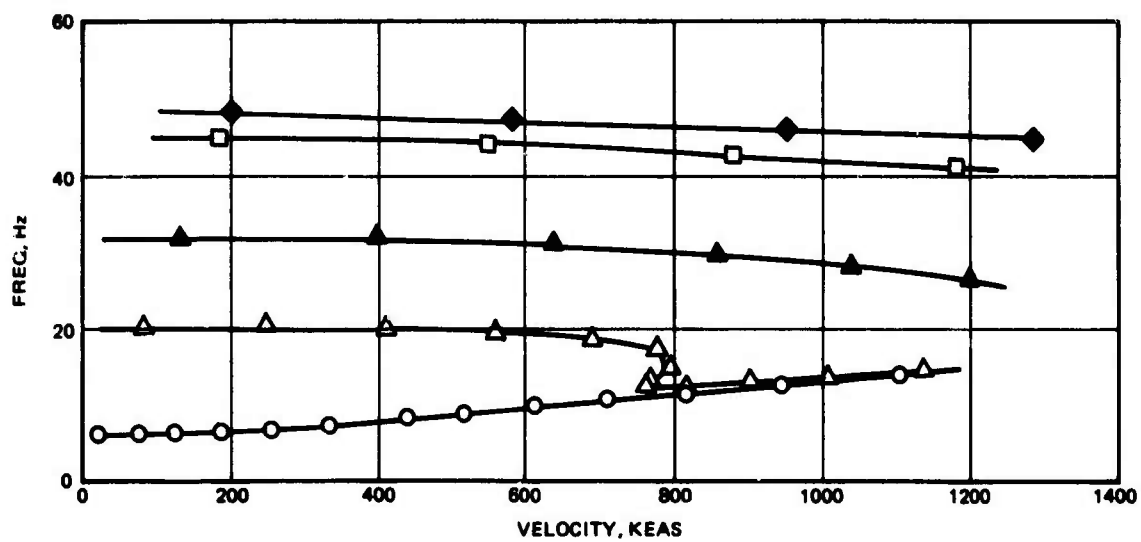
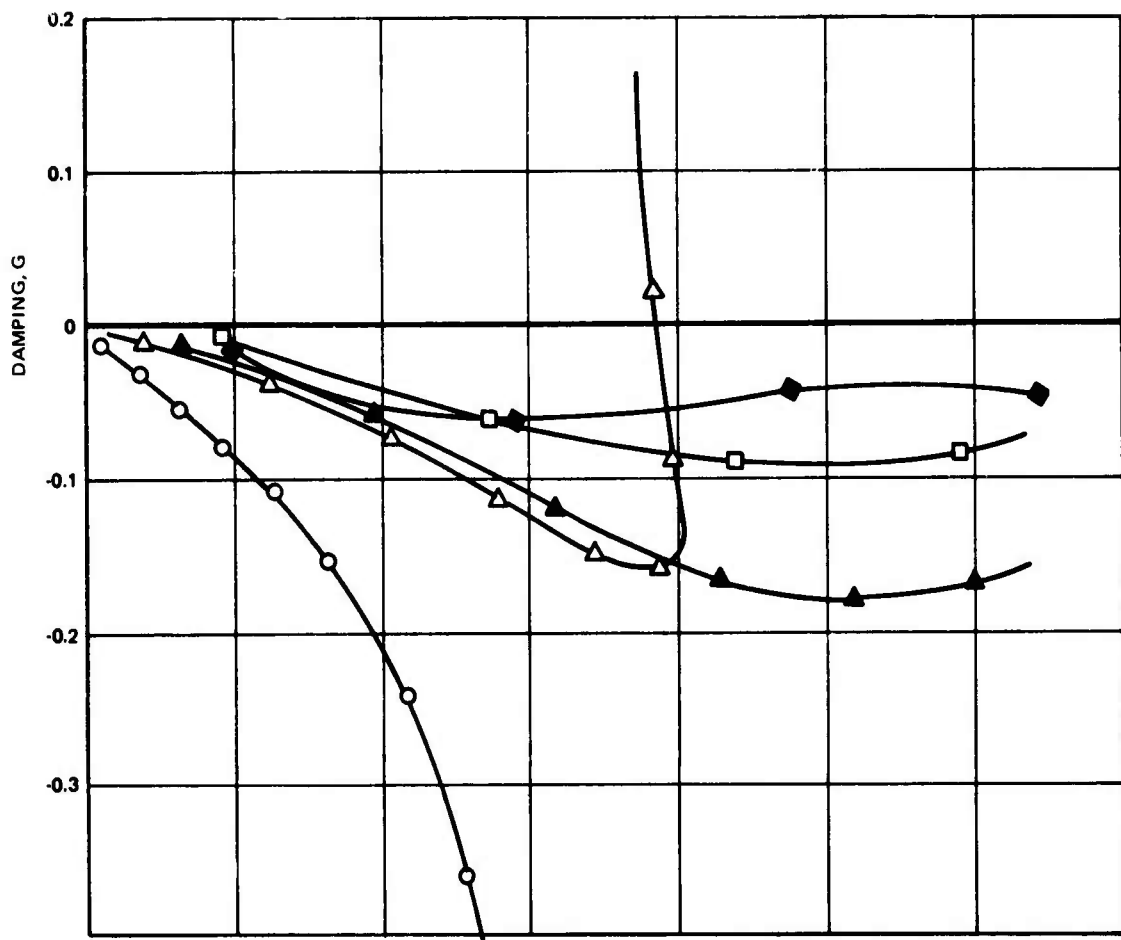


Figure 188. Wing Beam Model, Clean, No Fuel, $M = 0.8$, 20,000 Ft

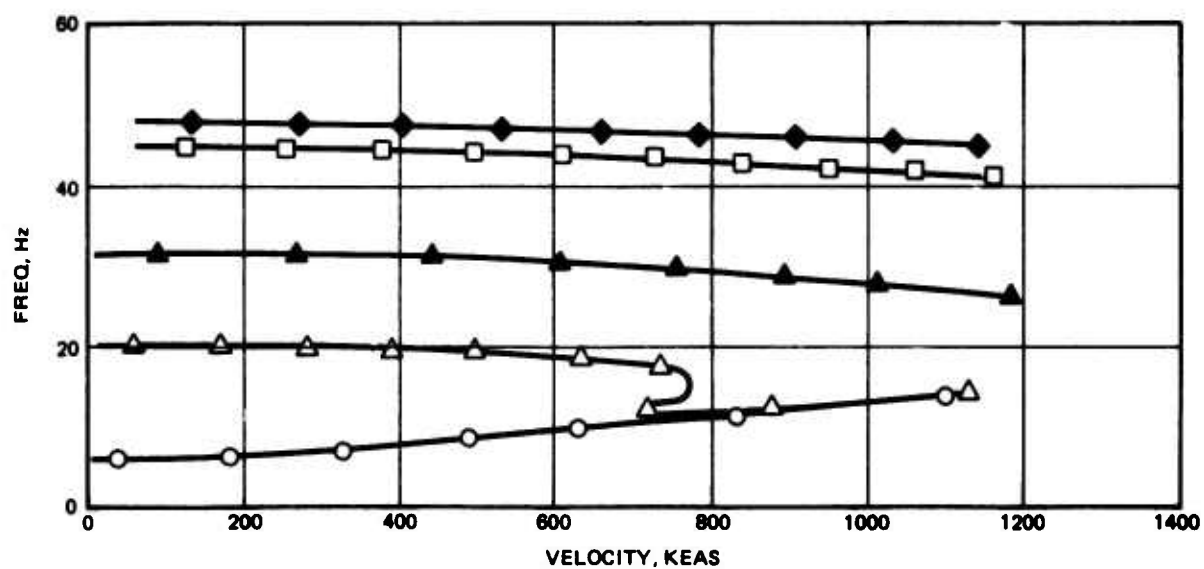
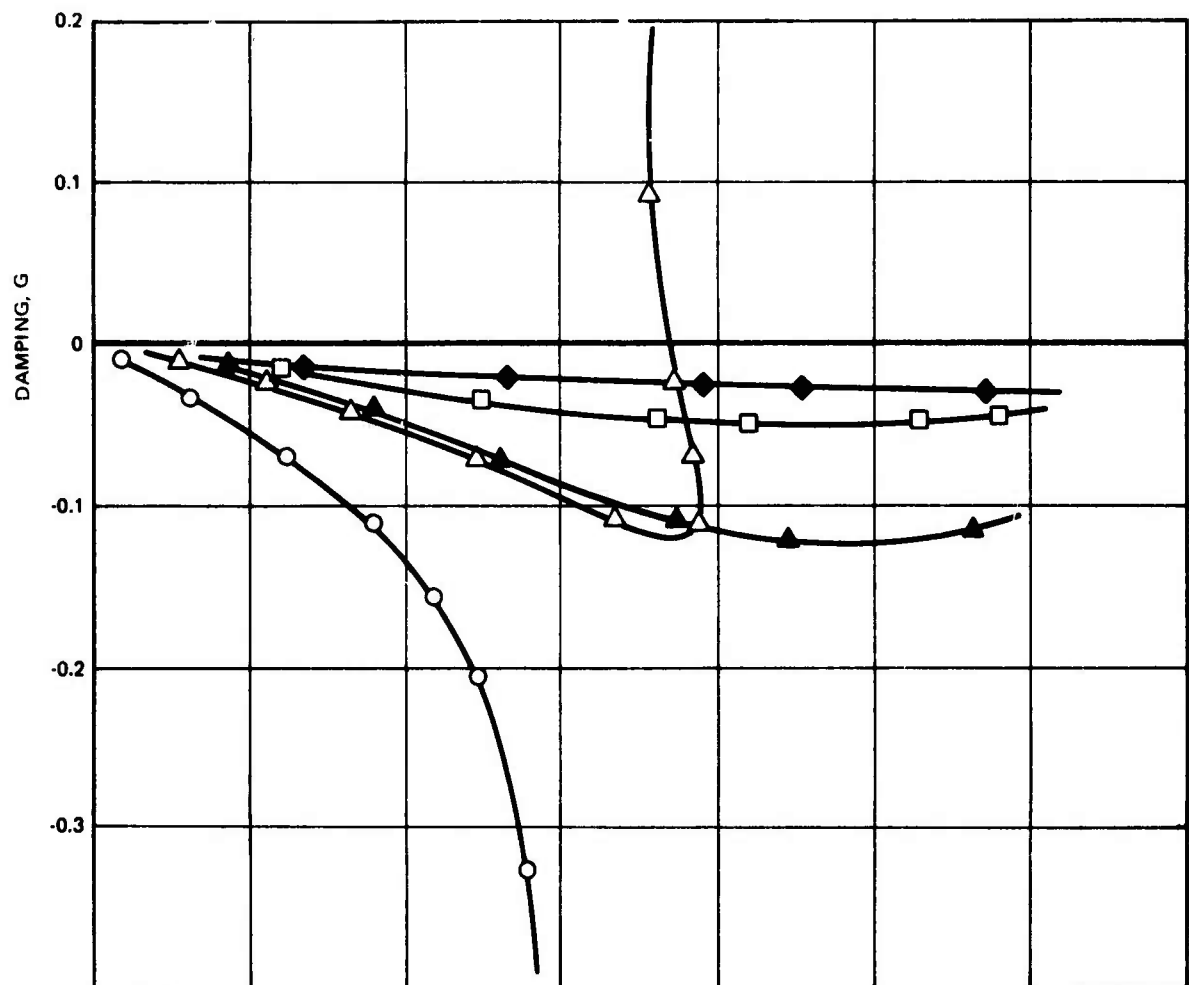


Figure 189. Wing Beam Model, Clean, No Fuel, $M = 0.8$, 40,000 Ft

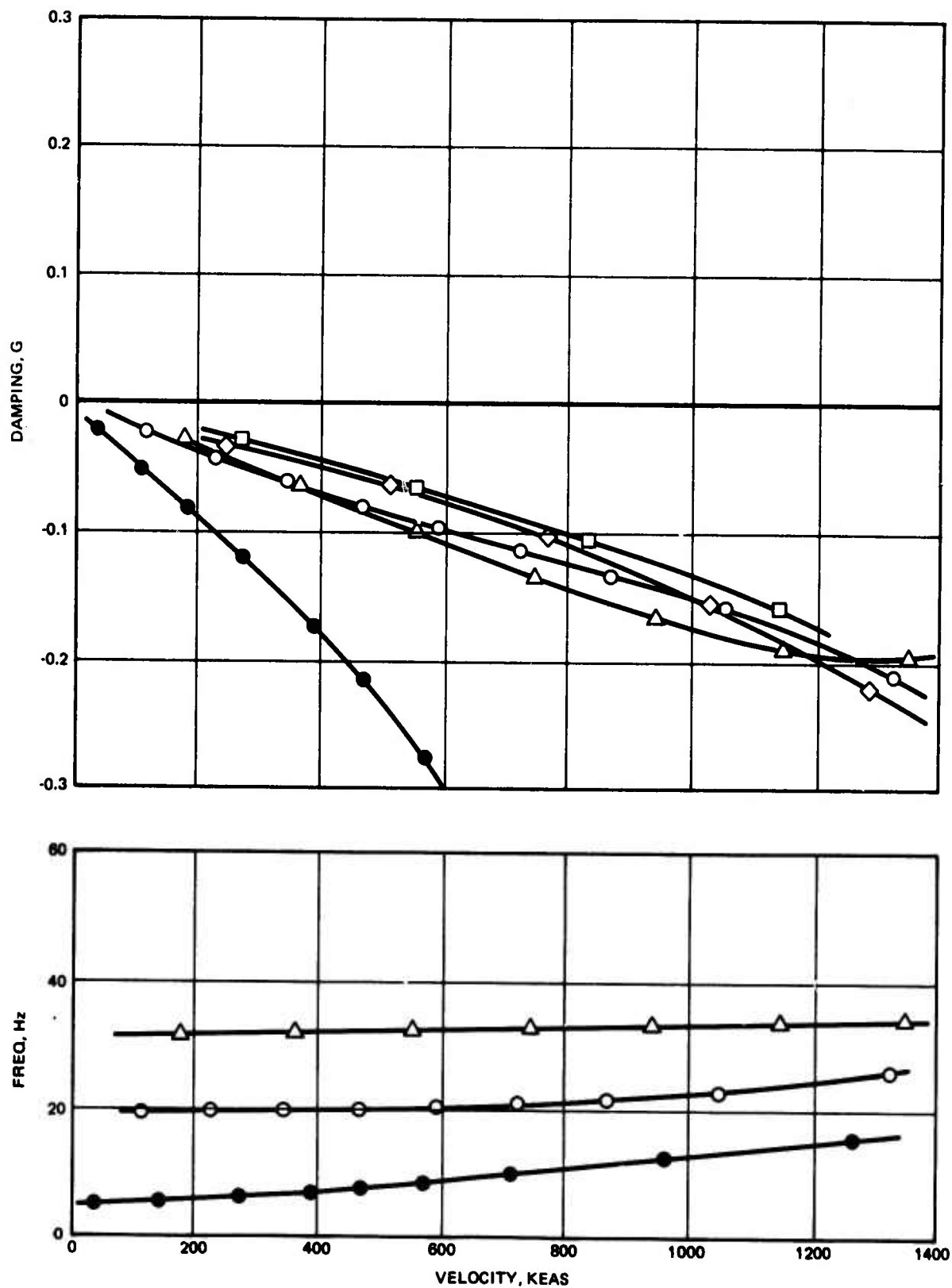


Figure 190. Wing Beam Model, Clean, No Fuel, $M = 1.3$, Sea Level

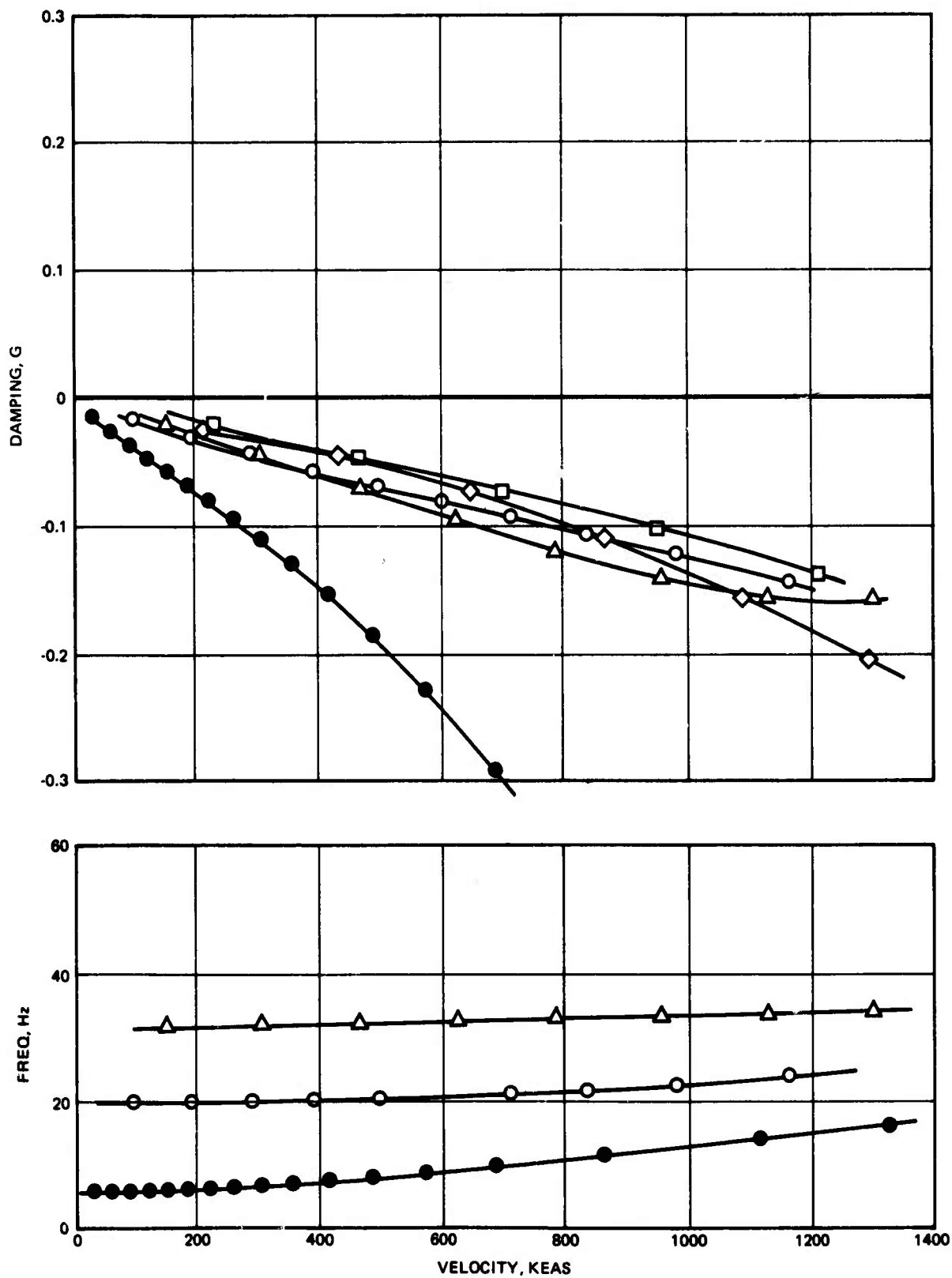


Figure 191. Wing Beam Model, Clean, No Fuel, M = 1.3, 11,000 Ft

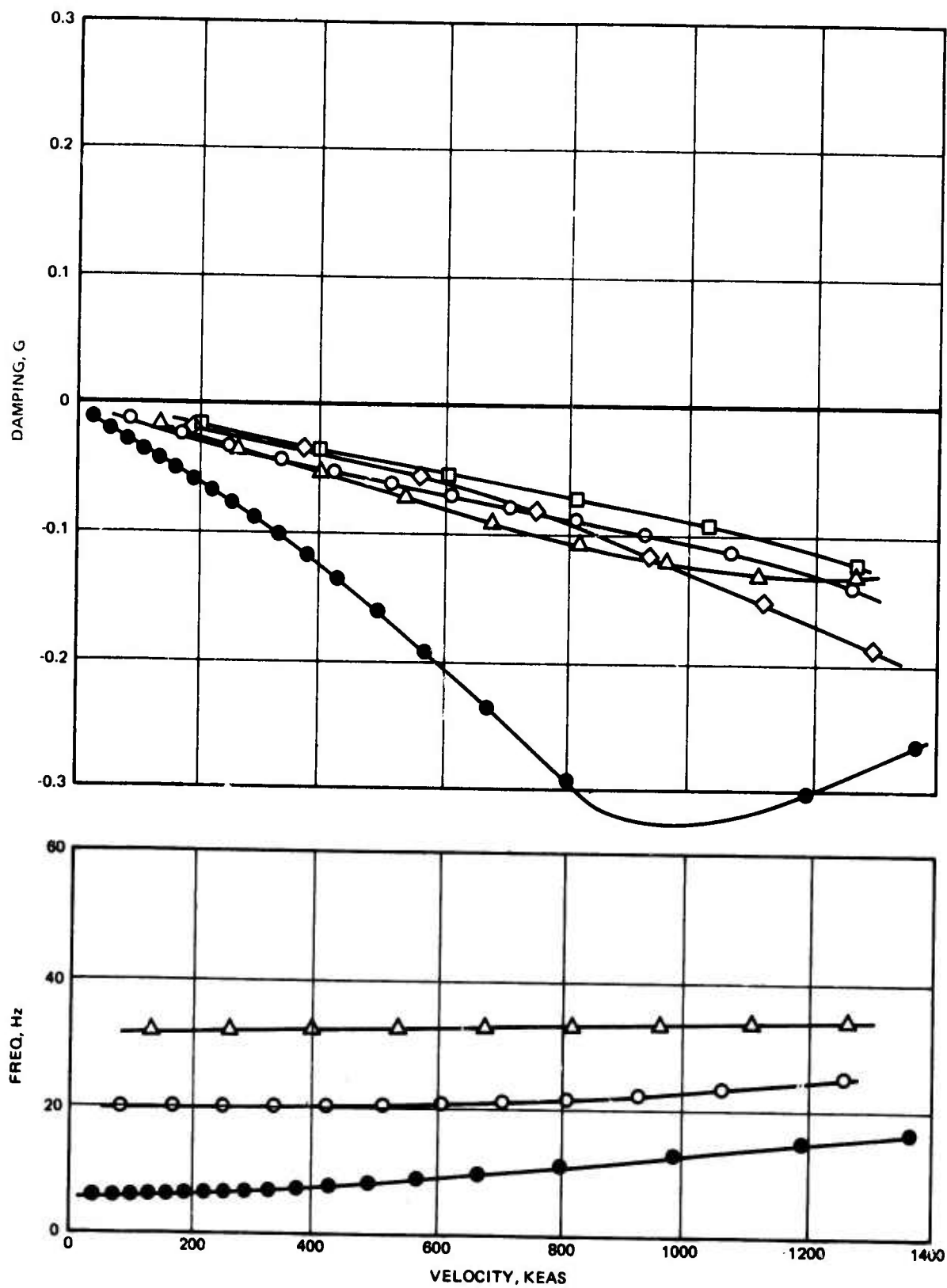


Figure 192. Wing Beam Model, Clean, No Fuel, M = 1.3, 20,000 Ft

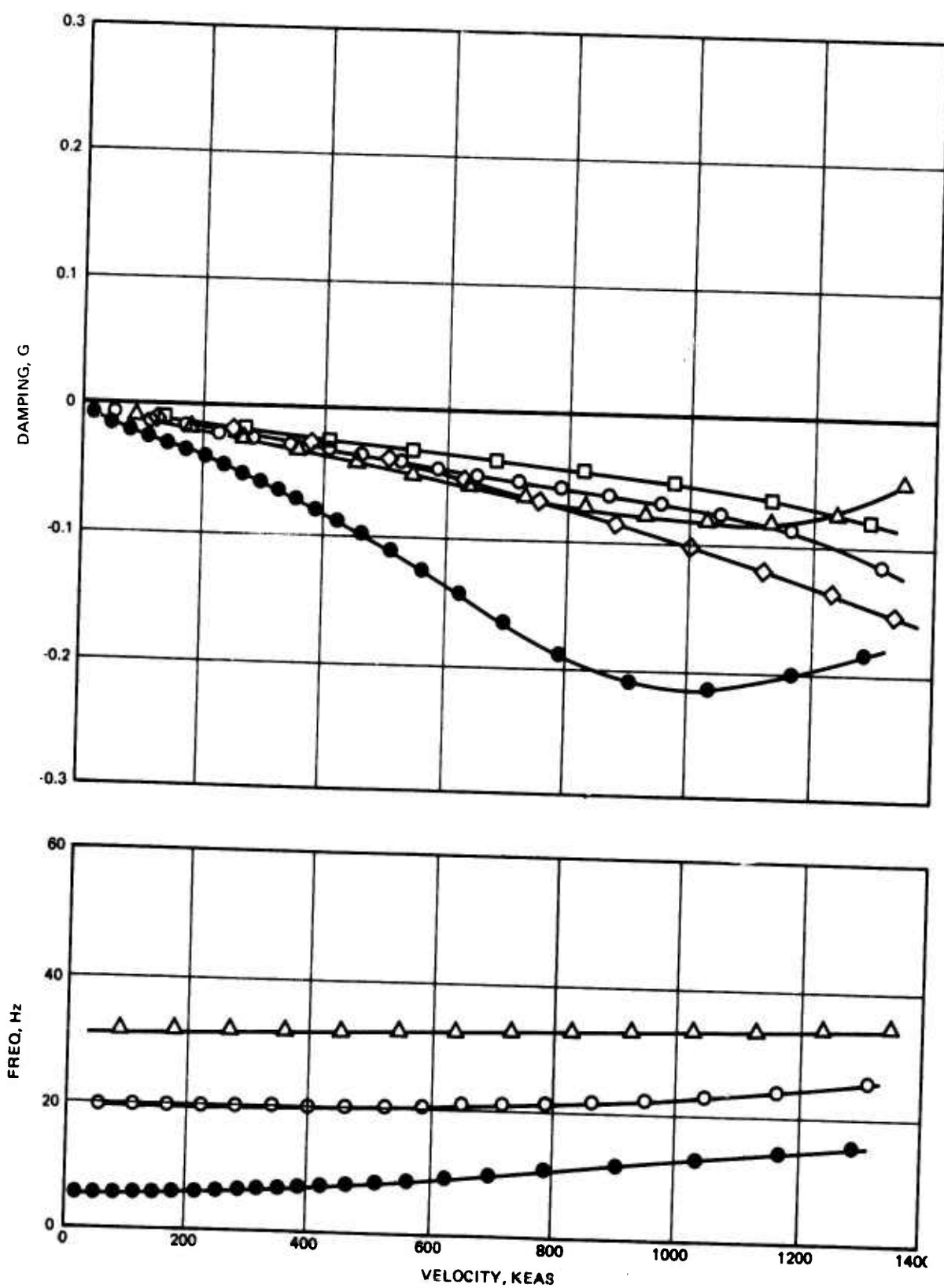


Figure 193. Wing Beam Model, Clean, No Fuel, $M = 1.3$, 40,000 Ft

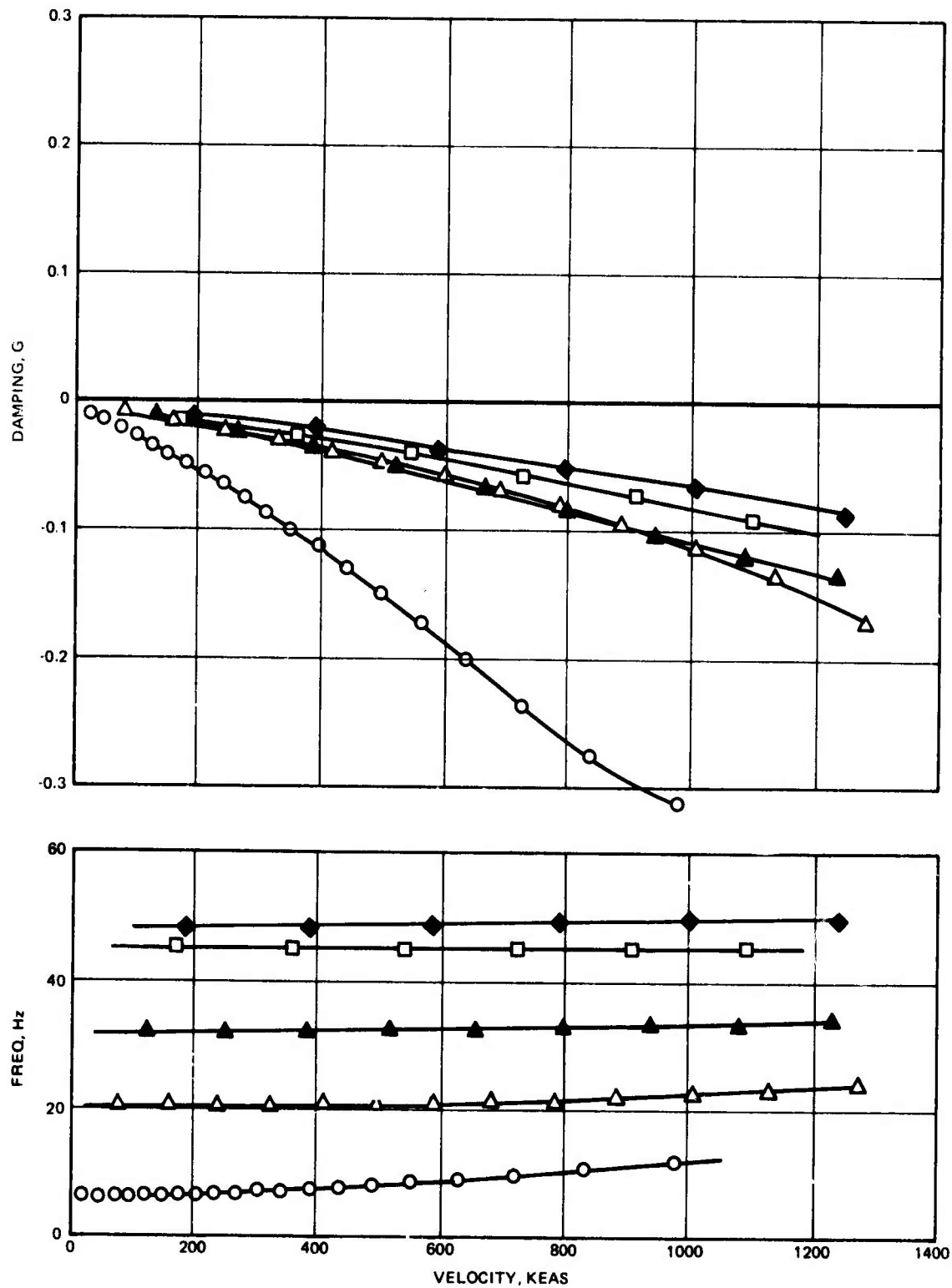


Figure 194. Wing Beam Model, Clean, No Fuel, M = 1.6, 21,500 Ft

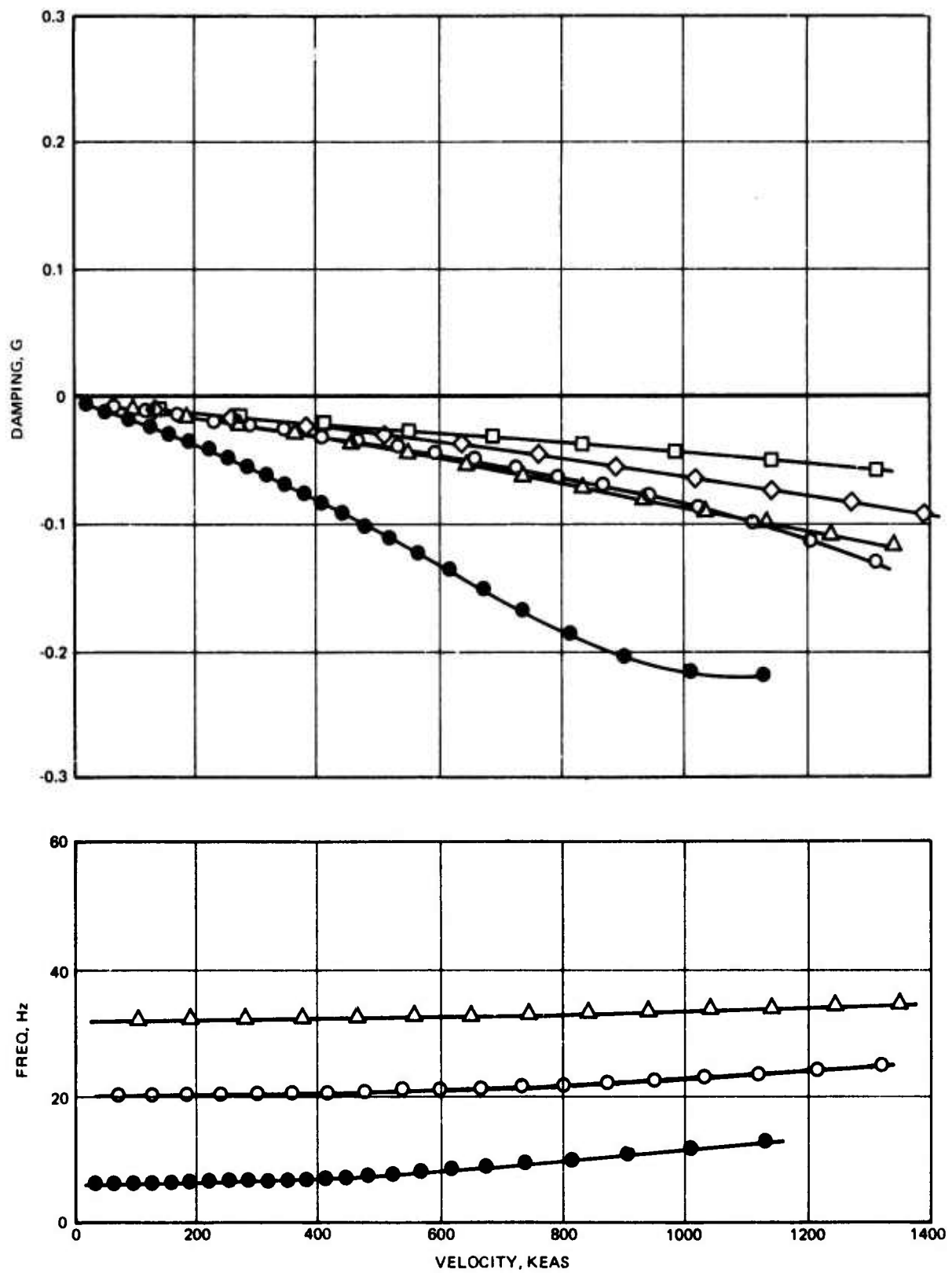


Figure 195. Wing Beam Model, Clean, No Fuel, $M = 1.6$, 40,000 Ft

Having thus achieved a preliminary verification of the flutter integrity of the clean, unloaded wing, the impact of fuel had to be investigated. The wing fuel tank extends to the geometric wing break. All but the three most outboard panels are, therefore, affected. The distributed weights data for the full-up case is summarized in Table 28.

**TABLE 28. WING MASS PROPERTIES
FULL FUEL**

Panel	Weight, lb	Arm*, in.	Unbalance, lb-in.	$I_{yy_{cg_2}}$, lb-in.	$I_{yy_{EA_2}}$, lb-in.
1	831.0	-5.7	-4736.7	1,630,307	1,657,306
2	624.75	0.7	437.2	871,788	872,094
3	249.0	-8.8	-2191.2	47,544	66,827
4	223.5	9.3	2078.6	78,825	98,156
5	186.3	6.8	1266.8	50,882	59,497
6	111.3	2.7	300.5	17,688	18,499
7	90.50	2.6	235.3	11,614	12,226
8	81.20	4.2	341.0	8,067	9,499

* Perpendicular distance from panel cg to beam reference axis; positive indicates aft cg

Results of the vibration calculations for the full fuel wing are summarized in Table 29. The corresponding nodelines are shown in Figure 196. Flutter analyses were completed at $M = 0.8$ and 1.3 . These results are given in Table 30 and the V - g - ω plots are included in Figures 197 through 203. The resultant flutter envelope is shown in Figure 196.

TABLE 29. WING FREQUENCY COMPARISON

Mode	Empty	Full Fuel
1st Bending	6.21	6.16
2nd Bending	20.31	18.80
Torsion	32.03	28.38

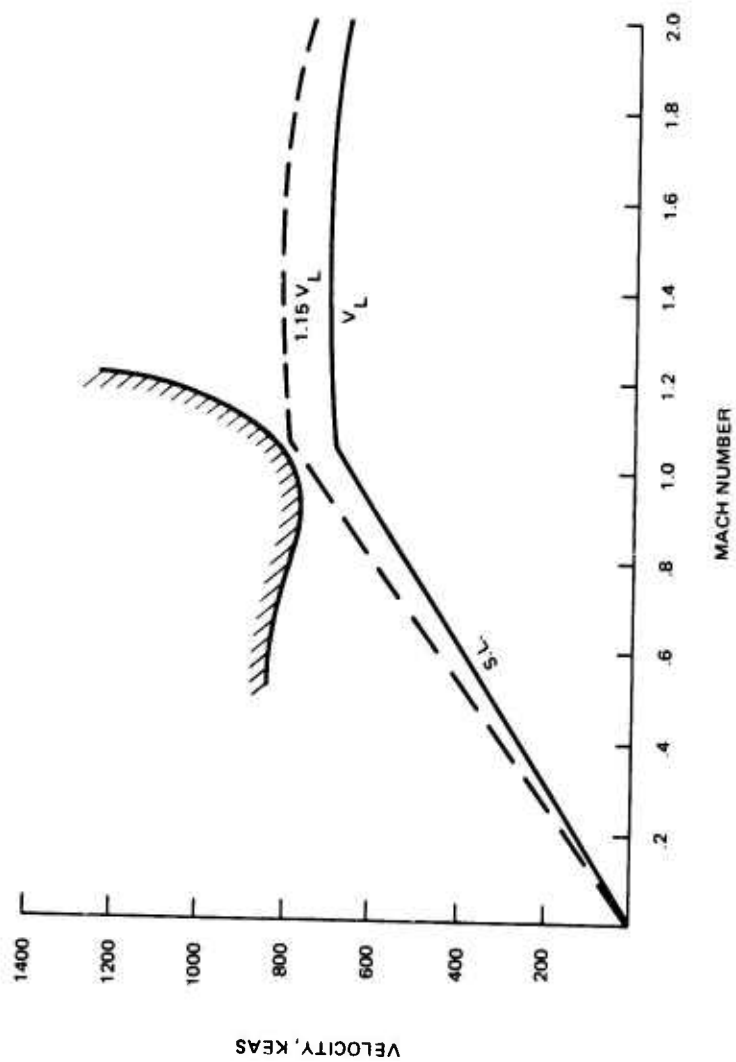
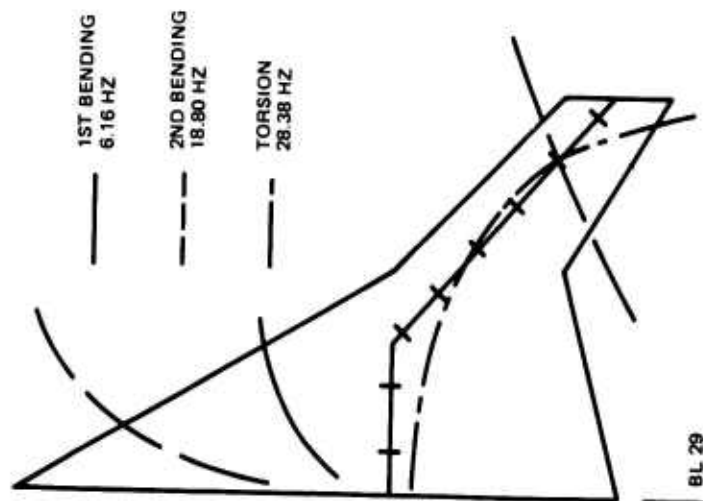


Figure 196. Wing Node Lines and Flutter Envelopes, Clean, Full Fuel

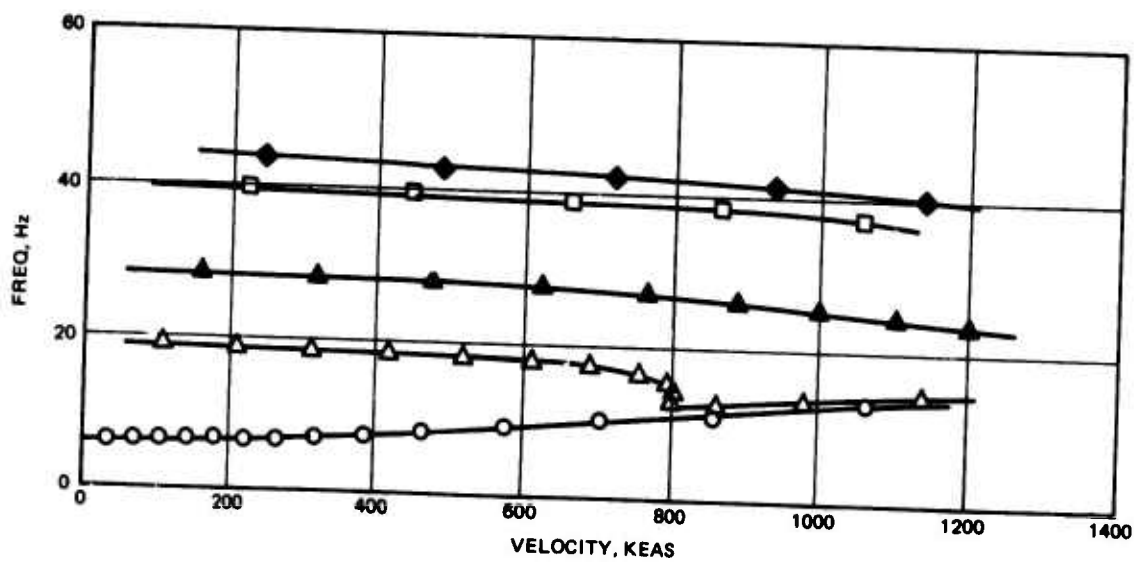
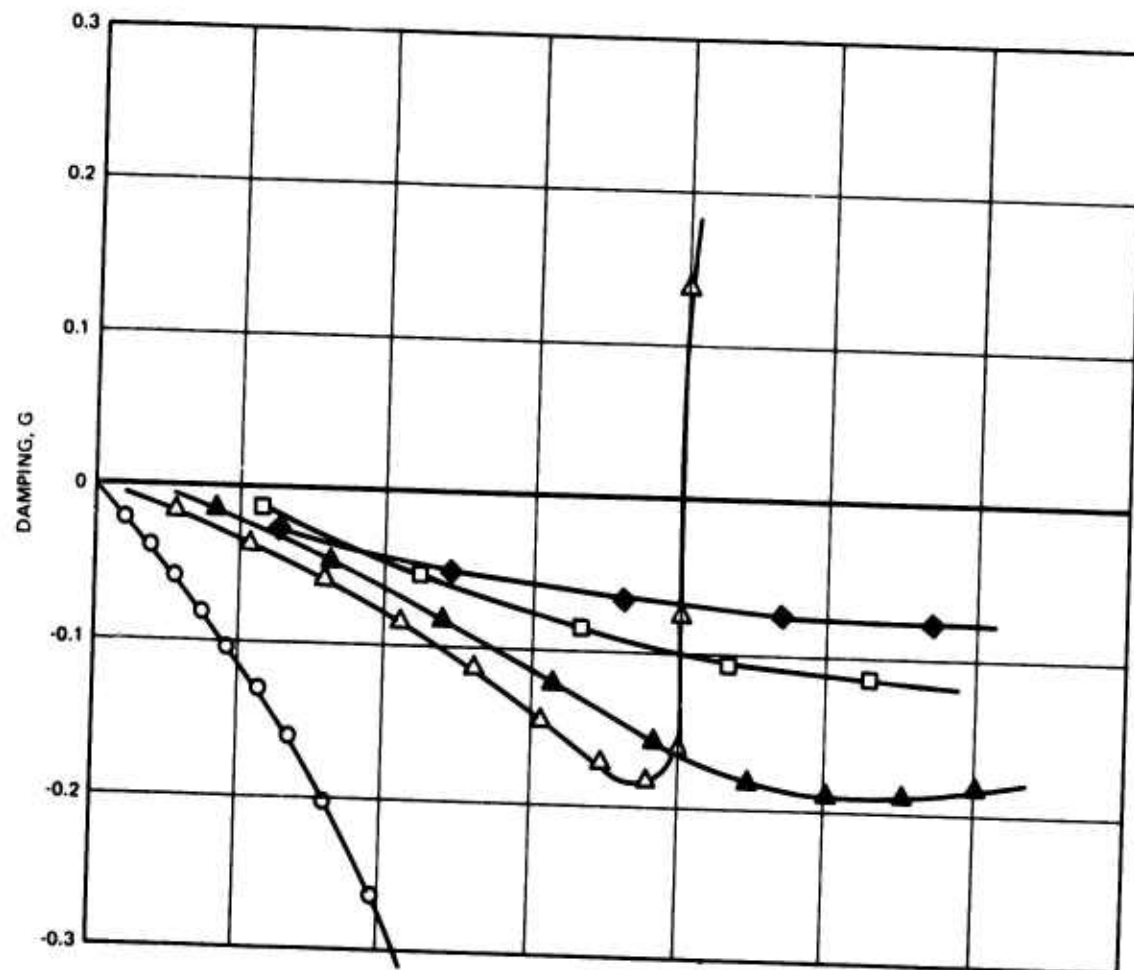


Figure 197. Wing Beam Model, Clean, Full Fuel, $M = 0.8$, Sea Level

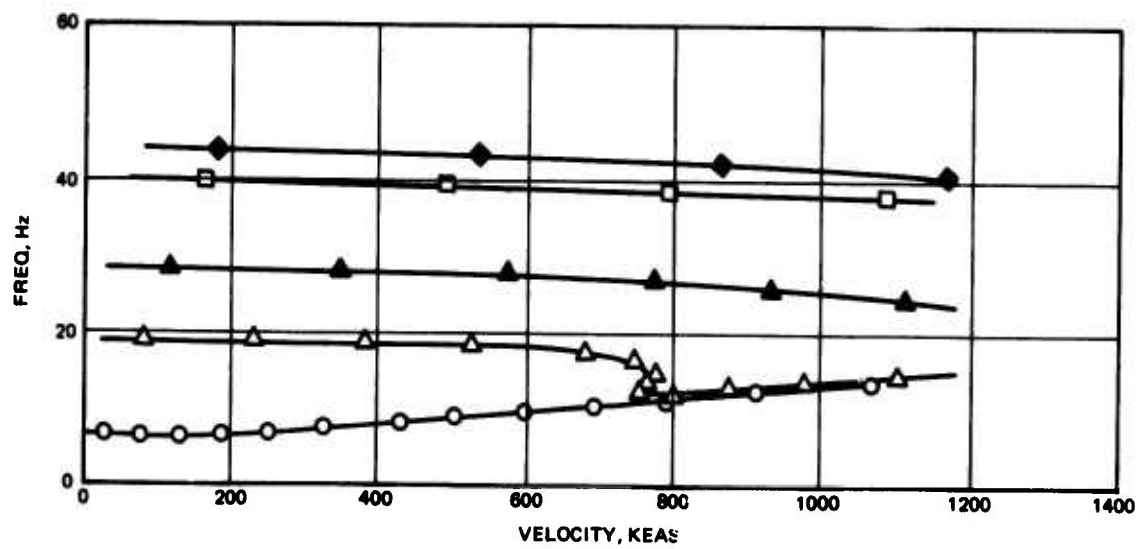
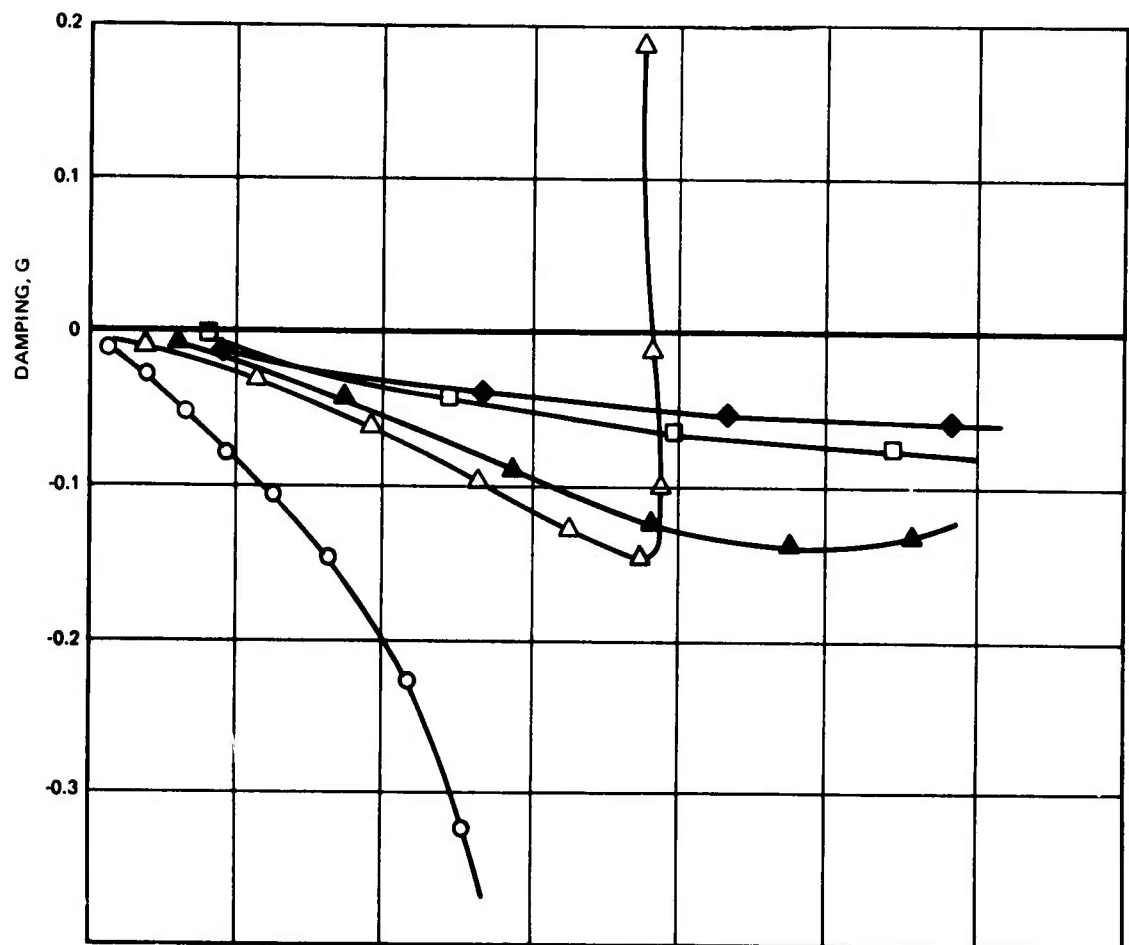


Figure 198. Wing Beam Model, Clean, Full Fuel, $M = 0.8$, 20,000 Ft

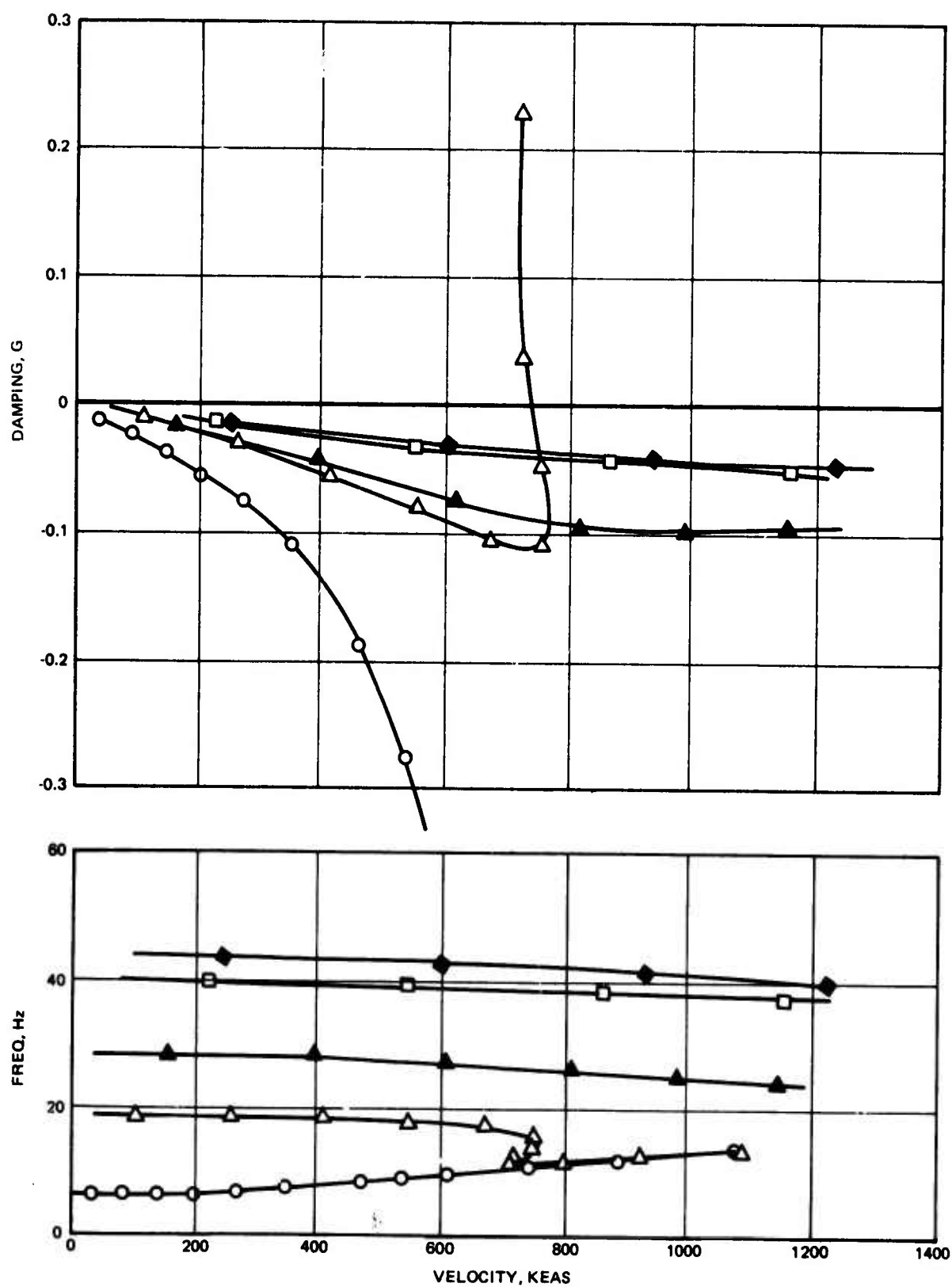


Figure 199. Wing Beam Model, Clean, Full Fuel, M = 0.8, 40,000 Ft

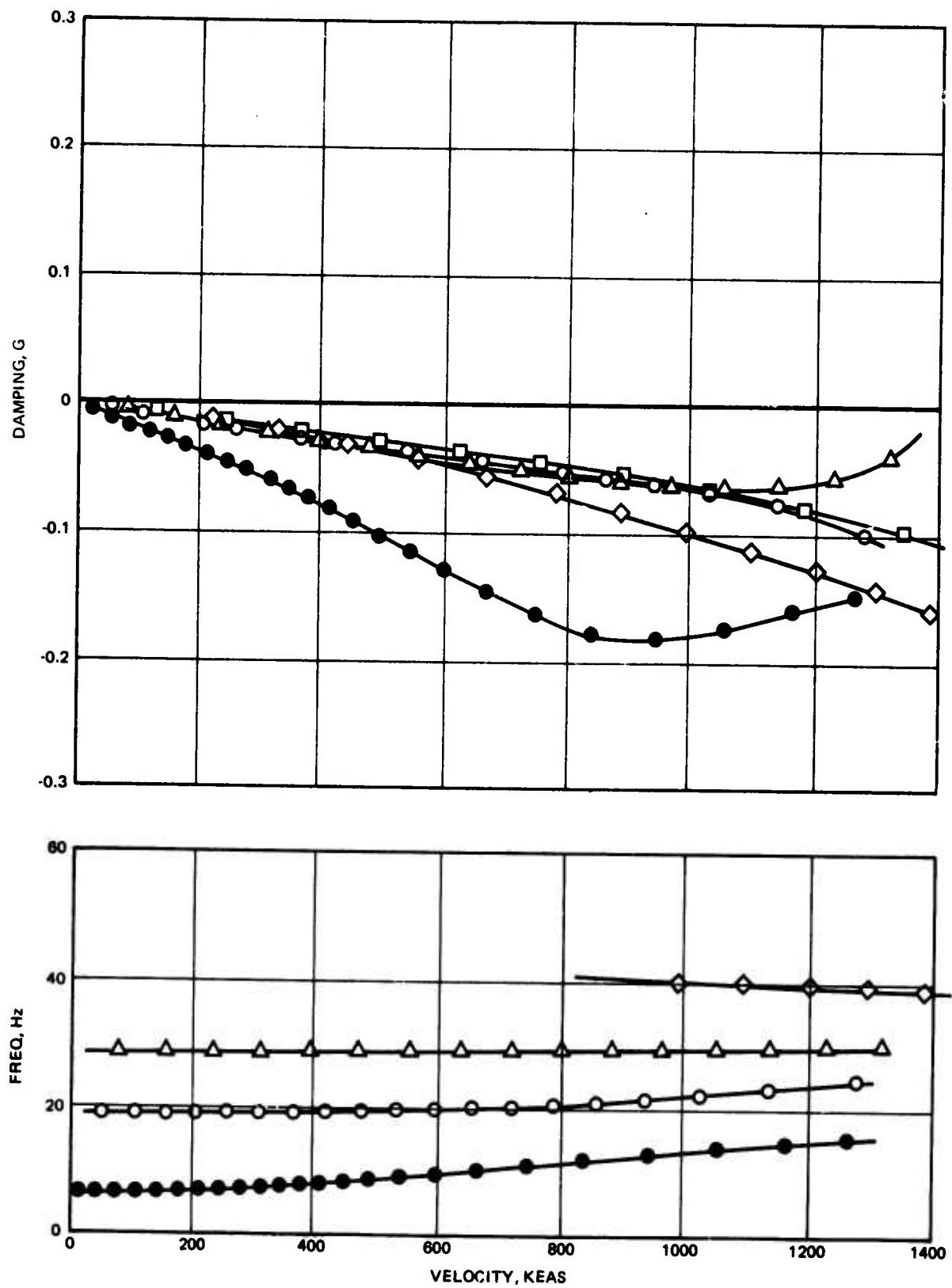


Figure 200. Wing Beam Model, Clean, Full Fuel, $M = 1.3$, Sea Level

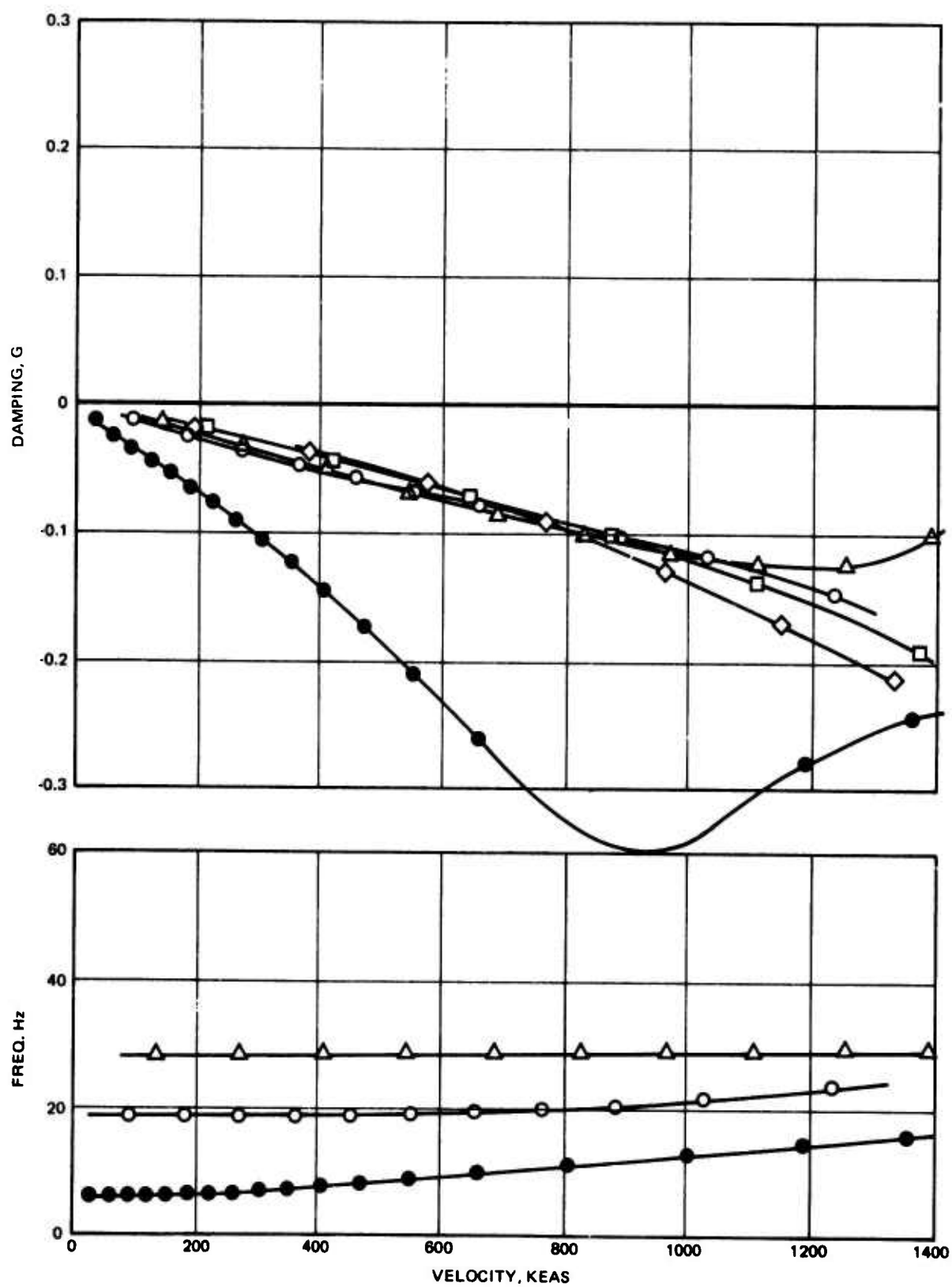


Figure 201. Wing Beam Model, Clean, Full Fuel, M = 1.3, 11,000 Ft

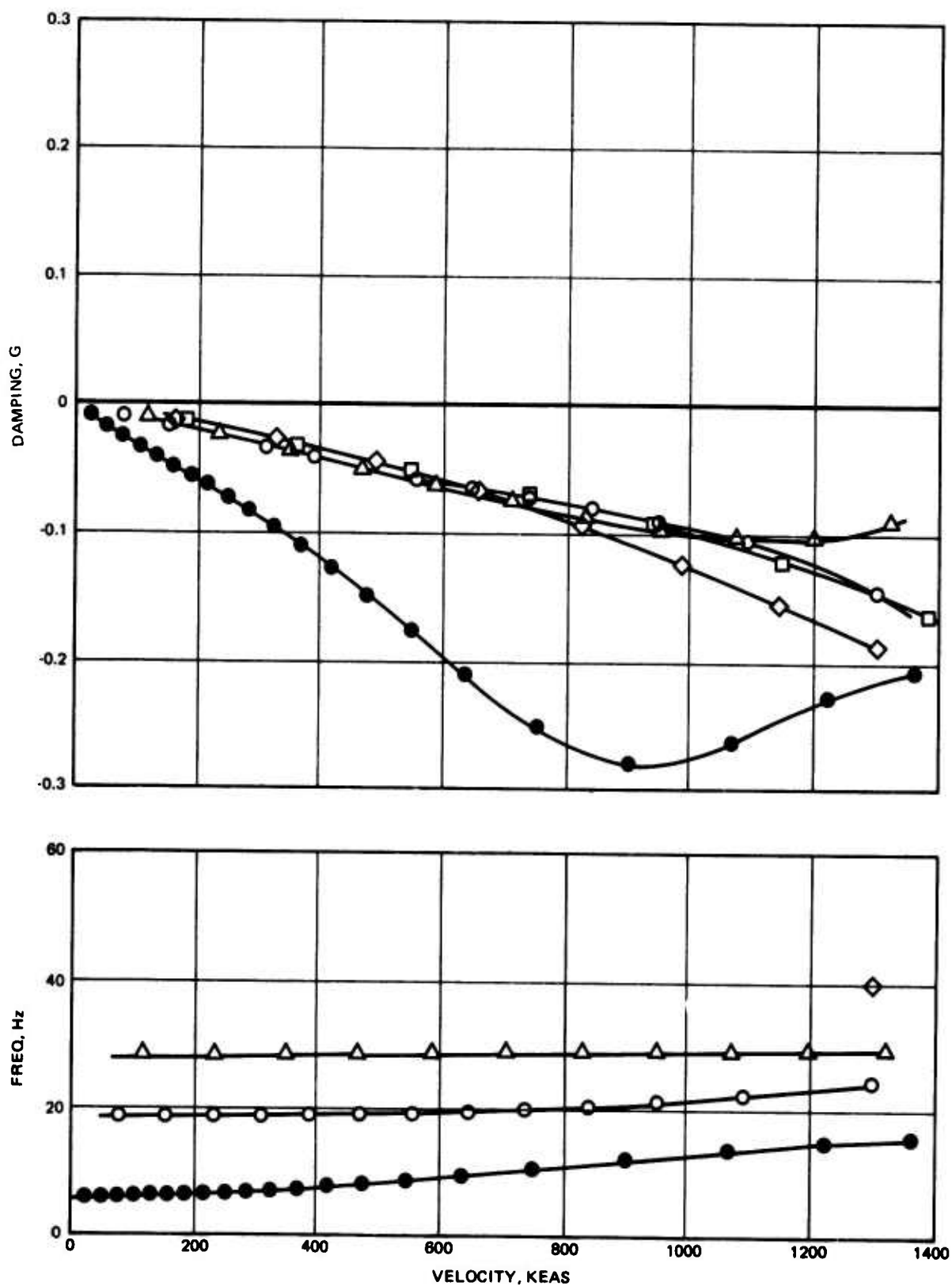


Figure 202. Wing Beam Model, Clean, Full Fuel, $M = 1.3$, 20,000 Ft

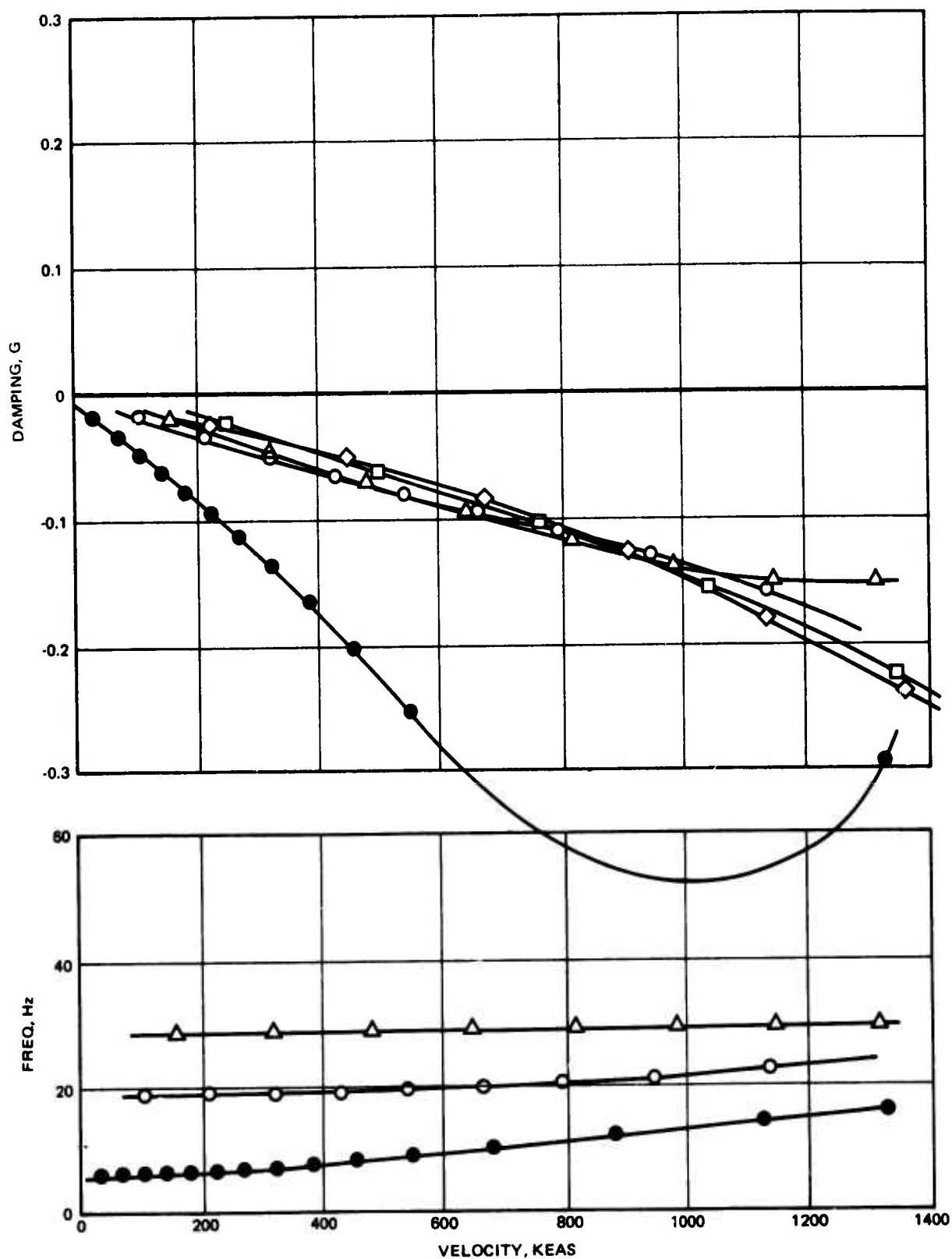


Figure 203. Wing Beam Model, Clean, Full Fuel, M = 1.3, 40,000 Ft

**TABLE 30. WING FLUTTER SPEED SUMMARY
FULL FUEL**

Mach	Altitude, 1000 ft	V _f , KEAS	V _f /V	Ref V-g- ω Plot, Figure
0.8	SL	794	1.51	5.4-50
	20	751	2.10	5.4-51
	40	720	3.19	5.4-52
1.3	SL	NF*	-	5.4-53
	11	NF	-	5.4-54
	20	NF	-	5.4-55
	40	NF	-	5.4-56
*No Flutter				

Finally, the effect of the tip-mounted Sidewinder had to be considered. A sketch of the tip installation is shown in Figure 204. The sidewinder was placed as far forward as possible for mass balance purposes. It was desired to locate the store fins aft of the wing trailing edge to avoid aerodynamic shocks onto the wing surface. The mass properties assumed for the sidewinder and launcher installation for dynamic calculations are given in Table 31.

TABLE 31. SIDEWINDER + LAUNCHER MASS PROPERTIES

Weight = 295 lb
Arm* = 18.55 in.
I _{yycg} = 209,726 lb-in. ²
I _{yycg} = 311,236 lb-in. ²

*Streamwise distance from store cg to the extended Elastic Axis.

Vibration analyses were completed assuming a rigid installation. The resultant frequencies are shown in Table 32 in comparison to the clean wing.

TABLE 32. WING FREQUENCY COMPARISON

Mode	Clean	Sidewinder Mounted
1st Bending	6.21 Hz	3.45 Hz
2nd Bending	20.31	11.85
Torsion	32.03	16.60

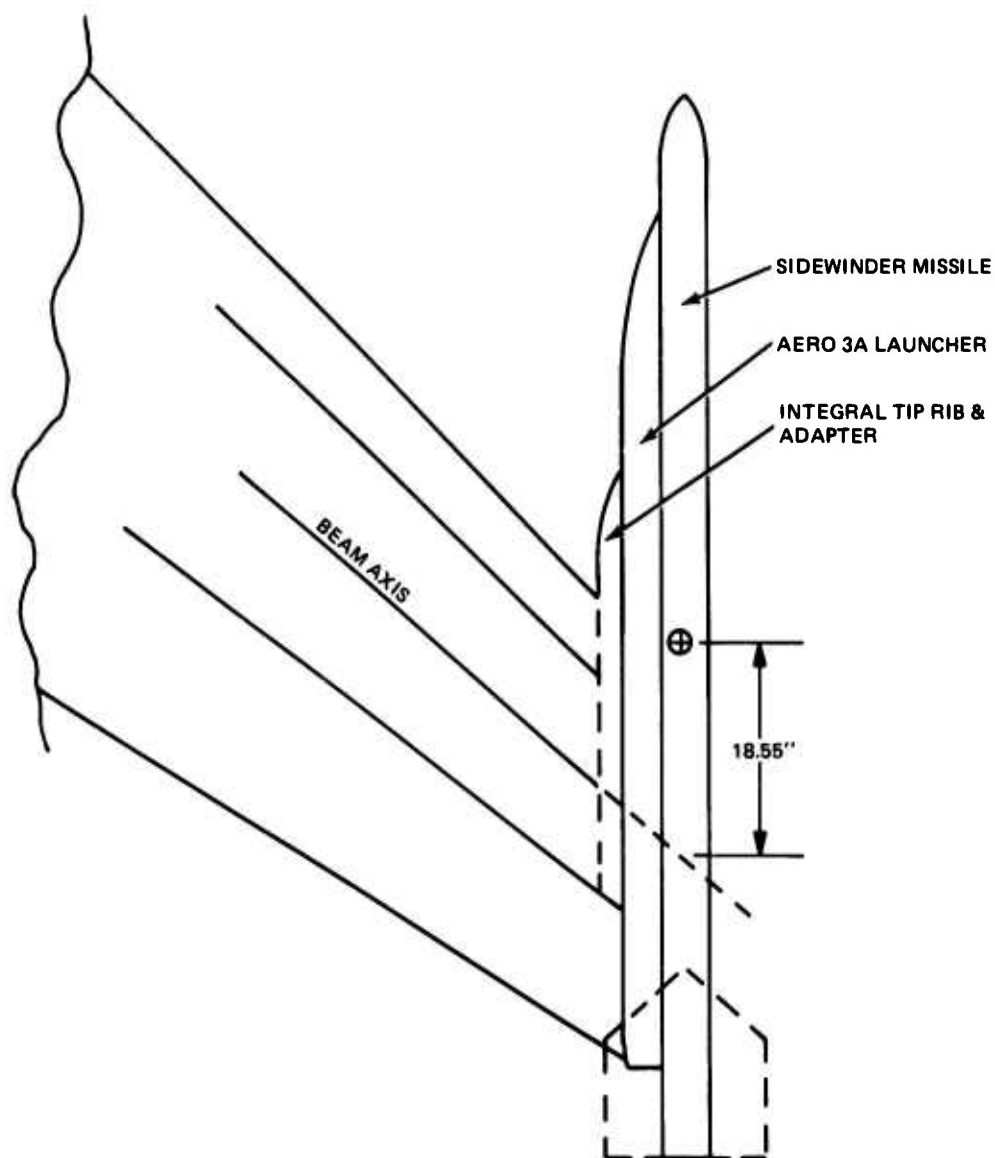


Figure 204. ADCA Wing - Sidewinder Installation

Node line plots and the calculated flutter envelope are shown in Figure 205 where adequate flutter margins are demonstrated. The corresponding V-g- ω plots are given in Figures 206 through 212. A summary of the flutter speeds is given below.

**TABLE 33. WING FLUTTER SPEED SUMMARY
SIDEWINDER MOUNTED, BEAM MODEL**

Maeh	Altitude, 1000 ft.	V _f , KEAS	V _f /V	Ref. V-g- ω Plot, Figure
0.8	SL	785	1.49	206
	20	749	2.10	207
	40	760	2.67	208
1.3	SL	NF*	-	209
	11	1341	1.92	210
	20	1280	2.20	211
	40	1151	3.13	212
*No Flutter				

Estimates of the store pylon installation flexibility are given in Table 34. They are referenced to the installed store cg location.

TABLE 34. WING TIP PYLON AND MOUNT FLEXIBILITIES

	Force	Torque
Deflection	**	-2.08 x 10 ⁻⁶
Rotation	-2.08 x 10 ⁻⁶	0.181 x 10 ⁻⁶
**Not considered		

The dimensions are rad/in.-lb and rad/lb. The sign convention is, again, force and deflection positive down, torque and rotation positive nose up.

The corresponding single degree of freedom pitch frequency is greater than 16 Hz. This is close to the coupled torsion frequency for the rigid case and well above the coupled bending modes, refer back to Table 32. Thus those margins presented for the Side-winder rigidly mounted will be maintained.

Verification of these preliminary wing analyses has been accomplished using a finite element model. Throughout the program those benefits associated with tailoring for increased washout under load have constantly been evaluated. This investigation had to

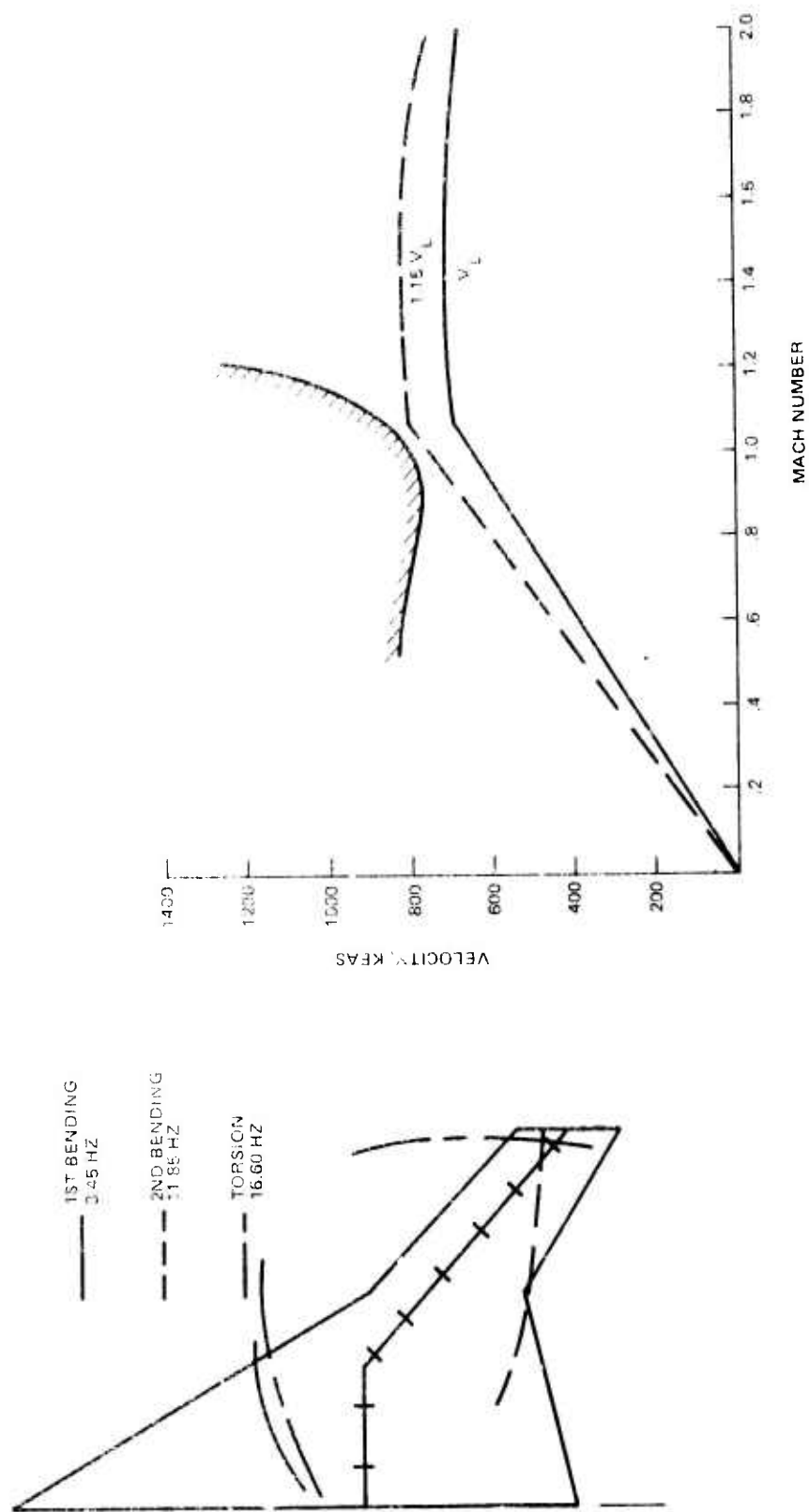


Figure 205. Wing Node Lines and Flutter Envelopes, Tip Mounted Sidewinder, Without Fuel

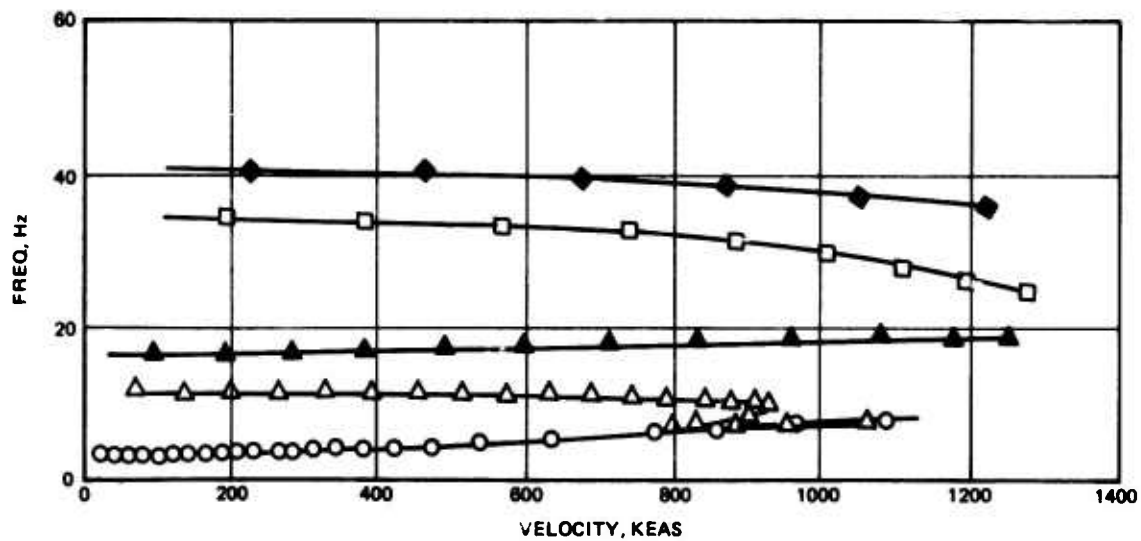
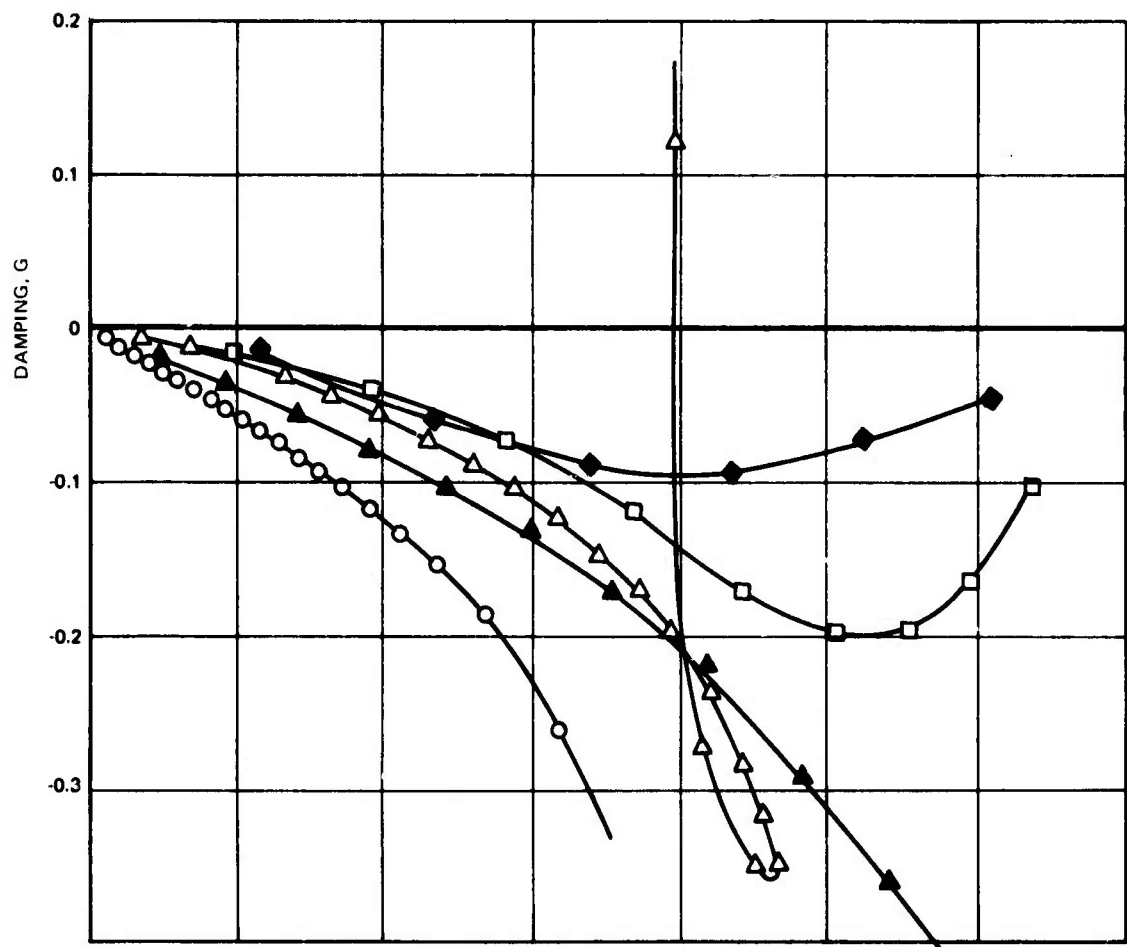


Figure 206. Wing Beam Model, Tip-Mounted Sidewinder, No Fuel, $M = 0.8$, Sea Level

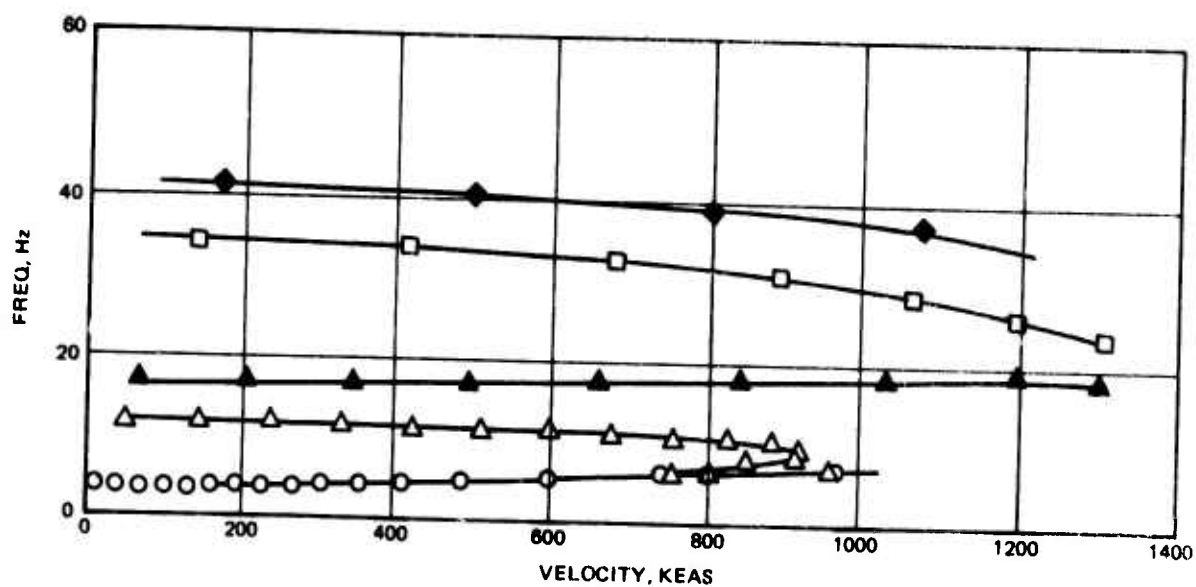
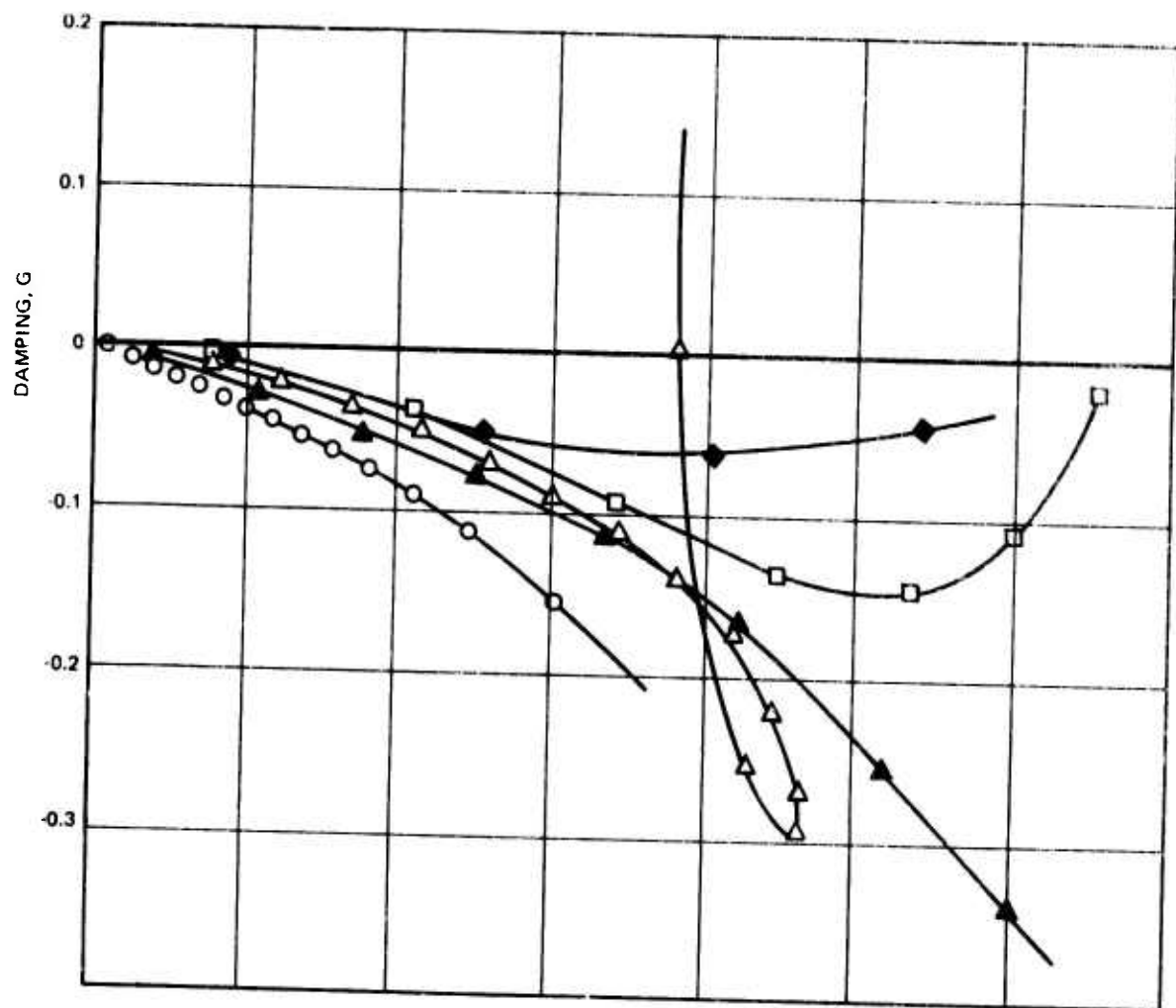


Figure 207. Wing Beam Model, Tip-Mounted Sidewinder, No Fuel, $M = 0.8$, 20,000 Ft

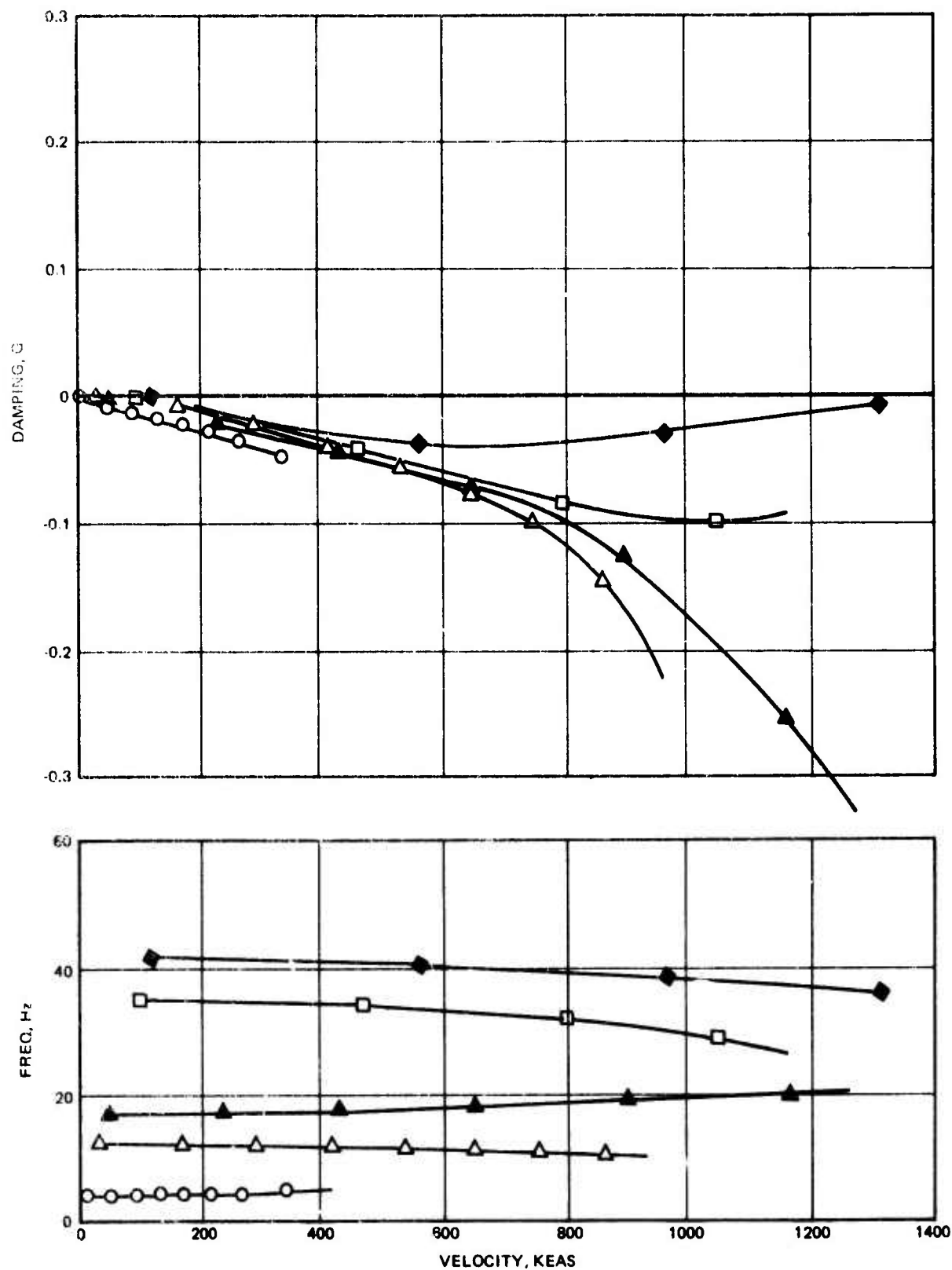


Figure 208. Wing Beam Model, Tip Mounted Sidewinder, No Fuel, M = 0.8, 40,000 Ft

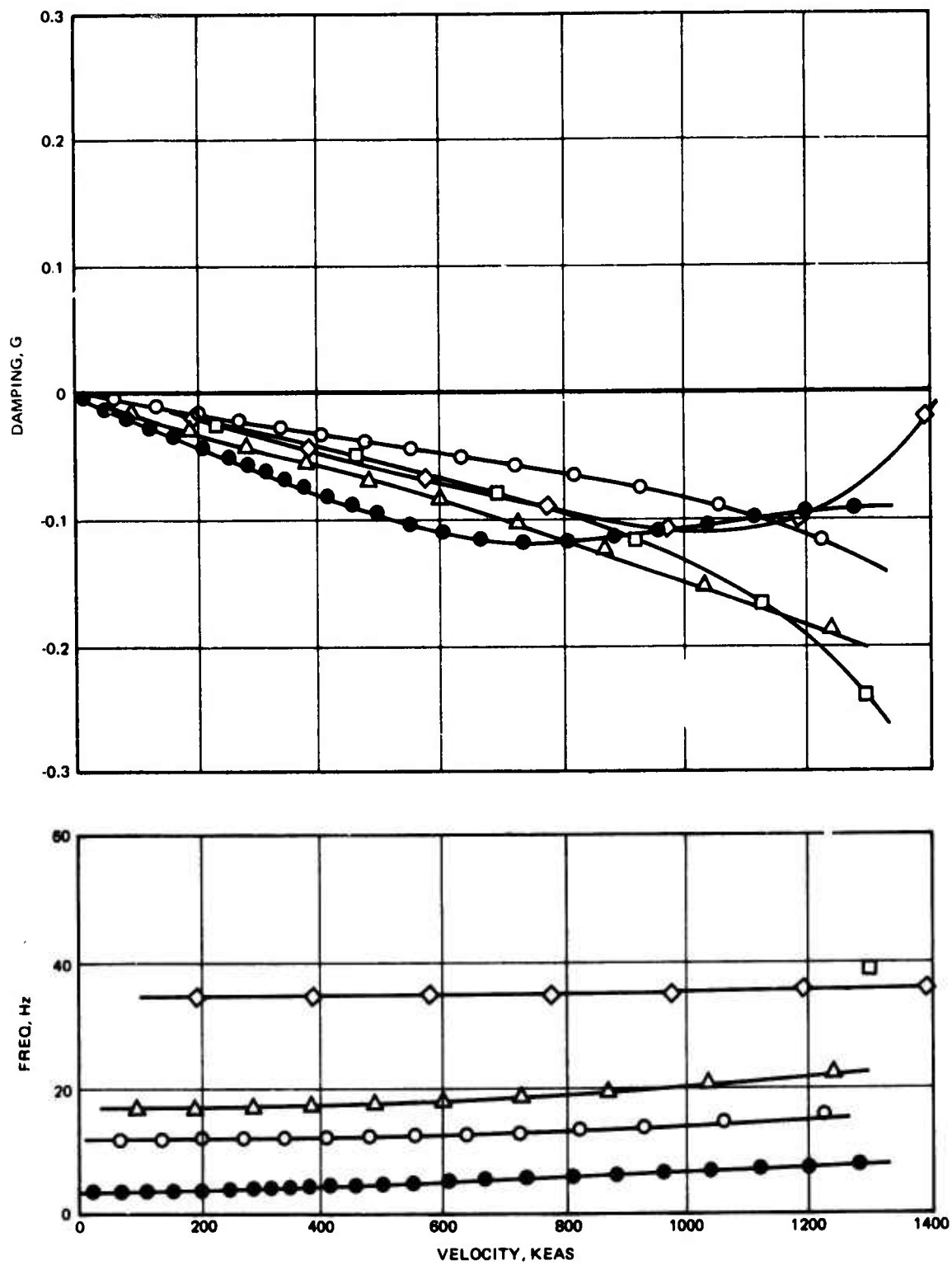


Figure 209. Wing Beam Model, Tip-Mounted Sidewinder, No Fuel, $M = 1.3$ Sea Level

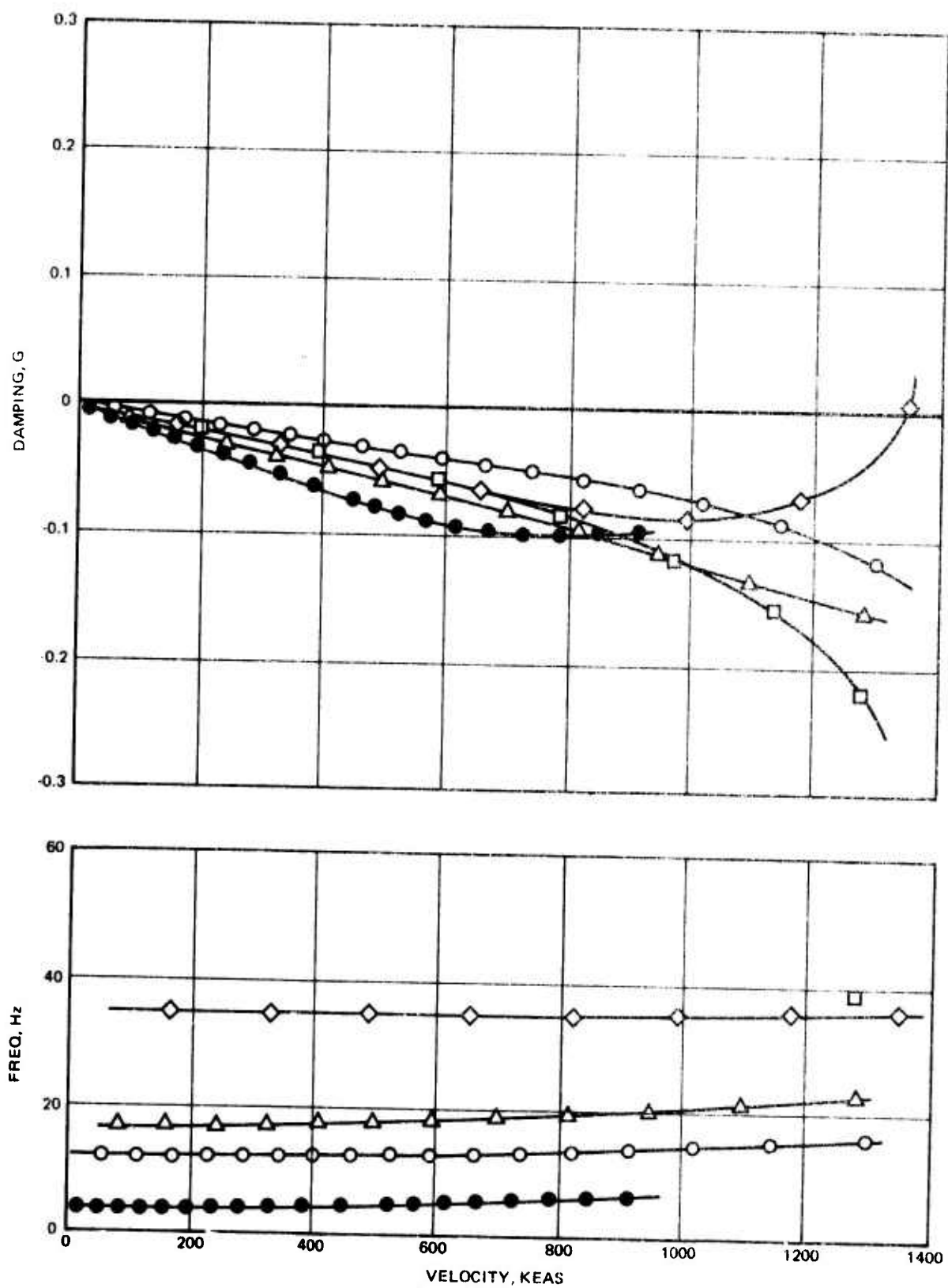


Figure 210. Wing Beam Model, Tip-Mounted Sidewinder, No Fuel, $M = 1.3$, 11,000 Ft

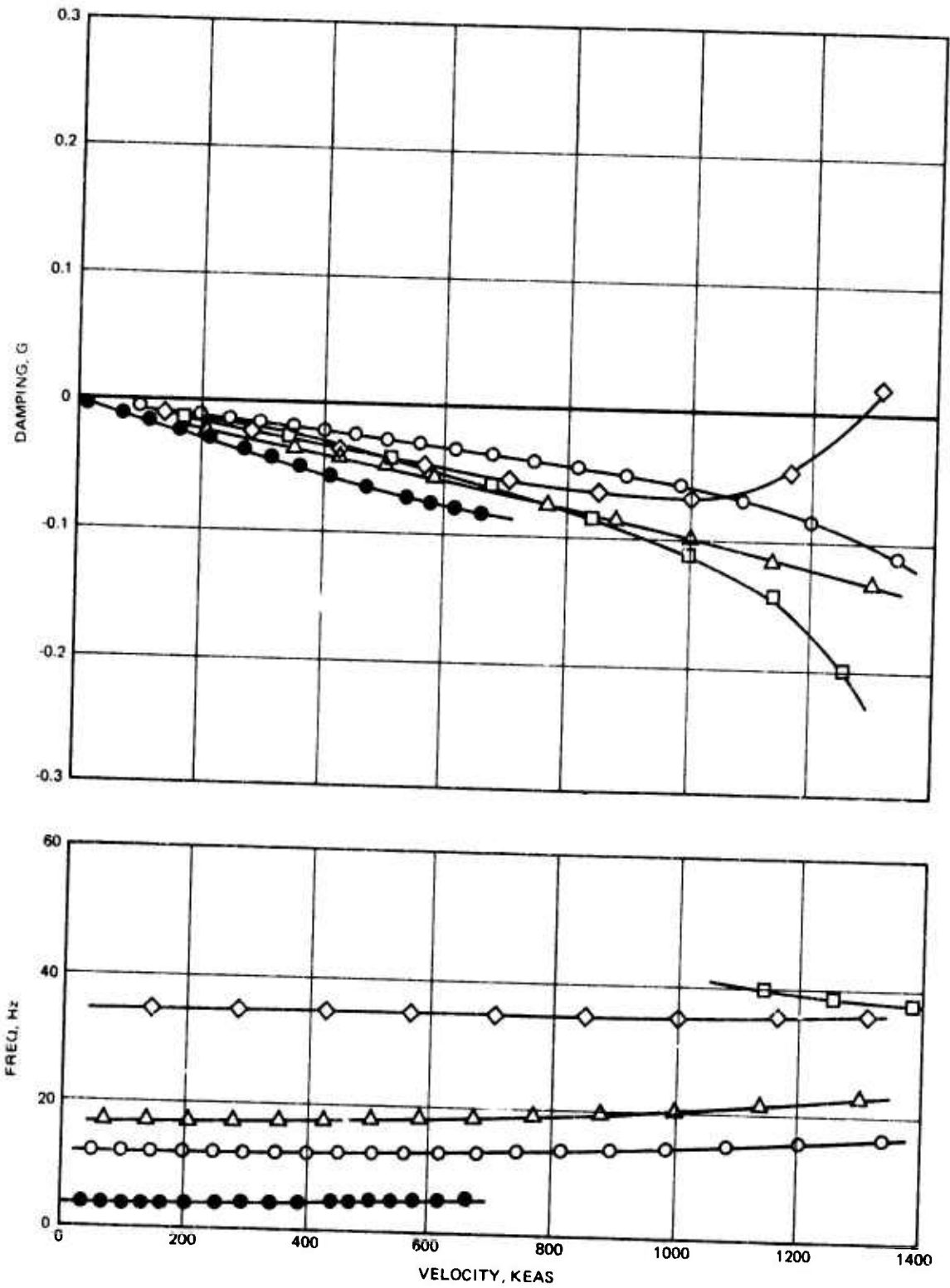


Figure 211. Wing Beam Model, Tip-Mounted Sidewinder, No Fuel, $M = 1.3$, 20,000 Ft

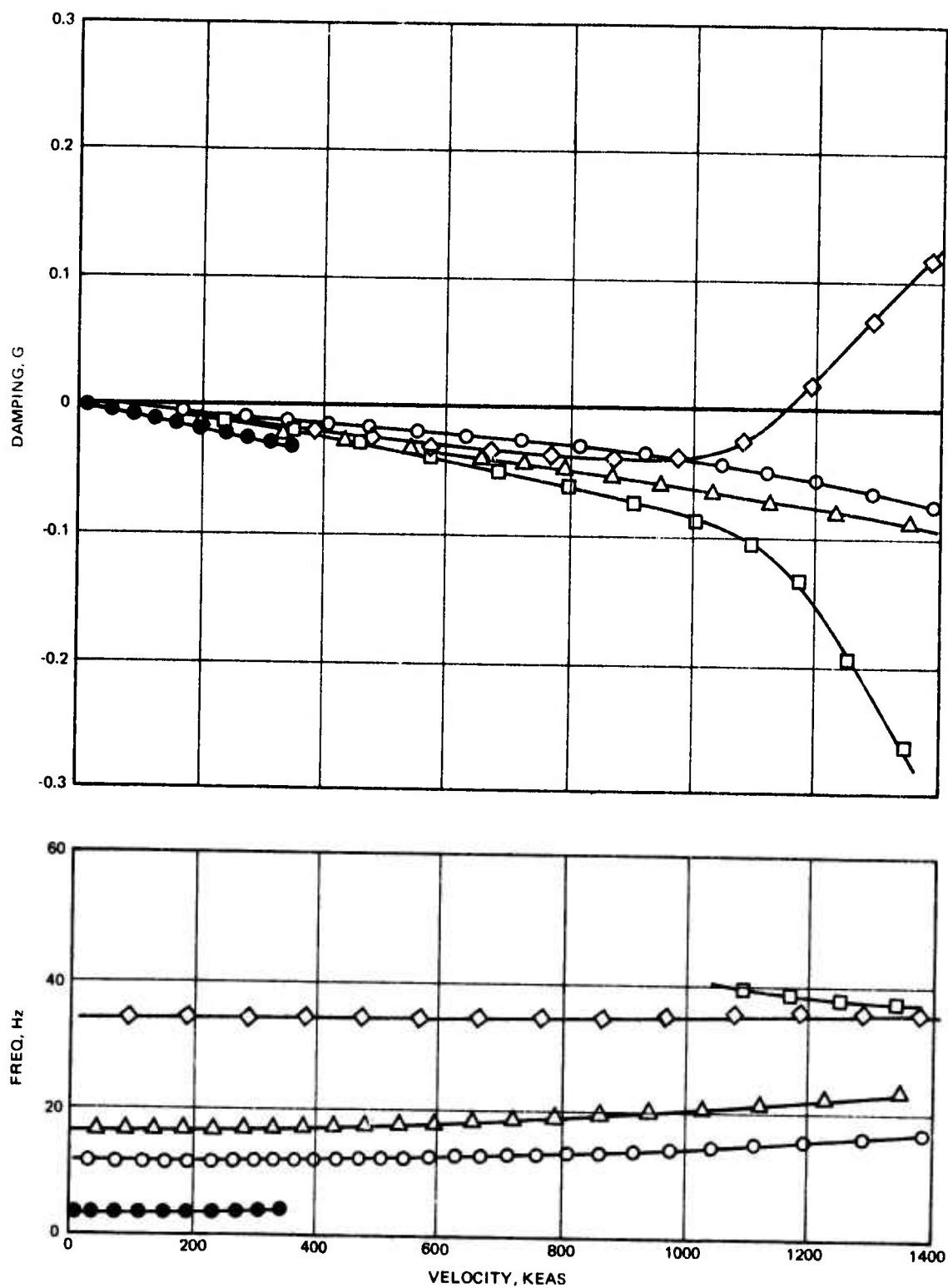


Figure 212. Wing Beam Model, Tip-Mounted Sidewinder, No Fuel, $M = 1.3$, 40,000 Ft

consider structural, as well as aerodynamic, benefits and impacts. The structural evaluation was accomplished using finite element multiple constraint optimization techniques. These studies and their results are presented in detail herein.

Largely because of the aerodynamic investigation, both theoretical and wind tunnel, the objectives of tailoring the ADCA wing for increased washout became secondary. Thus the current baseline ADCA wing design (CSMC) is unchanged in concept and dynamic characteristics from that preliminary beam design presented above.

The wing dynamic idealization for the finite element model is shown in Figure 213. Representation vibration and flutter results will be included for comparative purposes. The calculated frequencies, both symmetric and antisymmetric, are included in Table 35. Mode Shape plots for the symmetric case, the critical case for flutter, are included in Figures 214 and 215.

TABLE 35. WING FREQUENCY COMPARISON - CLEAN, NO FUEL

Mode	Beam Model, Cantilevered	Finite Element Model	
		Symmetric	Antisymmetric
1st Bending	6.21 Hz	6.81 Hz	7.78 Hz
2nd Bending	20.31	17.11	18.19
Torsion	32.03	31.77	32.18

Flutter analyses at $M = 0.8$ for both cases are included. V - g - ω plots at sea level are included in Figures 216 and 217. A flutter speed comparison is included in Table 36.

**TABLE 36. WING FLUTTER SPEED COMPARISON
 $M = 0.8$, CLEAN, NO FUEL**

Altitude, 1000 ft	Beam Model	Finite Element Model	
		Symmetric	Antisymmetric
SL	809 KEAS	800 KEAS	856 KEAS
20	771	774	848
40	739	757	842

Based on the excellent similarity demonstrated between the beam model and finite element model for the clean wing case, those beam model results for the full fuel and tip mounted Sidewinder cases are considered current. The flutter integrity of the ADCA wing design is, therefore, assured.

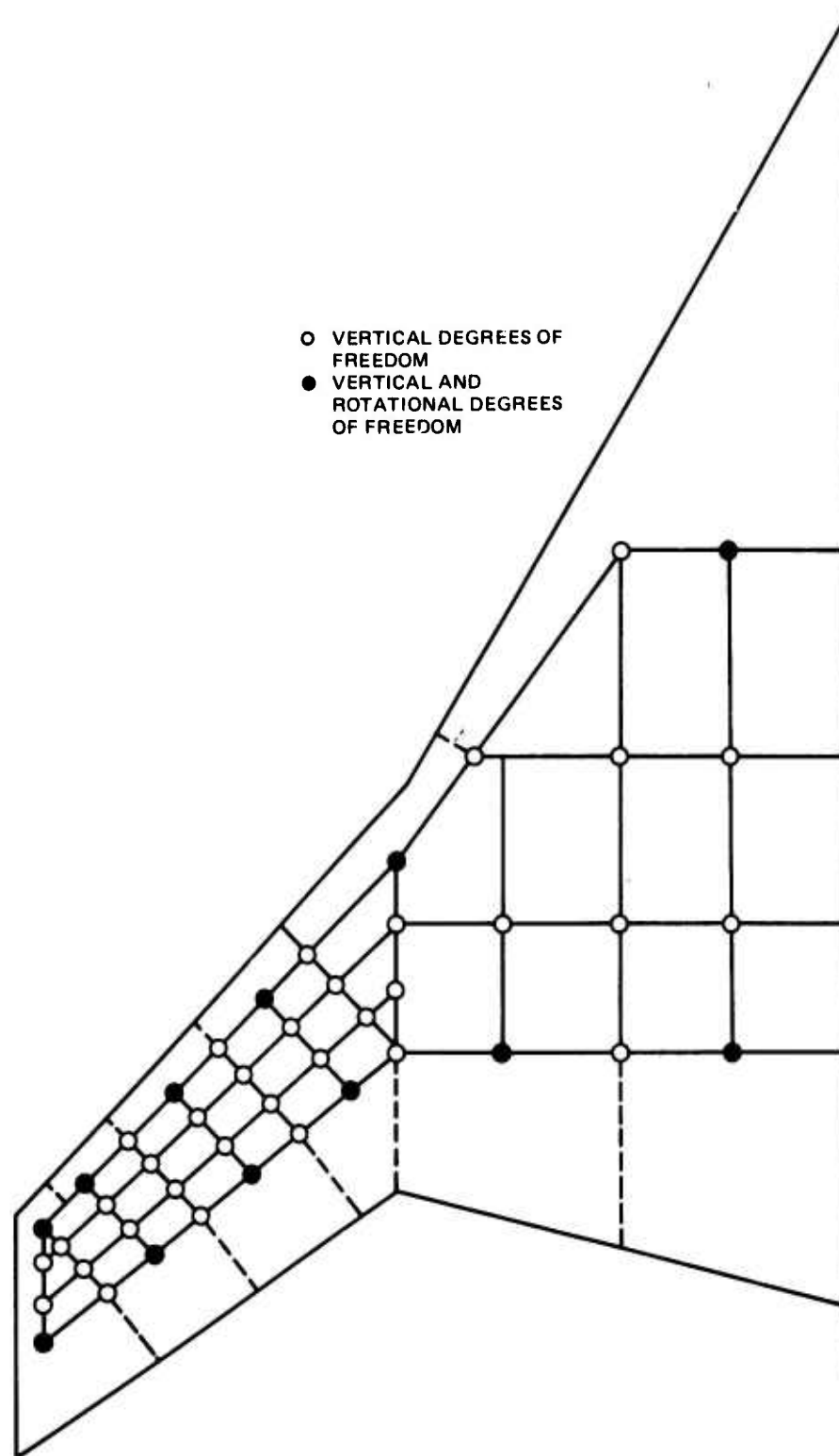


Figure 213. Wing Finite Element Dynamic Idealization

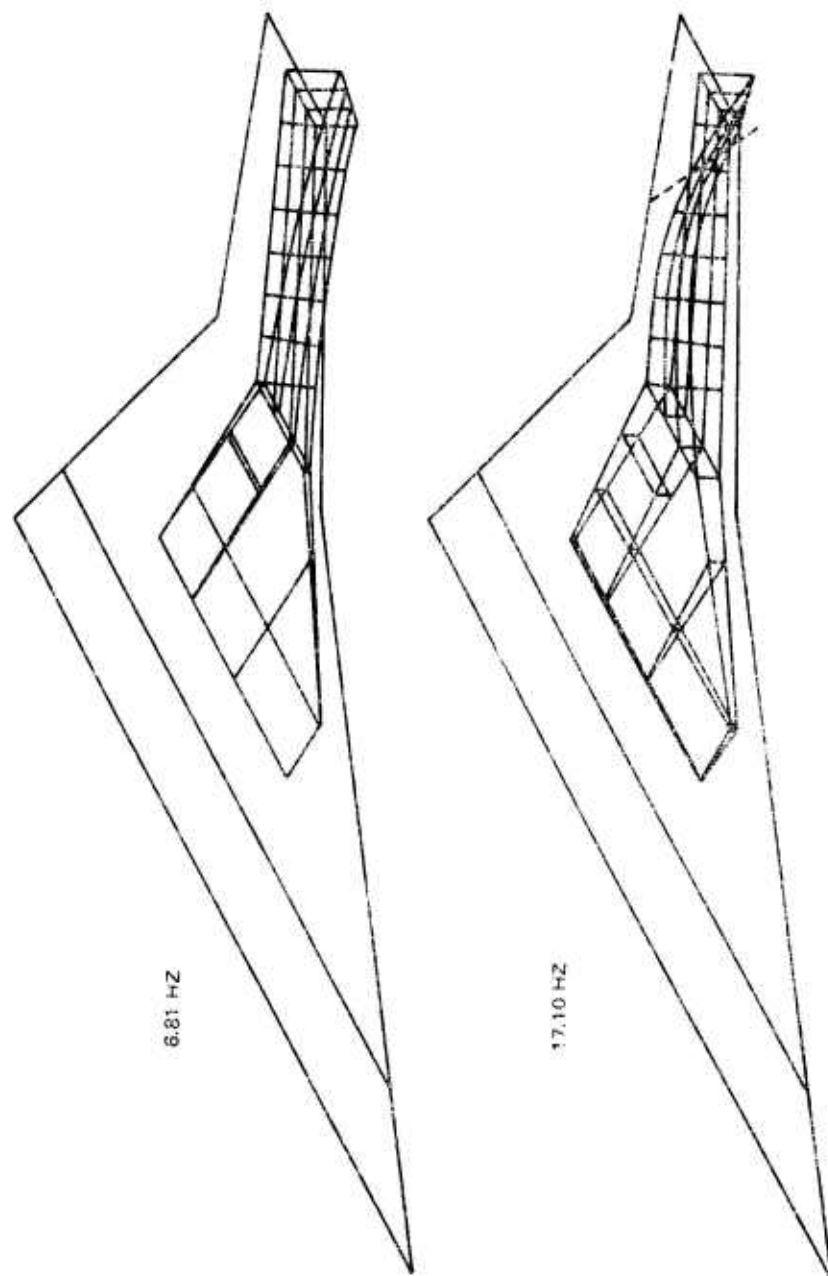


Figure 214. Wing Mode Shapes, Symmetric

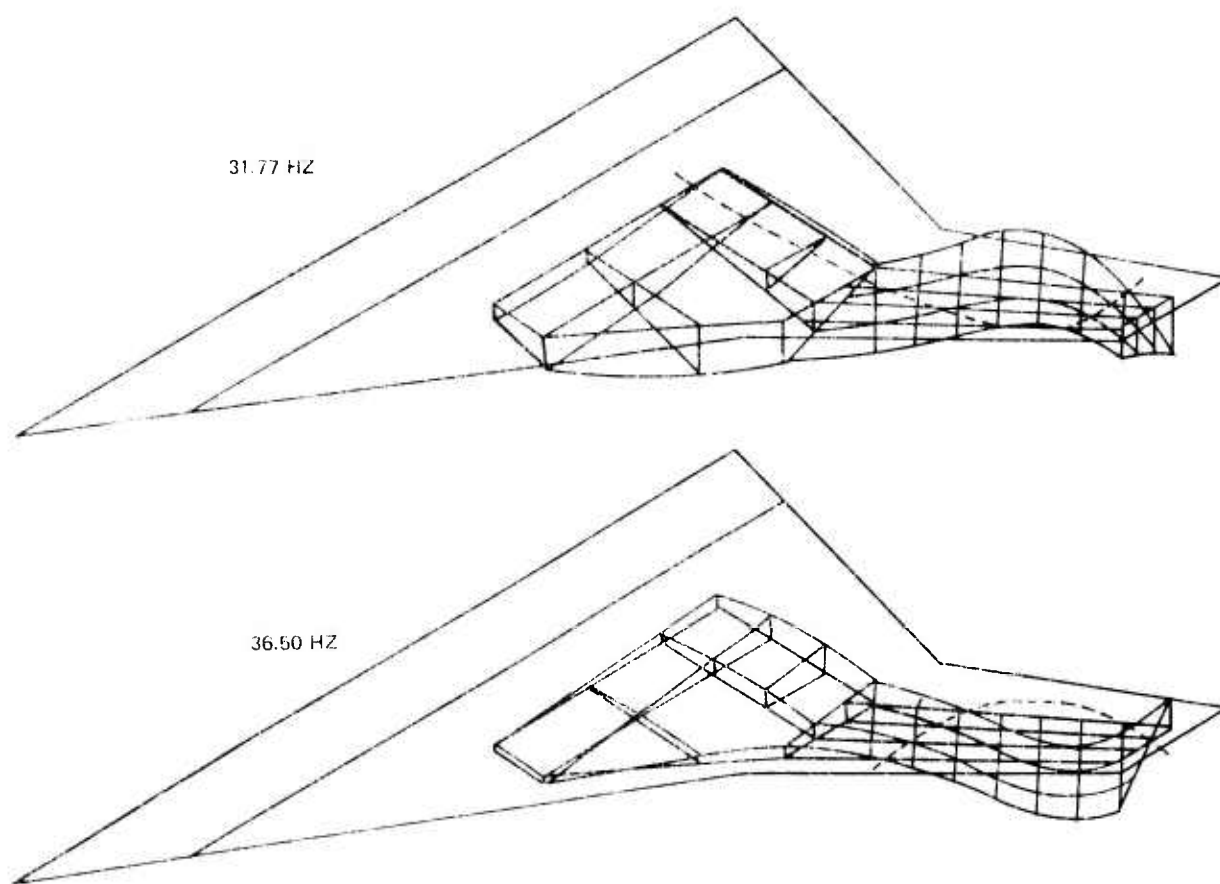


Figure 215. Wing Mode Shapes, Symmetric

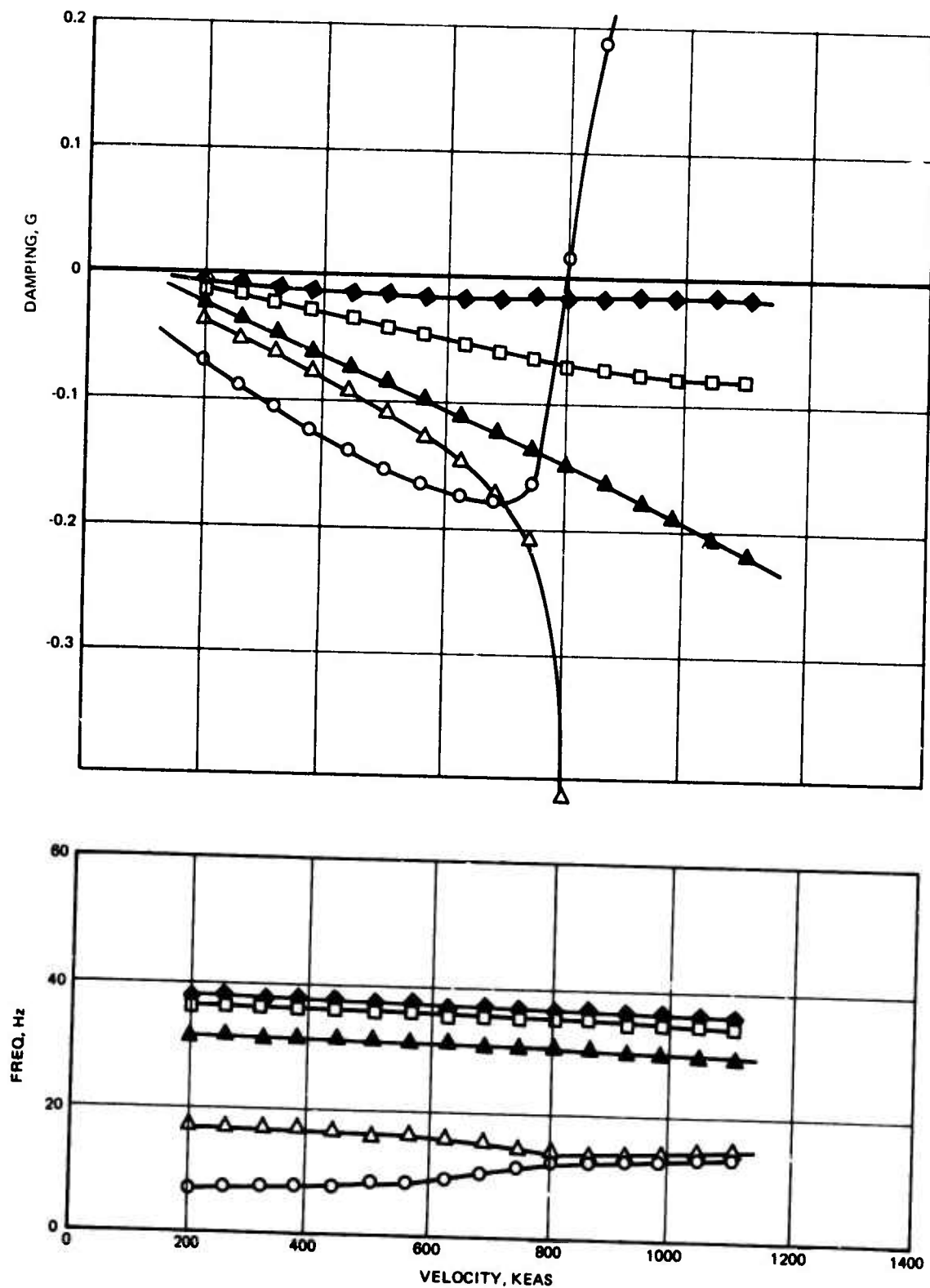


Figure 216. Wing Finite Element Model, Clean, No Fuel, Symmetric, $M = 0.8$, Sea Level

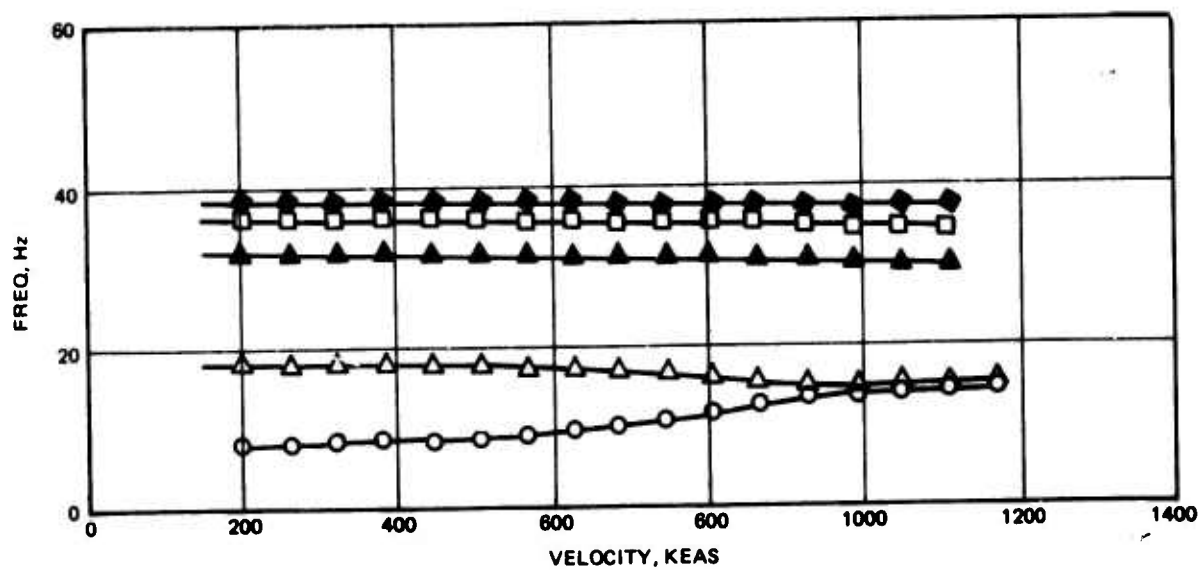
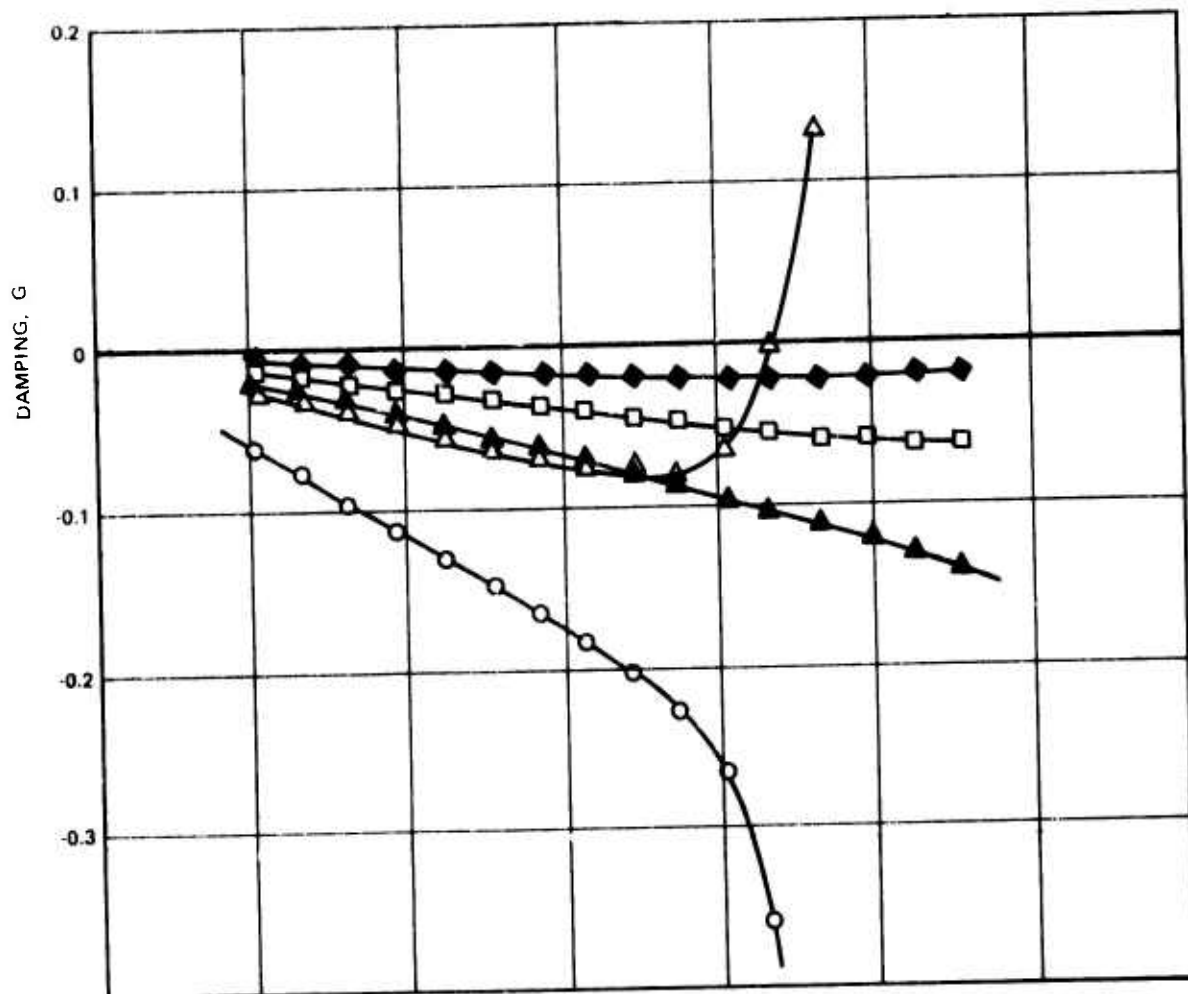


Figure 217. Wing Finite Element Model, Clean, No Fuel, Antisymmetric, $M = 0.8$, Sea Level

5.5 CANARD STRUCTURAL ARRANGEMENT AND DETAIL DESIGN CONCEPT

5.5.1 Canard Structural Arrangement

The canards are fully moveable, independently actuated, slab surfaces approximately 80 inches in span and 111 inches in chord at the root. Maximum depth at the fuselage side-wall is 4.4 inches. The main structural box is comprised of full depth honeycomb core supporting an upper and lower skin, a root rib, an outboard redistribution rib and an integral shaft/root fitting. The honeycomb core provides shear carrying capability to the canard box as well as stabilizing the skins against buckling. The skins, outboard of the shaft provide the basic axial and torsional shear load carrying material in addition to the required bending and torsional stiffness. The ribs allow major load redistribution to the shaft/root fitting, where the flight loads are ultimately collected and transmitted via the shaft to the fuselage which houses the shaft bearing support structure. The shaft enters the fuselage at FS 402.

5.5.2 Detail Structural Design Concept

The ADCA canard structural design concept is shown in Figure 218. The entire canard structure is fabricated with advanced composite materials, with the exception of the integral shaft/root fitting which is 220 ksi steel, and a small section at the root fitting, where a titanium stepped splice plate is co-cured in the skins. The basic concept employs Gr/Ep skins adhesively bonded to Heat Resistant Phenolic (HRP) full depth honeycomb core. The skins are attached to the steel root fitting with blind fasteners through a titanium stepped splice plate adhesively bonded within the skin. Axial load levels in this region are approximately 14,000 lb/in.

Prior to selection of the adhesive bonded root joint configuration design studies of this area were conducted which included an all-bolted concept. The chosen bonded configuration showed a weight advantage over the all-bolted design. This was due to the low bearing and net stress allowables in the Gr/Ep covers. The net stress allowable is reduced because of the interaction with the highly loaded bolts. A higher effective depth is also achieved with the bonded joint since the local titanium thickness is much less than that required for the bolted joint.

Graphite epoxy ribs are located at the root of the canard where the surface meets the fuselage and at the outboard end of the steel root fitting. The outboard rib is bonded to the skins, while the root rib is mechanically fastened. Both ribs are channel sections.

BEST AVAILABLE COPY

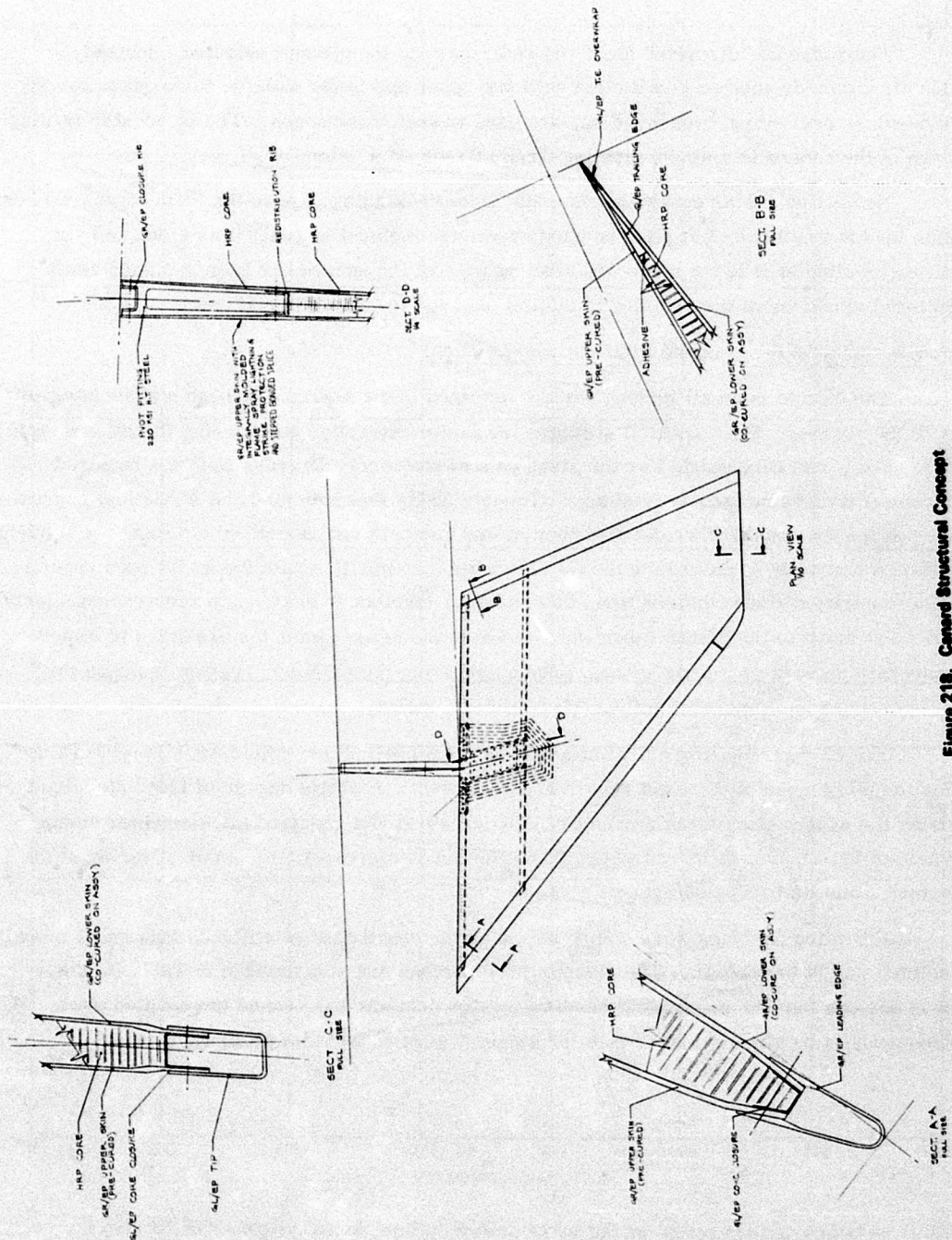


Figure 218. General Structural Concept

There are no "discrete" front and rear spars in the concept selected. Instead, densified core is used on conjunction with the upper and lower skins to form quasi spars. Fiberglass overwraps, wet layed up, are used to seal these edges. The removable leading edge of the canard is a single molding Gr/Ep U-shaped section.

No vertical shear connection is made from the leading edge to the main structural box. This load is reacted by flat plate bending, while the moment is reacted as a couple by a through-bolted joint to the box. The trailing edge of the canard has been designed as an integral extension of the skins, eliminating the need for an additional detail part.

5.5.3 Canard Vibration and Flutter Consideration

The canard is an all moving surface actuated in the fuselage through a shaft integral with the surface. The torsional stiffness for flutter integrity, considering the canard fixed at its root, was estimated. For the given canard planform and gross weight a required fundamental torsion frequency of approximately 32 Hz was indicated. A statistical approximation for the spanwise weight distribution was used, in conjunction with an inverse Rayleigh solution technique to determine the GJ distribution compatible with the 32 Hz requirement. The required stiffness distribution, thus defined, together with strength requirements form the basic input to the COMBO program, in which the cover laminates are sized to simultaneously meet these requirements. The output from the COMBO program includes the anisotropic panel flexibility influence coefficient matrix.

The 32 Hz frequency was similarly used as a preliminary minimum allowable value for the pitch mode of the rigid canard about its pivot. A single degree of freedom calculation using the canard pitch mass moment of inertia indicated a required pitch actuator spring value of 29.0×10^6 in. lb/rad where this value must represent the combined spring of the actuator and its backup structure.

Vibration analyses were completed using the above defined stiffness data and a more refined weight breakdown. The resulting frequencies are summarized in Table 37 where it is obvious that the mechanical bending-torsion coupling has caused the coupled pitch frequency to be slightly higher than the single degree of freedom prediction.

TABLE 37. PRELIMINARY CANARD CALCULATED FREQUENCIES

Actuator Spring = 29×10^6 in.-lb/rad	
Mode	Frequency
Canard 1st Bending	12.40
Torison-Pitch	36.24
2nd Bending	43.70

Node line plots as well as the calculated flutter speed envelope are shown in Figure 219. Two illustrative $V-g-\omega$ plots, corresponding to the envelope, are included in Figures 220 and 221. Examination of the $M=0.8$ curve, Figure 220, indicates that the torsion mode initially stiffens to couple with the second bending mode and cause the critical flutter mechanism. Subsequently the torsion mode destiffens and a classic flutter instability occurs. Supersonically, only the torsion-second bending mechanism occurs, see Figure 221 for $M=1.5$ at the V_L altitude. These observations led to an attempt to reduce the coupled torsion-pitch frequency such that the torsion-first bending coupling would become the critical mechanism for the subsonic case.

The actuator pitch spring was therefore reduced to 20.0×10^6 in.-lb/rad and vibration and flutter analyses were completed. The calculated frequencies are shown in Table 38 in comparison to those values for the 29.0×10^6 in.-lb/rad case.

TABLE 38. PRELIMINARY CANARD FREQUENCY COMPARISON

Mode	Effective Actuator Spring	
	20.0×10^6 in.-lb/rad	29.0×10^6 in.-lb/rad
1st Bending	12.05 Hz	12.40 Hz
Torison-Pitch	34.47	36.24
2nd Bending	43.56	43.70

As was expected, increased flutter margins were achieved through this reduction in the actuator pitch spring. $V-g-\omega$ plots are shown for $M=0.8$ and $M=1.5$ in Figures 222 and 223. A flutter speed comparison is shown in Table 39.

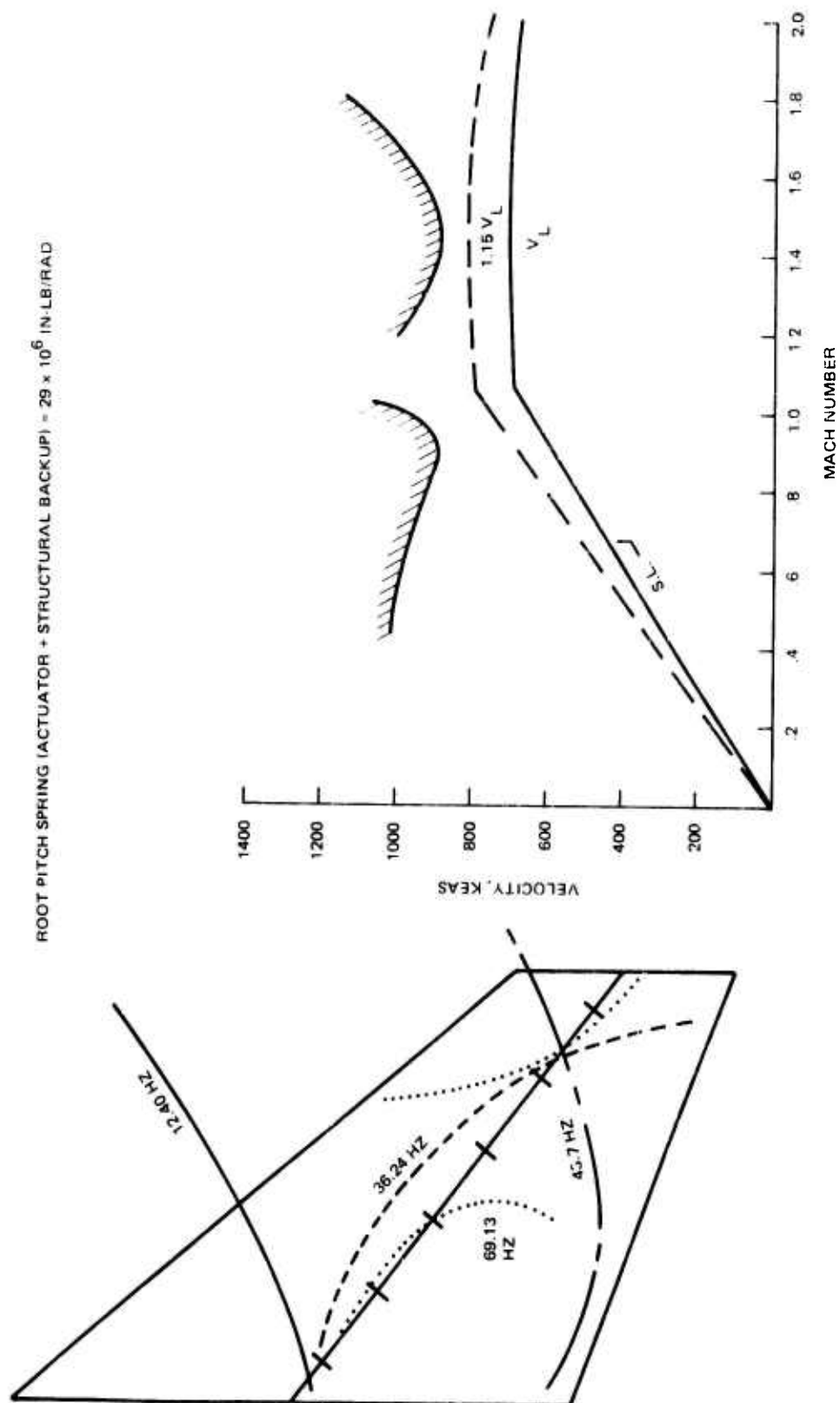


Figure 219. Canard, Preliminary Node Lines and Flutter Boundary

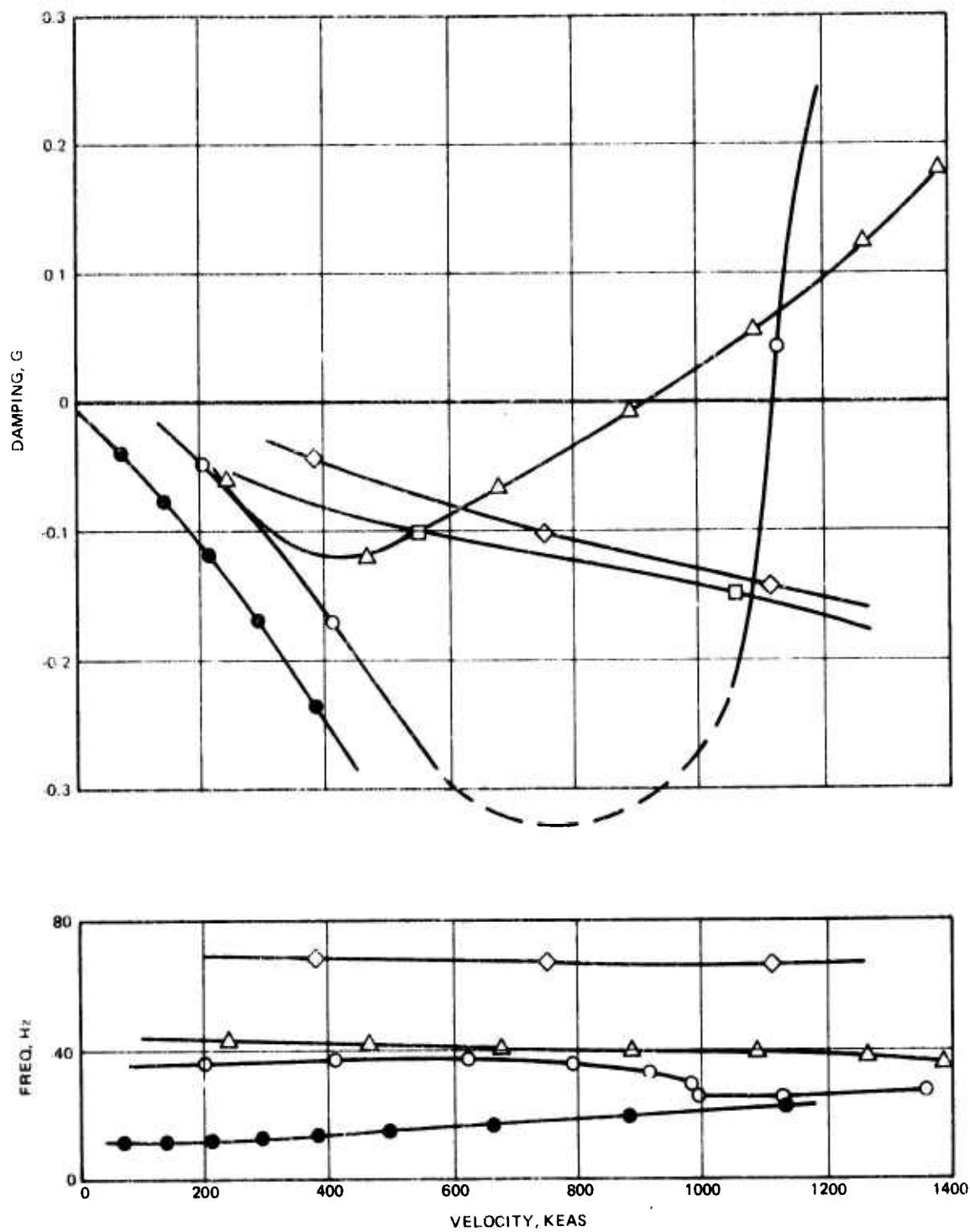


Figure 220. Preliminary Canard V-g Plot, $K(\text{Act.}) = 29 \times 10^6 \text{ In.} \cdot \text{lb/rad}$, $M = 0.8$, Sea Level

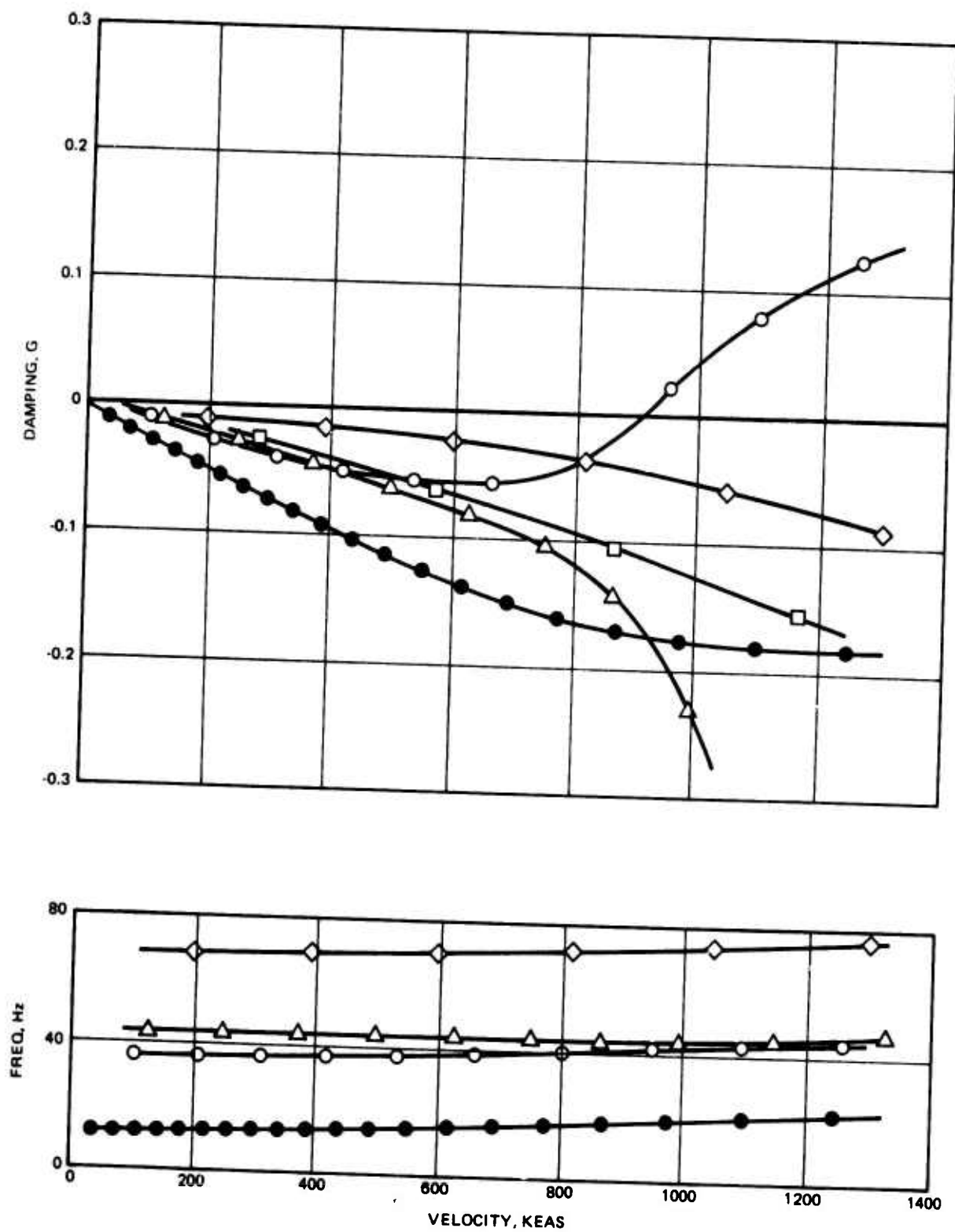


Figure 221. Preliminary Canard V-g Plot, $K(\text{Act.}) = 29 \times 10^6 \text{ in.} \cdot \text{lb/rad}$, $M = 1.5$, 17,750 ft

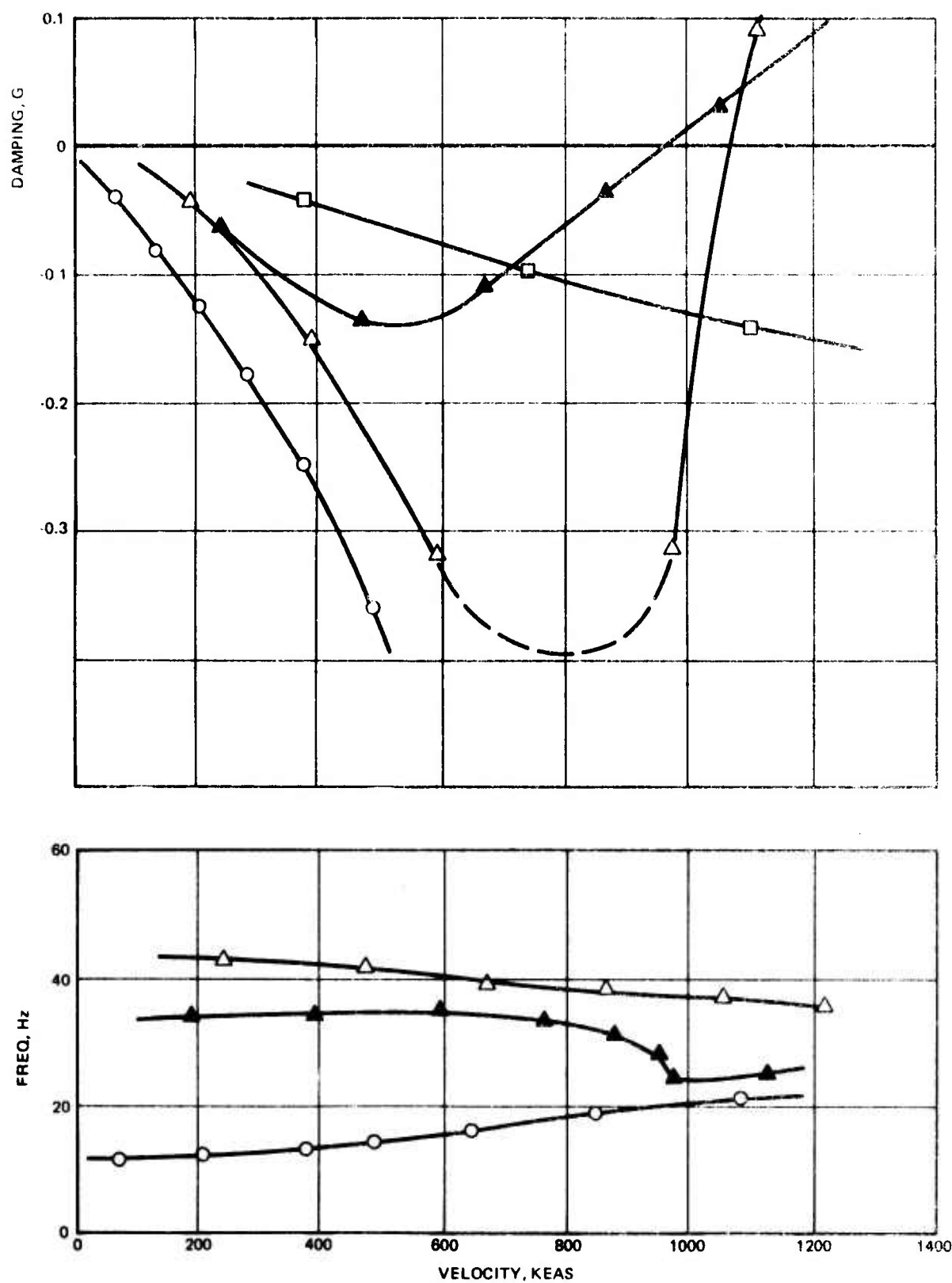


Figure 222. Preliminary Canard V-g Plot, $K(\text{Act.}) = 29 \times 10^6 \text{ In.} \cdot \text{lb/rad}$, $M = 0.8$, Sea Level

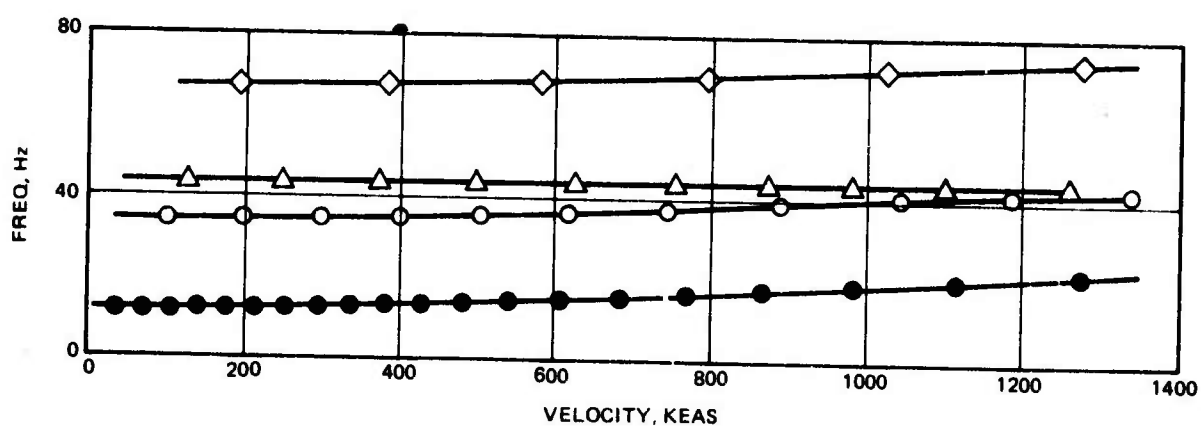
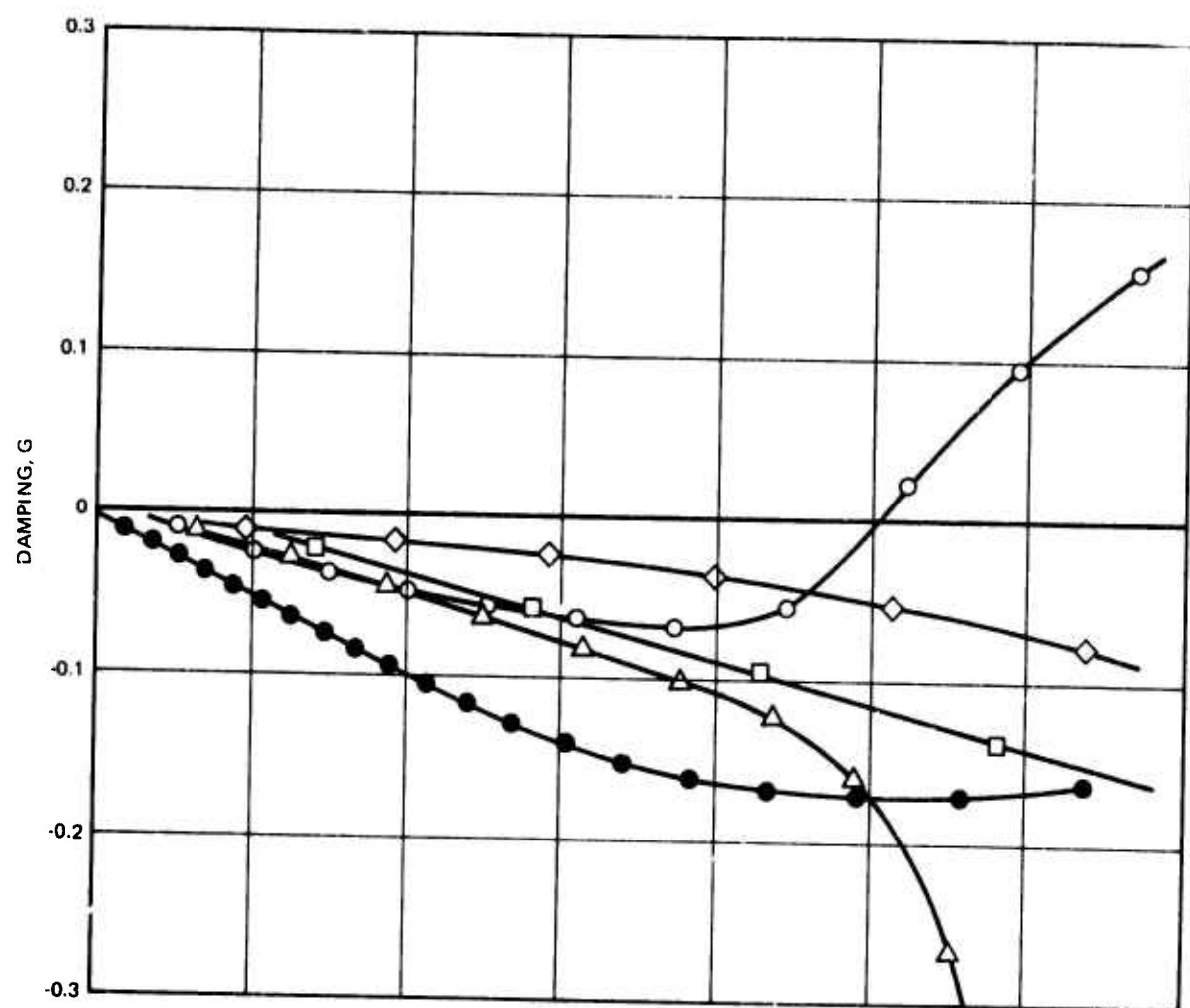


Figure 223. Preliminary Canard V-g Plot, $K(\text{Act.}) = 20 \times 10^6 \text{ In.} \cdot \text{lb/rad}$, $M = 1.5$, 17,750 ft

TABLE 39. PRELIMINARY CANARD FLUTTER SPEED COMPARISON

Case	Effective Actuator Pitch Spring	
	20.0×10^6 in.-lb/rad	29.0×10^6 in.-lb/rad
M = 0.8, SL	1015 KEAS	910 KEAS
M = 1.5, 17, 750 ft.	1000	900

As the design cycle dictated, various requirements were reiterated and the criteria discussed above was incorporated into the final canard design. The dynamic model idealization is shown in Figure 224, where the surface is divided into six panels, each having a deflection and rotational degree of freedom. The panels and rotational degrees of freedom are taken perpendicular to the beam reference axis.

The gross weight properties for the final canard design are summarized in Table 40.

TABLE 40. FINAL CANARD GROSS WEIGHT PROPERTIES

Values Given for One-Half Aircraft	
Weight	= 257lb
I _{yy} cg	= 274,400 lb in. ²
I _{yy} pivot	= 327,000 lb-in. ²

The distributed weight properties are included in Table 41 where the reader is again directed to the dynamic idealization shown in Figure 224.

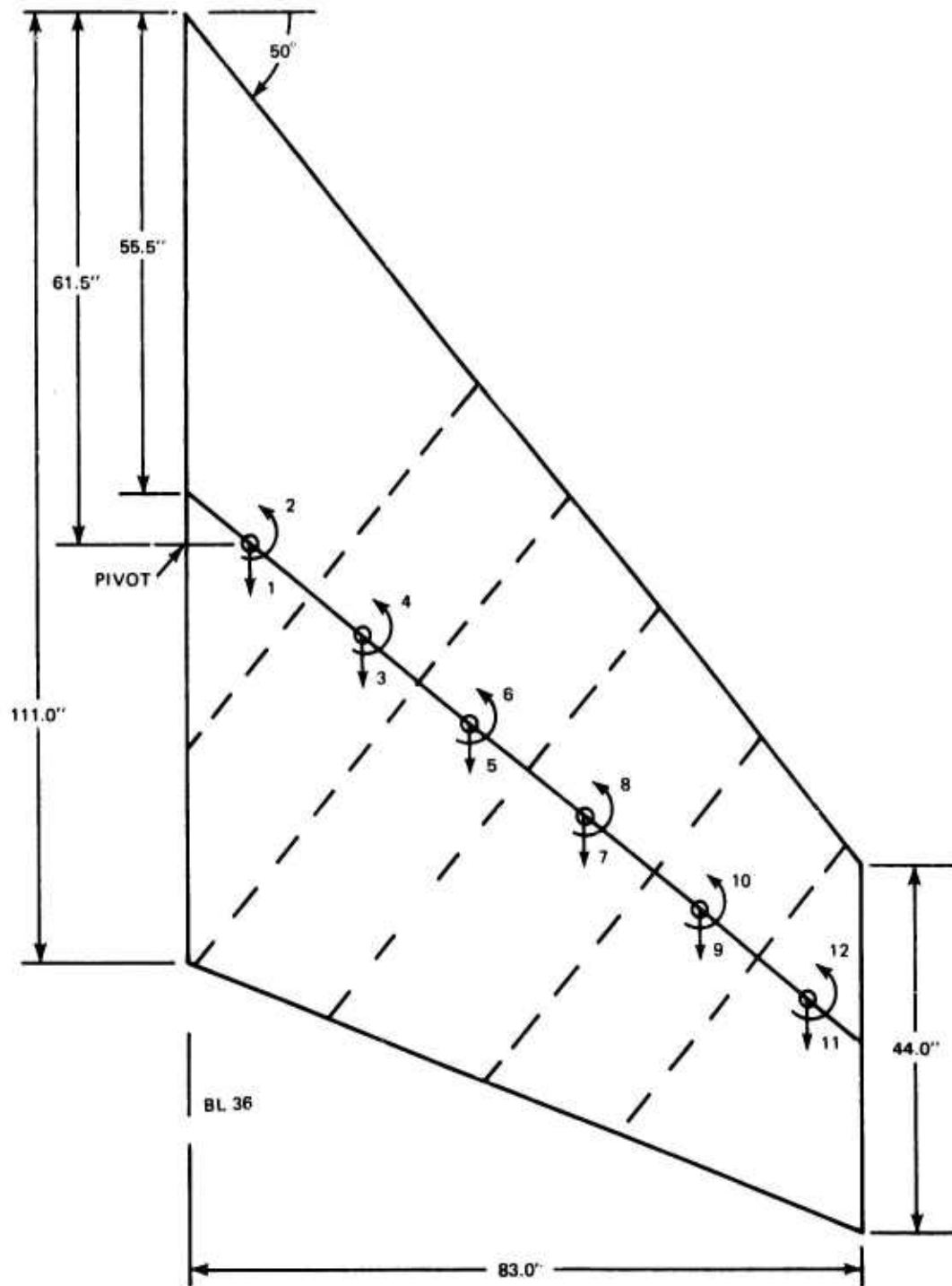


Figure 224. Canard Dynamic Idealization

TABLE 41. FINAL CANARD DISTRIBUTED MASS PROPERTIES

Panel	Weight, lb	Arm* in.	Unbalance lb.-in.	Iyy cg, lb.-in.	Iyy EA ₂ lb.-in. ²
1	191.1	-4.9	-936.4	22,877	27,465
2	46.4	1.8	83.5	14,276	14,426
3	39.2	3.5	137.2	11,141	11,621
4	30.9	2.4	74.2	6,722	6,900
5	24.7	2.4	59.3	3,912	4,054
6	24.7	2.4	108.7	2,495	2,973

*Perpendicular distance from panel cg to the beam reference axis. Positive indicates an aft cg.

It will be noted that the canard pivot shaft is located aft of the intersection of the reference beam axis with the root. The beam "root flexibilities" equivalent to the final 20×10^6 in.-lb/rad actuator pitch spring are given in Table 42. The sign convention is: deflection and load are positive down, rotation and torque are positive nose up. An aircraft reference axis is assumed.

TABLE 42. CANARD BEAM ROOT FLEXIBILITIES ($\times 10^6$)

Actuator Pitch Spring = 20.6×10^6 in.-lb/rad		
	Load	Torque
Deflection	1.25	-.25
Rotation	-.25	.05

The overall beam flexibility influence coefficients for the final canard design are included, for reference, in Table 43 the sign convention and units are the same as those mentioned above. The root flexibilities given above have been incorporated into the influence coefficients.

Vibration analyses for the final canard design were completed and the results are summarized in Table 44. Mode shape plots are included in Figure 225.

TABLE 43. ADCA CANARD BEAM MODEL INFLUENCE COEFFICIENTS* X10⁶

	1	2	3	4	5	6	7	3	9	10	11	12
1	0.42300	0.02824	1.9806	0.02824	3.4931	0.02824	5.0056	0.02824	6.5181	0.02824	8.0306	0.02824
2	0.02824	0.04556	0.4648	0.04556	0.88872	0.04556	1.3126	0.04556	1.7365	0.04556	2.1605	0.04556
3	1.9806	0.46480	17.491	0.46480	34.403	0.4648	51.388	0.46480	68.372	0.46480	85.356	0.46480
4	0.02824	0.04556	0.46480	0.08331	0.88872	0.08331	1.3126	0.08331	1.7365	0.08331	2.1605	0.08331
5	3.4931	0.88872	34.403	0.88872	78.632	0.88872	126.47	0.88872	174.30	0.88872	222.14	0.88872
6	0.02824	0.04556	0.46480	0.08331	0.88872	0.14488	1.3126	0.14488	1.7365	0.14488	2.1605	0.14488
7	5.0056	1.3126	51.388	1.3126	126.47	1.3126	228.81	1.3126	339.19	1.3126	449.58	1.3126
8	0.02824	0.04556	0.46480	0.08331	0.88872	0.14488	1.3126	0.24879	1.7355	0.24879	2.1605	0.24879
9	6.5181	1.7365	68.372	1.7365	174.30	1.7365	339.19	1.7365	570.64	1.7365	826.80	1.7365
10	0.02824	0.04556	0.46480	0.08331	0.88872	0.14488	1.3126	0.24879	1.7365	0.43670	2.1605	0.43670
11	8.0307	2.1605	85.356	2.1605	222.14	2.1605	449.58	2.1605	826.80	2.1605	1409.2	2.1605
12	0.02824	0.04556	0.46480	0.08331	0.88872	0.14488	1.3126	0.24879	1.7365	0.43670	2.1605	0.78690

*See Figure 224 for Coordinate Definition

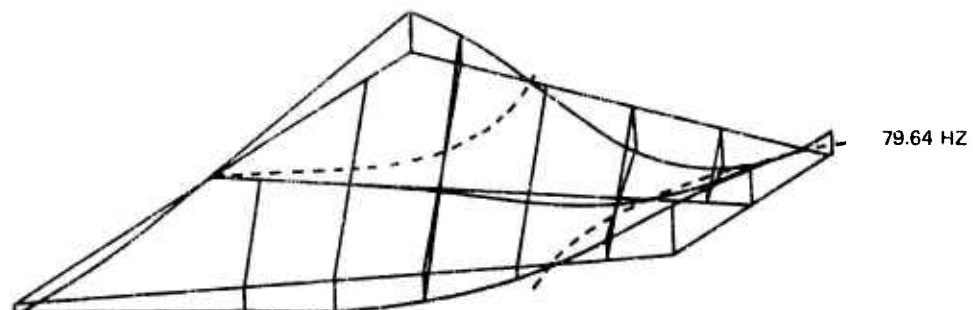
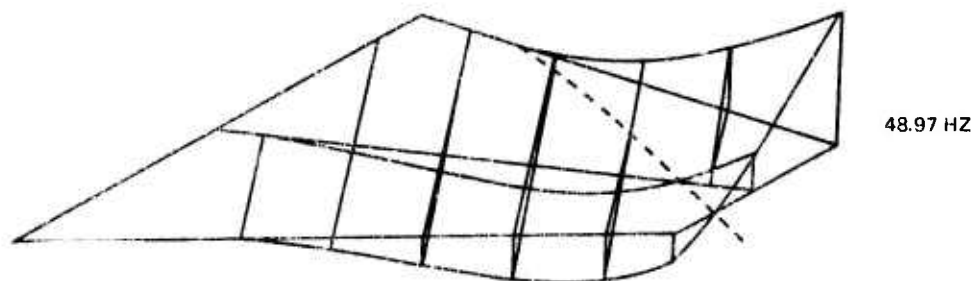
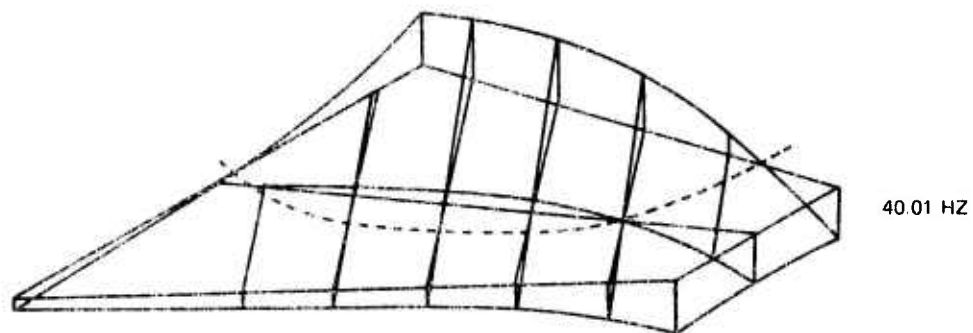
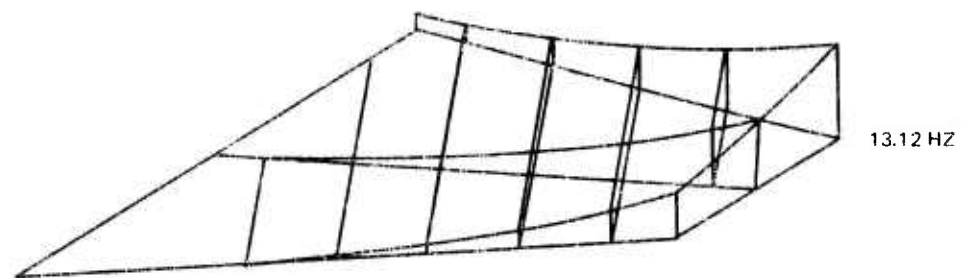


Figure 225. Final Canard Mode Shapes

TABLE 44. CANARD VIBRATION ANALYSES

Final Canard Design	
MODE	Calculated Frequencies, Hz
1st Bending	13.12
Torsion	40.01
2nd Bending	48.97

Comprehensive flutter analyses were completed throughout the flight envelope where-
in margins in excess of $1.15 V_L$ were demonstrated. Figures 226 through 240 are the
V-g- ω plots for Mach numbers 0.6 through 1.8. Final flutter envelopes are presented
in figures 241 through 243. The corresponding flutter speeds and margins are sum-
marized in Table 45.

TABLE 45. ADCA CANARD FLUTTER SPEED SUMMARY

Mach No.	Altitude Feet	V_f KEAS	V_f/V_L	Reference V-g- ω , Figure
.6	S.L.	1004	2.54	226
	20K	861	3.21	227
	40K	755	4.44	228
.8	S.L.	900	1.71	229
	20K	785	2.19	230
	40K	705	3.12	231
1.3	S.L.	1209	1.41	232
	11K*	1049	1.50	233
	20K	952	1.64	234
	40K	800	2.18	235
1.5	17.75K*	1032	1.46	236
	20K	1027	1.53	237
	40K	924	2.17	238
1.8	27.2K*	1180	1.72	239
	40K	1120	2.18	240

*Altitude appropriate to the V_L envelope.

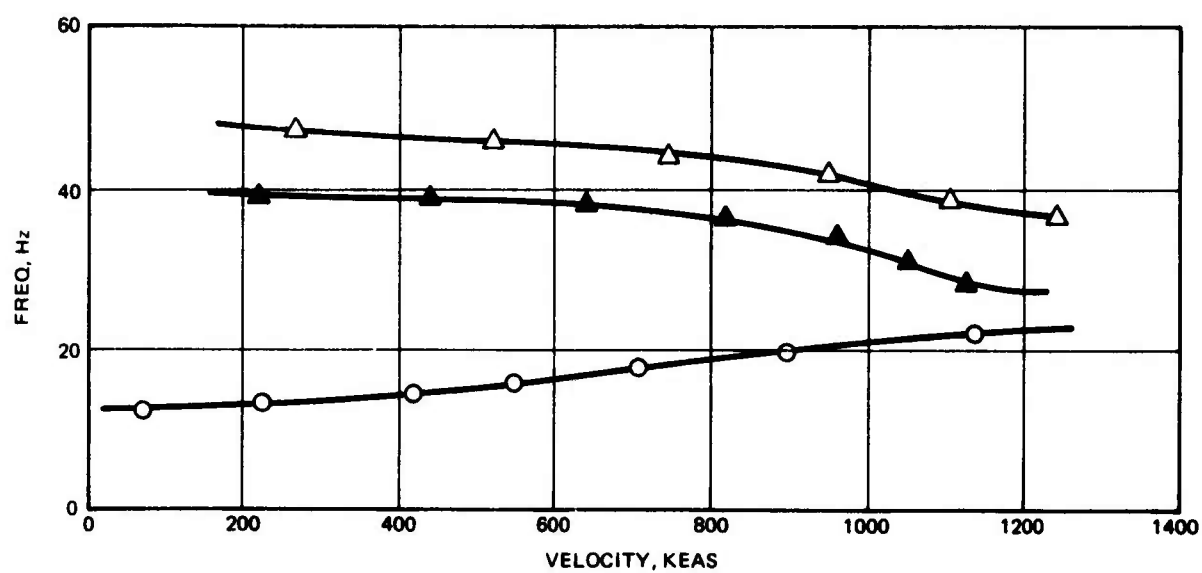
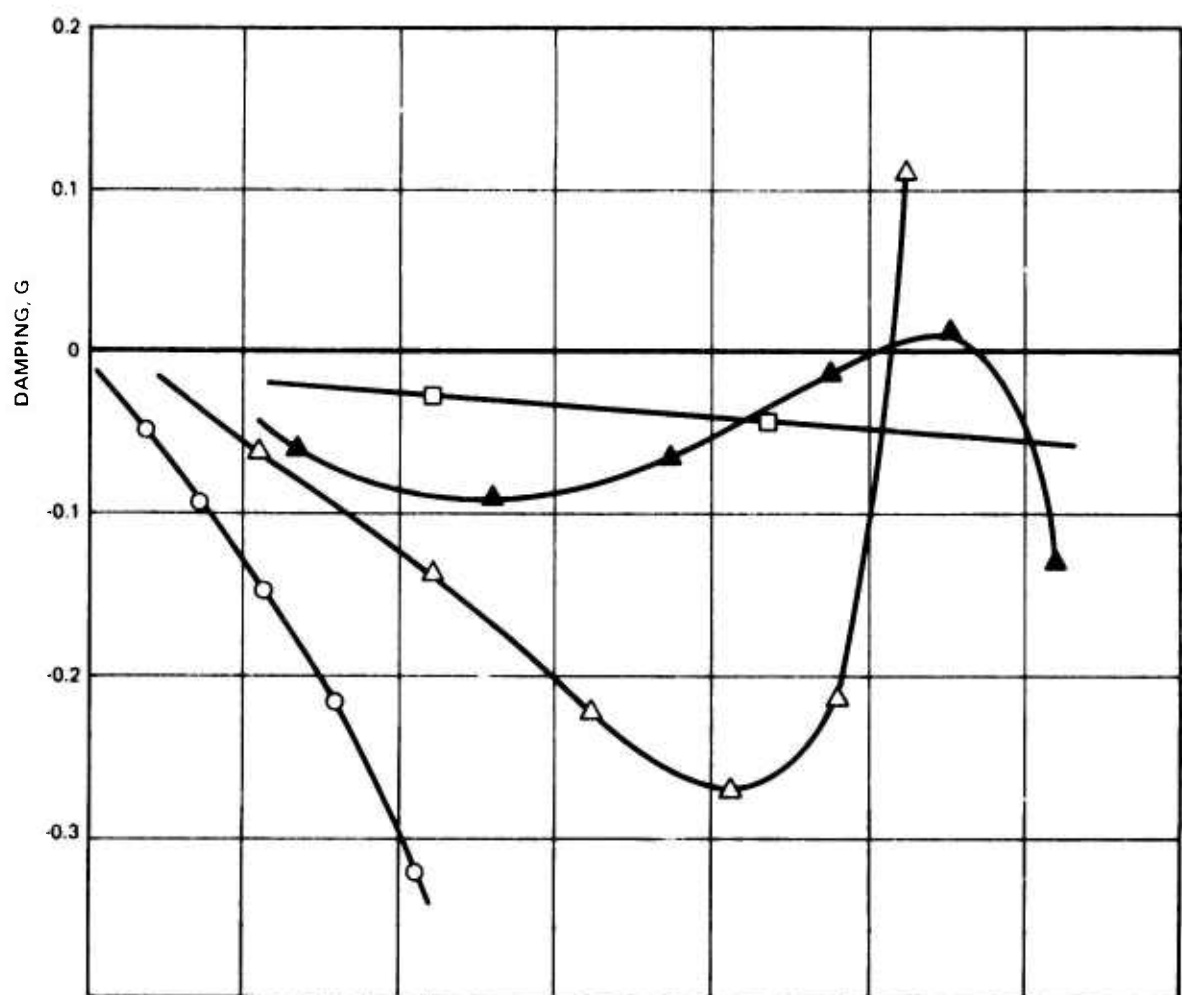


Figure 226. Preliminary Canard V-g Plot, $K(\text{Act.}) = 20 \times 10^6 \text{ In.} \cdot \text{lb/rad}$, $M = 0.6$, Sea Level

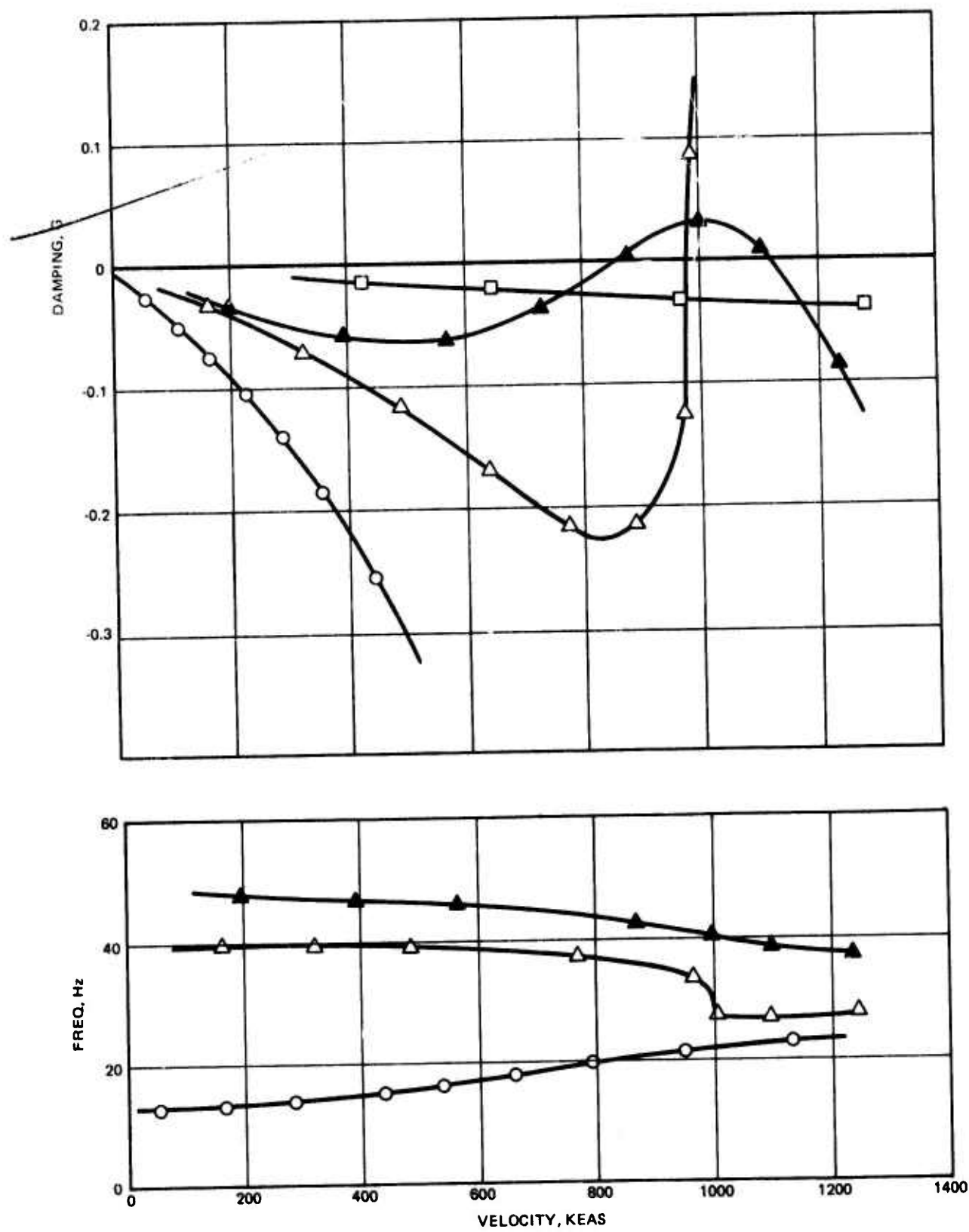


Figure 227. Preliminary Canard V-g Plot, $K(\text{Act.}) = 20 \times 10^6 \text{ In.} \cdot \text{lb/rad}$, $M = 0.6$, 20,000 ft

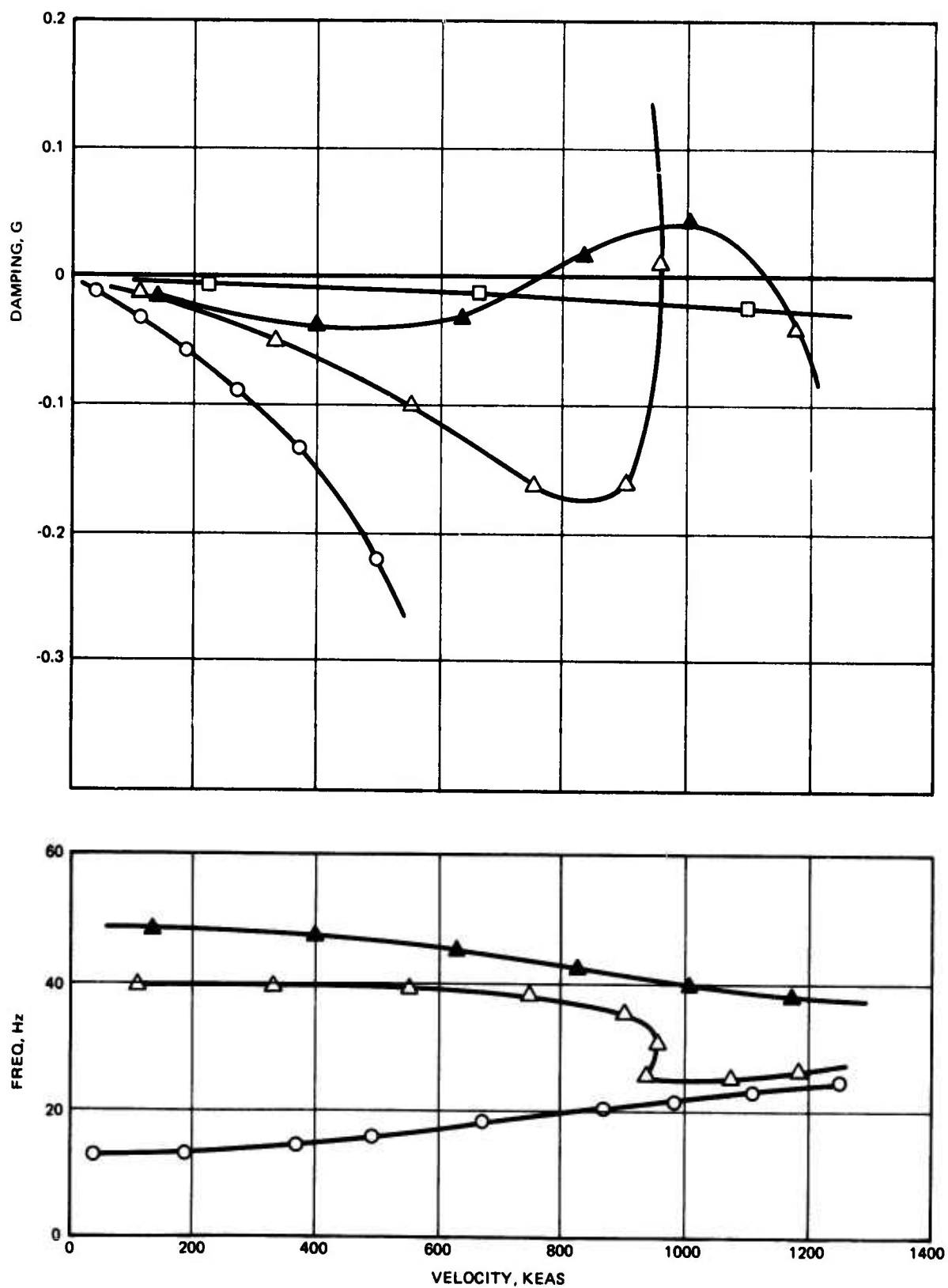


Figure 228. Preliminary Canard V-g Plot, $K(\text{Act.}) = 20 \times 10^6 \text{ In.} \cdot \text{lb/rad}$, $M = 0.6$, 40,000 Ft

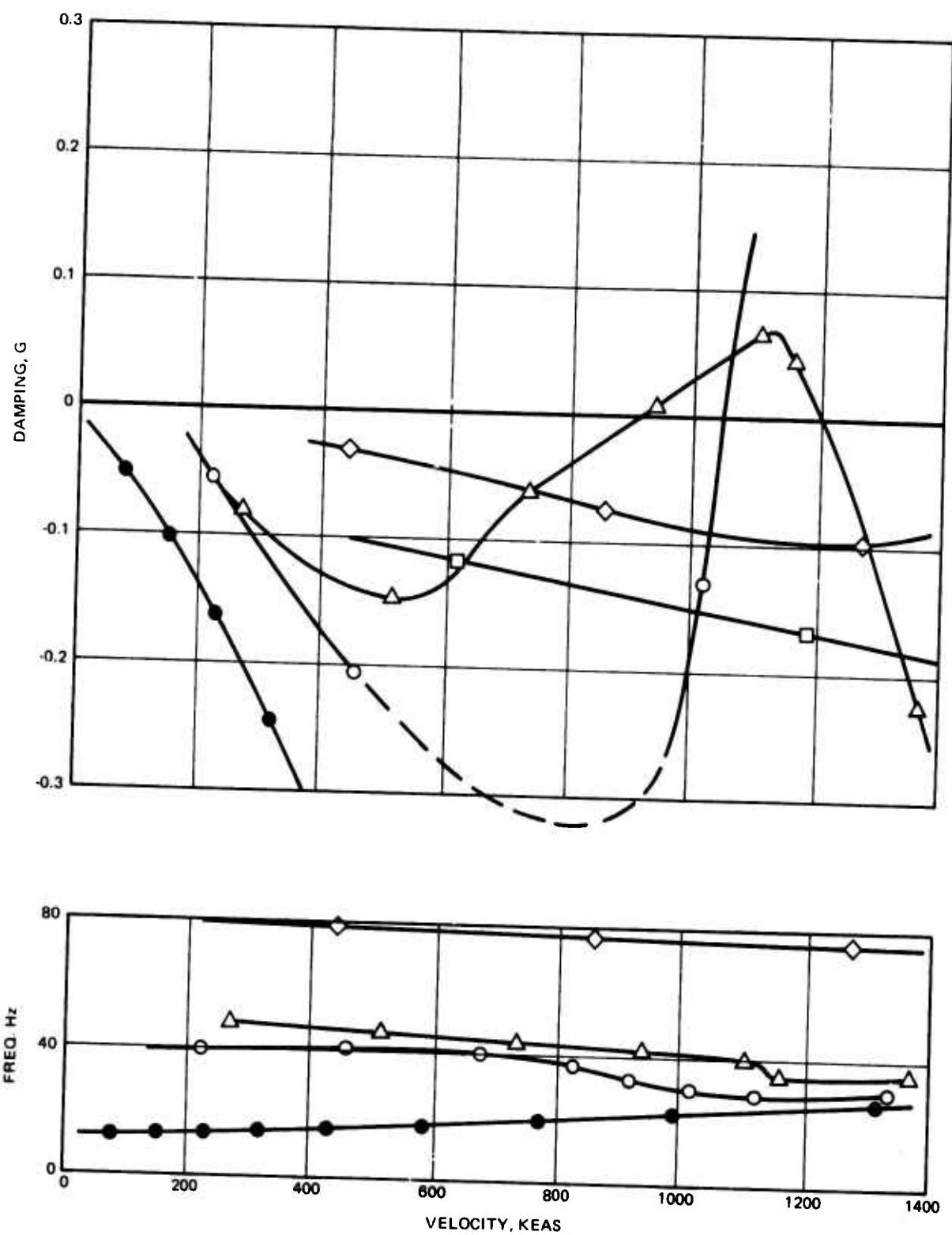


Figure 229. Final Canard V-g Plot, $K(\text{Act.}) = 20 \times 10^6 \text{ In.} \cdot \text{lb/rad}$, $M = 0.8$, Sea Level

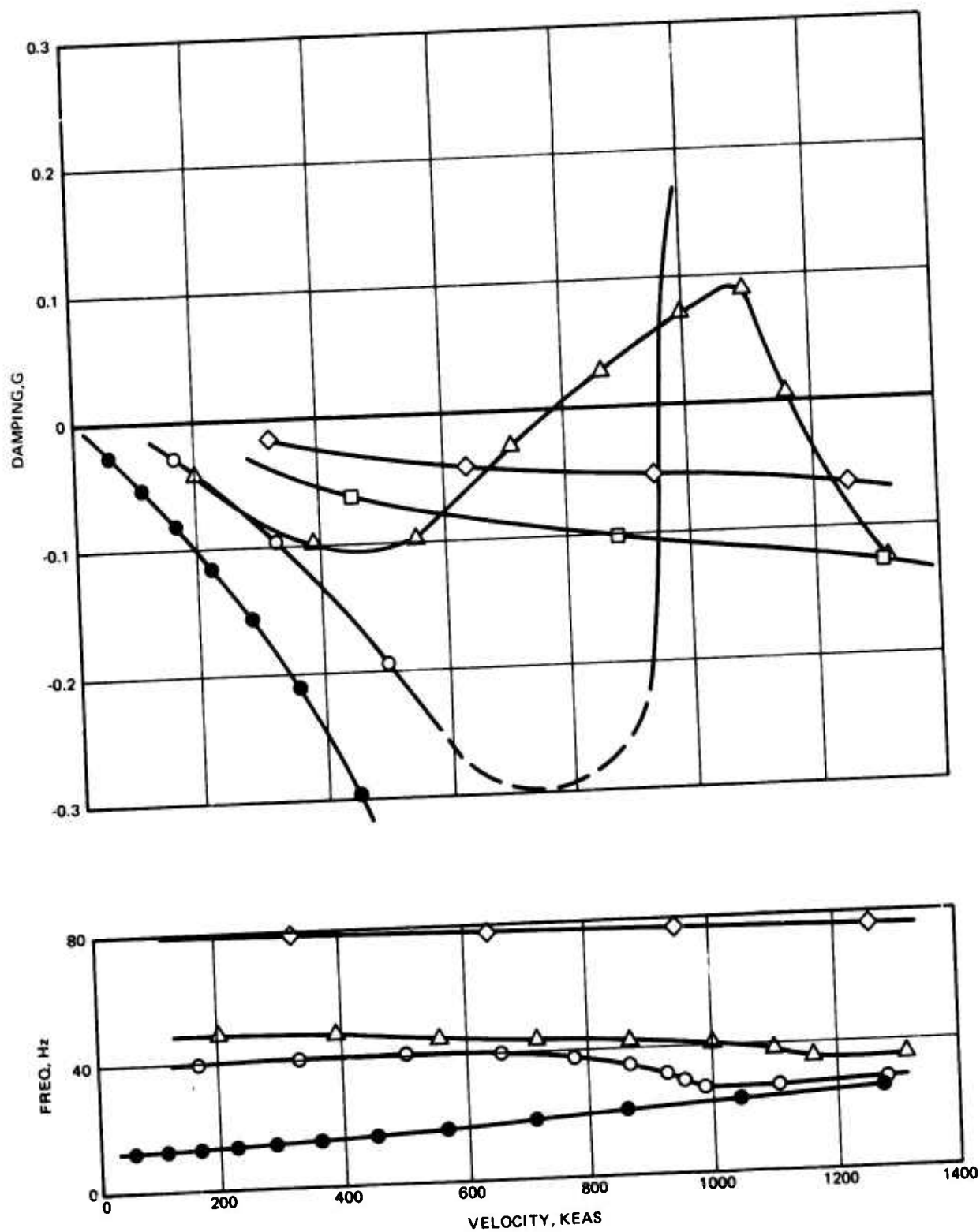


Figure 230. Final Canard V-g Plot, $K(\text{Act.}) = 20 \times 10^6 \text{ In.} \cdot \text{lb/rad}$, $M = 0.8$, 20,000 Ft

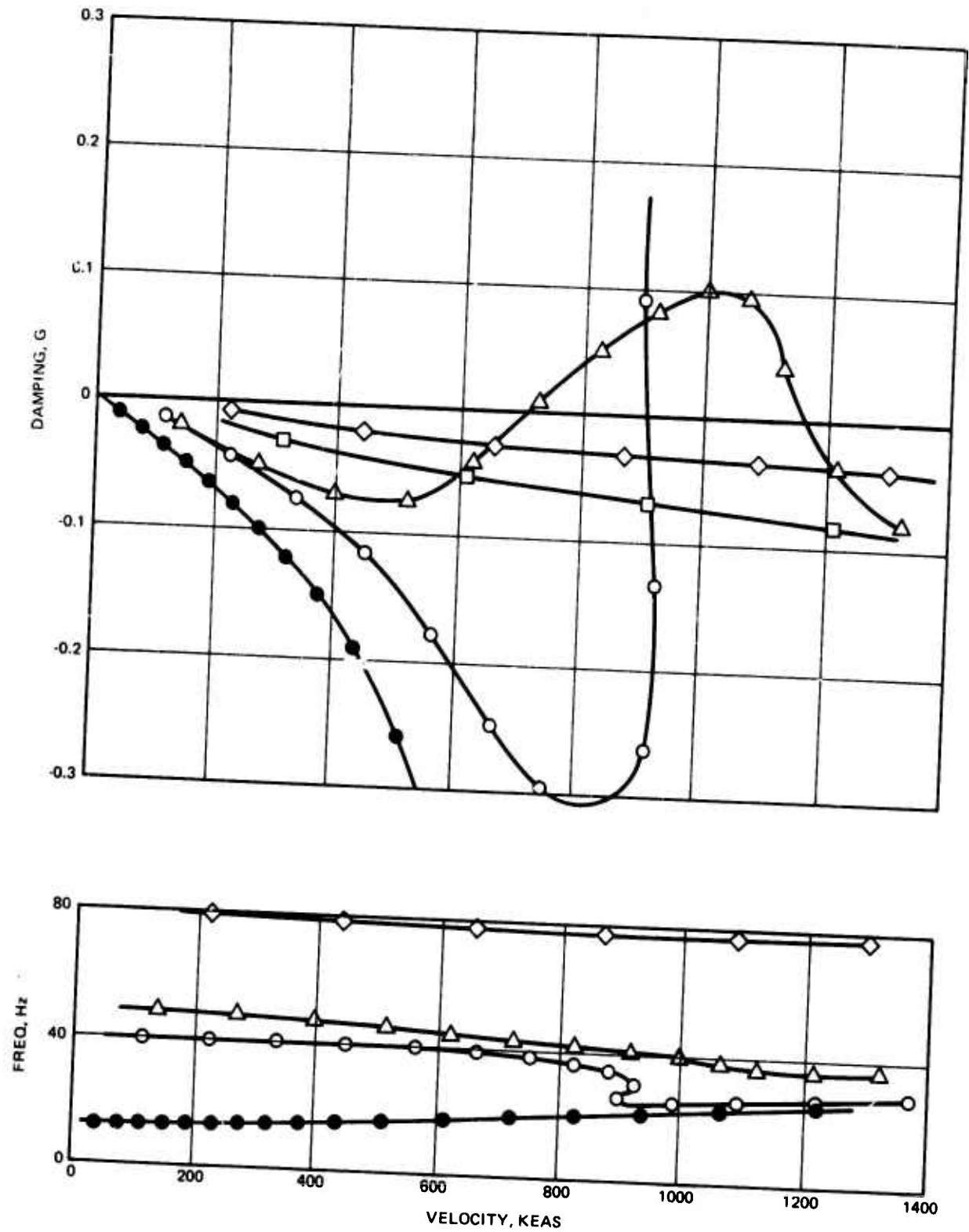


Figure 231. Final Canard V-g Plot, $K(\text{Act.}) = 20 \times 10^6 \text{ in.} \cdot \text{lb/rad}$, $M = 0.8$, 40,000 ft

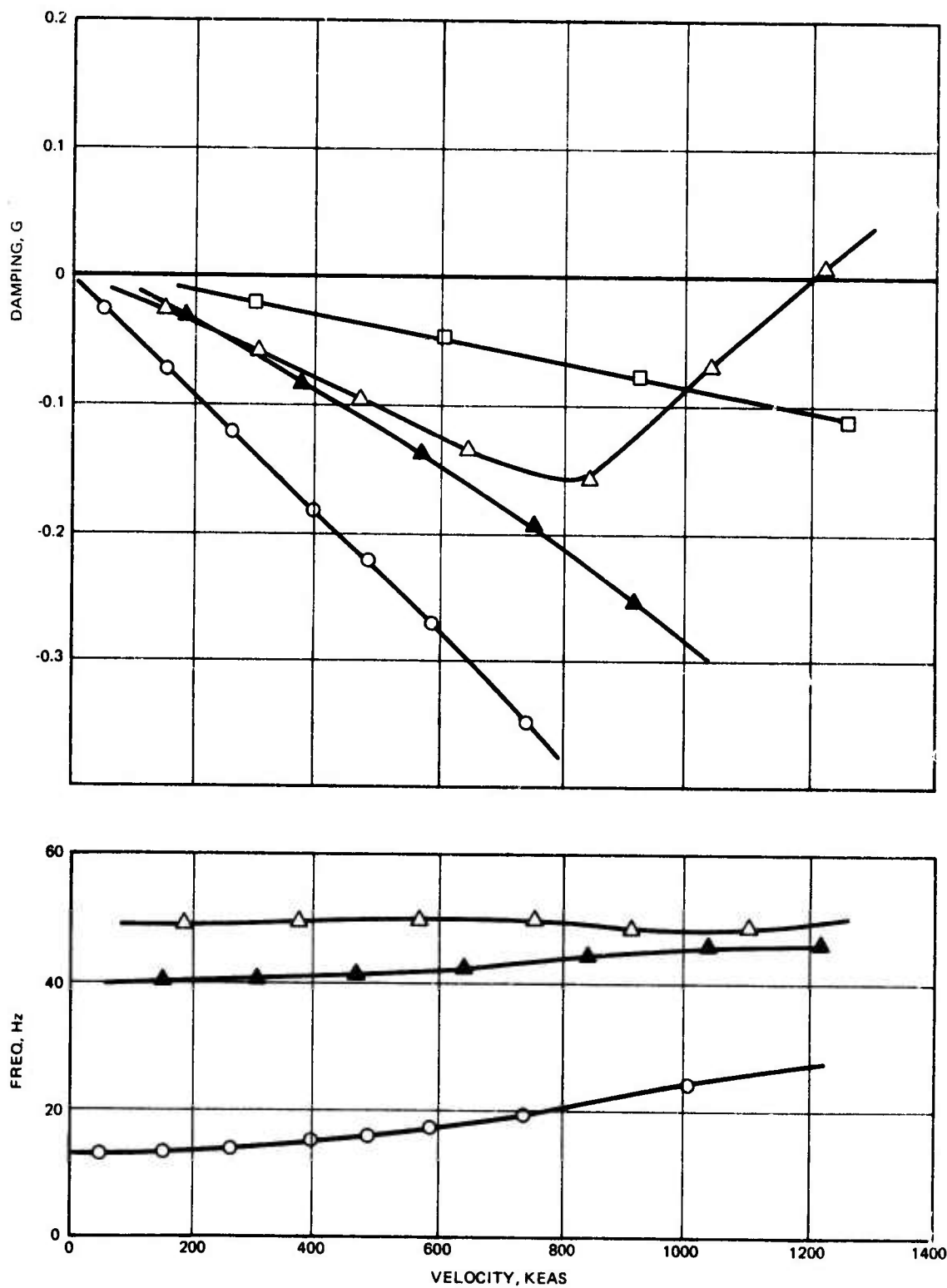


Figure 232. Final Canard V-g Plot, $K(\text{Act.}) = 20 \times 10^6 \text{ In.} \cdot \text{lb/rad}$, $M = 1.3$, Sea Level

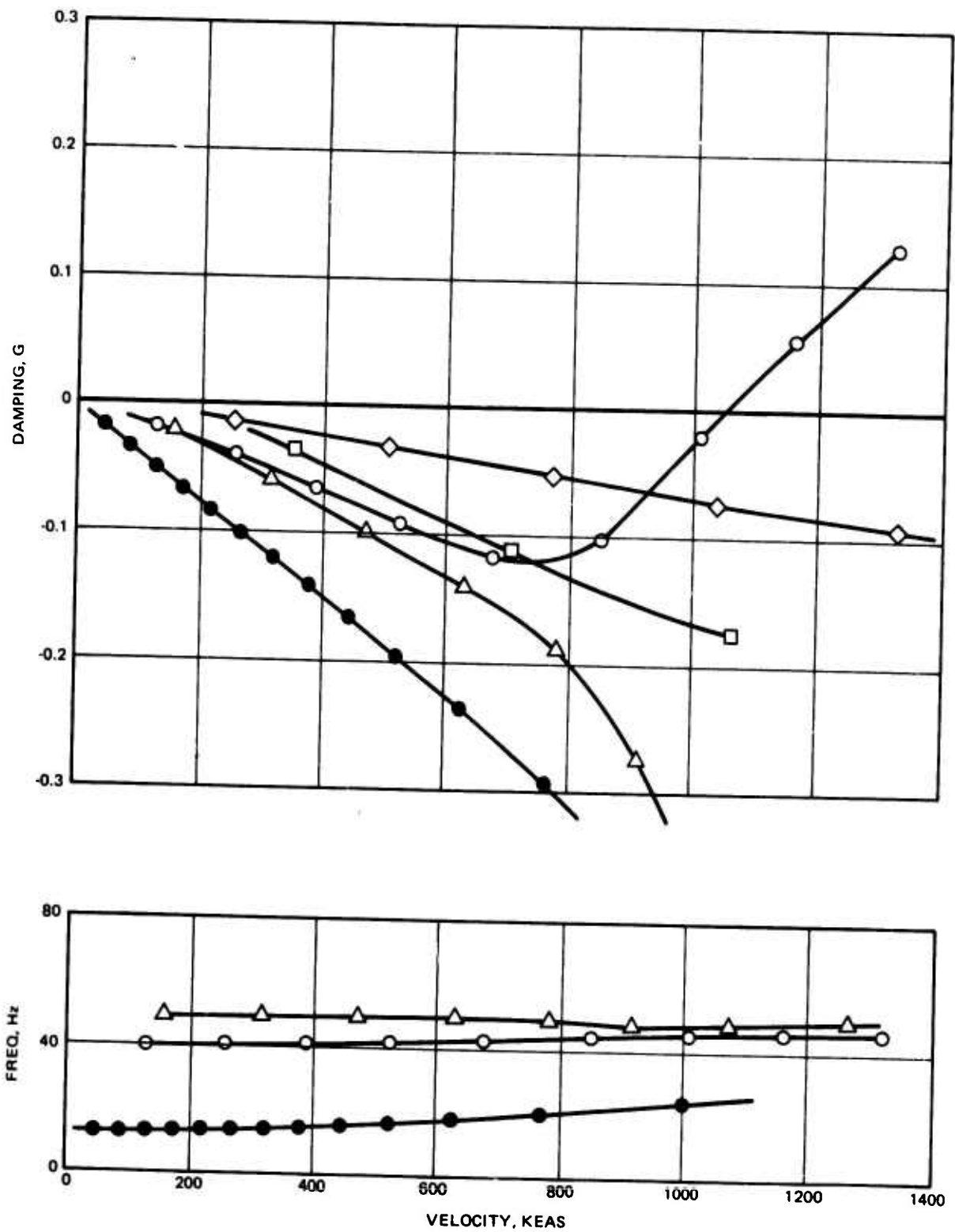


Figure 233. Final Canard V-g Plot, $K(\text{Act.}) = 20 \times 10^6 \text{ in.} \cdot \text{lb/rad}$, $M = 1.3$, 11,000 ft

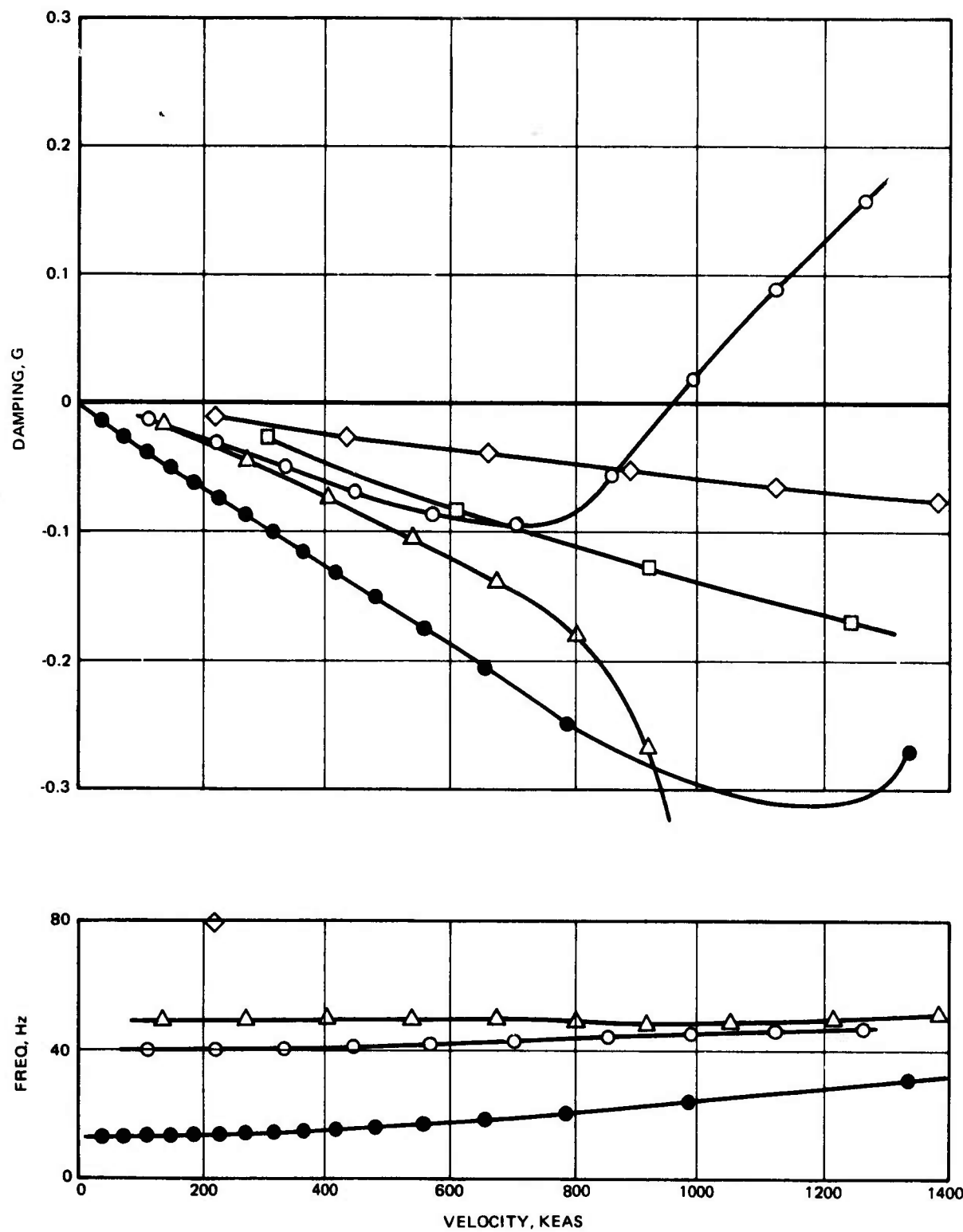


Figure 234. Final Canard V-g Plot, $K(\text{Act.}) = 20 \times 10^6 \text{ in.} \cdot \text{lb/rad}$, $M = 1.3$, 20,000 ft

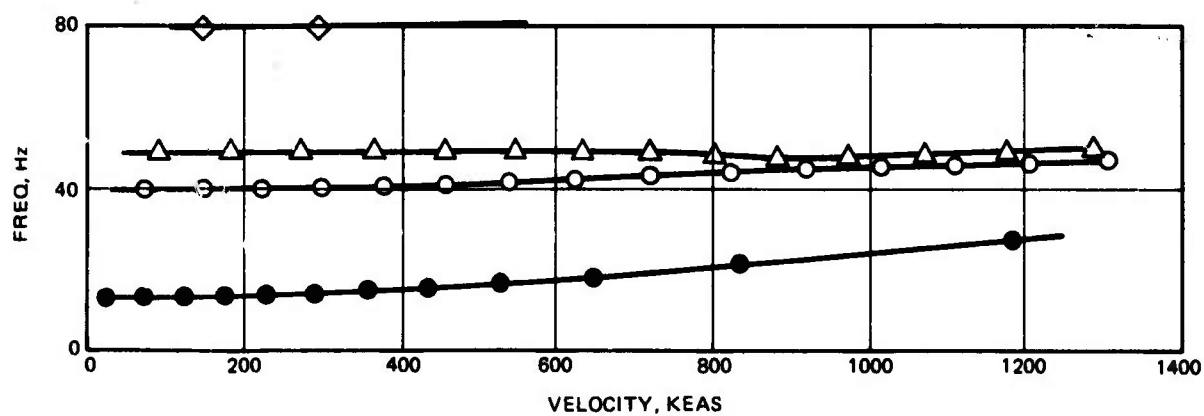
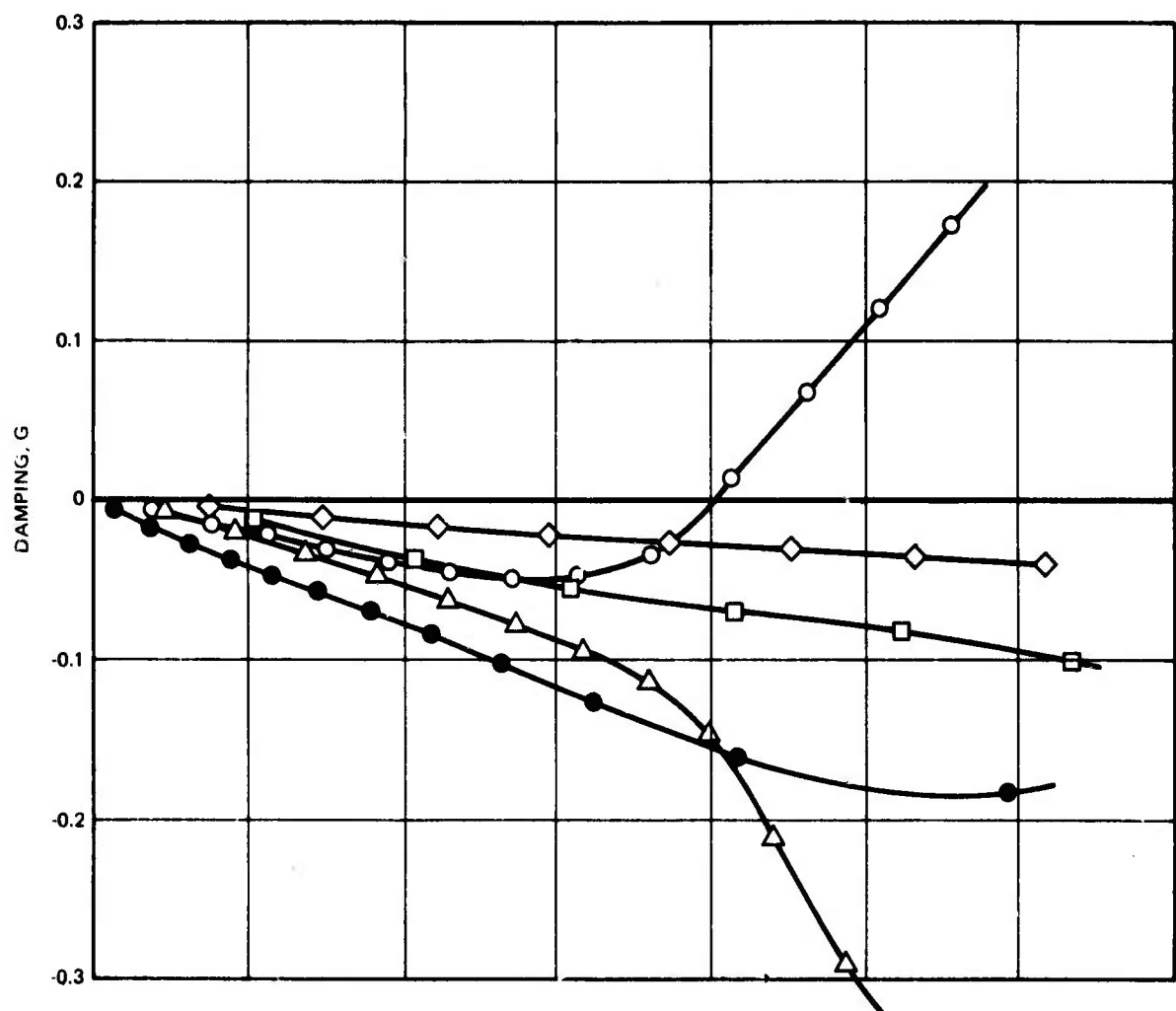


Figure 235. Final Canard V-g Plot, $K(\text{Act.}) = 20 \times 10^6 \text{ In.} \cdot \text{lb/rad}$, $M = 1.3$, 40,000 ft

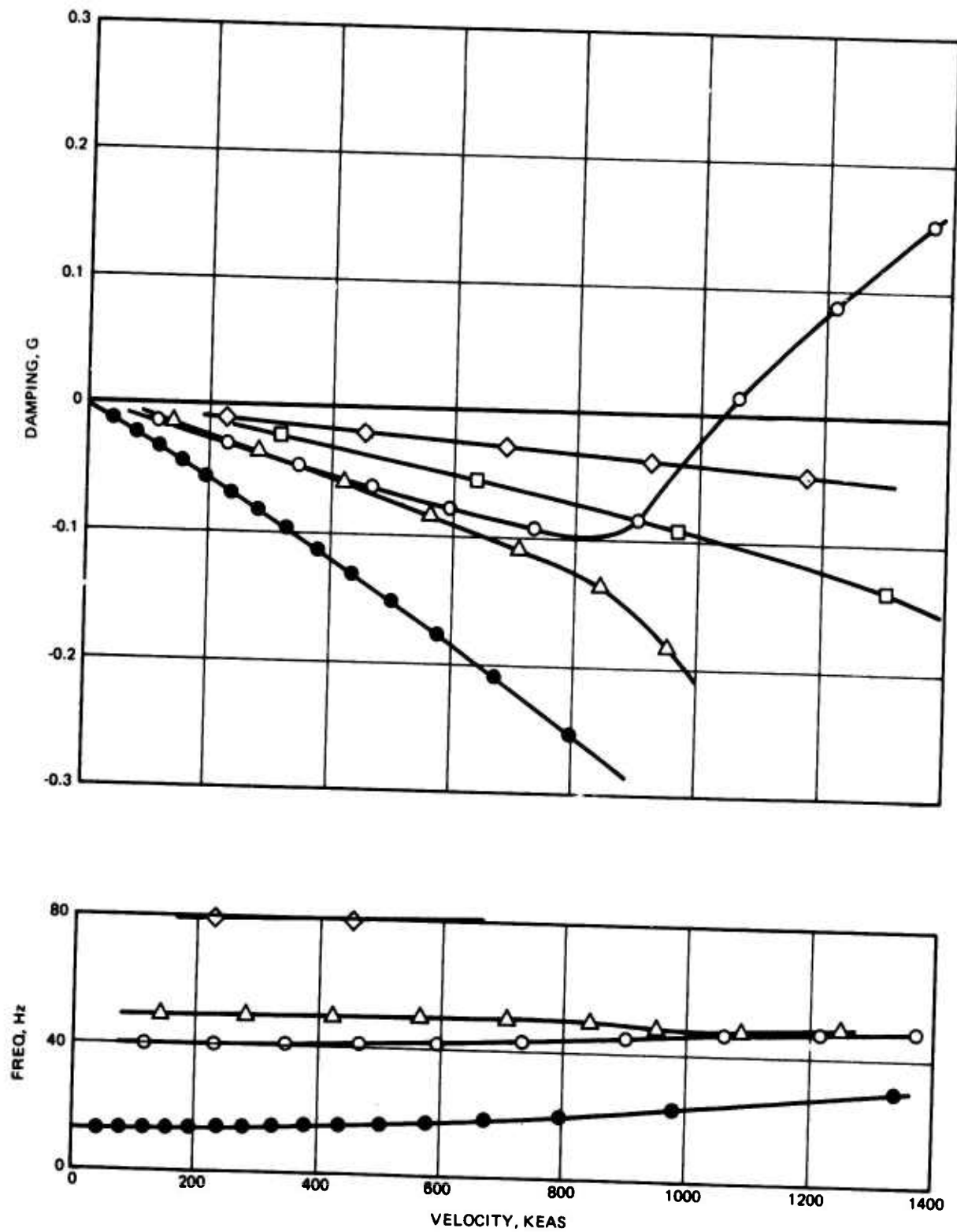


Figure 236. Final Canard V-g Plot, $K(\text{Act.}) = 20 \times 10^6 \text{ in.} \cdot \text{lb/rad}$, $M = 1.5$, 17,750 ft

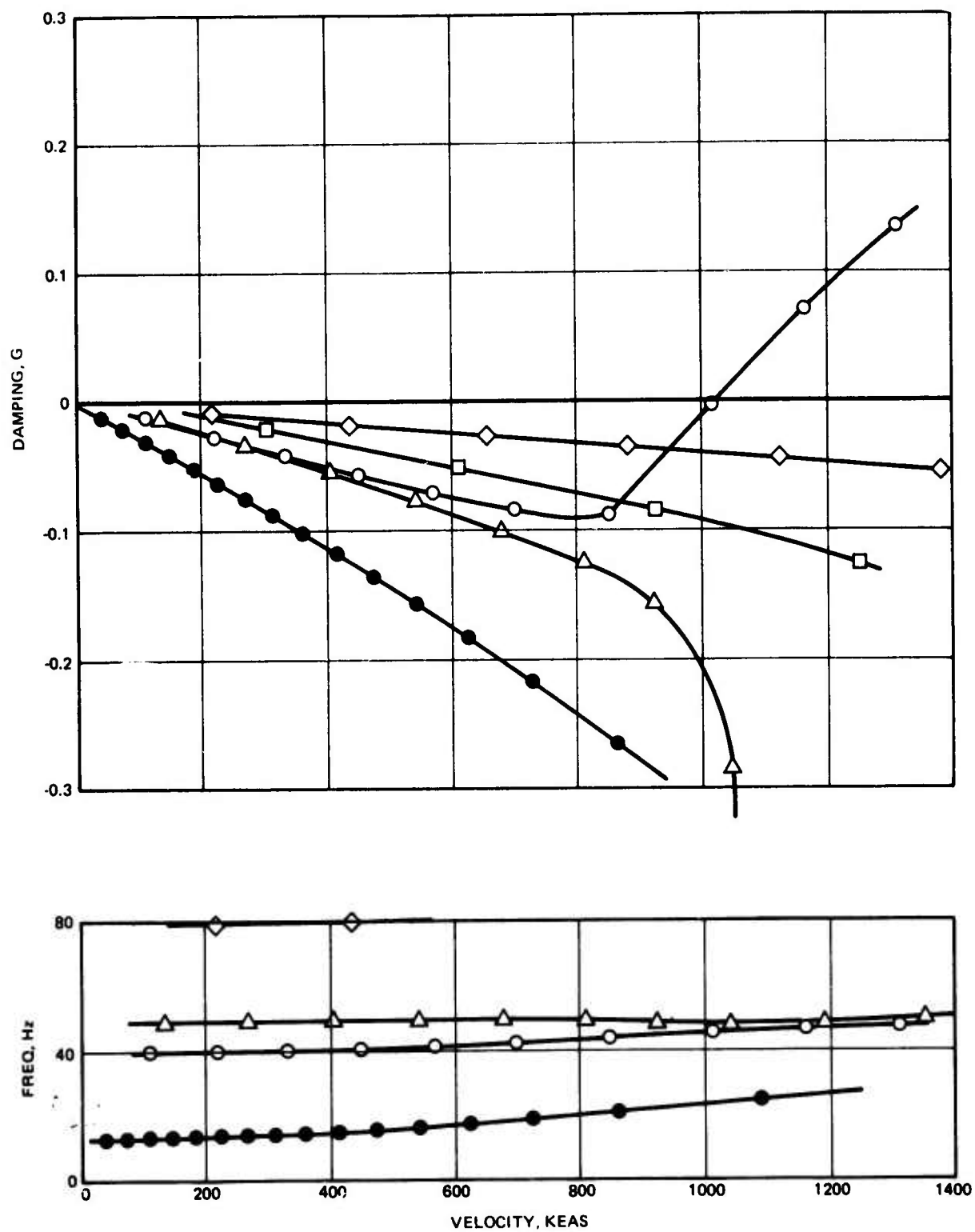


Figure 237. Final Canard V-g Plot, $K(\text{Act.}) = 20 \times 10^6 \text{ in.} \cdot \text{lb/rad}$, $M = 1.5$, 20,000 ft

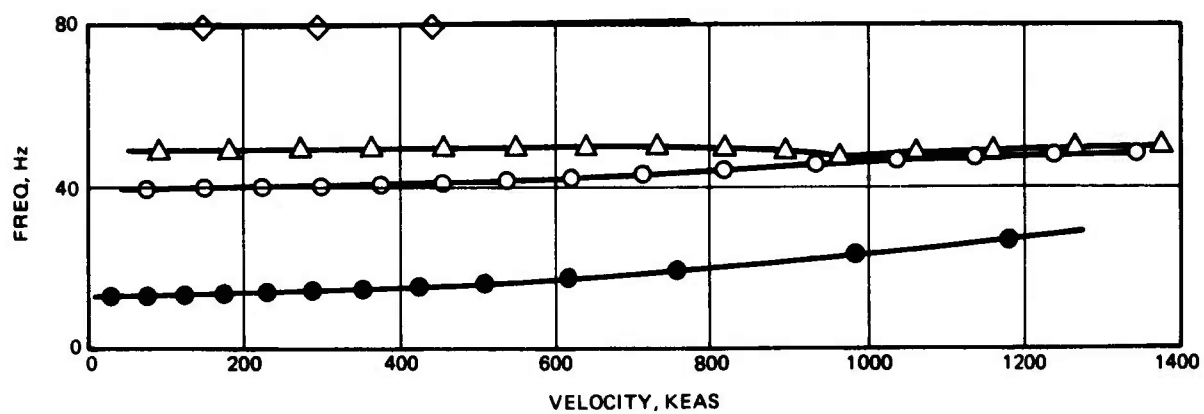
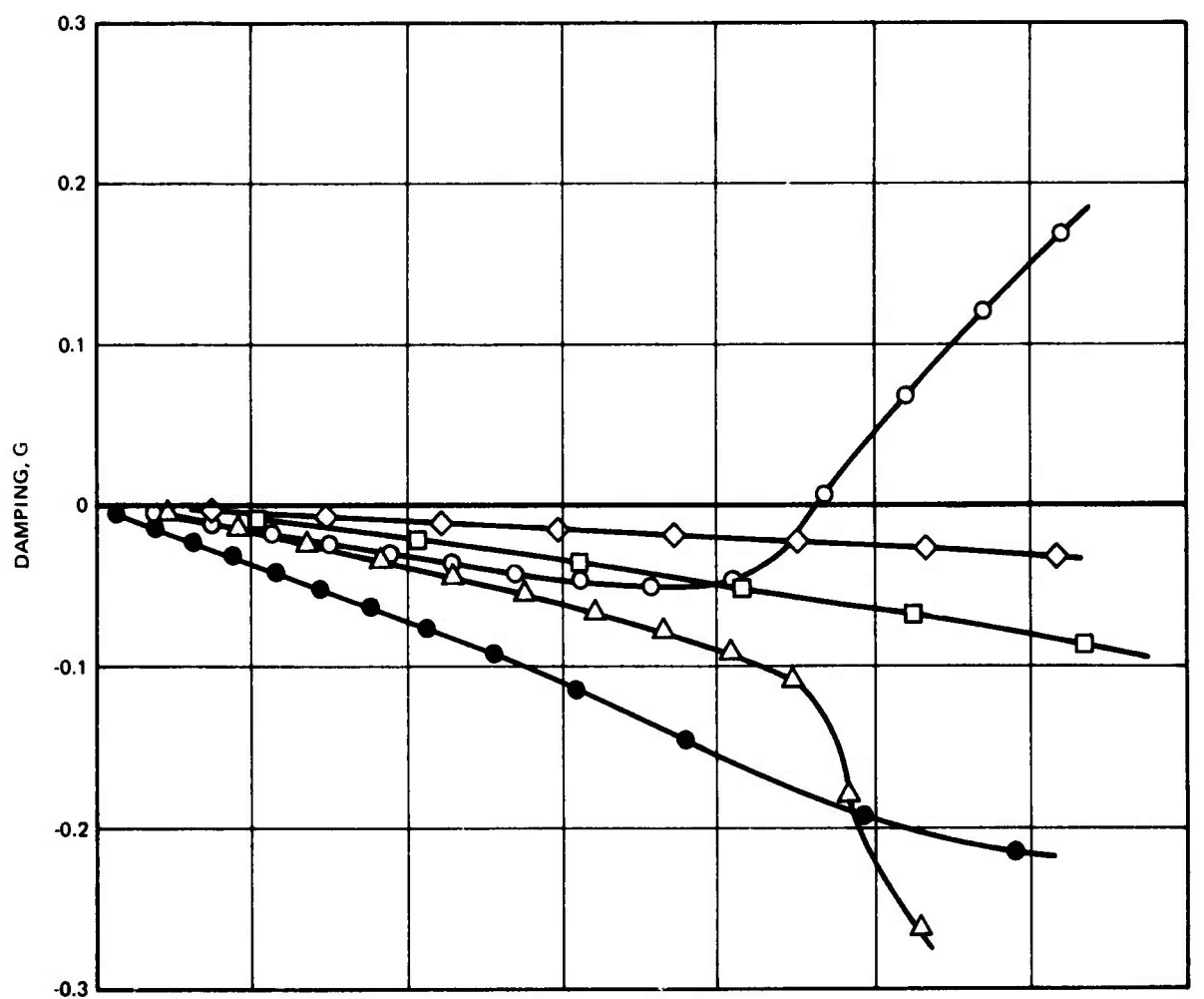


Figure 238. Final Canard V-g Plot, $K(\text{Act.}) = 20 \times 10^6 \text{ in.} \cdot \text{lb/rad}$, $M = 1.5$, 40,000 ft

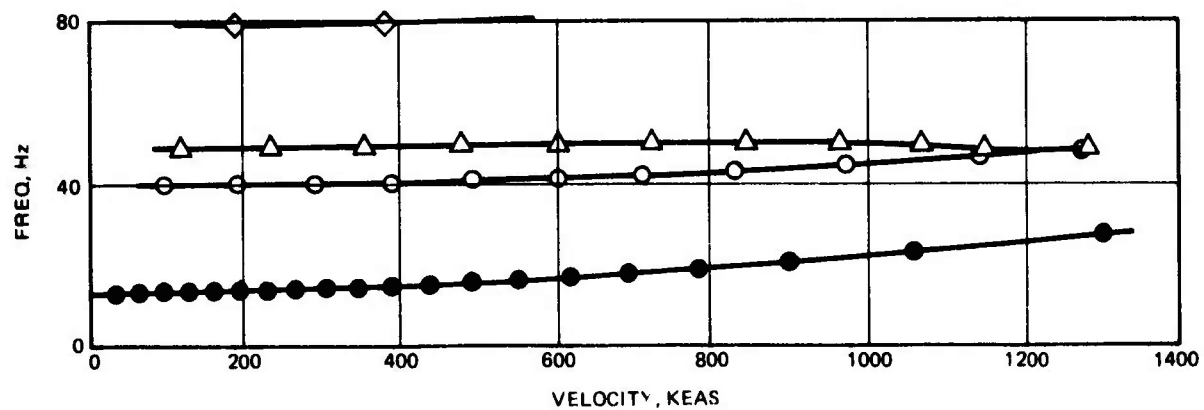
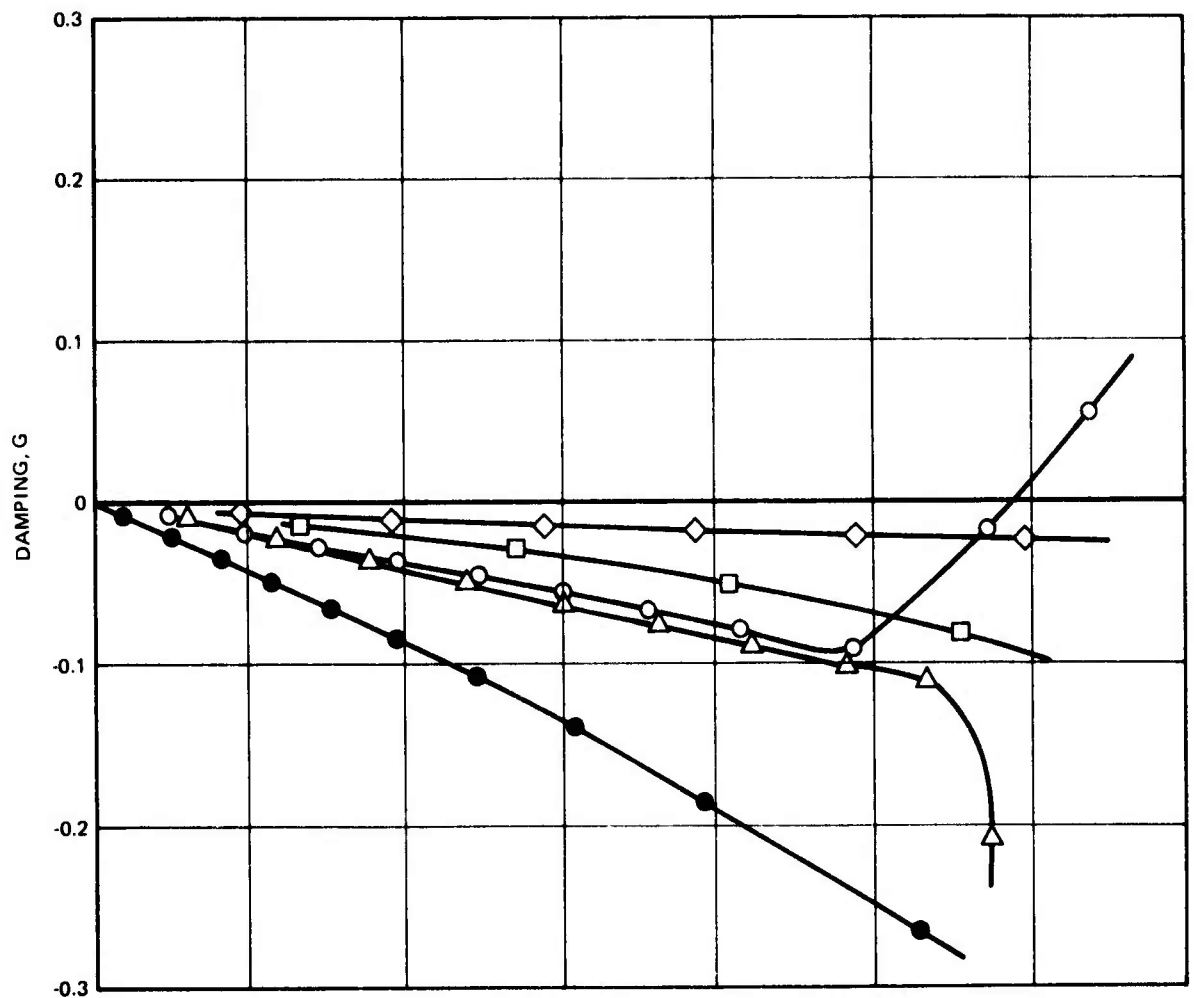


Figure 239. Final Canard V-g Plot, $K(\text{Act.}) = 20 \times 10 \text{ M} = 1.8$, 27,200 ft

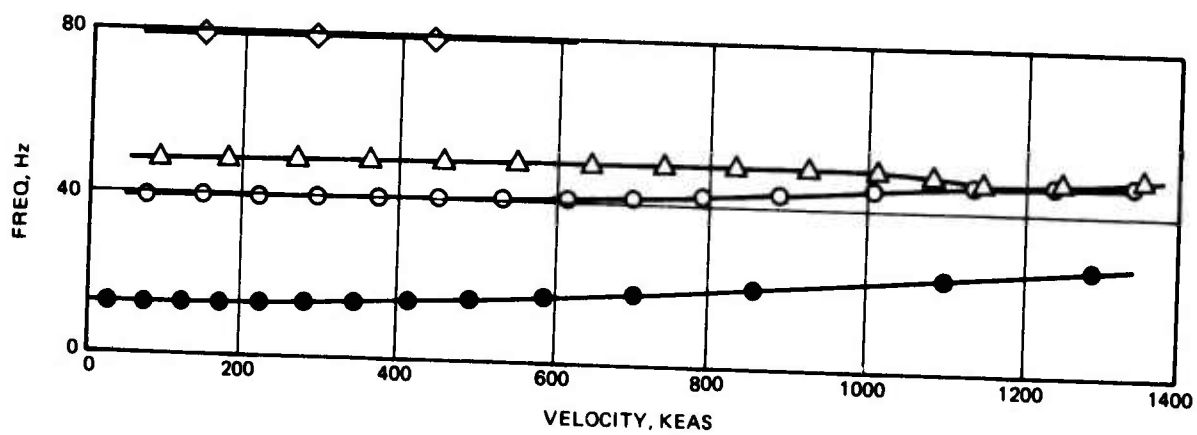
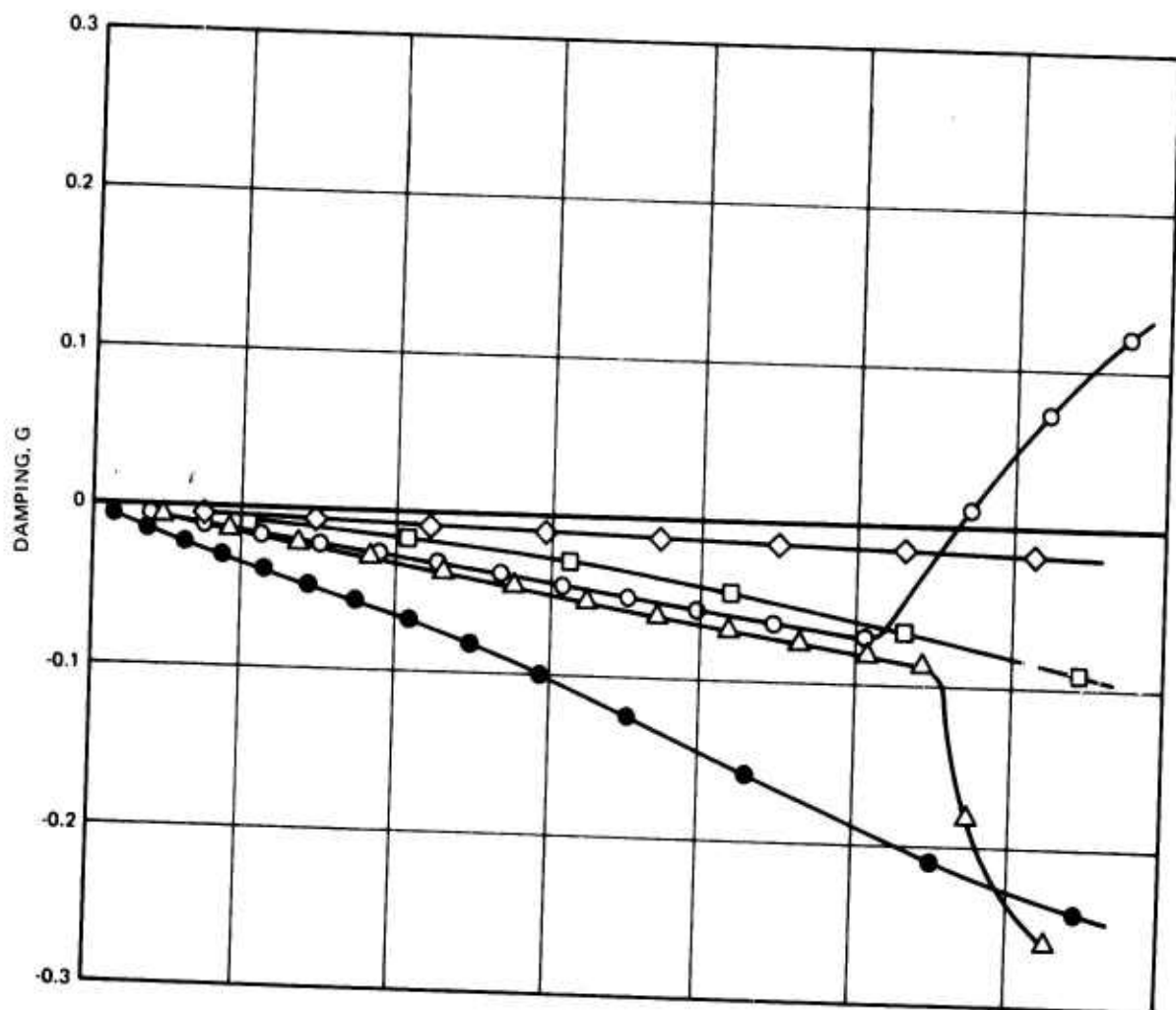


Figure 240. Final Canard V-g Plot, $K(\text{Act.}) = 20 \times 10^6 \text{ in.} \cdot \text{lb/rad}$, $M = 1.8$, 40,000 ft

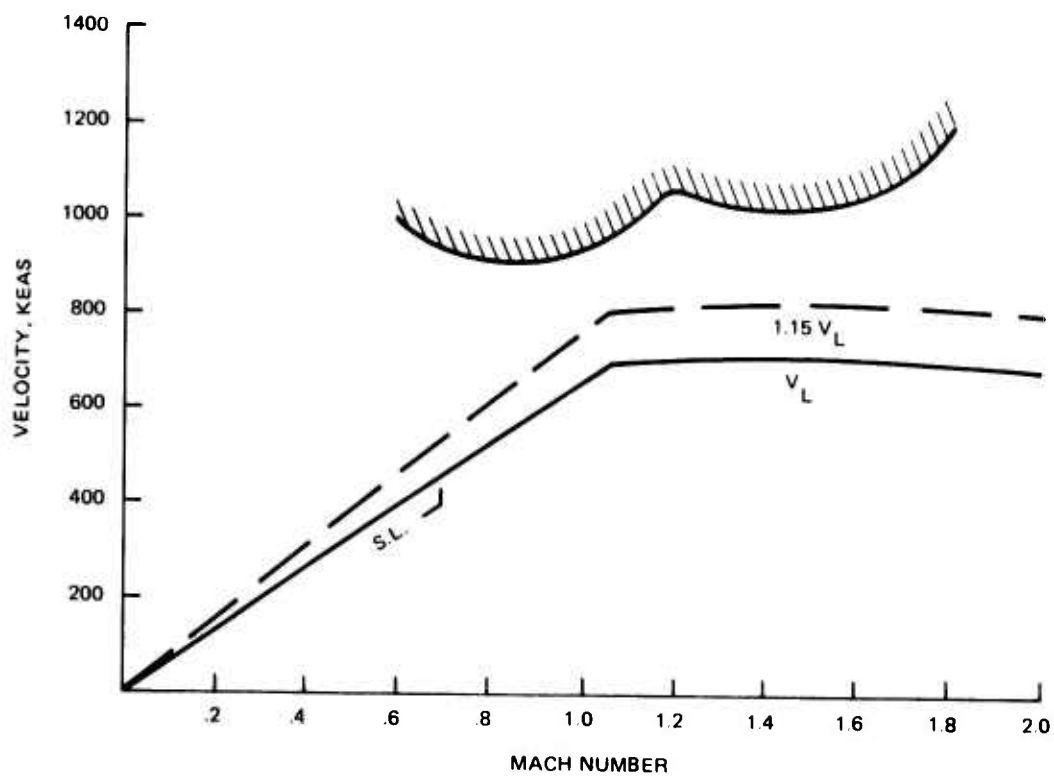


Figure 241. Final Canard V_L Flutter Envelope, Sea Level

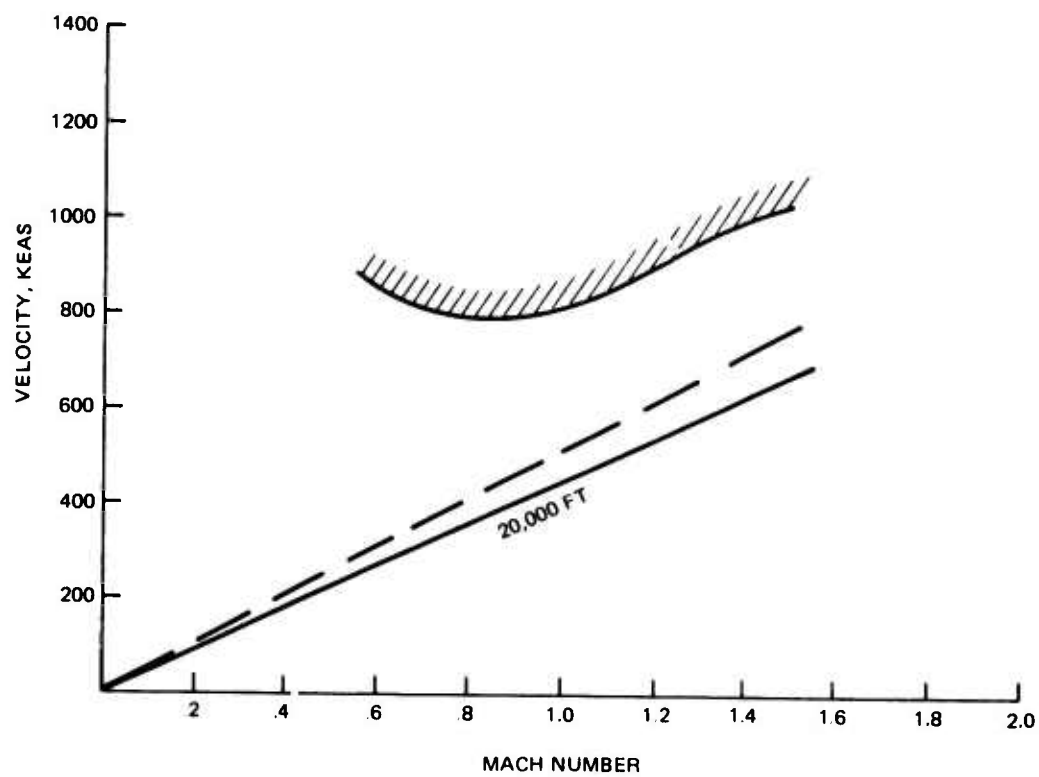


Figure 242. Final Canard Flutter Envelope, 20,000 Ft

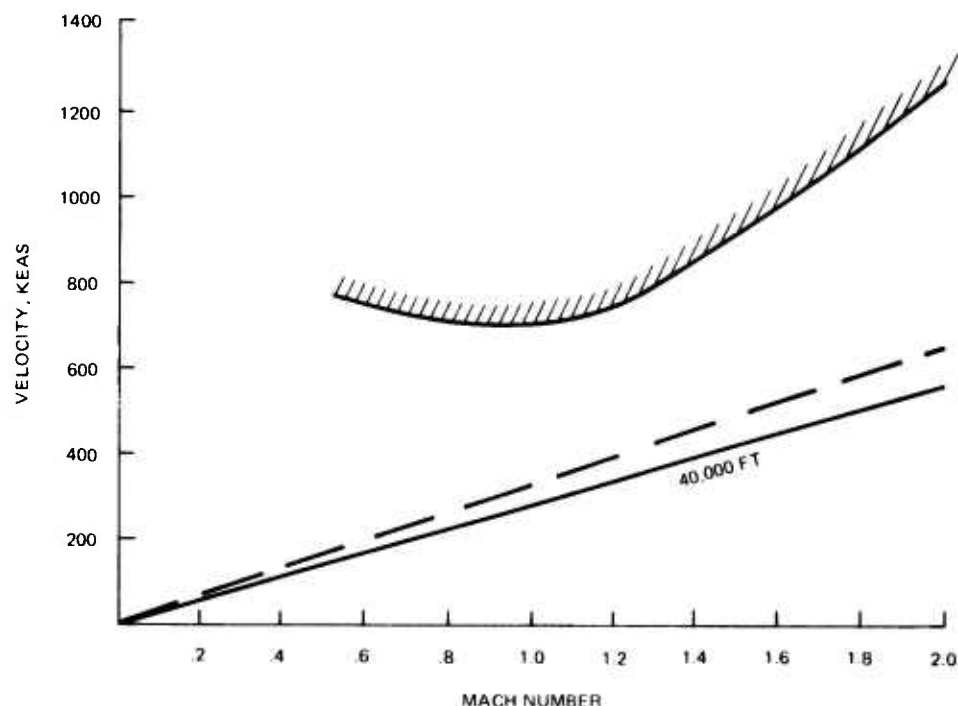


Figure 243. Final Canard Flutter Envelope, 40,000 Ft

5.6 VERTICAL FIN STRUCTURAL ARRANGEMENT AND DETAIL DESIGN

5.6.1 Vertical Fin Structural Arrangement

The vertical fin is a symmetrical, fixed stabilizing surface from which the moveable rudder control surface is mounted. It is approximately 105 inches in span, 130 inches in width, at the fuselage intersection, and has a maximum depth of 7.4 inches at the root. The main structural box, which lies between the 30 and 69% chord lines, is comprised of skins, full depth honeycomb core, three spars (front, mid-main and aft closure), two root ribs, a tip rib and three intermediate stub ribs located at the rudder hinge points. The primary attachment to the fuselage is accomplished between FS 741 and 759 with a horizontal shear only connection made at FS 704.

5.6.2 Detail Structural Design Concept

The ADCA vertical fin structural design concept is shown in Figures 244 and 245. The fin structure, including the leading edge and rudder is fabricated entirely with advanced composite materials. The design shown utilizes Gr/Ep skins bonded to and stabilized by

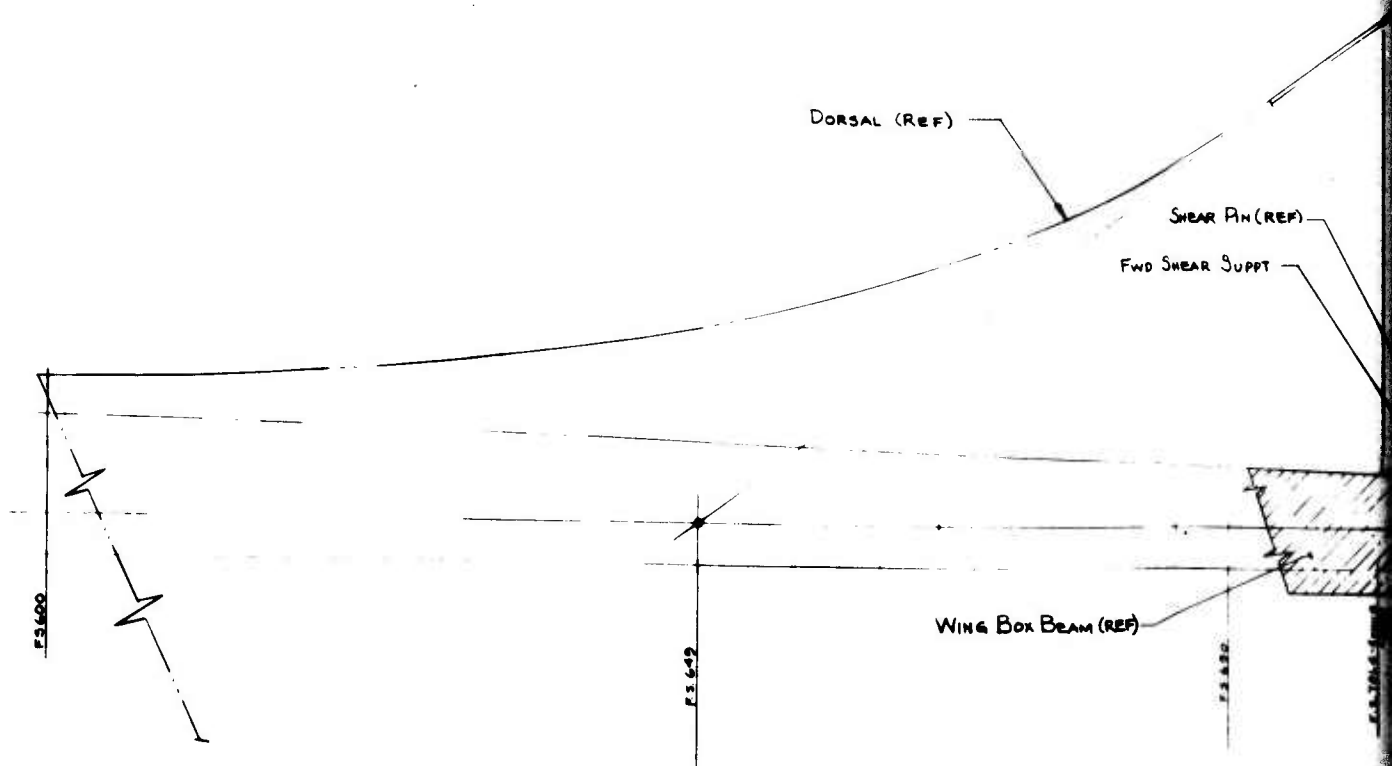
full depth IIRP honeycomb core. In the vicinity of the root attachment area the skin becomes a B/Gr/Ep hybrid in order to improve the material net stress allowables in the presence of high passing and bolt loads. Graphite epoxy spars (front, mid-main and aft closure) are located along the 30, 60 and 69% chord lines, respectively. All three spars are currently configured as channel sections and are bonded within the fin honeycomb assembly. Two Gr/Ep ribs are provided at the root of the fin for primary load redistribution. Both parts are channel sections, with the upper rib being bonded in place and the lower mechanically attached to the skins. An additional three Gr/Ep 'I' section riblets are utilized at each of the three rudder hinge support points. These ribs are bonded to the core and skins and provide redistribution capability for the concentrated load input.

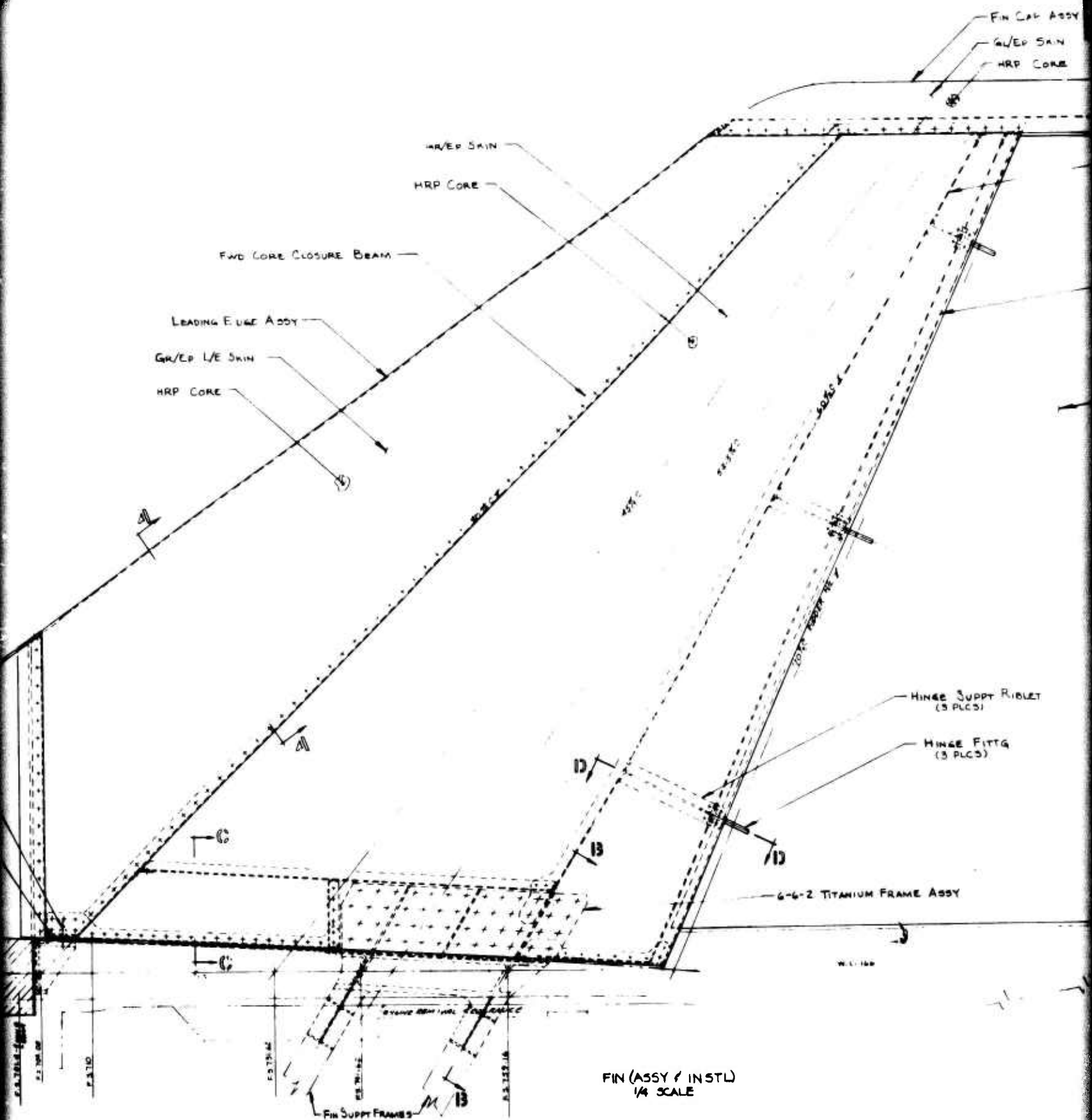
5.6.3 Fin Vibration and Flutter Considerations

The concept of aeroelastic tailoring through the use of advanced composite technology was beneficially exercised on the ADCA vertical fin. It has been demonstrated that tailoring towards decreased washout is beneficial for flutter. The extreme of such a design directive is a divergent, rather than flutter critical surface. Those benefits to be gained by tailoring for controlled twist to increase performance or reduce drag are minimal in the case of the fin. Thus, the objective of increasing flutter speed through tailoring was pursued.

The methods of reducing washout have been discussed previously. They include unbalancing the $\pm 45^\circ$ plies, rotating the laminate and rotating only the 0° layers through a small angle β . In the last method, rotating the 0° plies, the direct torsional stiffness remains virtually unaffected. Further, it has been shown that for β angles less than 15° the change in bending strength is negligible. It was this technique, therefore, that was selected for use in the ADCA vertical fin design.

The first cycle fin was sized to meet strength and stiffness requirements using the COMBO program. The number of layers in each direction and material, thus dictated, was kept constant and the angle of the 0° layers to the main beam axis, β , was parametrically increased. The 0° plies were rotated aft through 0, 5, 10 and 15° . Slab fin (i.e., no rudder degree of freedom) vibration and flutter analyses were completed for each of these cases. The results of these analyses are summarized in Table 46 where a 25% increase in flutter speed is demonstrated for the $\beta = 15^\circ$ case.





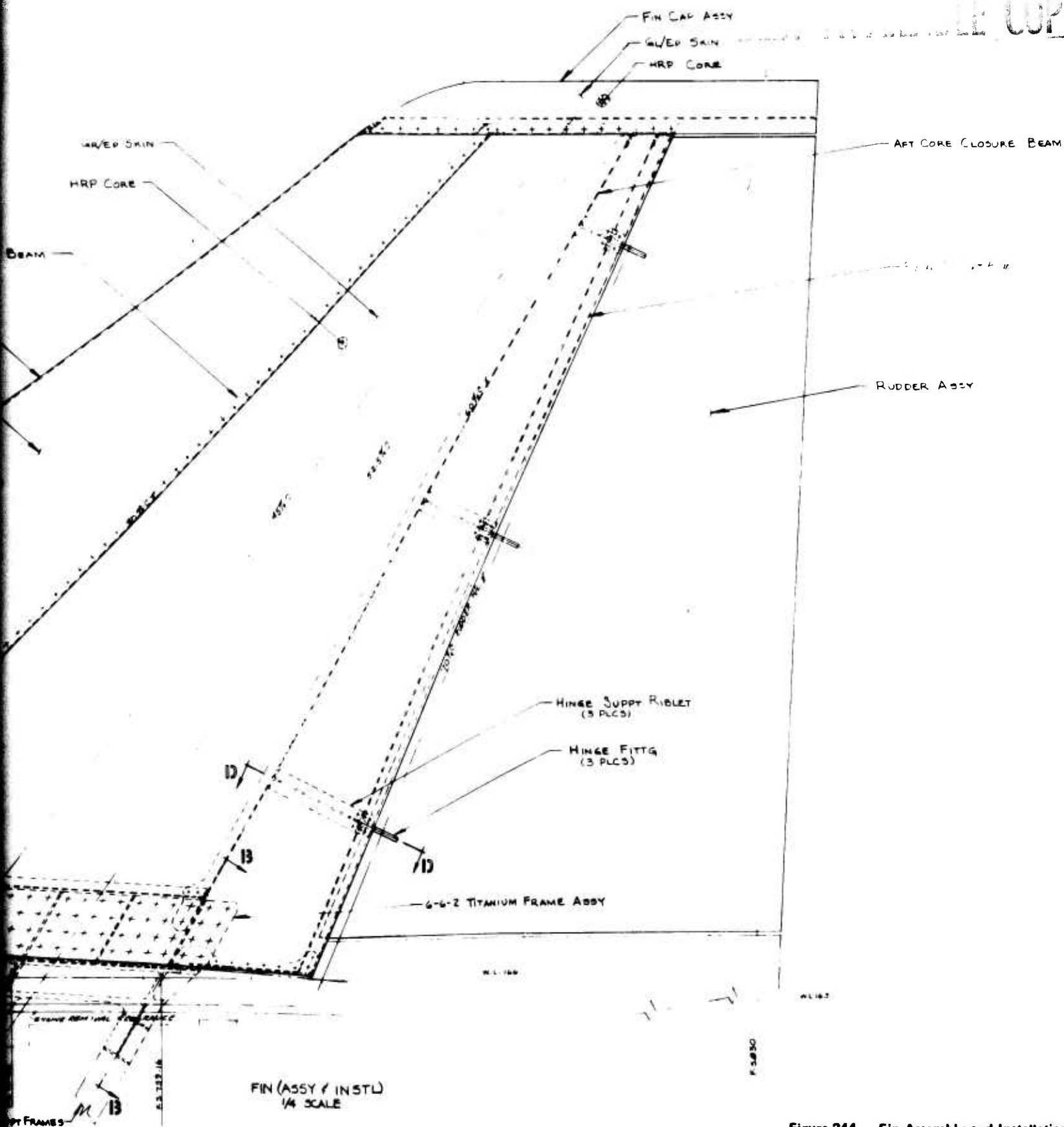
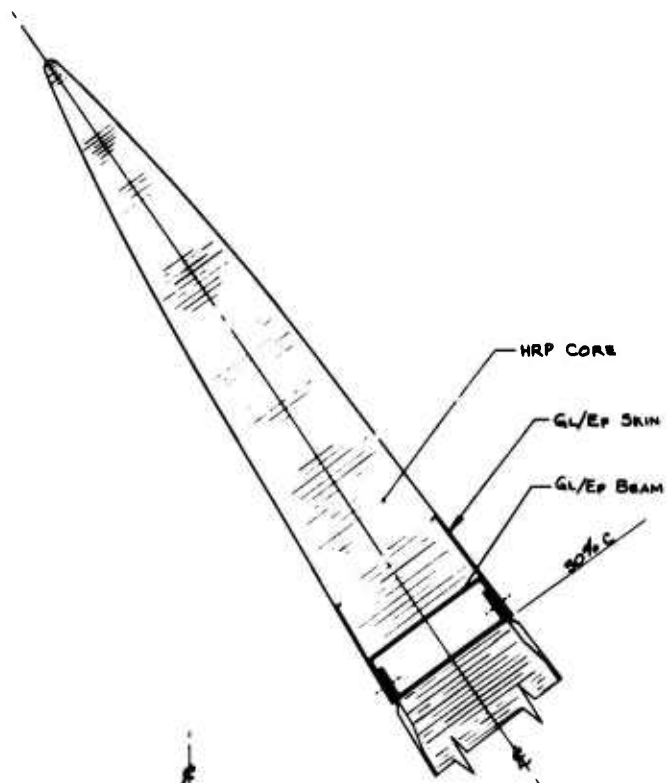
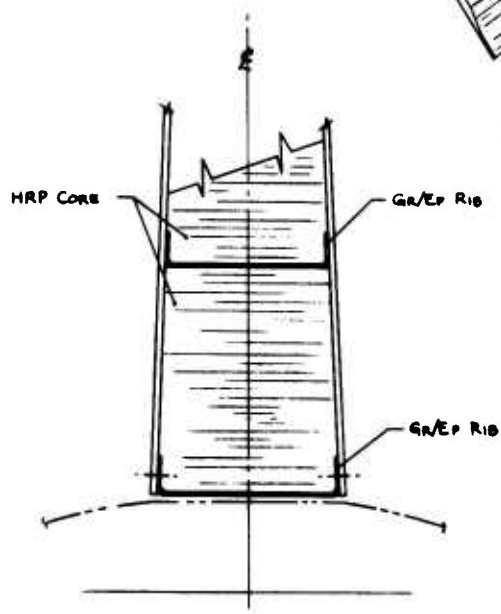


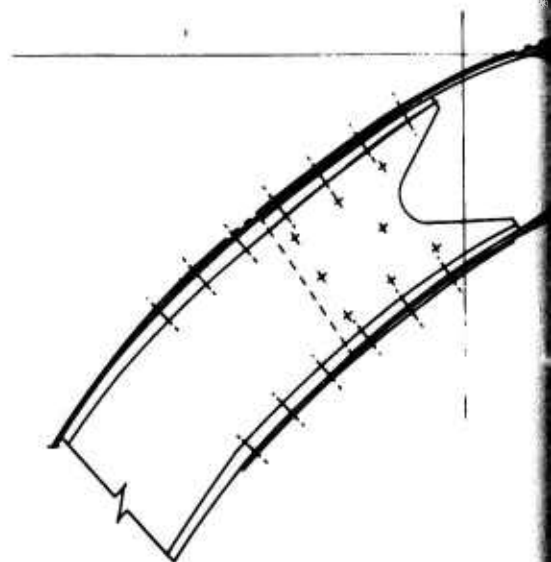
Figure 244.. Fin Assembly and Installation



SECT. A-A
HALF SCALE



SECT. C-C



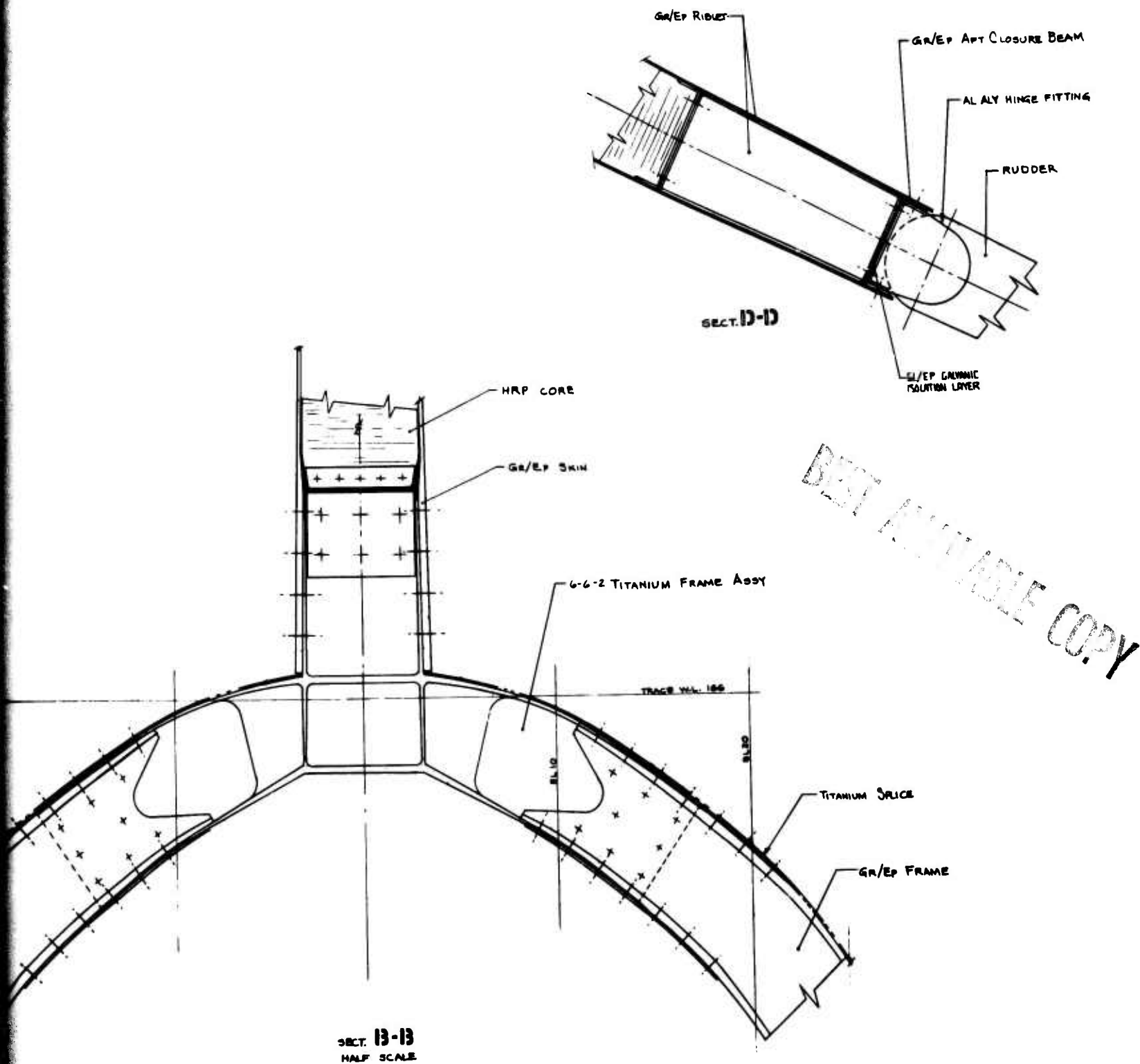


Figure 245. Fin Assembly and Installation

TABLE 46. PRELIMINARY ADCA FIN VIBRATION AND FLUTTER SPEED COMPARISON

β	Frequencies, Hz			V_f @ $M = 0.8, SL$	$V_f / V_{f\beta=0}$
	1st Bending	Torsion	2nd Bending		
0	14.35	33.20	44.01	740	1.0
5	14.32	33.08	44.21	759	1.03
10	13.98	33.26	43.64	785	1.06
15	13.33	33.75	42.12	926	1.25

It should be mentioned that in all cases, the flutter mechanism is a second bending - torsion coupling.

As the fin structural design was iterated, the findings from these preliminary studies were incorporated and the final fin design was checked for $\beta = 0^\circ$ and $\beta = 15^\circ$ only. The fin dynamic idealization is shown in Figure 246 where the panels and rotational degrees of freedom are taken perpendicular to the beam axis. The beam influence coefficients for the final fin design, $\beta = 15^\circ$, are given in Table 47. For comparative purposes the influence coefficients for $\beta = 0^\circ$ are also included. The sign convention is, bending and load are positive right, torque and rotation are positive nose left.

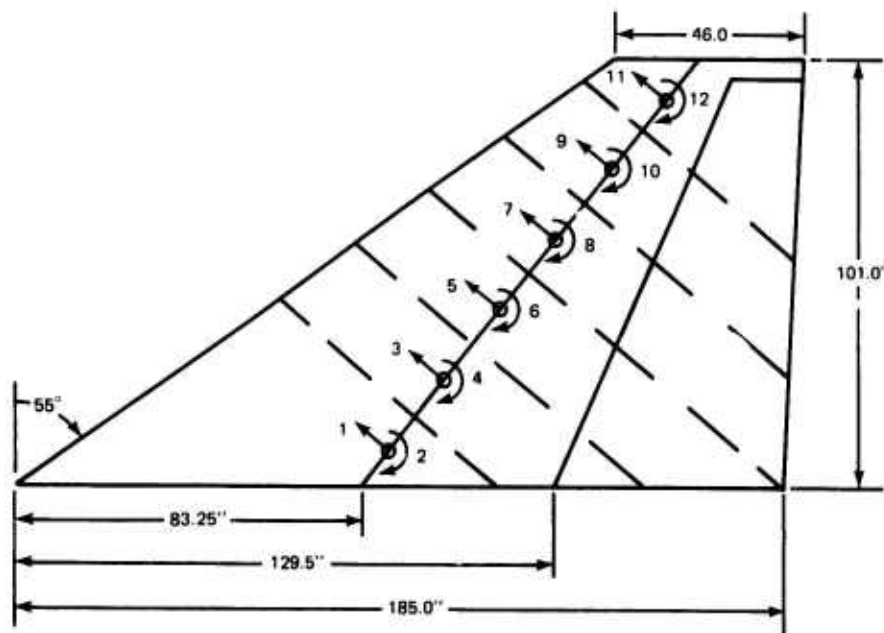


Figure 246. Fin-Rudder Dynamic Idealization

TABLE 47. ADCA VERTICAL TAIL BEAM MODEL INFLUENCE COEFFICIENTS*

 $\beta = 15^\circ$

	1	2	3	4	5	6	7	8	9	10	11	12
1	0.29270	-0.01410	1.1708	-0.01410	2.0489	-0.01410	2.9270	-0.01410	3.8051	-0.01410	4.6832	-0.01410
2	-0.01410	0.00732	0.07050	0.00732	-0.12689	0.00732	-0.18329	0.00732	-0.23968	0.00732	0.29608	0.00732
3	1.1708	-0.07050	8.1603	-0.13897	16.835	-0.13897	25.511	-0.13897	34.186	-0.13897	42.861	-0.13897
4	-0.01410	0.00732	-0.13897	0.02807	-0.35645	0.02807	-0.57394	0.02807	-0.79142	0.02807	-1.0089	0.02807
5	2.0489	-0.12689	16.835	-0.35645	44.121	-0.47944	74.775	-0.47944	105.43	-0.47944	136.08	-0.47944
6	-0.01410	0.00732	-0.13897	0.02807	-0.47944	0.06533	-0.97950	0.06533	-1.4796	0.06533	-1.9796	0.06533
7	2.9270	-0.18329	25.511	-0.57397	74.775	-0.97950	150.26	-1.2072	234.16	-1.2072	318.06	-1.2072
8	-0.01410	0.00732	-0.13897	0.02807	-0.47944	0.06533	-1.2072	0.14357	-2.2623	0.14357	-3.3173	0.14357
9	3.8051	-0.23968	34.186	-0.79142	105.43	-1.4796	234.16	-2.2623	433.22	-2.7390	657.12	-2.7390
10	-0.01410	0.00732	-0.13897	0.02807	-0.47944	0.06533	-1.2072	0.14357	-2.7390	0.32608	-4.9470	0.32608
11	4.6832	-0.29608	42.861	-1.0089	136.08	-1.9796	318.06	-3.3173	657.12	-4.9470	1218.7	-5.7616
12	-0.01410	0.00732	-0.13897	0.02807	-0.47944	0.06533	-1.2072	0.14357	-2.7390	0.32608	-5.7616	0.73754

 $\beta = 0^\circ$

	1	2	3	4	5	6	7	8	9	10	11	12
1	0.21813	0	0.87252	0	1.5269	0	2.1813	0	2.8357	0	3.4901	0
2	0	0.00794	0	0.00794	0	0.00794	0	0.00794	0	0.00794	0	0.00794
3	0.87252	0	6.0794	0	12.539	0	18.998	0	25.457	0	31.916	0
4	0	0.00794	0	0.03041	0	0.03041	0	0.03041	0	0.03041	0	0.03041
5	1.5269	0	12.539	0	32.856	0	55.732	0	78.609	0	101.48	0
6	0	0.00794	0	0.03041	0	0.07046	0	0.07046	0	0.07046	0	0.07046
7	2.1813	0	18.998	0	55.732	0	112.66	0	176.26	0	239.86	0
8	0	0.00794	0	0.03041	0	0.07046	0	0.15358	0	0.15358	0	0.15358
9	2.8357	0	25.457	0	78.609	0	176.26	0	330.57	0	505.60	0
10	0	0.00794	0	0.03041	0	0.07046	0	0.15358	0	0.34503	0	0.34503
11	3.4901	0	31.916	0	101.48	0	239.86	0	505.60	0	961.57	0
12	0	0.00794	0	0.03041	0	0.07046	0	0.15358	0	0.34503	0	0.76731

*See Figure 246 for Coordinate Definition
Units - IN./LB, RAD/IN. LB X 10⁻⁶

The distributed mass properties for the slab fin are included in Table 48.

TABLE 48. ADCA SLAB FIN MASS PROPERTIES

Panel	Weight, lb	Arm,* in.	Unbalance, lb-in.	I_{zzcg2} lb-in.	I_{zzEA2} lb-in.
1	82.8	-21.4	-1771.9	33557.	71476.
2	60.7	2.0	121.4	29134.	29377.
3	63.5	11.1	705.0	37374.	45198.
4	56.7	13.9	788.1	30496.	41451.
5	45.5	10.9	496.0	15210.	20616.
6	34.8	10.3	358.4	5386.	9078.
Total Weight	344.0				

*Perpendicular distance from panel cg to beam axis. Positive indicates an aft cg.

Vibration analyses were completed for both the $\beta = 0^\circ$ and $\beta = 15^\circ$ cases. A frequency comparison is shown in Table 49.

TABLE 49. ADCA SLAB FIN FREQUENCY COMPARISON

Mode	$\beta = 15^\circ$	$\beta = 0^\circ$
1st Bending	12.47	13.04
Torsion	29.08	29.21
2nd Bending	40.62	40.72

The accompanying mode shapes are shown in Figure 247 for the $\beta = 15^\circ$ case and Figure 248 for the $\beta = 0^\circ$ case. Of particular note, here, is the difference in the amount of rotation in the first bending mode. Since the twist is small, it is difficult to perceive its change with β . Table 50 gives a comparison of the calculated twist perpendicular to the beam axis in the first bending mode. In both cases the mode is normalized to a tip deflection of +1.

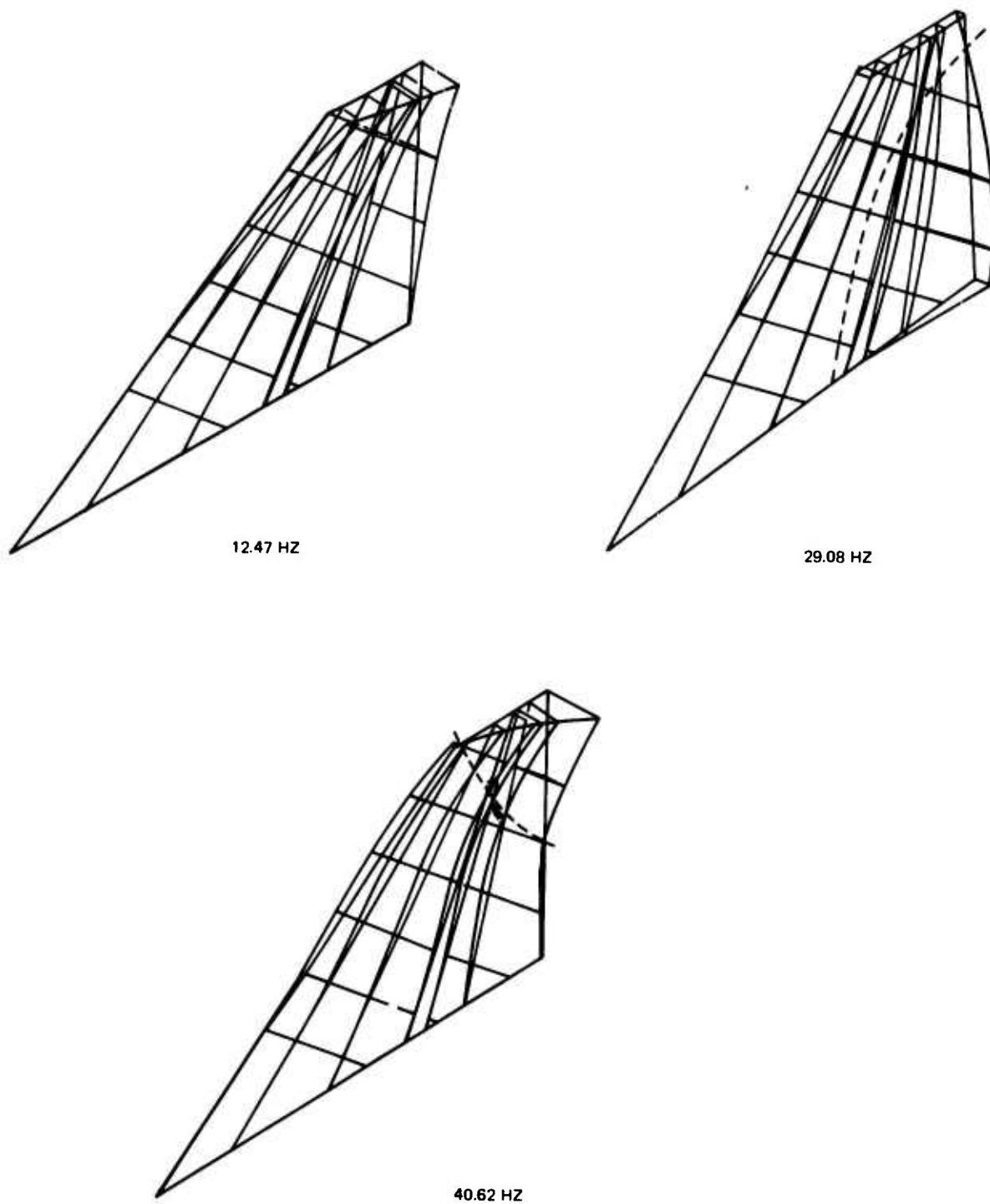
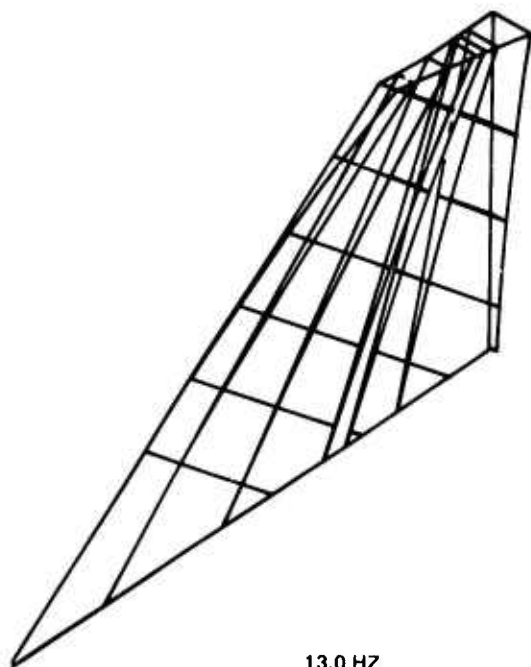
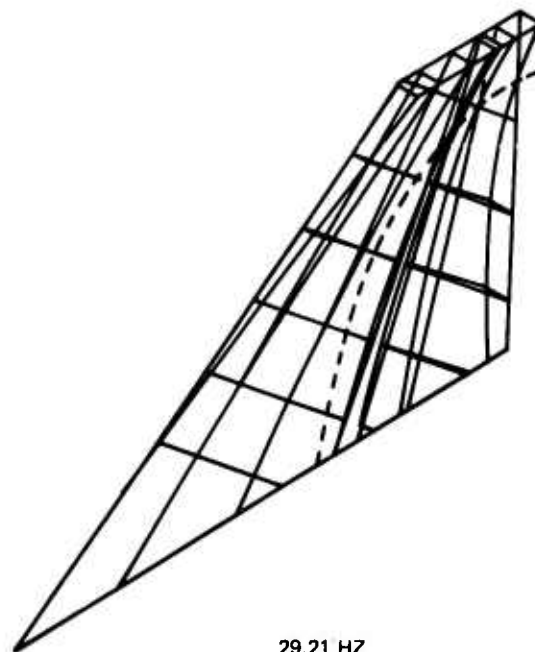


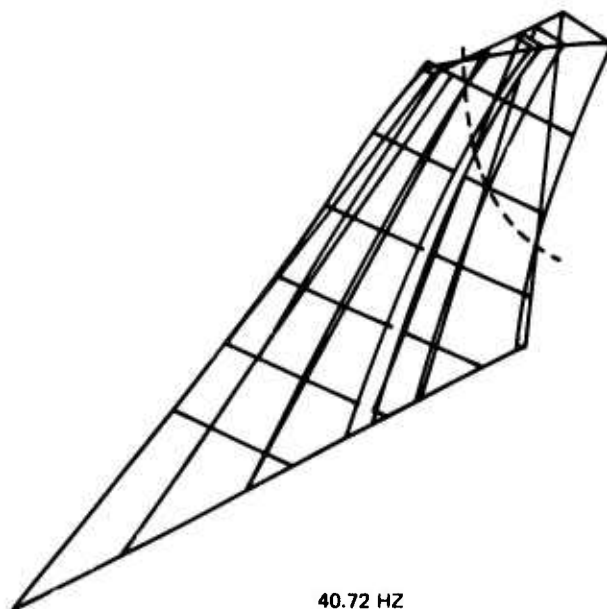
Figure 247. ADCA Fin Mode Shapes, $\beta = 15^\circ$, Slab



13.0 HZ



29.21 HZ



40.72 HZ

Figure 248. ADCA Fin Mode Shapes, $\beta = 0^\circ$, Slab

TABLE 50. ADCA SLAB FIN VIBRATION COMPARISON OF ROTATION IN FIRST BENDING MODE

Panel	$\beta = 15^\circ$	$\beta = 0^\circ$
1	-0.000247	0.000208
2	-0.000717	0.000767
3	-0.001145	0.001758
4	-0.001230	0.003563
5	-0.0004413	0.006447
6	+0.001534	0.009721

The calculated flutter speeds for these two cases are shown in Table 51 for $M = 0.8$ and $M = 1.3$ at sea level.

TABLE 51. ADCA SLAB FIN FLUTTER SPEED COMPARISON

	$M = 0.8$	$M = 1.3$
$\beta = 0^\circ$	771	769
$\beta = 15^\circ$	1050	941
$V_{f \beta = 15^\circ} / V_{f \beta = 0^\circ}$	1.36	1.22

It should be noted that the V_L altitude at $M = 1.3$ is 11,000 ft. Flutter speeds are shown at sea level to provide continuity across the transonic area, only. V - g - ω plots are included in Figures 249 and 250 for the $\beta = 15$ cases and in Figures 251 and 252 for the $\beta = 0$ cases. It can be seen that the torsion mode stiffens to couple with second bending to cause the critical flutter mechanism.

The rudder rotation degree of freedom was introduced using a modal mass-coupling technique. The design criteria were twofold. First, the slab flutter margins should not be degraded. Secondly, buzz criteria based on the fundamental coupled rudder rotation frequency should be met. Effective actuator spring rates from 2.0 to 2.9×10^6 in.-lb/rad were studied. This corresponds to uncoupled rudder rotation frequencies of up to 35 Hz. Because of the proximity to the fin torsion mode the mechanical coupling is strong. The relationship between the uncoupled rudder rotation frequency and the fundamental coupled

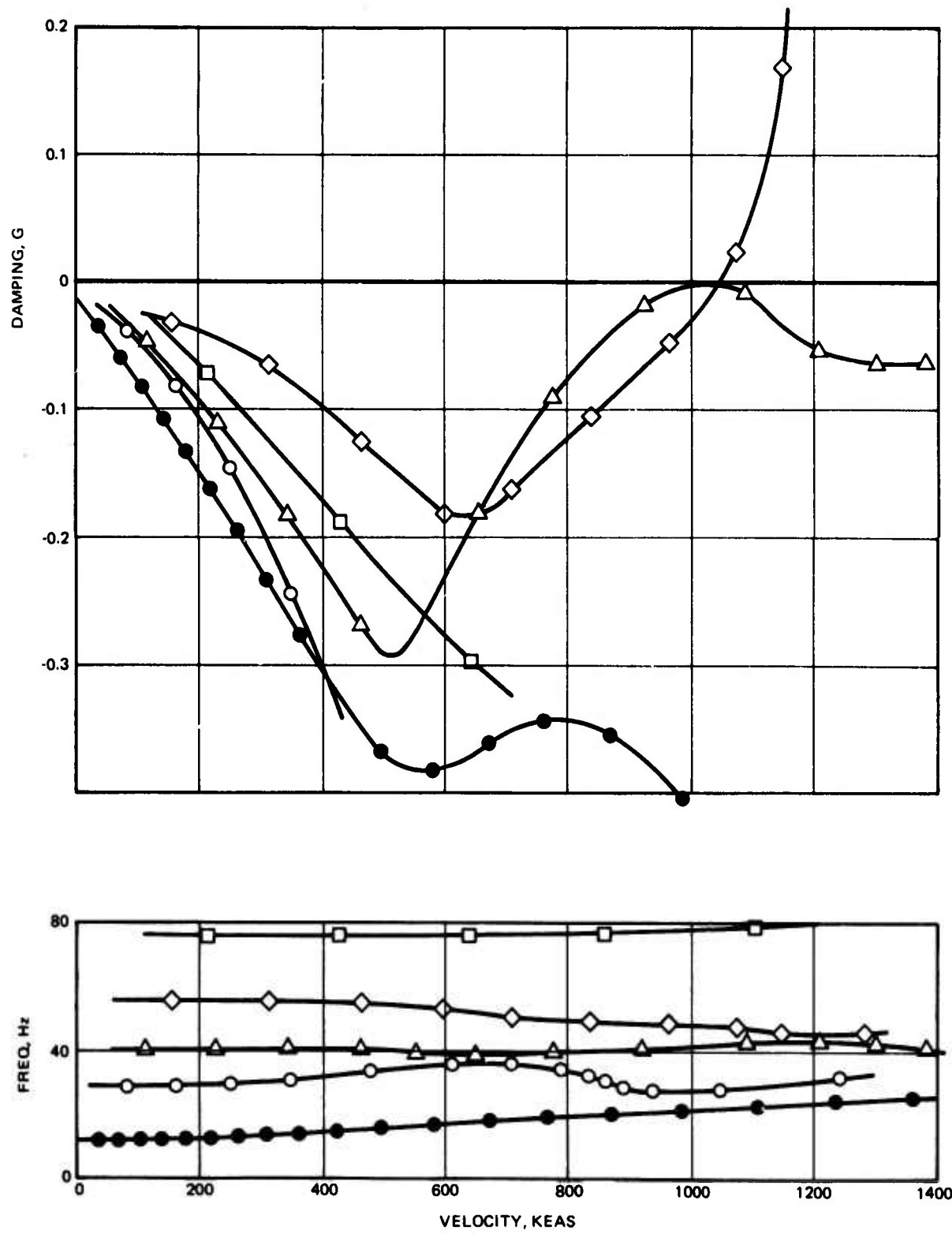


Figure 249. Slab Fin Tailored, $\beta = 15^\circ$, $M = 0.8$, Sea Level

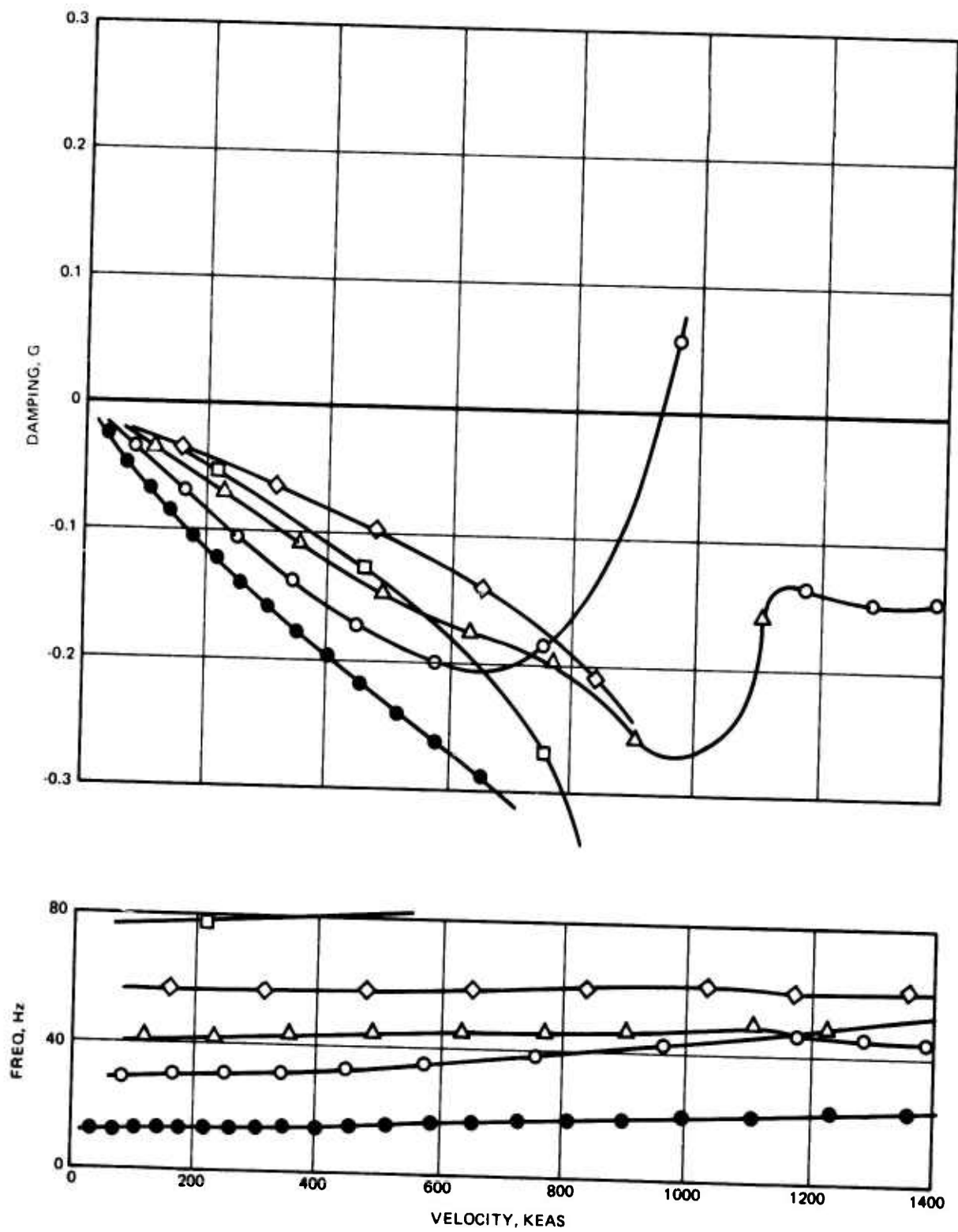


Figure 250. Slab Fin Tailored, $\beta = 15^\circ$, $M = 1.3$, Sea Level

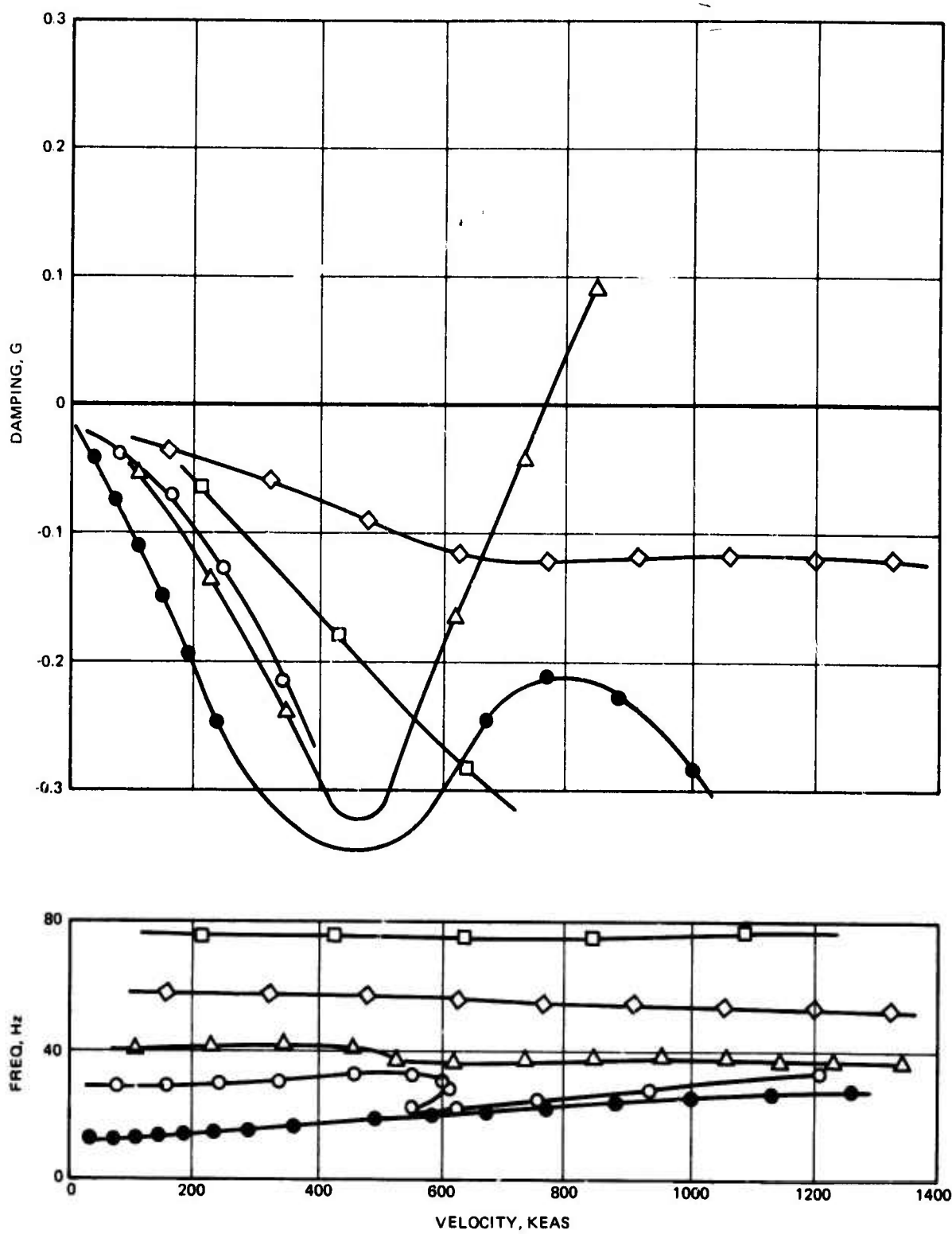


Figure 251. Slab Fin Untailored, $\beta = 0^\circ$, $M = 0.8$, Sea Level

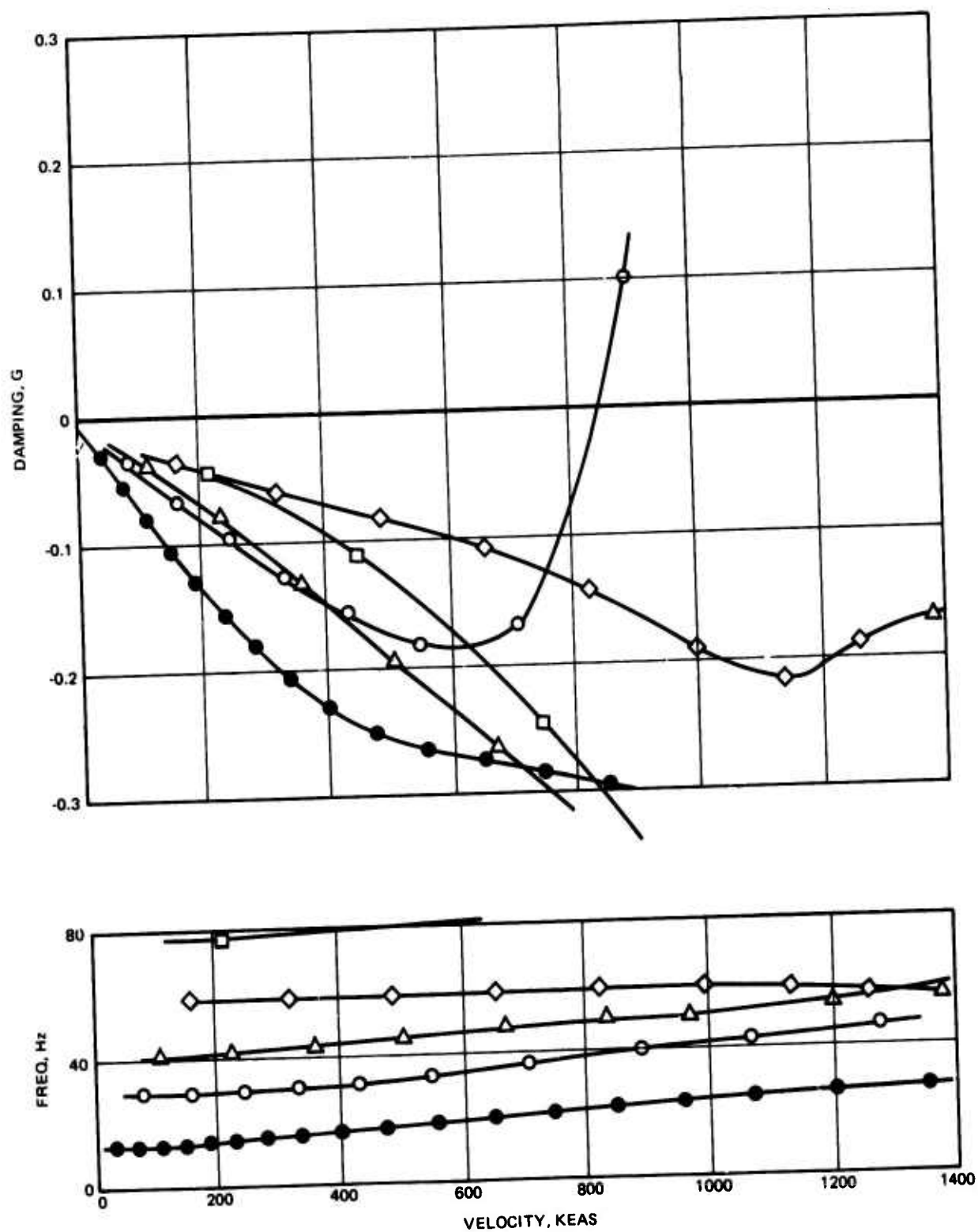


Figure 252. Slab Fin Untailored, $\beta = 0^\circ$, $M = 1.3$, Sea Level

rudder frequency is, therefore, non-linear. Figure 253 shows the coupled rudder rotation and fin torsion frequencies vs the effective actuator spring.

From Figure 253, the coupled rudder rotation frequency for an effective stiffness of 2.0×10^6 is 23.12 Hz. Taking the velocity at $M = 1.05$, sea level (the maximum q within the V_L envelope), $V/b \omega = 0.186$. This value was judged sufficiently high to meet buzz prevention criteria and the effective actuator spring of 2.0×10^6 in.-lb/rad was incorporated into the final fin design.

The rudder distributed weight breakdown is given in Table 52. The panels refer to those shown in the fin dynamic idealization, Figure 246, and are given perpendicular to the fin beam axis.

TABLE 52. ADCA RUDDER MASS PROPERTIES

Panel	Weight, lb	Unbalance*, lb-in.	Inertia*, lb-in. ²
3	23.0	411.0	13,825
4	16.0	234.0	6,346
5	12.0	130.0	2,635
6	8.0	60.0	813
Total Wt.	59.0		

*Unbalance and Inertia are taken at the hinge line about an axis parallel to the fin beam axis

The mass moment of inertia of the rudder about the hinge line corresponding to the above data, is 22,300 lb-in.².

The comprehensive results of the vibration analyses for the final fin-rudder design ($\beta = 15^\circ$, effective actuator spring = 2.0×10^6) are included. Table 53 shows a frequency comparison with the $\beta = 0^\circ$ case.

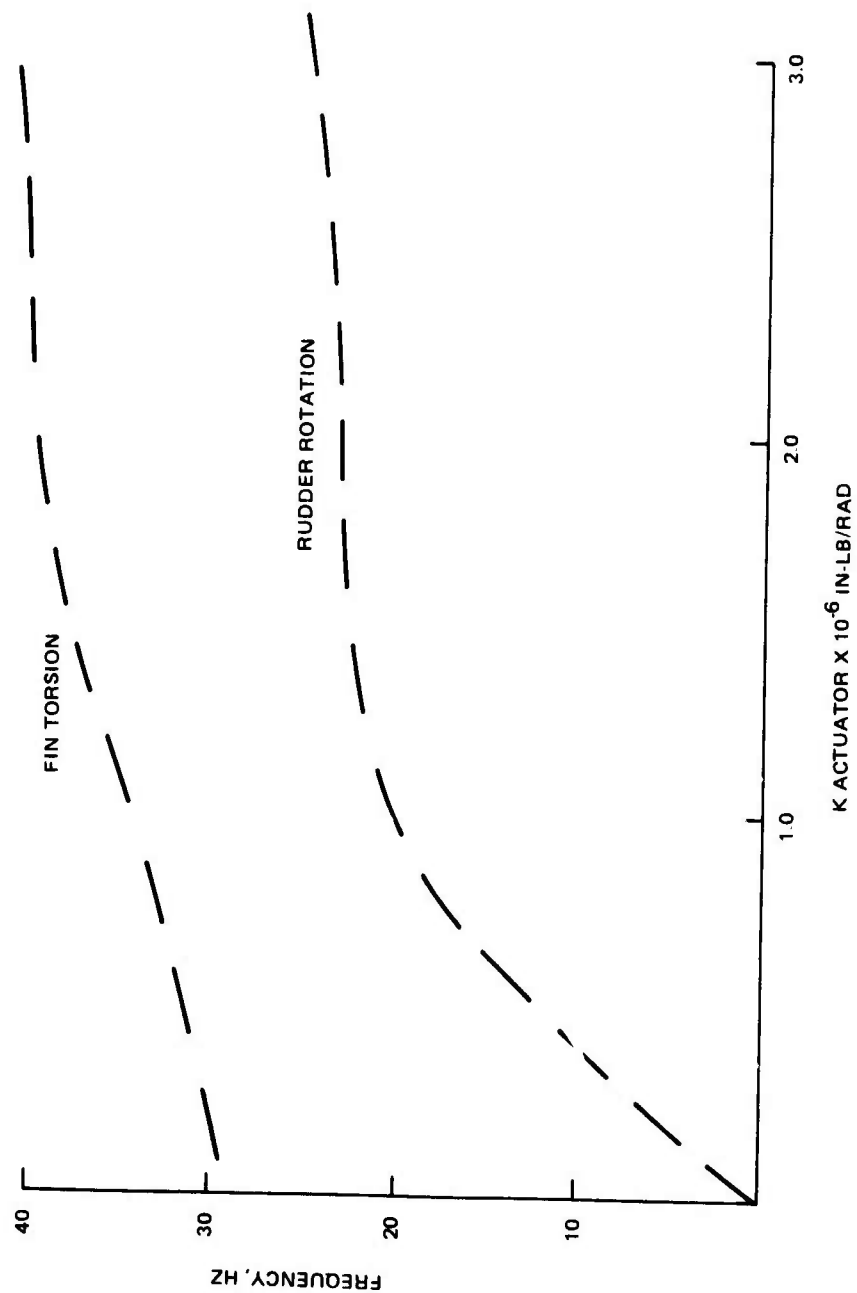


Figure 253. Fin-Rudder, Frequency Vs Actuator Stiffness

TABLE 53. ADCA FIN-RUDDER FREQUENCY COMPARISON

Mode	$\beta = 15^\circ$	$\beta = 0^\circ$
1st Bending	12.42 Hz	12.90 Hz
Rudder Rotation	23.12	23.52
Torsion	40.05	39.30
2nd Bending	43.71	47.26

Mode Shape plots are included for the $\beta = 15^\circ$ case in Figure 254. Those for the $\beta = 0^\circ$ case are shown in Figure 255. In both cases, torsion and second bending are highly coupled.

Comprehensive flutter analyses were completed for the $\beta = 15^\circ$ case. Similar analyses were completed for $\beta = 0^\circ$ at $M = 0.8$ and $M = 1.3$. The results are compared in Table 54. Because of the density dependency introduced with rudder rotation, a comparison is given at altitude as well as at sea level.

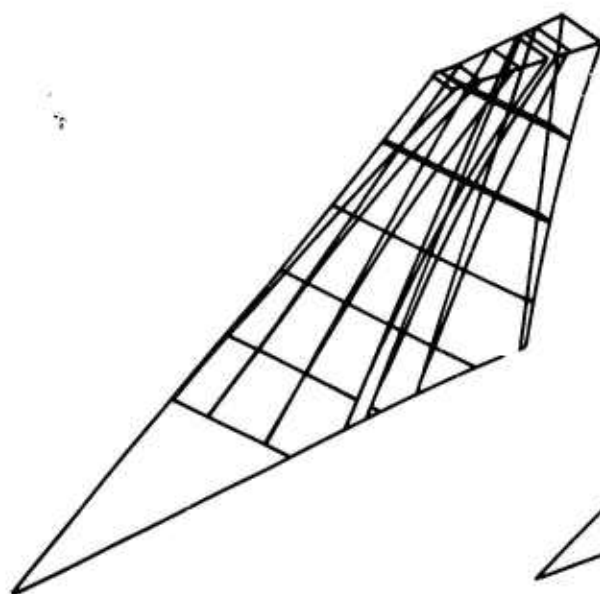
TABLE 54. ADCA FIN-RUDDER FLUTTER SPEED COMPARISON

Mach	Altitude, ft	$V_f \beta = 15^\circ$	$V_f \beta = 0^\circ$	$V_f \beta = 15^\circ / V_f \beta = 0^\circ$
0.8	SL	1074 KEAS	797 KEAS	1.35
0.8	20,000	840	675	1.24
0.8	40,000	672	598	1.12
1.3	SL	NF	1300	-
1.3	20,000	830	751	1.11
1.3	40,000	628	605	1.04

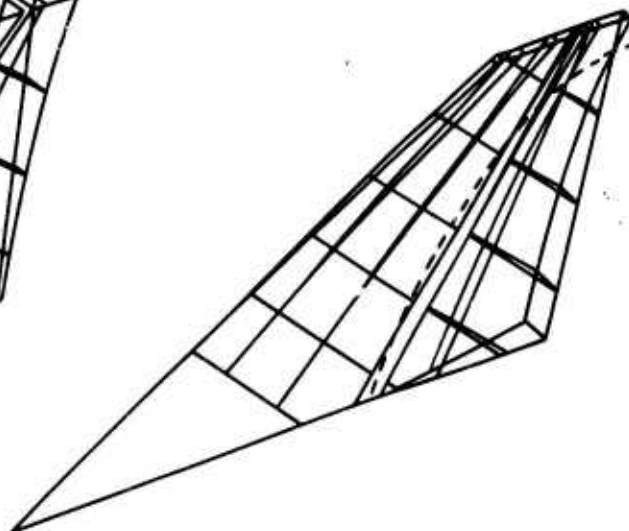
The corresponding V-g- ω plots for the $\beta = 0$ case are shown in Figures 256 through 261. Those for the $\beta = 15$ case are Figures 262 and 268.

The comprehensive analyses for the final fin design are summarized in Table 55 and the corresponding v-g- ω plots are shown in Figures 262 through 275.

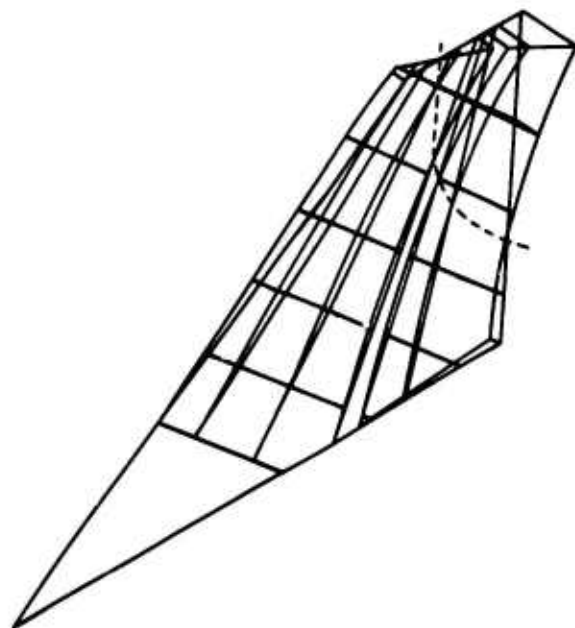
Flutter speed envelopes are shown in Figures 276 through 278.



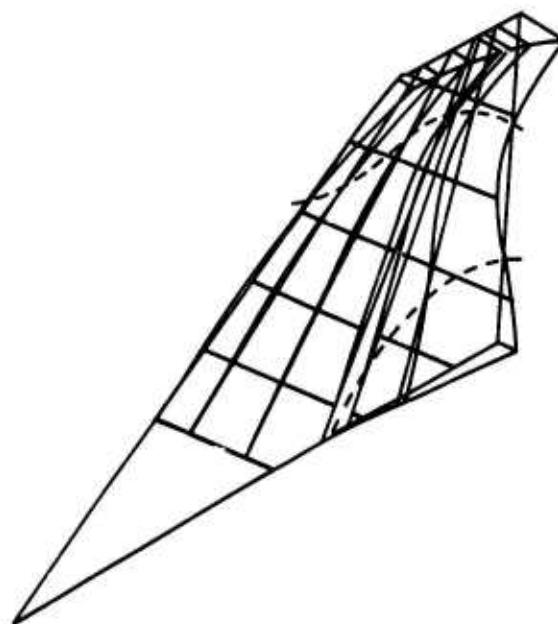
12.42 HZ



23.12 HZ

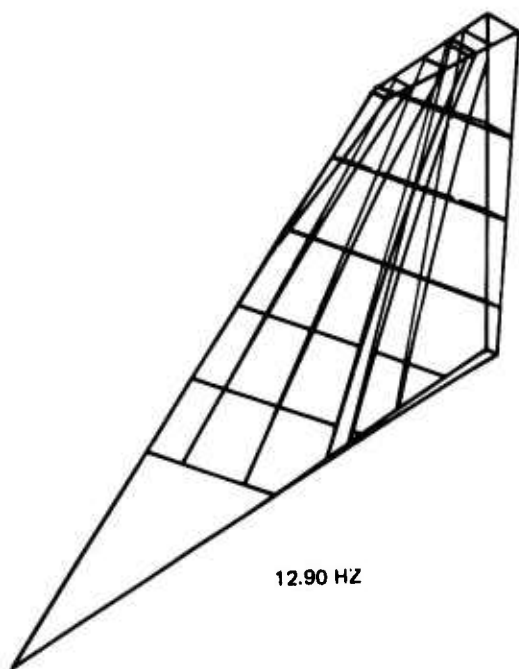


40.05 HZ

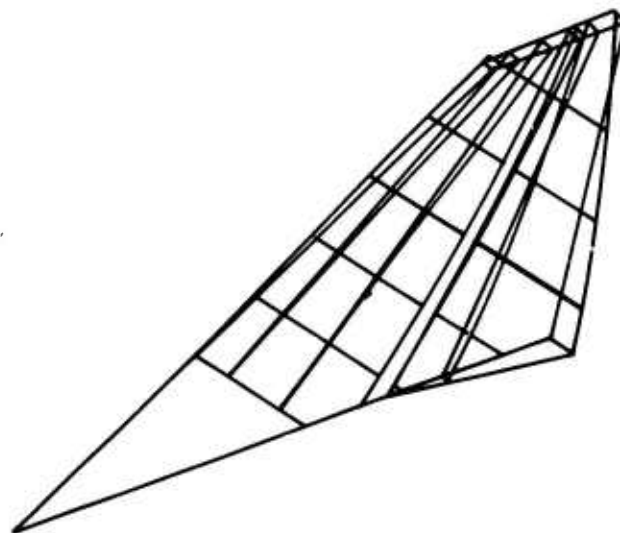


43.71 HZ

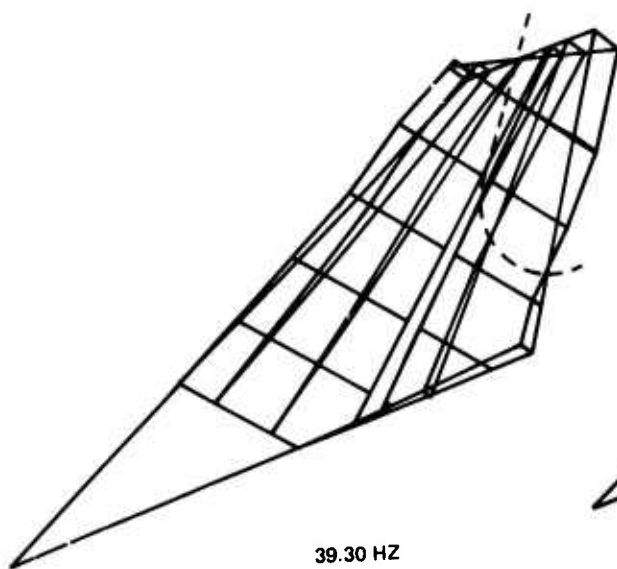
Figure 254. ADCA Fin-Rudder Mode Shapes, $\beta = 15^\circ$



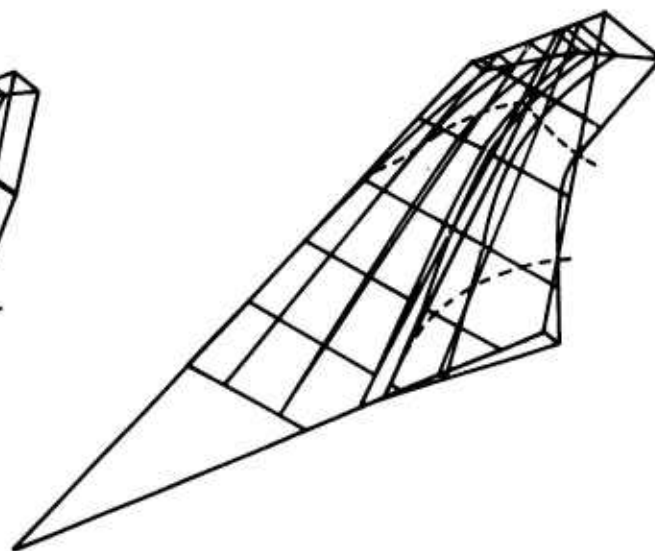
12.90 HZ



23.52 HZ



39.30 HZ



47.26 HZ

Figure 255. ADCA Fin-Rudder Mode Shapes, $\beta = 0^\circ$

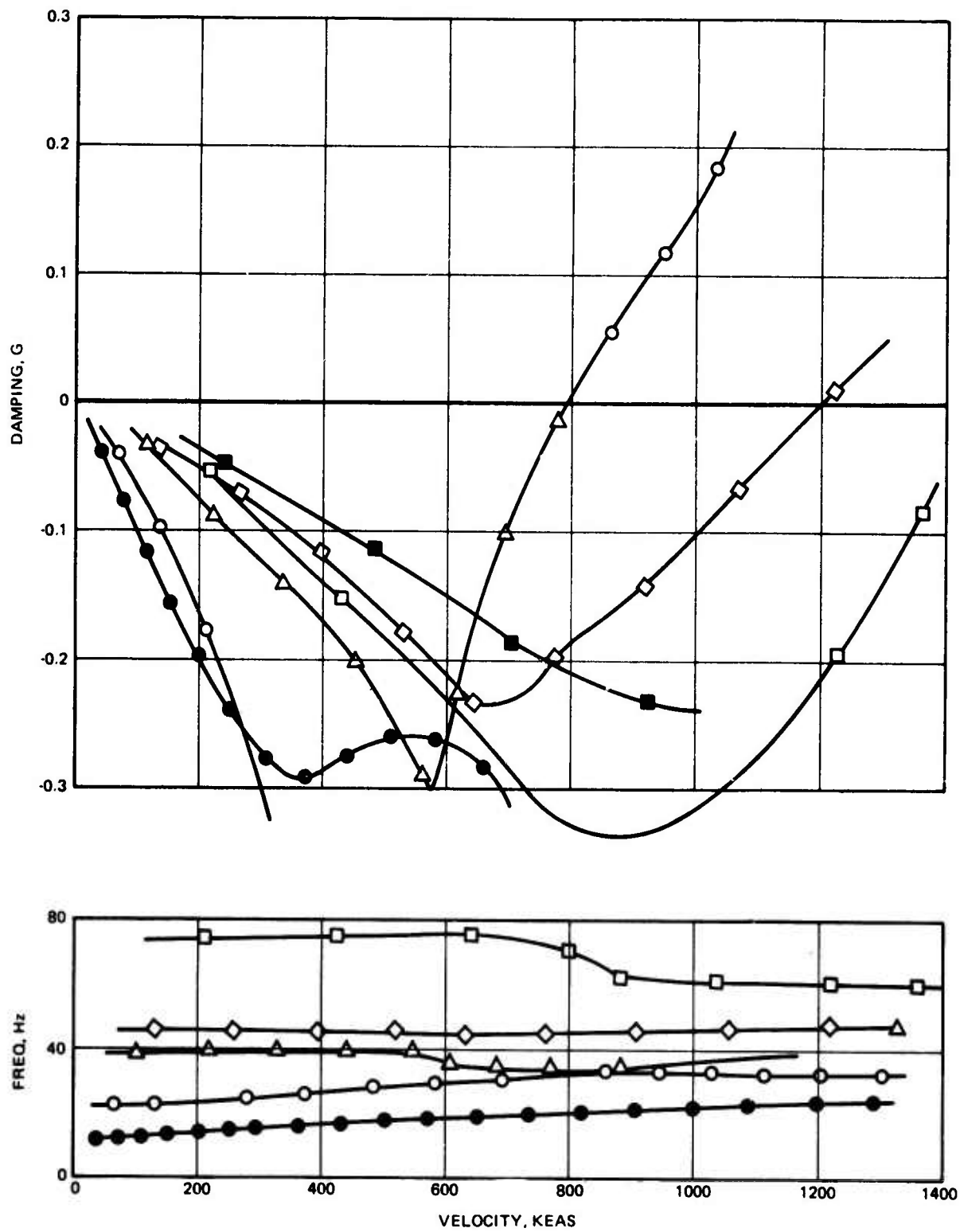


Figure 256. Fin-Rudder Untailed, $\beta = 0^\circ$, $M = 0.8$, Sea Level

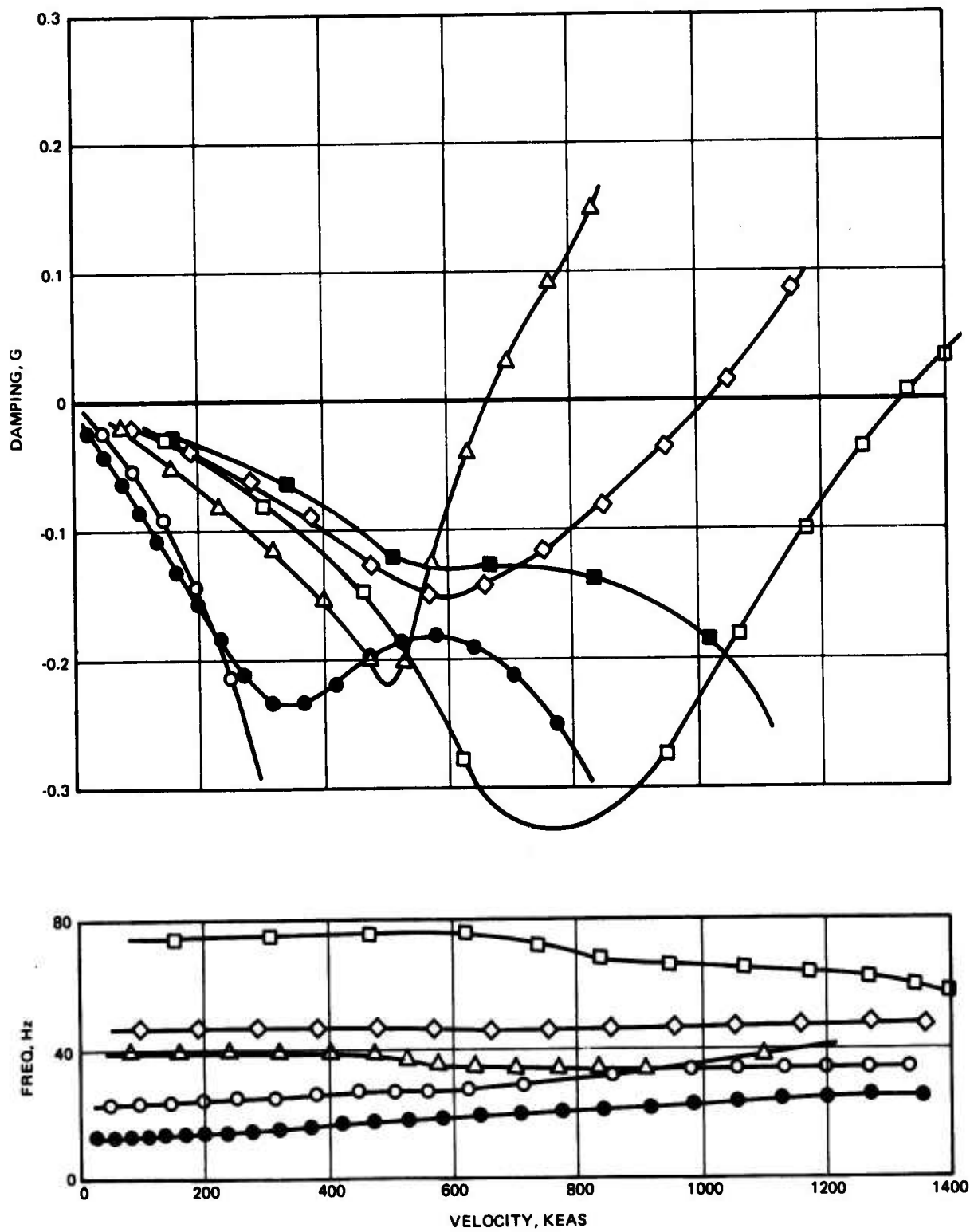


Figure 257. Fin-Rudder Untailored, $\beta = 0^\circ$, M - 0.8, 20,000 Ft

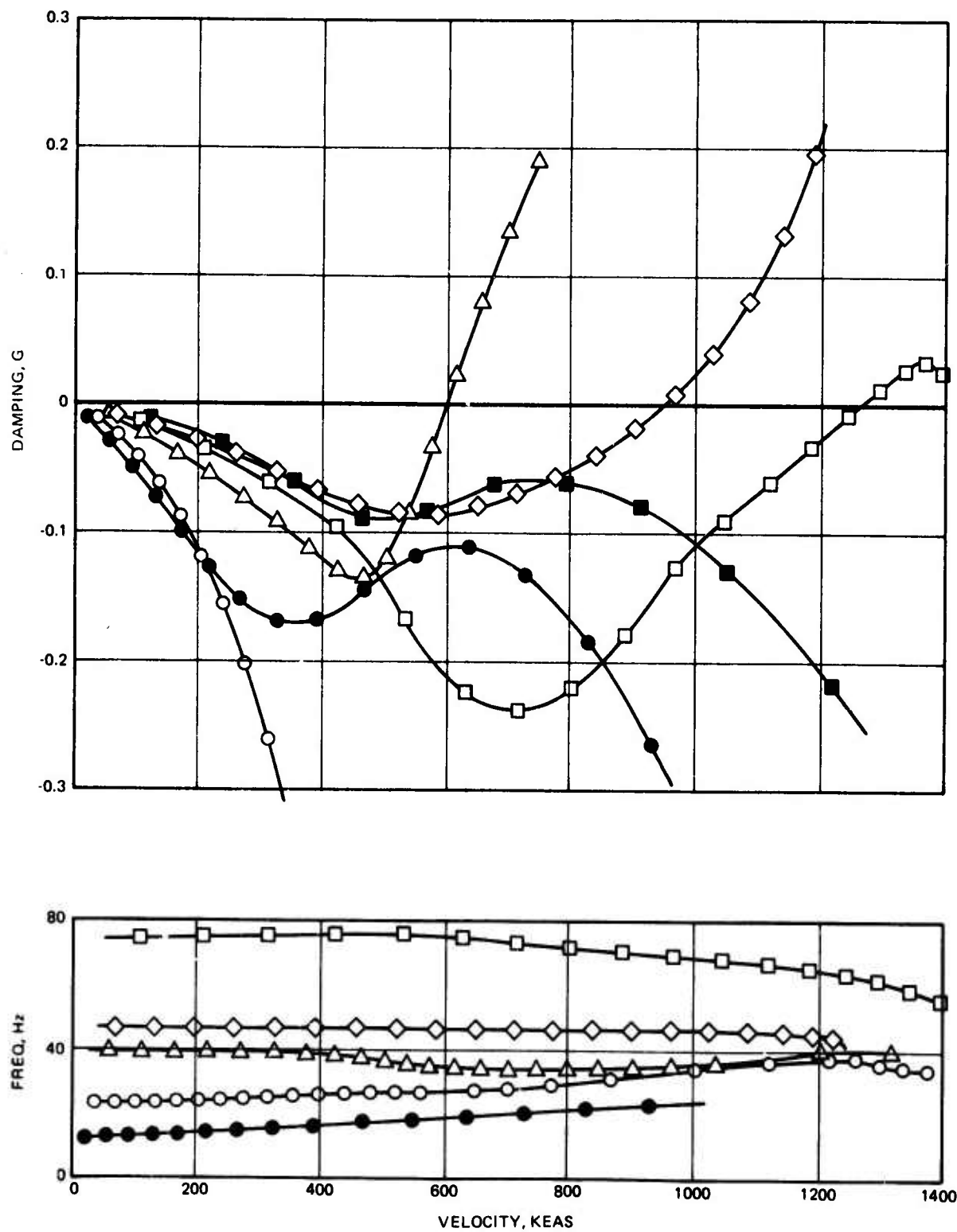


Figure 258. Fin-Rudder Untailored, $\beta = 0^\circ$, $M = 0.8$, 40,000 Ft

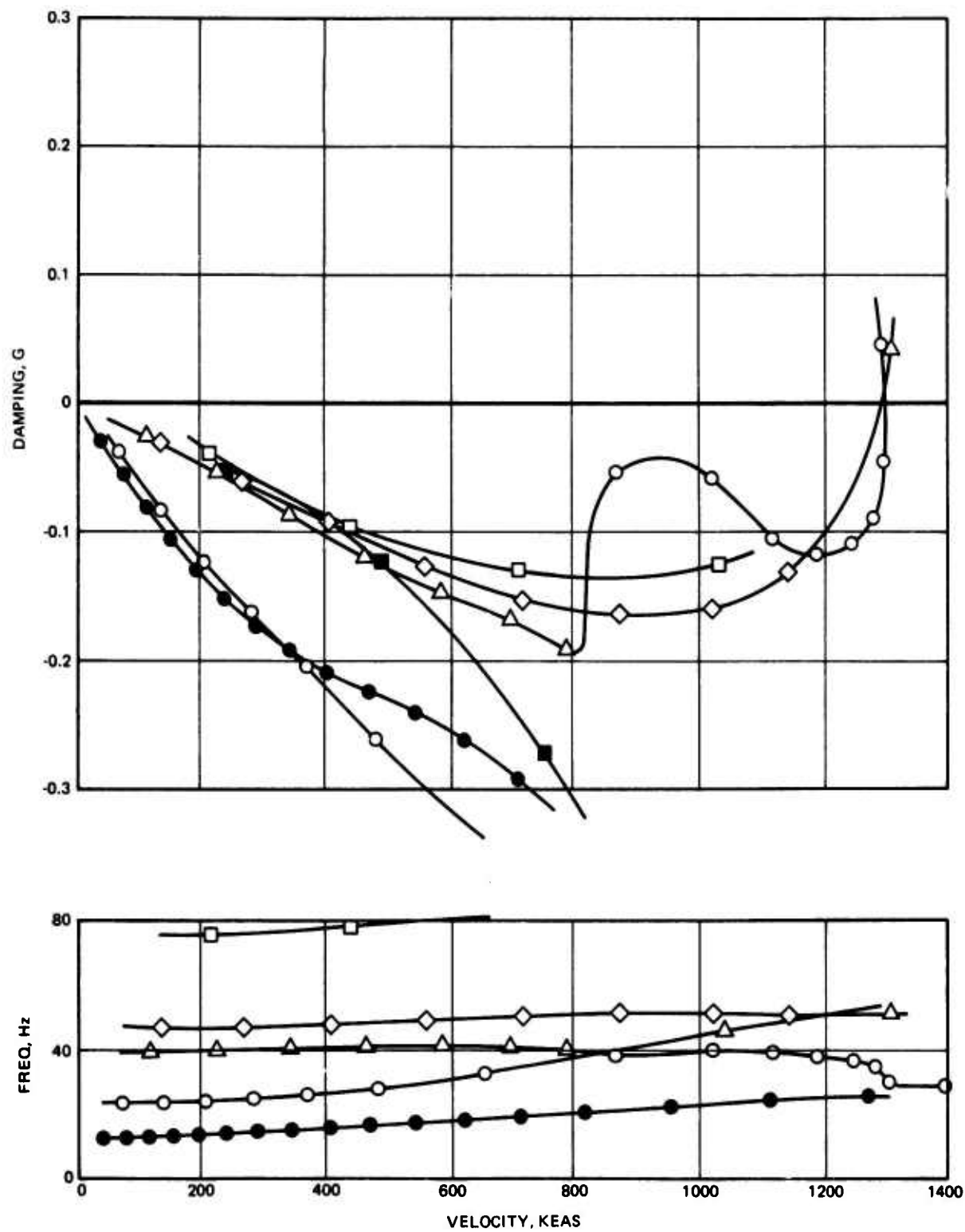


Figure 259. Fin-Rudder Untailored, $\beta = 0^\circ$, $M = 1.3$, Sea Level

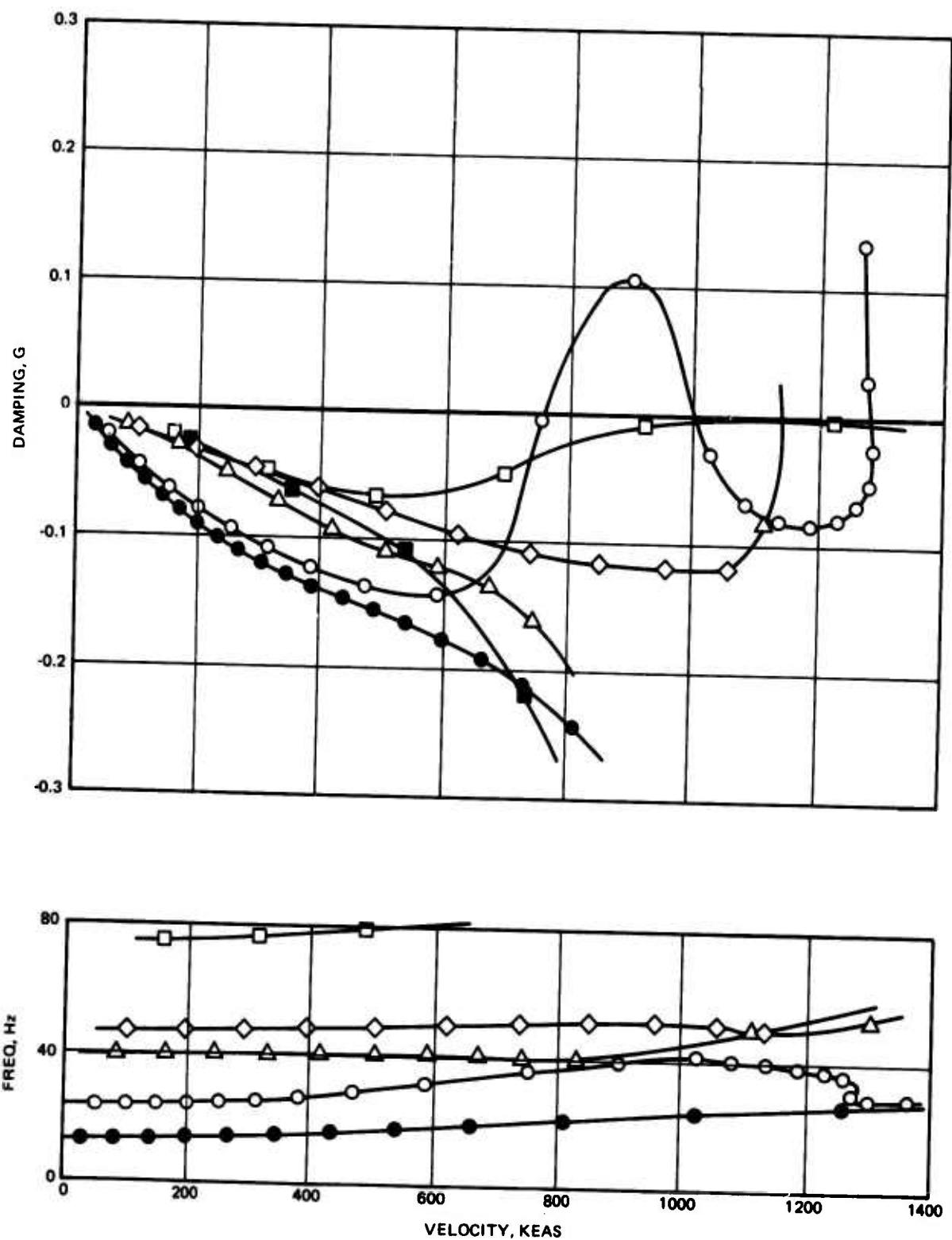


Figure 260. Fin-Rudder Untailored, $\beta = 0^\circ$, $M = 1.3$, 20,000 Ft

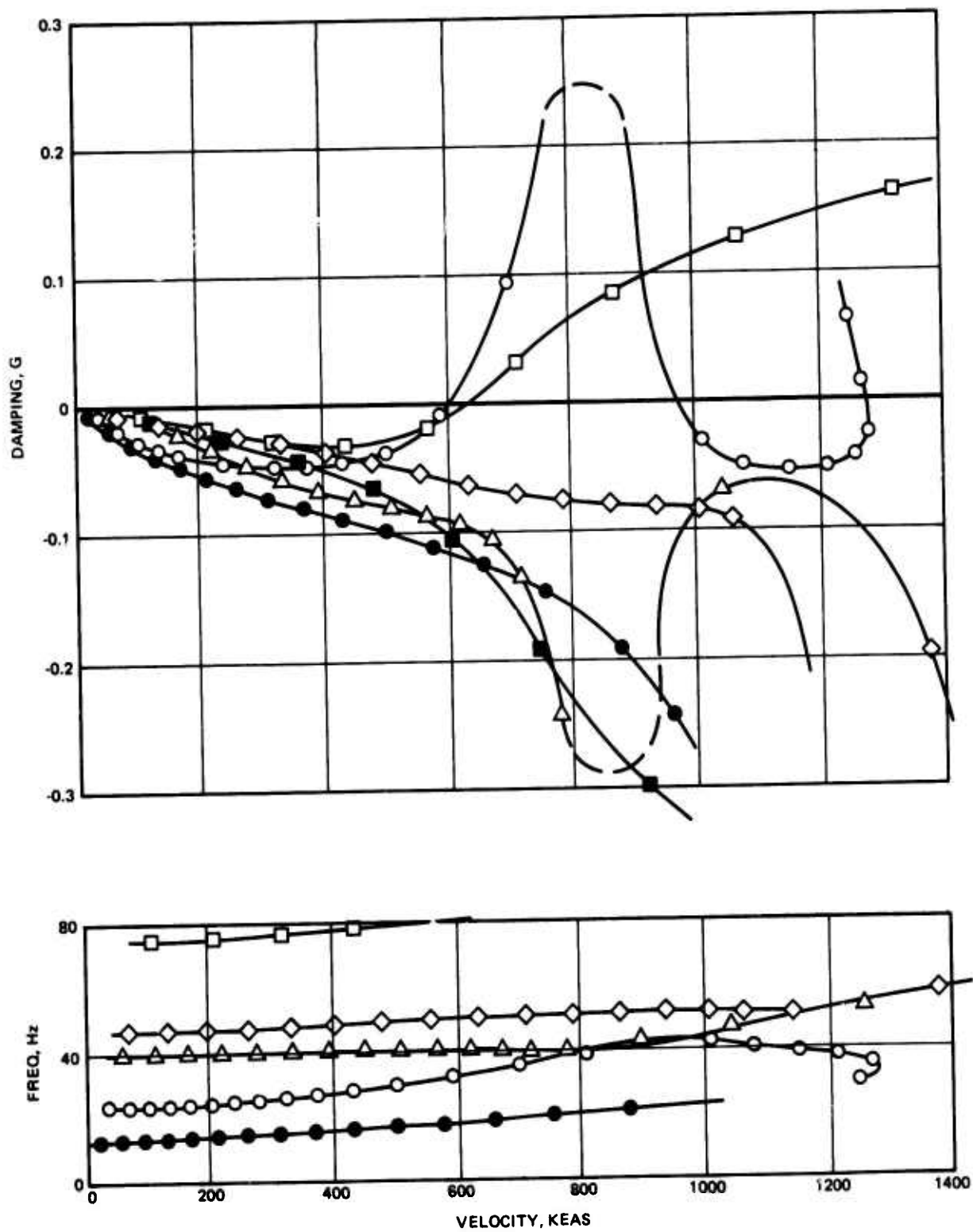


Figure 261. Fin-Rudder Untailored, $\beta = 0^\circ$, $M = 1.3$, 40,000 Ft

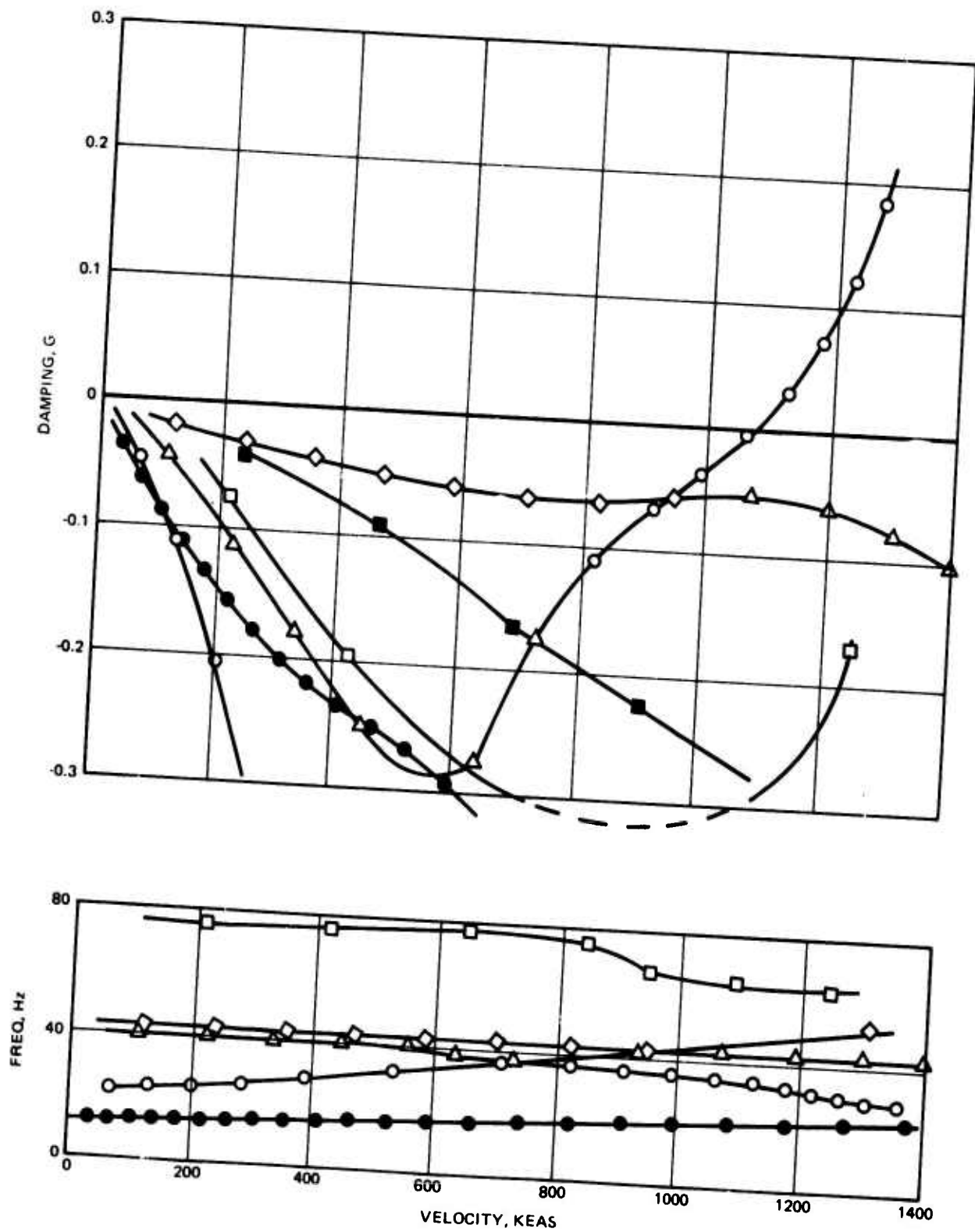


Figure 262. Fin-Rudder Tailored, $\beta = 15^\circ$, $M = 0.8$, Sea Level

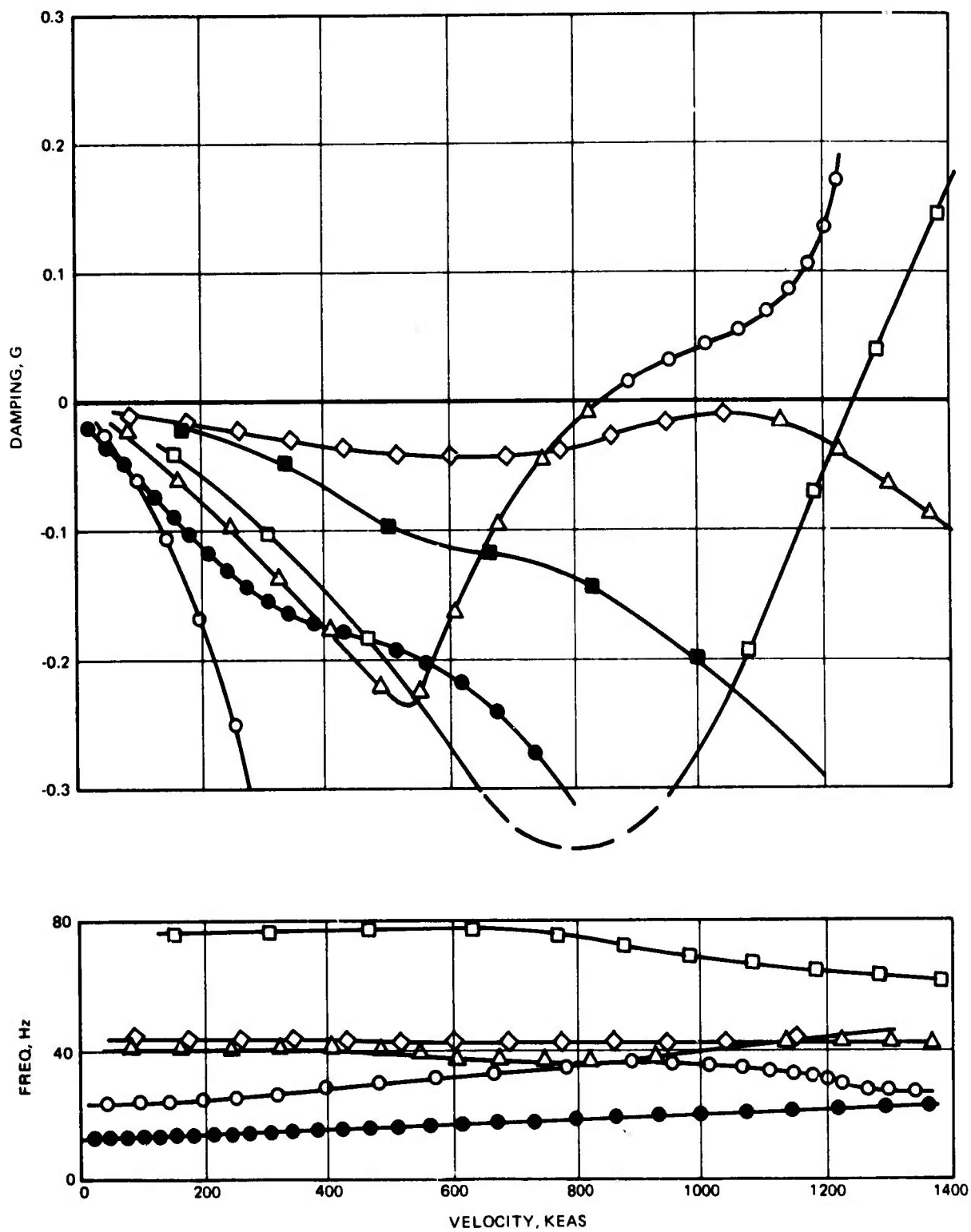


Figure 263. Fin-Rudder Tailored, $\beta = 15^\circ$, $M = 0.8$, 20,000 Ft

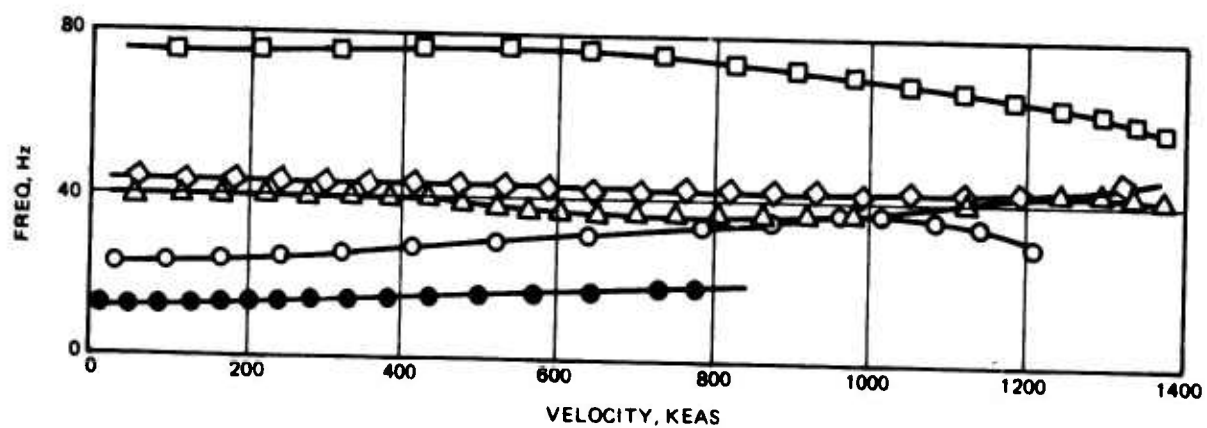
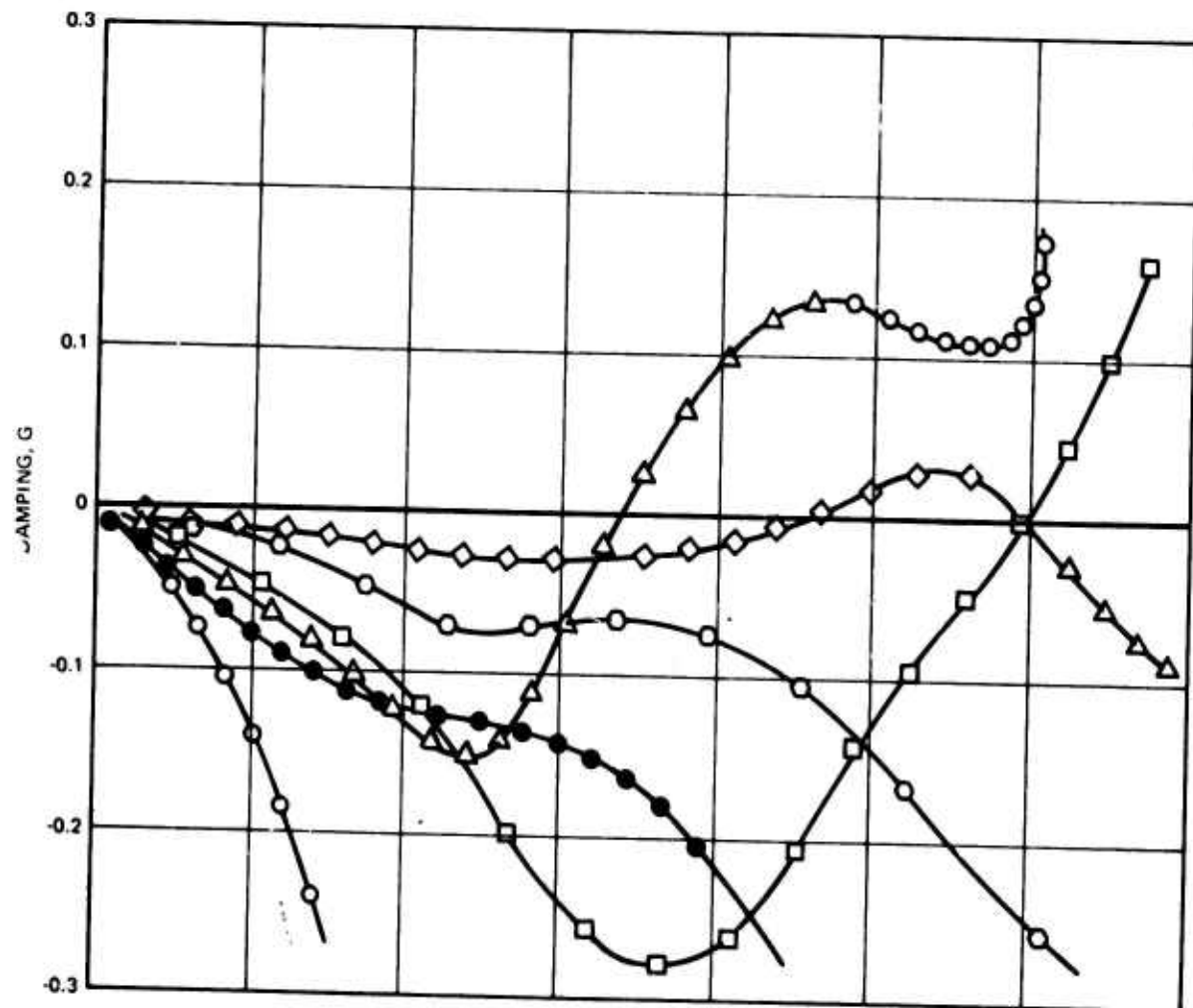


Figure 264. Fin-Rudder Tailored, $\beta = 15^\circ$, $M = 0.8$, 40,000 Ft

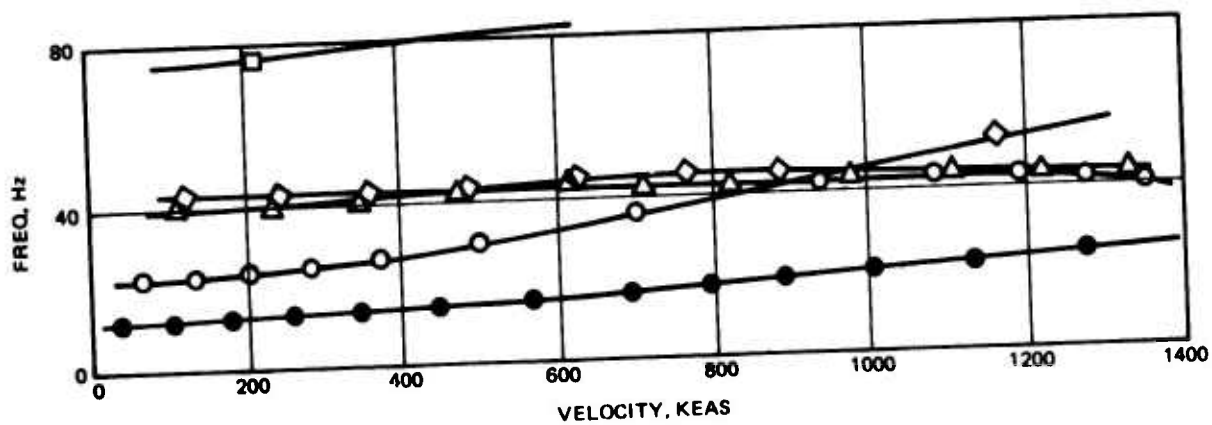
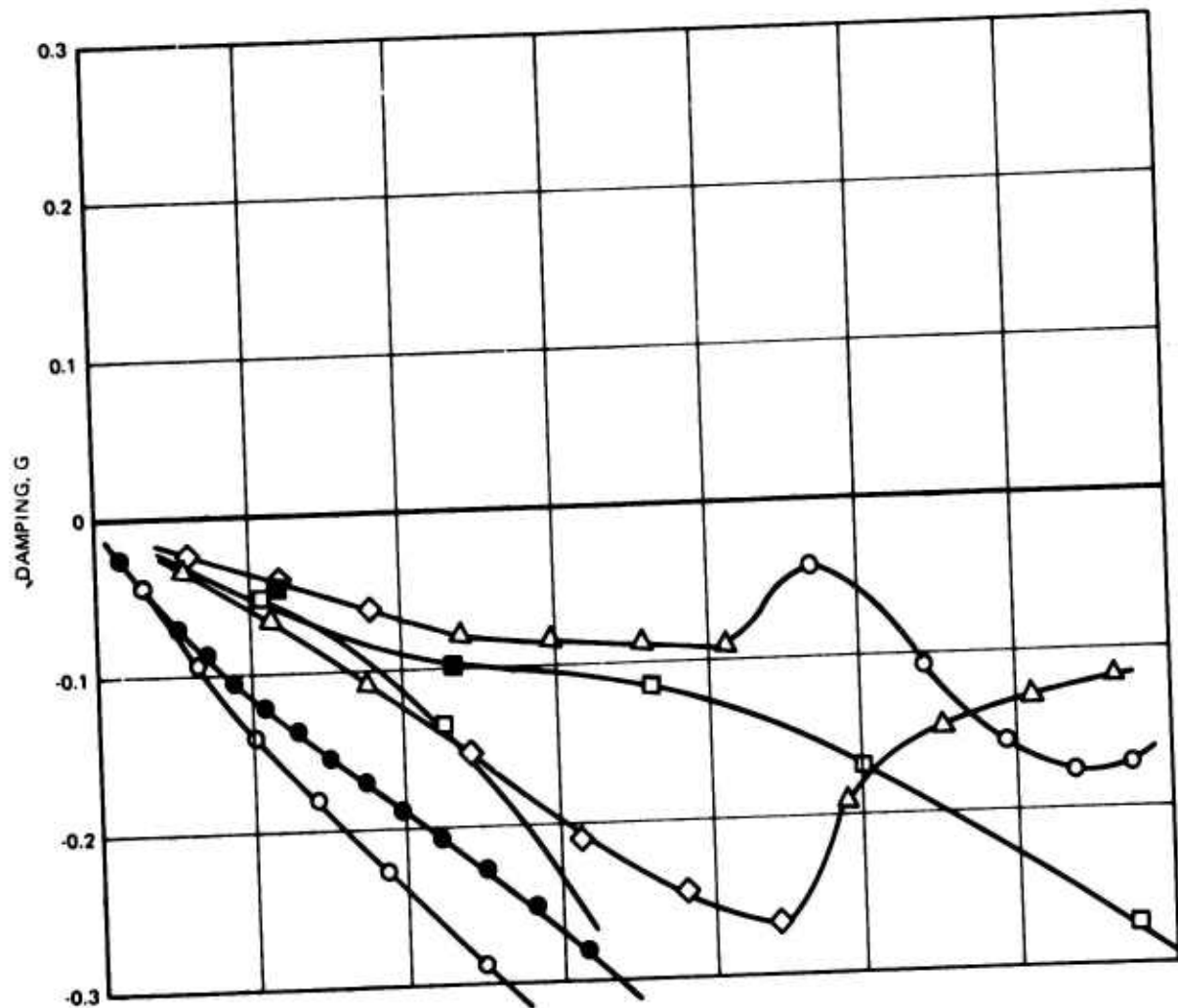


Figure 265. Fin-Rudder Tailored, $\beta - 15^\circ$, $M = 1.3$, Sea Level

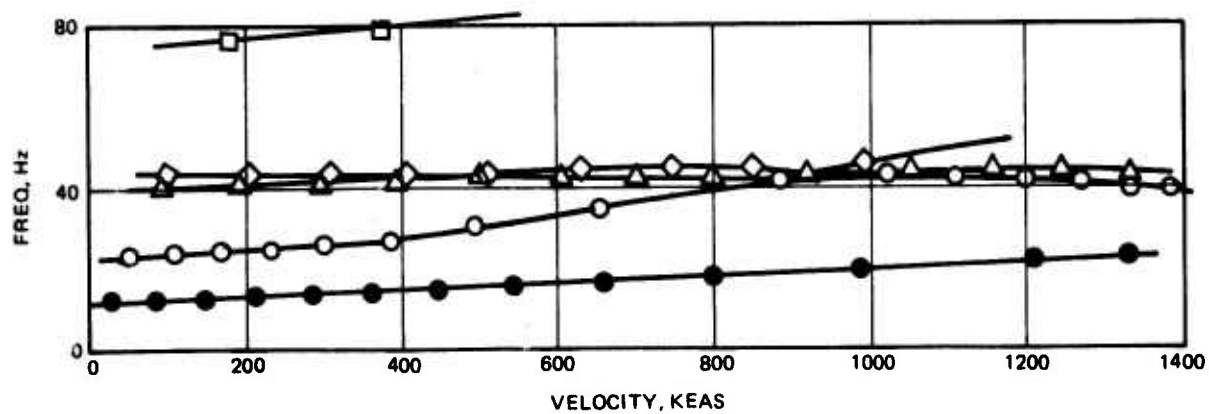
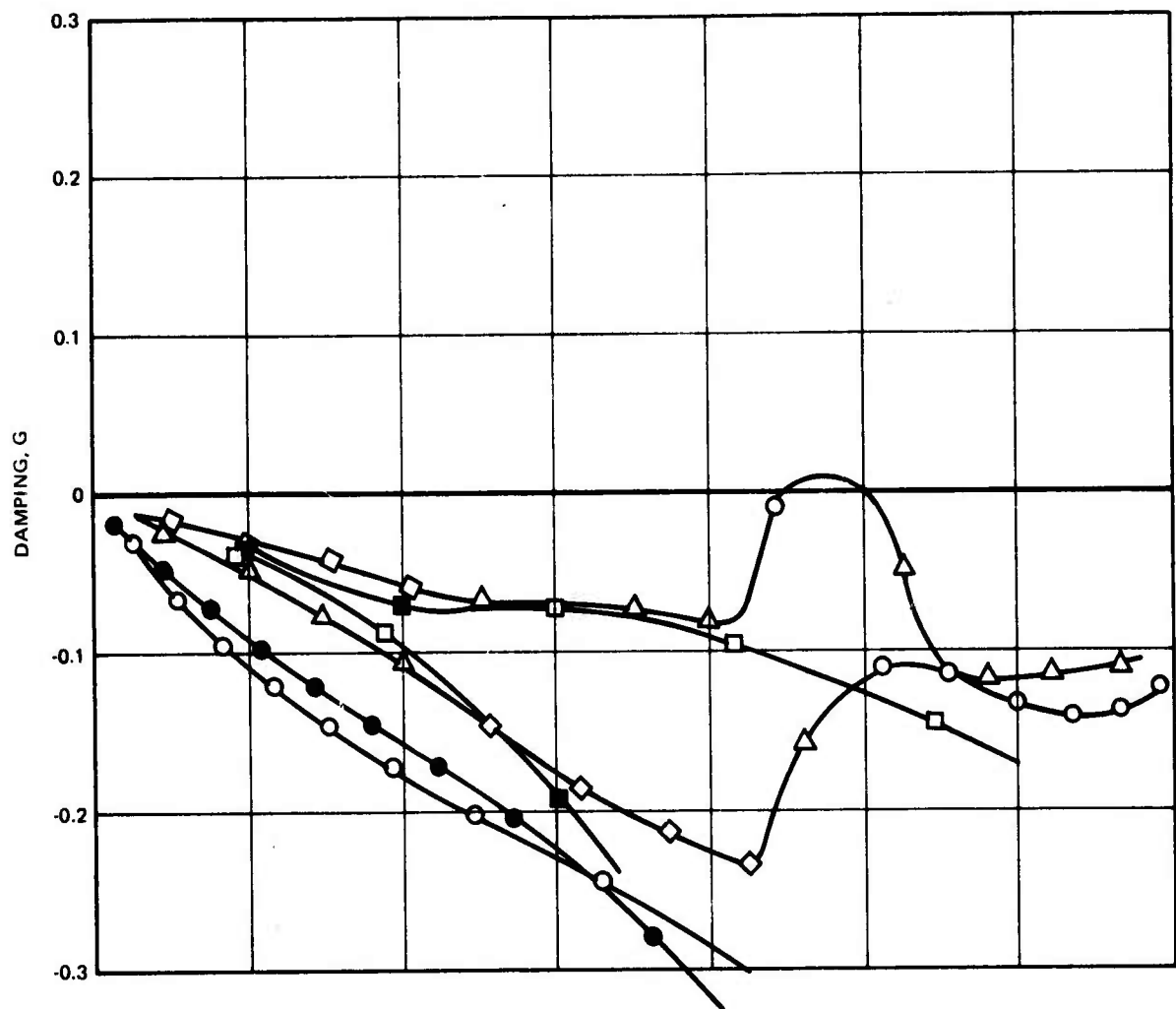


Figure 266. Fin-Rudder Tailored, $\beta = 15^\circ$, $M = 1.3$, 11,000 Ft

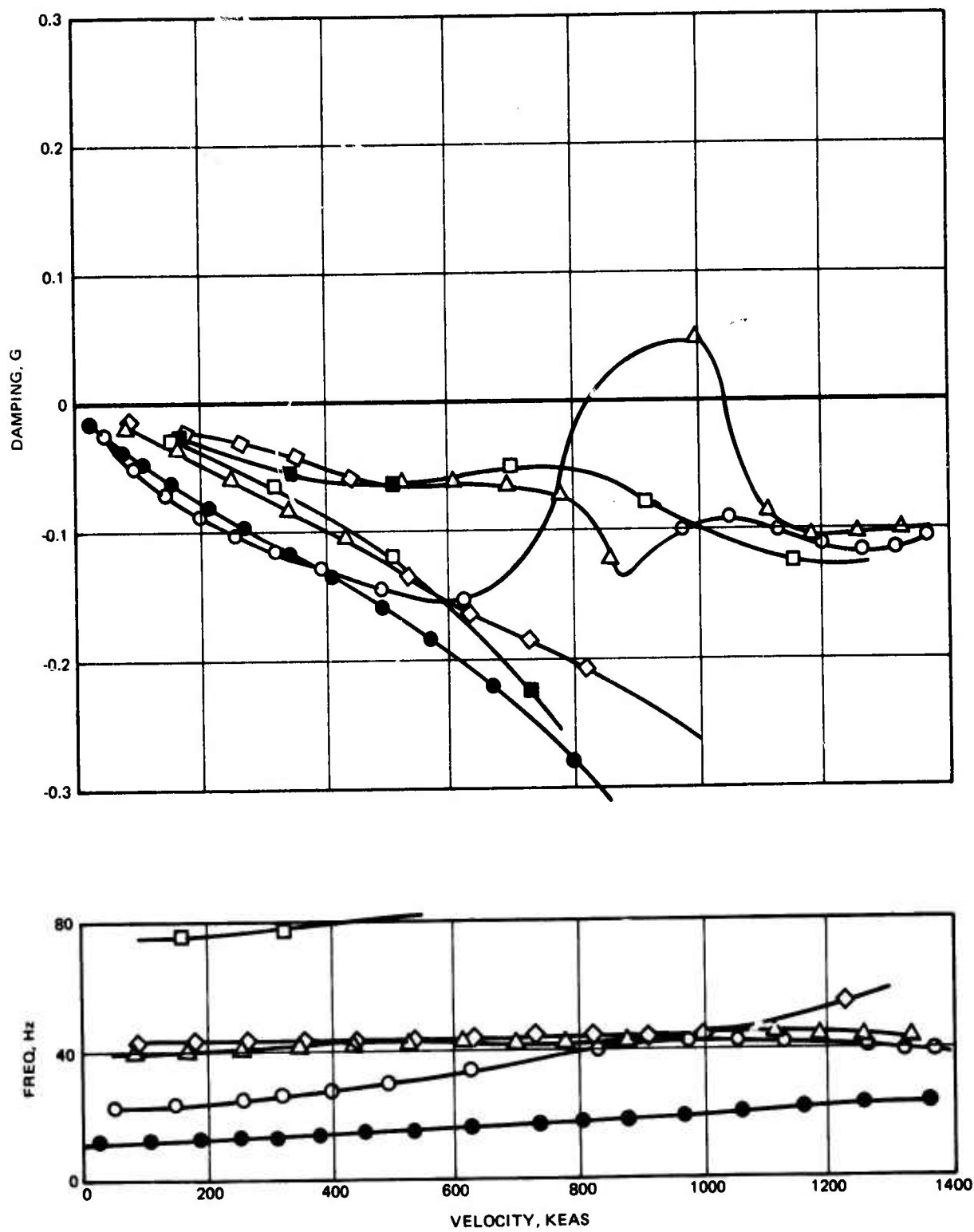


Figure 267. Fin-Rudder Tailored, $\beta = 15^\circ$, $M = 1.3$, 20,000 Ft

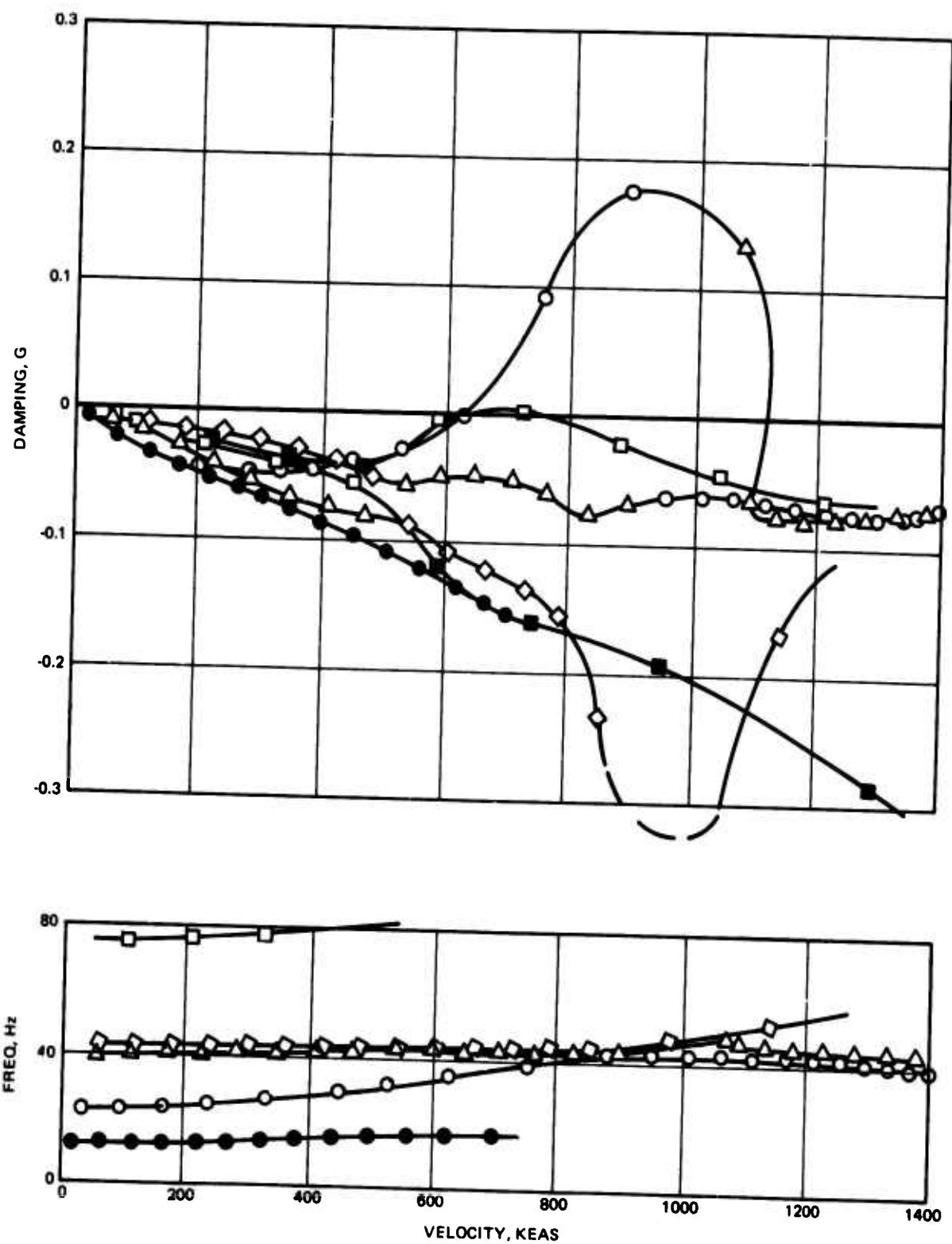


Figure 268. Fin-Rudder Tailored, $\beta = 15^\circ$, $M = 1.3$, 40,000 Ft

TABLE 55. ADCA FIN-RUDDER FLUTTER SPEED SUMMARY

Mach No.	Altitude, ft	V_f , KEAS	V_f/v	Reference V-g- ω Figure No.
0.6	SL	937	2.37	273
	20K	783	2.93	274
	40K	699	4.11	275
0.8	SL	1347	2.04	262
	20K	840	2.35	263
	40K	672	2.97	264
1.3	SL	NF	-	265
	11K*	895	1.27	266
	20K	830	1.42	267
	40K	628	1.71	268
1.6	21.5K*	NF	-	269
	40K	685	1.50	270
1.8	27.2K*	NF	-	271
	40K	735	1.39	272

*Altitude appropriate to V_L envelope.

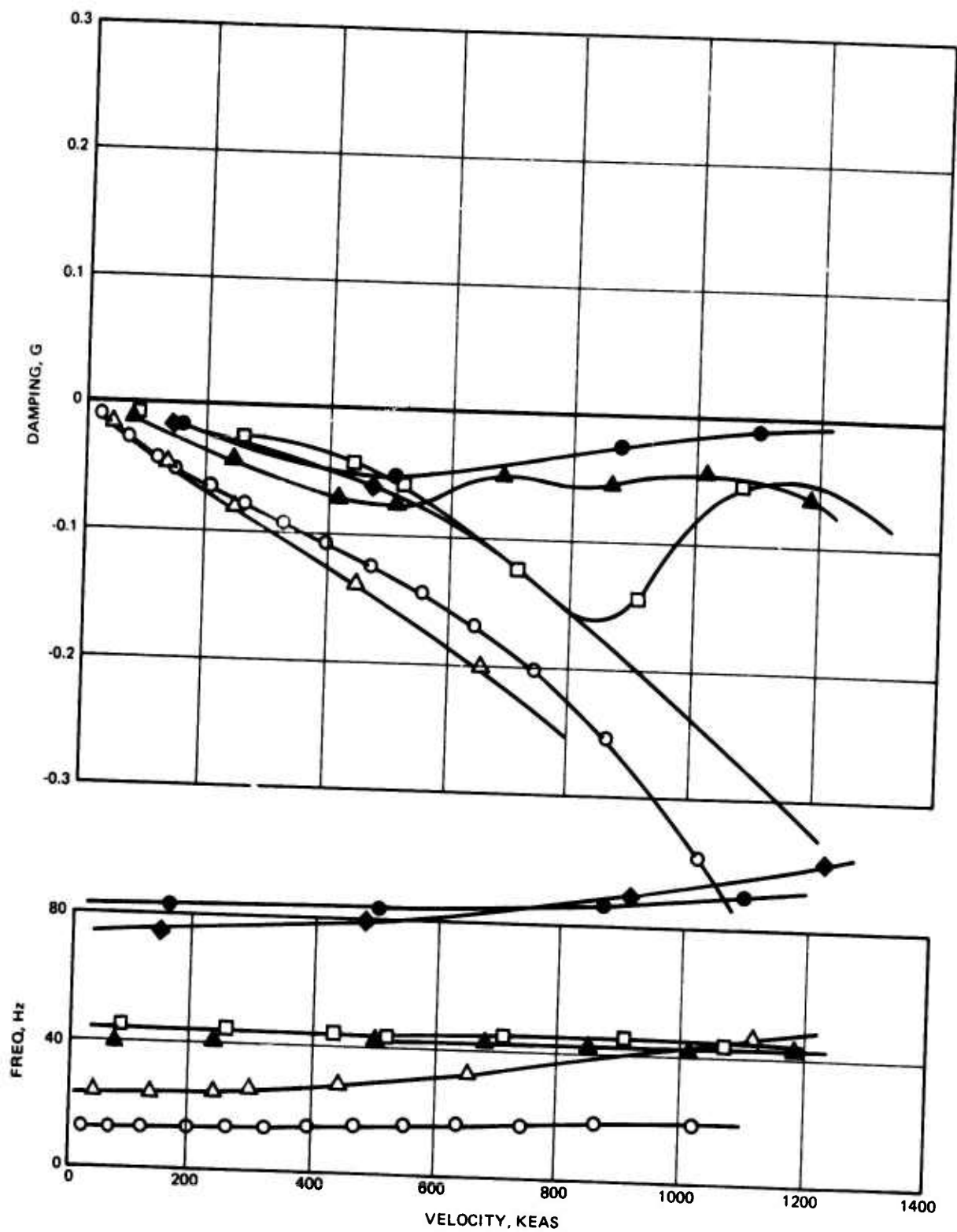


Figure 269. Fin-Rudder Tailored, $\beta = 15^\circ$, $M = 1.6$, 21,500 Ft

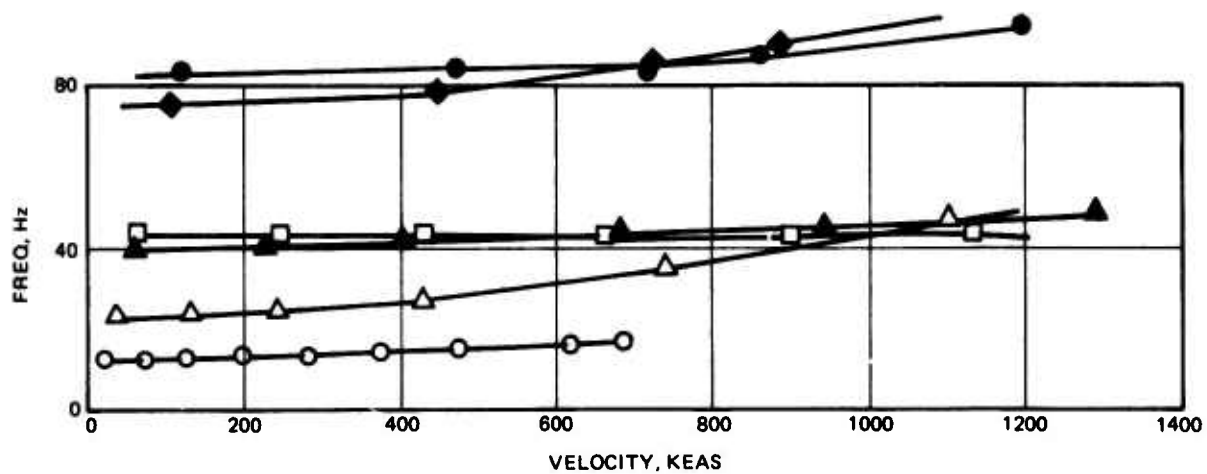
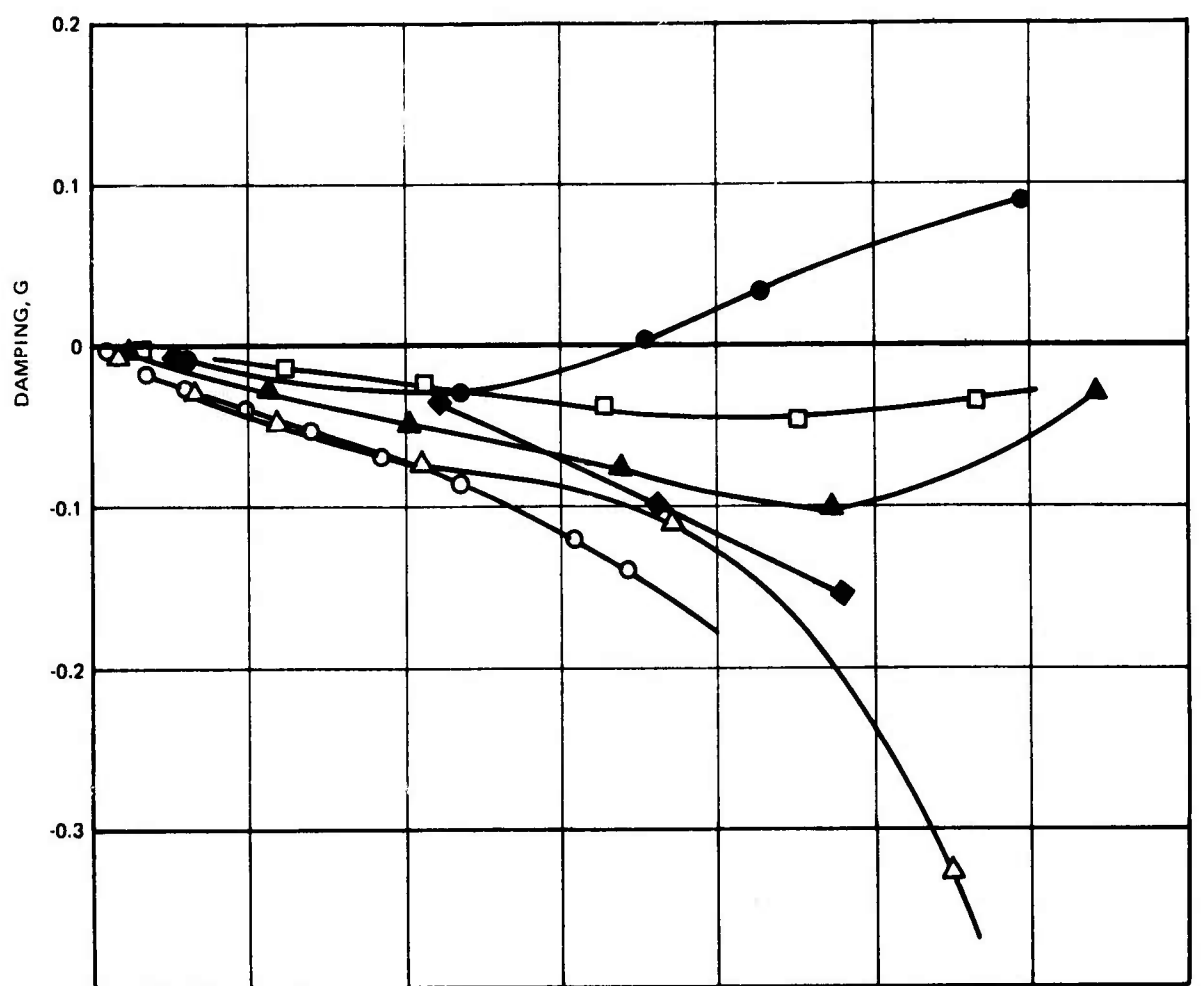


Figure 270. Fin-Rudder Tailored, $\beta = 15^\circ$, $M = 1.6$, 40,000 Ft

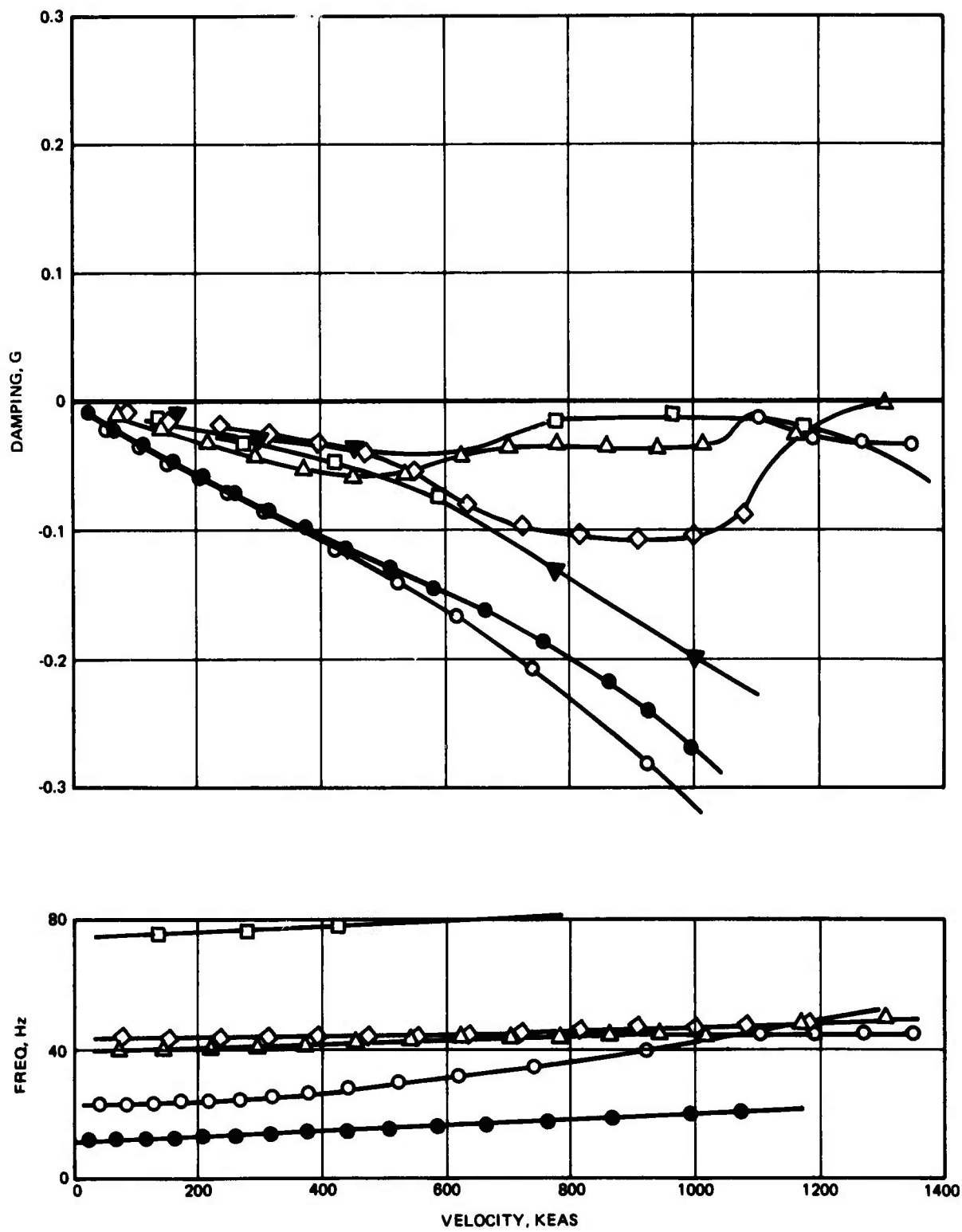


Figure 271. Fin-Rudder Tailored, $\beta = 15^\circ$, $M = 1.8$, 27,200 Ft

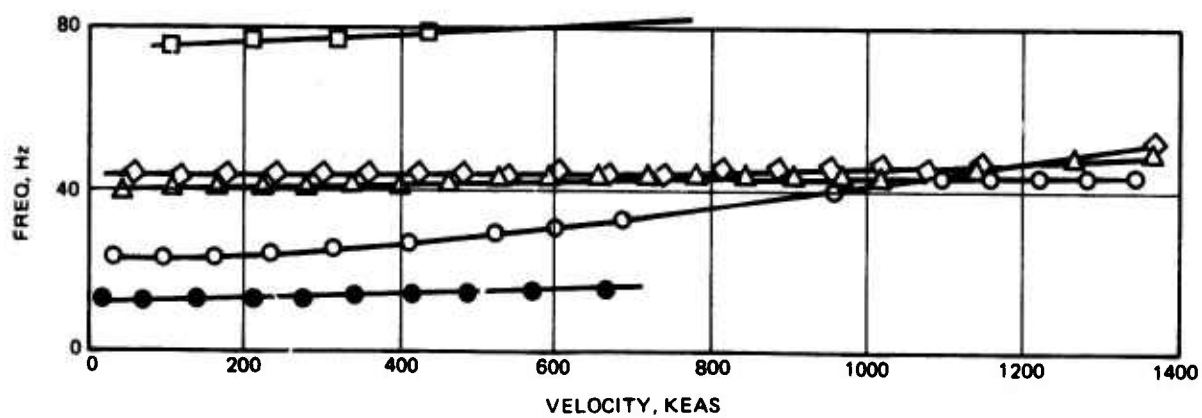


Figure 272. Fin-Rudder Tailored, $\beta = 15^\circ$, $M = 1.8$, 40,000 Ft

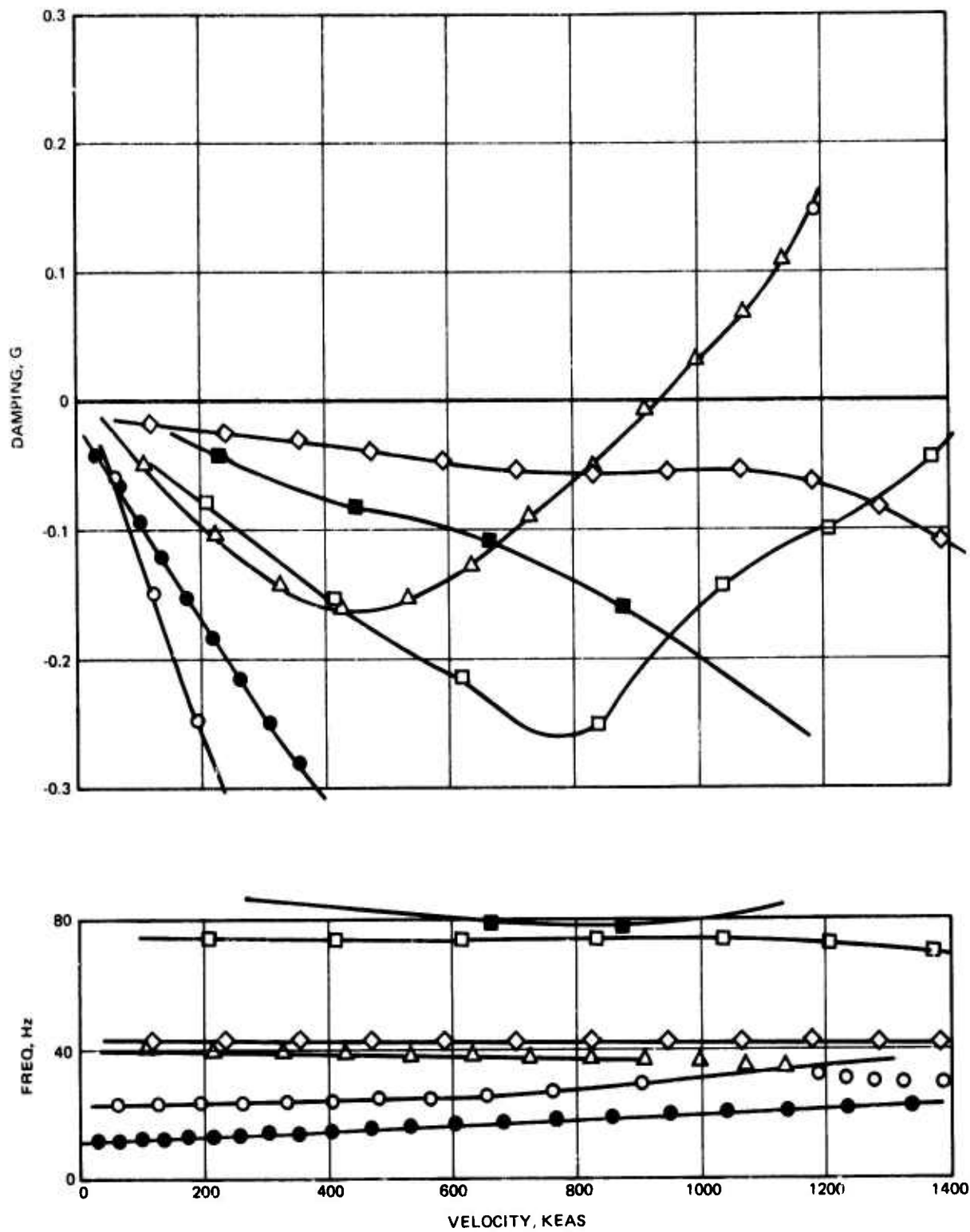


Figure 273. Fin-Rudder Tailored, $\beta = 15^\circ$, $M = 0.6$, Sea Level

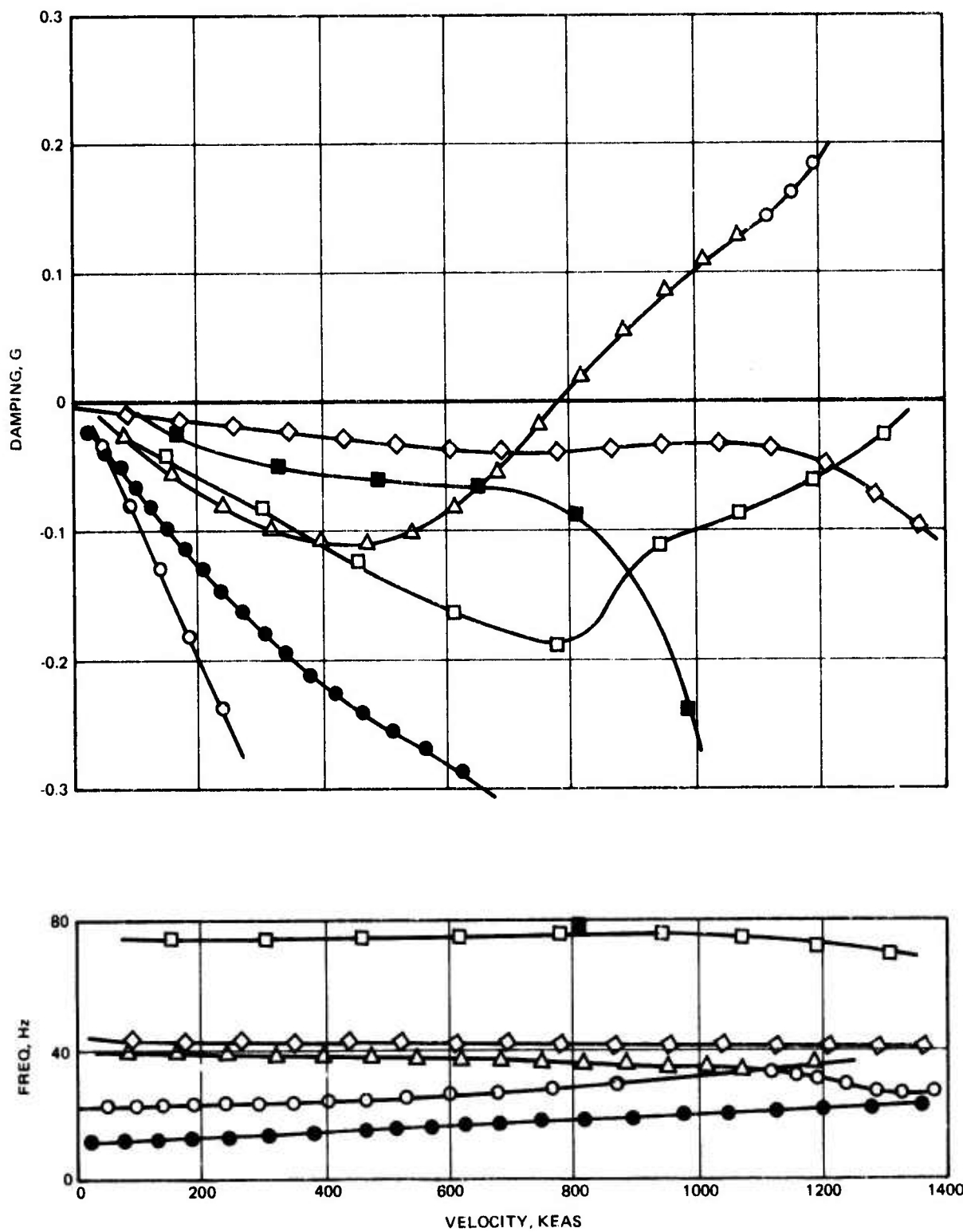


Figure 274. Fin-Rudder Tailored, $\beta = 15^\circ$, $M = 0.6$, 20,000 Ft

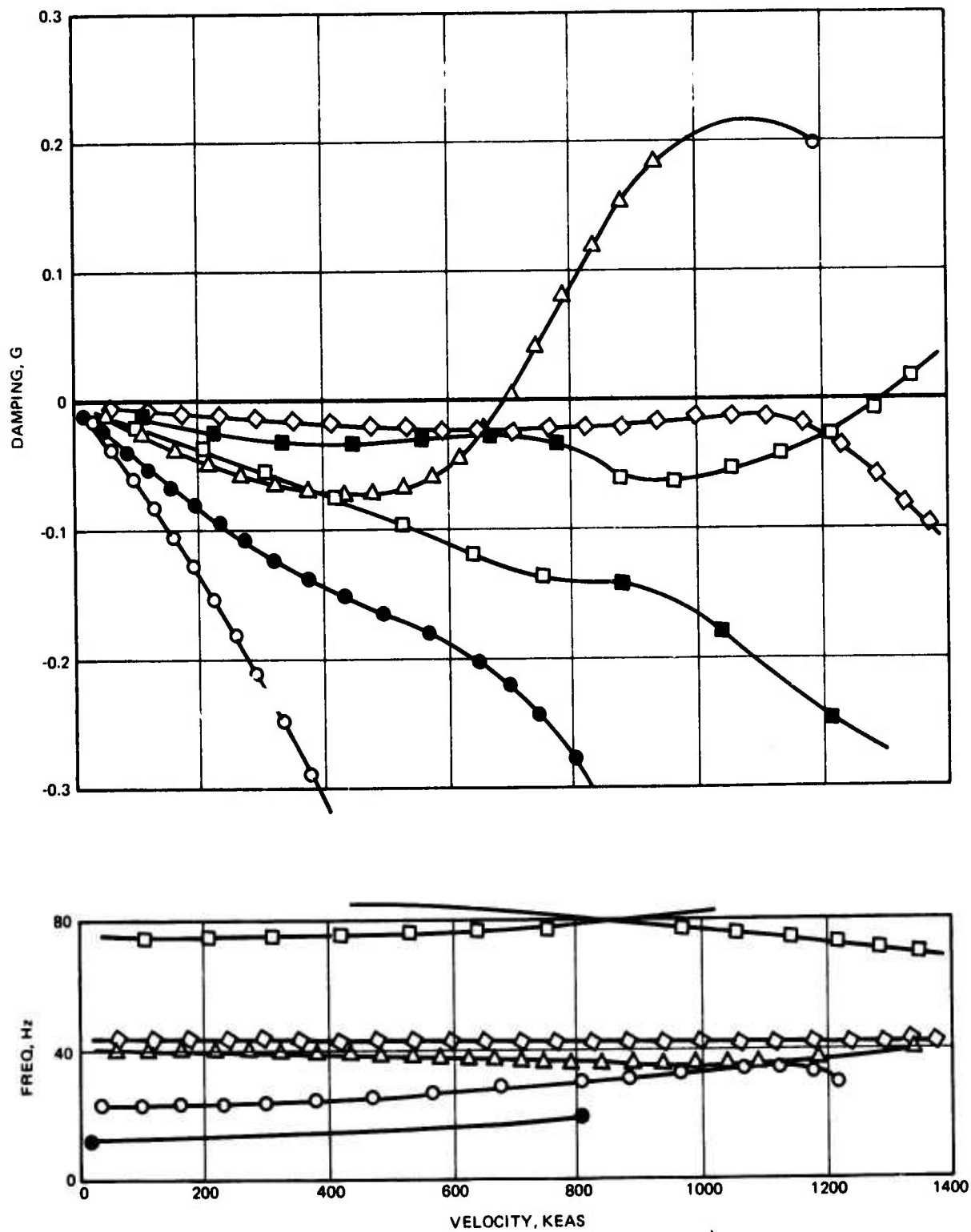


Figure 275. Fin-Rudder Tailored, $\beta = 15^\circ$, $M = 0.6$, 40,000 Ft

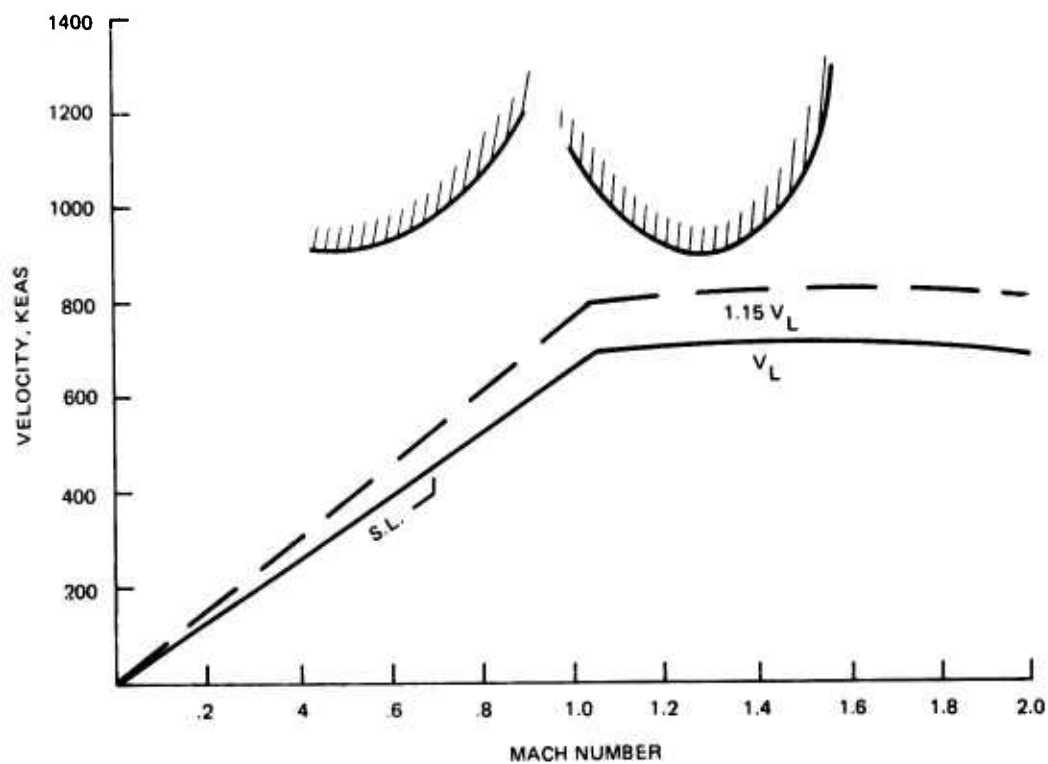


Figure 276. Fin-Rudder V_L Flutter Speed Envelope, Sea Level

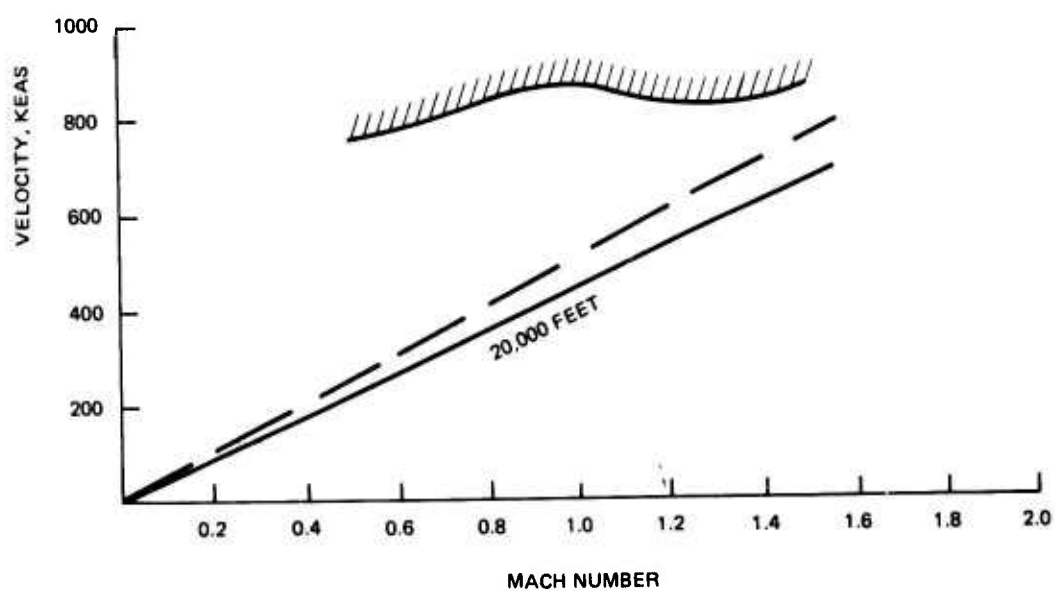


Figure 277. Fin-Rudder Flutter Envelope, 20,000 Ft

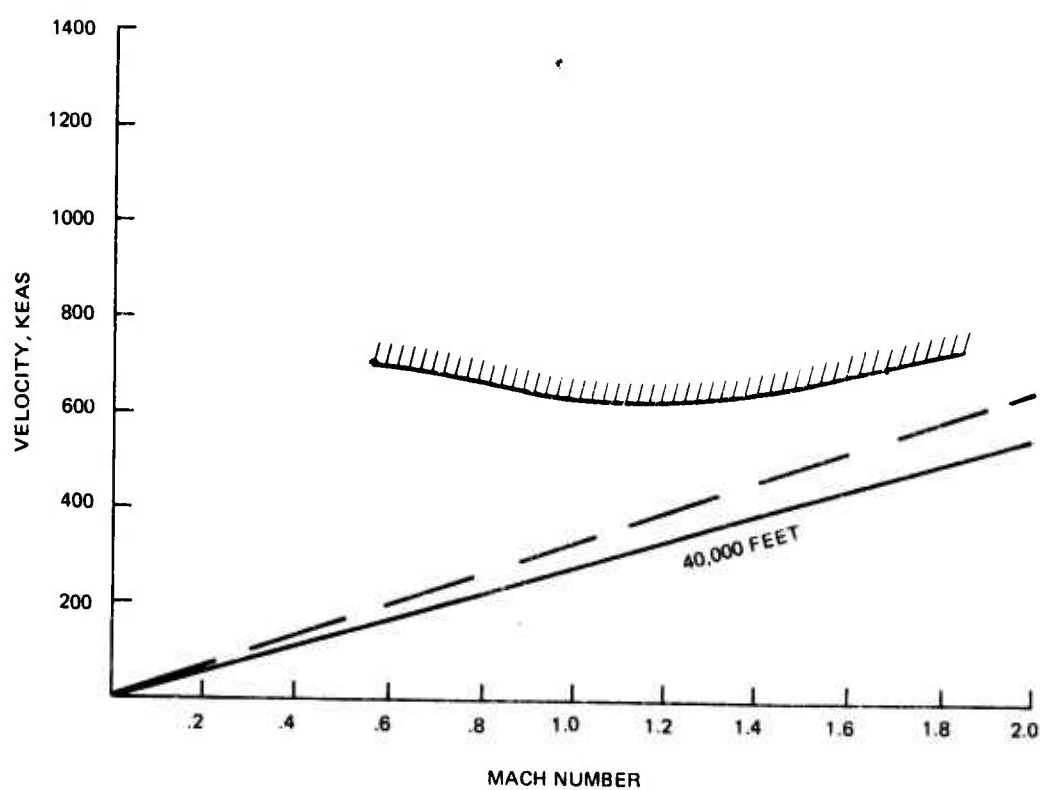


Figure 278. Fin-Rudder Flutter Envelope, 40,000 Ft

5.7 FUSELAGE STRUCTURAL ARRANGEMENT AND DETAIL DESIGN

The fuselage, which is strength designed primarily by symmetric and asymmetric high g flight maneuvers and 10 fps landing conditions, must also meet many other design requirements as indicated in Figure 279. The pressurization of the cockpit dictates the detail design of a large portion of the fuselage. Hinged actuated doors are provided for the nose landing gear and a portion of the forward fuselage structure is designed by hard nose-down landings. Quick opening access doors and panels are required for the gun, gun drum, and avionic equipment. The latter is located just aft of the cockpit.

Fuel tanks occupy most of the volume of the mid and aft fuselage. The surrounding structure must therefore be capable of supporting the fuel tank pressures which are a combination of a constant positive pressurization and pressure caused by maneuver translational and rotational accelerations. Fuel pressures encountered during in-flight refueling must also be considered. The inlet duct structure must be designed to withstand the very high inlet pressures associated with hammer shock waves generated during engine stalls at high Mach numbers.

The main landing gear is located in the mid-fuselage and is mounted off the bulkhead at Fuselage Station (FS) 600. Hinged actuated main landing gear doors are provided to close off the main gear stowage compartment. A trough for electrical and hydraulic lines is located at the top of the fuselage and removable panels cover this area. In addition, numerous access panels and doors must be provided to maintain the control surfaces actuators and oil and fuel pumps.

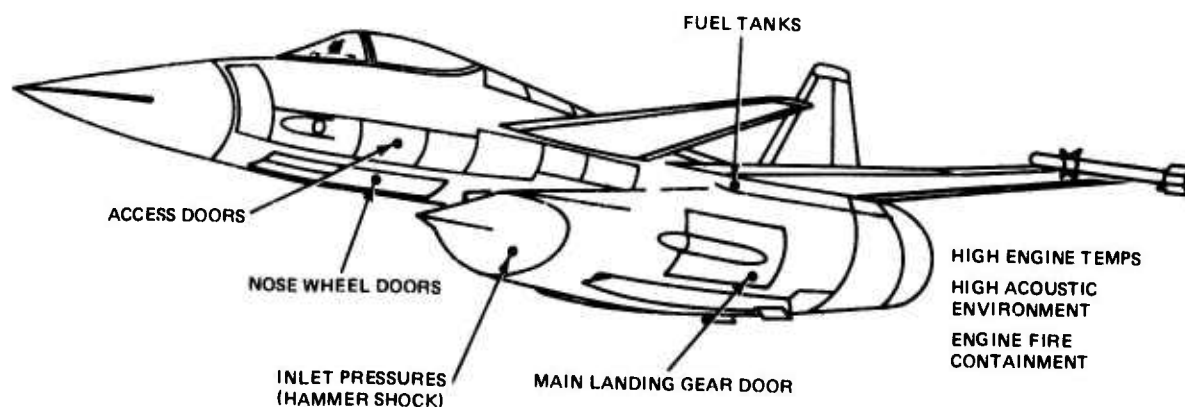


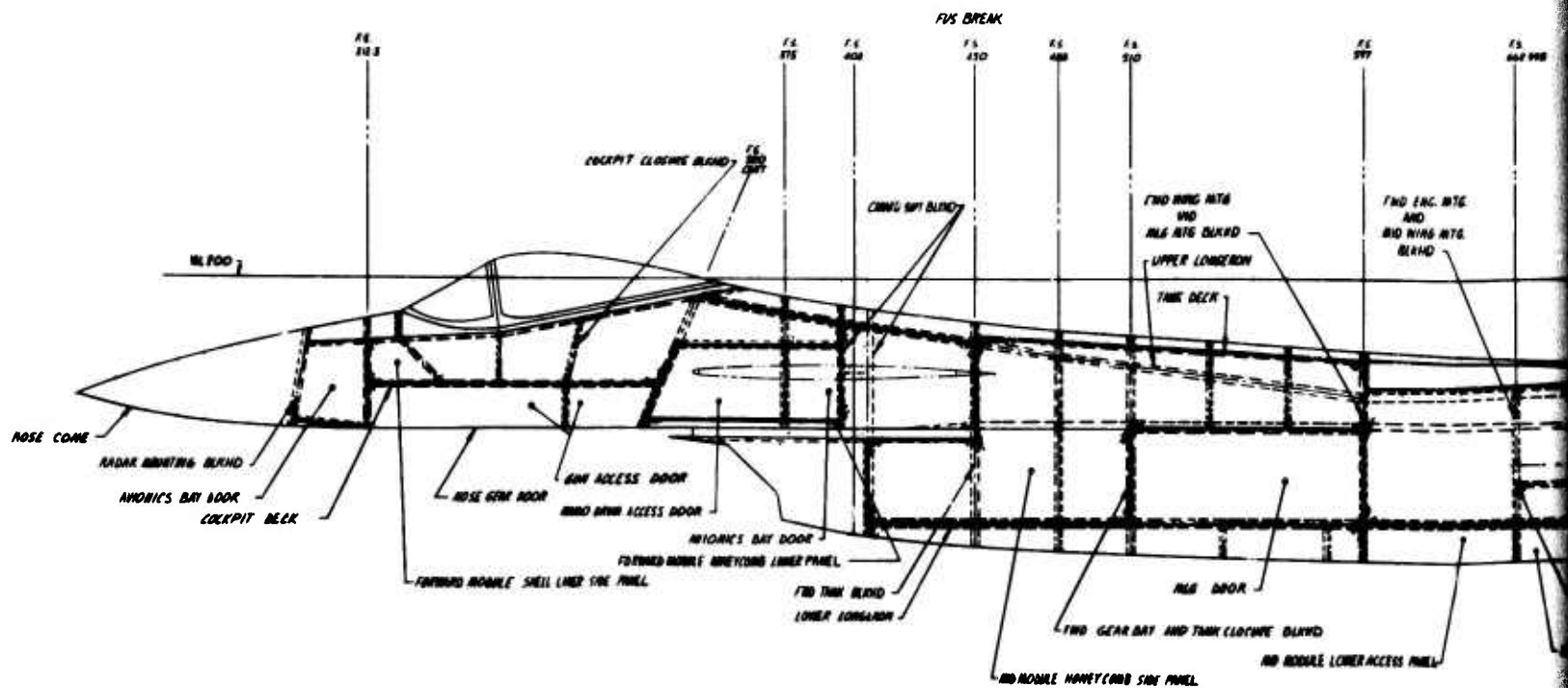
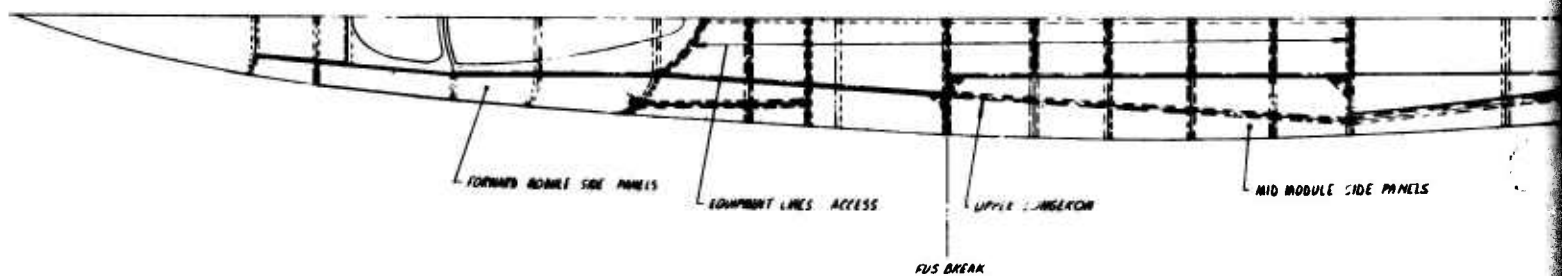
Figure 279. Fuselage Design Requirements

The extreme aft fuselage structure is designed by the extreme engine environment of high temperatures and acoustic levels. Consideration was given to fire containment by providing a fire containment shield. Access doors are needed for normal engine maintenance. Engine removal is accomplished by moving the engine directly aft so engine removal doors are not required.

5.7.1 Structural Arrangement

The fuselage structural arrangement, presented in Figure 280 is of semi-monocoque construction comprising 17 major Gr/Ep frames and bulkheads, a Gr/Ep structural outer shell and a Gr/Ep structural inlet duct. The bulkheads and frames serve to stabilize the shell, as well as provide shear redistribution and hard point attachment. Since several of the bulkheads perform multiple functions, the number of bulkheads and frames has been minimized. The outer shell is the primary shear carrying structure and also functions as a pressure vessel in the areas of the cockpit and integral fuel tanks. A structural inlet duct has been incorporated into the design, and was sized to transmit primary fuselage shear loads across the main landing gear well. Structural decks and webs tie the duct to the outer shell. The duct was designed to withstand hammershock pressure and fuel pressures where it forms walls of the integral fuel tanks.

The fuselage bending moments, vertical and lateral, are resisted primarily by six longerons, two upper, two lower and two mid. The fuselage shell panels are configured primarily as shear carrying with a relatively low longitudinal modulus of elasticity but due to strain compatibility with the longerons, a small percentage of the bending moment will be transmitted to the shell. The upper longeron in the structural arrangement was initially located such that it extended across the top of the wing. This location was originally selected because it provided maximum depth between longerons and a straight run without "kicking". This arrangement did present some problems. First, it meant that the longeron would have to be spliced at FS 597 and 701 to allow the wing box installation and, second, support of this compression longeron had to be considered. Design studies were conducted on this arrangement with two approaches. The first consisted of attaching the upper longeron directly to the upper wing box cover which would then become the upper longeron. This created a redundant load path for both vertical and lateral wing loads causing wing deflections to induce large transverse loads on the longeron splices at FS 597 and FS 701. The second approach consisted of splicing the longeron to a distinct member running over the wing box. This member would have to be connected to



6-11-64
BEST AVAILABLE COPY

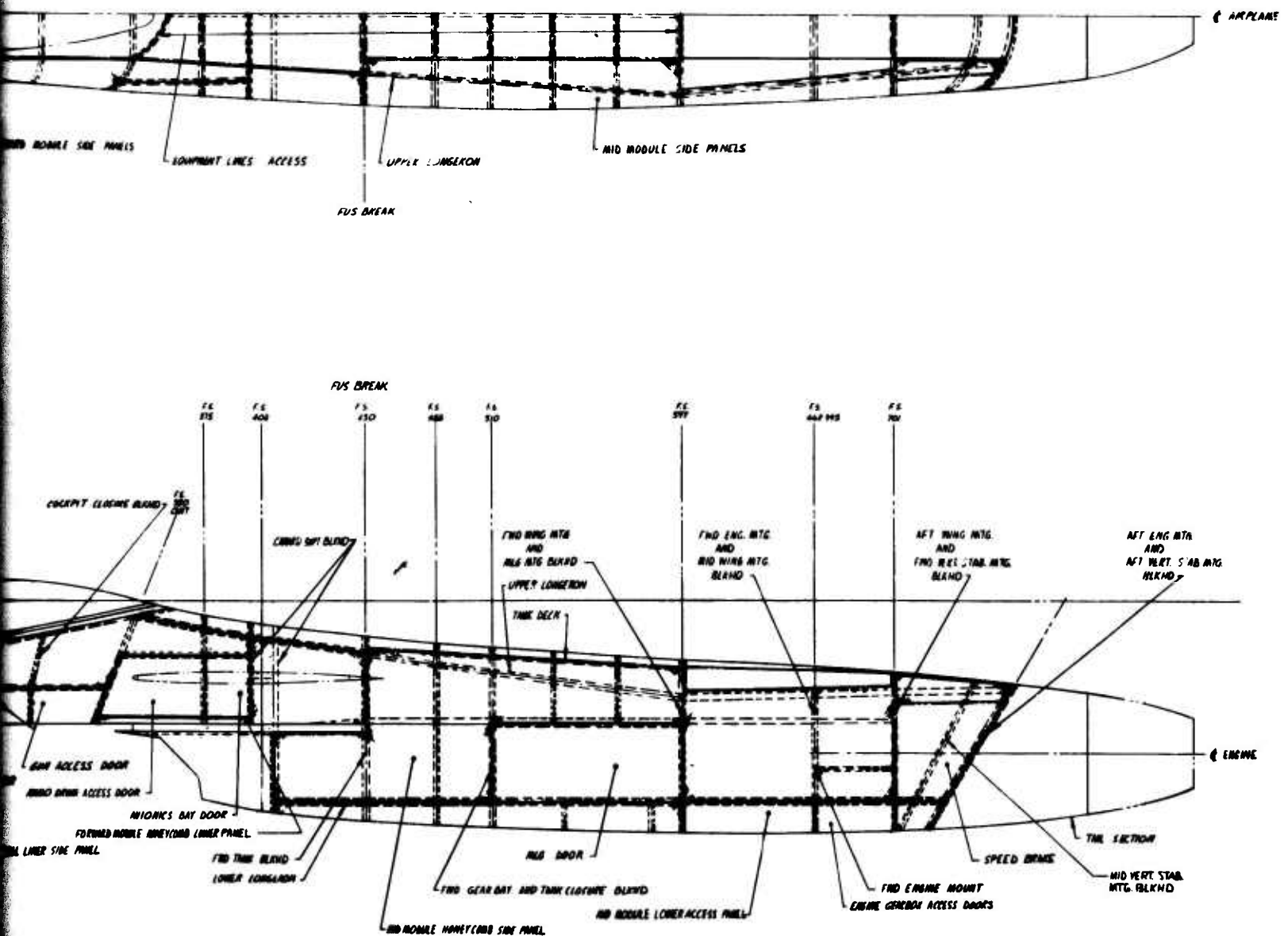


Figure 280. Fuselage Structural Arrangement

the wing by a flexible drag angle. The drawback in this arrangement was that the longeron is highly loaded in compression during flight maneuvers and would have to be designed as an unsupported column over a 102-in. length. It was, therefore, decided to reroute the longeron to pass under the wing where it could be supported by the fuselage shell structure and the attachment to the wing would be by means of a flexible drag angle. This introduces a "kick" at FS 600 but appears to be the most feasible arrangement.

Forward of FS 450 (which is the location of the manufacturing splice) a centerline keel is employed, running to the aft cockpit closure bulkhead. Incorporation of this member was necessary due to the many access doors required in the forward fuselage area for such items as avionics, gun, ammunition, etc.

5.7.2 Detail Structural Design Concept

The skin panel boundaries and type of construction for the fuselage are shown in Figure 280. The forward module outer shell is composed of four fixed panels; left and right hand side and lower panels plus a number of access panels and doors.

The side panel, Figure 281, utilizes the shell liner concept, with unidirectional Gr/Ep orientated circumferentially, to beam the cockpit internal pressure between the upper longeron and the cockpit floor. The upper longeron is integrally molded and consists of a high percentage of unidirectional Gr/Ep oriented longitudinally to carry the fuselage and local longeron bending loads.

The cockpit floor is an orthotropic honeycomb panel with greater transverse stiffness as it is supported by the side panels and nose wheel well beams. External ply build-ups on the face sheets permit the use of a constant depth core with densified core being used to accommodate the crushing loads from the supports.

The lower panel, Figure 282, is a honeycomb panel and permits integrally molding the mid longeron, which traverses from a horizontal plane where it splices to a discrete member at FS 320 to an almost vertical plane where it splices at FS 450. The duct is a thick honeycomb sandwich and has a non-circular cross section at this location. It is supported by transverse frames and the center keel.

The outer shell, Figure 283, of the mid module is comprised of three fixed panels: a left and right hand side panel and an aft upper panel, plus a number of access panels and doors. The side panels are large (25 ft) one-piece honeycomb panels with longitudinally oriented uni-directional Gr/Ep forming the integrally molded lower, mid and upper

[illegible]

5.7.3 Landing Gear and Landing Loads

Both the nose and main gear have a 10-in. stroke with 4-in. and 3-in. static positions respectively as measured from the fully compressed position. The stowage of the main gear was studied to determine a retraction system that would minimize the aircraft cross section. This requires rotation of the gear of approximately 180° during retraction. A rotation collar attached to the drag brace would rotate the collar approximately 90° and

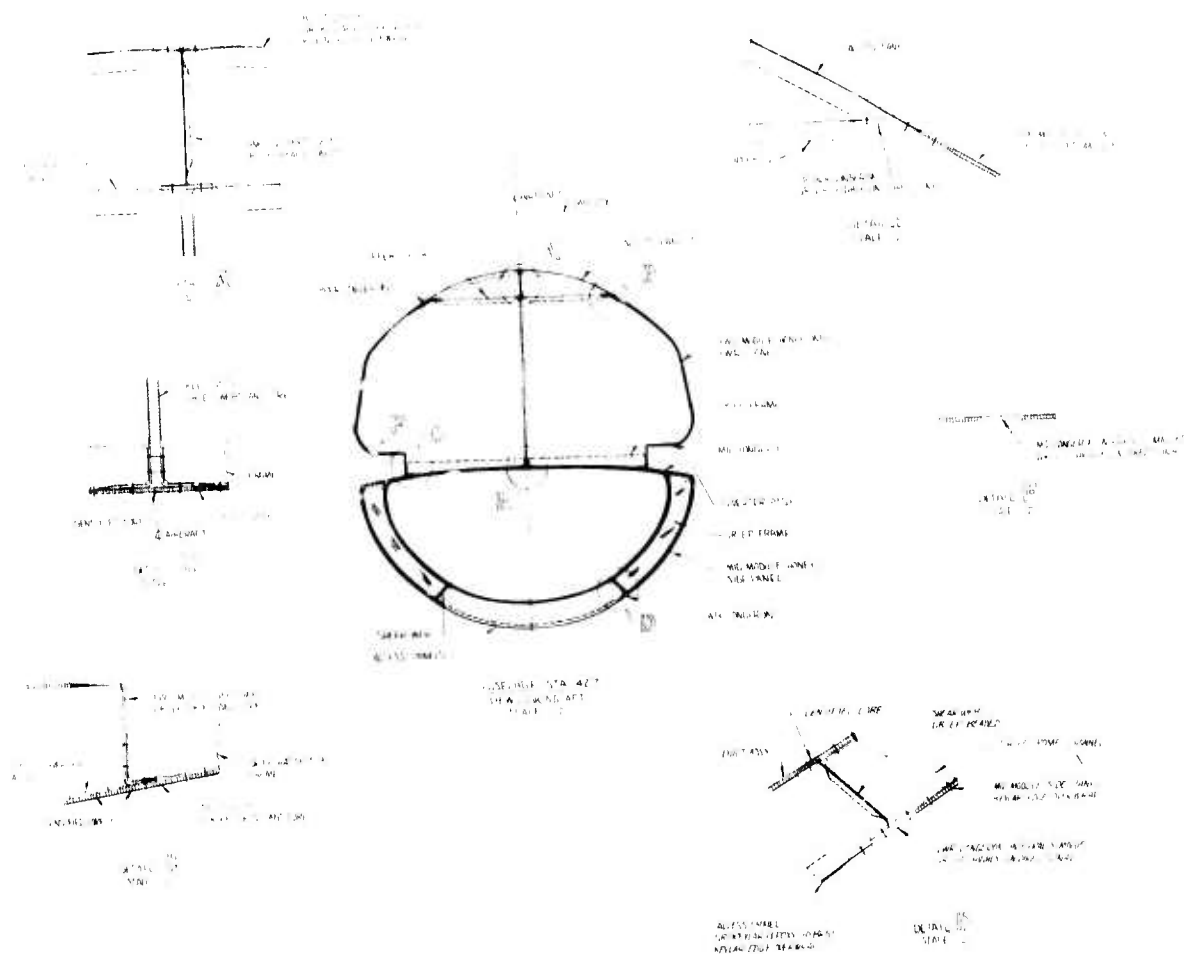


Figure 282. Fuselage Structural Arrangement — Station 427

TABLE 56. ADCA PRELIMINARY LANDING GEAR LOADS (LIMIT)

Condition	Nose Wheel	Main Left	Main Right	Remarks Loads Per Mil-A 008862A
2 Point Braked Roll $W = 1.2 \times 40017 = 48,020$ lb	$V_N = \dots$ $D_N = \dots$ $S_N = \dots$	$V_{ML} = 24,010$ $D_{ML} = 19,208$ $S_{ML} = \dots$	$V_{MR} = 24,010$ $D_{MR} = 19,208$ $S_{MR} = \dots$	Paragraph 3.3.1.1
3 Point Braked Roll $W = 1.2 \times 40017 = 48,020$ lb	$V_N = 12,298$ $D_N = \dots$ $S_N = \dots$	$V_{ML} = 17,863$ $D_{ML} = 14,290$ $S_{ML} = \dots$	$V_{MR} = 17,863$ $D_{MR} = 14,290$ $S_{MR} = \dots$	Paragraph 3.3.1.2
Unsymmetrical Braking $W = 47,720$ lb	$V_N = 8590$ $D_N = \dots$ $S_N = 3340$	$V_{ML} = 19,565$ $D_{ML} = 15,652$ $S_{ML} = 1670$	$V_{MR} = 19,565$ $D_{MR} = \dots$ $S_{MR} = 1670$	Paragraph 3.3.1.3
Reverse Braking $W = 47,720$ lb	$N = \dots$ $D_N = \dots$ $S_N = \dots$	$V_{ML} = 23,860$ $D_{ML} = -19,088$ $S_{ML} = \dots$	$V_{MR} = 23,860$ $D_{MR} = -19,088$ $S_{MR} = \dots$	Paragraph 3.3.1.4
Turning $W = 1.2 \times 40017 = 48,020$ lb	$V_N = \dots$ $D_N = \dots$ $S_N = 2016$	$V_{ML} = 5762$ $D_{ML} = \dots$ $S_{NL} = -2880$	$V_{MR} = 38,223$ $D_{MR} = \dots$ $S_{NR} = 19,112$	Paragraph 3.3.2
Turning + 625 μ Braking @ 48,020 lb	$V_N = 10,756$ $D_N = 5378$ $S_N = 5378$	$V_{ML} = 2401$ $D_{ML} = -1501$ $S_{ML} = -1200$	$V_{MR} = 34,862$ $D_{MR} = 21,789$ $S_{MR} = 17,431$	
Pivoting $W = 47,720$ lb	$V_N = 4008$ $D_N = \dots$ $S_N = \dots$	$V_{ML} = 21,855$ $D_{ML} = 17,484$ $S_{ML} = \dots$ $M_{ZL} = \dots$	$V_{MR} = 21,855$ $D_{MR} = \dots$ $S_{MR} = \dots$	Paragraph 3.3.3

Sign Convention: + V up, D Aft, S inbd

TABLE 57. ADCA PRELIMINARY LANDING GEAR LOADS

Condition	Nose Wheel	Main Wheel		Remarks
		Left	Right	
Taxiing W = 47,720 lb	$V_N = 12,025$	$V_{M_L} = 43,711$	$V_{M_R} = 43,711$	Paragraph 3.3.4.s Dyn. Analysis of 3.3.4.1 will have to be checked.
Towing W = 47,720 lb	$V_N = 1318$ $D_N = 10,519$ $S_N = \text{----}$	$V_M = 23,206$ $D_{M_L} = \text{----}$ $S_{M_L} = \text{----}$	$V_{M_R} = 23,206$ $D_{M_R} = \text{----}$ $S_{M_R} = \text{----}$	Paragraph 3.4.1
	$V_N = 6698$ $D_N = 10,519$ $S_N = \text{----}$	$V_{M_L} = 20,511$ $D_{M_L} = \text{----}$ $S_{M_L} = \text{----}$	$V_{M_R} = 20,511$ $D_{M_R} = \text{----}$ $S_{M_R} = \text{----}$	
Tow Load App. (From 0° to Max)	$V_N = 4008$ $D_N = \pm 5259$ $S_N = 0$	$V_{M_L} = 21,855$ $D_{M_L} = \text{----}$ $S_{M_L} = \text{----}$	$V_{M_R} = 21,855$ $D_{M_L} = \text{----}$ $S_{M_L} = \text{----}$	Tow Loads on Main Gear to be checked
Jacking W = 47,720 lb	Gear Points Vertical 1.35G, Horizontal 0.4G Other Points Vertical 2G, Horizontal 0.5G			Paragraph 3.4.2

Sign Convention + D(Aft), + S(Inbd)

TABLE 58. ADCA PRELIMINARY LANDING GEAR LOADS (LIMIT)

L.D. G.W. = 40,017 lb, $V_V = 10$ fps
 Loads are LIMIT per MIL-A-008862A

Main Strut Stroke = 10 in.
 Nose Strut Stroke = 10 in.

Attitude		Ground Loads	Strut Loads @ Axle
3 Point Level Nose Gear	Maximum Vertical	$V_N = 12,300$	$F_{SA} = 12,300$
	Spin Up	$V_N = 12,300$	$F_{SA} = 9899$
		$D_N = 5444$	$F_{SD} = 7622$
	Spring Back	$V_N = 12,300$	$F_{SA} = 12,300$ $F_{SD} = -6805$
2 Point Level	Spin Up	$V_{MLR} = 37,329$	$F_{SA} = 37,329$
		$D_{MLR} = 20,531$	$F_{SD} = 28,743$
	Spring Back	$V_{MLR} = 43,711$	$F_{SA} = 43,711$ $F_{SD} = -25,663$
12° Tail Down	Spin Up	$V_{MLR} = 37,329$	$F_{SA} = 40,990$
		$D_{MLR} = 20,531$	$F_{SD} = 16250$
	Spring Back	$V_{MLR} = 43,711$	$F_{SA} = 42,590$ $F_{SD} = -31898$
Drift Landing 2 Point Level		Left Main $V_{ML} = 21,855$ $D_{ML} = 0$ $S_{ML} = 17,484$	Right Main $V_{MR} = 21,855$ $D_{MR} = 0$ $S_{MR} = -13,113$

Ultimate net fuselage loads were calculated for the two most critical landing conditions and are presented in Figures 286 and 287. Landing condition (3) is a two-point level landing with maximum spin-up and is critical for the aft fuselage while condition (4) is a two-point 12° tail down landing with maximum spring back and is critical for the fuselage forward of FS 625. For comparison purposes, the ultimate net fuselage loads for the critical flight conditions are also shown. It can be seen that a good portion of the bottom fuselage (aft of FS 450) will be designed in compression by the landing conditions.

Preliminary sizing of the landing gear, tires and brakes have been completed. At the maximum takeoff gross weight of 47,720 lb, which includes 12,000 lb of external stores, the static loads (per gear) are 4008 lb and 21,855 lb for the nose and main gear respectively.

5.7.3.1 Nose Gear Tire

Maximum Static Load @ 47,720 lb = 4008 lb

Maximum Dynamic Load @ 47,720 lb = 8303 lb

(Braking @ 10 ft/sec²)

Per AFSC DH 2-1 - Dynamic Load $\leq 1.35 \times$ rated load DN 4A3 Paragraph 5.2.

Therefore: minimum rated load = $\frac{8303}{1.35} = 6150$ lb

Per AFSC DH 2-1 } - Requires allowance for 25% growth within same size tire.
DN 4A3 Paragraph 5.1.

Therefore; Growth Rated Load = $1.25 \times 6150 = 7687$ lb

Figure 284 presents nose tire information for two candidate tires. The tire that meets the growth rated load is the 22 x 6.6 -10 16 PR rated at 7960 lb and used on the F-111A and the F-15. Based on this preliminary study this tire would be the recommended selection but for a final design, further study should be made to determine if the 25% growth factor required by specification might be too conservative for this type of aircraft. On that basis, an alternate choice could be the 20 x 5.5 -10 12 PR tire, rated at 6150 lb and used on the A-6A and E-2A. Growth is available in 14 PR and 16 PR tires in production and used on the F-8H (and J) and EA-6B.

5.7.3.2 Main Gear Tire

Maximum Static Load @ 47,720 lb = 21,855 lb

Growth Rated Load = $1.25 \times 21,855 = 27,320$ lb

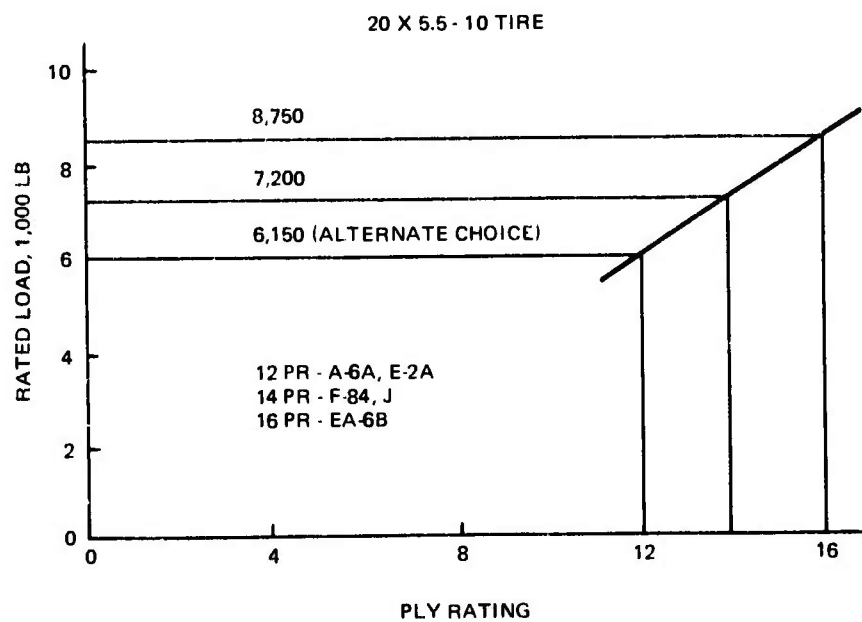
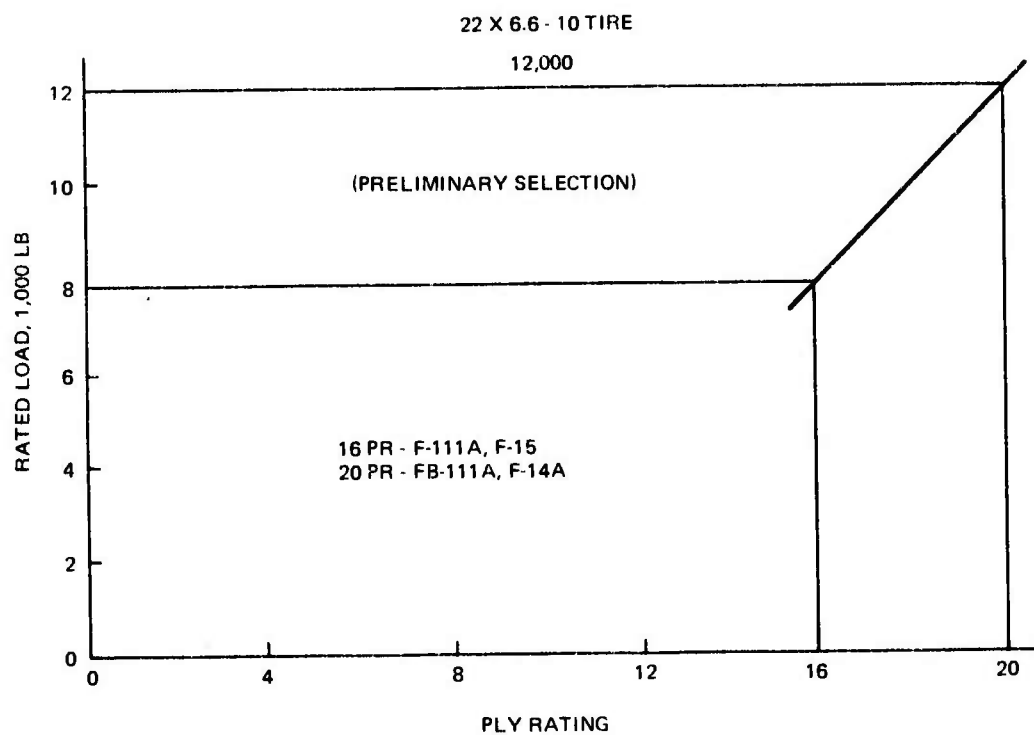


Figure 284. ADCA Nose Gear Tire Data

Three candidate tires would be the 30 x 8-18 26 PR, rated at 24,100 lb, the 32 x 8.8-16 24 PR, rated at 23,300 lb and the 34.5 x 9.75-18 22 PR rated at 23,400 lb. The recommendation would be to select one of these tires and allow for growth by increasing the ply rating. Subsequent brake sizing indicated that the 16-in. wheel was too small and an 18-in. wheel would be required to provide sufficient brake capacity. Based on this information, a 34.5 x 9.75-18 22 PR tire is recommended.

5.7.3.3 Brake Sizing

The preliminary brake sizing was based on a landing design gross weight of 39,759 lb and a maximum landing design gross weight of 47,302 lb. Three types of landings are considered: normal landing with chute; emergency landing with and without chute, and rejected takeoff with chute. A weight tradeoff was conducted to arrive at the minimum weight brake, assuming carbon brakes, and the results are summarized in Table 59.

**TABLE 59. PRELIMINARY BRAKE SIZING ENERGY REQUIREMENT - MIN.
WEIGHT BRAKE**

	Aircraft Kinetic Energy, 10 ⁶ Ft-Lb		Estimated Chute Energy, 10 ⁶ Ft-Lb	Brake Energy, 10 ⁶ Ft-Lb
Normal Landing @ 39,759 lbs; 188 kt 45 Stops	59.4		26.4	16.5
Emergency Landing @ 41,860 lb @ 193 kt 5 Stops with Chute 2 Stops Without Chute	65.5	5	29.3	18.3
		2	----	32.98
Rejected Takeoff @ 47,320 lb; 205 kt 2 Stops	84.12		37.3	23.4

To achieve this minimum weight brake, the chute is sized by the RTO requirement at 205 kt resulting in a maximum chute load of 12,572 lb. A chute diameter of 8.5 ft is needed which may be too large for this aircraft. The brake will have to accommodate 18.9 million ft-lb of normal energy which necessitates a wheel diameter no smaller than 18 in. The 34.5 x 9.75 - 18 tire with 18-in. rim is presently used on the F-15. Brake sizes are presented in Figure 285.

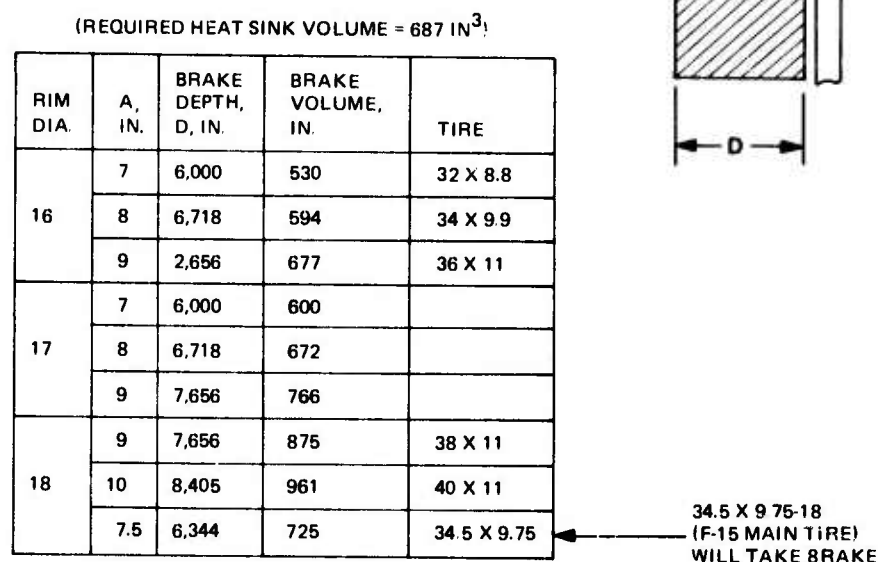


Figure 285. Brake Sizing

5.7.3.4 Composite Usage

Certain landing gear components such as drag braces or similar long parts are candidates for composite construction. Final determination of composite usage depends on the detail design of the landing gear.

5.7.4 Fuselage Flight Design Conditions

The applied air loads for the critical flight conditions are presented in the Loads and Criteria section. Distributed fuselage air loads for the symmetrical flight conditions and for the symmetrical portion of the rolling pullouts are also presented in that section. Two symmetrical conditions were selected as critical for the fuselage and were used for the design of the fuselage. Both are supersonic 6.5 g maneuvers ($M = 1.60$ at 50,000 ft); one balanced, and the other has a pitch acceleration of -6.2 rad/sec^2 . Net fuselage loads were calculated for the two conditions and are presented in Figures 286, 287 and 288.

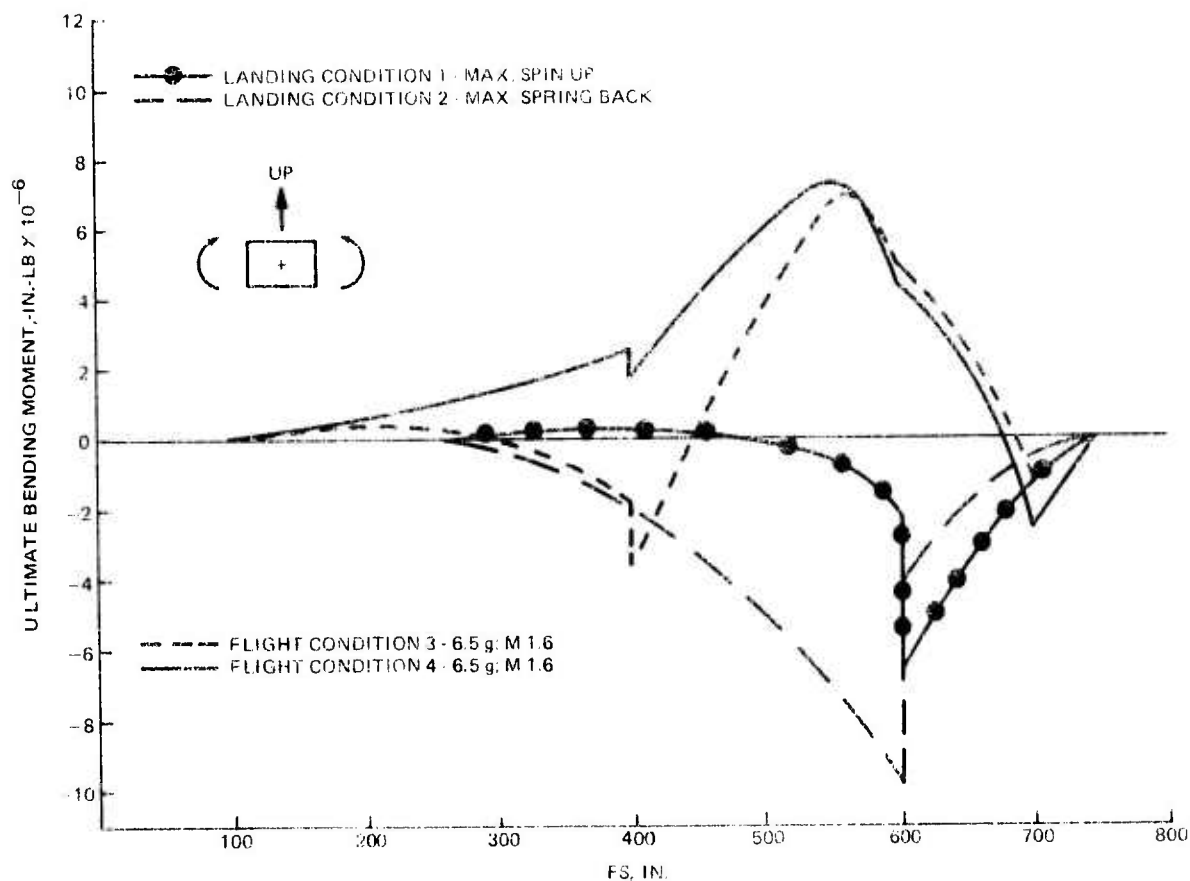


Figure 286. ADCA Fuselage Ultimate Vertical Bending Moment

Air loads for two rolling pullouts were calculated and are given in the Loads and Criteria section. Both conditions have a symmetrical load factor of 5.2 g. The first condition is at $M = 1.60$ at 50,000 ft and has the maximum antisymmetrical canard loads and thus imposes the critical torsion on the mid-fuselage. The second condition is at $M = 0.90$ at sea level and has the maximum antisymmetrical wing loads. The latter condition is critical for some parts of the wing/fuselage attachment.

5.7.5 Acoustic Levels

The predicted sound pressure levels at six zones on the ADCA for engine noise for a maximum afterburner ground run-up are shown in Figure 289. The free-field values were taken as a composite of the highest overall values derived using the GE Prediction (Figure 15 APP J CP45B002B) and USAF Rpt ASD TDR 62-26. These were then empirically corrected to account for the presence of the air vehicle.

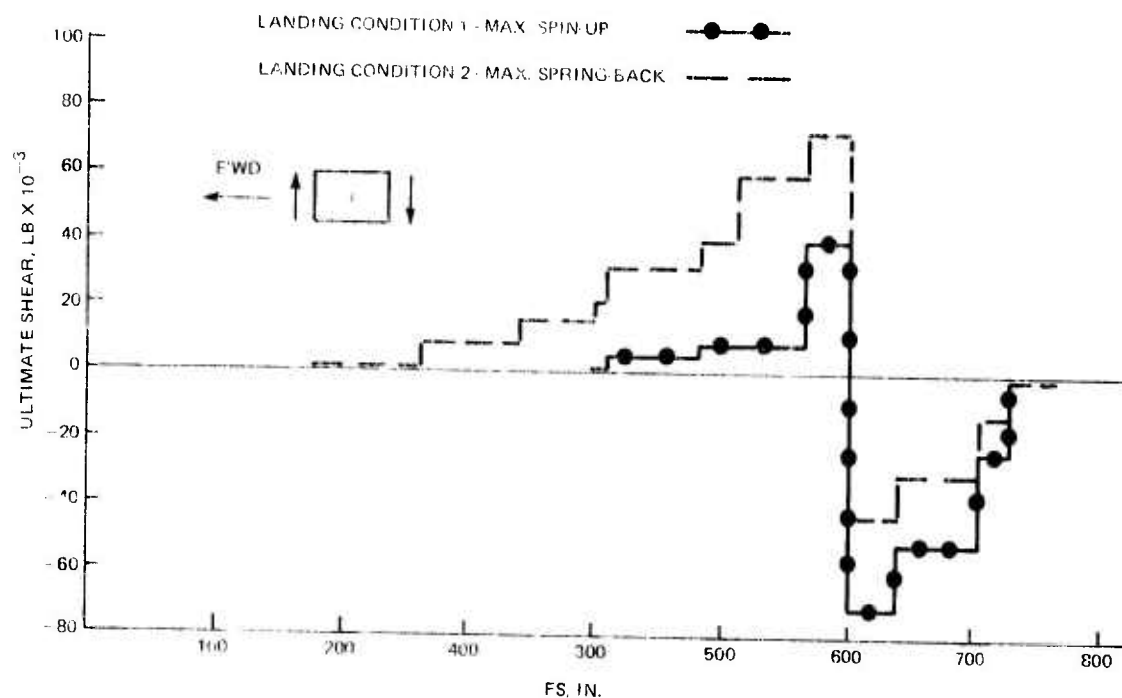


Figure 287. ADCA Fuselage Ultimate Vertical Shear

The db spectra for the six octave bands considered were derived using ASD TDR 62-26, Figure 4 and are shown in Figure 290.

Finally, the Mahaffey/Smith transformations (Ref. FZS-12-057, Pg. 59) originally derived for use on the B-58 program were used to establish the vibration levels (RMS G's) shown in Figure 291, based on the sound pressure levels given above. Eighty percent confidence levels were employed.

While boundary layer noise, engine noise in flight, and transonic shock-induced fluctuating pressures have yet to be considered, the data presented herein demonstrates the relatively low acoustic environment to be anticipated for all primary structure of the ADCA and assures that the design impact for acoustic stress and fatigue will be minimal.

5.7.6 Internal Pressurization

The fuselage shell, in addition to resisting the shears and bending moments of the critical landing and flight conditions, is also subjected to internal pressures. The cockpit is pressurized by the ESC system to maintain a particular altitude pressure; the inlet experi-

ences very high pressures from hammer shock during engine stalls at high Mach numbers and the fuel tank walls must sustain fuel pressures resulting from translational and rotational accelerations and from valve malfunctions during the fuel dump. These pressures have been determined and were included in the fuselage sizing and structural tradeoff calculations.

The cockpit pressure is established by MIL-E-38453 and MIL-A-008861A (USAF). For this class of aircraft, MIL-E-38453 specifies that an 8,000 ft altitude must be maintained in the cockpit up to 23,000 ft. Above that altitude, a differential pressure of 5 psi over ambient is held constant up to maximum altitude. The peak differential of 5.948 psi occurs at 23,000 ft. MIL-A-008861A (USAF) (Paragraph 3.10) requires that the pressurized differential between the structure and ambient shall be 1.33 times the maximum attainable. Thus the ultimate design cockpit pressure is $1.50 \times 1.33 \times 5.948$ which equals 11.87 psi.

The maximum limit hammer shock pressure that must be sustained by the inlet duct is estimated to be 42.4 psi which occurs at $M = 2.0$ at 31,500 ft. This estimate is based upon measured data from the F-111 and F-14A.

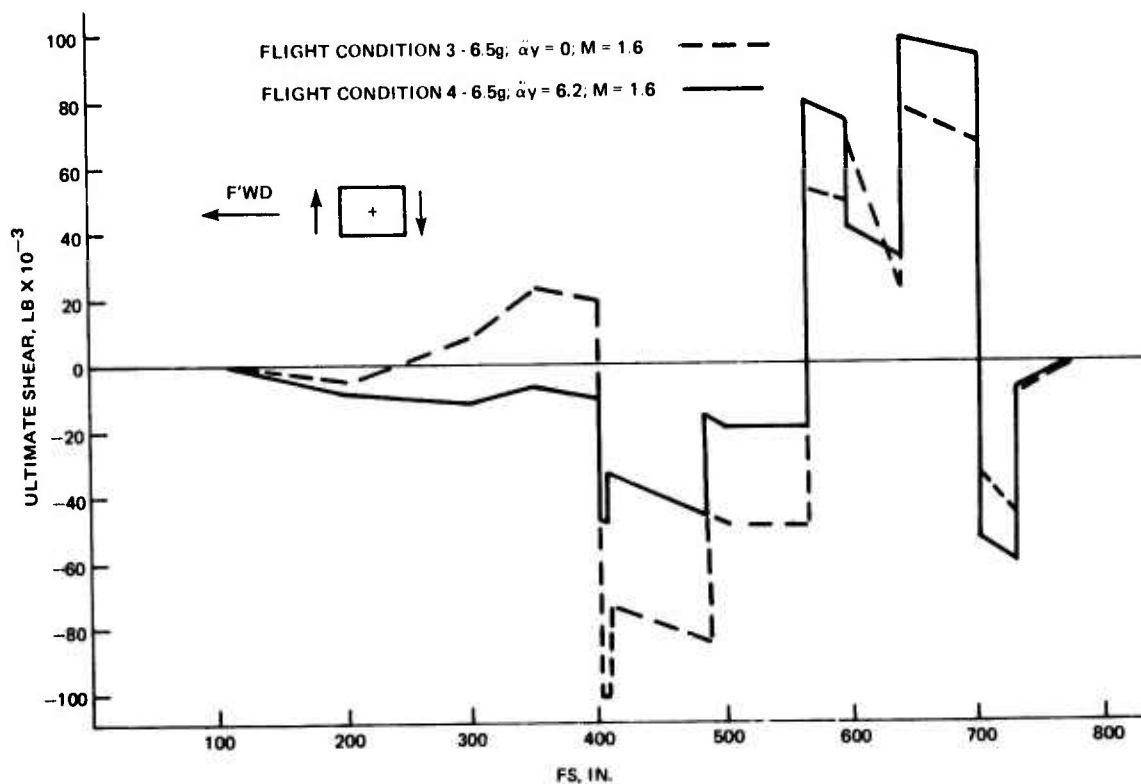


Figure 288. ADCA Fuselage Ultimate Vertical Shear

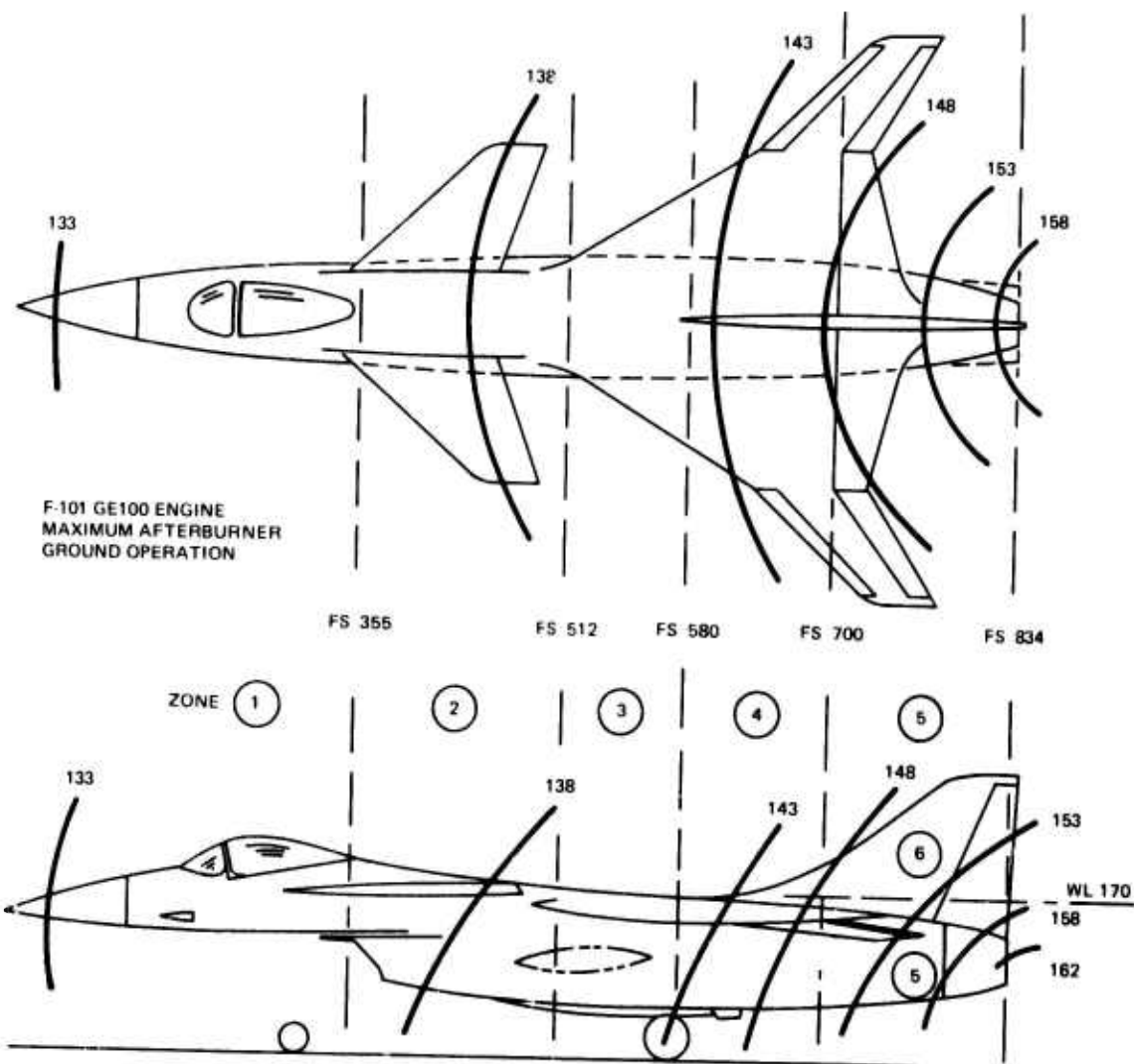


Figure 289. Overall ADCA Sound Pressure Levels

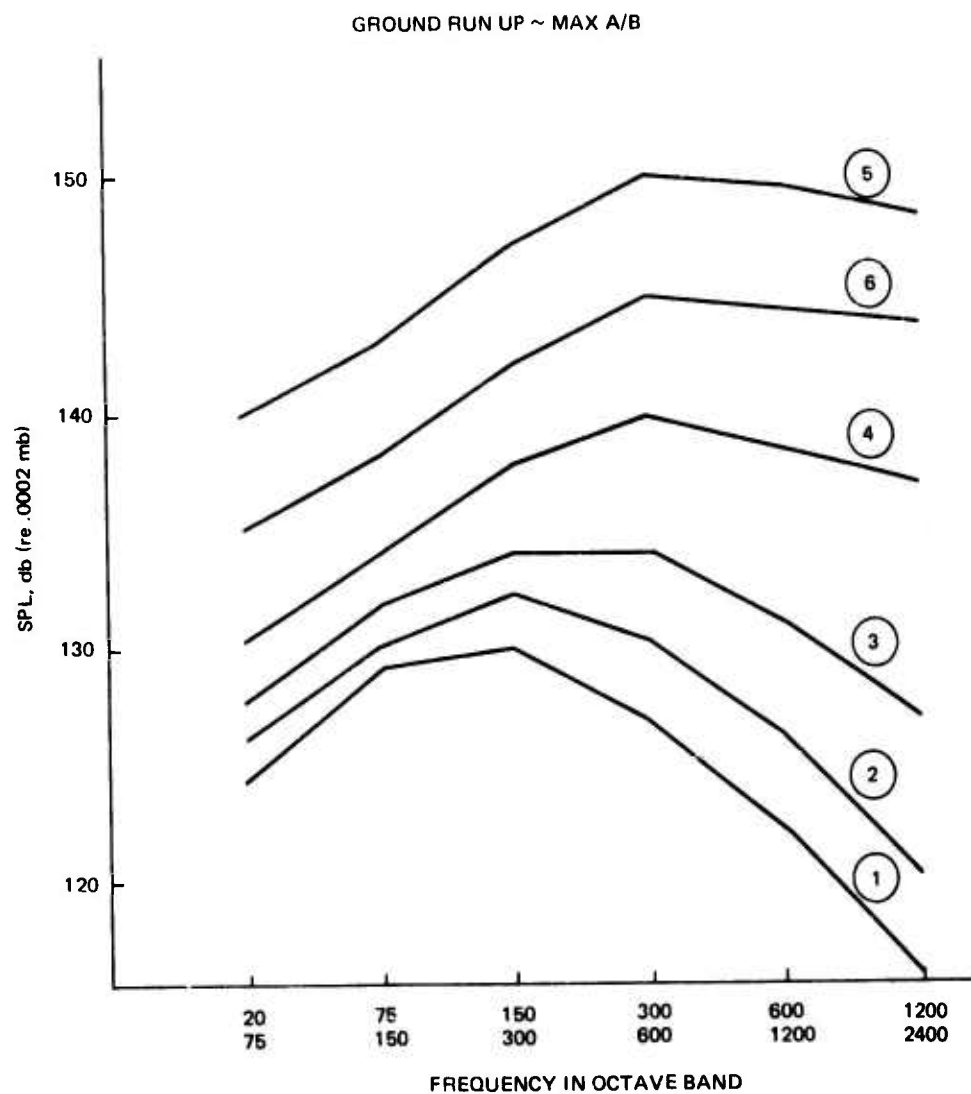


Figure 290. ADCA Predicted Sound Pressure Level for Aircraft Zones 1-6

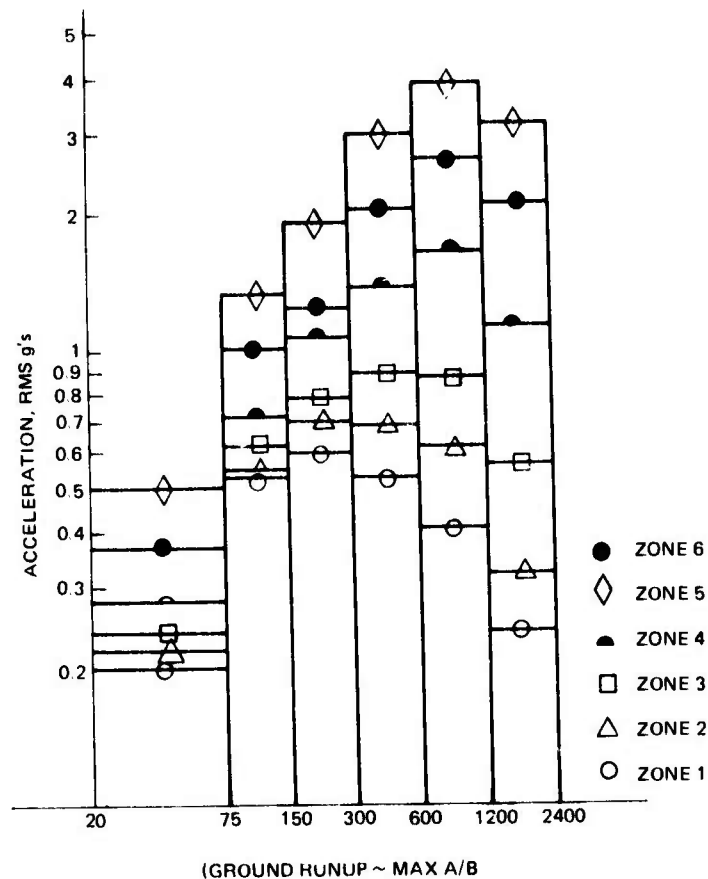


Figure 291. ADCA Predicted RMS Acceleration Levels for Aircraft Zones 1-6

During normal operation, the fuel system is unpressurized and thus the fuel pressures applied to the structure are simply a function of the hydrostatic head and the translational and rotational accelerations experienced by the aircraft. During fuel dump, a high fuel system pressure is a possibility in the event of a valve malfunction. This pressure is estimated to be 10 psi limit. This is combined with 1.0 g loading.

5.7.7 Engine Nacelle Structure Temperatures

An estimate was made of the engine nacelle structure temperatures for the maximum speed envelope. The results are shown in Figure 292 where a temperature range is given for each altitude/Mach number condition. The lower temperature represents the external surface structure and the higher temperature is representative of internal elements such as frames. The temperature at which absorbed moisture begins to seriously degrade the com-

pression strength of composite structure is generally considered to be 260°F. Examining the structural temperatures defined in Figure 292 it can be seen that most of the values are below 260°F except for a small portion of the speed envelope in the vicinity of the corner at Mach 2.0 and 31,500 ft. The calculations are conservative since they did not include the presence of the engine shroud which completely surrounds the engine and has been provided for fire control. This shroud, which is included in the ADCA weight estimate, consists of two titanium sheets (0.004 and 0.005-in. thick) separated by a 0.25-in. layer of RF 600 (quartz) insulation.

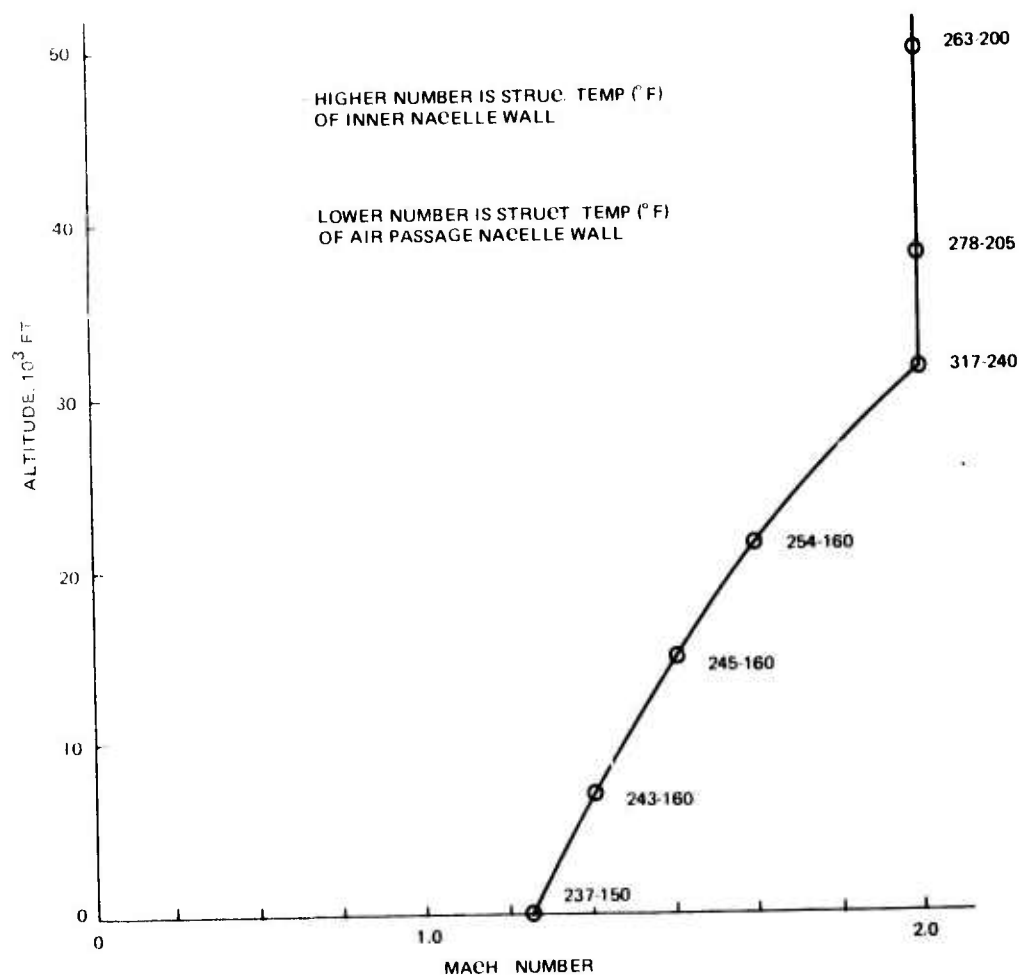


Figure 292. ADCA Nacelle Structural Temperatures at ADCA Design Speed Envelope F-101-GE-100 Engine Standard Day-Steady State-No Shroud

To obtain these temperatures several approximations had to be made. It was necessary to extrapolate the F101-GE-100 engine surface temperature given in Figure 293 to the specific flight conditions representative of the speed envelope. Since this engine surface is actually the fan air duct it was assumed that its temperature was strongly dependent on total temperature for the flight condition in question. The extent to which this engine surface exceeds total temperature was assumed to depend on the convective heat transfer coefficient in

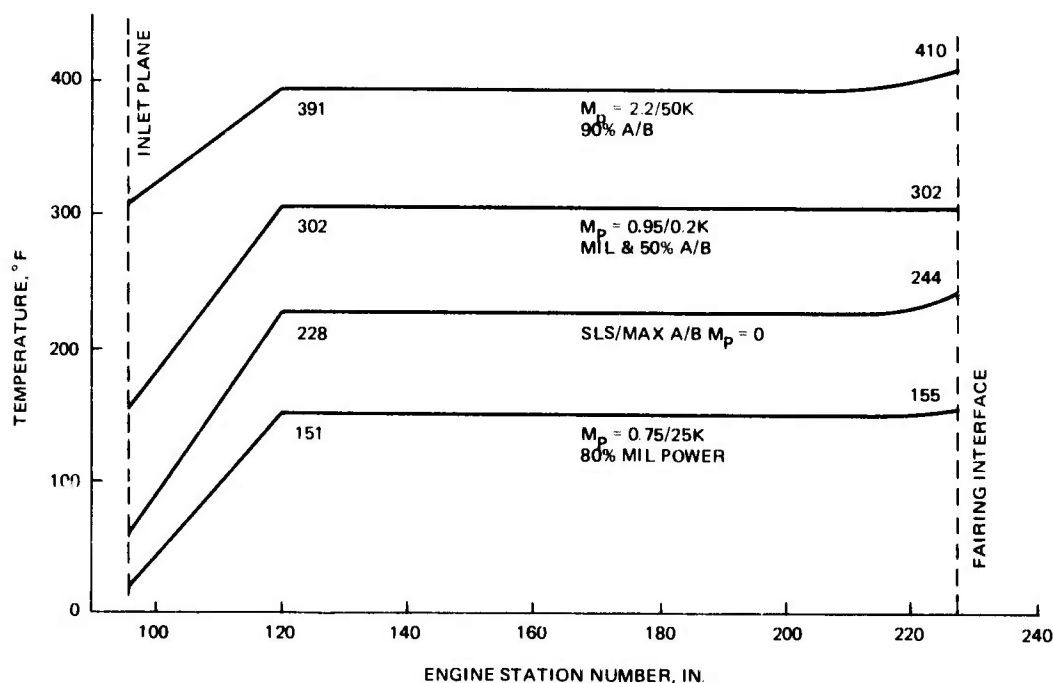


Figure 293. F101-GE-100 Estimated Engine Surface Temperature, Standard Day

the duct. This in turn is dependent mostly on altitude. The term T_E which is defined as:

$$T_E = T_{\text{Eng Surf}} - T_{\text{Total}}$$

is plotted vs altitude for the conditions given in Figure 294. The T_E was assumed to be valid for the range of Mach numbers encountered at the maximum level of the speed envelope (1.0 to 2.0) varying only with altitude as shown in Figure 294.

The structural temperatures were then obtained by assuming that the external nacelle surfaces would reach the equilibrium temperature due to aerodynamic heating from a

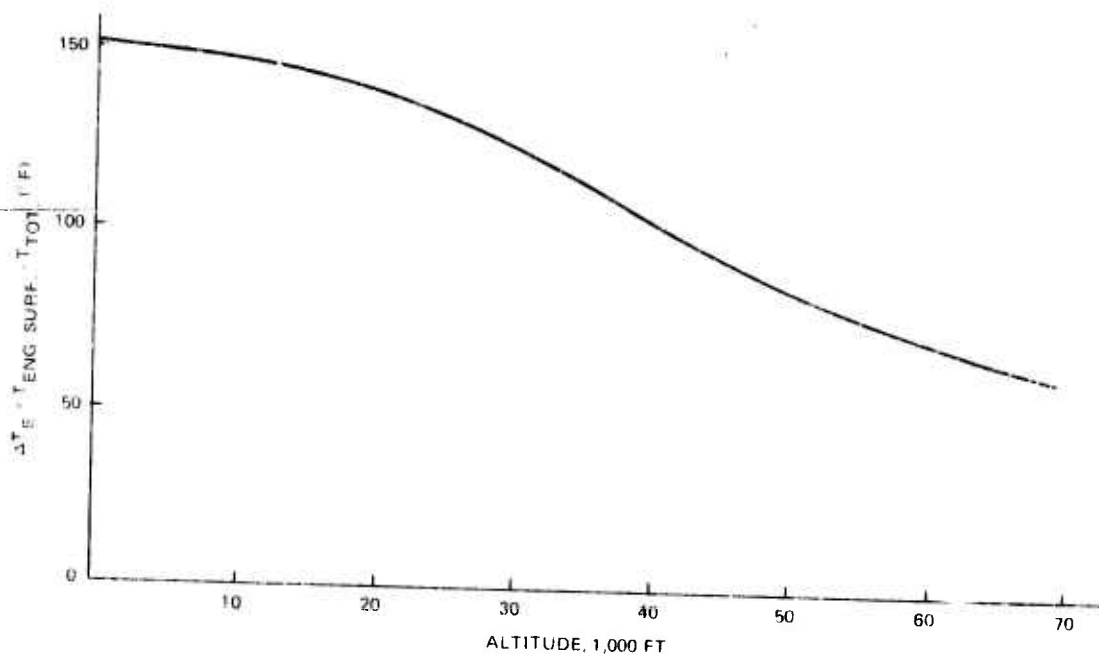


Figure 294. Estimated Effect of Altitude on Engine Surface Temperature

turbulent boundary layer, while the inner surfaces would attain a temperature that was midway between the nacelle external surface temperature and the engine surface temperature presented in Figure 293.

All conditions shown assume a standard atmosphere.

5.7.8 Fuselage Internal Load Distribution

The fuselage internal load distribution was determined by use of a computer program called "Semi-Analytical Fuselage Estimate - W9 Program" which is part of the Grumman RAVES system. This program was developed by the weights section as a tool for estimating fuselage weights during the preliminary design phase. The program, at present, is programmed for metallic allowables but these can be used for calculating internal load distribution. The fuselage must first be divided into modules up to a maximum of ten. The ADCA fuselage was divided into nine modules. Utilizing the net applied loads and fuselage geometry, Mc/I distribution is used for sizing the fuselage longitudinal elements (longerons and/or stiffeners) and shear panels (skin, decks, keels). Provision is made for including non-optimum factors to account for fuselage discontinuities or the application of longitudinal

concentrated loads. Four critical design conditions were selected for input to the W9 Program, two symmetrical landing conditions and two symmetrical flight conditions. The conditions are as follows:

- Two-Point Landing, Maximum Spin-Up (Figures 286 and 287)
- Two-Point Landing, Maximum Spring-Back (Figures 286 and 287)
- Supersonic 6.5 g Maneuver; M 1.60 @ 50,000 ft; $\alpha y = 0$ (Figures 286 and 288)
- Supersonic 6.5 g Maneuver; M 1.60 @ 50,000 ft; $\alpha y = 6.2 \text{ rad/sec}^2$ (Figures 286 and 288)

The critical longeron axial loads and shell, deck and keel shear loads are presented in Tables 60 and 61.

TABLE 60. CRITICAL ULTIMATE LONGERON LOADS (LB)

FS	Upper (1) Longeron	Cond.	Mid (1) Longeron	Cond.	Lower (1) Longeron	Cond.
212	-9301.	4	9159.	4	-	-
297	-18730.	4	14479.	4	-	-
342	-11493.	4	11330.	4	-	-
402	43498.	3	-43172.	3	0	-
450	-30154.	4	1308.	4	28846.	4
510	-52601.	4	-2004.	4	54605.	4
600	88519.	2	17500.	2	-106019.	2
663	21808.	1	8846.	1	-30654.	1
701	19466.	4	6516.	4	-25982.	4
756	0	-	0	-	0	-

Note:

(1) The designation upper, mid, and lower corresponds to the Overall Structural arrangement, Figure 280.

TABLE 61. CRITICAL ULTIMATE SIDE PANEL SHEARS (LBS/IN.)

FS to FS	Between Upper & Mid Long.	Cond.	Between Mid & Lower Long.	Cond.
212 - 297	-183.	4	-	-
297 - 342	199.	2	-	-
342 - 402	402.	3	-	-
402 - 450	-1223.	3	-687	4
450 - 510	-490.	3	-610.	3
510 - 600	882.	2	681.	2
600 - 663	-582.	1	-617.	1
663 - 701	1080.	4	1116.	4
701 - 756	-354.	4	-472.	4

A separate elastic analysis was conducted to calculate the redundant wing-to-fuselage attachment loads for the critical wing design condition. The ADCA wing is joined to the fuselage by six attachment fittings which transfer the wing loads to three bulkheads at FS 600, 663, and 702. The flexibilities of the three wing attachment bulkheads and the fuselage shell and longerons between FS 600 and 702 were included in the analysis. The flexible fuselage was then coupled to the wing finite element model. The resulting ultimate attachment loads for the final wing design condition were:

- FS 600 - 14,000 lb (compression)
- FS 663 - 65,000 lb (tension)
- FS 702 - 53,000 lb (tension)

These loads were used for the detail design studies of the wing-to-fuselage attachments.

5.7.9 Fuselage Bending and Torsional Stiffnesses

The fuselage bending (EI) and torsional (GJ) stiffnesses are based on strength design to meet the four critical flight conditions (two symmetrical and two asymmetrical) and the two critical landing conditions. These stiffnesses were calculated as a required input to the FLEXSTAB Program. Plots of the fuselage EI and GJ distribution are presented in Figures 295 and 296.

The vertical bending stiffness (EI_{yy}) curve was determined by assuming a specified longeron axial strain at the maximum ultimate vertical bending moment. The structural temperature used in establishing the specified strain was 240°F which corresponds to a speed of $M = 2.0$ at 31,500 ft. This is the extreme point on the ADCA design speed envelope. Although the critical supersonic flight maneuvers were calculated at $M = 1.60$ at 50,000 ft, this maximum structural temperature was assumed because the maneuver loads at Mach 2.0 would not be significantly lower. The room temperature allowable for Gr/Ep 0° layers in the presence of an open hole is 76,000 psi (see Section 5.1.3.2 of this report) in compression or tension. This corresponds to an allowable room temperature strain of $4,190 \mu$ in. or $3,900 \mu$ in. at 240°F. The latter value is the upper limit of the permissible longeron axial strain at 240°F. Since both the upper and lower portions of the fuselage are critical for compression loading, flight conditions for the upper and landing conditions for the lower, fuselage shell compression instability must also be considered. Based on the results of the COMFU (Composite Fuselage) runs, a maximum compression strain of $3,000 \mu$ in. appears to be a realistic number for design. This is the specified longeron axial strain used to

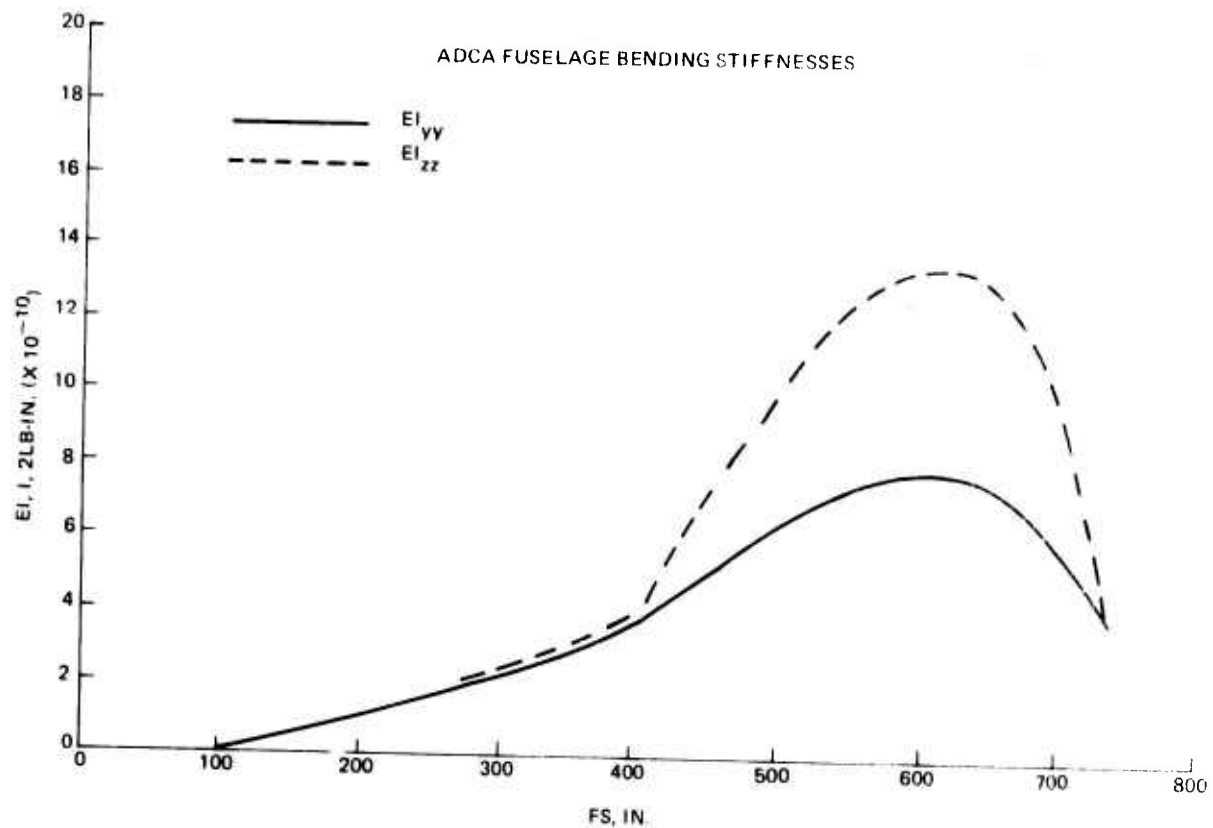


Figure 295. ADCA Fuselage Bending Stiffness

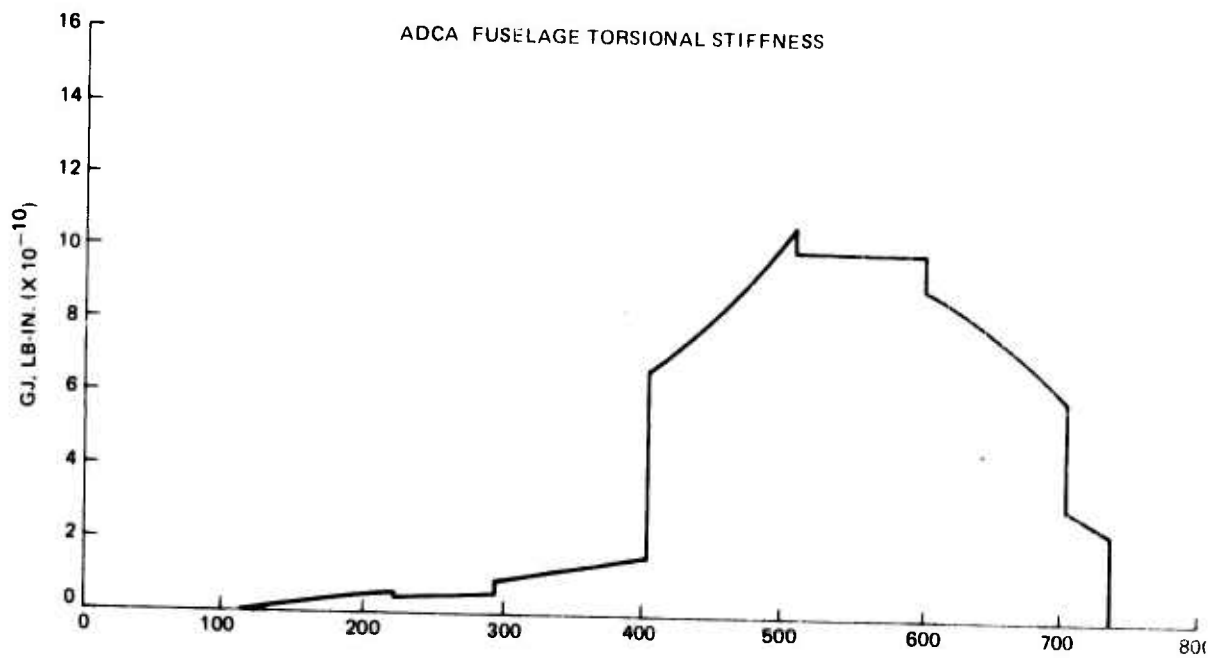


Figure 296. ADCA Fuselage Torsional Stiffness

calculate EI_{yy} . The lateral bending stiffness EI_{zz} is based on the longeron areas determined in calculating EI_{yy} .

The torsional stiffness (GJ) distribution was calculated by sizing the fuselage shell panels for the critical shear loads. In many cases, the shear loads were so low that the shell torsional stiffness was governed by the minimum layup.

5.7.10 Fuselage Shell Sizing and Tradeoffs

5.7.10.1 Side Panels

A weight comparison study was conducted for three different graphite/epoxy structural configurations: shell liner, sheet stringer, and honeycomb sandwich. Weights for these three configurations were calculated as a function of shear load intensity and the results are presented in Figure 297. The ground rule for the calculations was that the loading of the panels should not exceed the shear buckling allowable. A curve for buckled shell liner is presented for comparison purposes. A brief description of each configuration follows:

Unbuckled Shell Liner - The shell liner concept for the fuselage side was analyzed by idealizing the construction into an orthotropic cylinder by "smearing" the ring stiffnesses and adding these to the shell stiffnesses. The instability analysis used the buckling equations for an orthotropic cylinder from NASA SP-8007. These equations were used to check the stability of the shell between rings and the overall instability where the rings buckle with the shell.

By choosing a shell laminate and varying the ring bending stiffness and spacing, a curve can be drawn of the weight versus the shear buckling load. Repeating this procedure for a number of shell laminates produced the envelope curve shown in Figure 297.

It was found that for any practical ring sizing, the shell buckling between rings was always critical. A curve is included in Figure 297 for a buckled shell liner working the buckled skin to an ultimate shear stress of 19,500 psi.

Sheet Stringer - The sheet stringer configuration incorporated longitudinal hat section stiffeners at spacings varying from 3.0 to 9.0 in. The frame spacing for all calculations was assumed to be 21.0 in. which is consistent with the calculations made for the upper compression panel. See Figure 297.

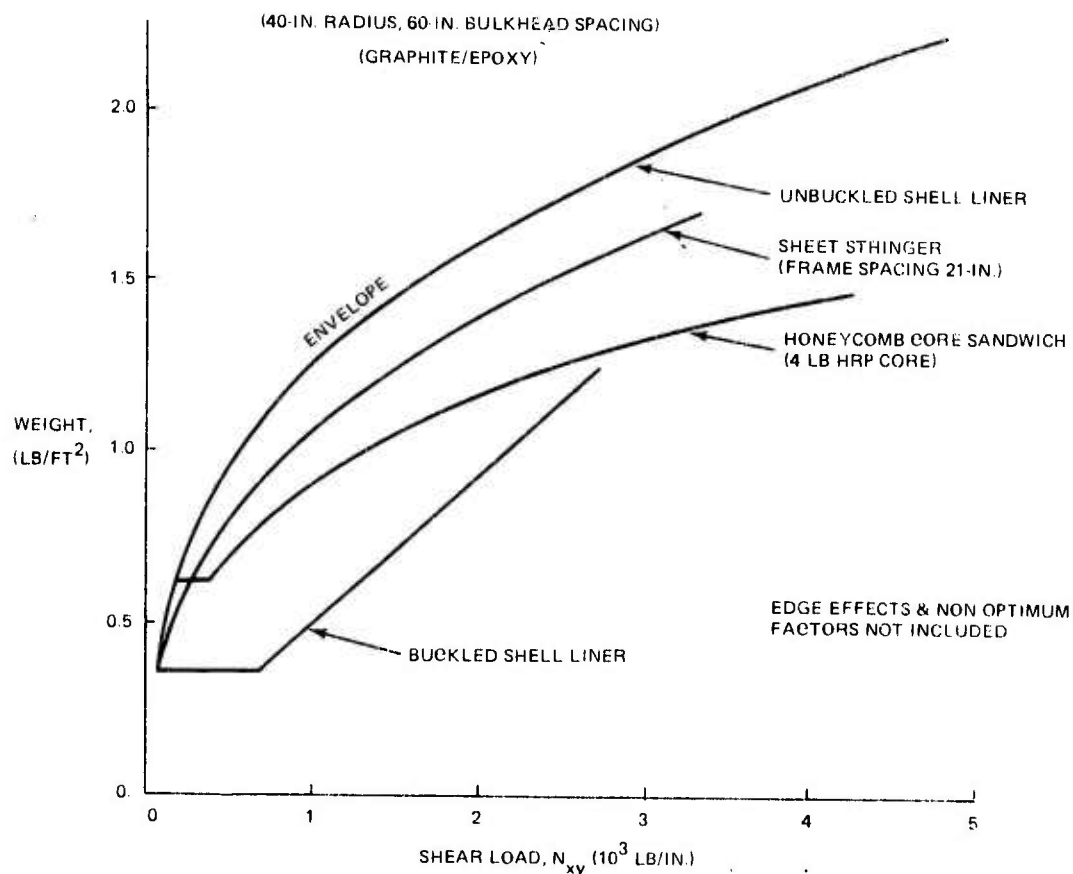


Figure 297. ADCA Fuselage Side Panel Weight Study

Honeycomb Sandwich - To evaluate the design concept which utilizes a honeycomb construction for the fuselage side panels a cylinder with a 40-in. radius and a bulkhead spacing of 60-in. was chosen as representative of a portion of the ADCA fuselage.

Symmetrical honeycomb sandwich panels with Gr/Ep quasi-isotropic face sheets and 4 lb/ft³ HRP core were studied. The torsional buckling analysis for orthotropic cylinders given in NASA SP-8007 was used to check the general instability of fuselage panels with core thicknesses ranging from 1/4 to 7/8 and the face thicknesses ranging from 0.021 to 0.084. The weight per square foot of each panel was calculated and plotted vs N_{xy} with a strength cutoff for the face sheets included. The curve shown in Figure 297 represents the minimum weight panel for each value of N_{xy} .

5.7.10.2 Top Deck Structure

The top deck was studied in the region of FS 527-600. A central spine member is assumed as being required to support the airpassage access doors; thus the panel size is approximately 20-in. wide by 63-in. long. Estimated design load intensity is 3100 lb/in. A brief description of a honeycomb and stiffened-sheet configuration follows:

Honeycomb - Using the Panbue II program, a parametric study was made of a honeycomb panel 20 x 60-in. in compression, with graphite face sheets and 4.0 lb/ft³ HRP fiberglass core. A carpet plot was made of weight vs load intensity varying face thickness and core depth, and the envelope of the lightest weight vs. load was determined.

Stiffened-Sheet - An all graphite skin stiffened by a continuous hat-type corrugation was investigated. Due to the length of the panel, full depth frames were added at 21-in. spacing and one-half their weight added to that of the panels. All elements of the sheet stiffened panel were kept non-buckling to failure, and normal shear effects were considered in obtaining the column allowables.

The curves as plotted, Figure 298, are for the basic panels and do not include non-optimum factors or weight adjustments for edge conditions.

5.7.10.3 COMFU Program

A computer program for preliminary design of composite fuselages has been developed called COMFU which is capable of analyzing stiffened composite fuselage panels. To simplify the program and enable it to be useful during the ADCA study time period the following assumptions were used as a base for the program:

- Circular orthotropic cylindrical shell between bulkheads, stiffened by rings and stiffeners
- No cut-outs, constant wall thickness
- Loads: Axial compression (N_x), torsion (N_{xy}), internal pressure (carried by hoop tension).

Three design options are offered:

- Solid laminate $0^\circ/\pm 45^\circ/90^\circ$, reinforced by rings and stiffeners
- Thick honeycomb sandwich with longerons, and $0^\circ/\pm 45^\circ/90^\circ$ facings
- Thin honeycomb sandwich with rings and stiffeners, and $0^\circ/\pm 45^\circ/90^\circ$ facings.

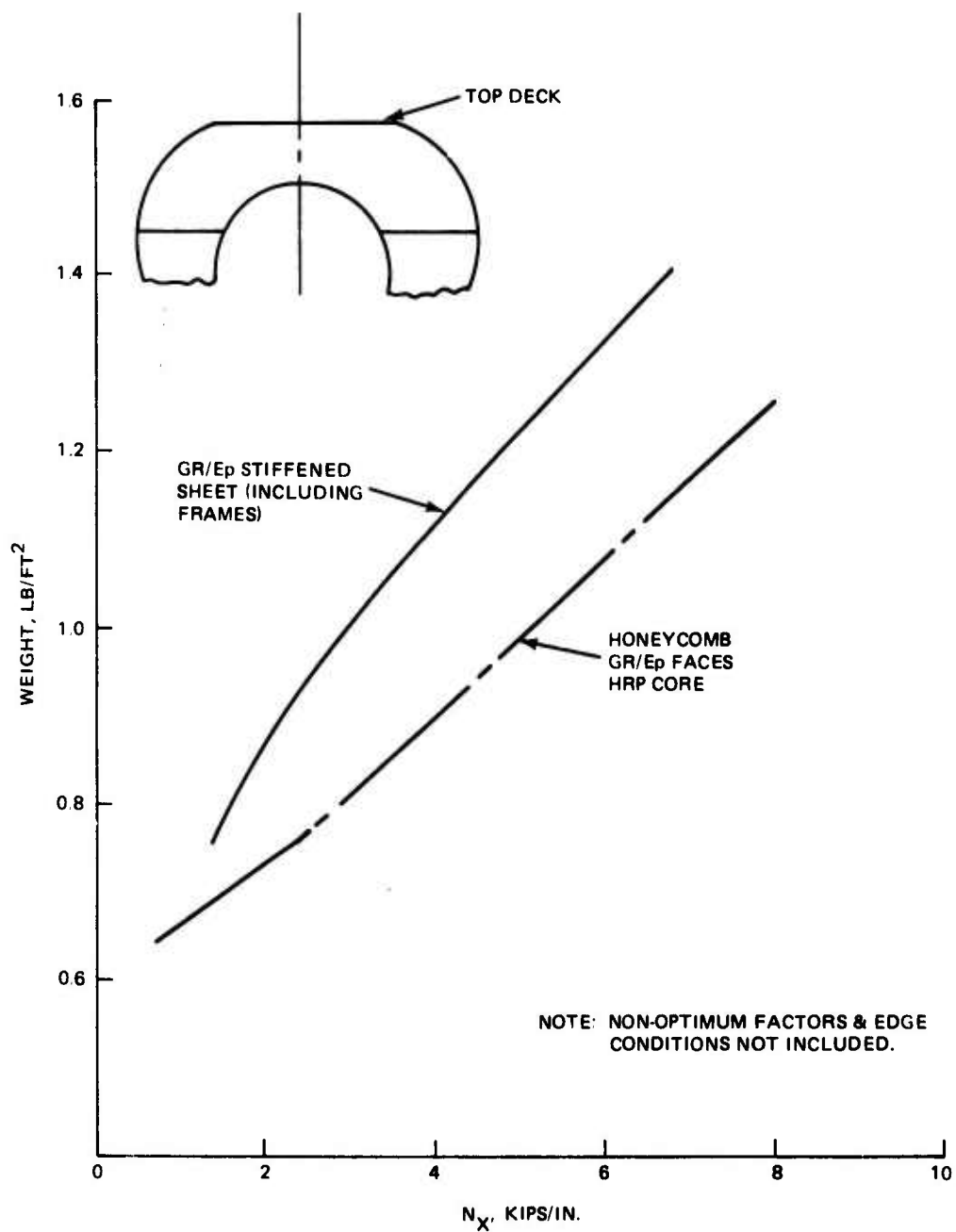


Figure 298. ADCA Fuselage Top Deck Weight vs Compressive Load Intensity

The program sizes the skin thickness by strength design and analysis for general instability, panel instability and plate instability for different combinations of compression and shear. The definitions of various instabilities are given as follows:

- General Instability: plate, rings and stiffeners buckle together
- Panel Instability: plate and stiffeners buckle between rings, rings do not buckle
- Plate Instability: plate buckles between rings and stiffeners, stiffeners and rings do not buckle.

In addition, the longitudinal stresses (stresses along the fiber direction of the layers), face laminate buckling, and shear strength are also calculated. Finally, the program also performs a preliminary weight analysis without non-optimum factors. The design cycle for the COMFU program is presented in Figure 299.

Three sections of the fuselage were selected for the initial runs:

- Cockpit sidewall: FS 212 - FS 297
- Inlet duct sidewall: FS 511 - FS 600
- Aft fuselage side panel: FS 600 - FS 663

These three fuselage panels were selected because they offered a variety of load and design requirements. All are subjected to combinations of shear, compression, and pressurization. Preliminary estimated internal loads were used and the results are presented in Table 62. The assumed criteria for buckling are as follows:

- Stiffened Laminate (i. e., shell liner): plate buckling between stiffening rings is permitted at limit load. Panel or general instability is not permitted at ultimate load
- Thin and Thick Honeycomb: buckling of any type is not permitted at ultimate load.

The weight figures presented do not include non-optimum factors. These relative weight figures are used for the preliminary stradeoff studies. In Case I, the cockpit sidewall, a comparison is made between stiffened laminate (shell liner) and thin honeycomb with stiffening rings. It was felt that the stiffened laminate would not be competitive with the honeycomb sandwich unless buckling was permitted so the shell liner was sized to buckle at limit load and a general instability and fiber failure check was made at ultimate

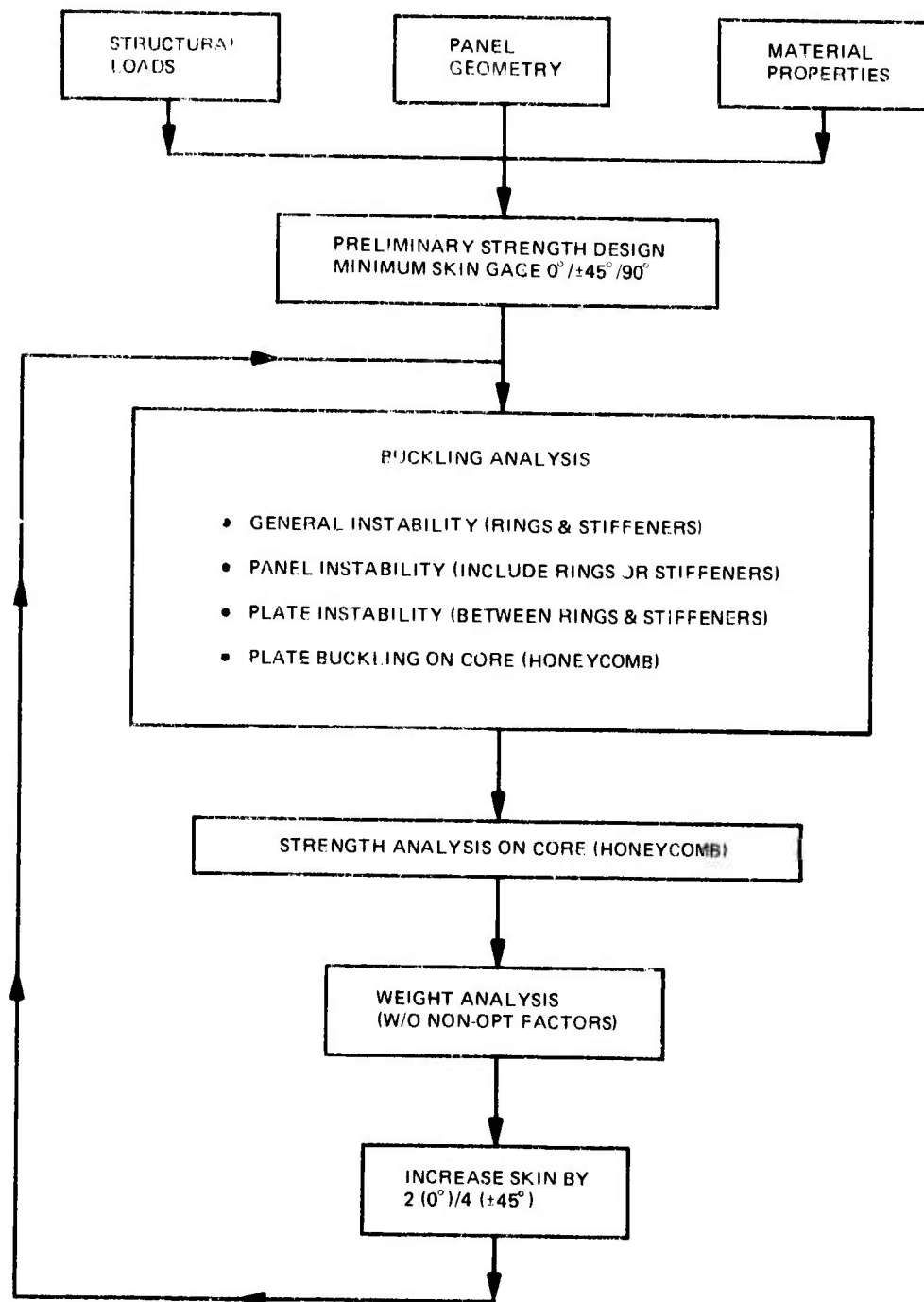


Figure 299. COMFU Program Design Cycle

TABLE 62. COMFU RESULTS

I (a) Cockpit Sidewall - Limit Flight Condition
(Material - Graphite/Epoxy)

Laminate with Rings & Stiffeners (Shell Liner)

Compression = 533 lb/in. Radius = 38.0
Shear = 167 lb/in. Length = 60.0

Check of Plate Buckling (between stiffening rings)

Skin Layup L/M/N	Stiffener Spacing, in.	Ring Spacing, in.	Weight, lb/ft ²
2/2/4	23.0	2.85	Buckled
4/2/8	23.0	2.85	Buckled
6/2/12 (1)	23.0	3.85	1.911
8/2/16	23.0	6.35	2.007
10/2/20	23.0	6.35	2.256
12/2/24	23.0	6.35	2.507
14/2/28	23.0	6.35	2.755

Note: (1) - Checked for general instability & fiber failure at ultimate load (Compression = 800 lb/in.; shear = 250 lb/in.). No instability or failure.

I (b) Cockpit Sidewall - Ultimate Flight Condition
(Material - Graphite/Epoxy)

Thin Honeycomb Sandwich with Rings

Compression = 800 lb/in. Radius = 38.0 in.
Shear = 250 lb/in. Length = 60.0
Longeron = 23.0 in. Core thickness = 0.20 in.
Spacing

Total Skin Layup L/M/N	Stiffener Spacing, in.	Ring Spacing, in.	Weight, lb/ft ²
2/2/4	23.0	6.0	1.471
4/2/8	23.0	10.0	1.647
6/2/12	23.0	10.0	1.897
8/2/16	23.0	10.0	2.146
10/2/20	23.0	10.0	2.396

TABLE 62. COMFU RESULTS (CONTINUED)

II (a) Inlet Duct Wall, Main Gear Well
(Material - Graphite/Epoxy)

Thick Honeycomb; No Rings

Radius = 24.0 in.
Length = 89.0 in.

Ultimate Flight Condition
Compression = 0
Shear = 755 lb/in.

Ultimate Landing Condition
Compression = 1226 lb/in.
Shear = 605 lb/in.

Skin Layup L/M/N	Stiffener Spacing, in.	Core Thickness, in.	Weight, lb/ft ²
2/4/8	25.0	0.50	1.582
	25.0	0.75	1.666
	25.0	1.00	1.749
	25.0	1.25	1.832

II (b) Inlet Duct Wall, Main Gear Well
(Material - Graphite/Epoxy)

Thin Honeycomb with Rings

Radius = 24.0 in.
Length = 89.0 in.

Ultimate Flight Condition
Compression = 0
Shear = 755 lb/in.

Ultimate Landing Condition
Compression = 1226 lb/in.
Shear = 605 lb/in.

Skin Layup L/M/N	Stiffener Spacing, in.	Ring Spacing, in.	Core Thickness, in.	Weight, lb/ft ²
2/4/8	25.0	10.0	0.25	1.609
			0.35	1.642
			0.45	1.676

TABLE 62. COMFU RESULTS (CONTINUED)

III (a) External Fuel Tank Wall - FS 600-FS 663

Thick Honeycomb; No Rings

Radius = 39.0 in.

Length = 63.0 in.

Ultimate Landing Condition

Compression = 1594 lb/in.

Shear = 660 lb/in.

Skin Layup L/M/N	Stiffener Spacing, in.	Core Thickness, in.	Weight, lb/ft ²
4/2/8	52.0	1.00	1.420
	52.0	1.25	1.503
6/2/12	52.0	0.75	1.586
	52.0	1.00	1.669
	52.0	1.25	1.753

III (b) External Fuel Tank Wall - FS 600-FS 663

(Material - Graphite/Epoxy)

Thin Honeycomb with Rings

Radius = 39.0 in.

Length = 63.0 in.

Ultimate Landing Condition

Compression = 1594 lb/in.

Shear = 660 lb/in.

Skin Layup L/M/N	Stiffener Spacing, in.	Ring Spacing, in.	Core Thickness, in.	Weight, lb/ft ²
4/2/8	52.0	8.0	0.25	1.308
		10.0	0.35	1.313
		10.0	0.45	1.347
6/2/12	52.0	10.0	0.25	1.530

load. The honeycomb sandwich is, of course, not allowed to buckle at ultimate load. Despite this buckling criteria, there appears to be a distinct weight advantage of the thin honeycomb over the stiffened laminate. This conclusion is tentative since non-optimum factors are not included and the factors could be quite different for the two types of construction. Also pressure effects are not included. The initial choice was shell liner construction and is shown on the drawings. The final choice would have to include the non-optimum factors, effects of cockpit pressurization, and the practicality of mounting cockpit equipment.

The inlet duct wall in the region of the main gear wheel well was examined for thick honeycomb with no rings and thin honeycomb with stiffening rings. The weight difference is very small in favor of the thick honeycomb. Since the space is limited because of main gear stowage, thick honeycomb is the logical choice. Both types of construction were also compared for the external fuel tank wall between FS 600 and FS 663. Here the weight advantage favored the thin honeycomb with stiffening rings but since this tank is the bladder tank and would require a liner across the stiffening rings, the choice was thick honeycomb with no rings.

COMFU was also used in a study of the upper fuselage between FS 510 and FS 600 and the results are discussed in Section 5.7.10.4.

5.7.10.4 Upper Structure - FS 510 to FS 600

The fuselage structure between FS 510 and FS 600 is subjected to the maximum bending moments during the critical flight and landing design conditions as shown in Figure 286. The maximum compression loads are applied to the upper structure during the flight conditions and to the lower structure during landing conditions. The lower longerons are located at the intersection of the outer fuselage shell and the lower sloping tank deck and are thus well stabilized against the Euler column mode of failure. The upper longerons are not geometrically stabilized except in the plane of the upper outer tank wall. For ease of fabrication, the upper longerons are integral with the tank wall which is of full depth honeycomb sandwich construction with graphite/epoxy skins. Since the depth of the upper longerons (normal to the plane of the tank wall) is limited to the depth of the honeycomb core, and the primary bulkheads are 90 inches apart, column failure is the critical mode.

Since the upper longerons are integral with the tank wall, stabilization against column failure can be achieved by the use of intermediate ring frames, against the inboard tank wall skins, which do not require notches to maintain longeron continuity. Alternate structural arrangements were analyzed with variations in honeycomb depth, ring spacing, and longeron material. At FS 597.5, the entire bending compression load is carried by the two upper longerons since the top portion of the fuselage shell is interrupted by the wing structural box. Moving forward of FS 597.5, the top shell begins to become effective in resisting the compression load but for the initial analysis, it was conservatively assumed that the upper longerons carry the entire compression load between FS 510 and FS 600.

With this assumption, the upper longerons were sized to withstand Euler column failure (including the effect of interlaminar shear stiffness) with honeycomb panel depths of 1.0 and 1.5-in. and with intermediate stiffening rings spaced at 15.0 and 22.5-in. respectively. The longeron material in one case was assumed to be Gr/Ep and in the alternate case hybrid with B/Ep used for the 0° layers and Gr/Ep for the 90° and ±45° layers. A summary table is presented below:

Longeron Material	Core Depth, in.	Ring Spacing, in.	Longeron Area, in.	Longeron E, 10 ⁶ psi	Longeron Strain, in./in.	Longeron Wt, lb/A/C	Ring Wt, lb/A/C	Core Wt, lb/A/C	Total Wt, lb/A/C
Gr/Ep	1.0	15.0	1.90	15.5	0.00204	18.80	14.40	13.07	46.27
Gr/Ep	1.5	22.5	1.87	15.5	0.00206	18.56	8.64	19.60	46.80
Hybrid	1.0	15.0	1.10	25.5	0.00214	14.06	14.40	13.07	41.53
Hybrid	1.5	22.5	1.12	25.5	0.00209	14.38	8.64	19.60	42.62

The skin weight was not included because the weight difference was not considered to be significant. There does not appear to be a clear weight advantage between the 1.0-in. depth and 1.5-in. depth. The lower stiffening ring weight associated with the 1.5-in. panel is offset by the higher honeycomb core weight. There is a small weight advantage gained by using the hybrid longeron material but whether it would be cost effective is doubtful.

In the previous analysis, the longerons were conservatively assumed to be carrying the entire compression load with no assistance from the shell structures. For the final sizing, the COMFU program was used to check for general and panel instability. The objective here was to determine if an ultimate strain of 0.003 in./in. could be attained. In this analysis, the shell is considered fully effective in carrying axial load and the out of plane

stabilizing effect of the fuselage shell on the longerons is accounted for by the compression buckling equations of the COMFU Program. A honeycomb depth of 1.50 in. was assumed and the longeron area was calculated assuming a minimum skin layup of 2/2/4 layers. These values were used as inputs to the COMFU program and the required skin layup and stiffening ring spacing were calculated. The results are presented in the table below:

Longeron Material	Longeron Area, in. ²	Skin Layup	Ring Spacing, in.	Weight, lb/ft ²	E (Skin), 10 ⁶ psi	Skin Strain, in./in.
Gr/Ep	0.615	6/2/4	45.0	1.325	11.0	0.00252
Gr/Ep	0.615	8/2/8	----	1.55	10.1	0.001833
Hybrid	0.375	6/2/4	45.0	1.309	11.0	0.00252
Hybrid	0.375	8/2/8	----	1.534	10.0	0.001833

The lightest combination with both longeron materials is the 6/2/4 layup with one stiffening ring. The strain of 0.00252 in./in. is quite close to the goal of 0.003 in./in. These two analyses bracket the final design of this area of the fuselage. For the final design, a finite element model would be required to define the transfer of axial load in the shell at FS 510 to the longerons at FS 600.

5.8 DETAIL DESIGN OF CRITICAL AREAS

5.8.1 Wing to Fuselage Attachment

The wing to fuselage attachment is accomplished at three bulkheads at FS 600, FS 663, and FS 702 through six attachment points. All points fall on BL 30. In addition to the transfer of large concentrated loads, the avoidance of secondary loads induced by wing deflections must be considered in the design. Replaceability of the fittings was also felt to be an essential feature. The final design meets all three of these requirements. The front and rear beam attachment designs, which are basically similar, are shown in Figures 300 through 302. Both designs incorporate steel shear pins located at the neutral axis of the wing to eliminate wing deflection secondary loads. The rear beam shear pin is inserted in a titanium fitting integral with the root rib while the front beam fitting is bolted to the front beam. All the socket action is taken in the wing fittings. On the fuselage side, the shear pins are inserted into titanium dagger fittings which transfer the loads to graphite/epoxy bulkheads by means of double shear bolted connections. Lateral tangs

BEST AVAILABLE COPY

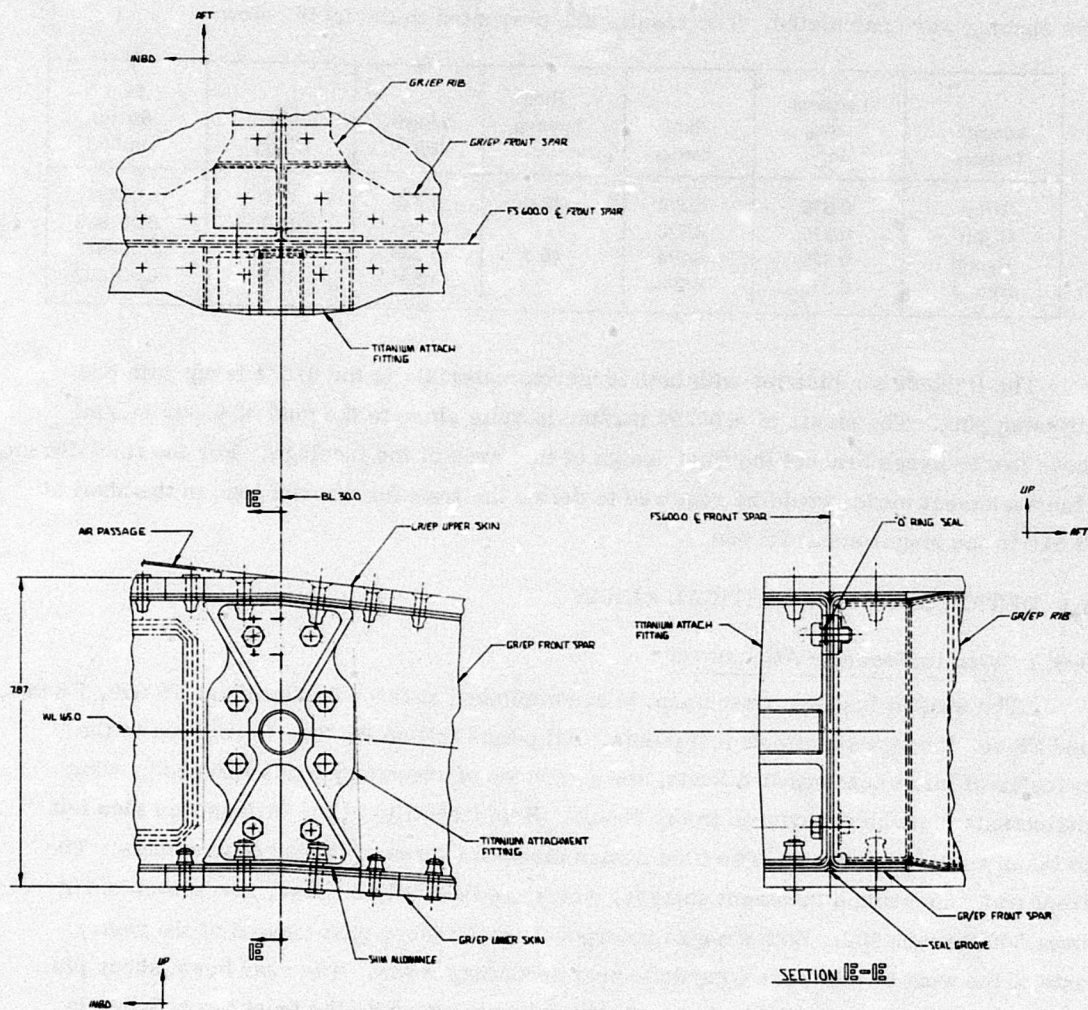


Figure 300. Wing/Fuselage Attachment-Front Spar

BEST AVAILABLE COPY

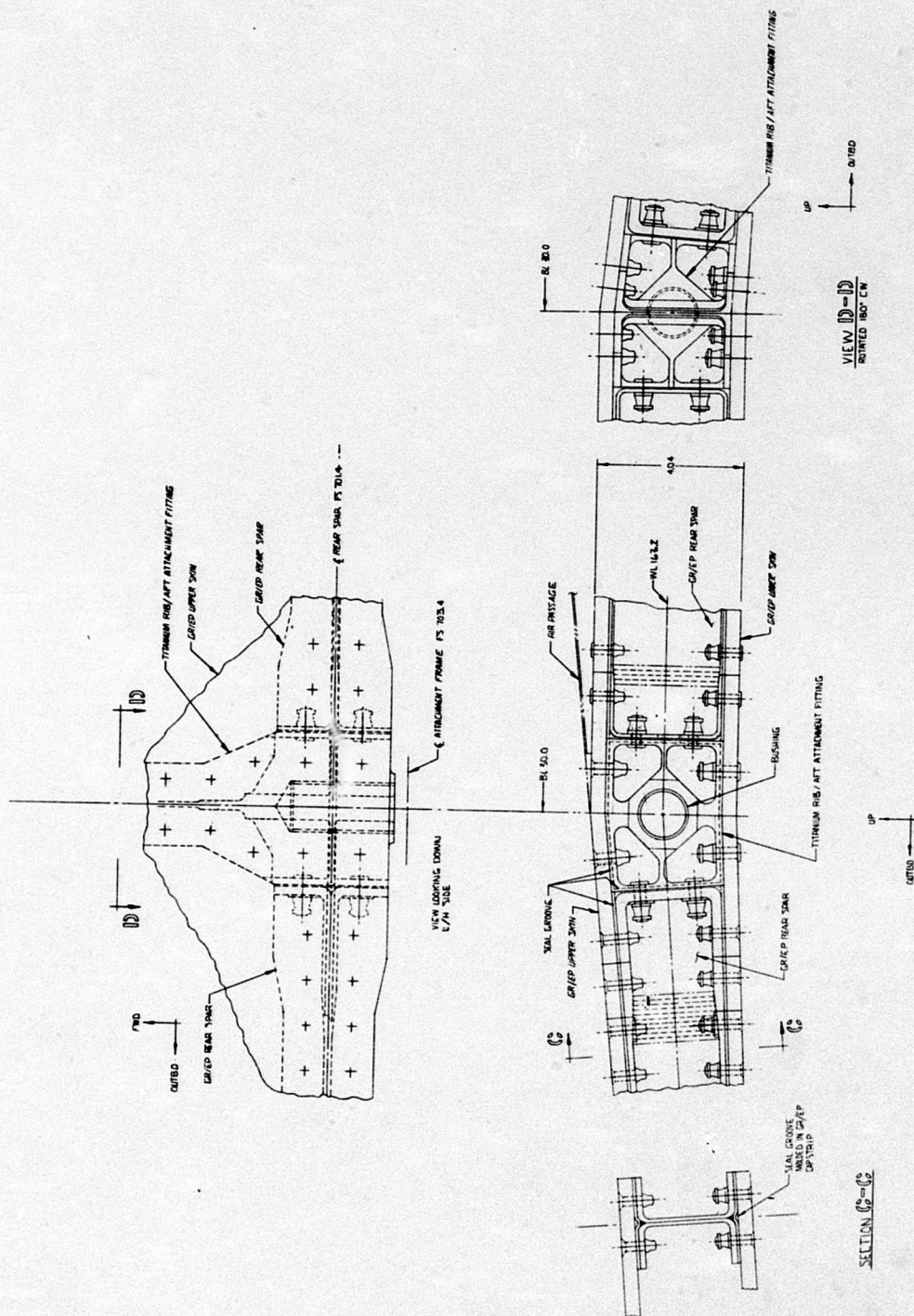
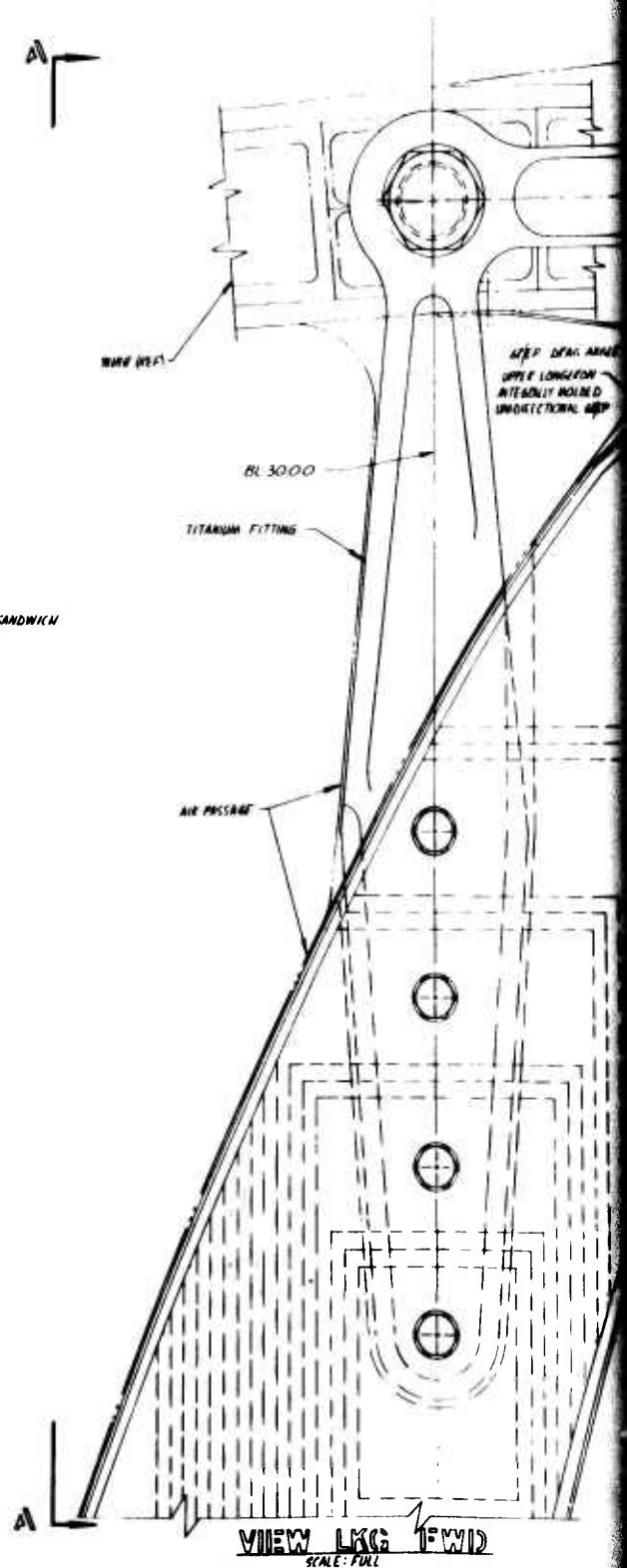
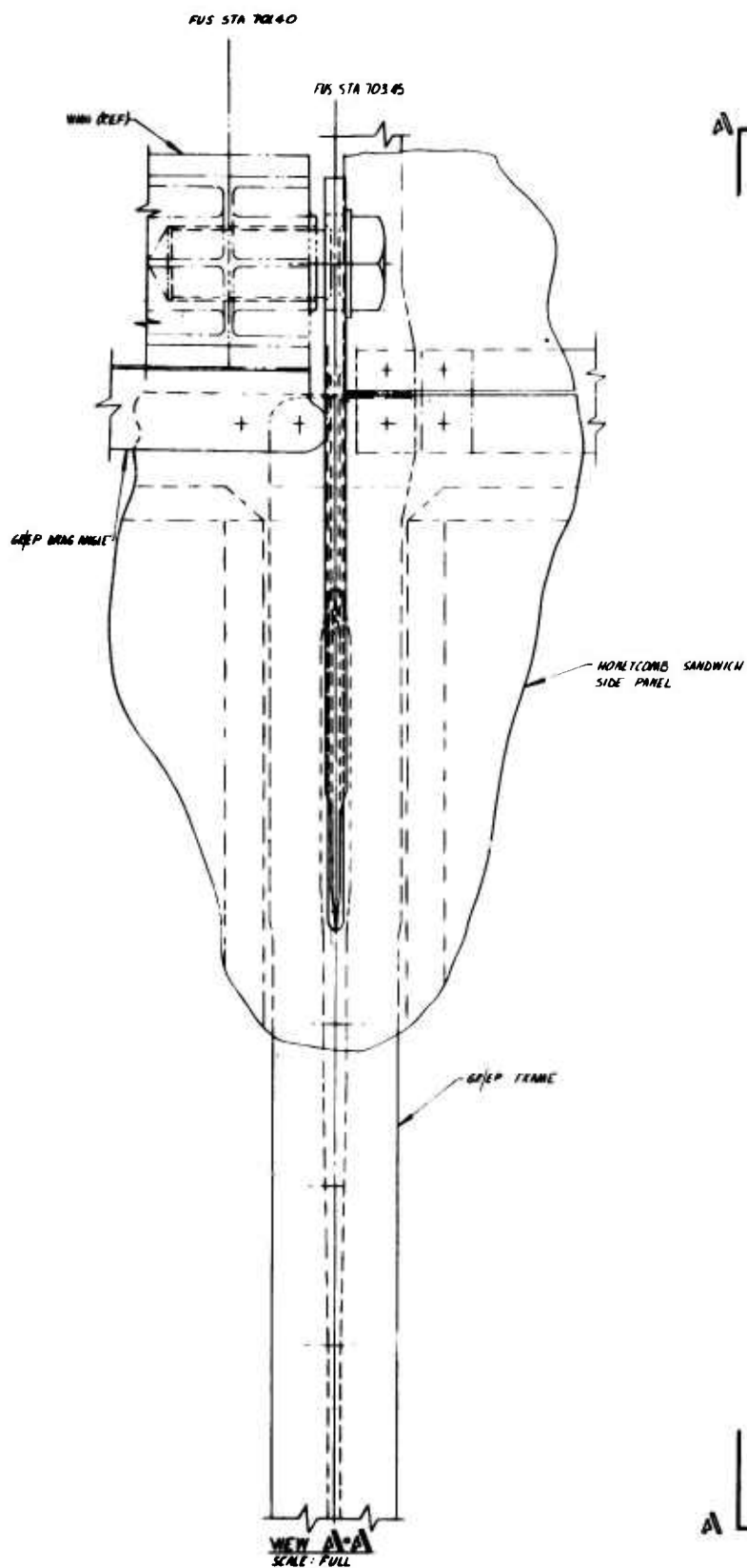


Figure 301. Wing/Fuselage Attachment-Rear Spar



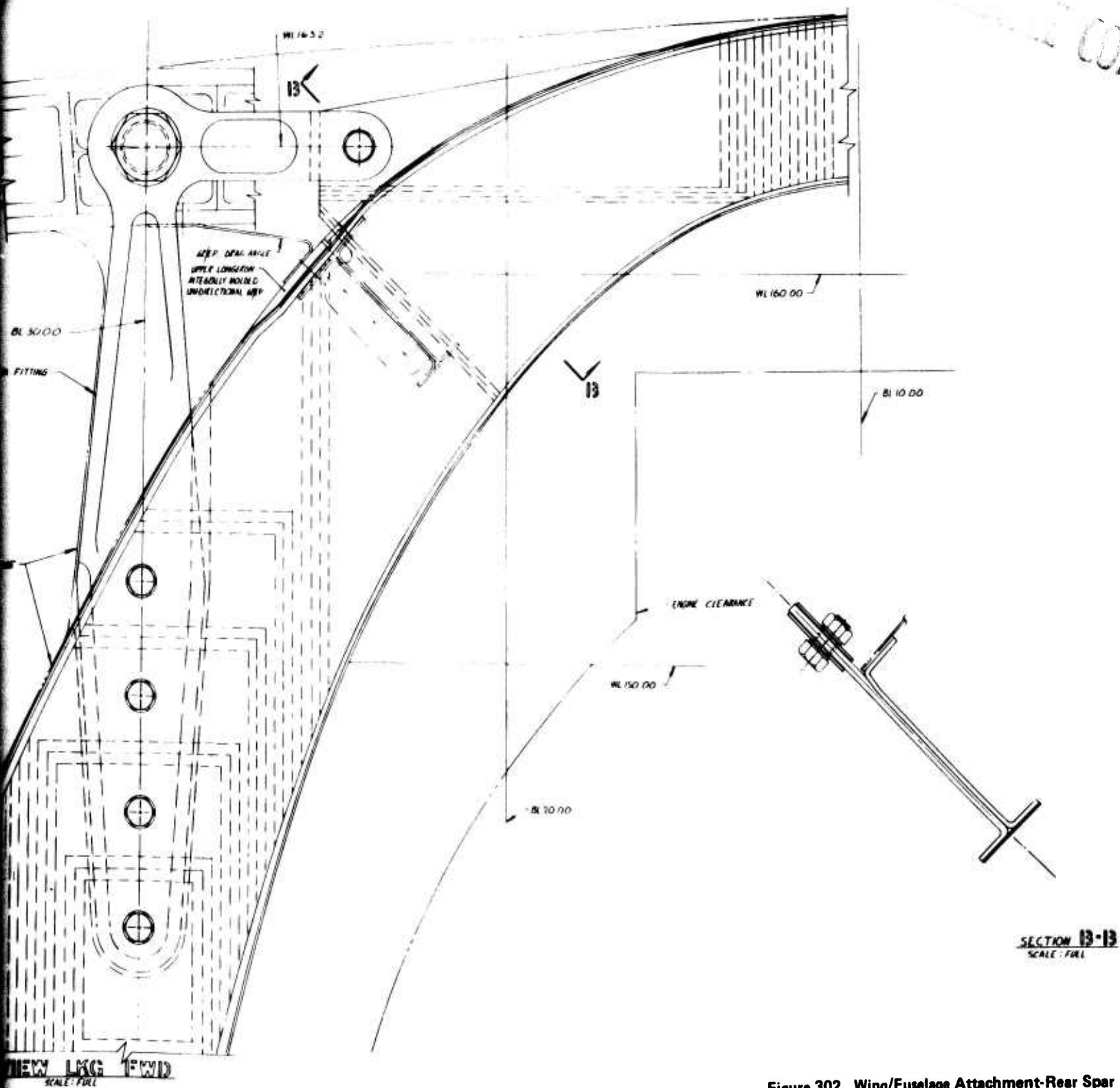


Figure 302. Wing/Fuselage Attachment-Rear Spar

on the dagger fittings transfer side loads from the wing to the bulkheads and maintain shear continuity across the top of the fuselage. Fore and aft loads are carried entirely by drag angles attaching the lower wing cover to the upper longerons.

The mid attachments, shown in Figures 303 and 304, are designed to carry vertical loads only. A titanium fitting is sandwiched between the mid beam shear webs and connected by steel bolts. The loads are transferred from this fitting to the graphite/epoxy bulkhead by means of two parallel links. The links eliminate any side loads generated by wing lateral loads or deflection. All-composite wing/fuselage attachments were initially looked at but it was apparent that the resulting structure would be more complex and less efficient than the utilization of metallic fittings.

5.8.2 Canard to Fuselage Attachment

The canard-to-fuselage attachment is shown in Figure 305. Due to the shallow depth of the canard, the bearings have been located in the fuselage. The outboard bearing housing is installed in the fuselage side wall at FS 402 and secured by a bolted retaining ring. The bolt holes are through the bearing housing and ring only, not through the composite. The inboard bearing housing is supported by an aluminum or titanium spider fitting attached to the centerline keel. The canard shaft thrust loads are reacted at the inboard bearing. The canard shaft is straddled by two graphite/epoxy bulkheads at FS 397 and FS 407. The vertical bearing loads are beamed to these bulkheads by the fuselage side wall and the centerline keel. The splined actuator arm extends down from the canard shaft and attaches to the forward end of the actuator. The aft end of the actuator is attached to the bulkhead at FS 450. A boron cradle fitting is used to balance the actuator load in a self balancing system. One end of the cradle fitting is attached to the aft end of the actuator fitting at FS 450 and the forward end is attached to two bearings on the canard shaft. The cradle fitting then transmits the axial actuator load directly to the canard shaft where it balances the load applied to the actuator horn. The torsion applied to the shaft is balanced by vertical kick loads at FS 402 and FS 450. Boron was selected for the cradle fitting because maximum stiffness was desired to meet the pitch stiffness required for flutter prevention. The cradle fitting was sized to meet this stiffness requirement and as a column when loaded in compression by the actuator. The cradle lugs that attach to the shaft bearings are made of wraparound boron layers which feather out at the aft end.

BEST AVAILABLE COPY

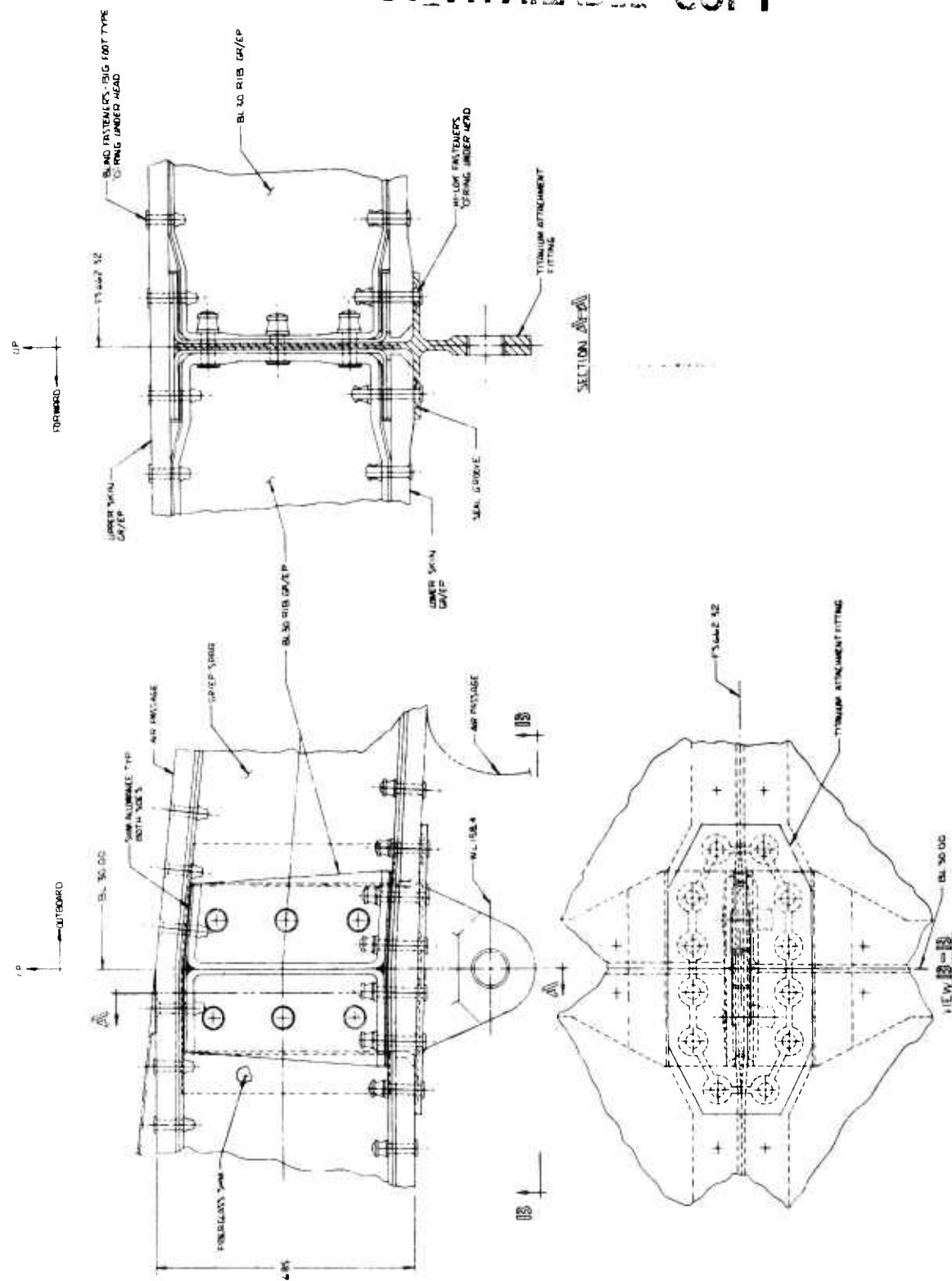
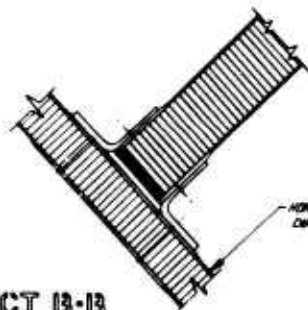


Figure 303. Wing/Fuselage Attachment-Mid Spar

SECT 13-13
SCALE: FULL



HONEYCOMB SANDWICH
DECK

BLADDER TANK SUPPORT BEAM

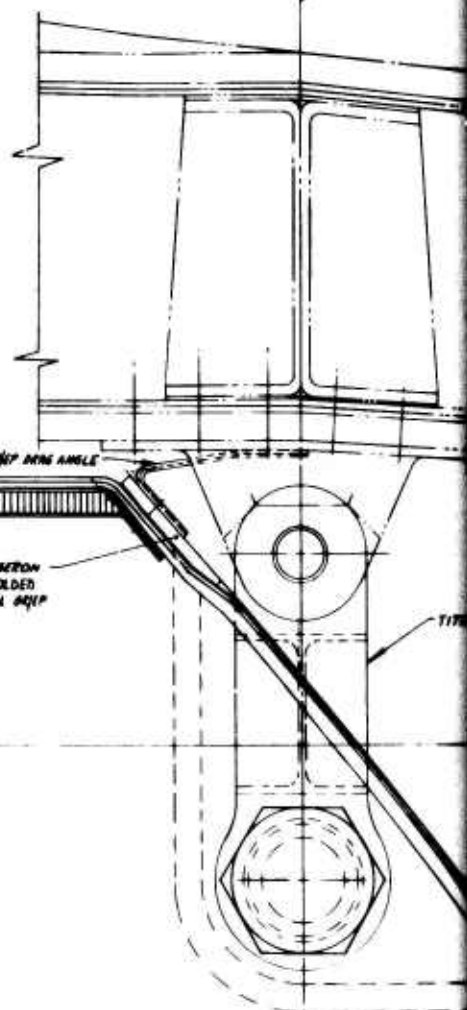
SHIP BOW ANGLE

UPPER LONGERON
INTEGRALLY MOLDED
UNIDIRECTIONAL GFRP

BL 30.00

BL 20.00

VIEW LKG AFT
SCALE: FULL



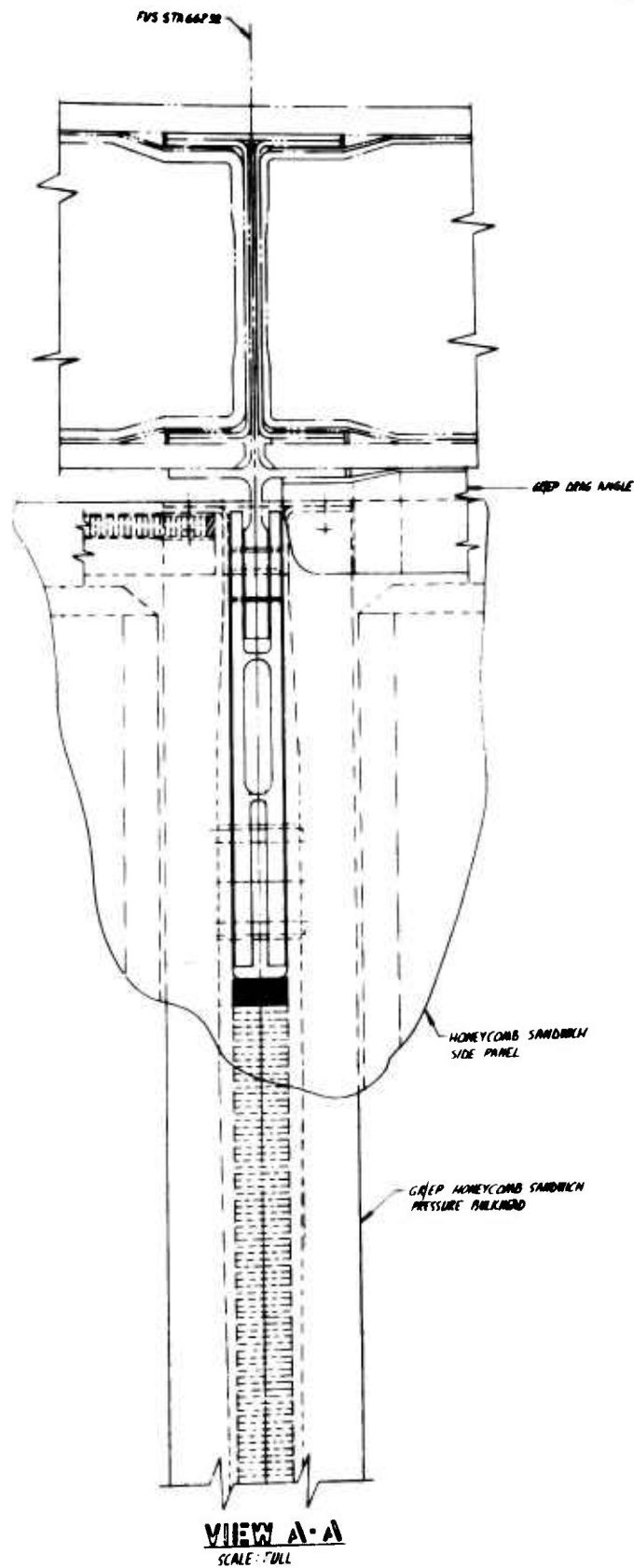
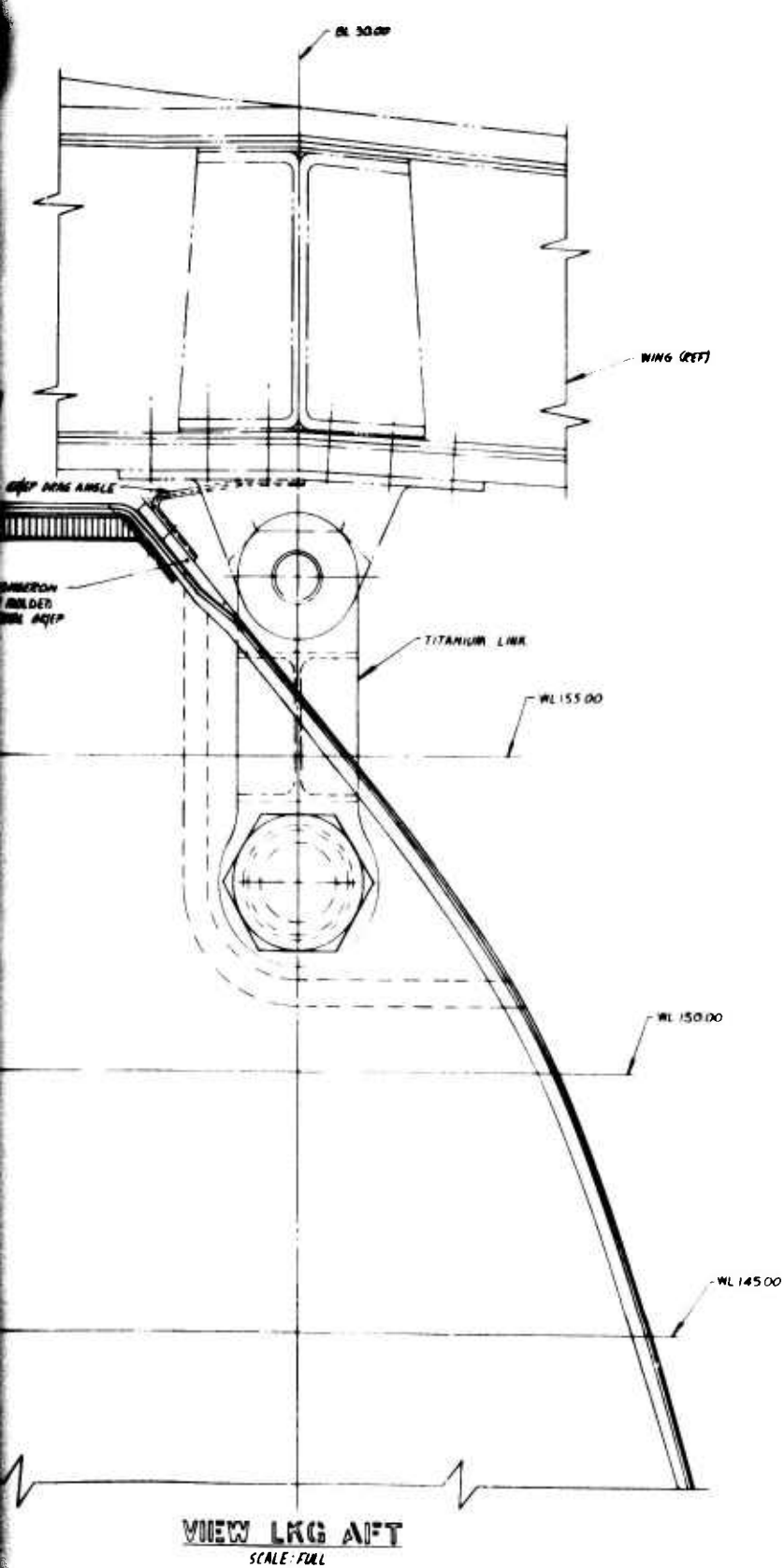
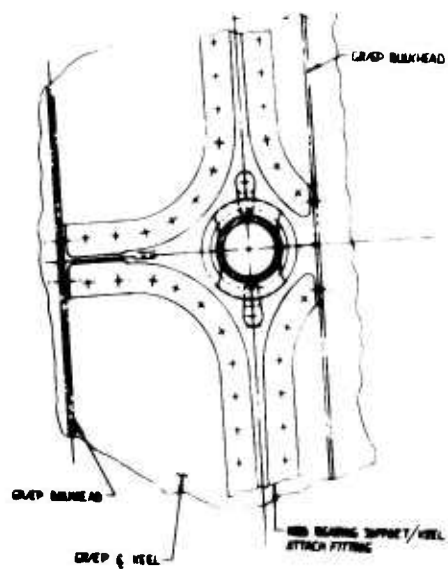


Figure 304. Wing/Fuselage Attachment-Mid Spar



VIEW C-C

← AIRCRAFT

HUB BEARING

ST

ST

PIST SHAFT

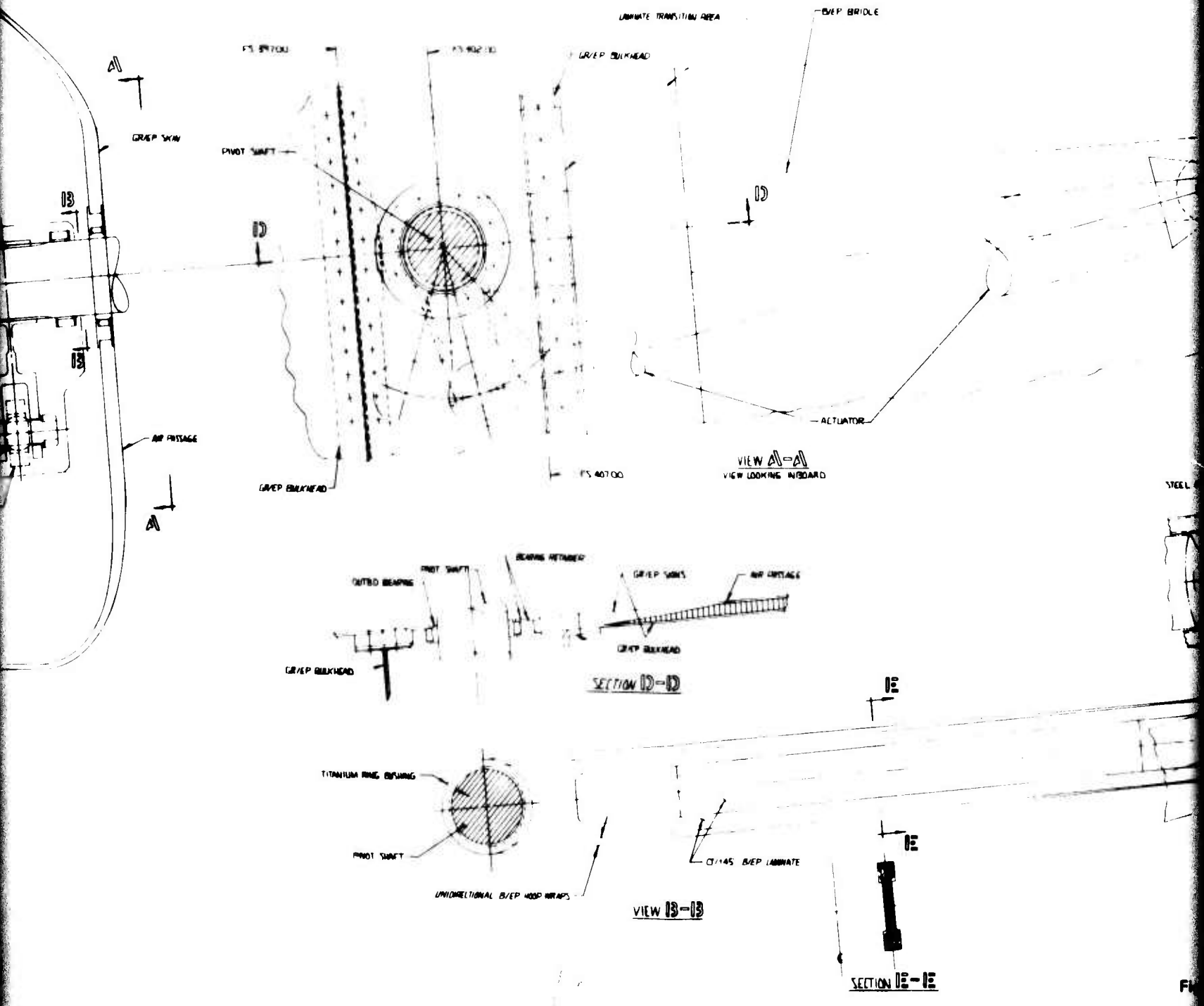
B/E P BRG

TIMBER FITTING

SHOULDER BOLT

← KEEL

SECTION THRU G OF PIST SHAFT
LOOKING AFT



2

CLIP COPY

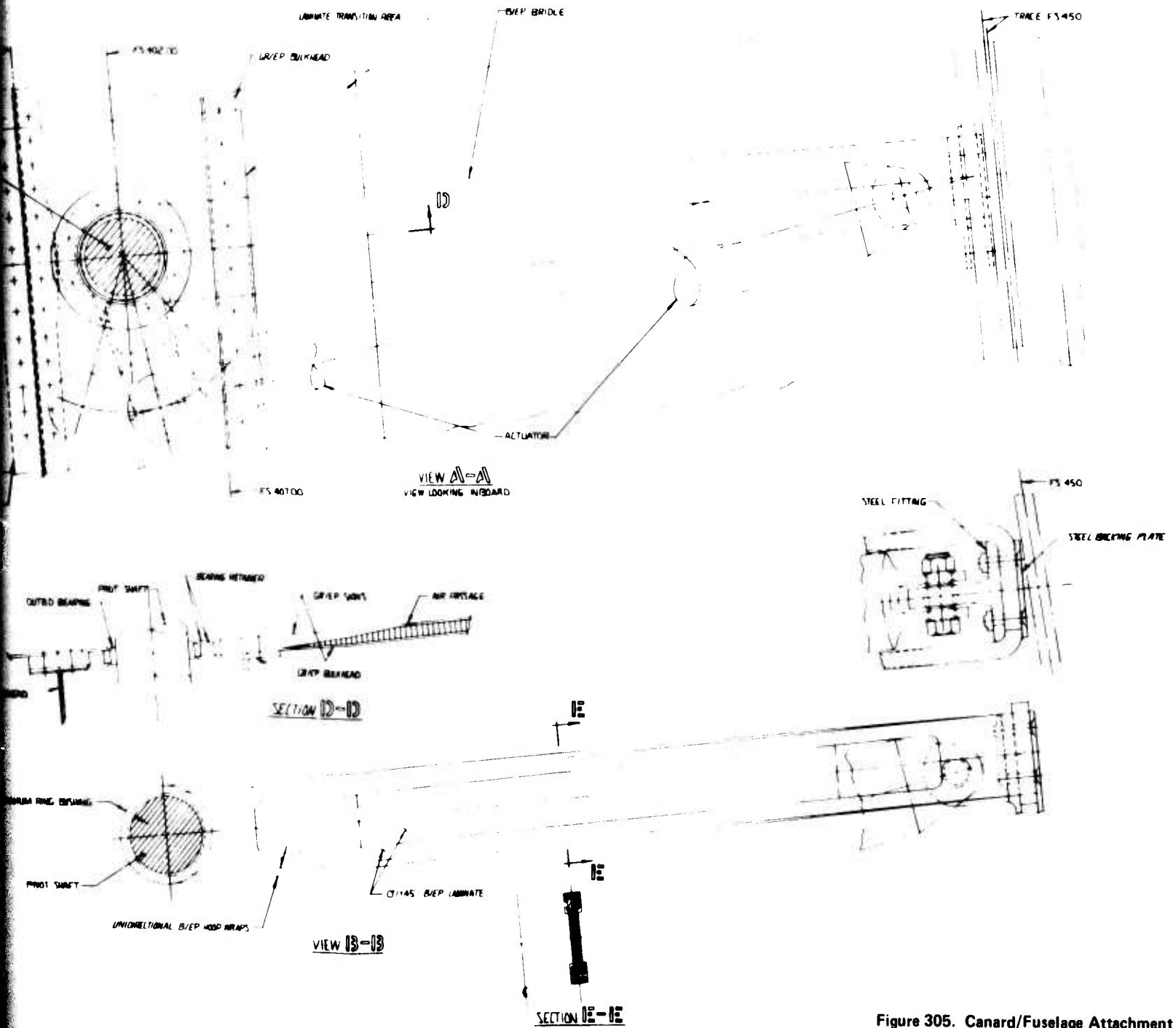


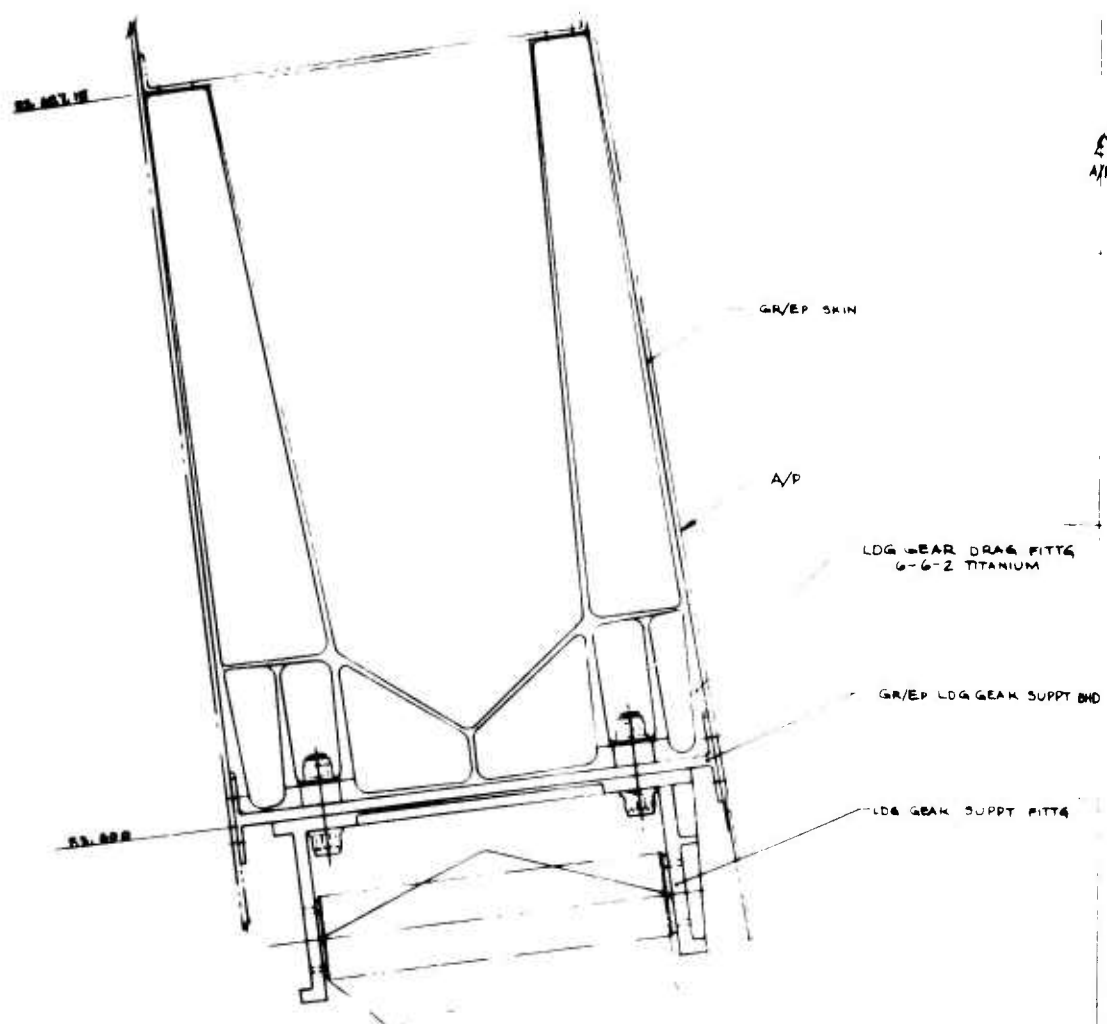
Figure 305. Canard/Fuselage Attachment

5.8.3 Vertical Fin to Fuselage Attachment

The vertical fin-to-fuselage attachment is accomplished through the use of a titanium root fitting. The attachment is shown in Figures 244 and 245. Being a highly swept surface, most of the bending moment is concentrated near the rear beam of the fin and it was decided to design for the entire bending moment at that attachment with the front beam attachment designed to carry only shear. The design problem is to transfer a large, highly concentrated, bending moment into a shallow ring bulkhead. Here again, an all composite approach was initially examined but the design became very complex and impractical. It was obvious that metallic structure should be used for the transfer of the fin cover loads to the bulkhead. Two canted, graphite/epoxy, bulkheads at FS 742 and FS 759 are utilized. The upper portion of both bulkheads consists of a titanium fitting bolted to the graphite/epoxy portion. The vertical fin covers, which are B/Gr/Ep hybrid locally to improve the composite net tension allowable, are bolted to splice plates integral with the titanium fitting. The fitting also doubles as a torque box, enabling the development of load in the fitting between frames in resisting the applied bending moment. Running cover loads in this area are on the order of 14,000 lb/in. At the front spar a shear pin oriented vertically attaches the root rib to a fitting, which in turn attaches to the FS 703 frame and reacts lateral shear. Drag shear is resisted at the main fitting.

5.8.4 Main Landing Gear Attachment

The main landing gear support installation is presented in Figure 306. The landing gear trunnion is supported by a steel fitting bolted to the forward face of the bulkhead at FS 600 which also functions as the forward wing beam attachment bulkhead. The steel attachment fitting is also attached to the horizontal deck at WL 144 which extends forward to FS 510. Aft of the main attachment fitting, a back-up fitting, (landing gear drag fitting) is provided which distributes fore and aft loads into the outer fuselage side wall and the inlet duct wall. Vertical landing gear loads are transferred to Bulkhead 600 by the landing gear support fitting. The centerline of the trunnion is offset from the bulkhead base by 4.64 in. The couple created by transferring the vertical load from the trunnion centerline to the plane of Bulkhead 600 is balanced by a couple in the WL 144 deck and the back-up fitting. The landing gear side load applied at the trunnion centerline is transferred to Bulkhead 600 by the landing gear support fitting and the couple is balanced by the landing gear drag fitting which transfers the couple into the outer side wall and the inlet duct wall.



VIEW 03-03
VIEW LOOKING DOWN

5
AIR

WL 135

LDG GEAR DRAG FITTS
G-6-2 TITANIUM

GR/EP LDG GEAR SUPPT BHD

LDG GEAR SUPPT FITTS

INNER DUCT WALL

R 35.5% -

145

MASS

NP

FS 600

LDG GEAR SUPPORT FITTS
220 KSI STEEL

LDG GEAR TRUNNION

BL + 2 REF

L (RETRACTED STRUT (REF))

LDG GEAR SUPPORT FITTS

(TRUNNION

LONGERON (REF)

LDG GEAR
STRUT

LDG GEAR SUPPORT STRUCTURE INSTL
@ FS 600
VIEW LOOKING AFT

027

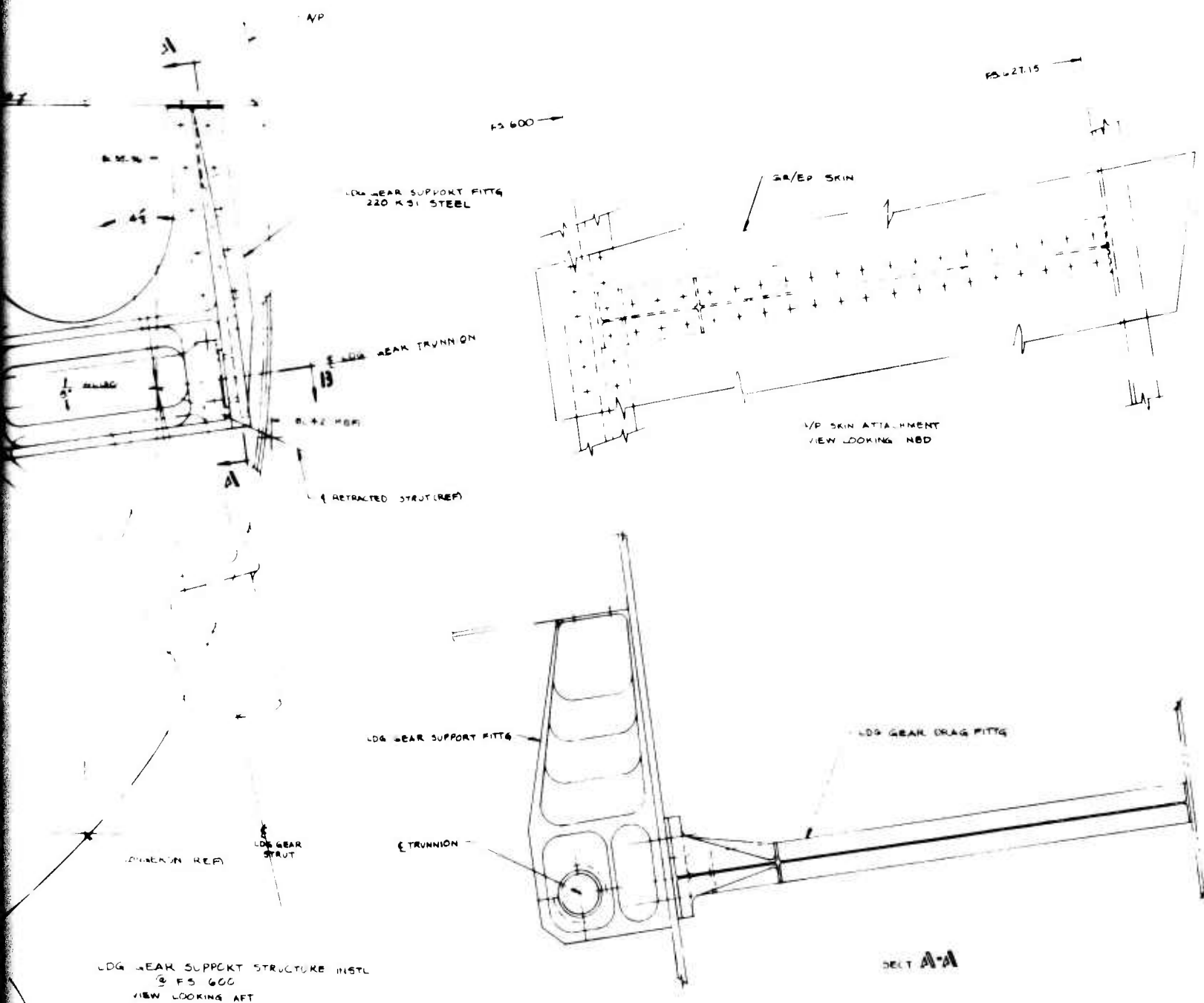


Figure 306 ADCA Main Landing Gear Support Installation

5.8.5 Engine Mounts

The ADCA engine is supported at three locations, two forward and one aft.

The left forward mount supports all three components of load, thrust, vertical and side loads. It is a quick connect fitting at the engine interface and rigidly attached to the FS 662,32 bulkhead. The vertical and side loads are transmitted to the side panel and structural duct by the bulkhead and the thrust load by the sloping lower pressure deck. Bathtub fittings are utilized to introduce the thrust load into the deck.

The right forward mount, Figure 307, though having an identical interface with the engine has the added requirement of not carrying side load. This is accomplished by utilizing spherical bearings in the plane of the vertical load which permits the mount to rotate about a fore and aft axis. The vertical and thrust loads are distributed to the side panel and structural duct by the bulkhead and sloping lower pressure deck. A truss fitting and upper and lower bathtub fittings are used to introduce the loads into the bulkhead, deck and side panel. The kick loads in the bathtub fittings require the addition of a lower partial frame, from the left to right lower sloping deck, at FS 643.

The aft left mount is simply a link with a spherical bearing on each end. This permits fore and aft, and side motion and limits the mounts function to supporting vertical load only.

5.8.6 Fuselage Manufacturing Splice - FS 450

The main manufacturing splice at FS 450, joins the forward and mid fuselage modules, Figure 308. The side panel of the mid fuselage module is a one piece honeycomb panel extending from FS 402 to FS 755. The lower portion of this panel is joined to the forward module at FS 402 and the upper portion at FS 450. The lower longeron of the forward module is spliced at FS 450 and becomes the mid longeron of the mid fuselage. The lower longeron splice at FS 450 is accomplished by a single shear scarfed splice plate of boron or graphite/epoxy which is integral with the capstrip of the FS 450 bulkhead. The upper longeron is spliced by a single shear scarfed titanium splice angle. An integral fuel tank is located aft of FS 450 making the pressure checking of the mid module, prior to joining, a primary design consideration.

The joining sequence consists of the bringing together of the forward and mid modules with the forward module lower honeycomb skin panel being off. This facilitates the

shimming of the upper longeron to the titanium splice angle, and allows the upper portion of bulkhead at FS 407 to be spliced to the lower portion which is a part of the mid module. The lower honeycomb skin panel which integrally contains the forward lower longeron is installed next with the longeron being spliced. The joint is completed by installing the upper deck between FS 407 and FS 450.

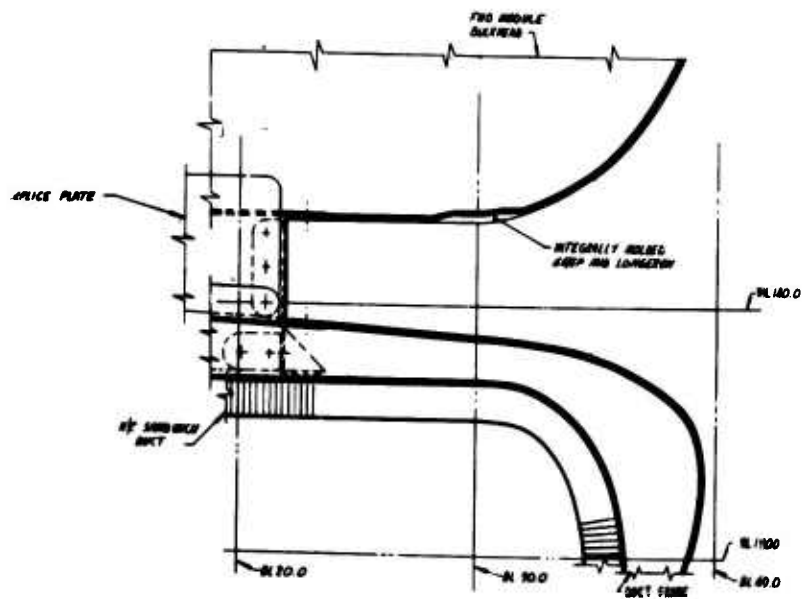
5.8.7 Hoist Fitting

The ADCA utilizes a three point hoist system as depicted in Figure 309. The forward hoist provision has been positioned at the centerline of the aircraft and FS 408, attaching to the aft canard support bulkhead. The two aft hoist points are placed on the wing either side of the aircraft centerline at BL 57 and FS 703. They have been positioned just aft of the wing box fuel tank such that complex sealing requirements are avoided. In addition, the two points also serve as two of the three points required for the wing hoisting.

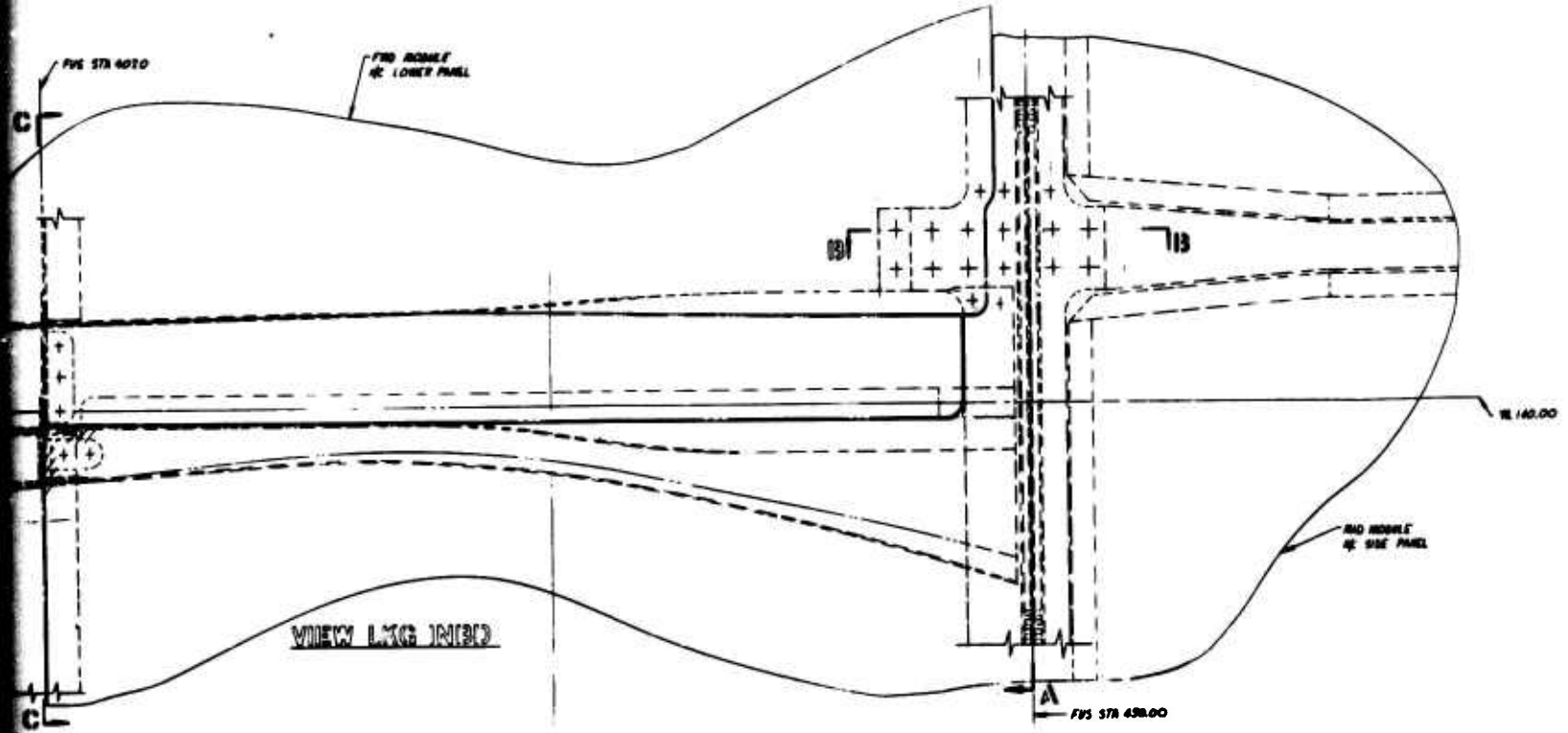
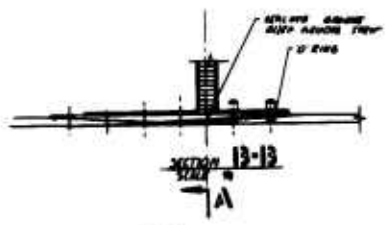
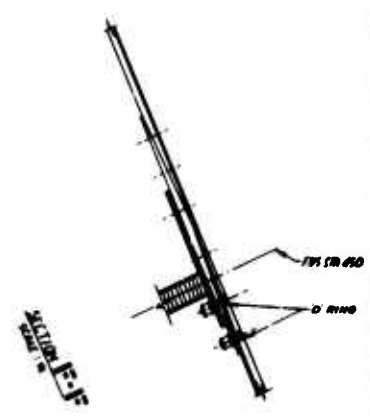
The hoist fitting attachment concept depicted in the figure is typical and utilizes a metallic fitting bolted to the wing box rear spar and skins. The fitting has a threaded hole, into which a helicoil insert is located. The insert is easily replaceable without fitting removal should the threads become damaged. For hoisting, the hoisting hardware is screwed into the fitting and the hoisting rig attached. A bolt simply fills the hole during flight. Loads during hoisting result in a vertical shear in the rear spar and a couple in the skins. Consideration had been given to an all composite hoist fitting, in lieu of the metallic design shown, however due to the compactness required, magnitude of load (approximately 17,000 lb with a 3g load factor), the threading requirement and the necessity of clearing a control system mechanism, it became complicated and impractical.

5.8.8 Control Surface Attachment

A typical control surface attachment, shown in Figure 310, depicts an inboard flaperon hinge support. Both hinge fittings, the wing side and the flaperon side, have been designed as metallic parts due to the minimum envelope into which they must fit, the magnitude of the concentrated load input and for simplicity. The concentrated load applied at the lug ends is reacted as a vertical shear in the rear spar, with the overturning moment coming off as axial loads in the wing skins. The spar web attachment fasteners are sealed at the spar/fitting faying surface by "O" rings secured in retaining grooves machined in the fitting. A removable Gr/GI/Ep trailing edge sealing plate is provided for access to the lug attachment bolt.



FWD RADAR
OF LOWER



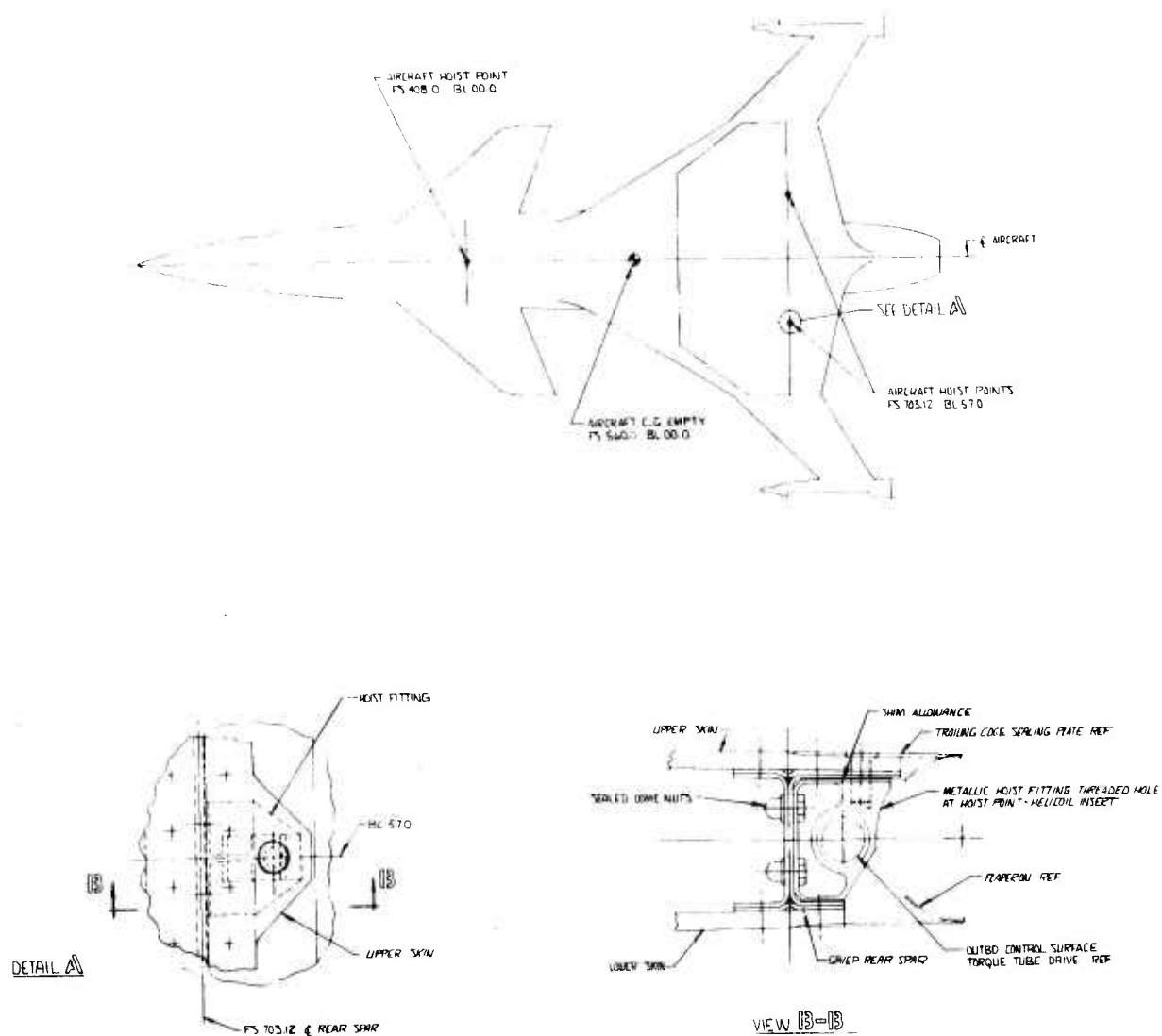


Figure 309. Hoist Fitting Attachment

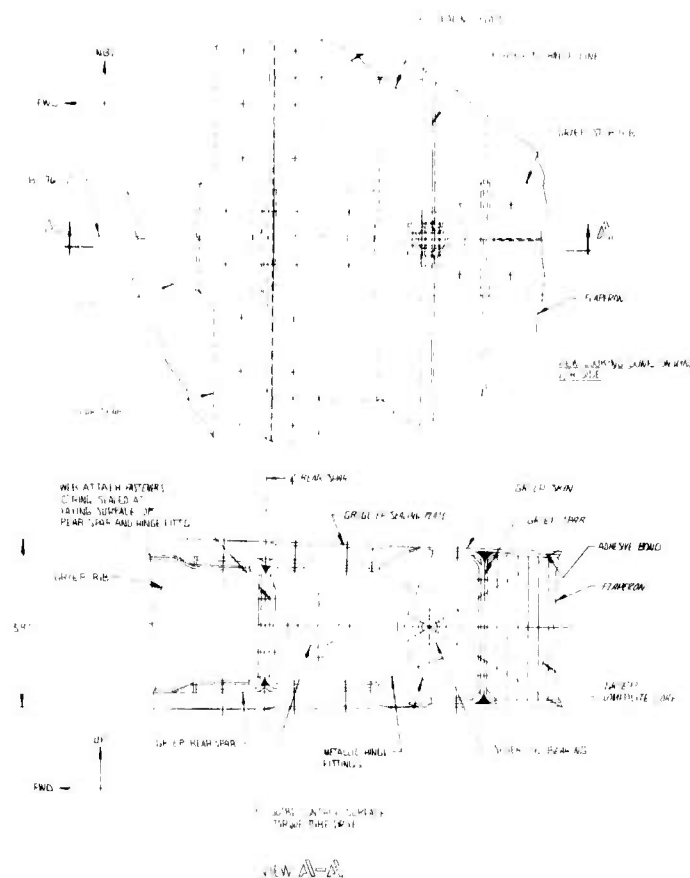


Figure 310. Control Surface Attachment

5.9 MANUFACTURING PLAN

The ADCA aircraft design study was conducted using a design-manufacturing interface to develop a producible structure which met all design requirements. Emphasis was placed on low vehicle acquisition cost to be consistent with current budgetary restrictions. Therefore, this study began with the review of the high cost centers in the fabrication of current high performance metal aircraft. Although metalworking technology is highly advanced, production costs are high due to the extremely large number of complex detail parts which must be produced and delivered on schedule to the assembly areas. The assembly flow is complicated by the installation of countless fasteners as the detail parts are assembled into modules which in turn are mated into the basic structural components

of the vehicle. Additional costs accrue from the fixturing, mechanical fastening equipment, and factory space required for assembly operations.

Therefore, a design-manufacturing philosophy for the ADCA vehicle was developed which significantly reduced part and fastener count. Wherever possible, cocuring of large assemblies was used to reduce part count to lower tooling, fastening, and production tracking costs. The currently available composite fabrication and tooling technology was reviewed to assess areas requiring further improvement. Two new concepts were developed. The translaminar reinforcement (TLR) concept uses stitching through the laminate to eliminate the anti-peel fasteners required for integrally molded skin to angle attachments. Thus, the cocured Gr/Ep assembly provides for joining a skin to substructure components with significantly fewer fasteners and detail parts with lower cost tooling. Also, the conformal molding process was developed so that mating parts which must be subsequently fastened, are molded concurrently. This process eliminates fit up problems requiring shimming, and enhances the structural efficiency of the joint so that fewer fasteners may be used. These two concepts are used in the fabrication of the wing center box.

Numerous sandwich panels are cocured in one operation. The cocuring process is also used to integrally mold surface protection systems for lightning strike, foreign object impact, and damage during maintenance to further simplify fabrication flow. Secondary bonding is limited to the wing spars and the vertical fin torque box to minimize manufacturing risk.

The major structural attachment fittings are titanium/steel machined parts due to the triaxial state of stress that occurs in highly loaded fittings. This is the only limitation on composite utilization in the airframe.

Manufacturing plans were prepared for fabrication of the wing, vertical and dorsal fins, rudder, canard, and fuselage assemblies. Each plan includes a tooling concept, an evaluation of various production schemes, and a description of the manufacturing sequence for the process selected. A final assembly plan was generated to cover the joining of the various components. An inspection plan was also prepared to provide confidence in the inspectability of the structure.

The fabrication sequences studied for the ADCA aircraft are all feasible, cost effective and minimize manufacturing risk. With available technology, the vehicle will cost less than its metal counterpart due to reductions in part and fastener count. In the

B-1 Horizontal Stabilizer programs, a similar approach led to projected cost savings of 14.5%. Future savings will accrue as the differential between composite and metal raw materials costs is reduced and composite material forms with increased processability are introduced. Innovative manufacturing techniques under current development may also simplify the fabrication flow.

In summary, the fabrication of an essentially all composite aircraft has been shown to be both feasible and cost effective. Manufacturing process confirmation would be obtained during fabrication of design verification components so that the full scale aircraft can be produced with confidence.

5.10 ENVIRONMENTAL CONSIDERATIONS

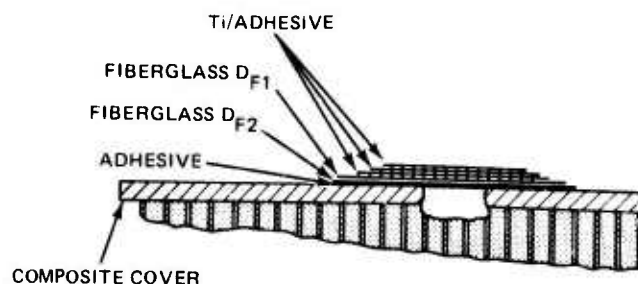
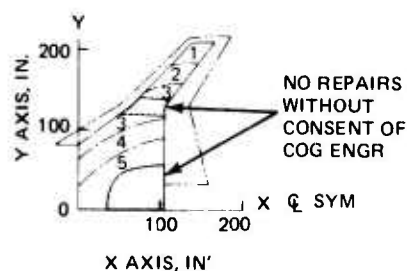
5.10.1 Repair Techniques

Since all production programs must provide for in-process errors and in-service damage it becomes essential that repair techniques be available to deal with these eventualities.

Two distinct situations can arise; errors and defects occurring at a major manufacturing center and damage occurring in the field. The repair techniques to deal with the latter should ideally be simple, inexpensive, reliable and portable. Figure 311 shows a procedure developed under an Air Force contract which meets these criteria. It utilizes alternate layers of titanium shim stock and adhesive on a fiberglass base cured directly over the damaged area. With this method the entire structure can be broken up into repair zones and a distinct repair configuration assigned to each zone or specify the requirement of a review of the damage by a cognizant engineer.

Repair procedures for in-process errors or defects have been developed for the composite B-1 horizontal stabilizer (R-100) and are being developed for the F-14A composite overwing fairing and main landing gear door. R-100 addresses a wide variety of discrepancies falling into four major categories as follows: dimensional discrepancies, visually apparent surface discrepancies, bonding discrepancies and voids and cure cycle discrepancies. Once the defect or damage has been characterized and its extent determined, the part is checked to a set of criteria which dispositions it in one of three ways. The part may be used as is, it may be repaired as specified or it may be presented to the Material Review Board (MRB) for action.

REPAIR ZONES FOR
DAMAGE OF DIAMETER
LESS THAN 1.0 IN.



REPAIR ZONE	TITANIUM LAYER DIAMETER							FIBER- GLASS DIA.	
	2.0	2.8	3.6	4.4	5.2	6.0	6.8	D _{F1}	D _{F2}
1	•	•						3.6	4.4
2		•	•	•				5.2	6.0
3		•	•	•	•			6.0	6.8
4		•	•	•	•	•		6.8	7.6
5		•	•	•	•	•	•	7.6	8.4

Figure 311. Repair Procedure ADCA Wing

One example of a visually apparent surface discrepancy is a delamination at the edge of a trimmed part. The spec (R-100) states that delaminations which are up to two plies deep, not more than 0.25-in. in from the edge, less than 1-in. in length, and comprise up to 20% of the perimeter shall be repaired by bonding the loose layers in place. EA-956 adhesive shall be injected into the voids and the repair cured for 24 hours at ambient temperature under clamp pressure. Delaminations which exceed the limits specified above shall be cause for MRB action.

5.10.2 Impact Resistance

The impact resistance of composites has been addressed in various advanced composite programs in the past with an indication that impact resistance of most composites are sufficient to withstand low energy impacts such as dropped tools.

The impact resistance of laminate edges has only recently become of interest. Edge impact tests performed at Grumman indicate that the edge treatment of composites can be a major requirement for composite laminates used in areas where bare edges are exposed, such as access doors. Various approaches to eliminate, alleviate or minimize the problem

can be pursued. One approach is to investigate the door to body interface seeking a door edge concept which is less susceptible to damage. Another is to attempt to improve the conventional door edge by overwrapping it with Kevlar, woven graphite or wrought metallic foil. Finally if it is found that neither of these approaches result in a satisfactory solution replaceability would become a major design criteria for those structural components which are more likely to be damaged.

5.10.3 Lightning Strike Protection Systems

An assessment has been made of the three readily available lightning strike surface protection systems for application on the ADCA. The three systems are:

- Integrally Molded Flame Sprayed Aluminum
- Integrally Molded Aluminum Wire Mesh
- Integrally Molded Co-Cured Aluminum Foil

All three systems are currently being employed on aircraft components; the flame spray system on the B-1 composite horizontal stabilizer box, the foil system on the F-14 composite horizontal stabilizer box and the mesh system on the leading and trailing edges of the B-1 horizontal stabilizer. The flame spray and foil systems cover approximately 50% of the total surface area while the mesh system covers 100% of the surface area.

The basic drivers for system selection are weight, cost, survivability and aerodynamic smoothness. Generally speaking, all three systems will afford adequate lightning protection characteristics (to the standard of MIL-B5087B Para. 3.3.4.5) and aerodynamic smoothness. Therefore, selection becomes a question of which system can perform at minimum weight and cost. In terms of weight and cost for 100% surface coverage the aluminum wire mesh system is the lightest but most expensive, followed by the flame spray system which is heavier but significantly less expensive. Weight/cost comparison conducted for the aluminum foil system place it on a par weightwise with the flame spray system and somewhere between the flame spray and mesh systems on a cost basis. Table 63 shows the relative weight and cost factors for the flame spray versus mesh systems, with the flame spray system at the baseline.

5.10.4 Erosion Protection Coatings

Currently, there are two basic erosion protection systems in aerospace use. The older neoprene rubber and the new polyurethane coating systems. These coatings were primarily developed for rain erosion, such as that experienced on the leading edges of

TABLE 63. MESH SYSTEMS COMPARED WITH FLAME SPRAY

	Labor Cost	Material Cost	Total Labor & Material Cost	Weight
Aluminum Flame Spray	1	1	1	1
Aluminum Wire Mesh	1.55	14.3	7.13	0.46

flight surfaces, radomes, etc., but they also have applicability in areas such as the underbelly of the aircraft where grit and gravel would be thrown from the landing gear. The maximum operating temperature of the neoprene system is 250°F, while the polyurethane system is useable to 400°F. Of the two systems, the polyurethane exhibits superior erosion characteristics. Two of the polyurethane materials are currently in use at Grumman, Astrocoat per MIL-C-83231 and M312/Chemglaze II. The former system is anti-static the latter is not. The M312 is lower cost, both from a material and labor point of view.

5.10.5 Moisture Absorption Protection Systems

The major problem of moisture absorption with advanced composite materials appears to be for structures operating at temperatures in excess of 260°F. For the ADCA mission as defined, the structural temperatures are 250°F maximum allowing use of organic matrix composites with only minor adjustment to design properties and without special moisture barriers. For application at temperatures in excess of 250°F one of four approaches can be considered - use reduced allowables for design, use currently available moisture barrier systems with weight penalties, develop a new, simple, light-weight barrier system or obtain a moisture resistant organic matrix. Based on currently available data, using reduced allowables would impose significant weight penalties. Development of a new barrier system or new organic matrix requires greater emphasis to be timely for the near future composite structures.

A readily available solution might be the moisture barrier system presented in Figure 312. This is really a combination system, in that it provides lightning strike protection as well. The system utilizes four mils of wrought aluminum foil and one mil of style 104/SP298 adhesive (0.001-in. thick) for surfaces to be protected from lightning,

followed by wet layup of the composite laminate. For surfaces that do not require lightning strike protection (internal) the two mil wrought aluminum foil is secondary bonded to the cured composite skin using the 0.001-in. adhesive. The other technique depicted would use electro-deposited nickel subsequent to part completion. This technique, if found to provide adequate protection, should be much easier to apply and less costly. This technique may also provide wear protection at edges and fastener holes in access panels.

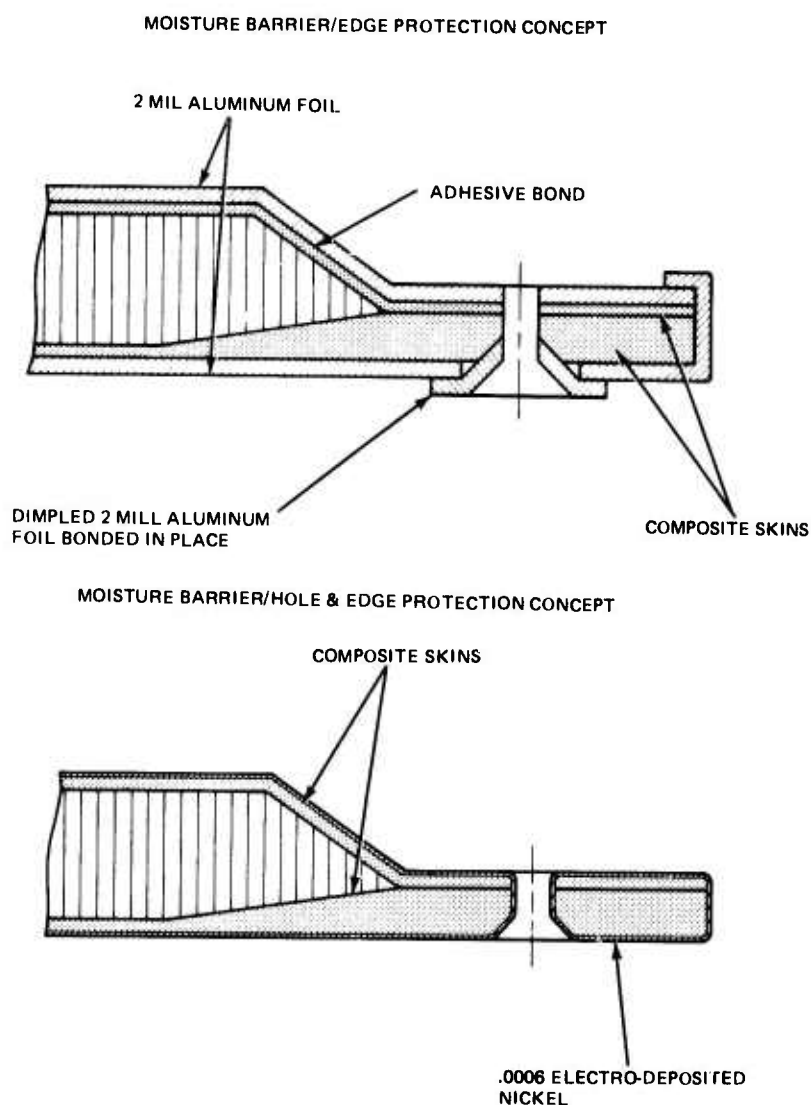


Figure 312. Moisture Barrier/Edge Protection Concept

Section VI

COST

6.1 COST ESTIMATING METHODOLOGY

6.1.1 Airframe Cost

The computerized models used by Grumman to estimate airframe cost are Resource Management Corp (RMC), RAND and Parametric Cost Estimating (PACE). The first two are based on industry-wide cost data and are used for comparative purposes only. They are sensitive to a limited number of design parameters, including weight and speed, but are not sensitive to material type and distribution.

PACE model was derived from historical Grumman Data. The Cost Estimating Relationships (CER's) used in the model were developed by performing a multiple regression analysis on data available from past Grumman programs. These CER's are sensitive to design parameters such as weight, speed, load factor, structural density, wing loading, engine thrust and weight, and material type and distribution.

PACE has been updated to reflect the specific requirements of ADCA. Projected costs for boron and graphite materials shown in Figure 313 have been incorporated. Cost modification factors have been introduced in accordance with savings afforded by reduction in the number of parts and fasteners inherent in composite designs. These are based on data gathered from such programs as the F-14 composite overwing fairing and the B-1 composite horizontal stabilizer. Cost modification factors have also been introduced that reflect projected cost savings offered by the Integrated Laminating Center currently in development at Grumman. This center will be operational in the ADCA time period.

6.1.2 Propulsion Cost

Propulsion costs were estimated for both off-the-shelf, modified and new engine designs. Wherever feasible, engine manufacturer cost projections were used. All other estimates were prepared using the 1974 revision of the RAND engine cost model (R-1288-PE).

6.1.3 Avionics Cost

A baseline avionics system cost was derived from studies performed recently by Grumman of aircraft with similar mission and performance requirements. The system included communication, navigation, weapon delivery, display and electronic warfare capabilities (Section III). This cost was an input to the PACE model.

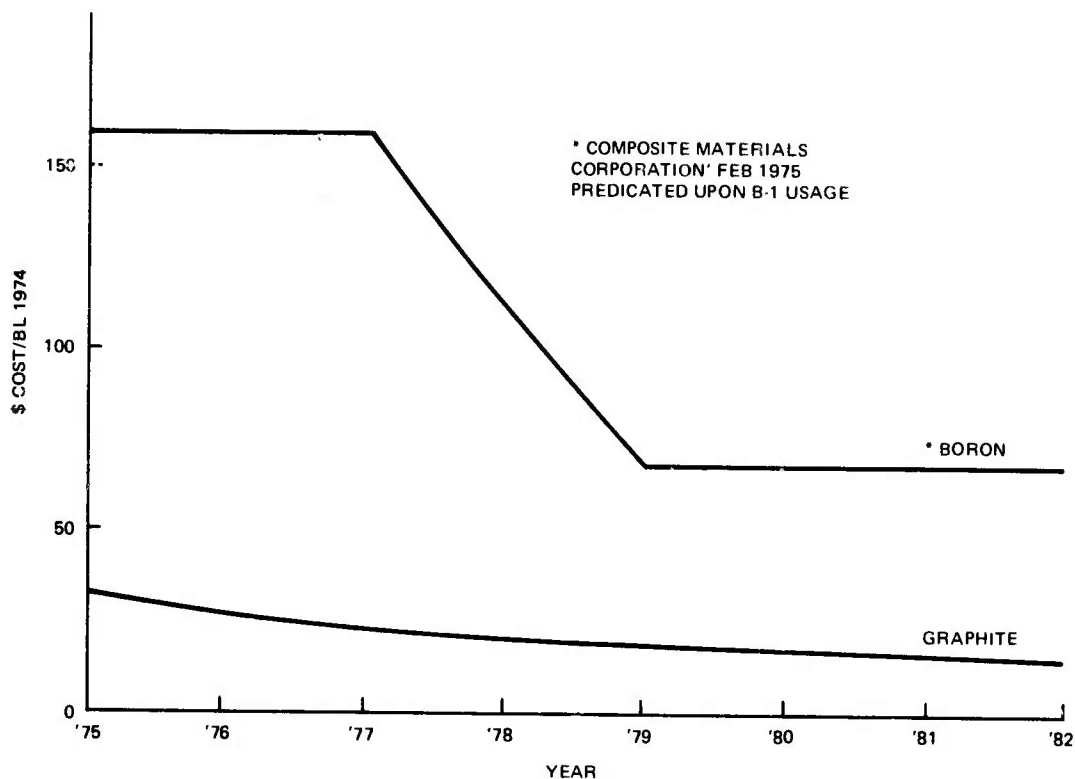


Figure 313 Boron and A/S Graphite Materials Cost Trends

6.1.4 Spares and Support Costs

PACE estimates the initial spares and support costs as a function of the number of production aircraft and the flyaway costs. Indirectly, it reflects the complexity of the aircraft through the flyaway costs. Factors have been applied to reflect improved reliability characteristics projected by the reliability and maintainability analyses. These factors were only applied to the final payoff assessment after the R and M analyses had been completed.

6.1.5 Operating Cost

Operating costs were derived parametrically by PACE, which is consistent with the "USAF Cost and Planning Factors" document (AFR 173-10). The costs are derived using selected aircraft performance characteristics. Factors have been applied to reflect a two-level maintenance approach forecasted for the 1980-1990 time frame, and for improved mean-time-between-failure manhours per flight hour forecast by the reliability and maintainability analyses. These factors were only applied to the final payoff assessment after the R and M analyses had been completed.

6.2 COST ANALYSIS

6.2.1 Initial Sizing and Tradeoff Studies

Cost analysis was initially performed for eight configurations with the following combination of materials and engines:

<u>Airframe Material</u>	<u>Quantity and Type of Engine</u>
*Composite	One F-101
Metal	One Rubberized F-101
Metal	Two F-101's
*Metal	Threc F-404's
Metal	Two F-100's
Composite	One GE 16/F8-A18
Composite Replacement	Three F-404's
Composite Replacement	One Rubberized F-101

In the latter two configurations, composite materials were substituted directly for the metal without consideration for redesign to take advantage of the overall iterated effects. The starred (*) configurations were baselined for all comparative studies.

6.2.2 Initial Cost Comparisons

Figure 314 shows relative cumulative average flyaway costs for the six most promising of the candidate configurations. It shows that the metal baseline of comparable performance, using off-the-shelf engines, would be 25% more expensive than the composite baseline. Some cost reduction may be achieved by composite replacement of metal parts and by rubberizing the engine. A 5% reduction may be achieved by designing an ADCA using an advanced engine.

Figure 315 shows relative life cycle costs for the candidate configurations. Most configurations are 20% more expensive than the composite baseline. The RDT&E costs for the composite design with the advanced engine makes this configuration less favorable than indicated by the cumulative average flyaway cost.

Tradeoffs were performed to identify optimum cruise speed and configuration. Figure 316 compares TOGW and costs for varying cruise speeds for two different

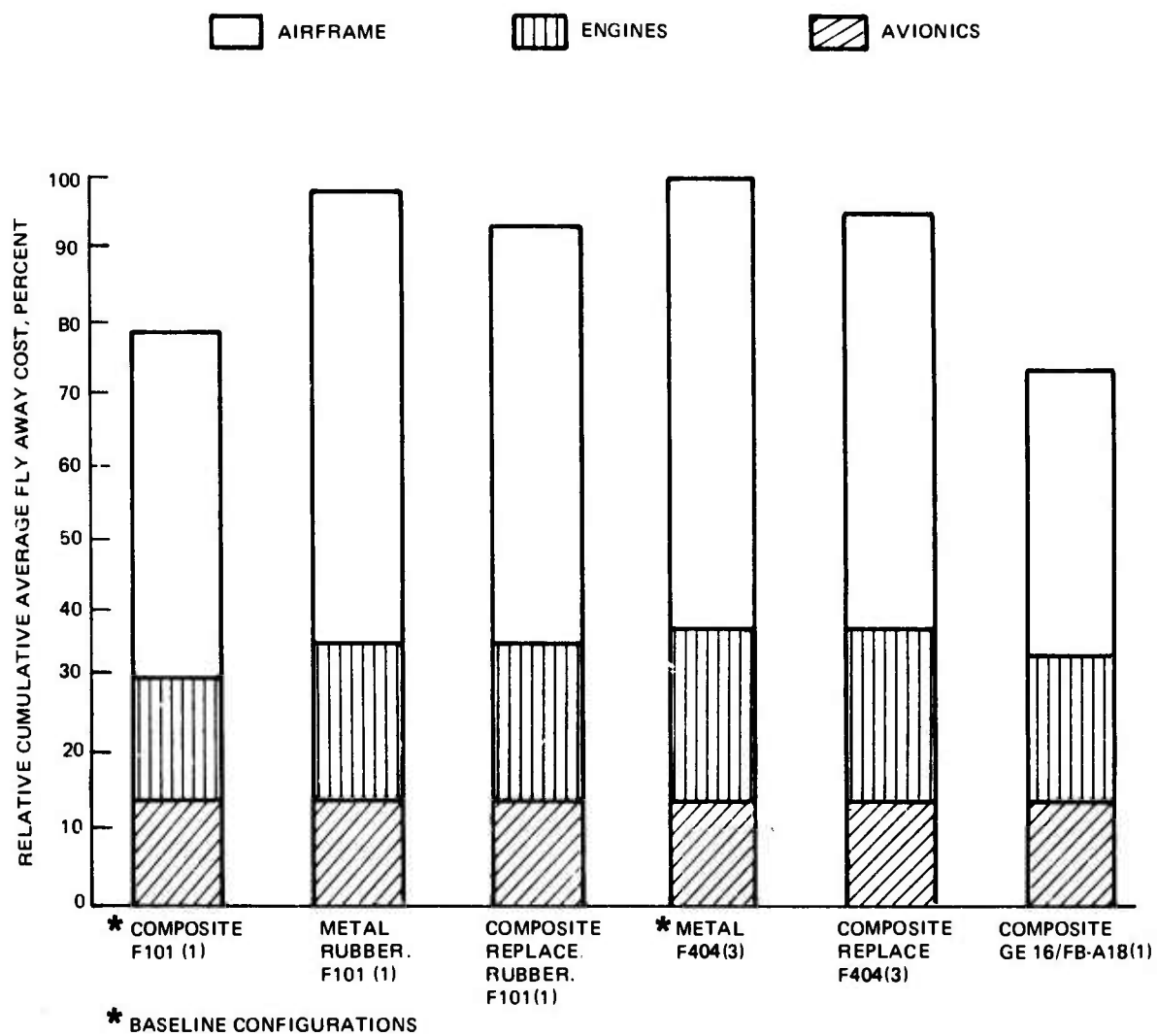


Figure 314. Cumulative Average Flyaway Costs

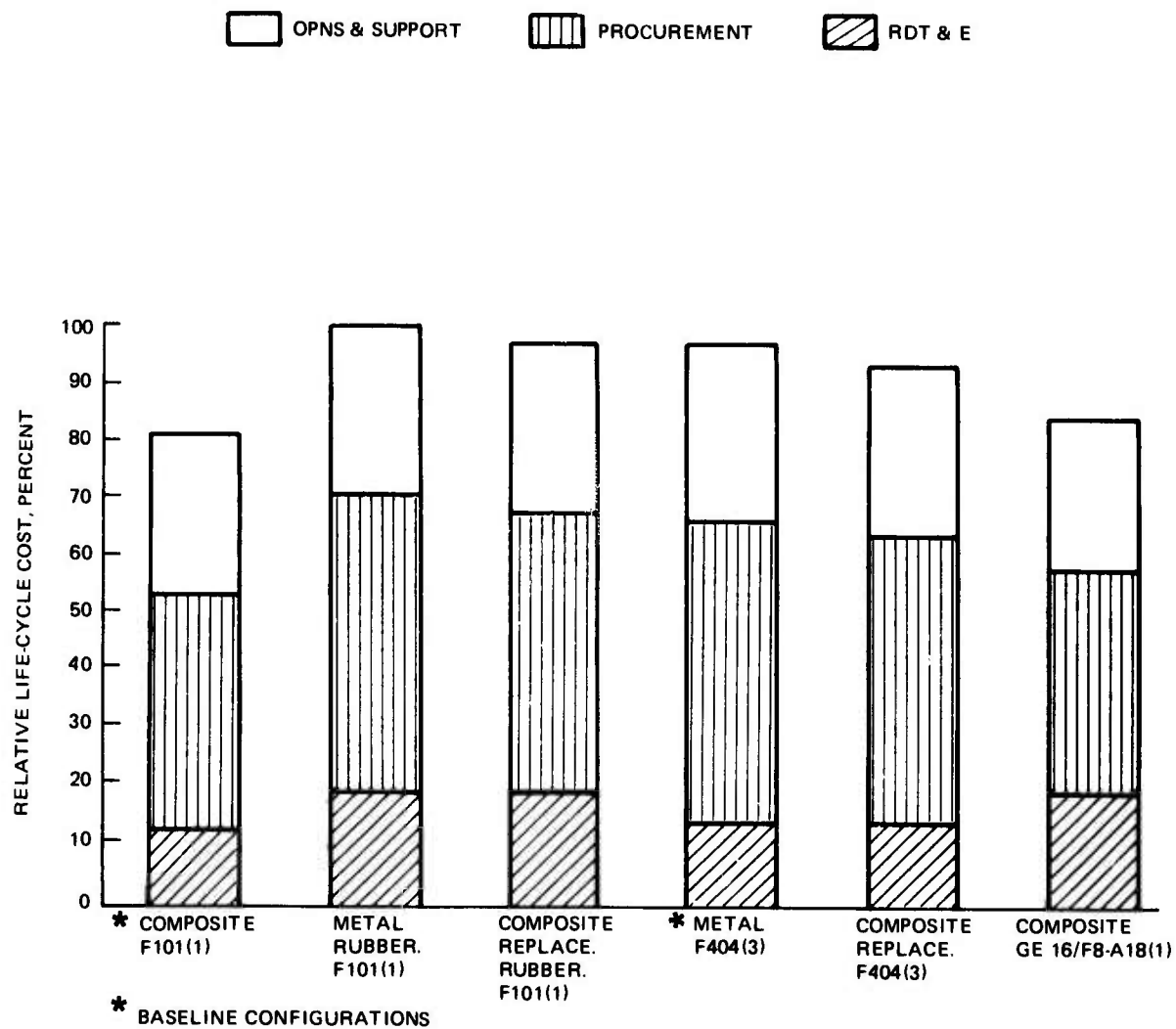


Figure 315. Life-Cycle Costs

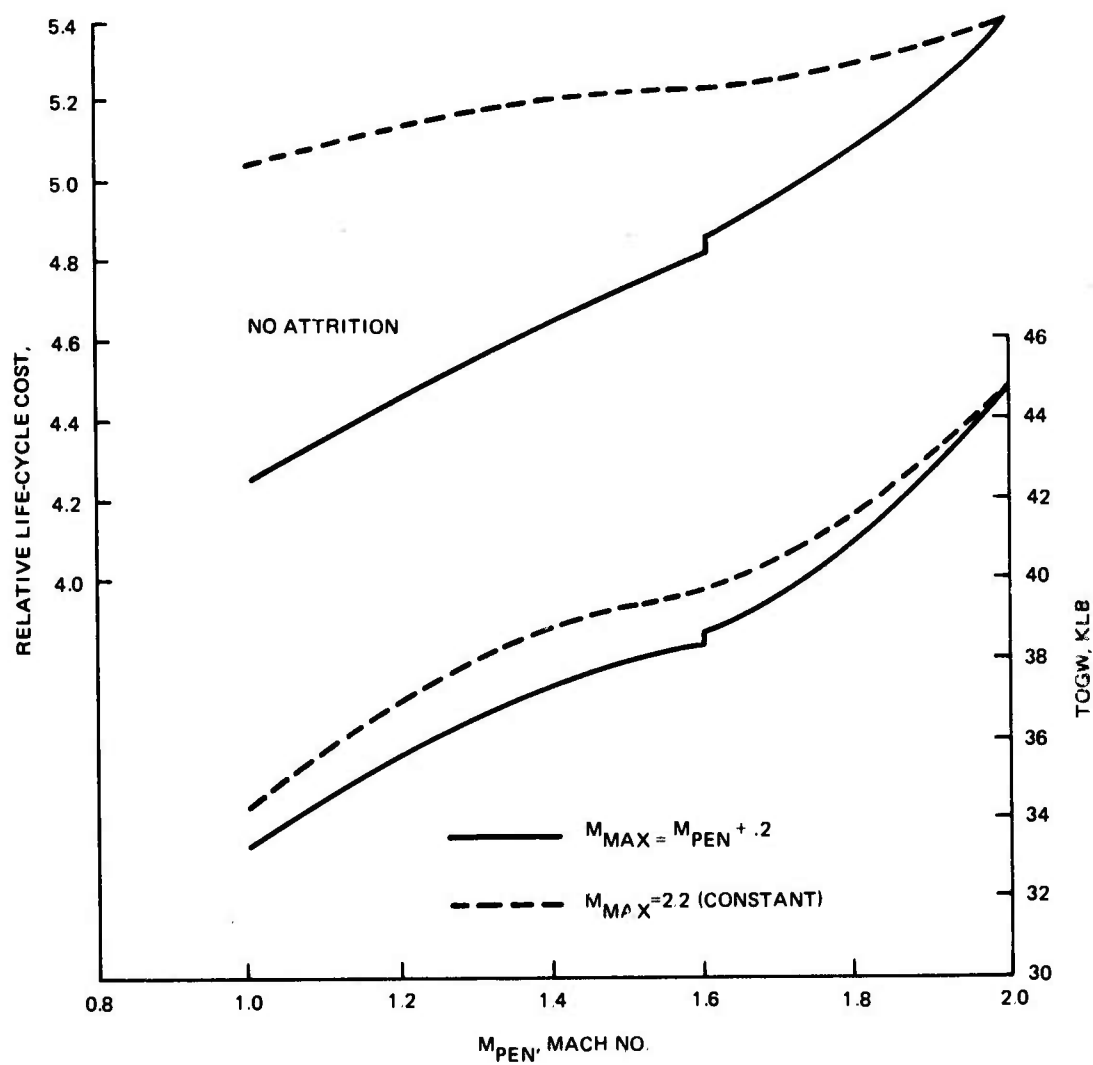


Figure 316. Cruise Mach No. Sensitivity, Composite Baseline F101(1), Baseline Mission

configurations. In one, M_{\max} is maintained at 2.2 and in the other, M_{\max} is varied with the penetration speed. Maintaining $M = 2.2$, while not a great penalty weightwise, incurs a considerable cost penalty, particularly when the lower penetration Mach numbers are selected.

Figure 317 shows that increasing the cruise Mach number from 1.6 to 2.0 incurs a 15% penalty in both cumulative average flyaway and life cycle costs. However, when attrition is considered, as shown in Section 2, the speeds can be on a par. As described in Section 2, selection of a cruise speed is sensitive to the number of sorties flown.

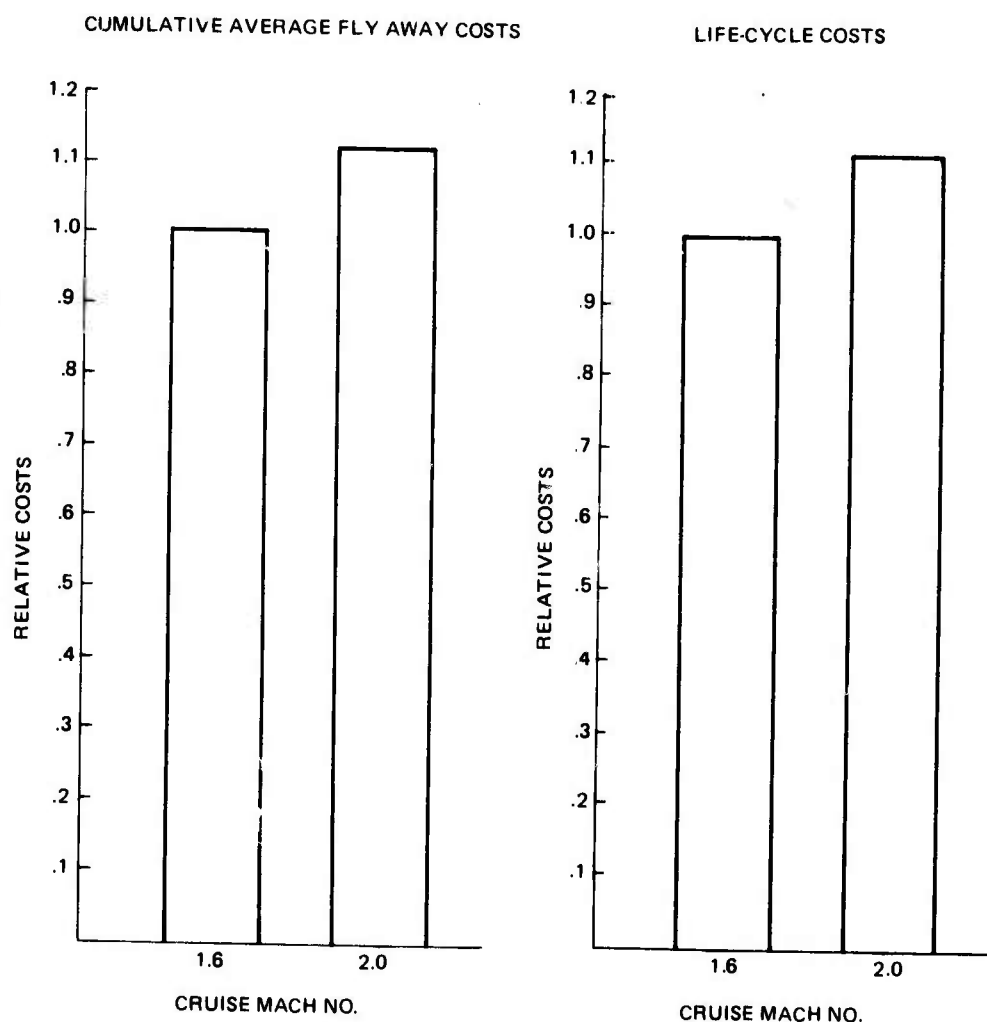


Figure 317. ADCA Mach 2 Cruise Cost Comparison

6.2.3 Reliability and Maintainability Analysis

The estimating technique used to develop ADCA maintenance manhours per flight hour (MMH/FH) estimates is sensitive to performance/design characteristics, responsive to design technology improvements, and provides realistic values which can be achieved in the field. The approach is based upon the use of correlation analysis to develop a model which relates historical maintenance data for current USAF tactical fighters to design/performance parameters. Maintenance estimating relationships were derived in Reference (5) from an investigation of correlations between MMH/FH and system design parameters of ten tactical USAF fighter aircraft*. Regression analysis-generated formulas are used in this study to project the historical baseline MMH/FH for each subsystem and the total aircraft configuration. The impact of technology improvement on each subsystem, expressed as a "technology improvement factor", reduces the baseline MMH/FH value to reflect improved reliability and reduced time to repair.

6.2.3.1 Maintenance Concept

The maintenance management concept for the ADCA is based upon a dual level system - organizational and depot - to insure high operational readiness. By properly designing ADCA for dual level maintenance, a reduction in DMMH/FH can be realized simply by the elimination of intermediate level maintenance alone. These design features, which include onboard health monitoring built-in-test, and modularity, lead to further reductions in organizational level maintenance and scheduled maintenance.

6.2.3.2 Technology Improvements

Realistic projections of MMH/FH goals must take into consideration technological advances which reduce maintenance resources and maintenance frequency. This was done by an engineering evaluation of the impact of technology improvements (technology cutoff 1980-1982) on the MMH/FH of each aircraft subsystem as shown in Table 64. Based on the evaluation, a technology improvement factor" was assigned to each subsystem which was used to adjust the baseline MMH/FH

Technology improvement factors for composite airframe, fuselage, and part of the flight control subsystems were based upon an evaluation of the R&M characteristics

*F-111, F-4E, F-4C, F-105, F-100, F-104, A-7D, F-5A, T-38 and A-37

of advanced composite structures. Studies conducted by Grumman and other aircraft manufacturers (References (6), (7) and (8)) provide the basis for the evaluation.

6.2.3.3 Reliability

Advanced composite designs are expected to exhibit improved reliability characteristics compared to equivalent metal designs. This is due primarily to reduction in the total number of parts and mechanical fasteners, and increased resistance to cracks, fractures, buckling, dents and punctures. The following reduction in failures/malfunction categories is projected:

- 70% for broken/loose/missing hardware failures
- 30% for crack/fracture/buckling failures
- 25% for foreign object damage and puncture/tear failures
- 30% for corrosion failures

The analysis indicates the advanced composite designs are expected to show an increase in MTBF of approximately 60 percent. This improvement has been reflected in the "technology improvement factor".

6.2.3.4 Maintainability

There is no essential difference between airframe maintenance manhours per repair for metal and advanced composite construction.

Using the regression analysis formulas in Reference (5) and the technology improvement factors in Table 64, R&M forecasts were derived and are summarized in Table 65. The analysis estimates an improvement of 1.7 MMH/FH for the composite baseline over the metal baseline. The factors for each configuration will be used in calculating their total life cycle costs.

6.2.4 Updated Vehicle Sizing Studies

Subsequent to the initial tradeoff studies, the vehicle was resized for increased payload. Comparisons of the resized vehicle were limited to four configurations.

<u>Airframe Material</u>	<u>Quantity and Type of Engine</u>
Metal	Three F-404
Composite	One F-101
Composite Substitution	Three F-404
Composite	One high T/W Adv. Engine

TABLE 64. SUBSYSTEM TECHNOLOGY IMPROVEMENT FACTORS

Subsystem	WUC	Technological Advances Impacting R & M	Technology Improvement Factors			
			Composite Baseline	Metal Baseline	Composite Substitute	Composite Advanced Engine
Airframe	1,100	Composites	0.8	0.95	0.8	0.8
Fuselage	12,000	Composites	0.8	0.95	0.8	0.8
Landing Gear	13,000	Improved Materials for Tires & Brakes	0.9	0.9	0.9	0.9
Flight Controls	14,000	Composites; BIT; Fly-by-Wire Digital Servo Valves, Integ. Servo	0.95	0.95	0.95	0.95
Power Plant	23,000	Onboard Health Monitoring Modularity	0.75	0.75	0.75	0.75
Environmental Controls	41,000	BIT; Advanced Cooling, Rotating Heat Exchangers	0.9	0.9	0.9	0.9
Electrical	42,000	VSCF; HVDC; Wild Freq; BIT; Fibre Optics; Battery Chrg. Control	0.9	0.95	0.95	0.95
Lighting	44,000	Fibre Optics	0.95	0.95	0.95	0.95
Hydraulic	45,000	BIT; Seals	0.9	0.9	0.9	0.9
Fuel	46,000	BIT; Sealing	0.9	0.9	0.9	0.9
Oxygen	47,000	Onboard Oxygen-Nitrogen Separator	0.95	0.95	0.95	0.95
Fire Detection	49,000		0.95	0.95	0.95	0.95
Instruments	51,000	Digital Processing; LSI; Integrate Display; Liquid Crystals	0.8	0.8	0.8	0.8
Auto Pilot	52,000	Digital Processing; BIT; LSI Strapdown Gyros	0.85	0.85	0.85	0.85
VHF	62,000	BIT; LSI	0.85	0.85	0.85	0.85
UHF	63,000	BIT; LSI	0.85	0.85	0.85	0.85
Interphone	64,000		0.9	0.9	0.9	0.9
IFF/SIF	65,000	Digital Processing;	0.85	0.85	0.85	0.85

TABLE 64. SUBSYSTEM TECHNOLOGY IMPROVEMENT FACTORS (CONTINUED)

Subsystem	WUC	Technological Advances Impacting R & M	Technology Improvement Factors			
			Composite Baseline	Metal Baseline	Composite Substitute	Composite Advanced Engine
Radio NAV	71,000	8IT; LSI; GPS	0.85	0.85	0.85	0.85
Radar NAV	72,000	8IT; LSI; Digital Processing Electronically scanned arrays	0.85	0.85	0.85	0.85
Bombing NAV	73,000	8IT; LSI	0.85	0.85	0.85	0.85
Fire Control	74,000	8IT; LSI	0.85	0.85	0.85	0.85
Weapons DLVY	75,000	8IT	0.95	0.95	0.95	0.95
ECM	76,000	Digital Programmable Processing; 8IT; LSI	0.8	0.8	0.8	0.8
Gun	84,000	Liquid Propellant; Long Life Barrels	0.8	0.8	0.8	0.8
Miscellaneous	90,000		0.95	0.95	0.95	0.95
Pre-Flight	03,100	Onboard Health Monitoring	0.9	0.9	0.9	0.9
Post-Flight	03,200	Onboard Health Monitoring	0.9	0.9	0.9	0.9
Periodic	03,400		0.1	0.1	0.1	0.1
Special	04,000		0.0	0.0	0.0	0.0
Periodic (SHOP)	03,400	Eliminated by Maintenance Concept	0.0	0.0	0.0	0.0

TABLE 65. R & M PARAMETER FORECASTS

Aircraft Configuration	MMH/FH	MFHBMA	MFHBF
Composite Baseline	10.6	0.28	0.56
Metal Baseline	12.3	0.24	0.48
Composite Substitute	11.7	0.26	0.52
Composite Adv. Engine	10.3	0.29	0.58

Figure 318 lists those parameters which were constant for all configurations. Table 66 also lists material distribution, and Figure 319, the vehicle design parameters for all configurations. These data represent the prime inputs to the PACE cost model.

•	V _{MAX} _____	1.8M, 2.0 FALLOUT
•	LOAD FACTOR _____	6.5g
•	NO. OF DESIGN MISSIONS _____	2
•	INSTALLED ELECTRONICS WEIGHT _____	1700 LB
•	AVIONICS COSTS NON-RECURRING _____	\$85M
	RECURRING _____	\$1.17 M/AC
•	NO. OF DEVELOPMENT A/C _____	12
•	PRODUCTION SCHED _____	300 A/C @ 60 YR (30, 60, 60, 60, 60, 30)
•	DOLLAR YEAR _____	1975

Figure 318, Cost Analysis Input Constants

TABLE 66. COST ANALYSIS INPUT VARIABLES

Material Distribution, % of AMPR Weight						
Configuration	Composite*		Ti	ST	AL	Misc
	Gr/Ep	B/Ep				
Composite	54.0	6.1	6.9	6.3	4.4	1.2
Metal (All)	0	0	15.0	18.0	42.0	5.0

*76.2% of structural weight

CONFIGURATION	TOGW, LB	WT EMPTY, LB	AMPR WT, LB	W/S PSF	STRUCT DENSITY PCF
METAL BASELINE F404 (3)	52,994	30,105	20,097	107.9	9.04
COMPOSITE BASELINE F101 (1)	40,553	21,556	13,519	95.5	8.00
COMPOSITE SUBST. F404 (3)	50,183	28,172	17,286	104.2	8.02
COMPOSITE ADV. ENGINE	38,288	19,347	12,912	95.9	7.84

ENGINE PARAMETERS				
ENGINE MODEL	THRUST, CLASS LB.	THRUST/WT	COSTS, N-RECUR	1976 \$M RECUR
F-101	30,000	7.0	0	1.28
F-404	16,000	8.0	0	.58
ADVANCED ENG	33,300	11.7	500	1.60

Figure 319. Vehicle Design Parameters

6.2.5 Resized Vehicle Cost Comparisons

In Figure 320 comparisons are shown in life cycle and cumulative average flyaway costs for the four configurations. It shows that a composite configuration has a clear advantage over the metal one, and that cost savings are optimum when the configuration is designed to utilize all the advantages of composites. The penalty for using an off-the-shelf engine was found to be minor and was offset by increased development and procurement costs for an advanced high thrust-to-weight engine.

Figure 321 provides additional perspective into cost advantages of composites by comparing unit costs for average procurement including development costs, cumulative average flyaway and 300th unit flyaway. All costs are compared to average procurement cost for the metal baseline.

6.2.6 Composite Airframe Cost Breakdown

Using the Grumman developed parametric cost estimating model, PACE, previously described, composite airframe costs have been broken down according to phase and cost element. These costs are expressed in 1975 dollars and do not include G and A or fee.

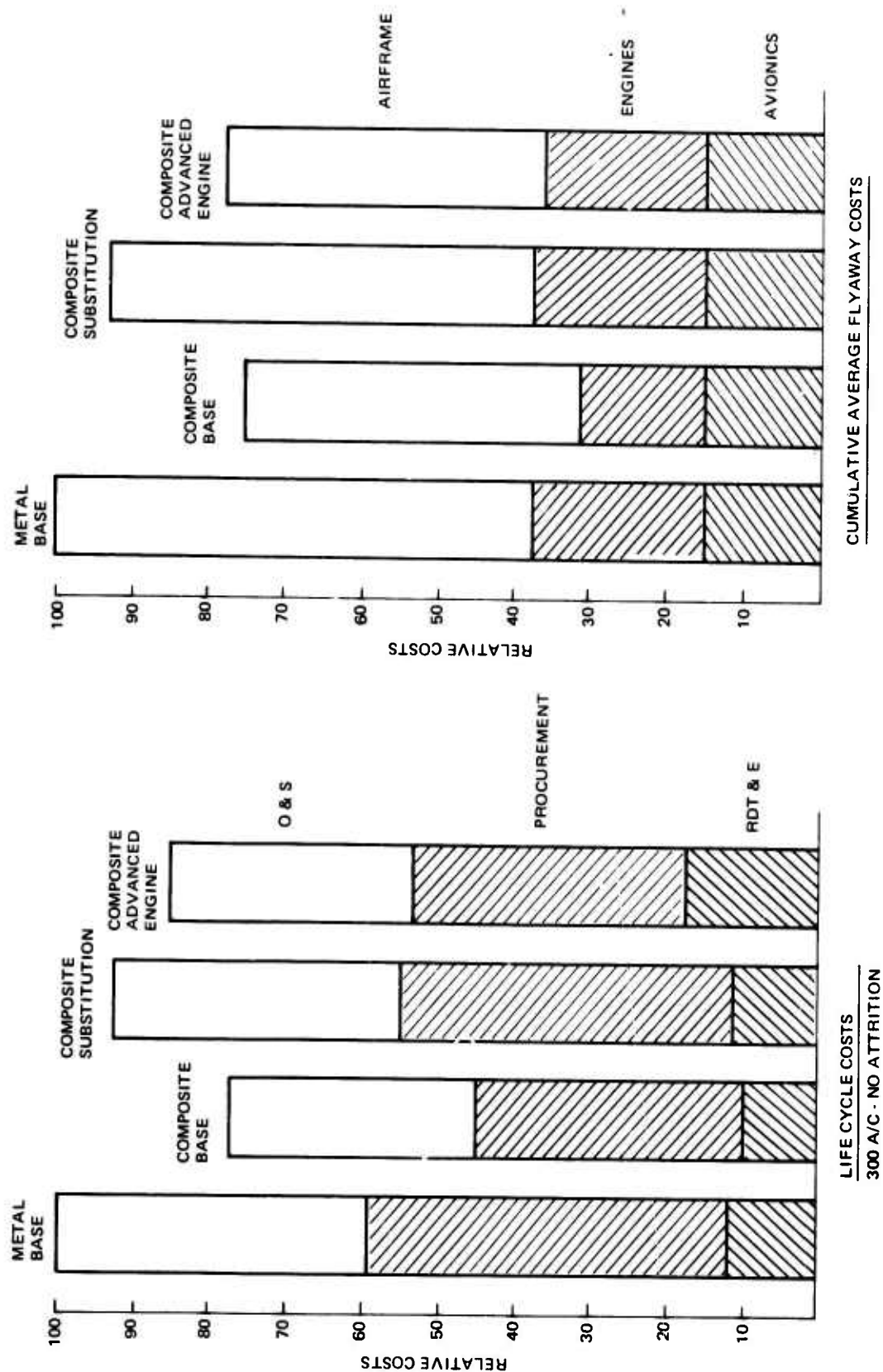


Figure 320. ADCA Cost Comparisons

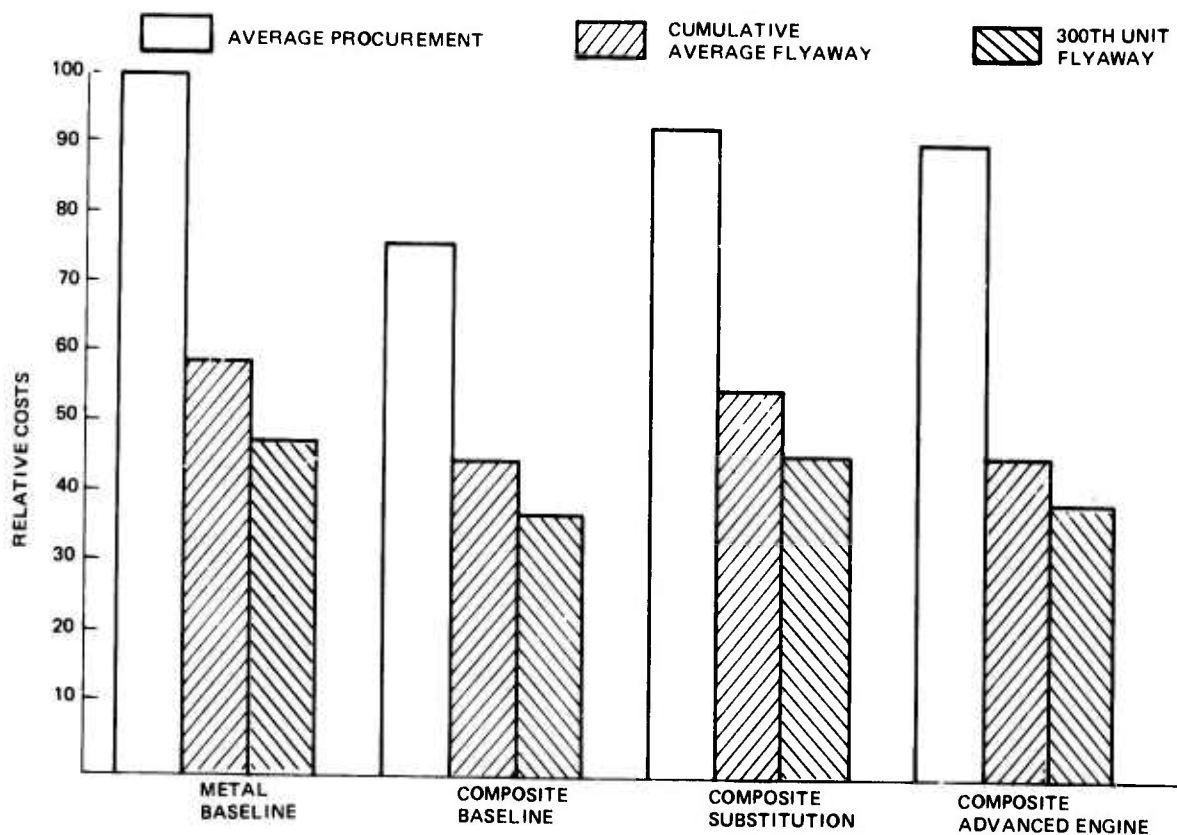


Figure 321. ADCA Unit Cost Comparisons

Table 67 shows the breakdown for the development phase during which 12 development aircraft are planned to be built and tested. Total dollars by cost element are further subdivided into direct and indirect costs and the direct costs for the labor cost elements are further translated into manhours. Table 68 provides similar cost data for a production run of 300 aircraft.

Tables 69, 70, 71 and 72 break down the costs of fabricating the major components, wing, body, fin and canard, and air induction section. Material costs are provided for each according to type. PACE is structured to provide costs for tail surfaces. The canard, being of a similar type structure as a stabilizer, has been included with the fin.

**TABLE 67. ADCA COMPOSITE AIRFRAMES RDT & E COST BREAKDOWN
(12 DEVELOPMENT AIRCRAFT, NO G & A, NO FEE)**

Cost Element	Total \$M	Direct \$M	Indirect \$M	Direct Hrs M
Engineering	126.2	64.4	61.8	6.12
Flight Test	27.4	14.0	13.4	1.40
Tooling	64.1	26.5	37.6	3.64
Fabrication/Subassembly	80.6	33.3	47.3	5.71
Final Assembly	5.0	2.0	3.0	0.35
Coordination	4.5	2.3	2.2	0.32
QC	6.4	2.6	3.8	0.38
Raw Material	3.2	-	-	-
Landing Gear	1.5	-	-	-
Equipment	13.5	-	-	-
Totals	332.4	145.1	169.1	17.92

**TABLE 68. ADCA COMPOSITE AIRFRAME PRODUCTION COST BREAKDOWN
(300 AIRCRAFT, NO G & A, NO FEE)**

Cost Element	Total \$M	Direct \$M	Indirect \$M	Direct Hrs M
Engineering	68.4	34.9	33.5	3.31
Tooling	61.6	25.4	36.2	3.49
Fabrication/Subassembly	287.3	118.7	168.6	20.38
Final Assembly	37.4	19.1	18.3	2.65
Final Assembly Test	16.0	8.2	7.8	1.14
Coordination	69.7	35.6	34.1	4.95
Quality Cont.	71.8	29.7	42.1	4.27
Raw Material	49.2	-	-	-
Landing Gear	17.0	-	-	-
Equipment	126.6	-	-	-
Totals	805.0	271.6	340.6	40.19

**TABLE 69. ADCA COMPONENT PRODUCTION COST BREAKDOWN
(300 AIRCRAFT, NO G & A, NO FEE)
WING**

Cost Element		Total \$M	Direct \$M	Indirect \$M	Direct Hrs M
Fabrication/Subassembly		106.7	44.1	62.6	7.57
Coordination		24.6	12.6	12.0	1.75
QC		27.3	11.3	16.0	1.62
Raw Material - 16.7	Aluminum Sheet Metal	0.02	—	—	—
	Aluminum Machined Parts	0.08	—	—	—
	Aluminum Honeycomb	0.01	—	—	—
	Steel Machined Parts	0.08	—	—	—
	Titanium	0.66	—	—	—
	Fiberglass	1.18	—	—	—
	Boron Composite	0	—	—	—
	Graphite Composite	14.68	—	—	—
Total		175.3	68.0	84.1	10.19

**TABLE 70. ADCA COMPONENT PRODUCTION COST BREAKDOWN
(300 AIRCRAFT, NO G & A, NO FEE)
BODY**

Cost Element		Total \$M	Direct \$M	Indirect \$M	Direct Hrs M
Fabrication/Subassembly		98.5	40.7	57.8	6.99
Coordination		24.6	12.6	12.0	1.75
QC		24.4	10.1	14.3	1.45
Raw Material - 21.0	Aluminum Sheet Metal	0.03	—	—	—
	Aluminum Machined Parts	0.12	—	—	—
	Aluminum Honeycomb	0.01	—	—	—
	Steel Machined Parts	0.23	—	—	—
	Titanium	3.02	—	—	—
	Fiberglass	0.94	—	—	—
	Boron Composite	5.87	—	—	—
	Graphite Composite	10.81	—	—	—
Total		168.5	63.4	84.1	10.19

**TABLE 71. ADCA COMPONENT PRODUCTION COST BREAKDOWN
(300 AIRCRAFT, NO G & A, NO FEE)
FIN AND CANARD**

Cost Element		Total \$M	Direct \$M	Indirect \$M	Direct Hrs M
Fabrication Subassembly		49.3	20.4	28.9	3.49
Coordination		12.3	6.3	6.0	.87
QC		12.2	5.0	7.2	.73
Raw Material - 7.4	Aluminum Sheet Metal	0.01			
	Aluminum Machined Parts	0.02			
	Aluminum Honeycomb	0.01			
	Steel Machined Parts	0.09			
	Titanium	0.56			
	Fiberglass	0.37			
	Boron Composite	0			
	Graphite Composite	6.36			
Total		81.2	31.7	42.1	5.09

**TABLE 72. ADCA COMPONENT PRODUCTION COST BREAKDOWN
(300 AIRCRAFT, NO G & A, NO FEE)
AIR INDUCTION SECTION**

Cost Element		Total \$M	Direct \$M	Indirect \$M	Direct Hrs M
Fabrication Subassembly		32.8	13.6	19.2	2.33
Coordination		8.2	4.2	4.0	.58
QC		7.9	3.3	4.6	.47
Raw Material - 4.2	Aluminum Sheet Metal	0.02			
	Aluminum Machined Parts	0.06			
	Aluminum Honeycomb	0.01			
	Steel Machined Parts	0.07			
	Titanium	0.01			
	Fiberglass	0.29			
	Boron Composite	0			
	Graphite Composite	3.73			
Total		53.1	21.1	27.8	3.38

6.2.7 Fuel Consumption Comparisons

Figure 322 compares the fuel consumption for each configuration both for ten years of peacetime operations and for a single wartime mission. The models used to derive these values are sensitive to vehicle design parameters such as weight. On this basis the advanced engine has only a minor fuel consumption advantage. An in-depth examination of engine performance by an engine manufacturer would be necessary to establish more realistic numbers.

6.2.8 Optimum Composite Usage Tradeoff

Figure 323 shows the results of the tradeoff to determine the optimum usage of composites. The almost constant improvement in costs with increased utilization of composites begins to reverse at about 75% and becomes negative beyond 80%. The last 20% of a structure consists primarily of high load concentration areas that, from weight and cost aspects, are best accommodated by high strength metal fittings and doublers. One hundred percent utilization cannot be achieved because of temperature considerations such as for engine firewalls.

6.2.9 Production Feasibility

An assessment of the effects of producing the ADCA in current facilities indicates that Grumman could proceed into quantity production with facilities, equipment and manpower currently available and/or in the process of activation.

At Grumman, advanced composite structures are fabricated in the production bonding facility, one of the most modern and best equipped in the country. Located in Plant 3, Bethpage, New York, this facility covers 86,500 sq ft and is mostly highbay (over 15 ft. high). It is used for development, prototype and production fabrication. Currently, 1600 pounds of boron and graphite/epoxy are processed per month. Four autoclaves are available: three are 10 ft in diameter x 30 ft long; the fourth is 42 in. x 10 ft.

All advanced composite materials are laid-up in the temperature and humidity-controlled adhesive bonding area. The 3-in. wide boron/epoxy tape currently used in production is laid-up by aid of a semi-automatic machine on mylar templates, which are subsequently transferred to a backlighted inspection table, then onto the production tools or mold forms.

Other equipment in this facility includes freezers for storing prepregs, a pneumatically operated tape cutter, layup and work benches, light tables for inspection, and

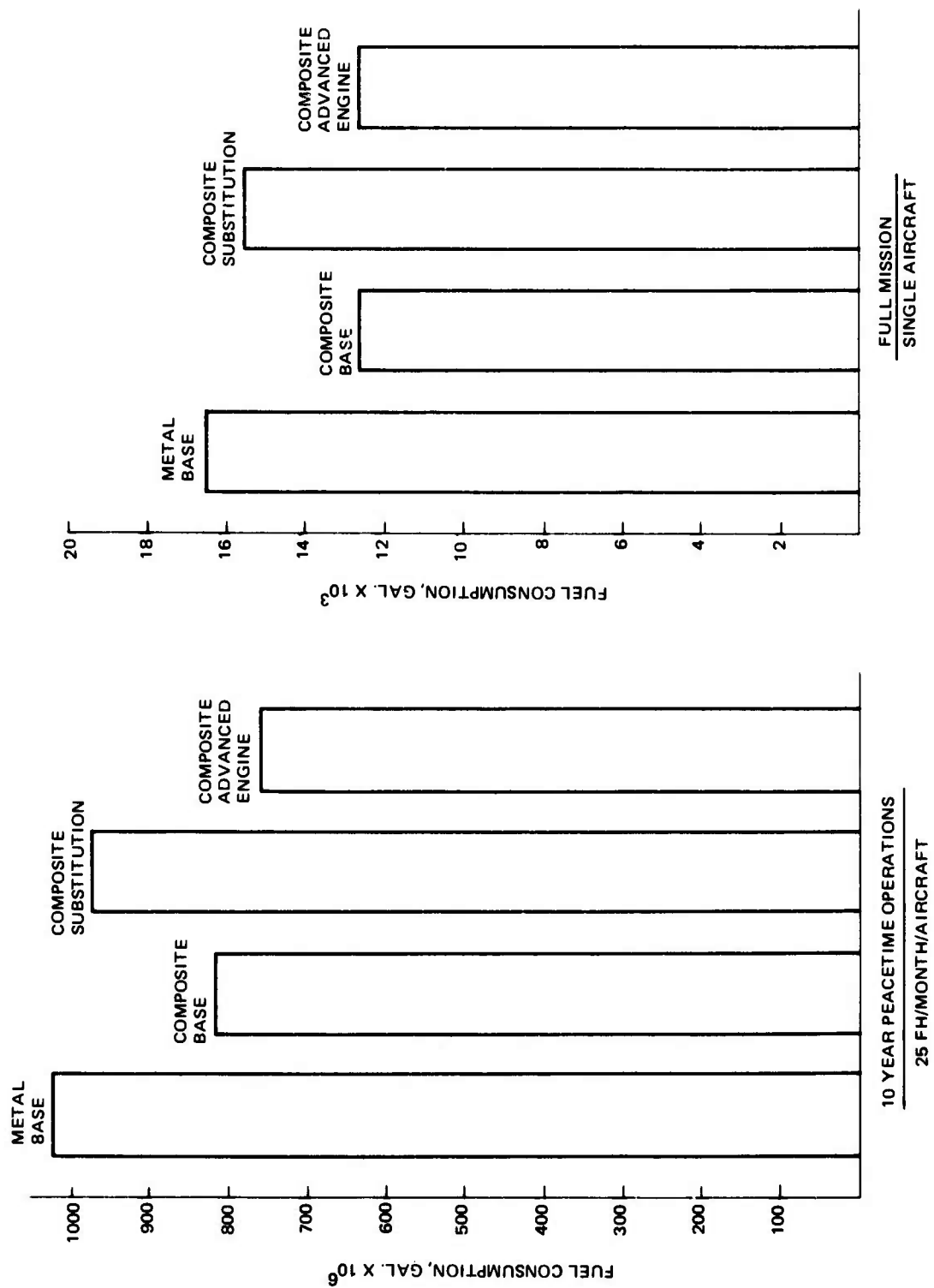


Figure 322. Fuel Consumption Comparison

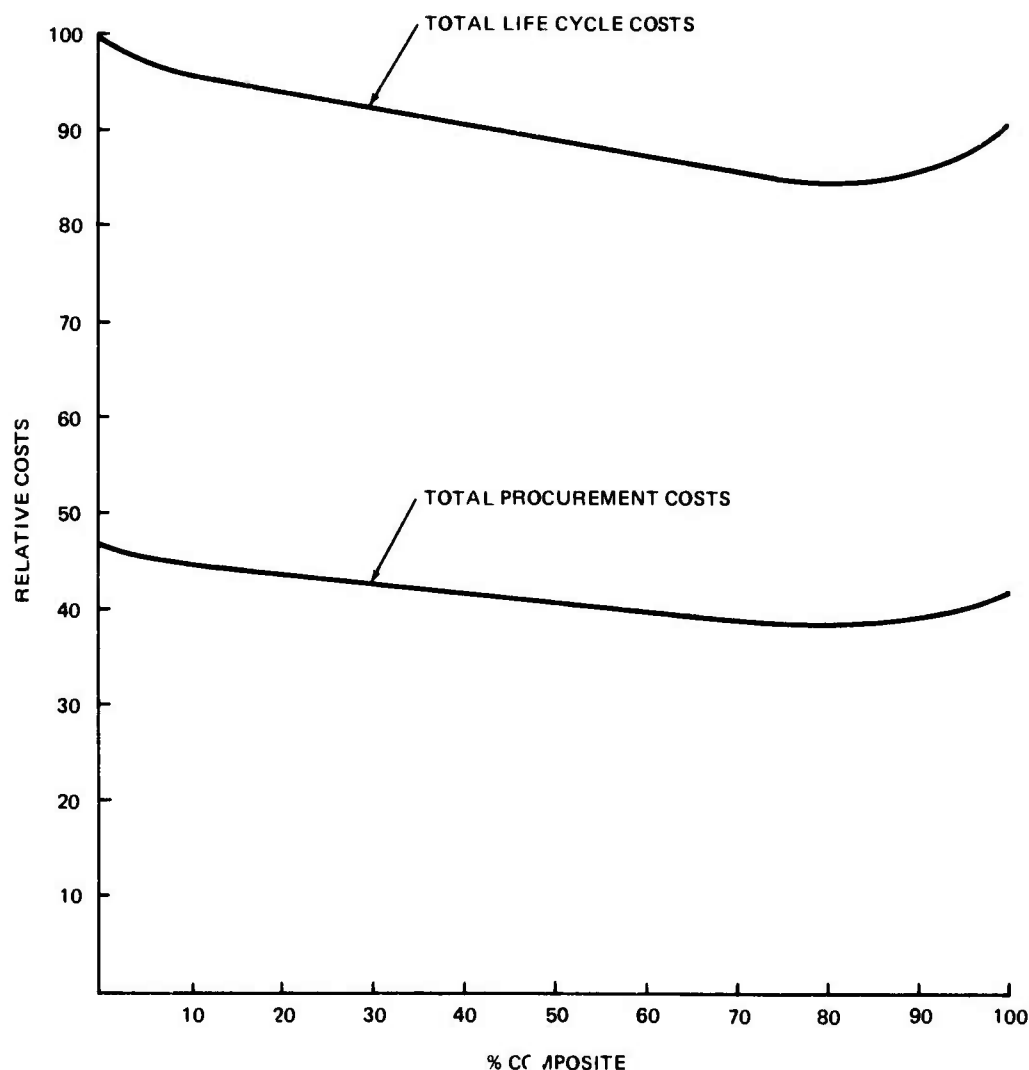


Figure 323. Composite Utilization Rate Payoff

platen presses with capacities to 5 x 8 ft. The Cramic core cutter is an example of the automatic core cutting machinery now being used at Grumman. The Craco tape-controlled riveter drills, reams, seals, and installs rivets in production assemblies.

In addition, Grumman is currently completing the activation of a fully integrated 170,000 ft facility at Milledgeville, Georgia, dedicated to the production of composite and plastic aerospace parts. Environmentally controlled layup rooms, walk-in freezer storage, core cutting facilities, a trim shop, mechanical assembly areas, and a tooling facility are provided. The largest autoclave is 10 ft x 35 ft, capable of operating at 600°F at 125 psi in either a conduction or convection mode. Five large ovens are being

installed, including a 10 ft x 10 ft x 30 ft unit with 600°F capability. Several platen presses, a 32-oz injection molding machine, capable of processing either thermoplastic or thermosetting materials, two vacuum-forming machines, and a canopy shop are being transferred from Bethpage. This facility is supported by a complete Quality Control Laboratory.

This facility will also be the new home of the integrated laminating center currently undergoing development proof testing at Bethpage. This center has been designed to integrate tape laying, ply handling, net trimming, inspection, and stacking of piles into one mechanized machine with a projected reduction of about 60% over conventional approaches.

Section VII

TECHNOLOGY DEVELOPMENT PLAN

The level of technology applied to the ADCA vehicle is consistent with technology readily available in the early 1980's time frame. The structural arrangement of the vehicle incorporates design concepts that, in most cases, have been verified by past composite programs. In the cases where the design concepts have not been verified, the weight/cost savings made possible by their application have not been included in the final analysis, so that the validity of the overall program results would not depend upon successful technology demonstration.

The ADCA program benefits, therefore, do not depend so much upon successful technology demonstration as the synergistic application of proven materials and design concepts. However, an assessment has been made to define the objectives of technology development programs, that will yield maximum payoff in overall reduced program costs and provide the required confidence for implementation, in those areas where sufficient development work has not been done.

The composite technology development thrusts, that have been identified to reduce overall program costs, have addressed both the procurement and life-cycle costs and include:

- Procurement Costs

The major thrusts to reduce procurement costs have been identified to be in the vehicle assembly phase of production, particularly in techniques to reduce the number of mechanical fasteners and in assembly techniques that will minimize shimming while maintaining critical air passage contours.

- Life-Cycle Costs

The major thrusts to reduce life-cycle costs have been identified to be the development of repairable fuel sealing concepts, both for faying surface sealing and individual fastener sealing and the development and verification of damage tolerant structural design concepts.

The emphasis on minimizing assembly costs, in order to reduce procurement cost, is based on an analysis of the cost drivers in the B-1 Composite Horizontal Stabilizer Program. This analysis indicated that, of the total recurring material costs on the

program, 22% is associated with drilling and fastening and includes the cost of hardware and drills. In addition, of the total manufacturing costs, 47% is associated with final assembly. Of the assembly costs, 66% is a result of the drilling and fastener installation costs. Although the Composite Horizontal Stabilizer contains 10,000 fewer fasteners than the metal stabilizer, it is apparent that final assembly costs, particularly drilling and fastener installations, are the major production cost drivers.

In conventional structures, a large number of fasteners are installed on a one-time basis only, never to be removed during the lifetime of the vehicle. All of these fasteners, however, suffer from the installation costs and are potential corrosion and fuel leakage sites. The justification for these fasteners, in composite structures, is a hold-over from metal fabrication techniques where the fasteners provided primarily shear transfer and secondary tension capability, to prevent skin stiffener separation due to buckling or fuel pressure loads.

In composite structure, the primary shear capability could be provided by a bonded joint, if some technique could be developed to resist the normal (tension) load components. A potential technique for accomplishing this is to stitch the substructure to the skin prior to co-curing. In this technique, the stitches would be designed to provide the tension capability. Several potential sewn-joint techniques are illustrated in Figure 324.

In conjunction with this advanced skin-to-substructure fastening technique, an advanced assembly technique has been established, which may eliminate the costly shimming of cover-to-substructure requirement in order to maintain air passage contour. The technique, illustrated in Figure 325, basically consists of a lower cover with integrally stitched caps and a substructure co-cured with (but not bonded to) the upper cover. By placing a bead of liquid shim in the lower-cover cap slots and inserting the substructure details, the liquid shim, upon curing, will hold the substructure in the required position, defined by jig located upper cover air passage. In order to accomplish this, the upper cover is temporarily attached to the substructure. Upon cure of the liquid shim, the cover is removed and all substructure attachments made. The upper cover is then reinstalled and permanently attached.

The ADCA life-cycle cost savings, over the metal aircraft, are primarily a result of the reduced size of the vehicle and the inherent corrosion and fatigue resistance of composite materials. Technology gaps do exist that may impact the life-cycle cost of the

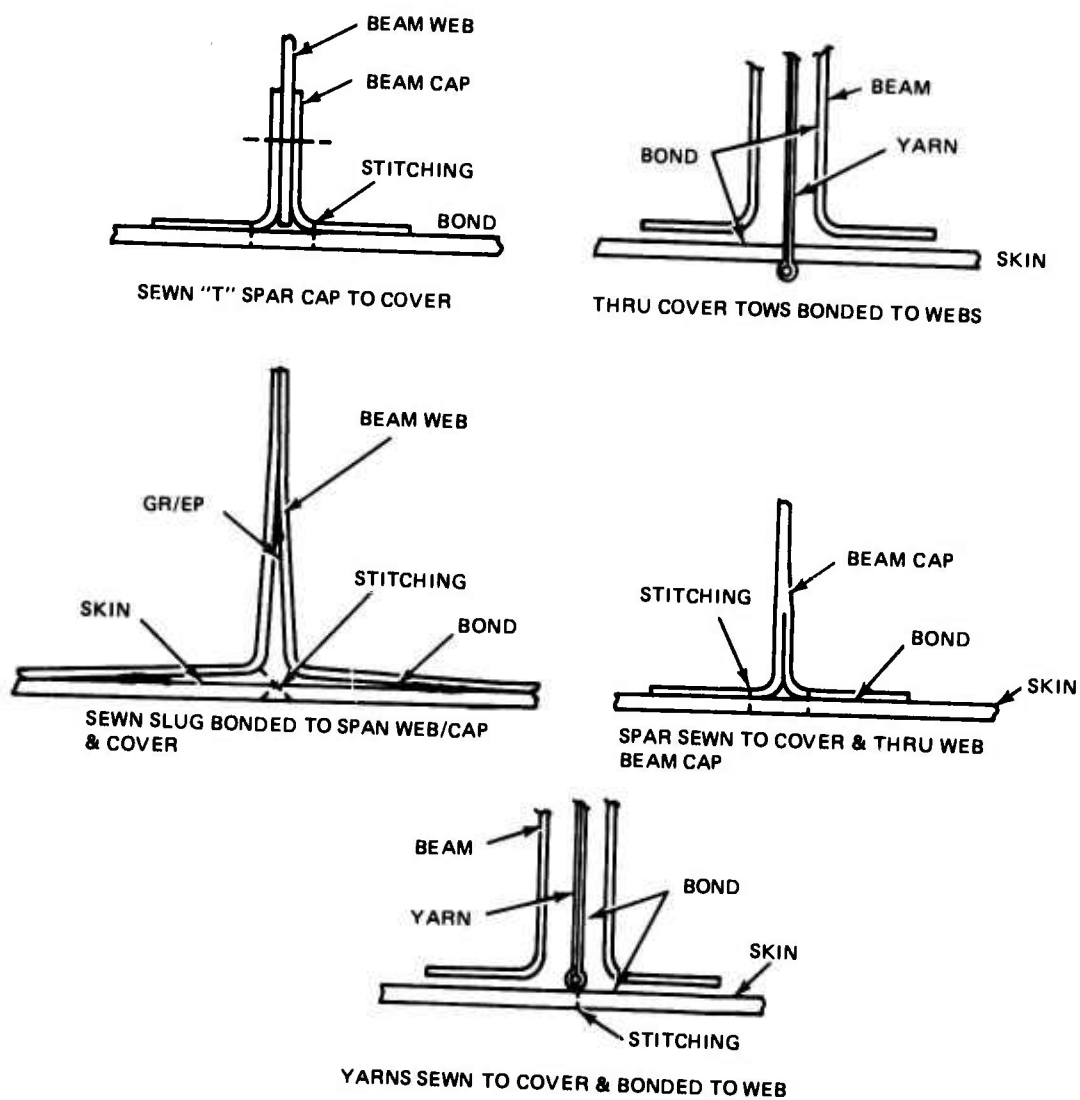


Figure 324. Cover-to-Substructure Attachment Techniques

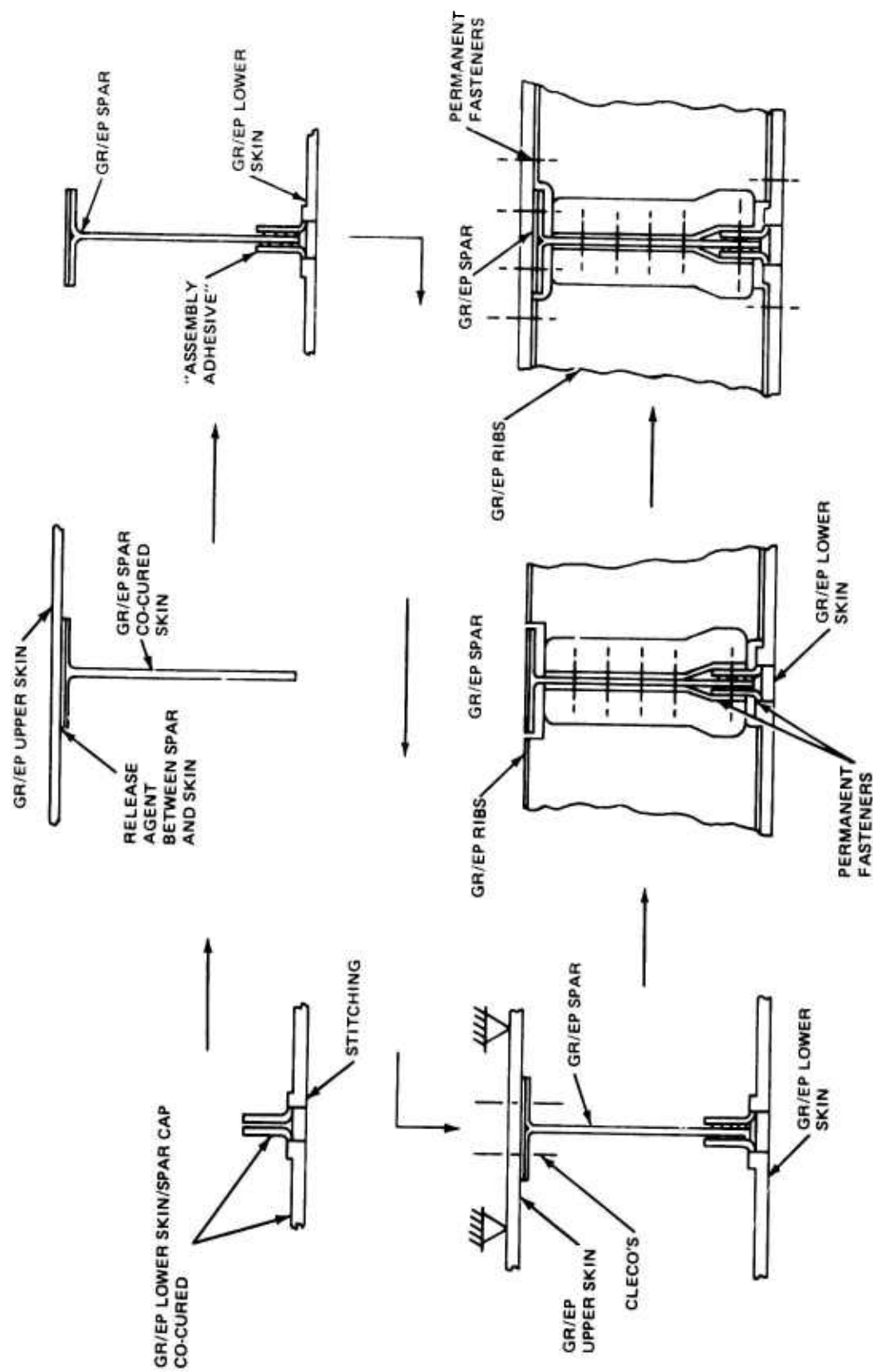


Figure 325. Advanced Assembly Technique for Skin to Substructure Fastening

vehicle, in particular the fuel sealing of integral composite fuel tanks. Although partially addressed on several past composite programs, a satisfactory, cost-effective, repairable, fuel sealing concept has not yet been developed, and the existing techniques do not completely satisfy the requirements.

Faying surface sealing is the least applicable of the existing techniques, in that the limited access of thin fighter wings does not permit repair of in-service fuel leaks, and external repair is not feasible. The injectable channel or groove seal technique, although repairable, has not been fully demonstrated on composite hardware, and the problems of injection ports and injection pressure effects, on the wider fastener spacing required on composite structures, have not been resolved.

A technique applicable to composite structure was established and is illustrated in Figure 326. In this technique, thermoplastic material is provided at the faying surface. Upon installation of the upper cover, preload is applied to the upper cover at the fuel seal joints, and local heat is applied to fuse the thermoplastic material. However, for this technique to be effective, cover removal techniques must be established, together with compatibility of the bonded/bolted joint flexibility and the ability to reseal after fuel-leak contamination.

As discussed previously in the report, damage tolerant design techniques are possible with composite components that could not be achieved with metallic structure. The concept of utilizing softening strips in wing panels, to confine the damage, can result in up to 200-pound structural weight savings on the ADCA vehicle. Although not baselined on the ADCA, the effectiveness of these techniques should be established, to provide the confidence necessary for composite implementation.

In addition to these technology areas that impact the program-cost of a vehicle, a whole host of environmental and service considerations exists that require development work, in order to achieve wholesale advanced composite material application. These areas include:

- Lightning-Strike Protection

Although addressed in several past advanced composite programs, the protection techniques have stressed only structural protection and not the associated problems of fuel-tank safety and avionics, fly-by-wire, system safety. This area requires detailed attention and resolution before an ADCA-type vehicle is feasible.

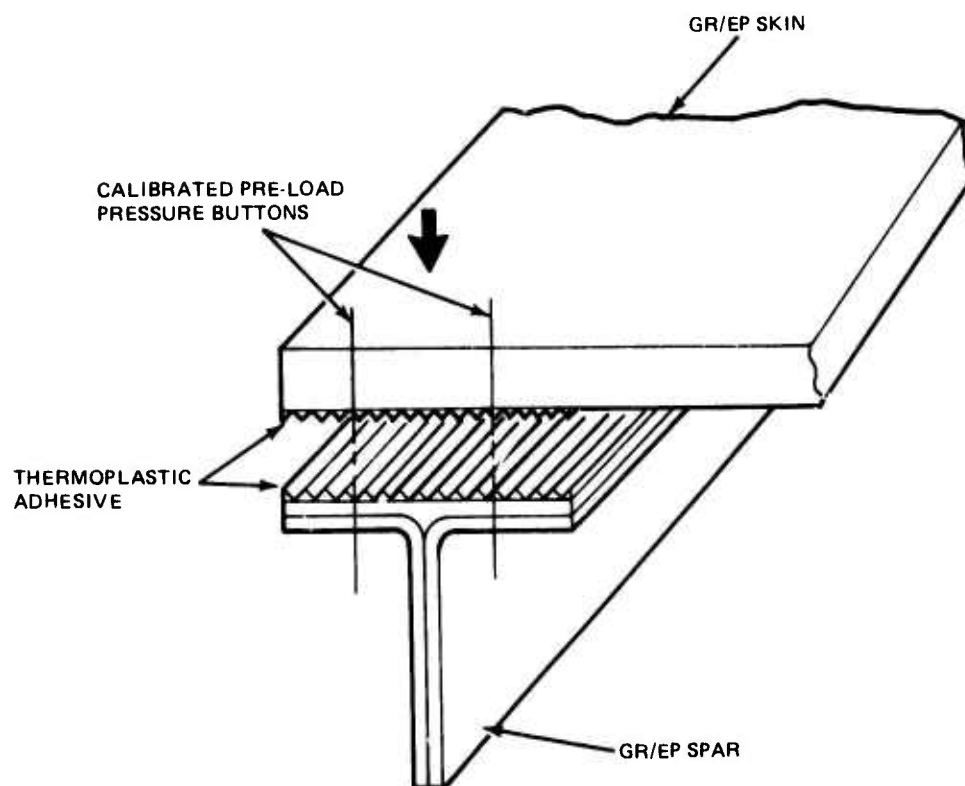


Figure 326. Advanced Sealing Concept

- Onboard Systems Grounding and Shielding

Although the ADCA vehicle provided for internal shielding and grounding, by means of metallic foil or flame spray, the effectiveness of these techniques has not yet been established. The effectiveness of the potential protection techniques should be established on realistic vehicle hardware and should include the electromagnetic effects resulting from lightning or nuclear pulse, the static discharge capability, and the vehicle/system grounding effectiveness. Particular attention must be given to the shielding of joints and the compatibility with weather sealing access doors.

- Environmental Compatibility

Along with the ongoing work on the moisture effects on composite structure, development work is required to establish the compatibility in a real-world environment, time/temperature, of composite materials with fuel, hydraulic fluid, cleaning agents, paint strippers, de-icing, and fire extinguishing fluids and the various gases anticipated in the vehicle such as oxygen, ozone and gun gasses.

- Erosion Protection

Although effective erosion protection systems exist for fiberglass structure, the wholesale application of advanced composites requires a detailed examination of the vehicle, to determine erosion protection requirements and the effectiveness of the current system.

- Acoustic Environment

Although not critical to the ADCA vehicle, due to the low acoustic environment, analytic techniques to predict structural capability of composites, in the acoustic environment, should be generated and correlated with test data. The response of metal structure in an acoustic environment is just barely understood, and composite structure response is not understood at all. In order to produce an optimum structure from the outset of the design, the effect of the acoustic environment must be understood.

- Laser Sensitivity

The potential implementation of air-to-air laser weapons makes it mandatory that a development plan be established, to determine the sensitivity of composites to laser weapons, and define and verify appropriate protection systems.

- Major Component Structural Interface Compatibility

The major problem, hindering the large-scale use of advanced composite materials, is that the vehicle program offices lack the confidence or background data to commit to advanced composites from the outset. This confidence can only be established in two ways: by the in-service data provided by current flight hardware, and by the structural demonstration and verification of a large-scale real vehicle component, incorporating as many of the critical structural areas of the vehicle as possible. The structural arrangement of the ADCA, Figure 155, indicates that a major component which includes the fuselage from Station 600 to 702 and the wing box above this area of the fuselage and running out to the wing planform break at B-L. 120.95 would incorporate a large portion of the critical structural regions of the vehicle.

These would include:

- Wing fuselage attachments
- Landing gear bulkhead and attachment
- Wing integral fuel tank
- Fuselage integral fuel tank
- Engine inlet and mount
- Control system attachment

This component would also include such detail design problems as the loading and laminate property variations around curved frames, detail joint design and verification, and the detail interaction between major components.

A full-scale component of this type, based on a realistic vehicle, would provide a large measure of the confidence needed, to commit to wholesale application of advanced composites to wing fuselage structure, on the next generation vehicle.

Section VIII
REFERENCES

1. Whitney, J.M. and Nuismer, R.J., "Stress Fracture Criteria for Laminated Composites Containing Stress Concentrations", J. Composite Materials, pp 253-265, Volume 8, July, 1974.
2. Savin, G.N., "Stress Concentration Around Holes", NASA TT F-607, November, 1970.
3. "Graphite/Epoxy and Boron-Graphite/Epoxy Hybrid Design Allowables", Grumman Aerospace Corp. CTN-75.1, Dec. 1975.
4. F. Austin et al "Aeroelastic Tailoring of Advanced Composite Lifting Surfaces in Preliminary Design" presented at AIAR/ASME/SAE 17th Structures, Structural Dynamics, and Materials Conference, Valley Forge, Pa., May 1976.
5. "Extension of Automated Structural Optimization Program (ASOP)" (R & D project currently being performed by Grumman Aerospace Corporation under Contract No. F33615-75-C-3146).
6. Wilkinson, K., et al., "Structural Optimization of Military Aircraft Subject to Aeroelastic and Strength Requirements", AFFDL-TR-75-137, December, 1975 (prepared by Grumman Aerospace Corporation under Contract No. F33615-72-C-1101).